

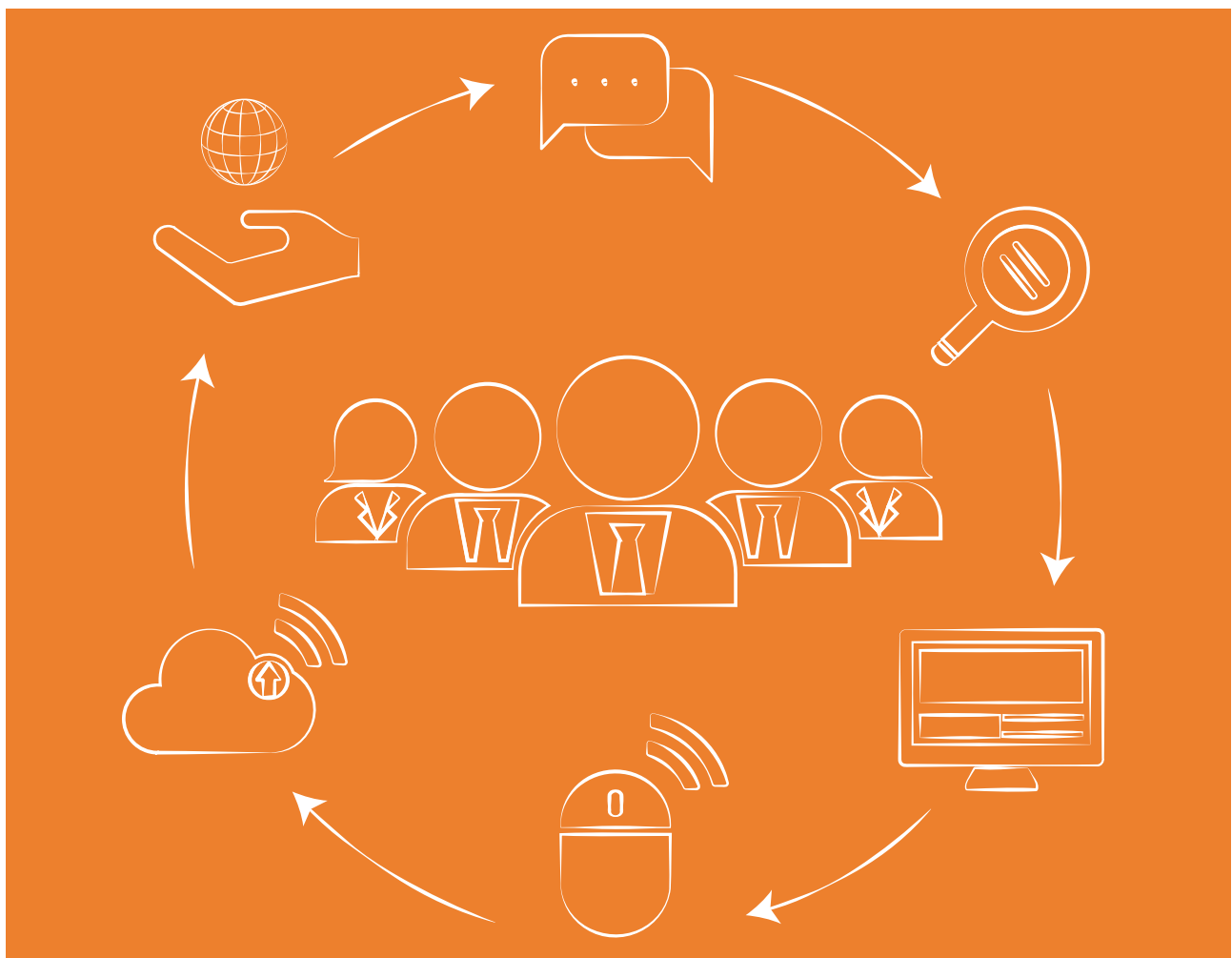


tic

Cuadernos de desarrollo aplicados a las TIC

Ed.42 | Vol.12 | N.1
January - March 2023

ISSN: 2254-6529



3C TIC. Cuadernos de desarrollo aplicados a las TIC.

Quarterly periodicity.

Edition 42, Volume 12, Issue 1 (January - March 2023).

National and international circulation.

Articles reviewed by the double blind peer evaluation method.

ISSN: 2254 - 6529

Legal: A 268 - 2012

DOI: <https://doi.org/10.17993/3ctic.2023.121>

Edita:

Área de Innovación y Desarrollo by UP4 Institute of Sciences, S.L.

info@3ciencias.com _ www.3ciencias.com



This publication may be reproduced by mentioning the source and the authors.

Copyright © Área de Innovación y Desarrollo by UP4 Institute of Sciences, S.L.



EDITORIAL BOARD

| | |
|-------------------|--|
| Director | Víctor Gisbert Soler |
| Editors | María J. Vilaplana Aparicio Maria Vela Garcia |
| Associate Editors | David Juárez Varón F. Javier Cárcel Carrasco |

DRAFTING BOARD

Dr. David Juárez Varón. *Universitat Politècnica de València (España)*
Dra. Úrsula Faura Martínez. *Universidad de Murcia (España)*
Dr. Martín León Santiesteban. *Universidad Autónoma de Occidente (México)*
Dra. Inmaculada Bel Oms. *Universitat de València (España)*
Dr. F. Javier Cárcel Carrasco. *Universitat Politècnica de València (España)*
Dra. Ivonne Burguet Lago. *Universidad de las Ciencias Informáticas (La Habana, Cuba)*
Dr. Alberto Rodríguez Rodríguez. *Universidad Estatal del Sur de Manabí (Ecuador)*

ADVISORY BOARD

Dra. Ana Isabel Pérez Molina. *Universitat Politècnica de València (España)*
Dr. Julio C. Pino Tarragó. *Universidad Estatal del Sur de Manabí (Ecuador)*
Dra. Irene Belmonte Martín. *Universidad Miguel Hernández (España)*
Dr. Jorge Francisco Bernal Peralta. *Universidad de Tarapacá (Chile)*
Dra. Mariana Alfaro Cendejas. *Instituto Tecnológico de Monterrey (México)*
Dr. Roberth O. Zambrano Santos. *Instituto Tecnológico Superior de Portoviejo (Ecuador)*
Dra. Nilda Delgado Yanes. *Universidad de las Ciencias Informáticas (La Habana, Cuba)*
Dr. Sebastián Sánchez Castillo. *Universitat de València (España)*
Dra. Sonia P. Ubillús Saltos. *Instituto Tecnológico Superior de Portoviejo (Ecuador)*
Dr. Jorge Alejandro Silva Rodríguez de San Miguel. *Instituto Politécnico Nacional (México)*

EDITORIAL BOARD

| | |
|---|---|
| Área financiera | Dr. Juan Ángel Lafuente Luengo <i>Universidad Jaime I (España)</i> |
| Área textil | Dr. Josep Valdeperas Morell <i>Universitat Politècnica de Catalunya (España)</i> |
| Ciencias de la Salud | Dra. Mar Arlandis Domingo <i>Hospital San Juan de Alicante (España)</i> |
| Derecho | Dra. María del Carmen Pastor Sempere <i>Universidad de Alicante (España)</i> |
| Economía y empresariales | Dr. José Joaquín García Gómez <i>Universidad de Almería (España)</i> |
| Estadística y Investigación operativa | Dra. Elena Pérez Bernabeu <i>Universitat Politècnica de València (España)</i> |
| Ingeniería y Tecnología | Dr. David Juárez Varón <i>Universitat Politècnica de València (España)</i> |
| Organización de empresas y RRHH | Dr. Francisco Llopis Vañó <i>Universidad de Alicante (España)</i> |
| Sinología | Dr. Gabriel Terol Rojo <i>Universitat de València (España)</i> |
| Sociología y Ciencias Políticas | Dr. Rodrigo Martínez Béjar <i>Universidad de Murcia (España)</i> |
| Tecnologías de la Información y la Comunicación | Dr. Manuel Llorca Alcón <i>Universitat Politècnica de València (España)</i> |

AIMS AND SCOPE

PUBLISHING GOAL

3C Ciencias wants to transmit to society innovative projects and ideas. This goal is reached through the publication of original articles which are subjected to peer review or through the publication of scientific books.

THEMATIC COVERAGE

3C Empresa is a scientific - social journal, where original works are spread, written in English, for dissemination with empirical and theoretical analyzes on financial markets, leadership, human resources, market microstructure, public accounting and business management.

OUR TARGET

- Research staff.
- PhD students.
- Professors.
- Research Results Transfer Office.
- Companies that develop research and want to publish some of their works.

SUBMISSION GUIDELINES

3C Empresa is an arbitrated journal that uses the double-blind peer review system, where external experts in the field on which a paper deals evaluate it, always maintaining the anonymity of both the authors and of the reviewers. The journal follows the standards of publication of the APA (American Psychological Association) for indexing in the main international databases.

Each issue of the journal is published in electronic version (e-ISSN: 2254-3376), each work being identified with its respective DOI (Digital Object Identifier System) code.

STRUCTURE

The original works will tend to respect the following structure: introduction, methods, results, discussion/ conclusions, notes, acknowledgments and bibliographical references.

The inclusion of references is mandatory, while notes and acknowledgments are optional. The correct citation will be assessed according to the 7th edition of the APA standards.

PRESENTATION WORK

All the information, as well as the templates to which the works must adhere, can be found at:

<https://www.3ciencias.com/en/journals/infromation-for-authors/>

<https://www.3ciencias.com/en/regulations/templates/>

ETHICAL RESPONSIBILITIES

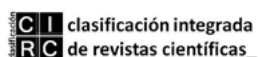
Previously published material is not accepted (they must be unpublished works). The list of signatory authors should include only and exclusively those who have contributed intellectually (authorship), with a maximum of 4 authors per work. Articles that do not strictly comply with the standards are not accepted.

STATISTICAL INFORMATION ON ACCEPTANCE AND INTERNATIONALIZATION FEES

- Number of accepted papers published: 19.
- Level of acceptance of manuscripts in this number: 66,7%.
- Level of rejection of manuscripts: 33,3%.
- Internationalization of authors: 3 countries (India, Spain, China).

Guidelines for authors: <https://www.3ciencias.com/en/regulations/instructions/>

INDEXATIONS



INDEXATIONS



/SUMMARY/

| | |
|---|-----|
| <i>Dielectric Properties of (GO-MgO-PoPDA- PVA) nanocomposite films</i> | 15 |
| A. J., Tabark and F. D., Amir | |
| <i>The Effect of Soil Characteristics On NFGM and FFGM Ground Motion Response Spectra</i> | 29 |
| H. R., Ghada and K. R., Hussam | |
| <i>Performance of column-to-column mechanical connection in precast concrete building under seismic loading</i> | 46 |
| A., Ahmed D. and A. R., Ammar A. | |
| <i>Study of finfet transistor: critical and literature review in finfet transistor in the active filter</i> | 65 |
| A.M., Arsen, K.M., Zaidoon and D. Hüseyin | |
| <i>Synthesis, identification of some new tetrazoline, thiazolidin-4-one and imidazolidin-4-one derivatives and evaluation anticancer of their molecular docking and anti-oxidant experimental</i> | 83 |
| Mohammed B. wathiq AL-tamimi and Suaad M. H. Al-Majidi. | |
| <i>Effect of method nano application with NPK fertilizer on the vegetative growth of two grape cultivars (Vitis Vinifera L.)</i> | 118 |
| Mohammed B. wathiq AL-tamimi and Suaad M. H. Al-Majidi. | |
| <i>Analysis of the impact of lake environmental water pollution on the health of outdoor swimmers based on STIRPAT environmental impact assessment model</i> | 132 |
| G., Xiaogang, W., Xinyu and Z. Xuxiang | |
| <i>Calculation and analysis of the impact of microsoft security- assisted physical education model on college basketball teaching in the Internet information era</i> | 152 |
| Z., Chenjing | |
| <i>Application of AR virtual implantation technology based on deep learning and emotional technology in the creation of interactive picture books</i> | 176 |
| L., Sidan, P., Peng and C., Lei. | |
| <i>Innovation of college pop music teaching in traditional music culture based on robot cognitive-emotional interaction model</i> | 200 |
| Z., Hua. | |
| <i>Exploring the direction of the English translation of environmental protection articles based on robot cognitive-emotional interaction model</i> | 222 |
| S., Shuai. | |
| <i>A strategy for building a smart sports platform based on machine learning models</i> | 248 |
| G., Mingchan | |
| <i>Reconstruction of physical dance teaching content and movement recognition based on a machine learning model</i> | 267 |
| L., Lei and Y., Tingting | |
| <i>Fabric yarn detection based on improved fast R-CNN model</i> | 287 |
| X., Haiyan | |

The Optimization Path of Higher Education Resource Allocation in China Based on Fuzzy Set Theory 308
Z., Yuqi

Quantization and application of low-rank tensor decomposition based on the deep learning model 330
Z., Jia

The role of social networking sites in promoting the culture of Iraqi rural women and empowering them 352
F.Z., Haider, K.Y., Noor and I.A., Saad

Particulate Matter Levels Classification Using Modified and Combined ResNet Models with Low Features Extraction 378
A.M., Rayan and A.S., Mohammed.



/01/

DIELECTRIC PROPERTIES OF (GO-MGO-POPDA- PVA) NANOCOMPOSITE FILMS

Tabark Ahmed Jassim*

Department of chemistry, College of Science, University of Diyala
scichems0@gmail.com

Amir Fadhil Dawood

Department of chemistry, College of Science, University of Diyala



Reception: 18/10/2022 **Acceptance:** 26/12/2022 **Publication:** 20/01/2023

Suggested citation:

A. J., Tabark and F. D., Amir. (2023). **Dielectric Properties of (GO-MgO-PoPDA- PVA) nanocomposite films.** *3C TIC. Cuadernos de desarrollo aplicados a las TIC*, 12(1), 15-27. <https://doi.org/10.17993/3ctic.2023.121.15-27>

ABSTRACT

In this work, a pure (PVA) polymer film reinforced with magnesium oxide, graphene oxide poly (o-phenylene diamine) (GO-MgO-PoPDA) was created utilizing the solution casting process in various weight ratios (0, 2, 4, 6, 8, 10 wt%). It was investigated how varied weight ratios of the nanoparticles magnesium oxide (MgO) and graphene oxide (GO) affected the Dielectric Properties of nano composite films. FTIR, SEM, X-RAY were used to characterize the nanocomposite. The results of the dielectric properties showed that the values of the alternating electrical conductivity of the prepared films increase when adding (GO-MgO-PoPDA) nanoparticles and with the increase of the frequency of the applied electric field and the increase of the particle content, while the values of the dielectric constant increase with the increase of each of the content of (GO-MgO-PoPDA) nanoparticles, but it decreases with increasing frequency. Whereas, the dielectric loss coefficient of the prepared films decreases when nanoparticles are added and with increasing frequency.

KEYWORDS

Dielectric Properties, Nanoparticles, Triple hybrid, Nanocomposite, Dielectric Constant, dielectric loss, Electrical Conductivity.

PAPER INDEX

ABSTRACT

KEYWORDS

1. INTRODUCTION

2. EXPERIMENTAL PART

2.1. Synthesis of binary nanocomposite

2.2. Synthesis of the ternary nanocomposites

2.3. Synthesis of the quaternary composites

3. RESULTS AND DISCUSSION

3.1. Infrared spectrum of the triple composites (GO-MgO-PoPDA)

3.2. Scanning electron microscope (SEM) of Triple Composite (GO-MgO-PoPDA)

3.3. X-ray diffraction of the Triple Composites (GO-MgO-PoPDA).

4. DIELECTRIC PROPERTIES:

4.1. Dielectric constant (ϵ')

4.2. Dielectric Loss Factor (ϵ'')

4.3. Electrical Conductivity ($\sigma_{a.c}$)

REFERENCES

1. INTRODUCTION

The research on polymer dielectrics (PD) For the past two decades, research has focused mostly on materials with high energy-storage density for dielectric applications due to their affordability, biocompatibility, flexibility, straightforward design, and ease of processing[1-6].This method of expansion employed insulating ferroelectric polymers, such as polyvinylidene fluoride and polyvinylidene fluoride tetrafluoroethylene. Polymer nanocomposites have recently attracted interest as energy storage materials [1-19], uses for electromagnetic interference shielding [20, 21] different kinds of nanofillers, such as CNT, CB, graphite, etc., are incorporated into the ferroelectric polymer matrices during the construction of these PNC [1-26]. These PNC fillers use a variety of fillers with various conductivities, sizes, forms, and co-functionalization [1-26]. These PD are made using either the classic mixed technique, which involves solution casting followed by heat molding, While most recently, our team created the cold pressing method, which safeguards the ferroelectric polymers' spherulites [9-12]. Since they have more interfaces in the PNC, the spherulites also store electrical charge, this causes increased interfacial polarization and raises the effective dielectric constant value. For enforcement in a more general scenario and the associated commercialization, we were competent to demonstrate the value of ferroelectric polymer matrices, the influence of filler surface area, the high value of (ϵ_{eff}) of 2400 in these PNC based on nanocrystalline nickel (n-Ni) filler, and the value of cold pressing in the development of PD. [9-12]. Polymer/metal composites, polymer/conductor composites, and polymer/ceramic composites are three examples of PNCs, are being developed as part of the development of these PD [7-26]. Interesting percolation behavior is displayed in one class [27].

2. EXPERIMENTAL PART

2.1. SYNTHESIS OF BINARY NANOCOMPOSITE

The (GO) prepared by the modified Hummer method [28].The(MgO) prepared through (sol-jel) method. The binary nanocomposite (GO-MgO) was synthesized by dispersing (0.5 g) of (GO) in 100ml of non-ionic water using an ultrasonic water bath at 25°C for 1 hour to form a GO solution.(0.5g) of MgO added to the GO solution. Moving for two hours at 25°C and then dispersing for another one hour, the precipitate was separated by centrifugation and dried at 80°C for two hours.[29].

2.2. SYNTHESIS OF THE TERNARY NANOCOMPOSITES

The triplet nanocomplex was prepared by dispersing (0.5g) of the GO-MgO binary complex in 50ml of non-ionic water by an ultrasonic bath at 25°C for 1 hour and then mixing with (1.62g) of o-PDA dissolved in 100ml of 0.1M (HCl) acid with constant stirring for 1 hour in an ice bath. The oxidizing agent solution was synthesized by dissolving (6g) of(APS) in 100 ml (HCl) at a concentration of 0.1M. It was gently added dropwise to the main mixture with vigorous moving. Then the new mixture was

kept in an ice bath under stirring for 4 hours and then removed from the ice bath. Then, moderate stirring for 20 hours at 25°C then the precipitate filtered washed with acetone and distilled water several times and dried in the oven at 80°C for 2 hours[29].

2.3. SYNTHESIS OF THE QUATERNARY COMPOSITES

The following six concentrations are used to create pure PVA polymer membranes that are reinforcement by the triple nanolayer (GO-MgO-POPDA):

| GO-MgO-PoPDA | PVA | The ratio |
|--------------|------|-----------|
| Zero | 1 | 0 % |
| 0.02 | 0.98 | 2 % |
| 0.04 | 0.96 | 4 % |
| 0.06 | 0.94 | 6 % |
| 0.08 | 0.92 | 8 % |
| 0.10 | 0.90 | 10 % |

The triple composite was dispersed in 3 ml of non-ionic water and gently added to PVA solution after the PVA had been thoroughly dissolved in (15 ml) of non-ionic water with constant stirring at (60 °C). The mixture heated to a temperature of (50°C) while being agitated for an additional hour and a half to create a homogenous solution. Transferred to a petridish and dried at (25°C). Finally, the nanocomposites' films were peeled off in order to examine their physical characteristics.

3. RESULTS AND DISCUSSION

3.1. INFRARED SPECTRUM OF THE TRIPLE COMPOSITES (GO-MGO-POPDA)

The infrared spectrum of the triple compound is depicted in the figure. It reveals the presence of several distinct bands for the triple hybrid compound, with the absorption bands at the region (3440.8 cm^{-1} - 3110 cm^{-1}) belonging to the group (NH-,NH₂) and the appearance of the band (1680.7 cm^{-1}) connected to the stretching vibrations of the (C=O) group (which is connected to graphene oxide). Two bands that are centered at (1617.7 cm^{-1} - 1531 cm^{-1}) are a result of the group's stretching vibrations. (C=C) Regarding the absorption bands, they are (C-N) in the quinoid and benzoide groups, together with the bundles (1137.3 cm^{-1} -1393 cm^{-1}) that belong to the alkoxy and epoxy groups, and the bundle at (436.29 cm^{-1}) that belongs to the magnesium oxide group MgO.

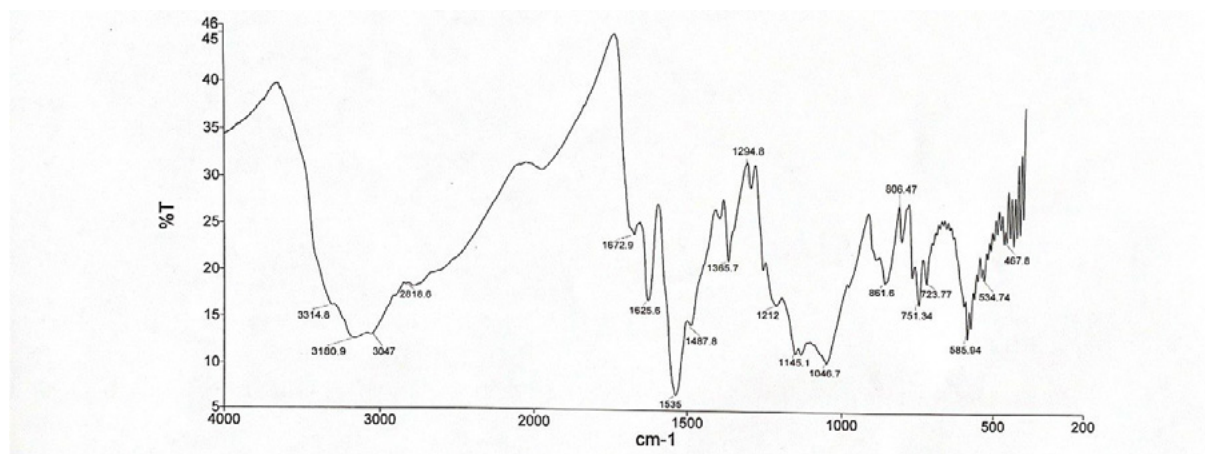


Figure 1. Infrared spectrum of the triple composite (GO-MgO-PoPDA).

3.2. SCANNING ELECTRON MICROSCOPE (SEM) OF TRIPLE COMPOSITE (GO-MGO-POPDA)

Scanning electron microscope with three composites (GO-MgO-PoPDA) SEM images of (GO-MgO-PoPDA) with magnification powers of (1 μm), (500nm), (200nm) and are shown in Figure (2). The investigation reveals that all of the photos contain asymmetrical structures, both in terms of shape and size. It should be highlighted that the polymerization of the monomer oPDA on the surface of the binary compound is the reason why graphene oxide and magnesium oxide did not appear clearly in this test (GO-MgO) and that these asymmetrical forms are the result of the monomer's haphazard diffusion across the oxide surfaces in the first step, which is followed by polymerization when APS is added to it in the second step.

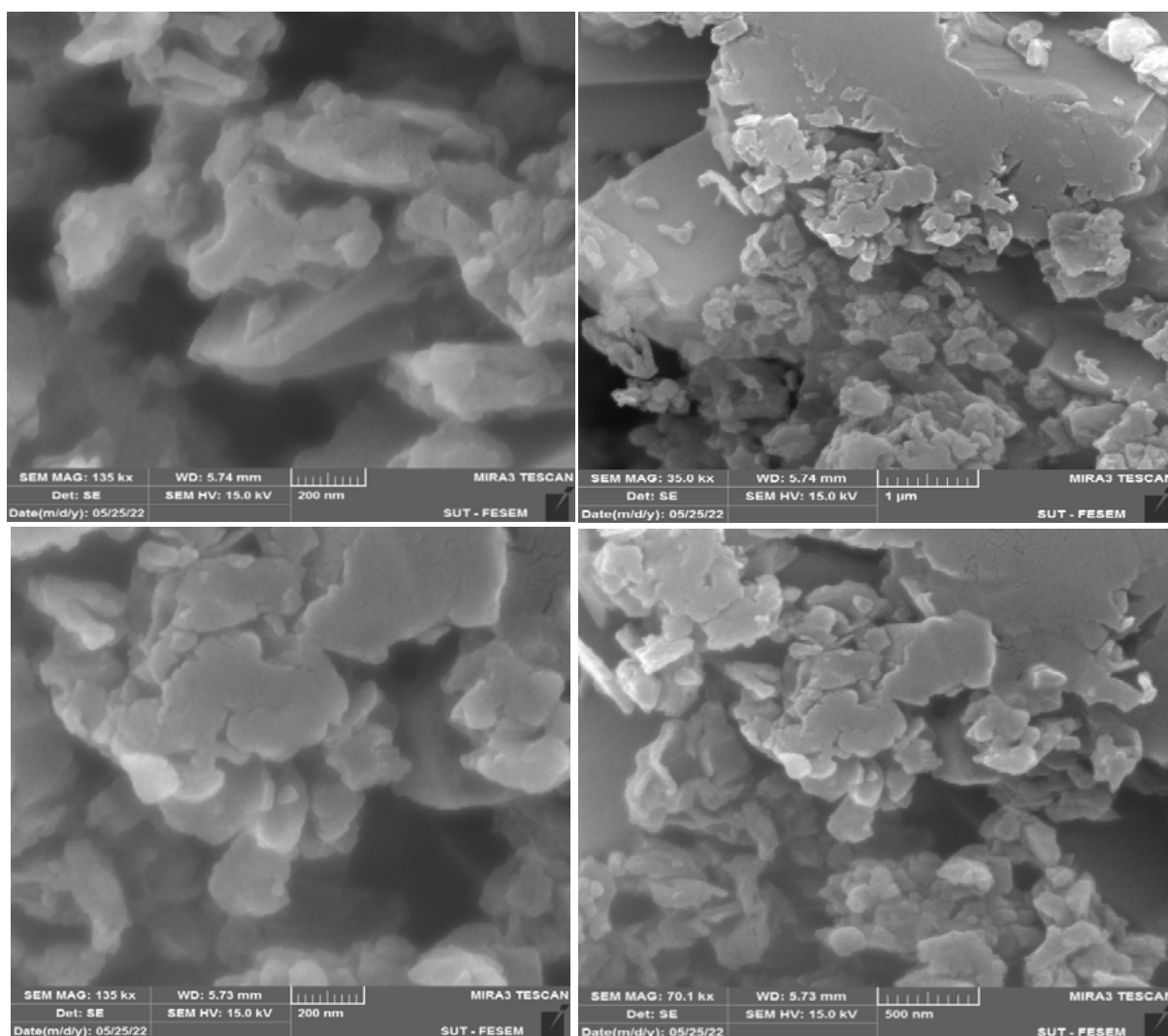


Figure 2. SEM of Triple Composites (GO-MgO-PoPDA).

3.3. X-RAY DIFFRACTION OF THE TRIPLE COMPOSITES (GO-MGO-POPDA).

The X-ray of the (GO-MgO-PoPDA) nanocomposite is depicted in Figure (3). The image below shows that the created triple nanocomposite can differentiate the peaks of magnesium oxide, and it is noteworthy that the maximum values of diffraction angles were obtained ($2\theta=26.7460, 27.9421, 19.7250$). The diffraction angles clearly overlap the PoPDA polymer, and no graphene oxide peaks are seen as a result of the overlap of the polymer and graphene oxide peaks.

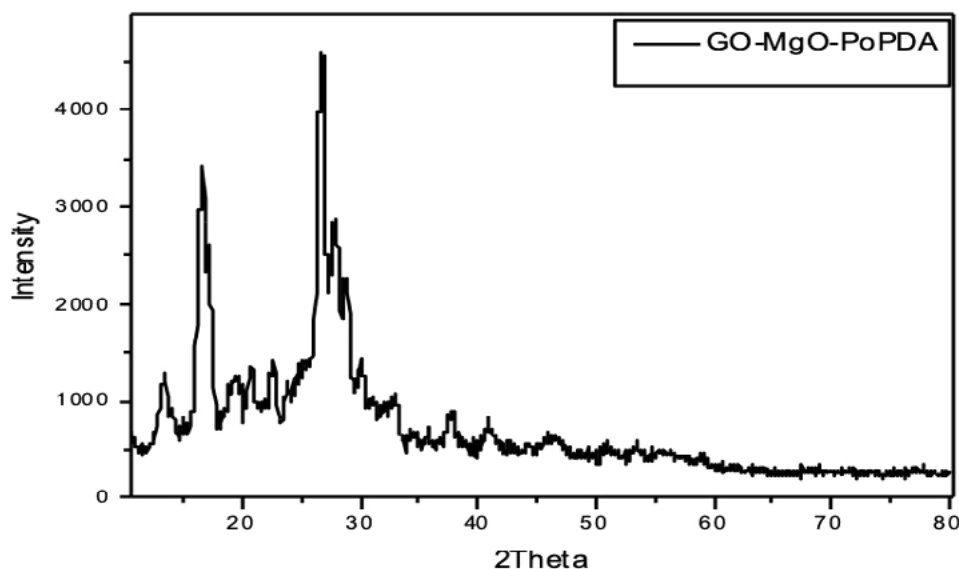


Figure 3. X-ray diffraction of the Triple Composites (GO-MgO-PoPDA).

4. DIELECTRIC PROPERTIES:

4.1. DIELECTRIC CONSTANT (ϵ')

The dielectric constant was calculated for the pure (PVA) polymer film and the (PVA:PoPDA-GO-MgO) nanocomposite films varying the weight ratios (2,4,6,8, 10wt%) at room temperature (25 °C) as shown in figure (4), when it can be seen from the graph that the dielectric constant drops as the frequency increases and for the films of all hybrid nanocomposites [30]. Dipolar groups in insulating polymers can arrange themselves in the direction of the electric field at low frequencies, but it is difficult for this group (Dipoles) when it is large to arrange itself towards the fast and time-varying electric field at high frequencies because the time period is short less than the time it takes for the molecules to be able to arrange themselves in the direction of the outgoing electric field, the electronic polarization occurs within a very short but longer period of time than the ionic polarization, while the dipole polarization takes a relatively long time compared to all polarizations, therefore the dielectric constant of non-polar polymers remains almost constant at high frequency and therefore (ϵ') values decrease dramatically and sharply with increasing frequency in low frequency regions [31], this may be the reason for the decrease in (ϵ') values with increasing frequency. Another reason for this decrease may be attributed to the decrease in the polarization of the space charges to the total polarization [32]. We also note from figure (4) that the dielectric constant (ϵ') of the hybrid composite (PVA:PoDA-GO-MgO) at the same frequency range rises with increasing weight ratios of the nano-oxides (Magnesium Oxide and Graphene Oxide) added. The insulation was recorded at the weight ratio (2 wt%) and its lowest value at the weight ratio (8 wt%), and all of these dielectric constant values are higher than the value of (ϵ') for pure

(PVA), and generally speaking, this rise in the dielectric constant value An increase in polarity and an increase in charge carriers are thought to be the causes of electricity [32].

Table 1. Dielectric constant of hybrid nanocomposite with different weight ratios of (GO, MgO).

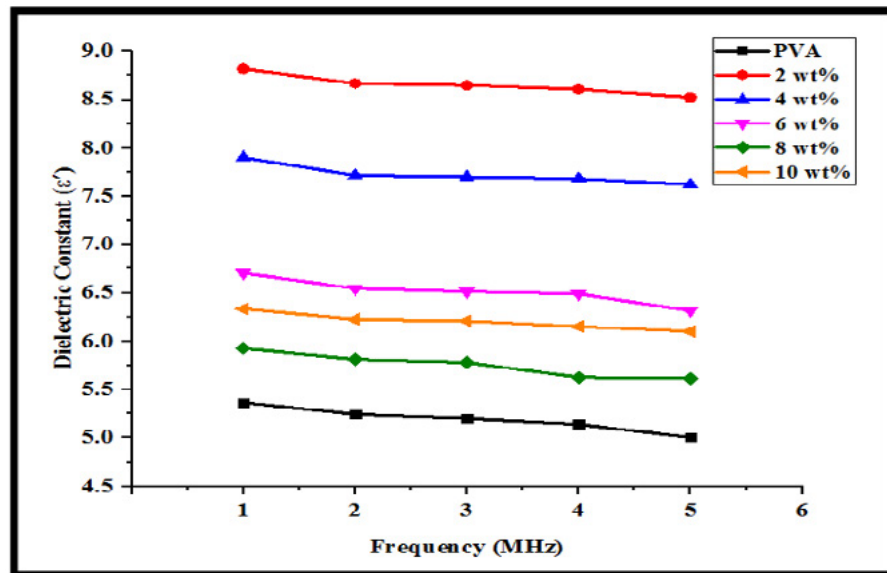


Figure 4. Dielectric constant as a function of hybrid nanocomposite films with different weight ratios of (GO, MgO).

4.2. DIELECTRIC LOSS FACTOR (ϵ'')

The energy dissipation in insulating materials is directly proportional to the dielectric loss factor, hence, understanding the importance of this component offers huge advantages in the use of composite materials. So that the behavior of polar polymers in an alternating electric field depends on the position of the dipoles, whether they are within the polymeric chain or in its side groups. The insulating loss factor was calculated for the prepared samples pure PVA polymer film and hybrid nanocomposites films (PVA:PoPDA-GO-MgO) varying the weight ratios (2, 4, 6, 8, 10 wt%) at room temperature (25 °C) and within the frequency range (1MHz-5MHz), from figure (5), It is evident that for all prepared samples, the dielectric loss factor decreases with increasing frequency. Additionally, we observe that as applied frequency rises, the dielectric loss first starts to decline at low frequencies, due to the decrease in the polarization of the vacuum charges (Space Charge Polarization) [32]. There is another reason for this decrease in (ϵ'') values with increasing frequency, which is because of the decrease of dipoles in nanocomposites [33]. The dielectric loss factor is characterized by a high level of polarization of space charges for the nanoparticles of oxides (Magnesium Oxide and Graphene Oxide), which leads to a decrease in the values of (ϵ'') with increasing frequency [34]. There is another reason for (ϵ'') to change with frequency because the dipoles absorb energy from the electric field in the system in order to overcome the resistance of the viscous materials that surround them during rotation, and this absorbed energy reduces the charge carriers

moving between the limits in the widening with the increase in the frequency of the applied field. Thus, these dipoles require high energy that is higher than the system to obtain relaxation and thus decreases (ϵ'') with increasing frequency [31]. Figure (5) note that the value of the dielectric loss factor (ϵ'') at the same frequency range increases when the weight ratios of nano-oxides (GO, MgO) increase, and that the highest value of (ϵ'') for the weight ratio (6 wt%) and the lowest value of the weight ratio (2 wt%) and the cause for this is due to the increase in the number of electrons in the nano-oxides used, and thus the dipole charge increases, which leads to an increase in electrical conductivity, thus increasing the value of (ϵ'') [32]. Table (2) shows the dielectric loss factor values for hybrid compounds with different weight ratios.

Table 2. Dielectric loss factor of hybrid with different weight ratios of (GO, MgO).

| Frequency (MHz) | Dissipation Factor (ϵ'') | | | | | |
|-----------------|-------------------------------------|------|------|------|------|-------|
| | PVA | 2wt% | 4wt% | 6wt% | 8wt% | 10wt% |
| 1 | 0.31 | 0.36 | 0.52 | 0.55 | 0.42 | 0.39 |
| 2 | 0.28 | 0.33 | 0.44 | 0.48 | 0.39 | 0.36 |
| 3 | 0.26 | 0.29 | 0.41 | 0.45 | 0.35 | 0.33 |
| 4 | 0.24 | 0.27 | 0.36 | 0.41 | 0.32 | 0.3 |
| 5 | 0.21 | 0.25 | 0.33 | 0.35 | 0.31 | 0.29 |

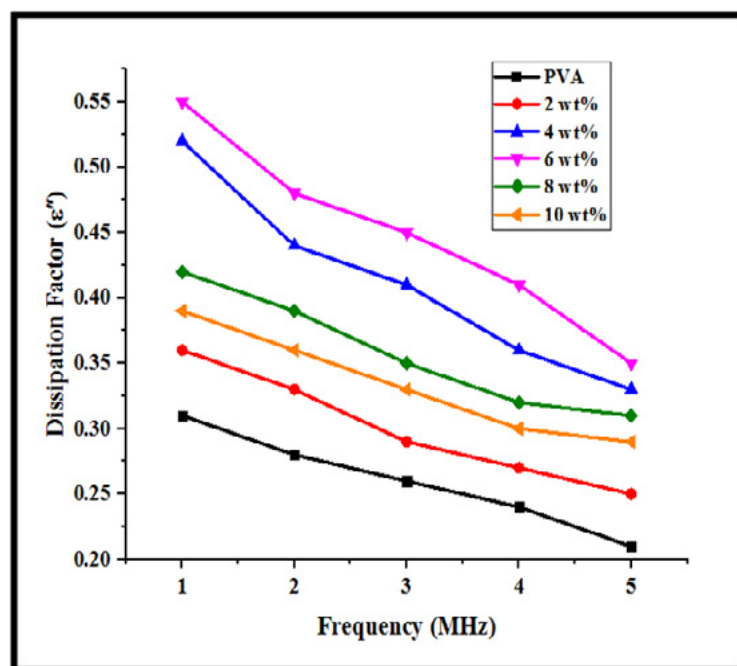


Figure 5. Dielectric loss factor as a function of frequency of hybrid nanocomposite films with different weight ratios of (GO, MgO).

4.3. ELECTRICAL CONDUCTIVITY ($\sigma_{a.c}$)

Electrical conductivity is defined as the process of moving electric charge from one place to another through a medium when an electric field is applied. Alternating electrical conductivity ($\sigma_{a.c}$) was calculated for the membrane of pure PVA polymer and hybrid nanocomposites films (PVA: PoPDA-GO-MgO) at room temperature (25 °C) and varying the weight ratios (2,4,6,8,10wt %) and in the frequency range (1MHz -

5MHz). As shown in figure (6), where we notice from the figure that the AC electrical conductivity ($\sigma_{a.c}$) increases with the rise in frequency and for all the prepared compounds, this increase in ($\sigma_{a.c}$) is attributed to the increase in the applied frequency to the polarization and the charge carriers (Carriers Charge) that It is transmitted by hopping process between electronic levels, and these hoppings of charge carriers across the voltage barrier and quantum tunneling increase the value of AC electrical conductivity [32]. From the figure, we also notice the absence of relaxation peaks, which indicates that the increase in ($\sigma_{a.c}$) is due to the rise in the density of ions (Ionic density) rather than the structural relaxation process in order to rearrange the dipoles in the system or molecular relaxation for polymer chains [35]. Alternating electrical conductivity (a.c.) in insulating materials is determined by power lost as a result of applying an alternating electric field, which appears as heat and rotates dipoles in their positions or causes charges to vibrate by changing the direction of the alternating electric field. For this reason, the amount of power lost determines the frequency of the applied field [36]. By increasing the weight ratios of the reinforcement with nano-oxides (MgO, GO), it is noted that the alternating electrical conductivity is high compared to the alternating electrical conductivity of the pure PVA membrane, which is few, as well as the formation of a continuous network in the form of agglomerates when the weight ratio of nano-oxides is increased, which it leads to the formation of a continuous path inside the hybrid nanocomposite films material as the weight ratio increases, Because of the formation of a continuous conductive path, this leads to an increase in the AC electrical conductivity, and its value is determined by the effect of polarization and electron movement in the substrate [32]. Table (3) shows the AC electrical conductivity values for all the prepared hybrid nanocomposites films.

Table 3. Electrical Conductivity values of the hybrid nanocomposites films with different weight ratios of (GO, MgO).

| Frequency (MHz) | (A.C) Electrical Conductivity ($\sigma_{a.c}$) (S/m) | | | | | |
|-----------------|--|-----------------------|-----------------------|-----------------------|-----------------------|-----------------------|
| | PVA | 2 wt% | 4 wt% | 6 wt% | 8 wt% | 10 wt% |
| 1 | 7.65×10^{-6} | 1.06×10^{-5} | 1.7×10^{-5} | 2.27×10^{-5} | 2.97×10^{-5} | 3.59×10^{-5} |
| 2 | 3.21×10^{-5} | 3.67×10^{-5} | 4.18×10^{-5} | 5.03×10^{-5} | 5.43×10^{-5} | 5.98×10^{-5} |
| 3 | 5.29×10^{-5} | 5.95×10^{-5} | 7.02×10^{-5} | 8.05×10^{-5} | 8.55×10^{-5} | 9.36×10^{-5} |
| 4 | 7.38×10^{-5} | 7.98×10^{-5} | 9.79×10^{-5} | 1.08×10^{-4} | 1.18×10^{-4} | 1.27×10^{-4} |
| 5 | 9.5×10^{-5} | 1.08×10^{-4} | 1.27×10^{-4} | 1.38×10^{-4} | 1.58×10^{-4} | 1.65×10^{-4} |

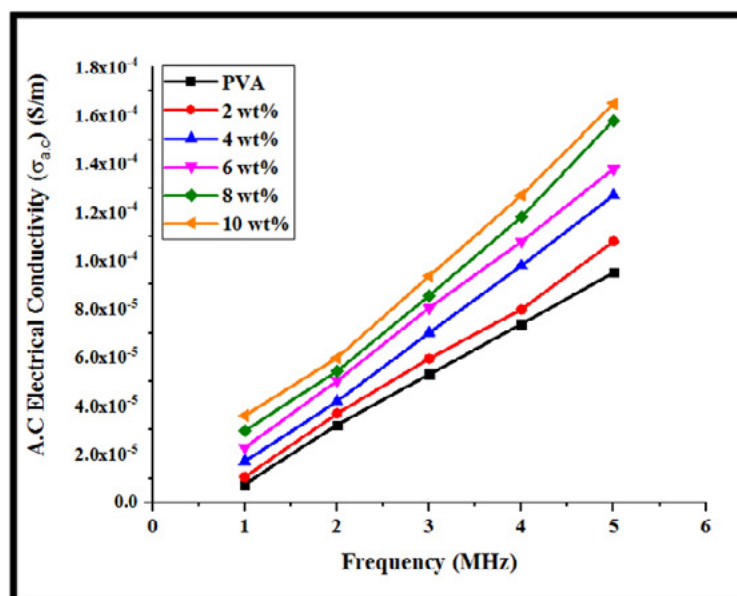


Figure 6. Electrical Conductivity as a function of frequency of hybrid nanocomposite films with different weight ratios of (GO, MgO).

REFERENCES

- (1) Dang, Z. M. (Ed.). (2018). **Dielectric polymer materials for high-density energy storage**. William Andrew.
- (2) Pan, H., Ma, J., Ma, J., Zhang, Q., Liu, X., Guan, B., ... & Nan, C. W. (2018). **Giant energy density and high efficiency achieved in bismuth ferrite-based film capacitors via domain engineering**. *Nature communications*, 9(1), 1813.
- (3) Thakur, V. K., & Kessler, M. R. (2014). Polymer nanocomposites: New advanced dielectric materials for energy storage applications. In *Advanced Energy Materials* (pp. 207-257). Wiley Blackwell.
- (4) Jiang, P., & Huang, X. (2017). **Dielectric materials for electrical energy storage**. *IEEE Transactions on Dielectrics and Electrical Insulation*, 24(2), 675-675.
- (5) Gao, J., Wang, Y., Liu, Y., Hu, X., Ke, X., Zhong, L., ... & Ren, X. (2017). **Enhancing dielectric permittivity for energy-storage devices through tricritical phenomenon**. *Scientific reports*, 7(1), 1-10.
- (6) Zhang, L. I. N., & Cheng, Z. Y. (2011). **Development of polymer-based 0–3 composites with high dielectric constant**. *Journal of Advanced Dielectrics*, 1(04), 389-406.
- (7) Kumar, T. V., & Kumar, G. R. (2016). **Recent Progress on Ferroelectric Polymer-Based Nanocomposites for High Energy Density Capacitors: Synthesis, Dielectric Properties, and Future Aspects**.
- (8) Zhang, L., Bass, P., & Cheng, Z. Y. (2014). **Revisiting the percolation phenomena in dielectric composites with conducting fillers**. *Applied Physics Letters*, 105(4), 042905.

- (9) Panda, M., Mishra, A., & Shukla, P. (2019). **Effective enhancement of dielectric properties in cold-pressed polyvinylidene fluoride/barium titanate nanocomposites**. *SN Applied Sciences*, 1, 1-7.
- (10) Panda, M., Srinivas, V., & Thakur, A. K. (2015). **Non-universal scaling behavior of polymer-metal composites across the percolation threshold**. *Results in Physics*, 5, 136-141.
- (11) Panda, M., Srinivas, V., & Thakur, A. K. (2014). **Universal microstructure and conductivity relaxation of polymer-conductor composites across the percolation threshold**. *Current Applied Physics*, 14(11), 1596-1606.
- (12) Li, Q., Chen, L., Gadinski, M. R., Zhang, S., Zhang, G., Li, H. U., ... & Wang, Q. (2015). **Flexible high-temperature dielectric materials from polymer nanocomposites**. *Nature*, 523(7562), 576-579.
- (13) Yang, M., Zhao, H., He, D., & Bai, J. (2016). **Largely enhanced dielectric properties of carbon nanotubes/polyvinylidene fluoride binary nanocomposites by loading a few boron nitride nanosheets**. *Applied Physics Letters*, 109(7), 072906.
- (14) Dang, Z. M., Yuan, J. K., Yao, S. H., & Liao, R. J. (2013). **Flexible nanodielectric materials with high permittivity for power energy storage**. *Advanced Materials*, 25(44), 6334-6365.
- (15) Li, Q., Yao, F. Z., Liu, Y., Zhang, G., Wang, H., & Wang, Q. (2018). **High-temperature dielectric materials for electrical energy storage**. *Annual Review of Materials Research*, 48, 219-243.
- (16) Nan, C. W., Shen, Y., & Ma, J. (2010). **Physical properties of composites near percolation**. *Annual Review of Materials Research*, 40, 131-151.
- (17) Dang, Z. M., Yuan, J. K., Zha, J. W., Zhou, T., Li, S. T., & Hu, G. H. (2012). **Fundamentals, processes and applications of high-permittivity polymer-matrix composites**. *Progress in materials science*, 57(4), 660-723.
- (18) Chen, Q., Shen, Y., Zhang, S., & Zhang, Q. M. (2015). **Polymer-based dielectrics with high energy storage density**. *Annual review of materials research*, 45, 433-458.
- (19) Gargama, H., Thakur, A. K., & Chaturvedi, S. K. (2016). **Polyvinylidene fluoride/nanocrystalline iron composite materials for EMI shielding and absorption applications**. *Journal of Alloys and Compounds*, 654, 209-215.
- (20) Gargama, H., Thakur, A. K., & Chaturvedi, S. K. (2015). **Polyvinylidene fluoride/nickel composite materials for charge storing, electromagnetic interference absorption, and shielding applications**. *Journal of Applied Physics*, 117(22), 224903.
- (21) Bertolazzi, S., Wünsche, J., Cicoira, F., & Santato, C. (2011). **Tetracene thin film transistors with polymer gate dielectrics**. *Applied Physics Letters*, 99(1), 126.
- (22) Dang, M. T., Hirsch, L., & Wantz, G. (2011). **P3HT: PCBM, best seller in polymer photovoltaic research**.
- (23) Toker, D., Azulay, D., Shimoni, N., Balberg, I., & Millo, O. (2003). **Tunneling and percolation in metal-insulator composite materials**. *Physical review B*, 68(4), 041403.

- (24) Bai, Y., Cheng, Z. Y., Bharti, V., Xu, H. S., & Zhang, Q. M. (2000). **High-dielectric-constant ceramic-powder polymer composites**. *Applied Physics Letters*, 76(25), 3804-3806.
- (25) Yamada, T., Ueda, T., & Kitayama, T. (1982). **Piezoelectricity of a high-content lead zirconate titanate/polymer composite**. *Journal of Applied Physics*, 53(6), 4328-4332.
- (26) Stauffer, D., & Aharony, A. (2018). **Introduction to percolation theory**. Taylor & Francis.
- (27) Hummers Jr, W. S., & Offeman, R. E. (1958). **Preparation of graphitic oxide**. *Journal of the american chemical society*, 80(6), 1339-1339.
- (28) Mohammed, L. A., Majeed, A. H., Hammoodi, O. G., Prakash, C., Alheety, M. A., Buddhi, D., ... & Mohammed, I. K. (2022). **Design and characterization of novel ternary nanocomposite (rGO-MnO₂-PoPDA) product and screening its dielectric properties**. *International Journal on Interactive Design and Manufacturing (IJIDeM)*, 1-15.
- (29) Rabee, B. H., & Hashim, A. (2011). **Synthesis and characterization of carbon nanotubes-polystyrene composites**. *European Journal of Scientific Research*, 60(2), 247-254.
- (30) Mohammed, M. I. (2022). **Controlling the optical properties and analyzing mechanical, dielectric characteristics of MgO doped (PVA-PVP) blend by altering the doping content for multifunctional microelectronic devices**. *Optical Materials*, 133, 112916.
- (31) Agool, I. R., Ali, M., & Hashim, A. (2014). **The Dielectric Properties of (PVA-PEG-PVP-MgO) and (PVA-PEG-PVP-CoO) Biomaterials**. *International Journal of Science and Research (IJSR) Volume*, 3.
- (32) Habeeb, M. A. (2013). **Effect of Nanosilver Particles on Thermal and Dielectric Properties of (PVA-PVP) Films**. *International Journal of Applied and Natural Sciences*, 2(4), 103-108.
- (33) Rasheed, H. S. (2021). **Study and Synthesis of Polymer-Blend PVA-PEG Doped with 5wt% Mgo and Different wt% of Co₃O₄ Thin Film**. *Egyptian Journal of Chemistry*, 64(9), 5093-5099.
- (34) Cyriac, V., Noor, I. M., Mishra, K., Chavan, C., Bhajantri, R. F., & Masti, S. P. (2022). **Ionic conductivity enhancement of PVA: carboxymethyl cellulose poly-blend electrolyte films through the doping of NaI salt**. *Cellulose*, 29(6), 3271-3291.
- (35) Popielarz, R., Chiang, C. K., Nozaki, R., & Obrzut, J. (2001). **Dielectric properties of polymer/ferroelectric ceramic composites from 100 Hz to 10 GHz**. *Macromolecules*, 34(17), 5910-5915.

/02/

THE EFFECT OF SOIL CHARACTERISTICS ON NFGM AND FFGM GROUND MOTION RESPONSE SPECTRA

Ghada Haitham Razzaq*

Civil Engineering Department, Al-Nahrain University, Baghdad1001, Iraq

Gedo0haitham@gmail.com

Hussam K. Risan

Civil Engineering Department, Al-Nahrain University, Baghdad1001, Iraq



Reception: 30/10/2022 **Acceptance:** 26/12/2022 **Publication:** 22/01/2023

Suggested citation:

H. R., Ghada and K. R., Hussam. (2023). **The Effect of Soil Characteristics On NFGM and FFGM Ground Motion Response Spectra**. *3C TIC. Cuadernos de desarrollo aplicados a las TIC*, 12(1), 29-45. <https://doi.org/10.17993/3ctic.2023.121.29-44>

ABSTRACT

This study aims to achieve the following goals: 1- To distinguish between the inelastic responses of buildings under earthquakes with NFGM and FFGM. 2- To inspect the effect of soil shear velocity on the response spectra. Several earthquake events, with different characteristics, are brought from the PEER website for “Pacific Earthquake Engineering Research” and analyzed using PRISM software to achieve these goals.

The research found that the acceleration, velocity, and displacement response of the selected near-fault ground motions on the structure has a higher effect than the far-field ground motion response in both types of soils and this difference is displayed more noticeably in long periods (periods after 0.2 sec). And when comparing responses of the two types of soils (the soft soil type and the rock type) it shows that the geological and geotechnical aspects of the soil deposits majorly affect the response spectra of the free field surface motions

KEYWORDS

Earthquake, near-fault ground motion, far-field ground motion, shear velocity, response spectra, PEER, PRISM.

PAPER INDEX

ABSTRACT

KEYWORDS

INTRODUCTION

METHOD OF RESPONSE SPECTRUM

CHOSEN GROUND MOTION RECORDS OF SPECIFIC EARTHQUAKES

ELASTIC RESPONSE OF NFGM AND FFGM

THE EFFECT OF SOIL TYPE ON SDOF ELASTIC SEISMIC RESPONSE

CONCLUSIONS

REFERENCES

INTRODUCTION

The concentration in this paper is on the seismic ground motion of a general single-degree-of-freedom structural system by comparing the change in the produced responses when varying several parameters like distance to the rupture plane, average soil shear velocity, earthquake components, etc.

From the “Pacific Earthquake Engineering Research Center” (PEER) Various numbers of earthquake events were taken to study, evaluate, process and compare with each other. These ground motions were divided into four groups. Each group is different from the other group in a certain aspect. the dynamic response spectrum is then calculated using PRISM software for all the ground motions in these groups and then a graph is drawn to better illustrates the results. Finally, the results will be discussed to get a broad understanding of the behavior of the structure under seismic ground motion.

An earthquake is an inevitable natural phenomenon that poses a great danger with the uncertainty of what time it is going to strike. Though, with preparation measures in place, the effects of disaster-destruction can be retained to a minimum and the effects of damage can be restricted, whereby emergency response and rescue labors can be made more effective during the outcome with a mixture of aid facilities, public spaces and shelters [1].

Tectonics-induced earthquakes are common and critical earthquakes. They will happen anyplace within the earth where adequate stored elastic strain energy is present to enterprise breakage propagation lengthwise a fault plane, and typically initiate by an initial rupture at a point on the fault plane [2].

Near-fault ground motions can be well-defined as the ground motions that occur near the fault of the earthquake. Near fault motions that get noted close to the epicenter are called near-epicenter records, whereas the ones that get recorded along the fault of the earthquake in the rupture direction can be arbitrated to being forward directivity [3].

Far-field ground motion is known as the ground motion that occurs far away from the fault of the earthquake. The distance by which the earthquake can be defined as NFGM or FFGM can vary from research to research but mostly we can take 20 m as an acceptable number to divide between the two. Even though in this paper the search is tightened to get a better result and to show the difference between the two types of GM better.

Zhang and Iwan (2002) discussed that the near-fault ground motions produce twice as high a dynamic response as the far field ground motion, and they also found that the damage resulting from NFGM earthquakes is done due to a small number of large inelastic deformation cycles, but the damage resulting from by FFGM earthquakes is due to many high-frequency cycles [4].

Anil K. Chopra and Chatpan Chintanapakdee studied the difference between the NFGM and FFGM. They studied two groups of ground motions, one with the characteristics of NFGM and the other with FFGM. They choose 15 NFGM and 15

FFGM and studied them concerning the linear response spectrum of pseudo-acceleration, pseudo-velocity, and displacement. And figured out that sensitivity regions in the cases of NFGM are much wider [5].

The research done by Hall et al. (1995) discussed that structures with a significant height are very weak against severe NFGM. The increase of the effect of high mode shapes and the wave propagation with its outcome on the deformation of the structure is reported, due to the exposure of the tall building to the 1994 Northridge earthquake [6].

Ali A. Muhsin and Hussam K. Risan also did a paper on the elastic response of a 35 stories reinforced concrete building under NF and FF excitation. And the results show that the NF excitations will cause the structure to surpass its life safety performance level. Also, the near-fault (NF) earthquake intensity measurements were explored in this paper for three different frame buildings with 6, 13, and 20 stories. And found that the building's vibration period and the equation that was used to calculate the IM highly affect the accuracy of the IM [7].

In this paper, a great number of earthquake events were taken randomly as a sample to evaluate this paper's goals. Four earthquake groups were made, each with specific characteristics. And analyzing these GM using PRISM to result in the responses that will be reviewed and discussed in this research.

METHOD OF RESPONSE SPECTRUM

The RSM expression is used to refer to the "Response spectrum method" and is known as the first logical act of scientific development of the design for earthquake-resistant. It can also be defined as an outline of absolute values of the structure's maximum response (that consist of displacement, accelerations, velocities, etc.) which is known as a function of the natural time period of the structure.

This method is the first actual technique for developing earthquake resistance design. For a structure to withstand an earthquake, it is required to be built around the notion that it is adept to endure a force equal to $m \times S_{a_{max}}$, where m is the mass of the structure and $S_{a_{max}}$ is the maximum expected acceleration that a structural body will be subjected to under a specific ground acceleration, and it is also the function of the individual time period of the structural body [8].

If a building system is considered an elastic system with MDOF (multiple degrees of freedom), then we can separate it into singular components of an SDOF (single degree of freedom). for each of these singular components, it is probable to find the peak response if we can measure the ground acceleration resulting from a shock-like earthquake, then The overall response can then be calculated by the superimposition of these singular responses. Using this method [8].

Fig.1 shows the acceleration time history of an NFGM for the " El Mayor-Cucapah" earthquake recorded in Mexico in 2010. This record is taken from PEER, having magnitude ($M_w = 7.2$), epicentral distance ($R_{rup} = 11.44$ Km), and PGA of 0.255g acceleration time history (near-fault). This acceleration time history is converted to an

elastic spectrum response using PRISM software to get the spectral (acceleration, velocity, and displacement) as in Fig.2. Three Damping ratios (ξ) values of 3%, 5%, and 10% to be used in the spectrum analysis and different values are taken because damping depends on the material used to build the structure as well as the number of joints and restraints. As for a typical value, 5% is correct for most concrete structures.

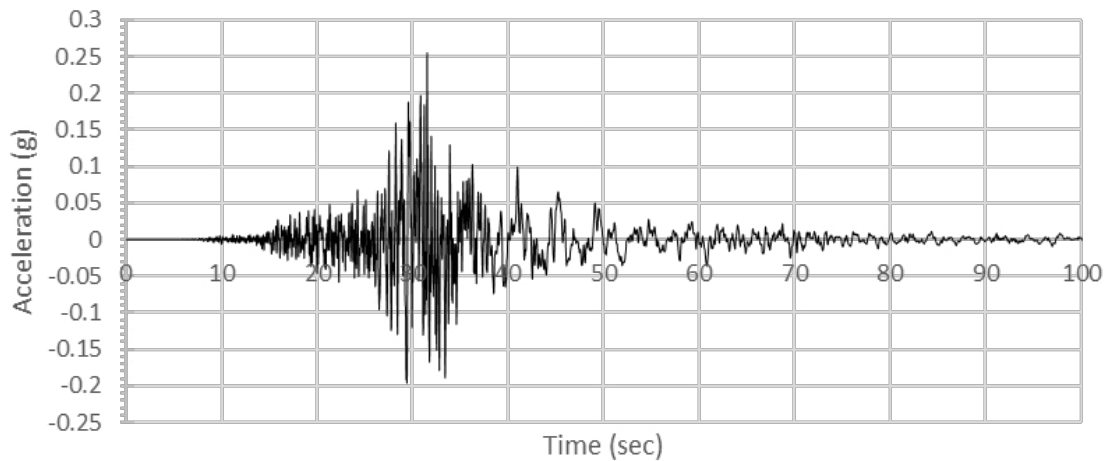


Figure 1. Acceleration time history of El Mayor-Cucapah (2010) earthquake

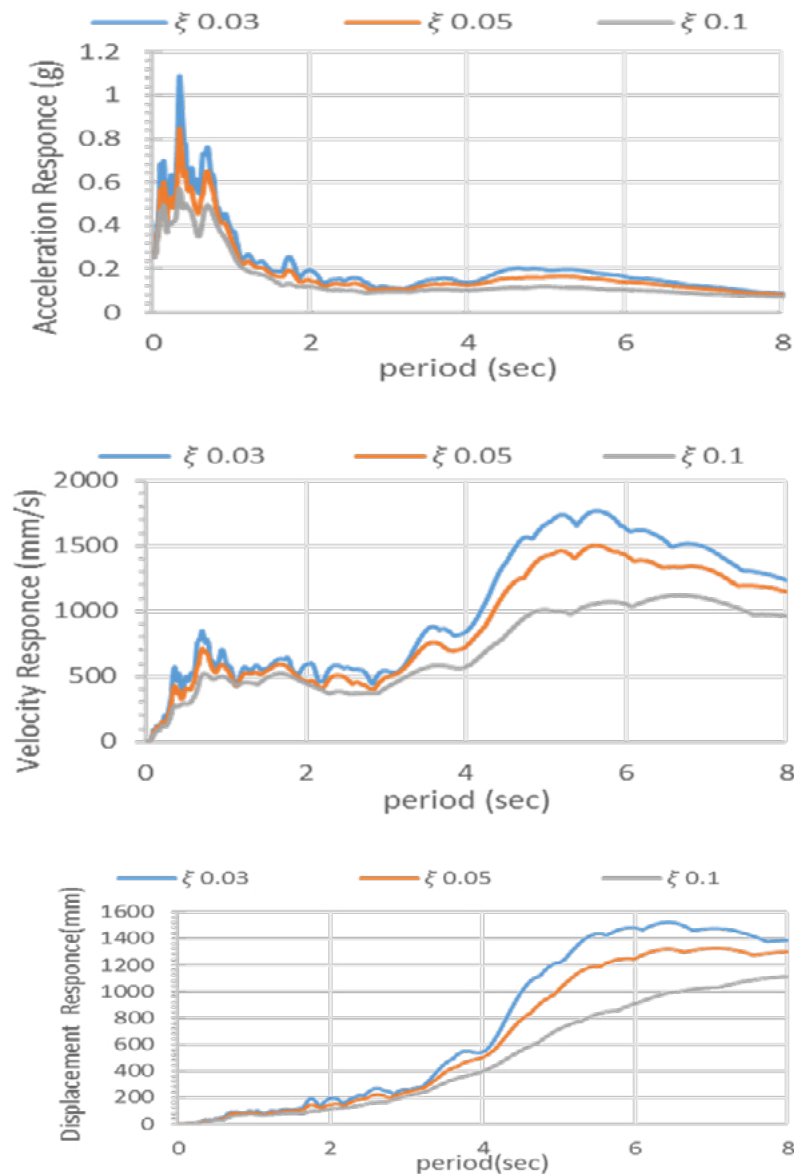


Figure 2. Acceleration, velocity, and displacement response spectrum of El Mayor-Cucapah (2010) earthquake

CHOSEN GROUND MOTION RECORDS OF SPECIFIC EARTHQUAKES

The data selected in this research are all shallow earthquakes in active tectonic areas (Shallow earthquakes are between 0 and 70 km deep) with a moment magnitude (M_w) in the range of (4-9) and all types of fault mechanisms were considered. Two soil types were chosen for this chapter with V_{s30} (soil shear velocity) values of (100-300) m/s for the first type (soft soil) and (600-800) m/s for the second type (soft rocks). Those ranges were taken because most of the shear velocity values for the Iraqi soils stand in those ranges. And for every type of soil NFGM and FFGM records are considered. For the NFGM distance of < 15 km and the events had to have a noticeable peak-like record to be considered whereas for the FFGM distance

of >50 km with no apparent peak was taken and this is to have a better comparison between the two ground motions.

By applying the conditions mentioned previously on the PEER search page four different groups of earthquake records are found, and the criteria for those groups as well as the number of events taken are listed in Table 1. To avoid the control of earthquakes with a large number of station records and satisfy the independent conditions, only one station was chosen for each earthquake event.

These earthquake event characteristics for groups 1 to 4 are listed in Tables 2 to 5 respectively. Groups 1 and 2 are built for Vs30 ranging from 100-300 m/s for both NFGM and FFGM. While groups 3 and 4 are built for Vs30 ranging from 600-800 m/s for both NFGM and FFGM. The fault type in all four groups was irrelevant to this research and that's why it was not specified.

Table 1. Ground motion groups' criteria

| Group | Magnitude | Vs30 | GM | No. of records |
|-------|-----------|---------|------|----------------|
| 1 | 4-9 | 100-300 | NFGM | 15 |
| 2 | | | FFGM | 11 |
| 3 | | 600-800 | NFGM | 20 |
| 4 | | | FFGM | 10 |

Table 2. the first group's earthquakes events

| NO. | Earthquake event | Year | Station | Magnitude | Rrup | Vs30 |
|-----|-----------------------------|------|-------------------------------|-----------|-------|--------|
| 1 | "Central Calif-02" | 1960 | "Hollister City Hall" | 5.00 | 09.02 | 198.77 |
| 2 | "Managua_ Nicaragua-02" | 1972 | "Managua_ ESSO" | 5.20 | 04.98 | 288.77 |
| 3 | "Hollister-03" | 1974 | "Hollister City Hall" | 5.14 | 09.39 | 198.77 |
| 4 | "Mammoth Lakes-09" | 1980 | "Hot Creek (HCF)" | 4.85 | 12.01 | 295.93 |
| 5 | "Westmorland" | 1981 | "Westmorland Fire Sta" | 5.90 | 06.50 | 193.67 |
| 6 | "Coalinga-02" | 1983 | "SUB (temp)" | 5.09 | 12.31 | 270.41 |
| 7 | "Imperial Valley-06" | 1979 | "EC County Center FF" | 6.53 | 07.31 | 192.05 |
| 8 | "Loma Prieta" | 1989 | "Gilroy Array #2" | 6.93 | 11.07 | 270.84 |
| 9 | "Chi-Chi_ Taiwan" | 1999 | "CHY101" | 7.62 | 09.94 | 258.89 |
| 10 | "Duzce_ Turkey" | 1999 | "Bolu" | 7.14 | 12.04 | 293.57 |
| 11 | "Tottori_ Japan" | 2000 | "TTR008" | 6.61 | 06.88 | 139.21 |
| 12 | "Parkfield-02_ CA" | 2004 | "Parkfield - Stone Corral 1E" | 6.00 | 03.79 | 260.63 |
| 13 | "Christchurch_ New Zealand" | 2011 | "Christchurch Resthaven " | 6.20 | 05.13 | 141.00 |
| 14 | "El Mayor-Cucapah_ Mexico" | 2010 | "El Centro Array #12" | 7.20 | 11.26 | 196.88 |
| 15 | "Darfield_ New Zealand" | 2010 | "TPLC" | 7.00 | 06.11 | 249.28 |

Table 3. the second group's earthquakes events

| NO. | Earthquake | Year | Station | Magnitude | Rrup | Vs30 |
|-----|----------------------|------|----------------------------|-----------|--------|--------|
| 1 | "Yorba Linda" | 2002 | "Calstate Bakersfield" | 4.265 | 199.89 | 275.00 |
| 2 | "Parkfield-02_ CA" | 2004 | "Milpitas Fire Station 4" | 6.000 | 195.59 | 263.76 |
| 3 | "El Alamo" | 1956 | "El Centro Array #9" | 6.800 | 121.70 | 213.44 |
| 4 | "Borrego Mtn" | 1968 | "LB - Terminal Island" | 6.630 | 199.84 | 217.92 |
| 5 | "Tabas_ Iran" | 1978 | "Kashmar" | 7.350 | 194.55 | 280.26 |
| 6 | "San Fernando" | 1971 | "Bakersfield - Harvey Aud" | 6.610 | 113.02 | 241.41 |
| 7 | "Landers" | 1992 | "Anaheim - W Ball Rd" | 7.280 | 144.90 | 269.29 |
| 8 | "Duzce_ Turkey" | 1999 | "Bursa Tofas" | 7.140 | 166.07 | 289.69 |
| 9 | "Hector Mine" | 1999 | "Newhall - Fire Sta" | 7.130 | 198.13 | 269.14 |
| 10 | "Chi-Chi_ Taiwan-03" | 1999 | "KAU066" | 6.200 | 123.57 | 214.97 |
| 11 | "Chi-Chi_ Taiwan-04" | 1999 | "KAU015" | 6.200 | 109.50 | 233.21 |

Table 4. the third group's earthquake events

| No. | Earthquake | Year | Station | Magnitude | Rrup | Vs30 |
|-----|--------------------------|------|---|-----------|-------|--------|
| 1 | "Morgan Hill" | 1984 | "Gilroy Array #6" | 6.19 | 09.87 | 663.31 |
| 2 | "L'Aquila_ Italy" | 2009 | "L'Aquila - Parking" | 6.30 | 05.38 | 717.00 |
| 3 | "10319993" | 2008 | "Hector" | 4.14 | 06.41 | 726.00 |
| 4 | "21522424" | 2006 | "Anderson Dam" | 4.30 | 13.62 | 600.00 |
| 5 | "Umbria Marche Italy" | 1997 | "Nocera Umbra-Salmata" | 5.50 | 12.45 | 694.00 |
| 6 | "Frulli_ Italy-03" | 1976 | "Tarcento" | 5.50 | 06.30 | 629.08 |
| 7 | "Chi-Chi_ Taiwan-02" | 1999 | "TCU089" | 5.90 | 12.02 | 671.52 |
| 8 | "Gilroy" | 2002 | "Gilroy Array #6" | 4.90 | 14.39 | 663.31 |
| 9 | "San Juan Bautista" | 1998 | "Hollister - SAGO Vault" | 5.17 | 07.04 | 621.20 |
| 10 | "14239764" | 2006 | "Joshua Ridge: China Lake" | 4.02 | 13.75 | 623.00 |
| 11 | "30226086" | 2003 | "Geyserville; Warm Springs Dam; Downstream" | 4.00 | 08.38 | 760.00 |
| 12 | "14282008" | 2007 | "Joshua Ridge: China Lake" | 4.11 | 06.72 | 623.00 |
| 13 | "21455182" | 2005 | "Atlas Peak" | 4.14 | 12.85 | 652.29 |
| 14 | "Sierra Madre" | 1991 | "Mt Wilson - CIT Seis Sta" | 5.61 | 10.36 | 680.37 |
| 15 | "Oroville-01" | 1975 | "Oroville Seismograph Station" | 5.89 | 07.99 | 680.37 |
| 16 | "Coyote Lake" | 1979 | "Gilroy Array #6" | 5.74 | 03.11 | 663.31 |
| 17 | "Anza (Horse Canyon)-01" | 1980 | "Anza - Terwilliger Valley" | 5.19 | 12.28 | 617.78 |
| 18 | "Mammoth Lakes-09" | 1980 | "USC McGee Creek" | 4.85 | 09.18 | 653.56 |
| 19 | "Coalinga-07" | 1983 | "Sulphur Baths (temp)" | 5.21 | 12.11 | 617.43 |
| 20 | "Hollister-04" | 1986 | "SAGO South - Surface" | 5.45 | 12.32 | 608.67 |

Table 5. the fourth group's earthquake events.

| No. | Earthquake | Year | Station | Magnitude | Rrup | Vs30 |
|-----|-----------------------------|------|-------------------------------|-----------|--------|--------|
| 1 | "Chi-Chi_ Taiwan-05" | 1999 | "TAP081" | 6.20 | 155.66 | 671.52 |
| 2 | "San Simeon_ CA" | 2003 | "Frazier Park - Post Office" | 6.52 | 186.24 | 643.91 |
| 3 | "El Mayor-Cucapah_ Mexico" | 2010 | "Silent Valley - Poppet Flat" | 7.20 | 167.65 | 659.09 |
| 4 | "Niigata_ Japan" | 2004 | "SIT012" | 6.63 | 156.93 | 710.53 |
| 5 | "Darfield_ New Zealand" | 2010 | "ODZ" | 7.00 | 180.55 | 638.39 |
| 6 | "Christchurch_ New Zealand" | 2011 | "RDCS" | 6.20 | 172.19 | 628.04 |
| 7 | "Parkfield-02_ CA" | 2004 | "Saint Joseph's Hill" | 6.00 | 181.51 | 690.97 |
| 8 | "Chi-Chi_ Taiwan-02" | 1999 | "TTN025" | 5.90 | 106.03 | 704.96 |
| 9 | "Molise-01_ Italy" | 2002 | "Norcia" | 5.70 | 183.86 | 678 |
| 10 | "L'Aquila_ Italy" | 2009 | "Cassino" | 5.40 | 116.68 | 630 |

ELASTIC RESPONSE OF NFGM AND FFGM

Elastic Seismic responses for the NFGM and FFGM are computed by scaling the chosen records in the four groups mentioned in the tables previously to a similar PGA (peak ground acceleration) which is chosen to be 0.3g then after processing all the data, the response spectra are then determined using Prism software as mentioned before. An average value of the SDOF response results of the spectral acceleration, spectral velocity, and spectral displacement ground motions for the earthquake events is done. Finally, the responses spectra are graphed using excel to better illustrate the results and to show the difference between NFGM and FFGM in acceleration, velocity, and displacement in elastic conditions.

Fig. 3 shows the differences in the Far-field ground motion and the near-fault ground motion for the soft soils (groups one and two). While Fig. 4 shows the difference in the Far-field ground motion and the near-fault ground motion for the soft rocks (groups three and four).

As illustrated above in Fig. 3 we can see that the general response of the near-fault ground motion in all three figures is much higher than the responses of far-field ground motion. Both the start of NFGM and FFGM are approximately equal in the short period where T is less than 0.3 sec. then, they start to depart from each other as the NFGM response starts to escalate until the end of the 4 sec period. It's obvious that the NFGM has the higher response on the structure with max NFGM acceleration, velocity, and displacement values being 18%, 182%, and 265% higher than the responses of FFGM for soft soils. As for the values of acceleration, velocity, and displacement of NFGM are 7%, 200%, and 501% higher than for FFGM for rocks as in fig. 4.

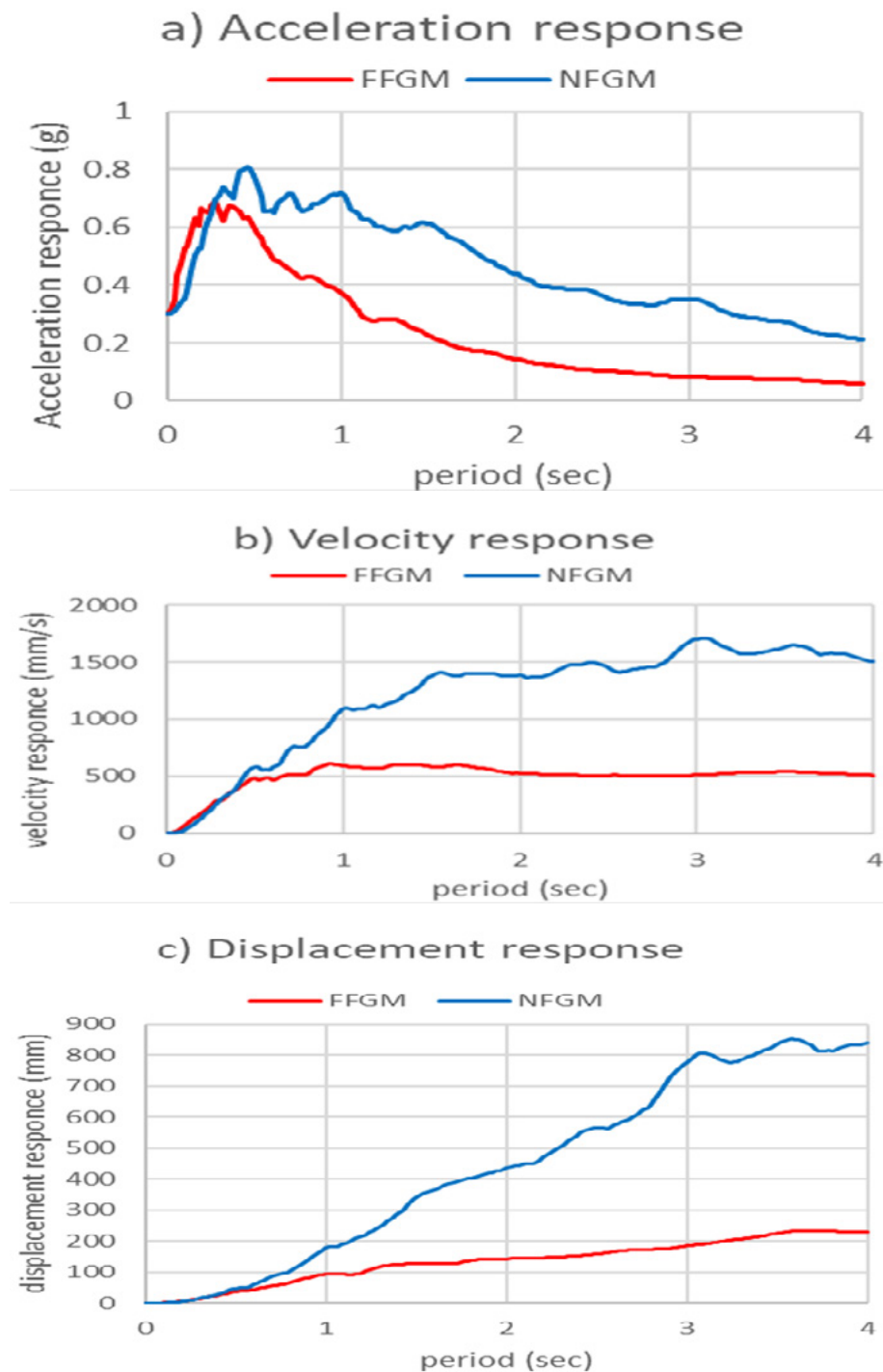


Figure 3. Comparison between NFGM and FFGM elastic response spectrum for the soft soils
a) Acceleration response, b) Velocity response, and c) Displacement response

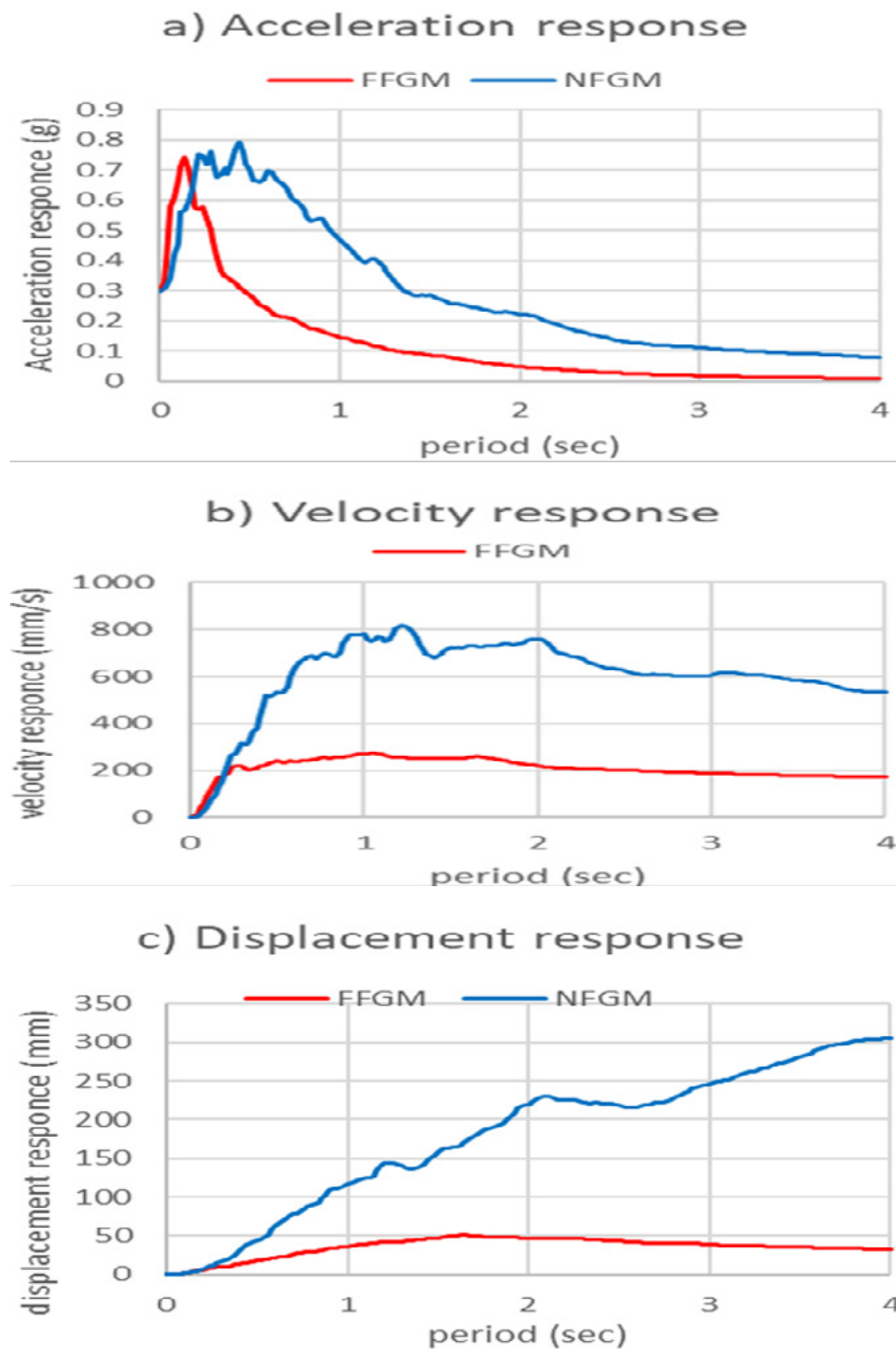


Figure 4. Comparison between NFGM and FFGM elastic response spectrum for the rock soil
a) Acceleration response, b) Velocity response, and c) Displacement response

THE EFFECT OF SOIL TYPE ON SDOF ELASTIC SEISMIC RESPONSE

For the last two decades, the studies of numerous travelling wave solutions to the nonlinear development equations have appealed the attentions of many scientist from all over the world. Nonlinear evolution equations (NLEEs) are used in explaining several complex phenomena that ascend on daily basis in the various fields of nonlinear sciences, such as, quantum mechanics, plasmas physics, earthquake waves and so on [9].

Seismic waves can cause shaking which can result in damage or failure of the structures. There are many characteristics of free field motion that can be considerably modified by the Local soil deposits such as the amplitude, duration, and frequency content. The nonlinear response of the site is displayed during the transmittal of high-intensity ground motion waves through the horizontal soil layers [10].

The records of acceleration in the near-field region are attained during earthquakes at somewhat short distances from the desired site and records in the far-field regions occurring far from the site demonstrated the huge influence of geotechnical site conditions such as properties of soil layers and soil stratification on strong motion characteristics at the ground surface.

In the near-field zones, the soil characteristics are very dominant and affect the directional properties of the earthquake GM. So the forward-directivity ground motions will enforce high deformation and high energy demands on structures.

As we can see in Fig.5, we can notice that the soft soil responses are much higher than the responses of the rock because the ground motion gets amplified much more in the regions where the soils are soft thus resulting in a higher structural response.

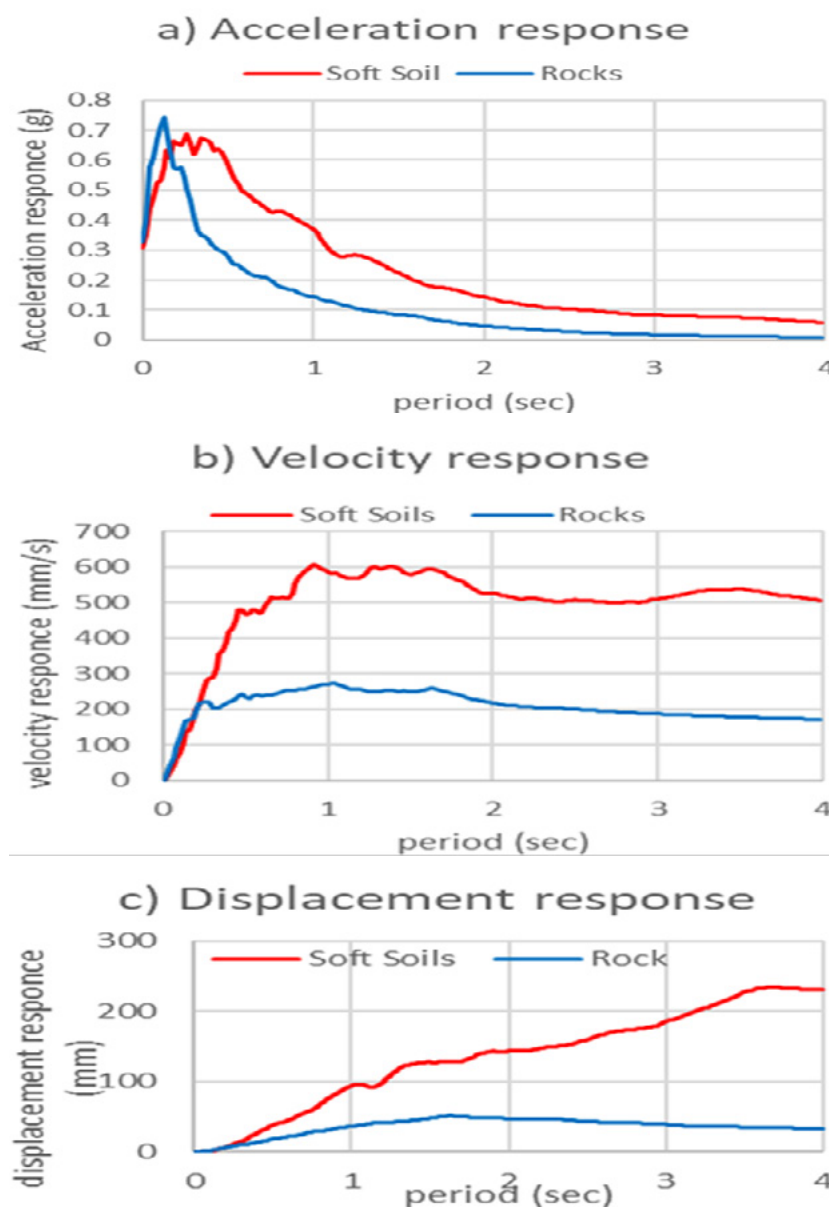


Figure 5. comparison between soft soils and rocks elastic response spectrum for NFGM in a) Acceleration response, b) Velocity response, and c) Displacement response.

CONCLUSIONS

from all the previous sections of the paper the following points are concluded:

- 1) The overall response of the near-fault ground motion in all three parameters (acceleration, velocity, displacement) is much higher than the responses of far-field ground motion in all conditions.
- 2) The start of NFGM and FFGM response graphs are roughly equal in the short period where T is less than 0.3 sec. after that, they begin to depart from each other as the NFGM response jumps to escalate until the end of the 4 sec period.
- 3) For both soft soils and rocks the NFGM responses are higher than the FFGM responses and the percentages of these differences are 18%, 182%, and 265% (acceleration, velocity, and displacement) higher for soft soils. As for the values of

acceleration, velocity, and displacement of NFGM are 7%, 200%, and 501% higher than for FFGM for rocks.

- 4) In the near-field regions, the soil characteristics are extremely governing and affect the directional properties of the earthquake GM.
- 5) The soft soil responses are more advanced than the responses of the rock because the ground motion becomes amplified further in the regions where the soils are soft thus causing a higher structural response.

REFERENCES

- (1) Caymaz, G. F. Y., & Komar, H. (2021). **Analysis of Earthquake Park Design Criteria: Cases in Ataşehir and Topkapı Parks, Istanbul.** *Architecture and Urban Planning*, 17(1), 88-102.
- (2) Liu, W., & Liu, Y. (2012). **Commonly used earthquake source models.** *Geologos*, 18(3), 197-209.
- (3) Somerville, P., Smith, N., Punyamurthula, S., & Sun, J. (1997). **Development of ground motion time histories for phase 2 of the FEMA/SAC steel project. SAC Background Document.** Report submitted to the Report SAC/DB-97/04, USA.
- (4) Zhang, Y., & Iwan, W. D. (2002). **Active interaction control of tall buildings subjected to near-field ground motions.** *Journal of Structural Engineering*, 128(1), 69-79.
- (5) Chopra, A. K., & Chintanapakdee, C. (2001). **Comparing response of SDF systems to near-fault and far-fault earthquake motions in the context of spectral regions.** *Earthquake engineering & structural dynamics*, 30(12), 1769-1789. <https://doi.org/10.1002/eqe.92>.
- (6) Hall, J. F., Heaton, T. H., Halling, M. W., & Wald, D. J. (1995). **Near-source ground motion and its effects on flexible buildings.** *Earthquake spectra*, 11(4), 569-605.
- (7) Chowdhury, I., & Dasgupta, S. P. (2019). **Earthquake Analysis and Design of Industrial Structures and Infra-structures.** Springer International Publishing.
- (8) Muhsin, A. A., & Risan, H. K. (2021). **Influence of near-fault characteristics on inelastic response of multi-storey building with intensity measurement analysis.** *Građevinar*, 73(11.), 1081-1092
- (9) Hall, J. F., Heaton, T. H., Halling, M. W., & Wald, D. J. (1995). **Near-source ground motion and its effects on flexible buildings.** *Earthquake spectra*, 11(4), 569-605.
- (10) Sulaiman, T. A., Bulut, H., & Baskonus, H. M. (2021). **On the exact solutions to some system of complex nonlinear models.** *Applied Mathematics and Nonlinear Sciences*, 6(1), 29-42. <https://doi.org/10.2478/amns.2020.2.00007>.
- (11) Dixit, J., Dewaikar, D. M., & Jangid, R. S. (2012). **Free field surface motion at different site types due to near-fault ground motions.** *International Scholarly Research Notices*, 2012.

/03/

PERFORMANCE OF COLUMN-TO-COLUMN MECHANICAL CONNECTION IN PRECAST CONCRETE BUILDING UNDER SEISMIC LOADING

Ahmed D. Abduleef*

College of Engineering, University of Samarra, Samarra 34010, Iraq.

ahmed.d.abd@uosamarra.edu.iq

Ammar A. Abdul Rahman

College of Engineering, Ashur University College, Baghdad10011, Iraq.



Reception: 17/10/2022 **Acceptance:** 24/12/2022 **Publication:** 13/01/2023

Suggested citation:

A., Ahmed D. and A. R., Ammar A. (2023). **Performance of column-to-column mechanical connection in precast concrete building under seismic loading**. *3C TIC. Cuadernos de desarrollo aplicados a las TIC*, 12(1), 46-63. <https://doi.org/10.17993/3ctic.2023.121.46-63>

ABSTRACT

Precast columns in precast concrete structures with floor heights require connections that need confident, reliable, and cost-effective design and implementation methods that can speed up both processes. At the same time, still ensure adequate strength, stiffness, and ductility to the column behavior. Columns specifically have the main role in structures for transmitting vertical and horizontal loads due to seismic effects to the base to fulfill life safety requirements, but the existence of a connection in the column cannot ensure the required. This work aims to study the performance and efficiency of mechanical bolted column connections under the action of seismic loading. In this regard, a column connection used in the precast structure of the new Karbala Provincial Council (KPC) under seismic loading is used as the case study. This building was analyzed and then designed employing special mechanical bolted connections produced by Peikko's products (Column-shoe & Anchor bolts). The analysis gave the exact forces at the connection location and the design using Peikko's column connection performed well under all loading cases including the seismic case. The analysis and design lead to smaller column section selection since it takes into account the interaction of applied loads using special equations.

KEYWORDS

Column Shoe, Column to column connection, Seismic design, bolted connection, Anchor bolts

PAPER INDEX

ABSTRACT

KEYWORDS

1. INTRODUCTION
 2. DISCRIPTION OF THE CONNECTION
 3. COMPONENTS OF THE BOLTED CONNECTION (PBC)
 - 3.1. Column Shoes
 - 3.2. Anchor Bolts
 4. MODELING
 - 4.1. Modeling of the Columns
 - 4.2. Selecting Column Connections Using Peikko Designer
 5. RESULTS AND DISCUSSION
 - 5.1. Run Analysis and Get the Results in ETABS
 6. DESIGN RESULTS FROM PEIKKO DESIGNER
 - 6.1. Corner Column (40x40 cm)
 - 6.2. Edge Column (60x60 cm)
 - 6.3. Corner Column (70x70 cm)
 - 6.4. Comparison with Manual Selection:
 7. CONCLUSIONS
- REFERENCES
- CONFLICT OF INTEREST

1. INTRODUCTION

In seismic-resistance structures with precast concrete (PC) members, the major challenge is to find, reliable economical, applicable, and structurally accepted methods to connect the precast elements in a way so that when subjected to cyclic seismic loads, these connections can provide not only sufficient strength and stiffness but also allow sufficient inelastic deformation capacity and stable hysteresis response of the structure [1]. In framed PC structures columns particularly play a fundamental role in transferring vertical and horizontal loads, to meet the requirement of life safety under seismic loads. Attention should be paid to the connections between precast columns to ensure the integrity of the building, load transfer, and the behavior under different load combinations [2]. The ultimate strength at the joint of precast concrete structures depends on the behavior of the material of joints between segments [3]. The connections between prefabricated elements are typically considered to be the weakest and most critical parts. Additionally, in seismic areas, the connections should ensure that the behavior of precast connections is equal to or even better than that of cast-in-place parts [4]. Peikko bolted column connections are considered an excellent solution for such purposes [5]. But was not verified clearly for earthquakes. A Study on an actual building (Karbala Provincial Council) made of precast concrete elements (columns, beams, and hollow core slabs) that are connected by mechanical joints (Column-shoe & Anchor bolts) will be conducted to check the adequacy and performance of these connections in sustaining the imposed loads on the building due to the seismic occurrence. Due to the different types of connections used in the building, a focus will be made here in this work on the column-to-column connections because very limited research work was published on the such connection under seismic effects. There are limited references that deal with the characterization of column-column connections of PC structures [6]. Also, there was limited access to studies that examined column shoe connections due to the privacy of the product's ownership. However, from the experimental data provided and the conclusions gained, it is obvious that this connection system can be used in connecting the parts of the column [7] but needs to check their performance under seismic action. Peikko initiated an extensive experimental research program in 2008 in collaboration with the Politecnico di Milano (Technical University of Milan) to study the performance of Peikko's bolted column-to-foundation connections made with the HPKM column and HPM anchor bolts. The aim was to produce and develop a prefabricated connection that replaces the monolithic connections with the same performance in terms of ductility, energy dissipation capacity, and stiffness [8]. The cyclic loading performance of the Peikko bolted connection for seismic conditions needs to be verified by extensive experimental investigations on full-scale concrete samples of precast and cast-in-place columns. Meanwhile, numerical verification needs to be concluded to check the adequacy of these bolted connections. The performance of the entire connection and its components under monotonic loadings were verified by experimental testing. The initial test with concrete column connections showed that rectangular cross-sections with at least four-column shoes behave rigidly or at least as stiff as in-situ concrete columns with continuous reinforcement under static loading [10]. The tests confirmed that the bolted connection with grout between the precast

elements behaves in the same way as the corresponding monolithic reinforced concrete column [11].

2. DISCRIPTION OF THE CONNECTION

A typical mechanical bolted column connection consists of column shoes and anchor bolts. The column shoe is placed in the formwork in the precast plant during the production of the column at the bottom end of the upper column and the anchor bolts are cast in the upper end of the lower column in case of column-column connection or cast in-site into the foundation in case of column-foundation connection as shown in Figure (1). The protruding threaded portion of the bolt allows the column shoe base plate to be tightened with a pair of washers and nuts. The tightening of the connection under seismic loading is also ensured by high-strength lock washers. The connection is completed by filling the joint between the columns or the column and the foundation with high-durability, non-shrinking mortar. Once the mortar has reached its design strength, the connection behaves as a reinforced concrete connection. The shear force transmission is done by anchor bolts with lock washers and mechanical locking between mortar and concrete. The design compressive strength of the grout should be at least one class higher than the highest concrete grade of the jointed elements, to avoid the brittle fracture of the concrete at the joint. [8]. Assembling the column shoes on the column requires steel boxes called Recess boxes containing two types (C and M) as shown in figure (2), their cost is low and they can be used multiple times to prevent concrete from filling the shoe hole during casting of the column.

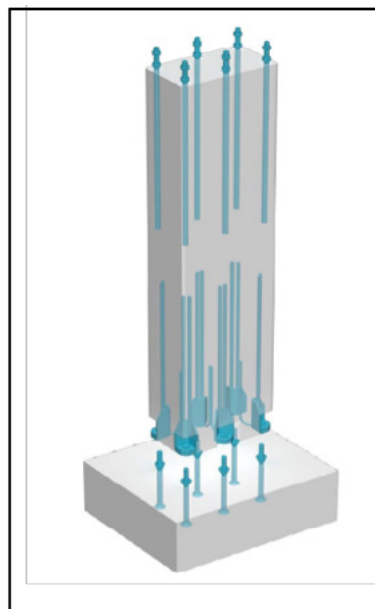


Figure 1. Typical bolted column connection [12]

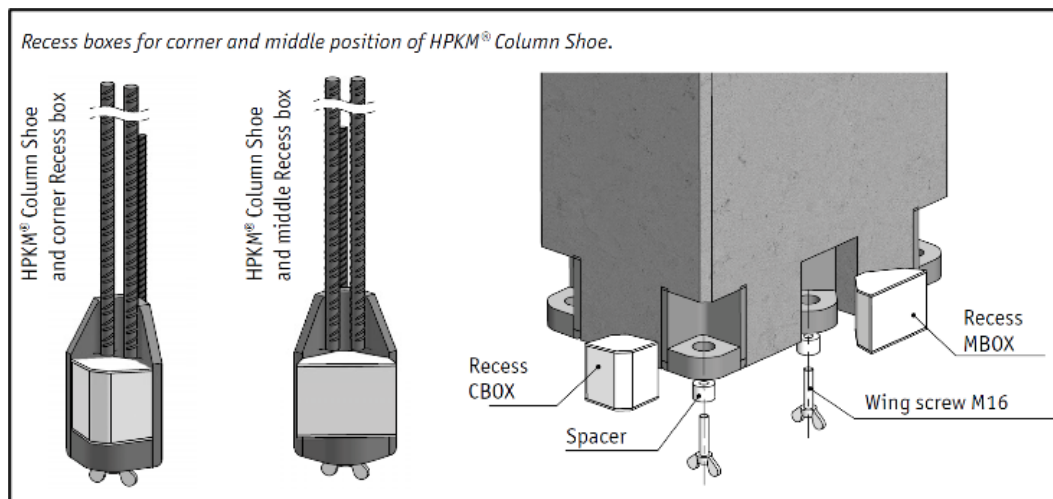


Figure 2. (C and M) types of Recess boxes [12]

3. COMPONENTS OF THE BOLTED CONNECTION (PBC)

3.1. COLUMN SHOES

Column shoes are products used to create moment-bearing connections between precast concrete elements, such as columns, foundations, and walls. The bolted column shoe connection is at least as stiff as a cast-in-place column connection with continuous reinforcement. The loads on the connection are first distributed to the individual column bases. The shear strength of a column shoe is equal to the shear strength of the corresponding anchor bolts [12]. The strength of the column shoe corresponds to the strength of the corresponding anchor bolts. Four or more column shoes can be used in one column cross-section [7]. figure (3) shows Peikko's column shoes that are used here.

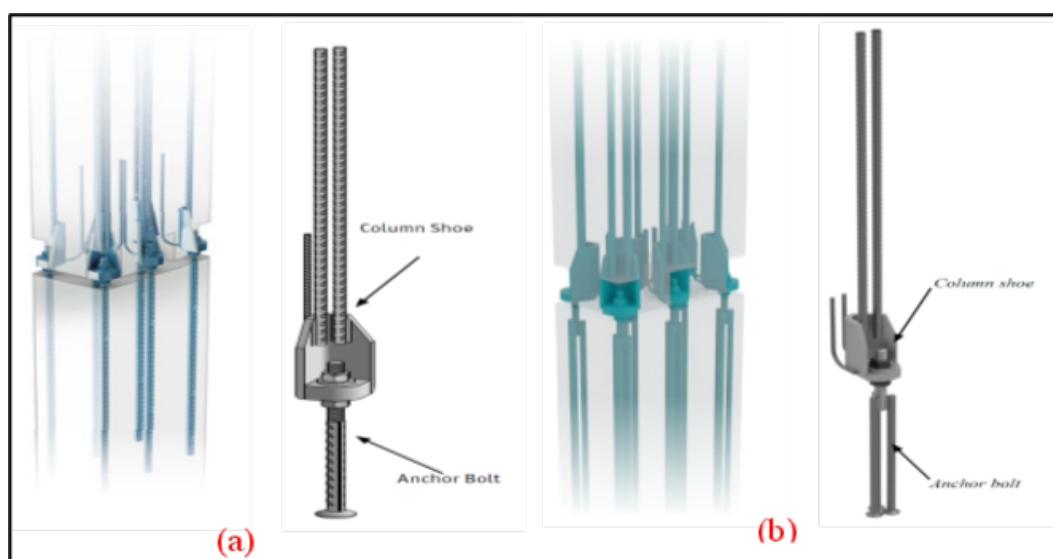


Figure 3. Peikko bolted connection (PBC) for column (a) HPKM column shoe [13], (b) BOLDA column shoe [14]

3.2. ANCHOR BOLTS

Anchor bolts can provide a solution for most precast connections (e.g., column - foundation, column - column, wall - foundation, wall - wall) as well as fastening of steel columns or even machine fastenings. It's available as L- a type use in shallow structures (e.g., foundations, slabs, beams) due to their relatively short anchor length and P-type for structures with sufficient depth (e.g., pedestals, and columns). if the tensile or shear strength of the anchor bolt steel is insufficient, additional reinforcement may be used to withstand the forces on the anchor bolt and if the concrete cone resistance is exceeded, supplementary reinforcement for the tension load should be provided. reinforcement arrangements can be calculated using the Peikko Designer software following EN 1992-4. With Peikko Designer software it is possible to select the appropriate type and number of anchor bolts to be used in a connection and to check the strength of the connection [13]. During the assembly phase, the forces acting on the anchor bolts are mainly caused by the weight of the column itself and the bending moment and shear force due to the wind load. Since the connection is not grouted, all forces from the column shoe are only absorbed by the anchor bolts. therefore, it must be designed for buckling and bending [12]. The anchor bolts used in column connections are shown in the figure. (4).

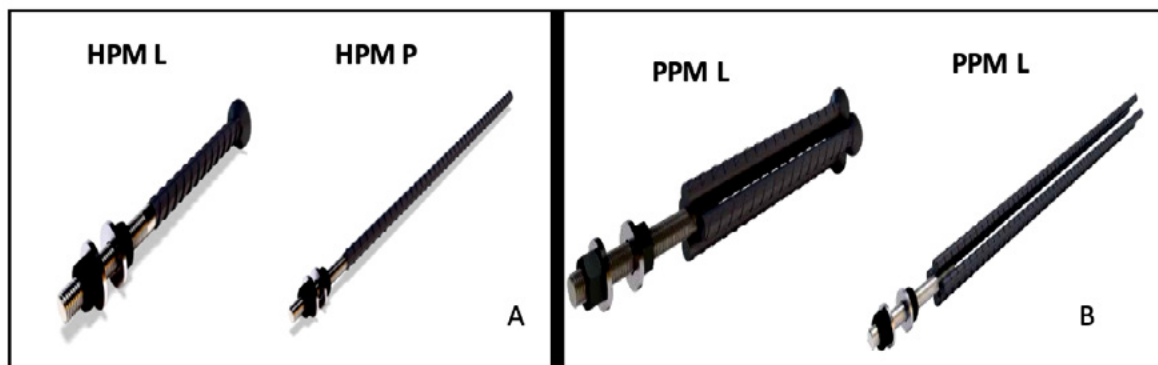


Figure 4. Anchor bolts. A) HPM Rebar Anchor Bolts Type L & type P [15]. B) High Strength Steel Anchor Bolts Type (L & P) [16]

4. MODELING

4.1. MODELING OF THE COLUMNS

Simulation models have the characteristic of being a technique for solving practical problems [17]. The whole structure of the building was divided into seven structures (Blocks) with expansion joints each part was modeled using CSI ETABS Software to analyze the effect of all external forces including seismic forces for the Karbala area according to the Iraqi Seismic Code. These forces were applied to the building and the magnitude of all internal forces acting on the columns at different stations through their total height was obtained. ETABS can give the magnitude of internal forces at

(0%, 25%,50%,75%, and 100%) of the column's height. This feature could be very useful in the design of the connection since it can help in identifying the magnitude of internal forces corresponding to desired connection location. There are three different column cross-sections in each of the seven blocks (40x40, 60x60, and 70x70 cm) respectively distributed at different positions on the plan (corner, edge, interior). In this work, Block number 7 figure (5) is considered only for these calculations. The seismic details defined in the ETABS model are shown in figure 6

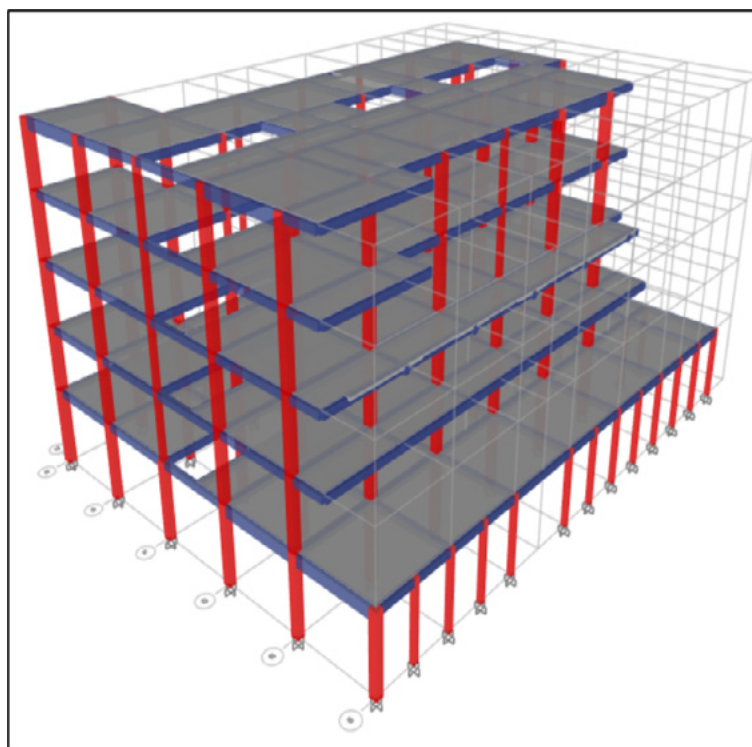


Figure 5. ETABS model of part 7

| Seismic Coefficients | |
|---------------------------------|-------|
| 0.2 Sec Spectral Accel, S_s | 0.3 |
| 1 Sec Spectral Accel, S_1 | 0.1 |
| Long-Period Transition Period | 6 |
| Site Class | D |
| Site Coefficient, F_a | 1.56 |
| Site Coefficient, F_v | 2.4 |
| Calculated Coefficients | |
| $SDS = (2/3) * F_a * S_s$ | 0.312 |
| $SD1 = (2/3) * F_v * S_1$ | 0.16 |
| Factors | |
| Response Modification, R | 5 |
| System Overstrength, Ω | 3 |
| Deflection Amplification, C_d | 4.5 |
| Occupancy Importance, I | 1 |

Figure 6. The seismic details defined in the ETABS model

4.2. SELECTING COLUMN CONNECTIONS USING PEIKKO DESIGNER

For column-to-column connection, HPKM & BOLDA column shoes with HPM & PPM anchor bolts were respectively chosen. The selection of the suitable size of column shoes and anchor bolts to be used for connecting the precast segments was first done manually based on the technical manual provided. The selection of the connection components was verified using Peikko designer software. The software contains a predefined module for different types of column shoes and their corresponding anchor bolts. In the software, there is an implemented design code selection. By selecting the required valid design code, it is possible to check the resistances of each column connection.

5. RESULTS AND DISCUSSION

5.1. RUN ANALYSIS AND GET THE RESULTS IN ETABS

After completing the modeling in ETABS, the analysis process will start to get the magnitude of all internal forces acting on the columns at the selected sections of the columns. After that, the analysis results were filtered, sorted, and rearranged to be used in the next step (Selection of Suitable connection items by Peikko designer). The analysis results used in the selection of the connection components (column shoes + anchor bolts) were selected based on the location of the column i.e., (corner 40x40, edge 40x40, 40x40 interior, 60x60 corner ...etc.). For simplicity and to avoid getting a huge number of designed connections for each column cross-section at each location and each story only the greatest values of internal forces on each column cross-section concerning its location due to the application of all types of loads including earthquakes were used to design the connections as shown in figures ((7) - (10)) and Table (1). The manufacturer can use any length of each segment that his factory can produce. The columns were made of three parts only taking into account that each column consists of three individual precast segments to be connected to cover the total height of the building.

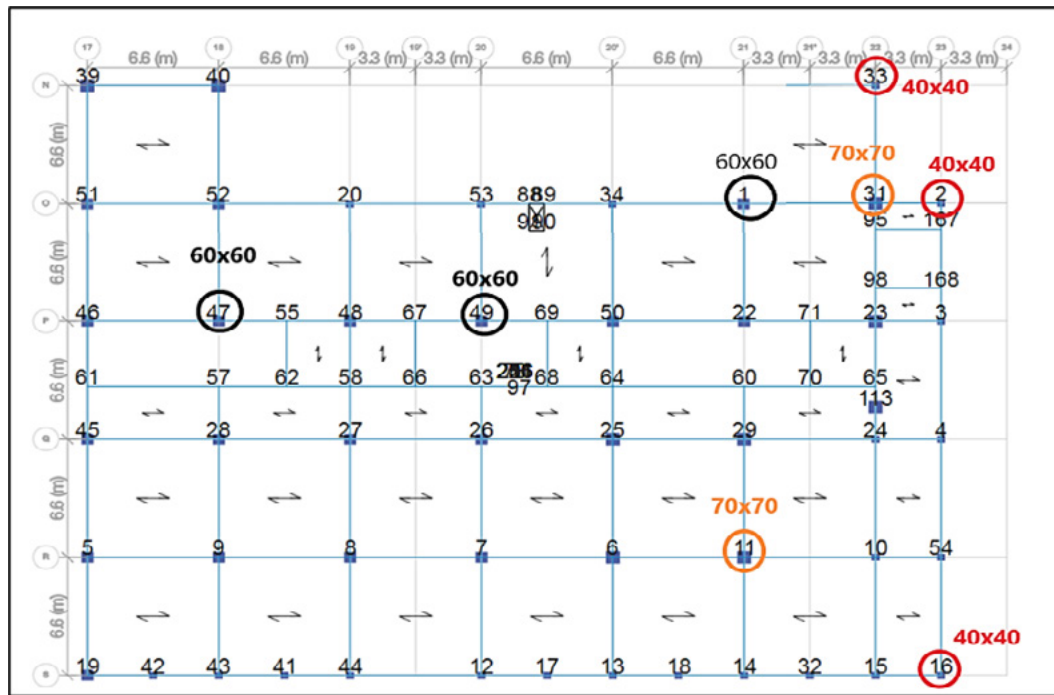


Figure 7. The Column that was subjected to the higher magnitude of internal forces & moments.

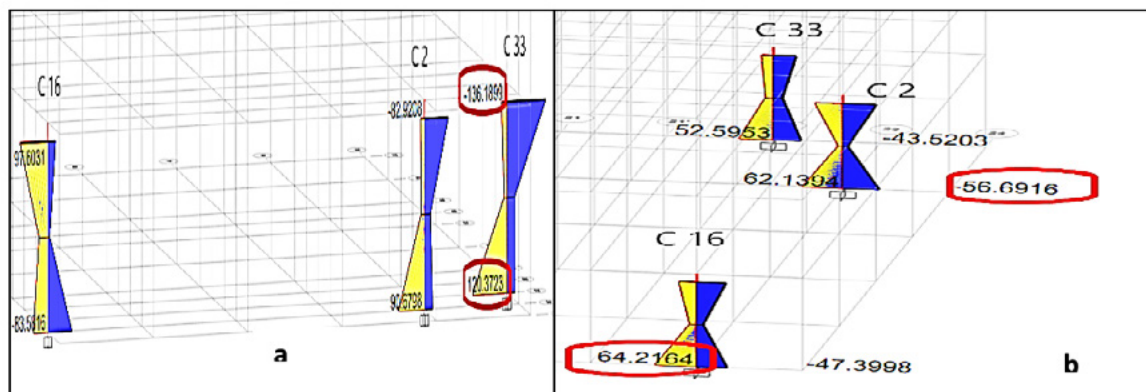


Figure 8. Corner Column 40x40 cm that was subjected to the highest magnitude of internal moments. (a) X-direction, (b) Y-direction.

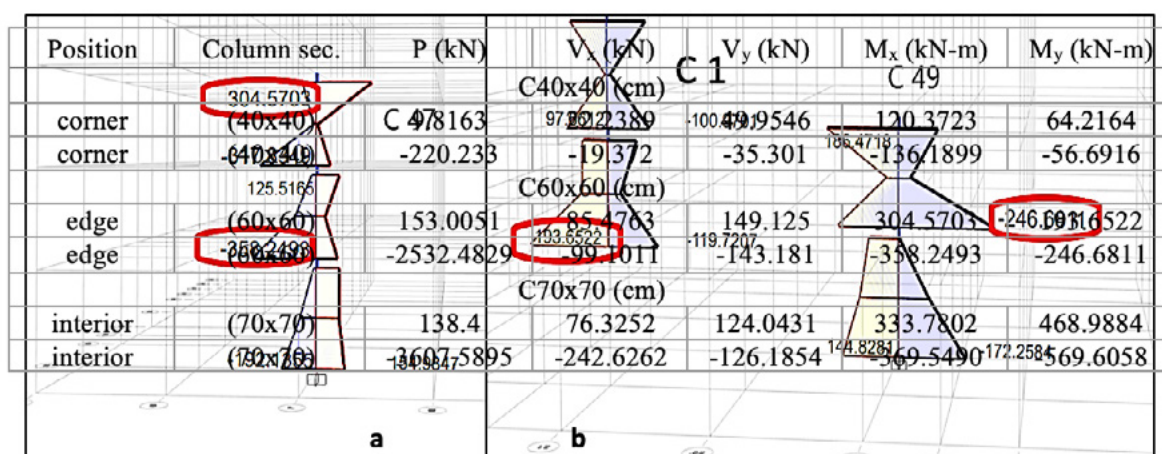


Figure 9. Edge Column 60x60 cm that was subjected to the highest magnitude of internal moments. (a) X-direction, (b) Y-direction.

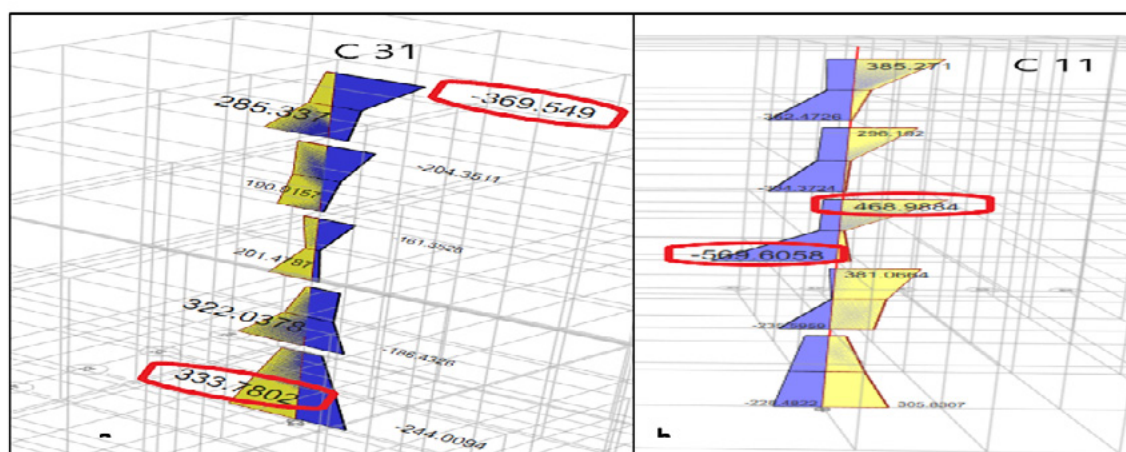


Figure 10. Interior Column 70x70 cm that was subjected to the highest magnitude of internal moments (a) X-direction, (b) Y-direction.

Table1. Analysis results of the building (Block-7) columns under the effect of all types of loadings including earthquake from ETABS software after filtering, sorting, and rearranging

| Position | Column sec. | P (kN) | V _x (kN) | V _y (kN) | M _x (kN-m) | M _y (kN-m) |
|-------------|-------------|------------|---------------------|---------------------|-----------------------|-----------------------|
| C40x40 (cm) | | | | | | |
| corner | (40x40) | 9.8163 | 22.2389 | 49.9546 | 120.3723 | 64.2164 |
| corner | (40x40) | -220.233 | -19.372 | -35.301 | -136.1899 | -56.6916 |
| C60x60 (cm) | | | | | | |
| edge | (60x60) | 153.0051 | 85.4763 | 149.125 | 304.5703 | 193.6522 |
| edge | (60x60) | -2532.4829 | -99.1011 | -143.181 | -358.2493 | -246.6811 |
| C70x70 (cm) | | | | | | |
| interior | (70x70) | 138.4 | 76.3252 | 124.0431 | 333.7802 | 468.9884 |
| interior | (70x70) | -3607.5895 | -242.6262 | -126.1854 | -369.5490 | -569.6058 |

The positive (+ve) values of axial forces (P) refer to tension forces due to seismic effect. However, their values were relatively small due to the weight of the entire building which tends to resist the tension forces. While the negative (-ve) values referred to compression forces due to both gravity load and seismic action. The shear forces sign referred to the direction of forces in the XY plane. While the Moments sign referred to whether the rotation will induce tension or compression forces on the column. The reason why there were (+ve) and (-ve) values were seismic action.

6. DESIGN RESULTS FROM PEIKKO DESIGNER

To Design the column connection (Choosing the right number and size of column shoes and anchor bolts to resist the Seismic loads) the analysis results of Table (1) were used in Peikko designer to check the chosen connection. Design results for one cross-section of each location (corner 40x40, edge 60x60, and interior 70x70) will be presented here. Peikko designer can provide a detailed report for the design process. When no more HPKM Column Shoes can fit in the cross-section to reach the required resistance BOLDA column shoes should be used instead.

6.1. CORNER COLUMN (40X40 CM)

Use 4 (HPKM column shoes - HPM anchor bolts) size 30 with 2 (HPKM column shoes - HPM anchor bolts) size 20 at the middle of the column lower face in the x-direction to satisfy the capacity requirements rather than using 6 (HPKM column shoes - HPM anchor bolts) size 30 for economic reasons and to provide more spacing for concrete as shown in figure (11). The design report indicates that the resistance of the connection was within the safe limits of the selected code provisions. And no failure in both the concrete or steel items (column shoes and anchor bolts). The green dot in the resistance diagram between the moments and the axial forces represents

the applied load of the column while the dashed line refers to the connection capacity. As shown in figure (12).

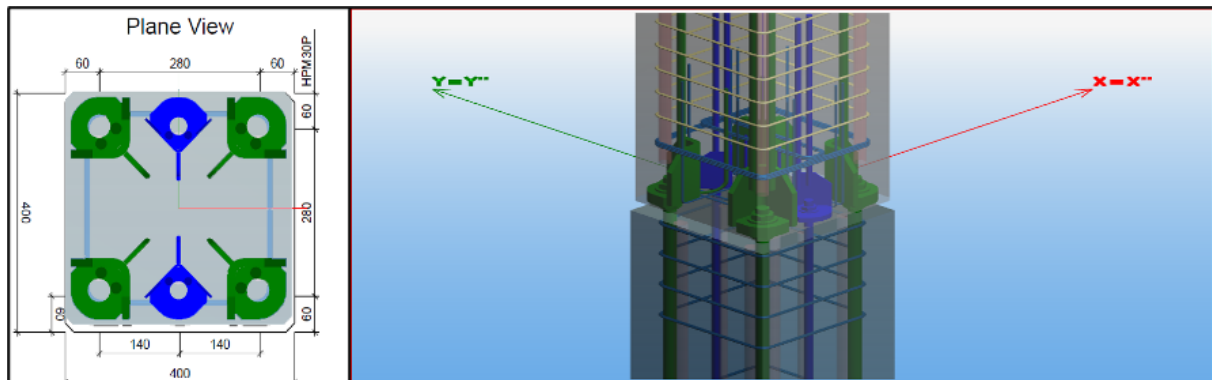


Figure 11. HPKM column shoe & HPM anchor bolts 1st configuration (4 size30 + 2 size20)

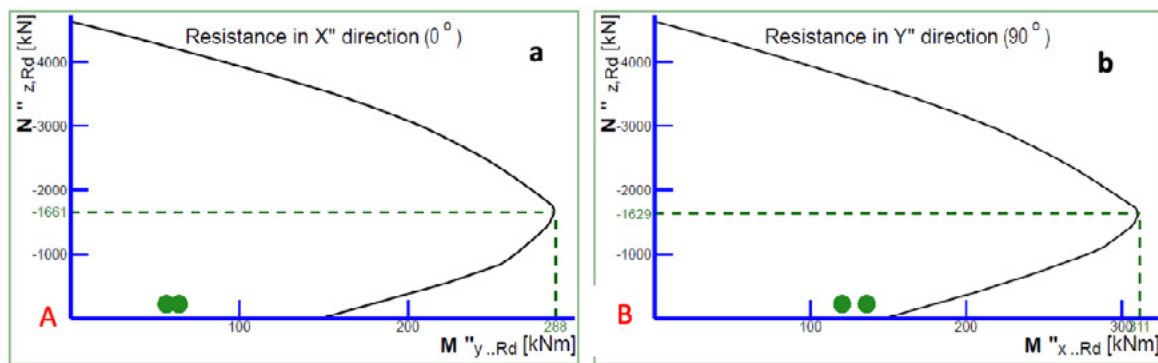


Figure 12. Resistance diagram of the connection, (a)- Resistance in the X direction, (b)- Resistance in the Y direction

6.2. EDGE COLUMN (60X60 CM)

Use 4 (BOLDA column shoe - PPM anchor bolts) size 39 as shown in figure (13). The design report indicates that the resistance of the connection was within the safe limits of the selected code provisions. And no failure in both the concrete or steel items (column shoes and anchor bolts). The green dot in the resistance diagram between the moments and the axial forces represents the applied load of the column while the dashed line refers to the connection capacity. As shown in figure (14).

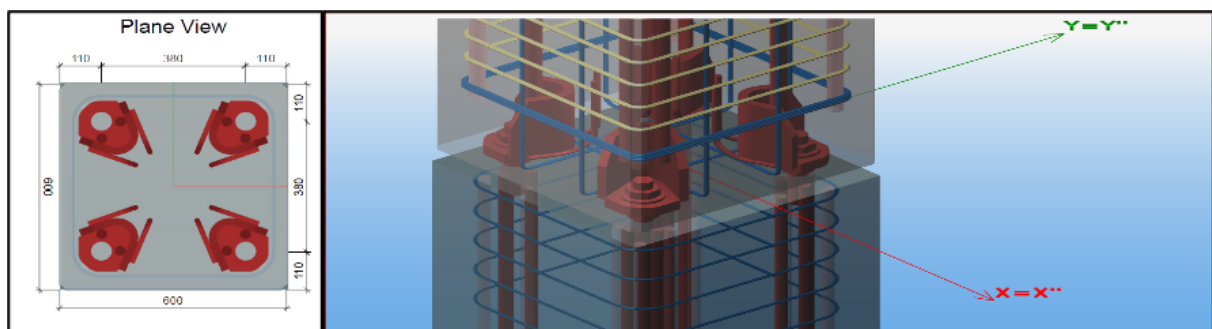


Figure 13. BOLDA column shoe & PPM anchor configuration (4 size39)

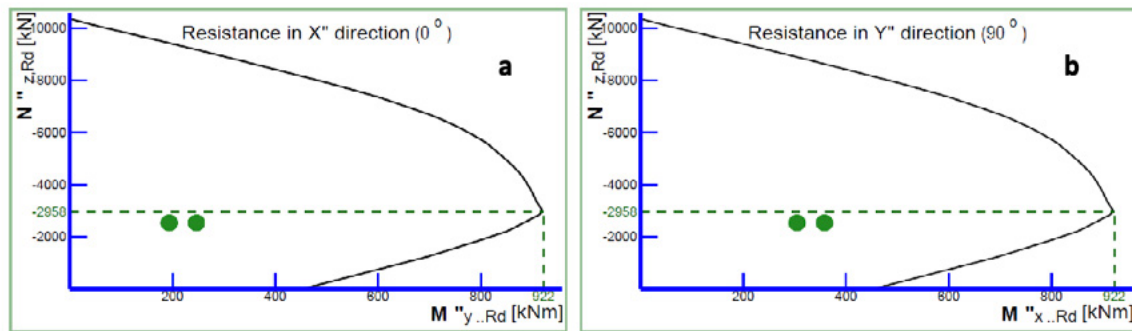


Figure 14. Resistance diagram of the connection. (a)- Resistance in the X direction, (b)- Resistance in the Y direction

6.3. CORNER COLUMN (70X70 CM)

Use 4 (PPM anchor bolts & BOLDA column shoe) size 45 as shown in figure (15). The design report indicates that the resistance of the connection was within the safe limits of the selected code provisions. And no failure in both the concrete or steel items (column shoes and anchor bolts). The green dot in the resistance diagram between the moments and the axial forces represents the applied load of the column while the dashed line refers to the connection capacity. As shown in figure (16).

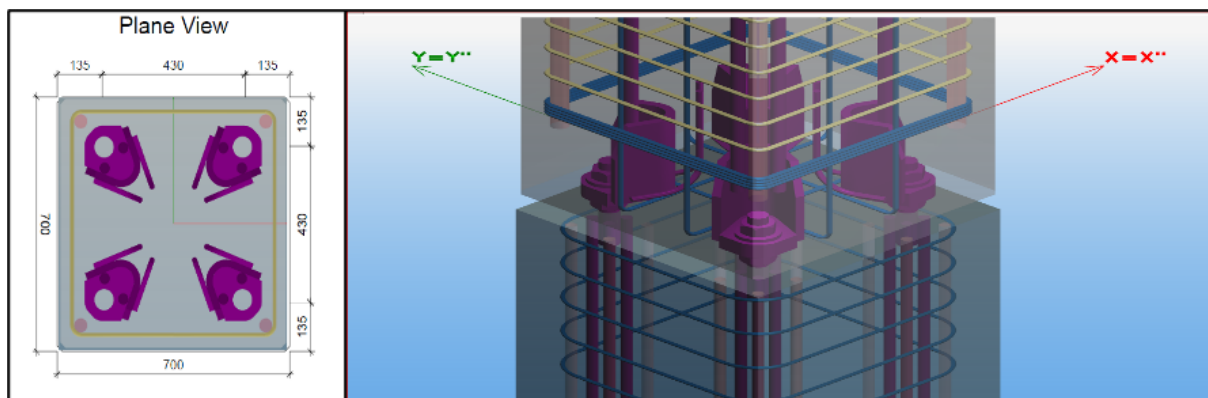


Figure 15. BOLDA column shoe & PPM anchor bolts (4 size45)

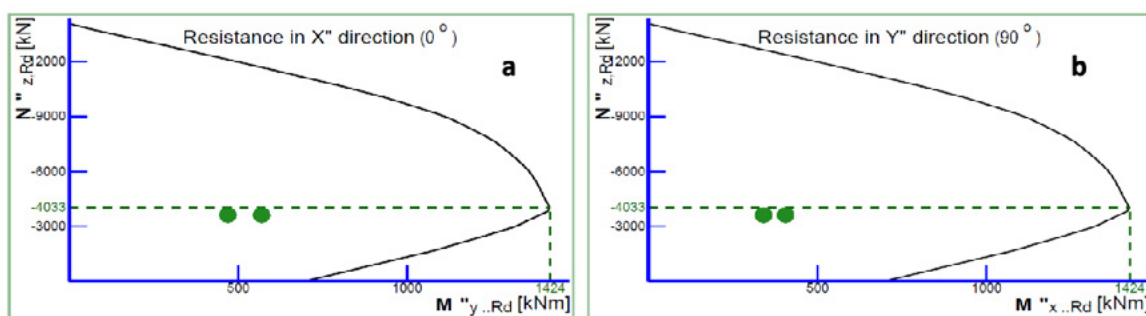


Figure 16. Resistance diagram of 4 - size - 45 configuration. (a)- Resistance in the X direction, (b)- Resistance in the Y direction

Or we can use 6 (PPM anchor bolts & BOLDA column shoes) size 39 as shown in figure (17). The design report indicates that the resistance of the connection was within the safe limits of the selected code provisions. And no failure in both the concrete or steel items (column shoes and anchor bolts). The green dot in the resistance diagram between the moments and the axial forces represents the applied load of the column while the dashed line refers to the connection capacity. As shown in figure (18). Whichever is more economical.

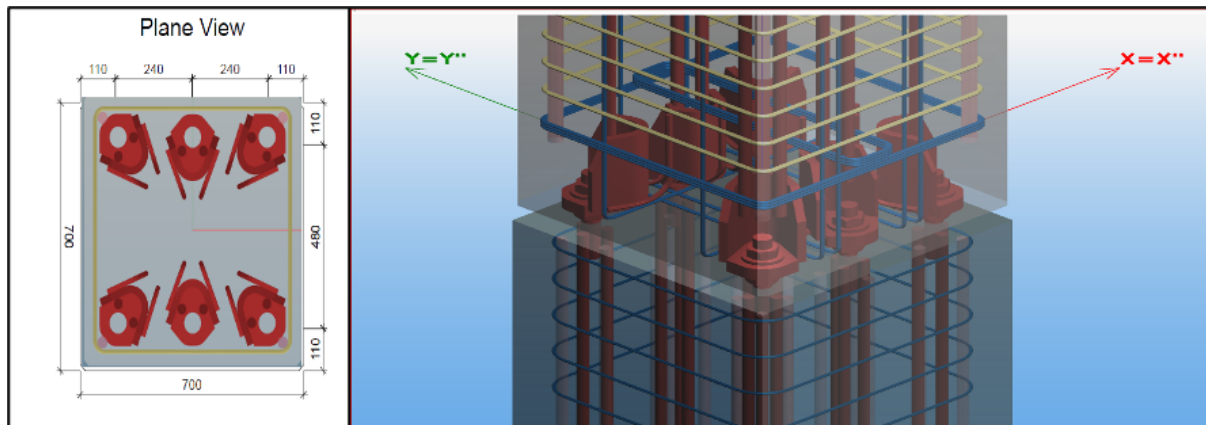


Figure 17. BOLDA column shoe & PPM anchor bolts 2nd configuration (6 size39)

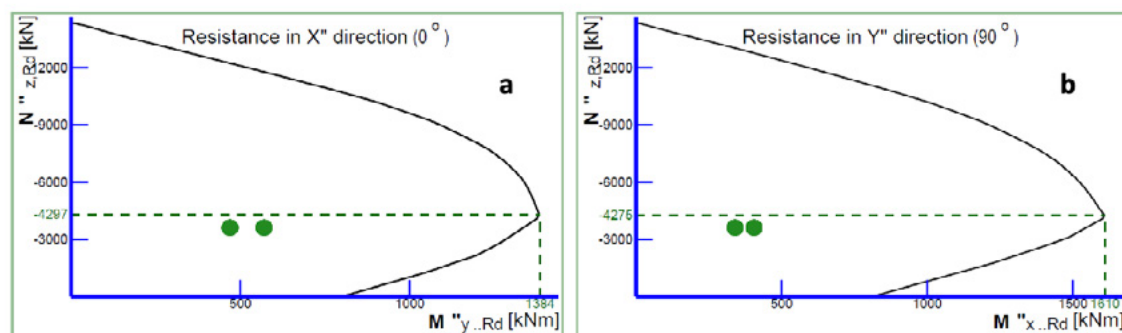


Figure 18. Resistance diagram of the 6 – size 39 configuration. (a)- Resistance in the X direction, (b)- Resistance in the Y direction

6.4. COMPARISON WITH MANUAL SELECTION:

The results from the Peikko designer for precast column-to-column connection were compared with those from a manual selection as follows. The manual selection was done by the capacity tables that the technical manuals of these items contain.

Table 2. Comparison with Manual Selection

| No | Column cross-section | Manual-selection | Peikko-selection |
|----|----------------------|--|---|
| 1 | Corner Column 40x40 | 4 (HPM anchor bolts & HPKM column shoes) size 39 | 4 (HPM anchor bolts & HPKM column shoes) size 30 with 2 (HPM anchor bolts & HPKM column shoes) size 20 at the |
| 2 | Edge Column 60x60 | 4 (PPM anchor bolts & BOLDA column shoe) size 45 | 4 (PPM anchor bolts & BOLDA column shoe) size 4 |
| 3 | Corner Column 70x70 | 4 (PPM anchor bolts & BOLDA column shoe) size 52 | 4 (PPM anchor bolts & BOLDA column shoe) size 45 or 6 (PPM anchor bolts & BOLDA column shoe) |

7. CONCLUSIONS

The column shoe connection system seems to have the same advantages as other connection types, but also very fewer disadvantages. The main drawback is that may be considered a relatively expensive solution, especially in certain markets. However, when choosing this solution, one should keep in mind that it saves materials since it ensures a much faster installation process than other solutions and a simple design process. These types of bolted connections (HPKM column shoes with HPM anchor bolts and BOLDS column shoes with PPM anchor bolts) do not require bracing due to the instantaneous mechanical fixing during assembly and a small amount of grouting is required for both types. A great advantage of Column shoes is considered a universal solution for connecting columns. Due to the existence of design tools, it is an easy, fast, and guaranteed way to create a design of this connection. This can lead to shorter duration and less cost in the project design work stage. In addition, it has good performance against seismic or dynamic loads, which gives additional security to the whole structure and was considered a shortage in all precast structures (not fulfilling the seismic requirements). It is necessary to choose a sufficiently strong column shoe and the appropriate anchor bolt in addition to a correct installation process to guarantee the performance of this type of connection system. From all of the above, the following can be concluded:

1. With the grouting mortar the shoe connection behavior is very similar to the behavior of the in-situ concrete column under seismic action.
2. The selection of column shoes and anchor bolts can be easily done with design tools such as Peikko Designer. However, it is very important to pay more attention when seismic, dynamic, or fatigue loads are considered.
3. Most of the stresses are concentrated on the shoe rods. Therefore, when using the column shoe system. this could provide a more economical use for the main reinforcement than a cast-in-place case
4. The column connection items chosen ensured that the principle of the strong column-weak beam is still valid since they provide a strong column connection.

5. The column connection items chosen can be used in demountable frames because they are removable.
6. More than one size of the same type of column shoe can be used at once in the same cross-section.

REFERENCES

- (1) Park, R. (1995). **A perspective on the seismic design of precast concrete structures in New Zealand**. *PCI journal*, 40(3).
- (2) Rodrigues, H., Arede, A., Varum, H., & Costa, A. (2012). **Behavior of RC building columns under cyclic loading: Experimental study**. *Journal of Earthquake and Tsunami*, 6(04), 1250026.
- (3) Ardiyati, P., Handika, N., & Purnomo, H. (2021). **Non-linear modelling of Ferro casting ductile shear key of L-Shaped concrete blocks with epoxy joint using Midas FEA**. *3c Tecnología: glosas de innovación aplicadas a la pyme*, 10(3), 101-117. <https://doi.org/10.17993/3ctecno/2021.v10n3e39.101-117>
- (4) Yu, J., Zhang, W., Tang, Z., Guo, X., & Pospíšil, S. (2020). **Seismic behavior of precast concrete beam-column joints with steel strand inserts under cyclic loading**. *Engineering Structures*, 216, 110766.
- (5) Camnasio E., Özer C. (2021). **Bolted Connections for Precast Structures in Seismic Areas Peikko Solutions and Design Examples**. Peikko White Paper, 1-12.
- (6) Rave-Arango, J. F., Blandón, C. A., Restrepo, J. I., & Carmona, F. (2018). **Seismic performance of precast concrete column-to-column lap-splice connections**. *Engineering structures*, 172, 687-699.
- (7) Abezgaus, S. (2020). **Investigation of column shoes (Doctoral dissertation, Vilniaus Gedimino technikos universitetas)**.
- (8) Camnasio E. (2017). **Bolted Column Connection for Seismic Applications**. *Peikko White Paper*, 1-4.
- (9) Paananen T. (2017). **Peikko is the first company to introduce seismic-proof precast bolted column connections**. <https://www.peikko.com/news/peikko-is-the-first-company-to-introduce-seismic-proof-precast-bolted-column-connections-2>
- (10) Peikko Group Technical Manual. (2019). **Bolted Column Connection (For Seismic Applications) Seismic-Proof Application of Bolted Connections**.
- (11) Kinnunen, J. (2017). **ETA tests and design of HPKM Column Shoe Connections**. *Procedia Engineering*, 172, 521-528.
- (12) Peikko Group Technical Manual. (2022). **HPM Rebar Anchor Bolt Easy and fast bolted connections European Technical Approval ETA-02/0006**.
- (13) Peikko Group Technical Manual. (2017). **HPKM Column Shoe Reliable Bolted Column Connections Designed according to ACI 318M-11**.
- (14) Peikko Group Technical Manual. (2021). **BOLDA Column Shoe Strong and Optimized Bolted Column Connections European Technical Assessment ETA-20/0529 Approved**.

- (15) Peikko Group Technical Manual. (2018). **PEC Column Shoe Heavy-duty Bolted Column Connections.**
- (16) Peikko Group Technical Manual. (2021). **PPM High-Strength Anchor Bolt Heavy-duty bolted connections.**
- (17) Kaseng, F., Condori, L. J. C., & Rodriguez, C. R. (2020). **Mix design with response surface methodology to optimize the flexural strength of concrete.** *3c Tecnología: glosas de innovación aplicadas a la pyme*, 9(3), 47-57. <https://doi.org/10.17993/3ctecno/2020.v9n3e35.47-57>

CONFLICT OF INTEREST

The authors declare that the research was conducted in the absence of any commercial or financial relationships that could be construed as a potential conflict of interest.

/04/

STUDY OF FINFET TRANSISTOR: CRITICAL AND LITERATURE REVIEW IN FINFET TRANSISTOR IN THE ACTIVE FILTER

Arsen Ahmed Mohammede

Engineering Faculty, Electrical Department, Kirkuk, Iraq

arsenahmed@uokirkuk.edu.iq

Zaidoon Khalaf Mahmood

University of Kirkuk, Iraq

Doç.Dr. Hüseyin Demirel

Engineering Faculty, Electrical Department, Karabuk, Türkiye



Reception: 28/10/2022 **Acceptance:** 25/12/2022 **Publication:** 18/02/2023

Suggested citation:

A.M., Arsen, K.M., Zaidoon and D. Hüseyin. (2023). **Study of finfet transistor: critical and literature review in finfet transistor in the active filter.** *3C TIC. Cuadernos de desarrollo aplicados a las TIC*, 12(1), 65-81. <https://doi.org/10.17993/3ctic.2023.121.65-81>

ABSTRACT

For several decades, the development of metal-oxide-semiconductor field-effect transistors have made available to us better circuit time and efficiency per function with each successive generation of CMOS technology. However, basic product and manufacturing technology limitations will make continuing transistor scaling difficult in the sub-32 nm zone. Field impact transistors with fins were developed. offered as a viable solution to the scalability difficulties. Fin field effect transistors can be made in the same way as regular CMOS transistors, allowing for a quick transition to production. The use of inserted-oxide FinFET technology was presented as a solution to continue transistor scaling. Due to gate fringing electric fields through the added oxide (SiO₂) layers, the electromagnetic integrity of an iFinFET is superior to that of a FinFET. We discovered that the proposed mobility model functions admirably and that the Joule effect mostly influences the drain current and the heat source. The major goal of this work is to compare the performance characteristics of combinational logic using CMOS and FinFET technology. The inverting gate is modelled in HSPICE simulation on a 32nm transistor size utilising CMOS and FinFET structures, and respective performances, such as energy consumed, are examined.

KEYWORDS

Approximation electronic conductivity, Metal-oxide-semiconductor field-effect transistors, Network for energy conversion, FinFET, Adder, Energy utilization, Simulation

PAPER INDEX

ABSTRACT

KEYWORDS

1. INTRODUCTION
2. WIRE SURVEY CIRCUITS
3. FINFET TECHNOLOGY
4. FINFET HAS UPSIDES OVER CLASSIC MATERIAL PADDOCK TRANSFORMER
 - 4.1. FINFETS CIRCUITS USED BY RESEARCHERS
5. INVESTIGATORS' MOSFETS DEVICES, METRICS, AND FACTS
6. OUTPUT WITH COMPUTATION
 - 6.1. FINFET BASED INVERTER
7. CONCLUSION

REFERENCES

1. INTRODUCTION

Larger quantities FinFET innovation is being employed for high-volume production of CMOS microchips in the sub-20 nm generation [1, 2]. A p-channel FinFET's output efficiency of the same fin height is exactly comparable even to an n-channel FinFET with same element size due to the 110 winglet crystalline phase and a higher level of deformation stimulated in the channel region by ingrained sio2 source/drain regions [1]. Though that is advantageous for applications that demand logic circuits, it reduces the write ability of a statically six mosfet recording cell with two individuals Mosfet carry FinFETs, and two lift FinFETs [3]. The insertion-oxide FinFET (iFinFET) technology has been presented as a solution to continue transistor scaling [4]. The atomic fidelity of an iFinFET is higher than that of a FinFET due additional gate surrounding electric fields created by the additional oxide sheets. The door field-effect semiconductor delivers improved electric purity at the cost of a greater intrinsic delay [4]. According to a slew of recent studies, triple gate (DG) gadgets are the best option. In comparison to planar double gate semiconductors, quasi-planar FinFET is the easiest to fabricate among the numerous types of DG devices.

Fin field effect transistors use an extremely thin undoped body to reduce SCEs by suppressing subsurface leakage channels. An undoped or lightly doped [6] body decreases V_t changes caused by Irregular dopant oscillations promote carrier concentration and lead to a higher on current.

The capacity of the gateway gate to control the prediction capability and current will flow in the inversion layer decreases as devices shrink in size, and undesired characteristics known as "relatively brief effects" begin frequently plague iron field-effect semiconductors. Scaling typical "bulk" titanium field-effect devices below 20nm looks to be impossible for a variety of reasons [5]. If the limitation could not be removed, Allen's law would come to end around a year.

The Voltage-Doping Transformation model is a basic tool that may reasonably be expected to convert the impacts of incorporating system variables including barrier height and depletion power [6,7] into design parameters. The following formulas can be generated from the concept in the case of the narrow effect and waste barrier reducing:

$$I_{D \cong I_{DSS}} \left[1 - \frac{V_{GS}}{V_{GS(off)}} \right]^2$$

where V_{GS} is the high voltage size of connexion with the built-in possibilities of the possible cause or drain, tox is the multi gate texture, is really the discharge and origin crossroad complexity, and tdep is the gate field absorption depth in the inversion layer, which is equitable to the complexity of the depletion region beneath the gate in noble metal field-effect transistors. The "Electrodynamic Integrity" factor is the name of the parameter. It's a measurement of how and why the draining's lines of force effect the stream zone [8], creating the relatively brief effect and fluid barrier lowering effects. It is dependent on the device design. The resistance value of an iron field-

effect diode with a particular gate length let can be computed by applying formulas based on the previous formulae.

$$I_D \cong I_{DSS} \left[1 - \frac{V_{GS}}{V_{GS(\text{off})}} \right]^2 = 40 \text{ mA} \left[1 - \frac{-2}{-6} \right]^2$$

where is the relationship? A lengthy device's duty ratio is V_{GS} . The "duty cycle roll-off" The drain current lowers as the size of the device falls, but it is a well relatively brief phenomenon. As indicated in any of these calculations, the overall impacts can be decreased by reducing the circuit length the multi - gate thicknesses. Symptoms can also be lowered by raising the intensity of doping and minimizing the depletion depth. However, due to the increased tunneling current associated with decreasing valve thicknesses, gate oxides can really be scaled beyond a certain point. Lower the depletion depth just under the [9] to the substrate as another method of mitigating short-channel effects. Shorter depletion zones and, as a result, lower parasitic capacitances are associated with a narrower depletion width. As a result, the leakage regime's sub-threshold slope improves. Reduced depletion width, on the other hand, correlates to reduced barrier impact on the canal, leading in a longer downstream section change on/off. When the gate's Electromagnetic wires from the emitter and collector effect channel area adjustment, short-channel effects occur.

Figure 1 depicts these field lines. In a macroscopic device, local equipotential lines flow over the depleting zone coupled with the contacts (Fig. 1). Their effects on the circuit can be reduced by increasing the sorption capacity in the inversion layer. Regrettably, in very embedded systems (1106 cm^{-3}) the pl intensity is now too strong for efficient transient conditions.

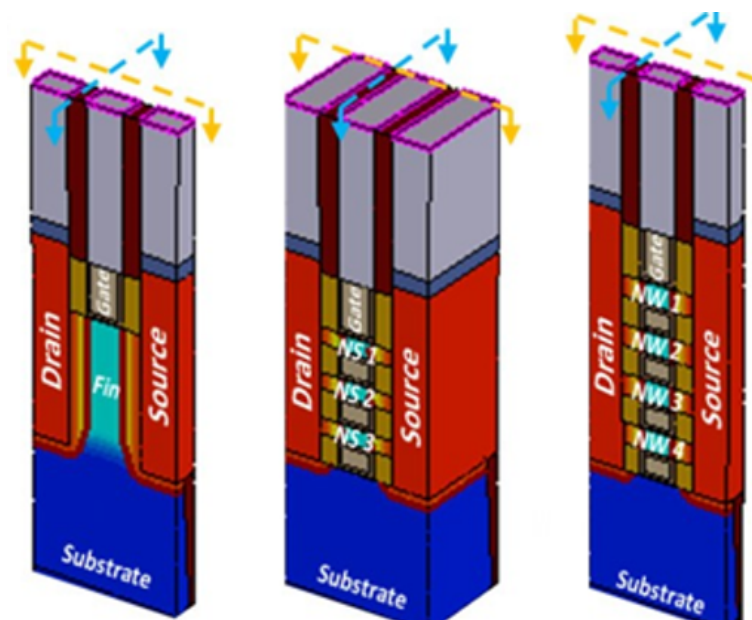


Figure 1. Metal-oxide-semiconductor paddock devices with two gates.

The Electro - static Ethics quotient of a bulk devices can be calculated using the Battery New methodology, which can really be described thus:

$$I_D \cong I_{DSS} \left[1 - \frac{V_{GS}}{V_{GS(\text{ff})}} \right]^2 = 40 \text{ mA} \left[1 - \frac{-5}{-6} \right]^2$$

Both valves of a double-gate mechanism are linked together. The electrical charge traces from the app's gate and source cease on the bottom positive terminal [10,11], preventing them from reaching the channel region Fig. 1. The only boundary layers that can encroach on the inversion layer and damage short-channel features are those that propagate through the si substrate itself [30]. The thickness of the silicon sheet can be lowered to decrease encroachment. The developing and developed field plus optimal circuit depths depth with each gate in a double-gate device are both equal to $t_{Si}/2$.

The Electrochemical Stability factor of that double device can be calculated using the Voltage-Doping Modeling approach, which can be expressed as

$$I_D = I_{DSS} \left[1 - \frac{-V_{GS}}{-V_{GS(Off)}} \right]^2$$

The facts in formula 1.8 leads to an essential conclusion: bulk semiconductors then when you've ran, they reach a maximum extent when they run out of energy. of 25-30 nm, while double arrangement is the only way to attain that all lengths.

Section 1 offered an overview of silver paddock circuits and FinFET [12-15] devices in Sections 2 and 3. FinFET's advantages over metal field-effect semiconductors and FinFET circuits are explored in Section 4. Important investigations and facts were reported in sections 5. Parameters and results used by investigators and the modeling results are reported in section 6. In Section 7 the conclusion of paper is given.

2. WIRE SURVEY CIRCUITS

Aside from Bipolar Junction Transistor, Metal-Oxide Semiconductor Field-Effect Transistors, or simply metal-oxide-semiconductor field-effect transistors [16], are another form of transistor (BJT). In 1960, Kahng and Atalla invented the very first metal-oxide-semiconductor field-effect transistors [17], which are more cost-effective than BJT a single crystal silicon chip with a huge transistor count Field-effect devices made on electrode materials have four terminals in the level of cash running seen among collector and emitter is determined by the power delivered to the inverting input. This semiconductor can be thought of as a switch to some extent. As between evaporator and the condenser, a conduction trench forms when the gate voltage applied is larger than the threshold voltage, electricity flows seen between two terminals [18-20].

If the gate voltage is less than the threshold voltage as shown in Fig. 2, no conducting channel will form, and the transistor will be deemed an open circuits. When strong reversal develops, the input impedance, The turnstile power is regulated in V_{out} .

Wire field-effect transistor come in a range of sizes. The n-type outflow, n-type supplier, and p-type framework make up an n-channel MOS or NMOS transistor.

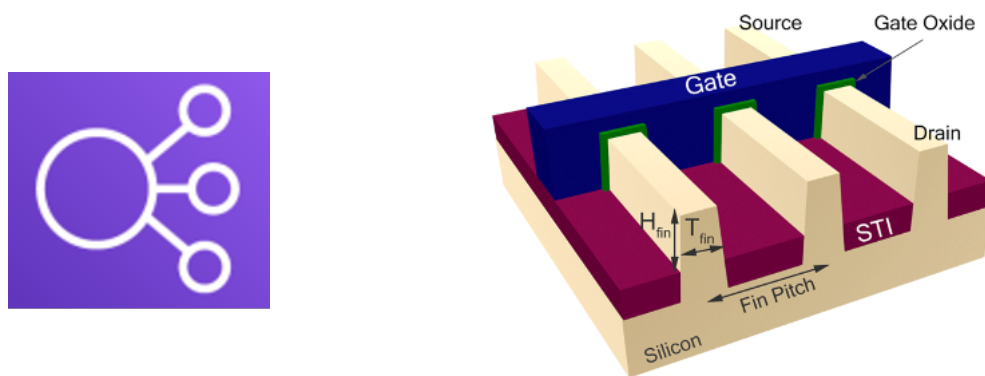


Figure 2. Brass ground diodes with N layers

PMOS, or p-channel, is another type of industrial practice area transistor with a c h base, p-type drains, and p-type sources.

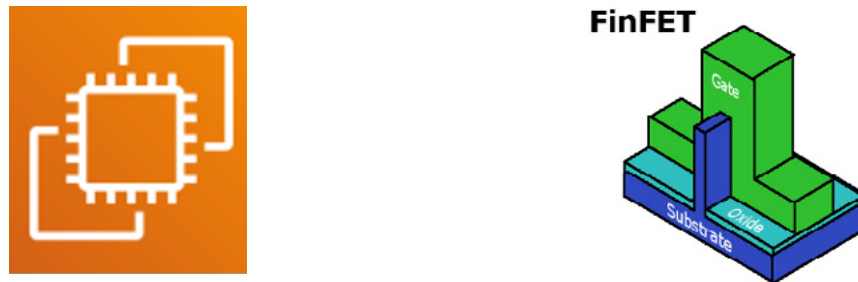


Figure 3. Brass ground diodes with P layers

Because both diodes are employed in a circuit, it is now referred to as Composite. Furthermore, as previously stated, each type of transistor can be categorized into two types: enrichment and degradation modes. Under the corrosion products that connects the drain and source in an enhancement mode transistor as in Fig 3, there is no channel. The source to drain wires would only be coupled [21-24] when a strong voltage was applied, forming of an e drift region behind corrosion products. The channel in a depletion mode transistor is readily available beneath the oxide layer. An electron result of adding or a doped impurity can serve as the channel. The presence of a channel allows the drain and source wires to be connected directly.

3. FINFET TECHNOLOGY

FinFET is an of pas' circuit with a "fin-like" form, the semiconductor channel is formed by the gated wrapping about over the fin. It's also characterized as a quasilinear route since the electricity passes transverse to the diamond surfaces and the channel is diagonal to the substrate line.

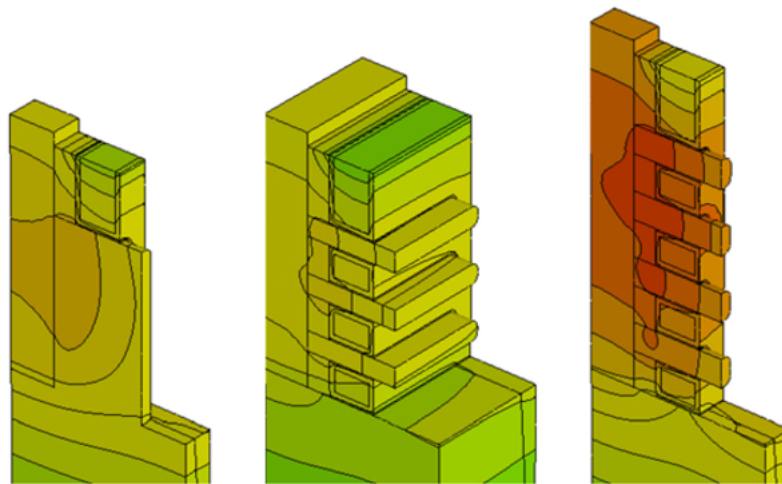


Figure 4. FinFET's Configuration

All of the devices in this paper were created using the Schematic capture Simulation Finite element analysis suite, which allows nano-scale mosfets to be appropriately modelled using particle corrected glide transport schema, rising 2D meshes, Vibrational energy facts, barrier tunneling modelling using the Hartree approximate solution, and peripheral cues mobility's [25]. As a result, the outcome of the analysis study combines two main subatomic particles consequences.

In a Fet, a conducts cell is formed by a super Si fin device, allowing electrons to flow from source to drain. The inputs come from a gate that arcs around the function held. As a result, even when the circuit is turned off, regulating electron flow avoids current leakage. The volume of charged particles and indeed the velocity at which these runs can sometimes increase, leading a single fin's secondary flow to break. This stops the electric current by interrupting the electron flow from the inlet to the outlet. The partial volume effect is enhanced by paddock semiconductors with many gates that have been built in line with each other. The quantity of fins controls the quantity of charged particles flowing from greater potential to reduced prospective. As a result, as the rate with which the particles flow is faster, the switch velocity is high. The main advantage of many fins is that they provide better switching speed over the conduction channel. Fig 4 shows a response; energy leaking is decreased. This produces a large quantity with on

operational voltage. Fin magnetic coil transistors are available in many different logic architectures. The amplifier can be constructed in the one of the following ways, dependent on the fin optoelectronic devices used:

- Impedance phase: In this method, both gates are shortened, resulting in greater drive force and best channel duration control.
- The impartial mode, wherein the on those gates are driven by different signals, may lower the quantity of semiconductors in the circuit.
- Reduced mode, where another the n-type is exposed to a voltage level. FinFETs while a voltage applied to p-type FinFETs. This changes the phone's input impedance, reducing leaky leakage power at the cost of increased latency.

4. FINFET HAS UPSIDES OVER CLASSIC MATERIAL PADDOCK TRANSFORMER

Following are the main advantages of Supervision over the channel is improved shown in Table 1:

- Narrow effects have been suppressed.
- Dynamic leakage current is reduced.
- Shifting speed is increased.
- Increased drain potential (More drive-current per footprint)
- Reduce the switching energy.
- Power usage is low.

Table 1. Advantages of FinFET over Traditional metal-oxide-semiconductor field-effect transistors

| Category | Portal FET | | Photovoltaic of Passivation Layer FET | | | |
|-----------|-------------------|------------------|---------------------------------------|--------------------|-----|-----|
| | Exhaustion Method | Shrinking Method | | Improvement Method | | |
| N-channel | OV | OFF | ON | OFF | ON | OFF |
| P-channel | OV | +ve | OV | +ve | -ve | oV |

4.1. FINFETS CIRCUITS USED BY RESEARCHERS

Chen et. al. [7] suggested a Nano-scale FinFET circuit sturdiness (reliability and scalability) analysis. One of the most difficult challenges for nanoscale VLSI designers is ensuring dependability. Circuit dependability is negatively impacted by smaller shapes, low output supply, and higher frequencies: these characteristics increase the incidence of soft errors, and larger degrees of device parameter variation transform the design challenge from predictable to probability. As a corollary, reducing fault rates and reducing variance influence has become extremely critical. The Transistors circuit was introduced as a beautiful dual FET version that enables for innovation growth in the future. [26] demonstrated that FinFET logic can be implemented at 160nm for the first time by demonstrating inverter-chain functionality. Joshi et al analyzed the behavior of FinFET SRAM and found that it has superior performance and lower power than standard planar PD-SOI. IBM was the first company to successfully convert an existing microprocessor design to 100 nm FinFET technology. [9] proved that an Inverter SRAM architecture had a 30% good disturbance margin than a traditional SRAM system than a bulk CMOS SRAM. The HSPICE tool from Synopsys is used to examine FinFET behavior. FinFET circuits are compared to include massive networks 21nm and 34nm technology in the studies. Over Bulk CMOS designs, FinFET-based designs reduce delay variation by an average of 83 percent and 43

percent for logic gates and memory cells, respectively. The findings suggest that FinFET circuits have superior reliability and scalability, as improved fault immunity and far less quality assured from process parameters are indications of this.. FinFET-based circuit design is found to be more robust than bulk CMOS-based circuit design [27]. With the upcoming FinFET technology, assessed a series of innovative memory circuit approaches. Storage durability, leaky energy usage, and cell area for individual FinFET Dynamic ram, cross level, and low-quality tied-gate In a 24angstrom FinFET innovation, Mosfets Memory cells were studied. When compared to the smaller quality paired gate FinFET dynamic ram seen in 41nm FinFET technology, the reading safety of the specifically relates dynamic unbiased FinFET SRAM cells improves by up to 92 percent. The task constructed multi-Vt FinFET SRAM cells reduce idle mode power losses and cell surface by up to 45X and 15.5 percent, however, when relative to a typical low cutoff bound FinFET SRAM cell scaled for equivalent read stability. [28] investigated the statistical reliability and power losses of FinFET SRAM cells with dynamic v_{th} tuning in the presence of process parameter variations. When the channel length of a single gate metal-oxide-semiconductor field-effect transistor is shortened and cascading improves quality by increasing impedance and gain while lowering series resistive loss. After executing the sequence to serial translation of the analogous circuit, cascading aids in the correction of given series, both lead to the concurrent resistive loss.

At the very least, the cascade device's overdrive voltage limits the output swing. In a cascade construction, the minimal power supply required is $4V_{sat}$, which is met in this design. The enhanced quality of the cascade arrangement causes the terminal voltage range limitation. The optimal current sources are replaced by device. The AI's total serial resistive loss is controlled by V_B . Variables in the AI's self-reflecting resonance can also be used to manipulate it. As a result, the proposed technique is the best fit for the situation.

We have really been able to prove basic gates and logic units based on such relatively basic yet foundational optimization of Cws levels via WFE, as addressed in our latest studies [29]. These static CMOS gates, as well as their logic features obtained by TCAD calculations, are briefly revisited in Fig.4. They show that designing absolutely lowest logic circuits in terms of device counts and area is doable by giving a maximum of two or three labor in the Super bowl and gate metals of FinFETs. These benefits translate to decreased energy consumption and 2 - 3 decades in these new gates, resulting in PDP statistics that are comparable to their typical FinFET counterparts, but being slower in switching due to the standalone gate configuration's lower electrical characteristics.

The researchers examined blended design as double FinFET technology using a voltammetric regulator oscillators as a research study. Due to increased Short-Channel Effects, using standard planar single gate metal-oxide-semiconductor field-effect transistors is becoming increasingly challenging (SCEs). Random dopant fluctuations (RDF) in the channel region of planar metal-oxide-semiconductor field-effect transistors, in addition to SCEs, are regarded to be the primary cause of baseline voltage variations between devices made on another wafer. The authors

introduce FinFETS technology, which reduces variability owing to Stochastic dopant variations thanks to a doped samples or weakly treated material and reduces carrier motion depreciation. Due to Sub - threshold fluctuations, the FinFET Controller has a 3.93 percent variability, but the Cmp VCO has 17.98 percentage variance, indicating that fin field effect transistors are so much more process time tolerant. The following are some of FinFET's key benefits: (1) Almost perfect sub-threshold slope (2) Inherent gate capacitance is low. (3) Junction capacitances that are smaller. (4) Increased resistance to SCEs. (5) A higher ratio of (ION/IOFF). (6) Shorted gate (SG) and independent gate (IG) choices provide circuit design freedom. Thermal issues will be investigated in future study, as fin field effect transistors suffer from self-heating[12]. [25] outlines an effort to investigate (1) A comparison of FinFET devices is viewed for analog signals schematic capture; (2) Output strain, impedance, Transparent gain, but instead transition rate are examined Gd FinFET operating including both significant invert and reduced load zones; (3) Statistical spatially varying evaluation for all the above FinFET specifications in both large and powerful distortion and low current regions of DG FinFET activity Vth fluctuation, small channel implications and manufacturing variances plague nanoscale bulk CMOS technology. FinFET technology is utilized to improve SCE and process variation immunity. If both selecting bits go low in the end state, the circuit presented in previous section gate can easily be adjusted to construct an Opcode function. While one of the pull-down mosfet connections is changed from S0 to S1, the circuit discharge its output anytime the inputs (A&B) go low, as shown in Fig.5. This only affects the situation where both select indicators are low, resulting in the Operands procedure in the last event. The two 4T circuits shown above show how the WFE may neatly effect the same network with modest input changes, boosting its performance and adding to the sequence set. Applying MTCMOS and SVL Leakage Reduction Technique, [30] designed and constructed a FinFET Based Inverter. Because of a substantial impact on a dedicated channel, which results in an actual growth in short channel effects and heightened attention to processing alterations, scaling of standard single-gate bulk metal-oxide-semiconductor field-effect transistors faces great hurdles in the nanoscale regime. When compared to standard CMOS, double-gate FinFETs have better SCEs performance [26,27,28], which encourages upgrading of tech. The article compares hang leaks, delay, and overall power usage of the logic gate in different settings of FinFET innovation. Simulations are carried out at 35angstroms using the Tcad tool. MTCMOS and Inefficiencies pragmatic circuit-level technologies are used to create a layout with provides speed and low power consumption and maximum volt devices. The fin field effect transistors based inverter using SVL approach has a 50-60% lower leakage power than a typical FinFETs based inverter and a 25-30% lower leakage power than a fin field effect transistors based inverter using MTCMOS technique, according to simulation results. Fin field effect transistors based inverters using the MTCMOS technology use 65-70 percent less power than standard inverters and 35-40 percent less power than fin field effect transistors based inverters using the SVL technique. The SVL technique is superior than the MTCMOS technique for minimizing leakage power and delay, however the SVL technique consumes more power than the

MTCMOS technique. This solution technique is found to be the greatest fit for the given problem [31].

5. INVESTIGATORS' MOSFETS DEVICES, METRICS, AND FACTS

In the meantime, each fin has its own breadth, thickness, and structure. Coating, etching, and other processes are used to create the fins. The gate, of naturally, has a number of properties, one of which is the turnstile length.

The foundation goes through numerous lithography processes, including provides a soft patterning, in one FinFET supply chain. The base is patterned with spacer-like features in this method. An etcher then carves vertical tunnels down into the floor between these structures, generating fins. The spaces are then replaced with oxide to use an epitaxial growth. After polishing the top section, the device is subjected to a recess etch stage. After that, a gate dioxide is applied, followed by the barrier development. Table 2 illustrates about devices, metric's and important facts. It is also clear from Fig. 5 that BJ is affected more in comparison to FET.

Table 2. Investigators' Mosfets Devices, Metrics, and Facts

| | Field Effect Transistor (FET) | Bipolar Junction Transistor (BJ) |
|----|--|--------------------------------------|
| 1 | Intensity at voltage level | Intensity at high frequency |
| 2 | Significant current gain | Less current gain |
| 3 | Highly Insertion loss | Less Insertion loss |
| 4 | Resistive output | Medium noise generation |
| 5 | Reduced noise generation | High noise generation |
| 6 | Fast switching time | Medium switching time |
| 7 | Electrical disruption is common | Robust |
| 8 | Some require an input to turn it "OFF" | Requires zero input to turn it "OFF" |
| 9 | Voltage controlled device | Current controlled device |
| 10 | Exhibits the properties of a Resistor | Cheap |
| 11 | More expensive than bipolar | Easy to bias |

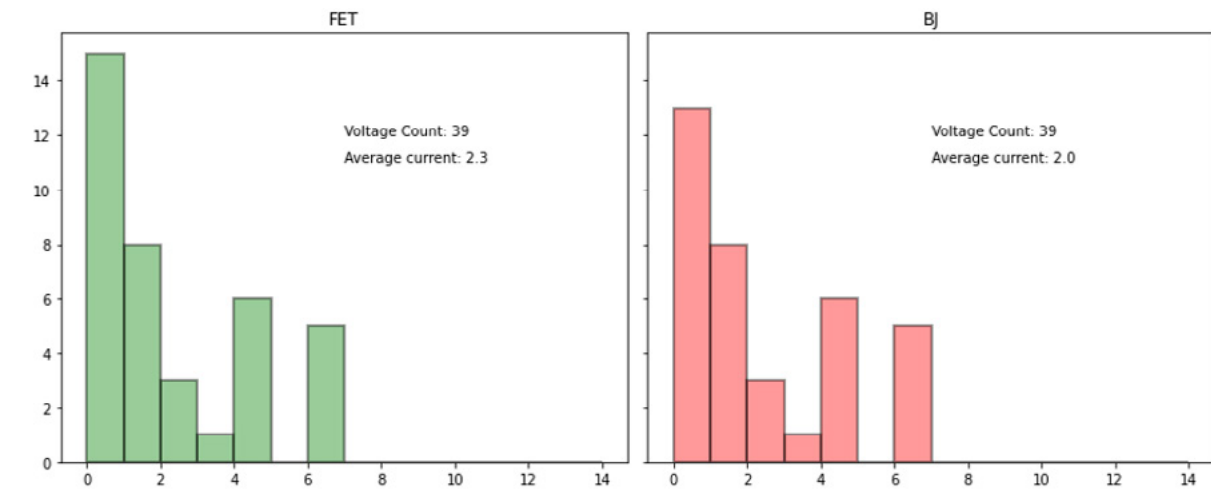


Figure 5. Comparison between FET and BJ on the basis of voltage count and average current

6. OUTPUT WITH COMPUTATION

In this part, we show simulated results for a 32nm FinFET-based converter and a 32nm wire field-effect transistor-based converter, as well as average output calculations for rectifier gates in various modes using HSPICE. Table 3 provides the parameters of FinFET and material field-effect devices that were employed in the Matlab simulation inverters simulation.

Table 3. Parameters used in Experimentation

| NPN | PNP | V_{CE} | $I_{C(max)}$ | P_d |
|---------|---------|----------|--------------|--------|
| BC547 | BC557 | 45v | 100 mA | 600 mW |
| BC447 | BC448 | 80v | 300 mA | 625 mW |
| 2 N3904 | 2 N3906 | 40v | 200 mA | 625 mW |
| 2 N2222 | 2 N2907 | 30v | 800 mA | 800 mW |
| BC140 | BC160 | 40v | 1.0 A | 800 mW |
| TIP29 | TIP30 | 100v | 1.0 A | 3 W |
| BD137 | BD138 | 60v | 1.5 A | 1.25 W |
| TIP3055 | TIP2955 | 60v | 15 A | 90 W |

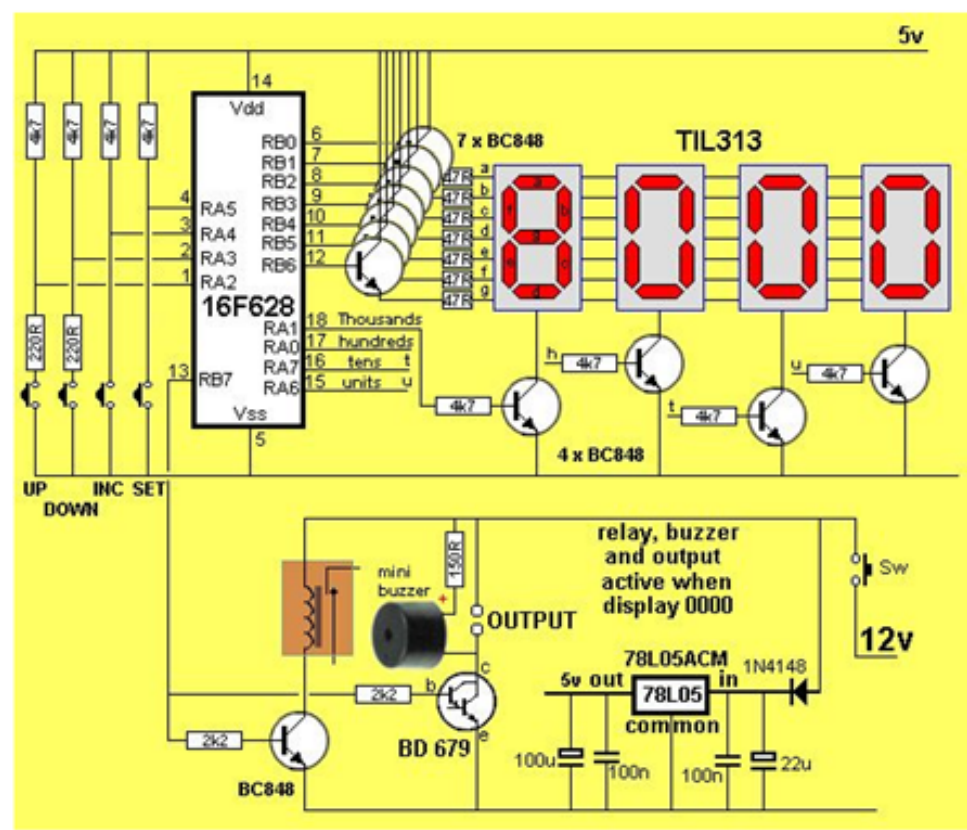


Figure 6. Steel field-effect devices are used in this bridge rectifier

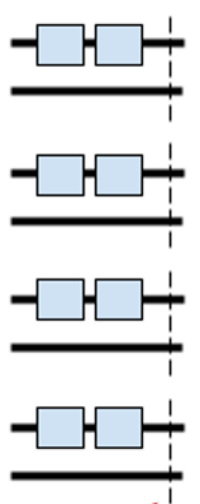


Figure 7. Found Using the following on Discharge Investigation in Metal-Oxide Vlsi Field-Effect Silicon chips

Figures 6 and 7 illustrate the circuit diagram and feedback characteristics of the inverter metal - oxide field-effect transistors. For the test, the supply voltages used were 0.6V for 52nm technologies. A pulse is often used to represent input input.

6.1. FINFET BASED INVERTER

Fig8, Fig9, Fig10, and Fig11 illustrate the circuit of an accelerator using FinFET architecture in the Quick (SG) mode, Reduced (LP) mode, Unbiased (IG) mode, and

Composite mode (IG/LP) modes, accordingly. H-SPIICE simulation was performed them in a 32-nm technology node. The inputs are applied to the inverter, they are propagated via the converter, and indeed the insight parameters of FinFET based reactors are presented in Fig12.

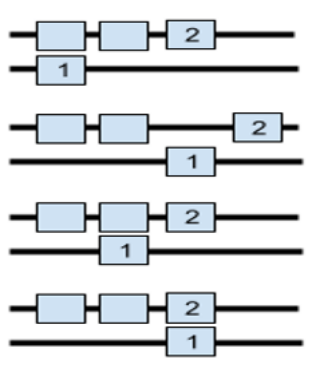


Figure 8. Amplifier Loop in Quick Mode

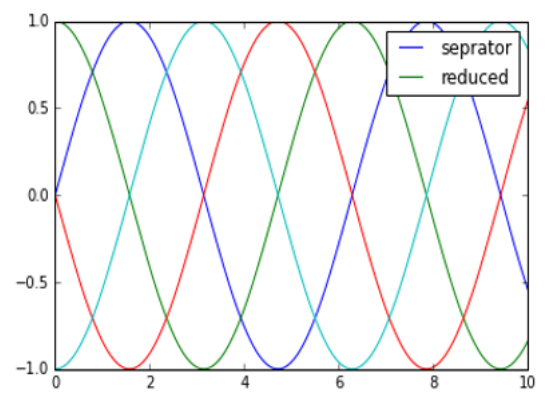


Figure 9. Separator Component Reduced Mode applying FinFET Technology

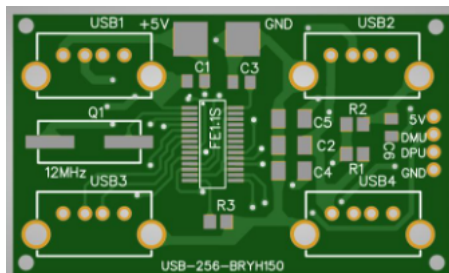


Figure 10. Concentrator with Unbiased Mode



Figure 11. Splitter Component in LP Configuration Circuit applying FinFET

Table 4. Total Energy Comparison

| S. No | Technology | Methodology | Average Power |
|-------|------------|----------------------|-----------------|
| 1 | 42nm | Massive Radial MOSFT | 2.4813E-04 watt |
| 2 | 42nm | FinFET(SG Mode) | 3.3988E-05 watt |
| 3 | 42nm | FinFET(LP Mode) | 7.1432E-05 watt |
| 4 | 42nm | FinFET(IG Mode) | 2.4868E-04 watt |
| 5 | 42nm | FinFET(IG/LP Mode) | 2.2091E-04 watt |

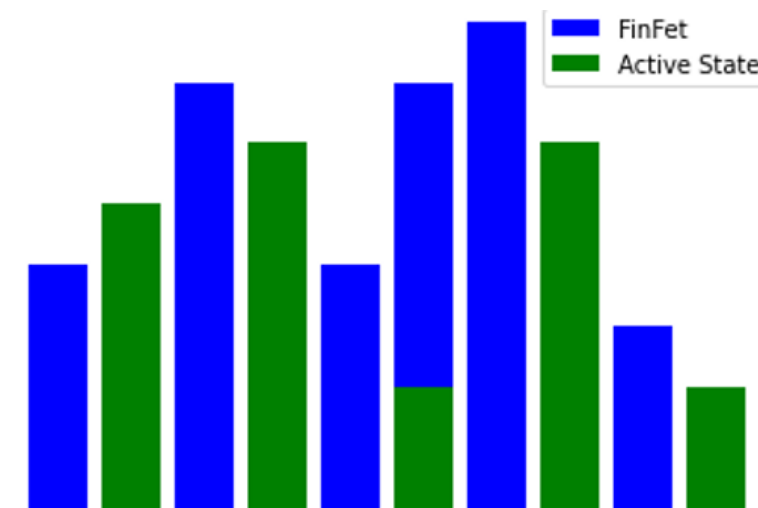


Figure 12. Pg, Lh, Gs, & Unmutated FinFET Converter Discharge Investigation

7. CONCLUSION

To brief, we constructed Au-gated pan FETs as well as Fin-FETs with variable fin-widths using Tio2 composite thin films including extreme density 2DEGs. We discover a mathematical gate impedance reduction in the constructed FinFETs when compared to planar FETs. We show that scaling down the Tio2 fin widths improves gate capacitance even further. We were able to increase the discharge capacity in the Mosfets with the shortest fin-widths when comparing to the produced planar FETs, resulting in a new dopant electron concentrations modulation. We expect that by narrowing the fin-widths even more, we will be able to modulate the 12 electron per unit cell 2DEG density completely. We believe that employing the FinFET technique to improve massive carrier content modulation in complicated oxides would eventually lead to reversible control of emerging phenomena in these materials. Using HSPICE, this research measured the effectiveness of an inverter generator to that of traditional silicon inverters brass field-effect transistors. The overall power consumption of the FinFET circuit is substantially lower than that of the planar iron field-effect passive components circuit.

REFERENCES

- (1) Kuhn, K. J. (2011, April). **CMOS scaling for the 22nm node and beyond: Device physics and technology**. In Proceedings of 2011 International Symposium on VLSI Technology, Systems and Applications (pp. 1-2). IEEE.
- (2) Roy, K., Mukhopadhyay, S., & Mahmoodi-Meimand, H. (2003). **Leakage current mechanisms and leakage reduction techniques in deep-submicrometer CMOS circuits**. *Proceedings of the IEEE*, 91(2), 305-327.
- (3) Frank, D. J., Dennard, R. H., Nowak, E., Solomon, P. M., Taur, Y., & Wong, H. S. P. (2001). **Device scaling limits of Si MOSFETs and their application dependencies**. *Proceedings of the IEEE*, 89(3), 259-288.
- (4) Hu, C. (1996). **Gate oxide scaling limits and projection**. In *International Electron Devices Meeting. Technical Digest* (pp. 319-322). IEEE.

- (5) Yeo, Y. C., King, T. J., & Hu, C. (2003). **MOSFET gate leakage modeling and selection guide for alternative gate dielectrics based on leakage considerations.** *IEEE Transactions on Electron Devices*, 50(4), 1027-1035.
- (6) Chen, J., Chan, T. Y., Chen, I. C., Ko, P. K., & Hu, C. (1987). Subbreakdown drain leakage current in MOSFET. *IEEE Electron Device Letters*, 8(11), 515-517.
- (7) Bandung, S. T. T., STT Bina Tunggal, and STT Dr Khez Muttaqien. (2013). International technology roadmap for semiconductors. <http://www.itrs.net>.
- (8) Skotnicki, T., Hutchby, J. A., King, T. J., Wong, H. S., & Boeuf, F. (2005). **The end of CMOS scaling: toward the introduction of new materials and structural changes to improve MOSFET performance.** *IEEE Circuits and Devices Magazine*, 21(1), 16-26.
- (9) Wong, H. S., Frank, D. J., & Solomon, P. M. (1998, December). **Device design considerations for double-gate, ground-plane, and single-gated ultra-thin SOI MOSFET's at the 25 nm channel length generation.** In *International Electron Devices Meeting 1998. Technical Digest (Cat. No. 98CH36217)* (pp. 407-410). IEEE.
- (10) Solomon, P. M., Guarini, K. W., Zhang, Y., Chan, K., Jones, E. C., Cohen, G. M., ... & Wong, H. S. (2003). **Two gates are better than one [double-gate MOSFET process].** *IEEE circuits and devices magazine*, 19(1), 48-62.
- (11) Suzuki, K., Tanaka, T., Tosaka, Y., Horie, H., & Arimoto, Y. (1993). **Scaling theory for double-gate SOI MOSFET's.** *IEEE Transactions on Electron Devices*, 40(12), 2326-2329.
- (12) Nowak, E. J., Aller, I., Ludwig, T., Kim, K., Joshi, R. V., Chuang, C. T., ... & Puri, R. (2004). **Turning silicon on its edge [double gate CMOS/FinFET technology].** *IEEE Circuits and Devices Magazine*, 20(1), 20-31.
- (13) Yan, R. H., Ourmazd, A., & Lee, K. F. (1992). **Scaling the Si MOSFET: From bulk to SOI to bulk.** *IEEE Transactions on Electron Devices*, 39(7), 1704-1710.
- (14) Choi, Y. K., Asano, K., Lindert, N., Subramanian, V., King, T. J., Bokor, J., & Hu, C. (1999, December). **Ultra-thin body SOI MOSFET for deep-sub-tenth micron era.** In *International Electron Devices Meeting 1999. Technical Digest (Cat. No. 99CH36318)* (pp. 919-921). IEEE.
- (15) Doris, B., Cheng, K., Khakifirooz, A., Liu, Q., & Vinet, M. (2013, April). **Device design considerations for next generation CMOS technology: Planar FDSOI and FinFET.** In *2013 International Symposium on VLSI Technology, Systems and Application (VLSI-TSA)* (pp. 1-2). IEEE.
- (16) Kong, B. S., Kim, S. S., & Jun, Y. H. (2001). **Conditional-capture flip-flop for statistical power reduction.** *IEEE Journal of Solid-State Circuits*, 36(8), 1263-1271.
- (17) Liu, B., & Wang, B. (2015). **Reconfiguration-based VLSI design for security.** *IEEE Journal on Emerging and Selected Topics in Circuits and Systems*, 5(1), 98-108.
- (18) Piguet, C. (2004). **Low-Power Electronics Design, Solid-State Circuits, New York.**
- (19) Ghai, D., Mohanty, S. P., & Thakral, G. (2013, August). **Comparative analysis of double gate FinFET configurations for analog circuit design.** In *2013*

- IEEE 56th International Midwest Symposium on Circuits and Systems (MWSCAS)* (pp. 809-812). IEEE.
- (20) Ghai, D., Mohanty, S. P., & Thakral, G. (2013, August). **Double gate FinFET based mixed-signal design: A VCO case study**. In *2013 IEEE 56th International Midwest Symposium on Circuits and Systems (MWSCAS)* (pp. 177-180). IEEE.
 - (21) Wang, F., Xie, Y., Bernstein, K., & Luo, Y. (2006, March). **Dependability analysis of nano-scale FinFET circuits**. In *IEEE Computer Society Annual Symposium on Emerging VLSI Technologies and Architectures (ISVLSI'06)* (pp. 6-pp). IEEE.
 - (22) Partovi, H., Burd, R., Salim, U., Weber, F., DiGregorio, L., & Draper, D. (1996, February). **Flow-through latch and edge-triggered flip-flop hybrid elements**. In *1996 IEEE International Solid-State Circuits Conference. Digest of Technical Papers, ISSCC* (pp. 138-139). IEEE.
 - (23) Mahmoodi-Meimand, H., & Roy, K. (2004, May). **Data-retention flip-flops for power-down applications**. In *2004 IEEE International Symposium on Circuits and Systems (IEEE Cat. No. 04CH37512)* (Vol. 2, pp. II-677). IEEE.
 - (24) Halter, J. P., & Najm, F. N. (1997, May). **A gate-level leakage power reduction method for ultra-low-power CMOS circuits**. In *Proceedings of CICC 97- Custom Integrated Circuits Conference* (pp. 475-478). IEEE.
 - (25) Tschanz, J., Narendra, S., Chen, Z., Borkar, S., Sachdev, M., & De, V. (2001, August). **Comparative delay and energy of single edge-triggered & dual edge-triggered pulsed flip-flops for high-performance microprocessors**. In *Proceedings of the 2001 international symposium on Low power electronics and design* (pp. 147-152).
 - (26) Moon, J. S., Athas, W. C., Beerel, P. A., & Draper, J. T. (2002, May). **Low-power sequential access memory design**. In *Proceedings of the IEEE 2002 Custom Integrated Circuits Conference (Cat. No. 02CH37285)* (pp. 111-114). IEEE.
 - (27) Rabaey, J. M., Chandrakasan, A. P., & Nikolic, B. (2002). **Digital integrated circuits (Vol. 2)**. Englewood Cliffs: Prentice hall.
 - (28) Hu, J., & Ye, L. (2010, August). **P-type complementary pass-transistor adiabatic logic circuits for active leakage reduction**. In *2010 Second Pacific-Asia Conference on Circuits, Communications and System* (Vol. 1, pp. 94-97). IEEE.
 - (29) Cao, K. M., Lee, W. C., Liu, W., Jin, X., Su, P., Fung, S. K. H., ... & Hu, C. (2000, December). **BSIM4 gate leakage model including source-drain partition**. In *International Electron Devices Meeting 2000. Technical Digest. IEDM (Cat. No. 00CH37138)* (pp. 815-818). IEEE.
 - (30) Benini, L., De Micheli, G., & Macii, E. (2001). **Designing low-power circuits: practical recipes**. *IEEE Circuits and Systems magazine*, 1(1), 6-25.
 - (31) Su, L., Zhang, W., Ye, L., Shi, X., & Hu, J. (2010, January). **An Investigation for Leakage Reduction of Dual Transmission Gate Adiabatic Logic Circuits with Power-Gating Schemes in Scaled CMOS Processes**. In *2010 International Conference on Innovative Computing and Communication and 2010 Asia-Pacific Conference on Information Technology and Ocean Engineering* (pp. 290-293). IEEE.

/05/

SYNTHESIS, IDENTIFICATION OF SOME NEW TETRAZOLINE, THIAZOLIDIN-4-ONE AND IMIDAZOLIDIN-4-ONE DERIVATIVES AND EVALUATION ANTICANCER OF THEIR MOLECULAR DOCKING AND ANTI-OXIDANT EXPERIMENTAL

Mohammed B. wathiq AL-tamimi

Department of Chemistry, College of Science, University of Baghdad,
Baghdad, Iraq

mohammed.baqer1205m@sc.uobaghdad.edu.iq

Suaad M. H. Al-Majidi

Department of Chemistry, College of Science, University of Baghdad,
Baghdad, Iraq



Reception: 25/10/2022 **Acceptance:** 26/12/2022 **Publication:** 21/02/2023

Suggested citation:

Mohammed B. wathiq AL-tamimi and Suaad M. H. Al-Majidi. (2023). **Synthesis, identification of some new tetrazoline, thiazolidin-4-one and imidazolidin-4-one derivatives and evaluation anticancer of their molecular docking and anti-oxidant experimental.** *3C TIC. Cuadernos de desarrollo aplicados a las TIC*, 12(1), 83-116. <https://doi.org/10.17993/3ctic.2023.121.83-116>

ABSTRACT

In this study, a new series of 1,3-dimethyl-6-(amino aceto hydrazine) pyrimidine-2,4-dione-6-yl with 4-substituted benzyldehyde, The compound (1-5) was synthesized in a single pot that cyclization by the addition of sodium azide, 2-mercapto acid & 2-amino acetic acid to produce five-membered heterocyclic rings includes: tetrazoline-1yl (6-10), thiazolidin-4-one (11-15) and imidazolidin-4-one (16-20) derivatives respectively. These compounds were characterized using spectral methods [FTIR and ¹HNMR, ¹³C-NMR for some of them] evaluations, measurements, and analyses of their physical qualities. Each molecule was evaluated for antioxidant activity in vitro to use the DPPH and phosphomolybdenum methods. When compared to the standard drug Ascorbic acid, (1-20) demonstrated promising antioxidant activity among the bioactive molecules synthesized. Furthermore, molecular docking against, substances showed superiority over the standard medication Exemestane in tests of the Aromatase enzyme.

KEYWORDS

Tetrazoline, Thiazolidin-4-one, Imidazolidin-4-one, molecular docking and Anti-oxidant

PAPER INDEX

ABSTRACT

KEYWORDS

1. INTRODUCTION

2. MATERIALS AND METHODS

2.1. SYNTHESIS OF 1,3-DIMETHYL-6- (AMINO ACETO HYDRAZIDE BENZYLIDENE)- PYRAMIDINE-2, 4-DIONE-6-YL.(1-5)[24, 25]

2.2. SYNTHESIS OF 1,3-DIMETHYL-6-AMINO ACETAMIDE[5-(4-SUBSTITUTED PHENYL)-2H-TETRAZOLINE-1-YL]-PYRAMIDINE-2,4-DIONE-6-YL.(6-10) [26, 27]

2.3. SYNTHESIS OF 1,3-DIMETHYL-6-AMINO ACETAMIDE[2-(4-SUBSTITUTED PHENYL)-THIAZOLIDIN-4-ONE-3-YL]- PYRAMIDINE-2,4-DIONE-6-YL.(11-15)[28]

2.4. SYNTHESIS OF 1,3-DIMETHYL-6-AMINO ACETAMIDE[2-(4-SUBSTITUTED PHENYL)-IMIDAZOLIDINE-4-ONE-3-YL]-PYRAMIDINE-2,4-DIONE-6-YL.(16-20)[29, 30]

2.5. ACTIVATION OF ANTIOXIDANT DEFENSES (DPPH RADICAL SCAVENGING ASSAY)[31, 32]

2.6. TOTAL ANTIOXIDANT CAPACITY[33]

2.7. IN SILICO STUDIES

2.7.1. PREPARATION OF THE LIGAND[2]

2.7.2. DETERMINING PROTEIN BINDING REGIONS

2.7.3. MOLECULAR DOCKING INVESTIGATION

3. RESULTS AND DISCUSSION

3.1. SCHEME-1 SYNTHESIS OF NEW TETRAZOLINE, THIAZOLIDIN-4-ONE, AND IMIDAZOLIDINE-4-ONE DERIVATIVES

3.2. DPPH SCAVENGING ACTIVITY

3.3. QUANTITATIVE MEASURE OF ANTIOXIDANT CAPACITY

3.4. DOCKING STUDIES

4. CONCLUSION

REFERENCES

1. INTRODUCTION

Uracil is an essential pyrimidine representative. It is one of the five nucleobases and a promising structure in many natural products [1]. Uracil derivatives are important intermediates in the purine synthesis. One of the four nucleobases that make up RNA, it is a pyrimidine derivative that occurs naturally. In RNA, uracil couples to adenine via two hydrogen bonds. DNA with thymine instead of uracil [2, 3].

Compounds containing a high nitrogen content constitute a distinct class of C-N heteroaromatic compounds [4]. The tetrazoline ring structure contains unsaturated bonds, which ensures good energy properties [5]. Due to its high nitrogen concentration, enthalpy of formation [6], and inclination toward lesser sensitivity, tetrazoline is commonly employed in the construction of high-energy density materials [7].

Thiazolidinone derivatives have a five-membered heterocyclic ring with one sulfur, one nitrogen, and three carbon atoms. Thiazolidinones are one of the most essential heterocyclic compounds [8], and their derivatives, which have a carbonyl group in the fourth position, are an integral part of many synthetic pharmaceuticals with diverse biological activities [9, 10].

4-Imidazolidinones are a class of nitrogen-rich saturated lactams with medicinal applications [11]. Imidazolidinone derivatives are currently of interest as organocatalysts in modern organic synthesis [12]. 4-Imidazolidinones are cyclic amides, whereas 2-Imidazolidinones are cyclic urea compounds. Illustrates imidazolidinone isomers [13]. The imidazolidin-2-one motif is frequently found in natural products^{1,2} as well as pharmaceutically interesting synthetic molecules [14].

As a result of their ease of synthesis, uracil derivatives are regarded as promising compounds in drug discovery. The pyrimidine core is an important pharmacophore moiety of biologically active natural and synthetic compounds that compete for the same binding sites [15]. The most common biological activities of uracil derivatives in the last years application: Antioxidant [2], Anti-inflammatory [16], Anticancer [17], Anti-leukemia [18], Antibacterial [19, 20], anti-tumour [21], anti-angiogenesis [22] and Anti-diabetic [23].

2. MATERIALS AND METHODS

The investigation relied on unpurified chemicals purchased from BDH, Fluka, Merck, and Sigma Aldrich. In addition, an Electro thermal melting point device was used to record the melting points, although no corrections were made. Using a SHIMAZU FTIR-8400 Fourier transform Infrared spectrophotometer, KBr discs were used to record the (4000-600) cm⁻¹ FTIR spectra of the produced compounds. Using a BRUKER 400MHz equipment, TMS was used as the internal standard, and DMSO-d₆ was used as the solvent in order to get ¹H- and ¹³C-NMR spectra in Iraq. The Adiwaniyah Technical Institute and the Al-Forat Alawsat University both employed Japanese Shimadzu 1900i spectrophotometers.

2.1. SYNTHESIS OF 1,3-DIMETHYL-6- (AMINO ACETO HYDRAZIDE BENZYLIDENE)- PYRAMIDINE-2, 4-DIONE-6-YL.(1-5)[24, 25]

A solution of (0.5 g, 0.022 mol.) 1,3-dimethyl-6-(amino aceto hydrazine) pyrimidine-2,4-dione-6-yl, (0.022 mol.) para substituted aromatic aldehydes in (10 mL) of ethanol absolute as a solvent were thoroughly mixed with glacial acetic acid as a catalytic three drops of, and the mixture was refluxed for (6-10) hours. The product was filtrated, water washed and recrystallized by ethanol Table-2 lists characteristics of compounds in terms of their physical properties (6-10) as well as FTIR spectral data.

2.2. SYNTHESIS OF 1,3-DIMETHYL-6-AMINO ACETAMIDE[5-(4-SUBSTITUTED PHENYL)-2H-TETRAZOLINE-1-YL]-PYRAMIDINE-2,4-DIONE-6-YL.(6-10) [26, 27]

Compounds (6-10) were obtained from reaction of an equimolar a combination of Schiff bases (1-5) (0.0009 mol.) in ethanol (10 mL). Sodium azide (0.05 g, 0.0009 mol.) dissolved in the same solvent was added and the solution was reflux for (18-20) hours. The product was filtrated, water washed and recrystallized by ethanol Table-2 lists some of the physical properties of compounds (6-10) as well as FTIR spectral data.

2.3. SYNTHESIS OF 1,3-DIMETHYL-6-AMINO ACETAMIDE[2-(4-SUBSTITUTED PHENYL)-THIAZOLIDIN-4-ONE-3-YL]-PYRAMIDINE-2,4-DIONE-6-YL.(11-15)[28]

Throughout this step, (0.0009 mol.) of compound (1-5) of Schiff bases and (0.06 mL, 0.0009 mol.) of 2-mercaptoacetic acid were added dropwise to THF (10 mL). After that, the reaction mixture was heated to reflux temperature (20-24). The mixture was filtered, washed, and purified further with ethanol to recrystallization. Table-3 contains a list of a variety of physical properties of compounds (11-15) as well as FTIR spectral data.

2.4. SYNTHESIS OF 1,3-DIMETHYL-6-AMINO ACETAMIDE[2-(4-SUBSTITUTED PHENYL)-IMIDAZOLIDINE-4-ONE-3-YL]-PYRAMIDINE-2,4-DIONE-6-YL.(16-20)[29, 30]

An equimolar amount of Schiff bases (1-5) is added to a mixture (0.0009 mol.) As a solvent, (10 mL) of ethanol was stirred in, with (0.25 g, 0.0009 mol.) 2-aminoacetic acid in the same solvent and the mixture solution was refluxed for (20-22) hours. The resulting mix was then result of filtering being reformed from acetone crystals after being allowed to cool to room temperature. Table-3 lists a variety of physical properties of compounds (16-20) as well as FTIR spectral data.

Table 1. the physical properties as well as the FTIR spectral data cm⁻¹ of the compounds that were produced (1-5).

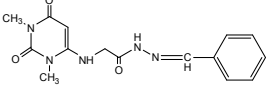
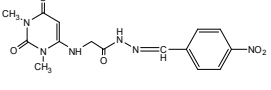
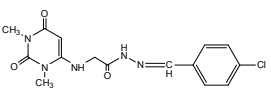
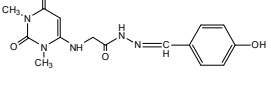
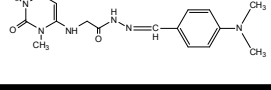
| Com. No. | Physical properties | | | | Major FTIR Absorptions cm ⁻¹ | | | | |
|----------|---|---------|---------|----------------|---|----------------------|--------------|------------------|---|
| | Compound Structure | m.p °C | Yield % | Color | νN-H | νC-H Arom. Aliph. | ν(C=O) | ν(C=N) ν(C=C) | Other bands |
| 1 |  | 88-90 | 80 | Pale gray | 3282 | 3053 2952 | 1701 1681 | 1639 1623 | - |
| 2 |  | 222-223 | 85 | yellow | 3294 | 3001 2975 | 1701 1683 | 1639 1620 | (NO ₂) Asym. 1521 Sym. 1346 |
| 3 |  | 187-188 | 77 | Light gray | 3294 | 3099 2997 2943 | 1731 1683 | 1649 1625 | (C-Cl) 1091 |
| 4 |  | 268-270 | 70 | Light yellow | 3301 | 3028 2960 | 1730 1656 | 1627 1619 | ν(-OH) 3433 |
| 5 |  | 250-251 | 85 | Reddish yellow | 3292 | 3060 2979 | 1699 1681 | 1639 1620 | - |

Table 2. the physical properties as well as the FTIR spectral data cm⁻¹ of the compounds that were produced (6-10).

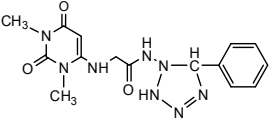
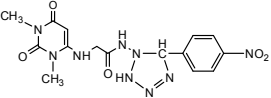
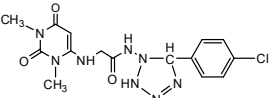
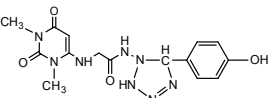
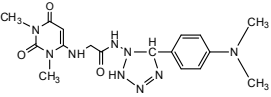
| Com. No. | Physical properties | | | | Major FTIR Absorptions cm ⁻¹ | | | | |
|----------|---|---------|---------|--------------|---|-------------------------|--------------|-------------|--|
| | Compound Structure | m.p °C | Yield % | Color | νN-H | νC-H Arom. Aliph. | ν(C=O)) | ν(C=C)) | Other bands |
| 6 |  | 359-360 | 80 | Deep yellow | 3275 | 3023 2923 | 1708 1668 | 1620 | ν(N=N) 1450 |
| 7 |  | 310-311 | 77 | Light yellow | 3290 | 3024 2975 | 1703 1687 | 1622 | ν(N=N) 1451 ν(NO ₂) Asym. 1523 Sym. 1346 |
| 8 |  | 359-360 | 75 | Yellow | 3286 | 3077 2997 | 1711 1685 | 1625 | ν(C-Cl) 1089 ν(N=N) 1453 |
| 9 |  | 260-261 | 84 | Deep gray | 3319 | 3028 2958 | 1710 1682 | 1608 | ν(N=N) 1448 ν(-OH) 3406 |
| 10 |  | 268-269 | 83 | Yellow | 3282 | 3050 2962 | 1703 1685 | 1625 | ν(N=N) 1457 |

Table 3. the physical properties as well as the FTIR spectral data cm⁻¹ of the compounds that were produced (11-15).

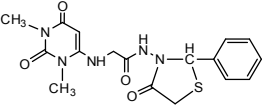
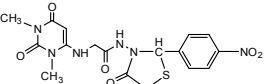
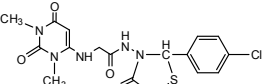
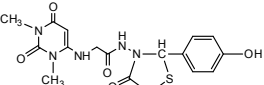
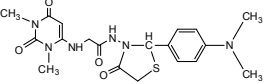
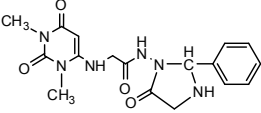
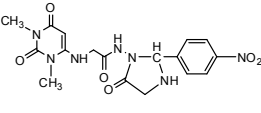
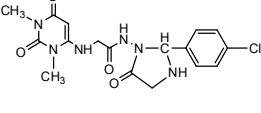
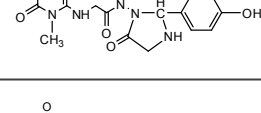
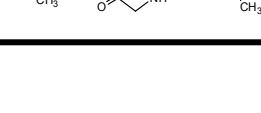
| Com. No. | Physical properties | | | | Major FTIR Absorptions cm ⁻¹ | | | | |
|----------|---|---------|---------|--------------|---|-------------------------|--------------|-------------|--|
| | Compound Structure | m.p °C | Yield % | Color | νN-H | νC-H Arom. Aliph. | ν(C=O)) | ν(C=C)) | Other bands |
| 11 |  | 270-271 | 81 | Light yellow | 3350 | 3060 2956 | 1699 1674 | 1620 | ν(C-S) 709 |
| 12 |  | 302-303 | 84 | Yellow | 3382 | 3002 2974 | 1701 1685 | 1618 | ν(NO2) Asym. 1521 Sym. 1346 ν(C-S) 702 |
| 13 |  | 212-213 | 78 | Deep gray | 3286 | 3097 2983 | 1733 1683 | 1625 | ν(C-Cl) 1091 ν(C-S) 700 |
| 14 |  | 230-231 | 79 | Deep gray | 3269 3253 | 3060 2974 | 1701 1683 | 1626 | ν(-OH) 3444 ν(C-S) 703 |
| 15 |  | 264-265 | 82 | Yellow | 3284 | 3060 2981 | 1701 1685 | 1628 | ν(C-S) 696 |

Table 4. the physical properties as well as the FTIR spectral data cm⁻¹ of the compounds that were produced (16-20).

| Com. No. | Physical properties | | | | Major FTIR Absorptions cm ⁻¹ | | | | |
|----------|---|---------|---------|----------------|---|-------------------|--------------|--------|--|
| | Compound Structure | m.p °C | Yield % | Color | νN-H | νC-H Arom. Aliph. | ν(C=O) | ν(C=C) | Other bands |
| 16 |  | 253-254 | 81 | Yellow | 3180 | 3051 2977 | 1731 1666 | 1612 | - |
| 17 |  | 270-271 | 86 | Deep yellow | 3211 | 3050 2958 | 1693 1672 | 1630 | ν(NO ₂) Asym. 1521 Sym. 1344 |
| 18 |  | 193-194 | 79 | Deep gray | 3180 | 3049 2995 | 1713 1662 | 1622 | ν(C-Cl) 1089 |
| 19 |  | 224-225 | 75 | Reddish yellow | 3180 | 3062 2987 | 1692 1662 | 1610 | ν(-OH) 3413 |
| 20 |  | 262-263 | 82 | Light yellow | 3298 | 3060 2977 | 1701 1683 | 1625 | - |

2.5. ACTIVATION OF ANTIOXIDANT DEFENSES (DPPH RADICAL SCAVENGING ASSAY)[31, 32]

Activation of antioxidant defenses was measured for a range of compounds (1-20) using a conventional method and the stable DPPH free radical. The compounds 1–20 were produced in DMSO at three different concentrations (50, 100, and 150) M, after which it was put to a methanol solution (of up to 2 milliliters) that contained 0.0002 grams per milliliter of DPPH radical. After 30 minutes of room temperature incubation, the spectrophotometer was utilized for determining the absorbance of the reaction mixture at a wavelength of 517 nm. Ascorbic acid served as a reference substance when evaluated at the same quantities as the other substances. To determine how effective ascorbic acid was in blocking DPPH radicals, we used the following formula: $((Ac-As)/Ac) * 100$. (percentage). An absorbance measurement taken from a control (Ac) and one taken from a sample (As) are shown.

2.6. TOTAL ANTIOXIDANT CAPACITY[33]

It was revealed that the compounds that were synthesized had a total antioxidant capability when they were tested with the phosphomolybdenum technique. An aliquot of a solution containing the chemical was combined with one milliliter of reagent that included 0.6 M sulphuric acid, 28 mM (Na₂HPO₄), and those were all included (4 mM ammonium molybdate). After that, a hermetic seal was placed on each of the test tubes that contained the reaction solution for the compounds that were being analyzed, and the tubes were then heated to 95 degrees Celsius for an hour and a half. After bringing the temperature in the room up to room temperature, a spectrophotometer was used to measure the absorbance of each tube at 695 nm in comparison to a blank. The total antioxidant activity is reported as the amount of ascorbic acid that is comparable to one gram. For the purpose of plotting the calibration curve, the following concentrations of ascorbic acid in DW were used: 10, 20, 30, 50, 70, 90, 120, 180, and 200 g/mL.

2.7. IN SILICO STUDIES

2.7.1. PREPARATION OF THE LIGAND[2]

Molecular docking research was carried out making use of the Small Drug Research Suites software package (Schrodinger 2020-3, LLC). The two-dimensional it was decided to draw out the structures of the freshly produced substances, and then Maestro 12.5 was used to turn those drawings into three-dimensional structures. Before docking, the ligands' pH levels were brought up to the physiological range using the OPLS2005 force field, and energy was reduced as much as possible. The Epik choice was made so that the ligand could remain in the correct protonation state throughout the process.

2.7.2. DETERMINING PROTEIN BINDING REGIONS

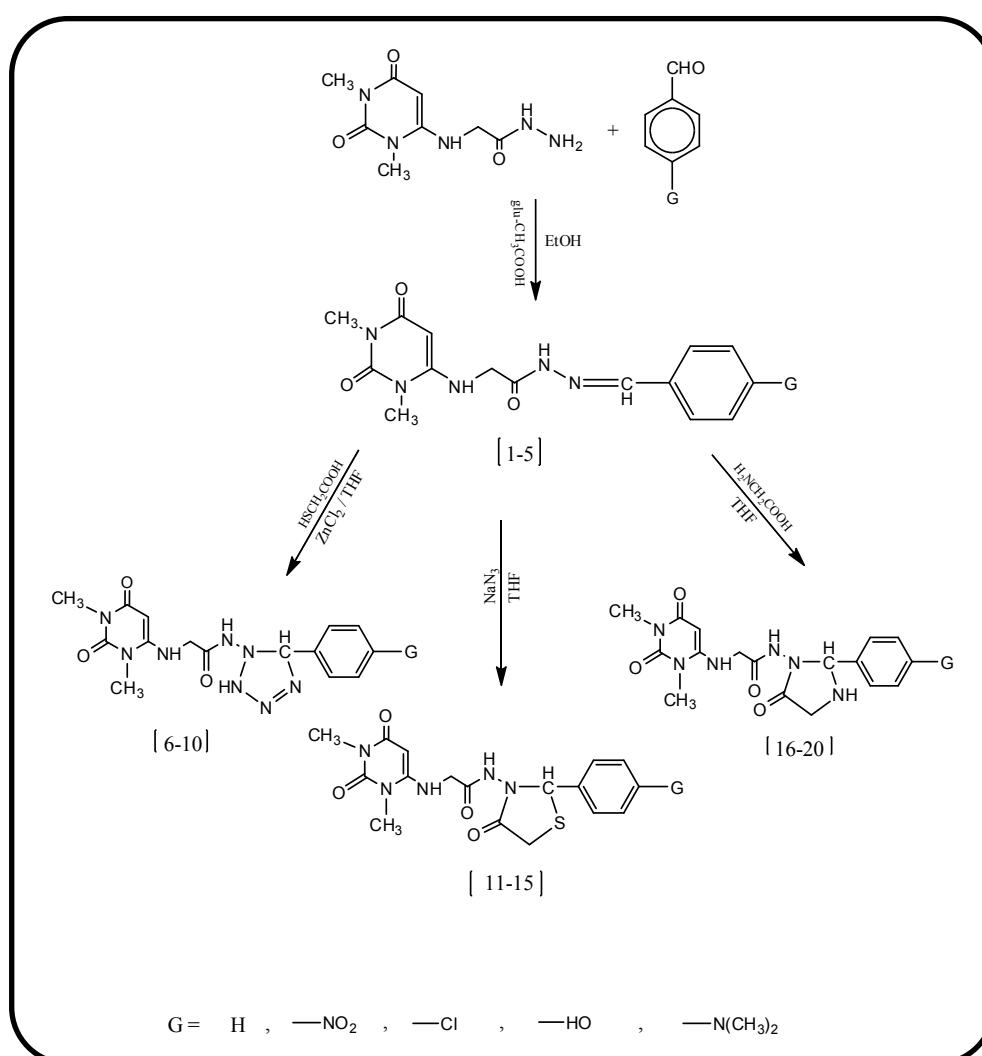
We uploaded the three-dimensional crystal structure of the aromatase enzyme, which may be found in the RCSB Protein Data Bank (PDB ID: 3S7S). The 3D crystal structure has been fixed and prepared with the help of Maestro 12.5's protein preparation wizard. To get started, the crystal structure had every last trace of water vapor evaporated. The protein's bond orders and charges were determined before any of the missing hydrogen atoms were added. Ionization of amino acids was achieved through adjustment of the physiological pH via the Propka software. As a final step, the OPLC force field was used for restrained minimization. For docking purposes, this streamlined structure worked wonderfully. After protein preparation, the best protein binding site was determined by identifying the highest-ranked potential protein binding sites utilizing the use of the maestro 12.5 glide grid program.

2.7.3. MOLECULAR DOCKING INVESTIGATION

Binding sites on the receptor were located using the glide grid tool, and the best ligand poses and binding energies were predicted using ligand docking. To begin, the Glide docking module in Maestro 12.5 was used to successfully dock all ligands onto their corresponding receptors. A grid box was generated using the receptor grid generation platform in the region of the co-crystallized ligand that is favored at the binding site. Maestro 12.5 was used to perform the simulations. Last but not least, the maestro 12.5 work space visualizer was used to visualize poses and analyze the resulting data.

3. RESULTS AND DISCUSSION

Synthesised Using Schiff bases of 1,3-dimethyl-6-(amino aceto hydrazine) pyrimidine-2,4-dione-6-yl and various reagents, a series of new heterocyclic rings with five members was synthesized Scheme-1. This series includes tetrazoline, thiazolidin-4-one and imidazolidine-4-one.



3.1. SCHEME-1 SYNTHESIS OF NEW TETRAZOLINE, THIAZOLIDIN-4-ONE, AND IMIDAZOLIDINE-4-ONE DERIVATIVES

The first step in the synthesis of new in Scheme-1 tetrazol, thiazolidin-4-one, and imidazolidine-4-one derivatives. A solution of 1,3-dimethyl-6-(amino aceto hydrazine) pyrimidine-2,4-dione-6-yl, para substituted aromatic aldehydes and absolute ethanol Its solvents were thoroughly combined with glacial acetic acid a catalytic three drops to synthesized Schiff bases derivatives (1-5) in table-1 showed the physical properties and FTIR of compound (1-5). The FTIR spectrum^[34] showing in figure(1-5) includes the presence of a $\nu(\text{N-H})$ at $(3301-3282) \text{ cm}^{-1}$; $\nu(\text{C-H})$ Arom. at $(3099-3001) \text{ cm}^{-1}$; $\nu(\text{C-H})$ Aliph. at $(2997-2941) \text{ cm}^{-1}$; $\nu(\text{C=O})$ at $(1731-1656) \text{ cm}^{-1}$, $\nu(\text{C=N})$ at $(1649-1627) \text{ cm}^{-1}$ and $\nu(\text{C=C})$ at $(1625-1619) \text{ cm}^{-1}$ of compound (1-5). The compound (2) have $\nu(\text{-NO}_2)$ in asym. at (1521 cm^{-1}) and sym. at (1346 cm^{-1}) ; compound (3) have $\nu(\text{C-Cl})$ at (1091 cm^{-1}) and compound (4) have $\nu(\text{-OH})$ at (3433 cm^{-1}) . Compound (5) $^1\text{H-NMR}$ spectra data, all signals shown in table-5 and showing in Figure 21 that contain signal 2.51 (s, 6H, $\text{N-(CH}_3)_2$); 2.96 (s, 3H, N-CH_3); 2.99 (s, 3H, $\text{O}=\text{N}(\text{CH}_3)=\text{O}$); 3.4 (s, 1H, NH); 3.51 (s, 2H, CH_2); 3.57 (s, 1H, $=\text{CH}$); 6.75 (s, 1H, N=C-H); 7.63-8.49 (m, 4H, Ar-H); 9.66 (s, 1H, HN-N). Table-6 shows the $^{13}\text{C-NMR}$ spectrum data of this compound (5) and showing in Figure 22.

Synthesised compounds (6-10) by cyclization compound (1-5) through sodium azide in ethanol as solvent as showing in scheme-1. In table-2 showed the physical properties and FTIR of compound (6-10). The FTIR spectrum of tetrazoline derivatives showing in figure(6-10) includes the presence of a $\nu(\text{N-H})$ at $(3319-3275) \text{ cm}^{-1}$; $\nu(\text{C-H})$ Arom. at $(3077-3023) \text{ cm}^{-1}$; $\nu(\text{C-H})$ Aliph. at $(2997-2923) \text{ cm}^{-1}$; $\nu(\text{C=O})$ at $(1711-1668) \text{ cm}^{-1}$, $\nu(\text{C=C})$ at $(1625-1608) \text{ cm}^{-1}$ and $\nu(\text{N=N})$ at $(1457-1448) \text{ cm}^{-1}$ of compound (6-10). The compound (7) have $\nu(\text{-NO}_2)$ in asym. at (1523 cm^{-1}) and sym. at (1346 cm^{-1}) ; compound (8) have $\nu(\text{C-Cl})$ at (1089 cm^{-1}) and compound (10) have $\nu(\text{-OH})$ at (3406 cm^{-1}) . Compound (7) $^1\text{H-NMR}$ spectra data, all signals shown in table-5 and showing in Figure 23 that contain signal at 2.5 (s, 3H, N-CH_3); 2.5 (s, 3H, $\text{O}=\text{N}(\text{CH}_3)=\text{O}$); 3.45 (s, 2H, CH_2); 3.46 (s, 1H, NH); 3.56 (s, 1H, N-CH tetrazoline ring); 3.62 (s, 1H, $=\text{CH}$); 4.9 (s, 1H, N-NH-N); 7.5-8.3 (m, 4H, Ar-H); 9.5 (s, 1H, HN-N).

Compounds (11-15) were synthesized by cyclizing compounds (1-5) through 2-mercaptoacetic in THF as the solvent, as in Scheme-1. In table-3 showed the physical properties and FTIR of compound (11-15). The FTIR spectrum of Thiazolidin-4-one derivatives showing in figure(11-15) includes the presence of a $\nu(\text{N-H})$ at $(3350-3253) \text{ cm}^{-1}$; $\nu(\text{C-H})$ Arom. at $(3097-3002) \text{ cm}^{-1}$; $\nu(\text{C-H})$ Aliph. at $(2983-2956) \text{ cm}^{-1}$; $\nu(\text{C=O})$ at $(1733-1683) \text{ cm}^{-1}$, $\nu(\text{C=C})$ at $(1628-1618) \text{ cm}^{-1}$ and $\nu(\text{C-S})$ at $(709-696) \text{ cm}^{-1}$ of compound (11-15). The compound (12) have $\nu(\text{-NO}_2)$ in asym.

at (1521 cm^{-1}) and sym. at (1346 cm^{-1}); compound (13) have $\nu(\text{C-Cl})$ at (1091 cm^{-1}) and compound (14) have $\nu(\text{-OH})$ at (3444 cm^{-1}). Compound (13) $^1\text{H-NMR}$ spectra data, all signals shown in table-5 and showing in Figure 24 that contain signal 2.5 (s, 3H, N-CH₃); 2.5 (s, 3H, $\text{O}=\text{N}(\text{CH}_3)=\text{O}$); 3.58 (s, 2H, CH₂); 3.83 (s, 2H, S-CH₂); 3.98 (s, 1H, NH); 4.1 (s, 1H, N-CH thiazolidinone ring); 4.2 (s, 1H, =CH); 7.5-8.3 (m, 4H, Ar-H); 8.7 (s, 1H, HN-N). Table-6 shows the $^{13}\text{C-NMR}$ spectrum data of this compound (13) and showing in Figure 25.

Synthesised compound (16-20) by cyclization compound (1-5) through glycine in ethanol as solvent as in scheme-1. In table-4 showed the physical properties and FTIR of compound (16-20). The FTIR spectrum of imidazolidine-4-one derivatives showing in figure(16-20) includes the presence of a $\nu(\text{N-H})$ at (3298-3180) cm^{-1} ; $\nu(\text{C-H})$ Arom. at (3062-3049) cm^{-1} ; $\nu(\text{C-H})$ Aliph. at (2995-2958) cm^{-1} ; $\nu(\text{C=O})$ at (1731-1662) cm^{-1} and $\nu(\text{C=C})$ at (1630-1610) cm^{-1} of compound (16-20). The compound (17) have $\nu(\text{-NO}_2)$ in asym. at (1521 cm^{-1}) and sym. at (1344 cm^{-1}); compound (18) have $\nu(\text{C-Cl})$ at (1089 cm^{-1}) and compound (19) have $\nu(\text{-OH})$ at (3413 cm^{-1}). Compound (16) $^1\text{H-NMR}$ spectra data, all signals shown in table-5 and showing in Figure 26 that contain signal 2.5 (s, 3H, N-CH₃); 2.5 (s, 3H, $\text{O}=\text{N}(\text{CH}_3)=\text{O}$); 3.17 (s, 2H, CH₂); 3.17 (s, 2H, CH₂-NH); 3.38 (s, 1H, NH); 3.57 (s, 1H, N-CH imidazolidinone ring); 3.59 (s, 2H, N-CH₂); 3.64 (s, 1H, =CH); 7.5-8.3 (m, 4H, Ar-H); 8.7 (s, 1H, HN-N).

Table 5. ¹H-NMR of compound (5, 7, 13 and 16)

| No. | Compound structure | ¹ H-NMR spectral data (δppm) |
|-----|--------------------|--|
| 5 | | 2.51 (s, 6H, N-(CH ₃) ₂); 2.96 (s, 3H, N-CH ₃); 2.99 (s, 3H, O=N(CH ₃)=O); 3.4 (s, 1H, NH); 3.51 (s, 2H, CH ₂); 3.57 (s, 1H, =CH); 6.75 (s, 1H, N=C-H); 7.63-8.49 (m, 4H, Ar-H); 9.66 (s, 1H, HN-N) |
| 7 | | 2.5 (s, 3H, N-CH ₃); 2.5 (s, 3H, O=N(CH ₃)=O); 3.45 (s, 2H, CH ₂); 3.46 (s, 1H, NH); 3.56 (s, 1H, N-CH tetrazoline ring); 3.62 (s, 1H, =CH); 4.9 (s, 1H, N-NH-N); 7.6-8.4 (m, 4H, Ar-H); 9.5 (s, 1H, HN-N) |
| 13 | | 2.5 (s, 3H, N-CH ₃); 2.5 (s, 3H, O=N(CH ₃)=O); 3.58 (s, 2H, CH ₂); 3.83 (s, 2H, S-CH ₂); 3.98 (s, 1H, NH); 4.1 (s, 1H, N-CH thiazolidinone ring); 4.2 (s, 1H, =CH); 7.5-8.2 (m, 4H, Ar-H); 8.7 (s, 1H, HN-N) |
| 16 | | 2.5 (s, 3H, N-CH ₃); 2.5 (s, 3H, O=N(CH ₃)=O); 3.17 (s, 2H, CH ₂); 3.17 (s, 2H, CH ₂ -NH); 3.38 (s, 1H, NH); 3.57 (s, 1H, N-CH imidazolidinone ring); 3.59 (s, 2H, N-CH ₂); 3.67 (s, 1H, =CH); 7.5-8.3 (m, 4H, Ar-H); 8.7 (s, 1H, HN-N) |

Table 6. ¹³C-NMR of compound (5 and 13)

| No. | Compound structure | ¹³ C-NMR spectral data (δppm) |
|-----|--------------------|--|
| 5 | | 28.31 (C ₁ , C ₃); 58.23 (C ₇); 65.03 (C ₅); 111.23 (C ₁₁); 112.35 (C ₁₂); 129.97 (C ₁₀); 152.54 (C ₆ , C ₉); 160.31 (C ₂ , C ₄); 165.14 (C ₈) |
| 13 | | 28.31 (C ₁ , C ₃); 38.23 (C ₁₀); 59.11 (C ₇); 61.13 (C ₁₁); 66.01 (C ₅); 129.18 (C ₁₃); 133.05 (C ₁₄); 136.17 (C ₁₂); 138.26 (C ₁₅); 152.12 (C ₆); 160.06 (C ₂ , C ₄); 166.93 (C ₈ , C ₉) |

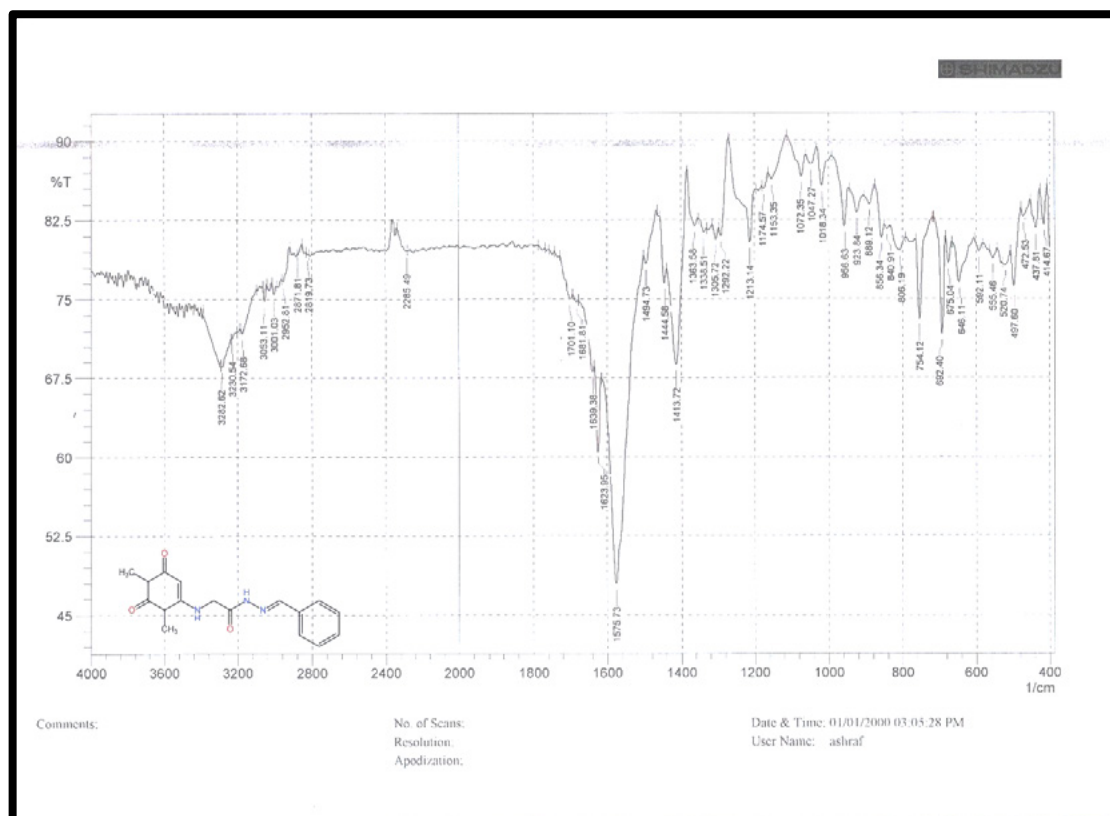


Figure 1. FTIR Soectrum of Compound (1)

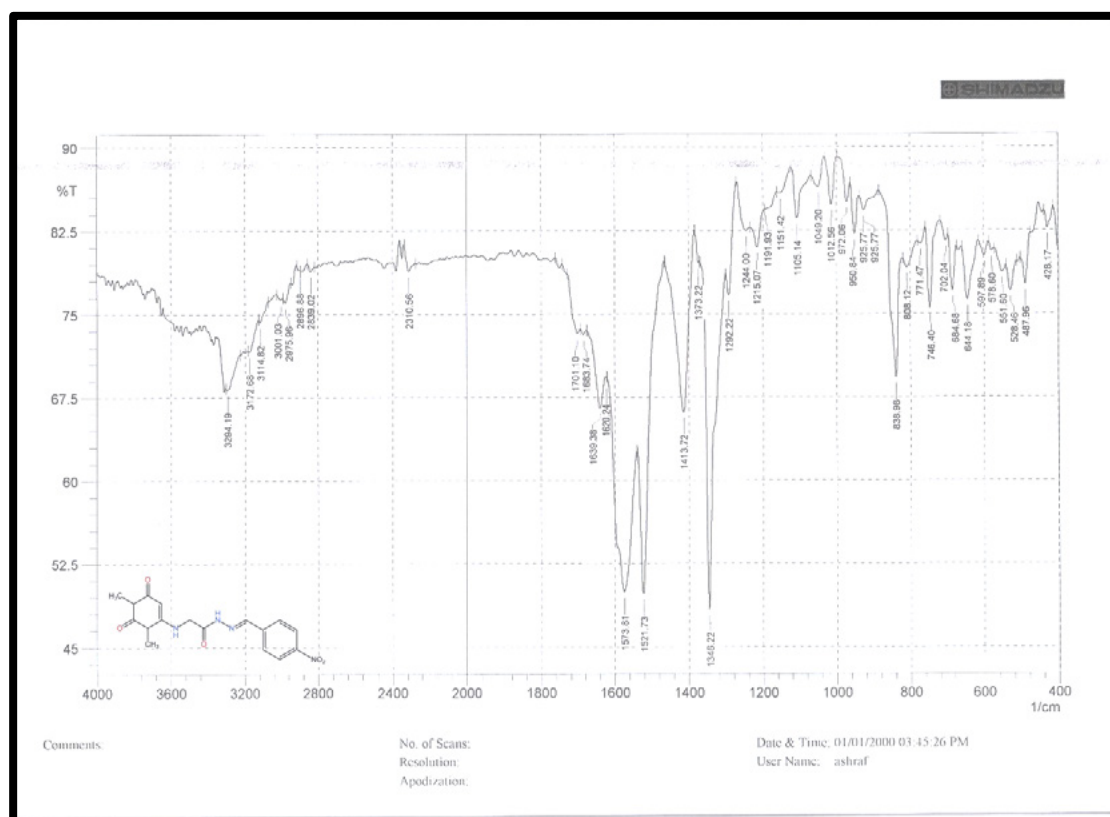


Figure 2. FTIR Soectrum of Compound (2)

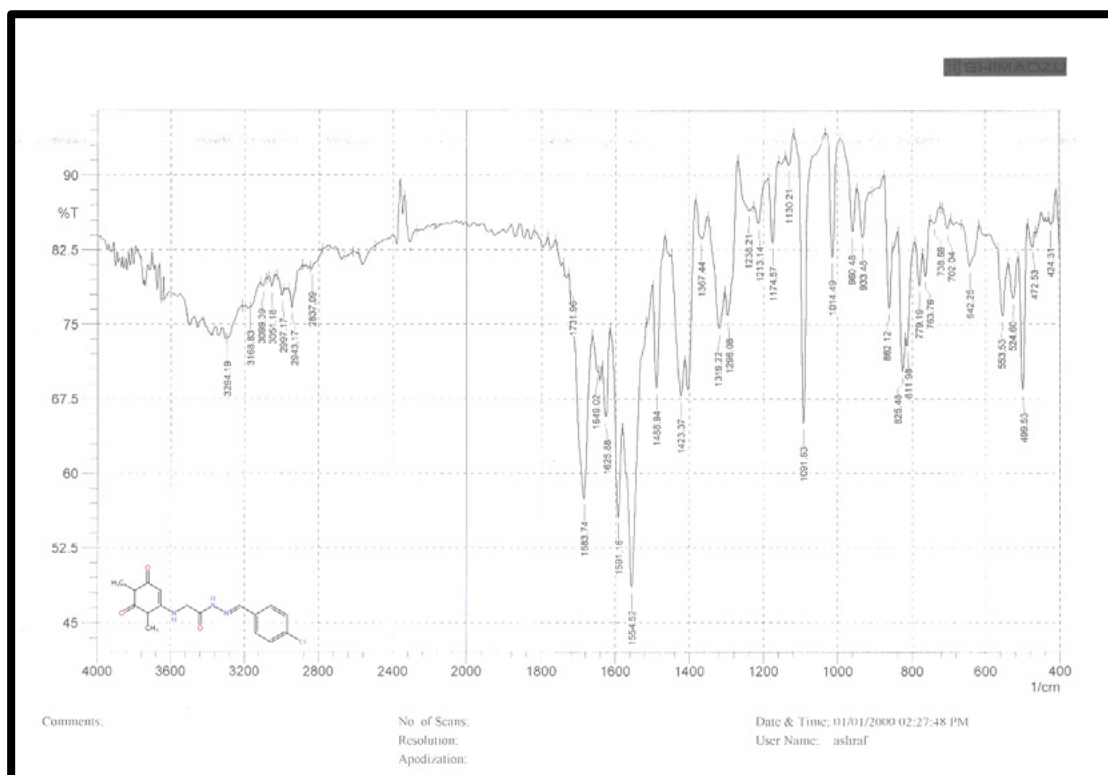


Figure 3. FTIR Soectrum of Compound (3)

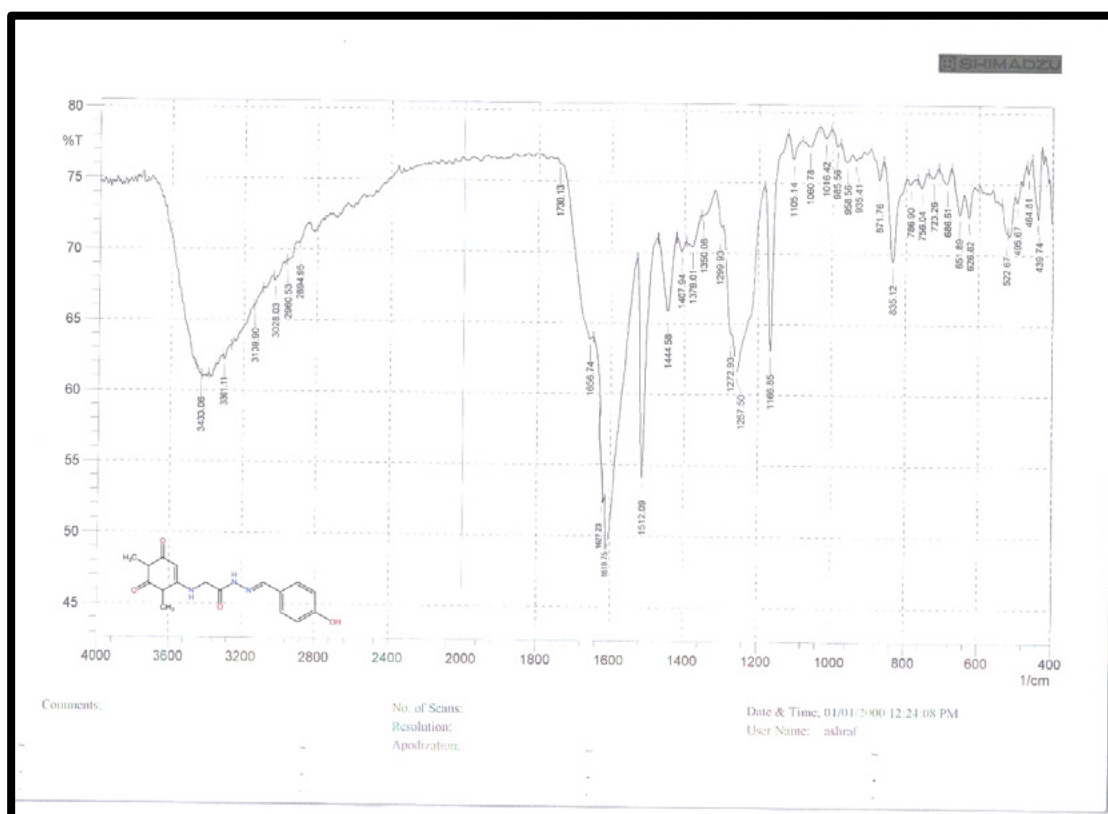


Figure 4. FTIR Soectrum of Compound (4)

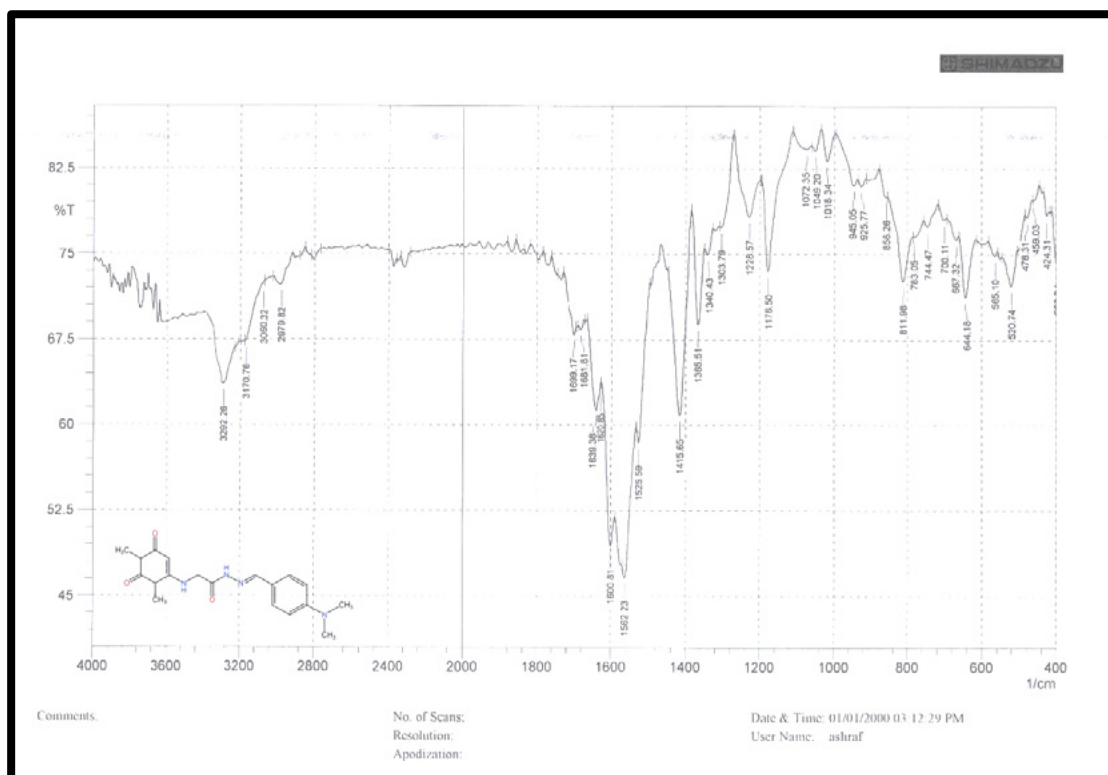


Figure 5. FTIR Soectrum of Compound (5)

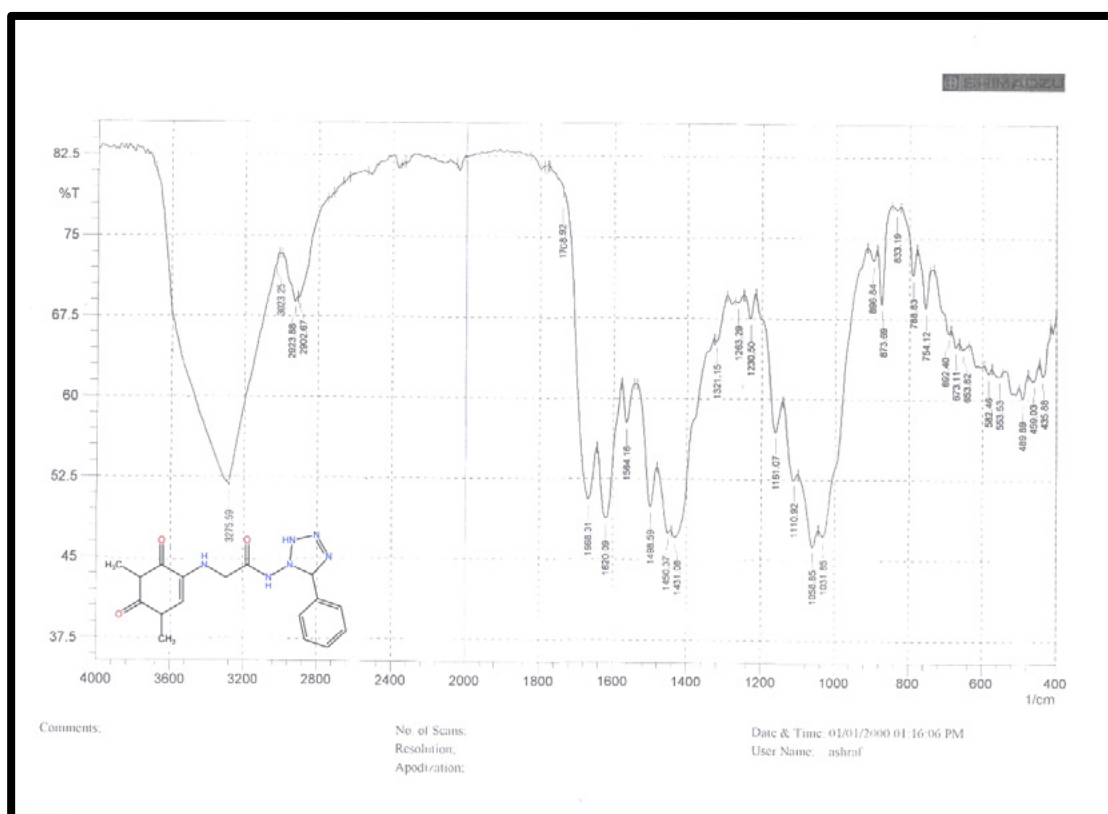


Figure 6. FTIR Soectrum of Compound (6)

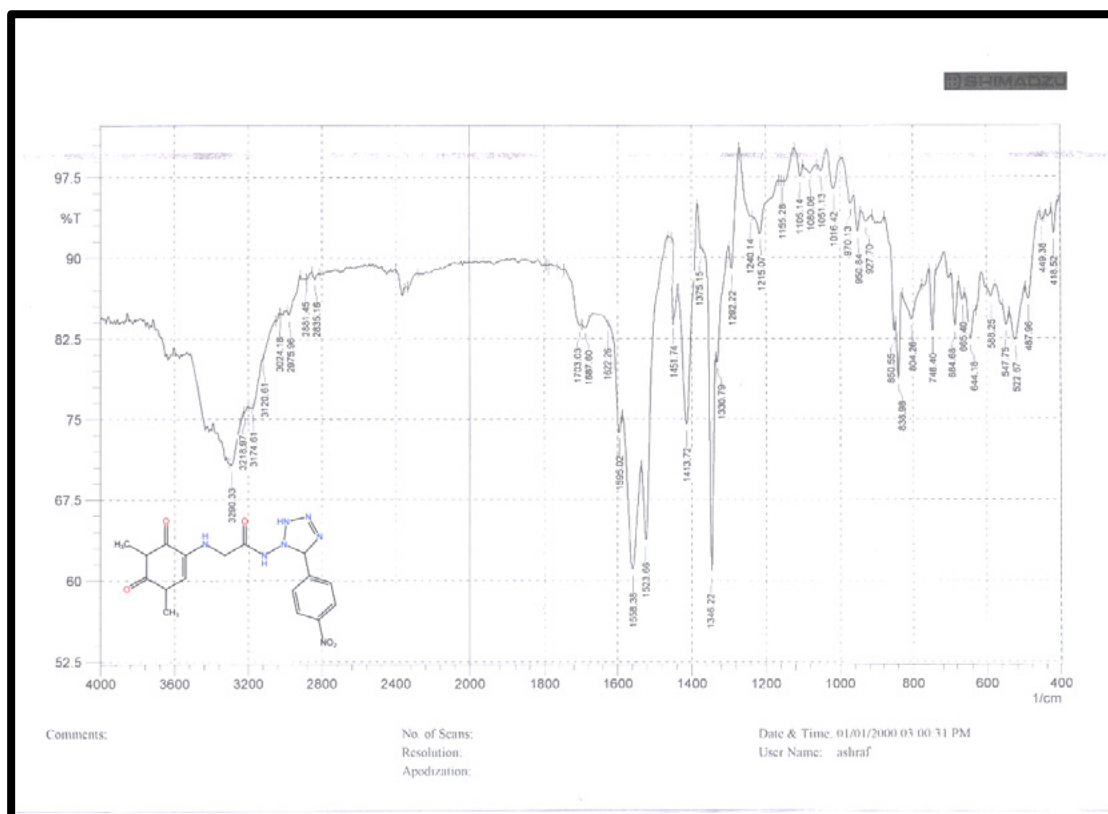


Figure 7. FTIR Soectrum of Compound (7)

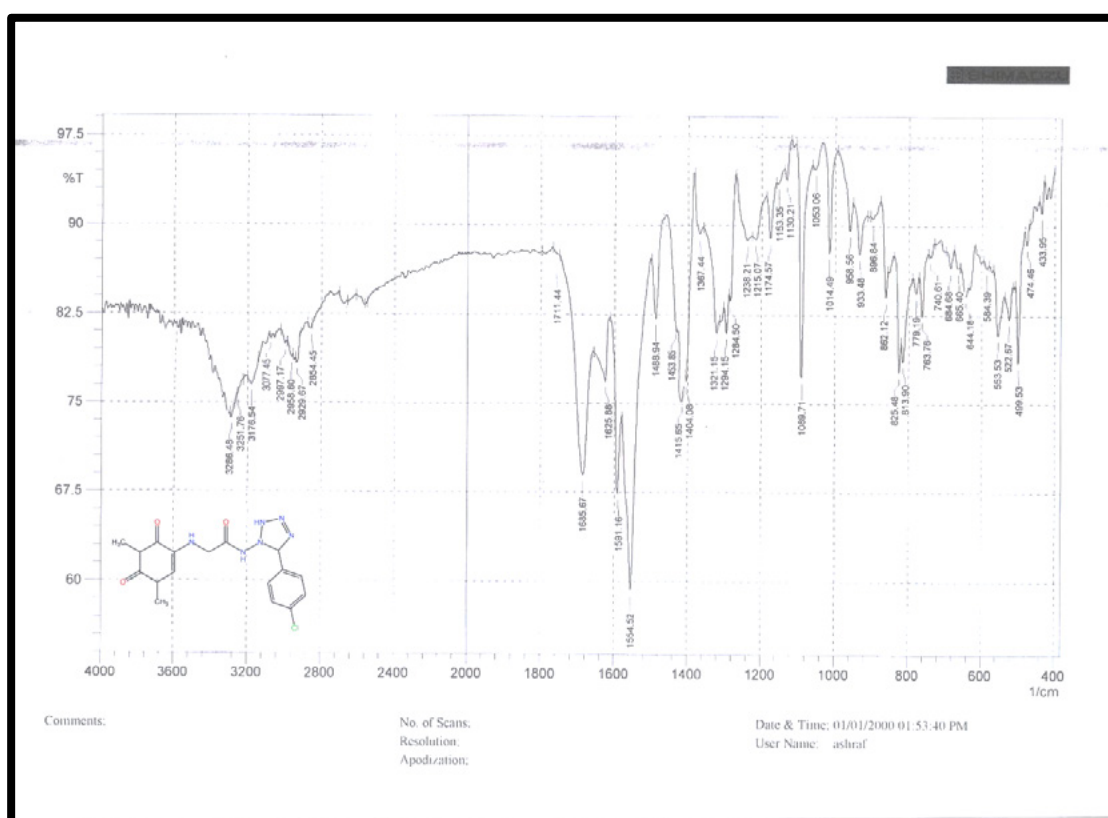


Figure 8. FTIR Soectrum of Compound (8)

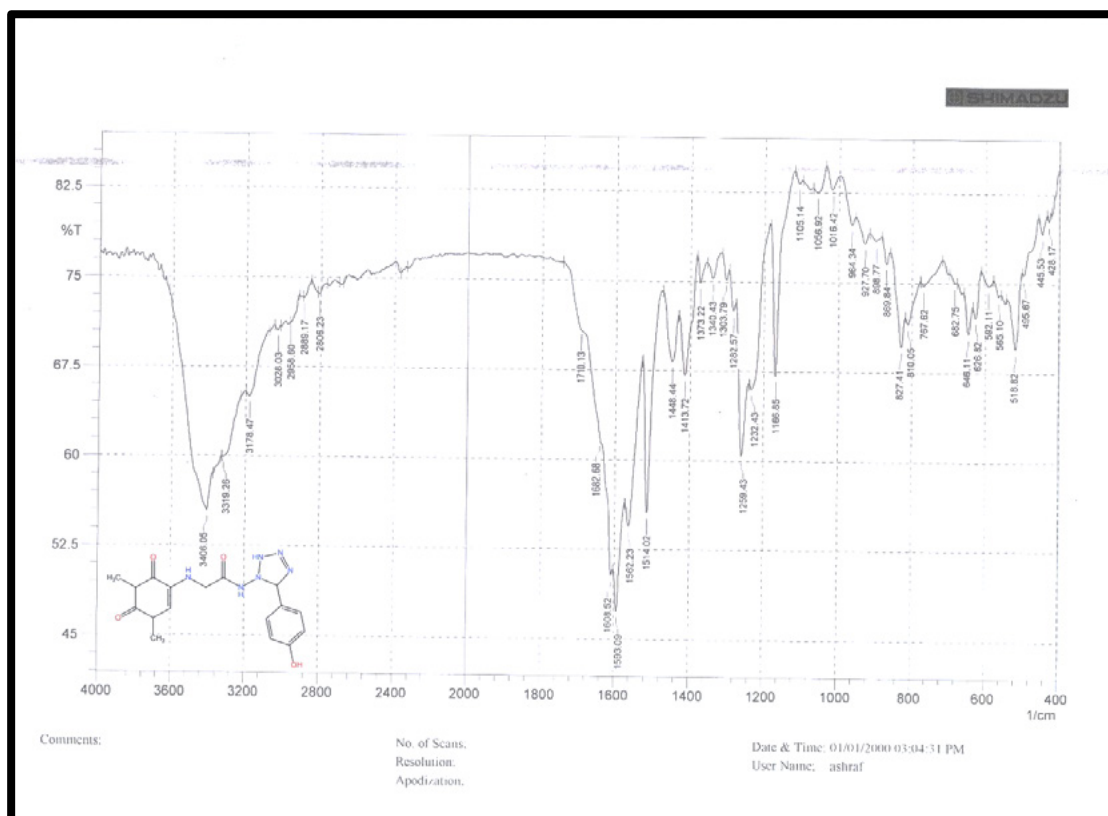


Figure 9. FTIR Soectrum of Compound (9)

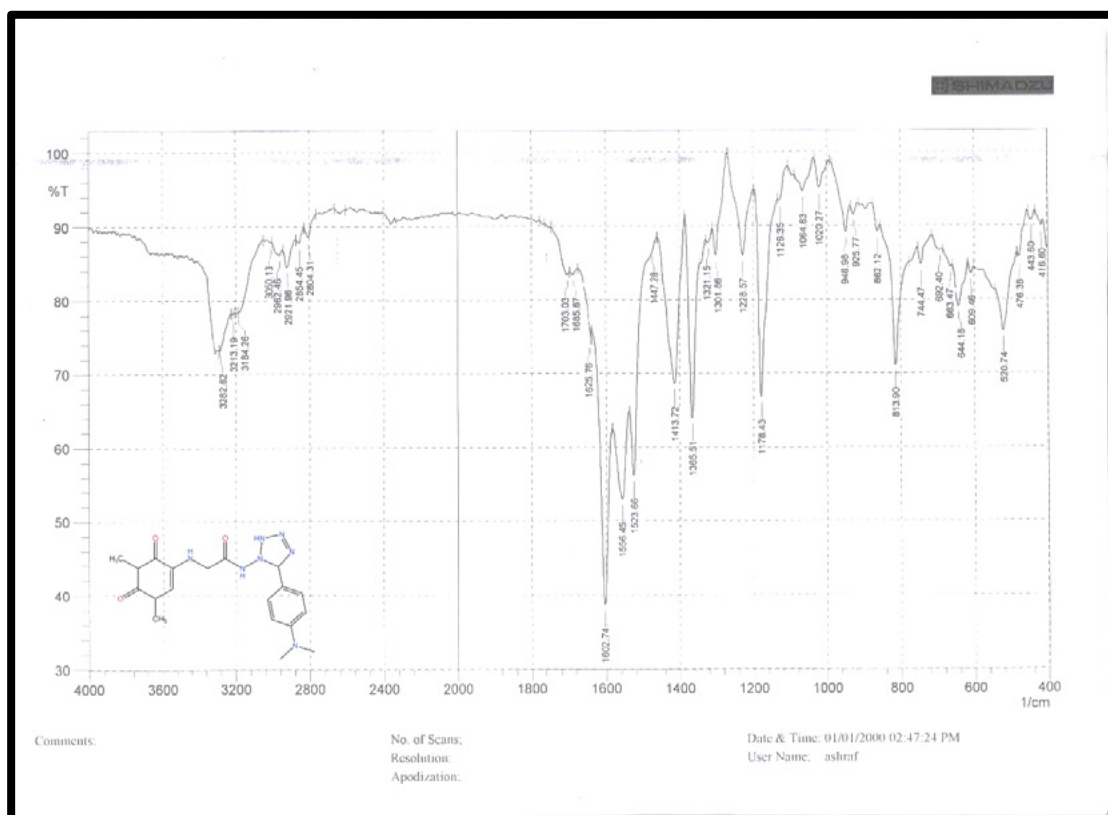


Figure 10. FTIR Soectrum of Compound (10)

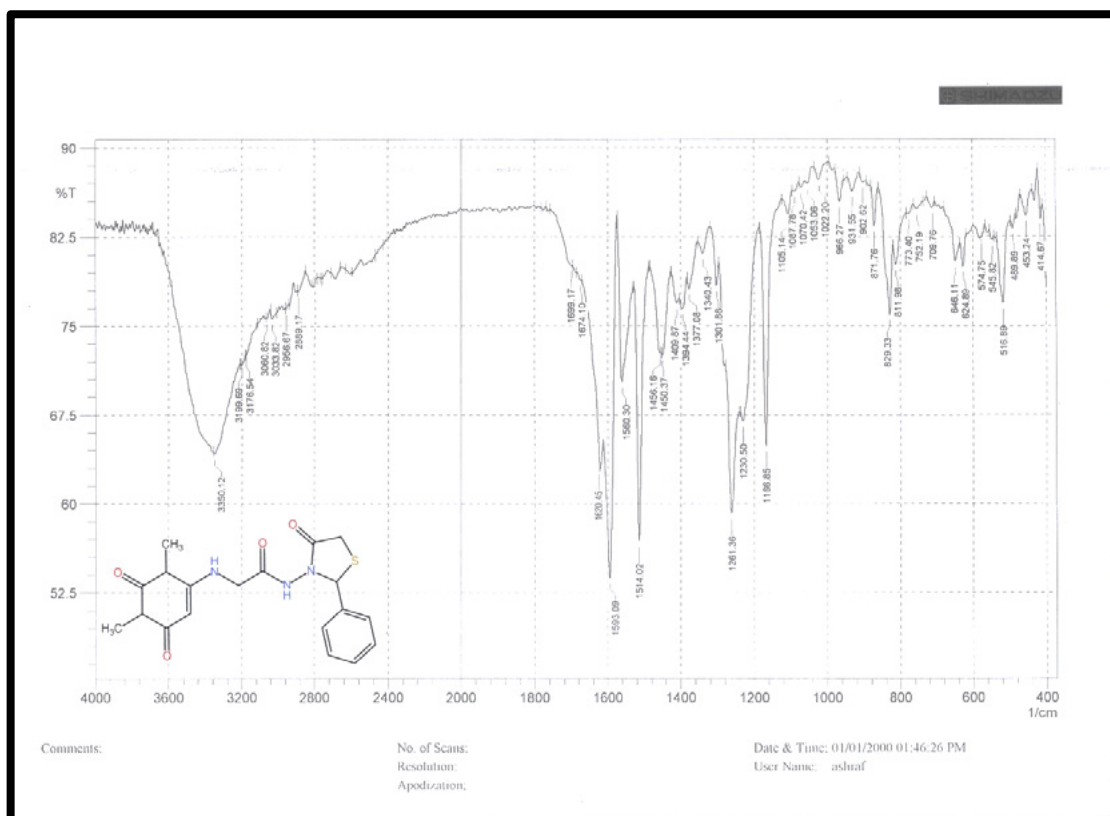


Figure 11. FTIR Soectrum of Compound (11)

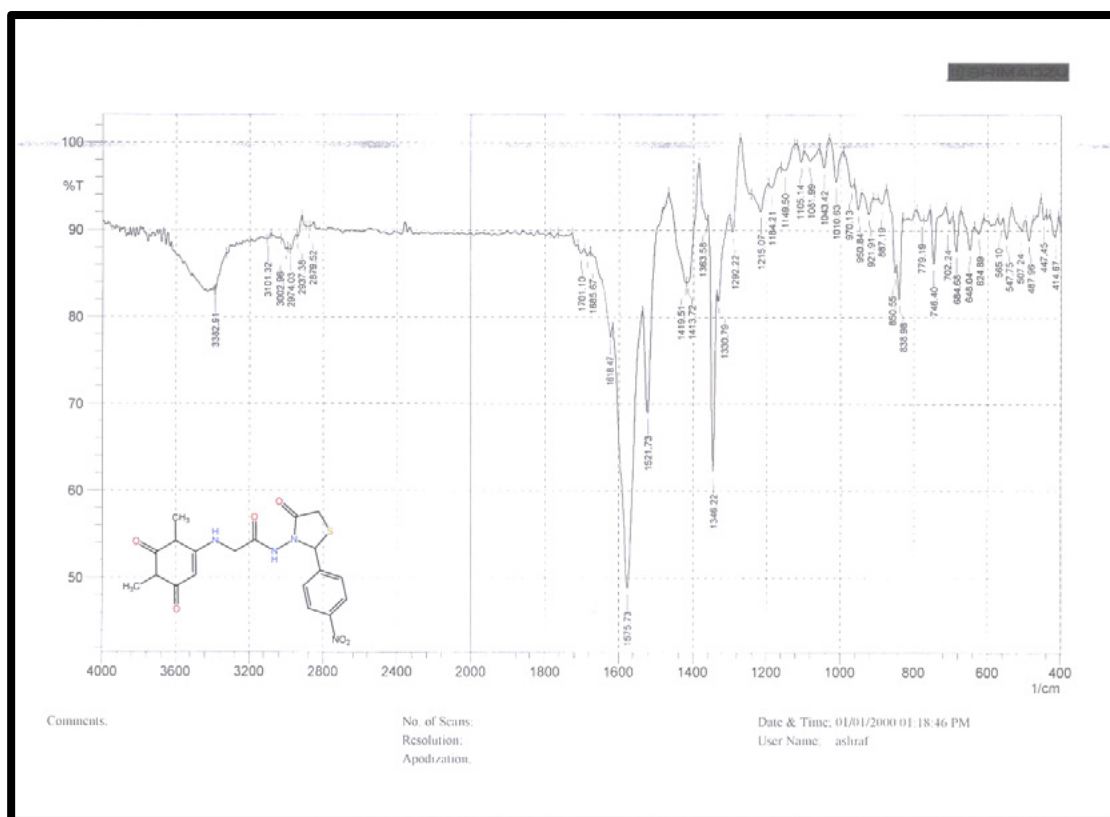


Figure 12. FTIR Soectrum of Compound (12)

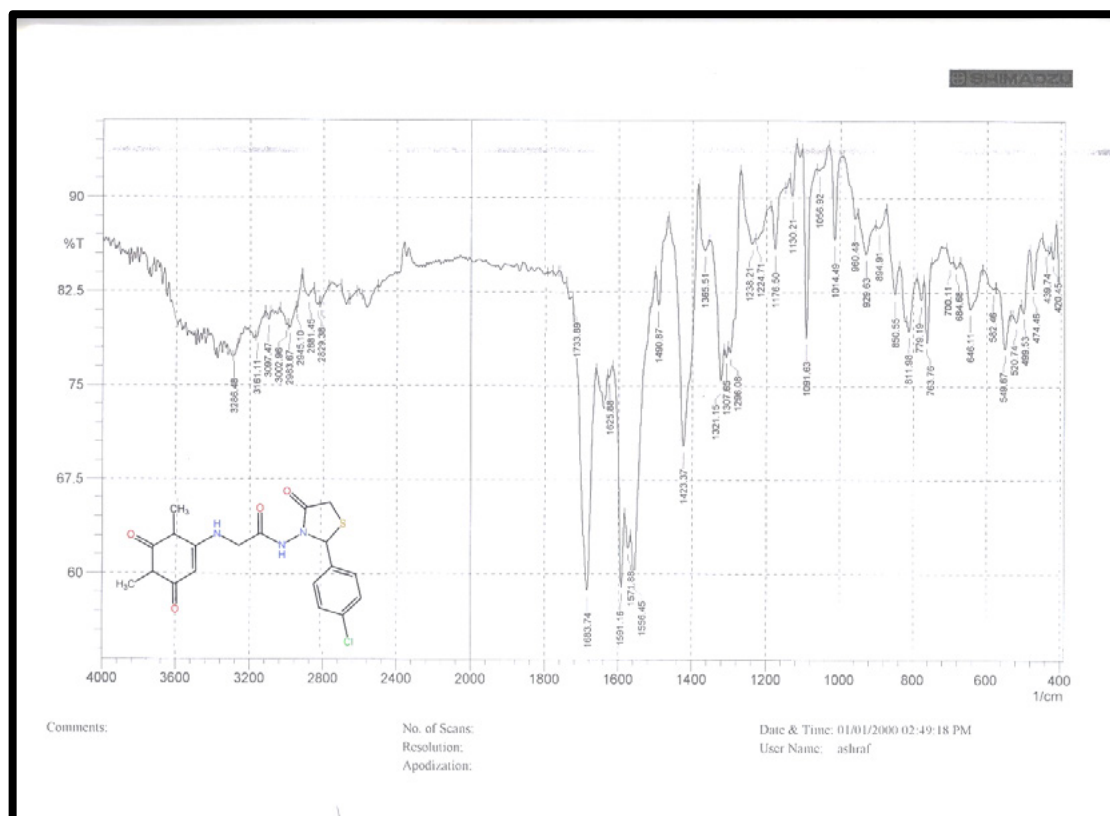


Figure 13. FTIR Soectrum of Compound (13)

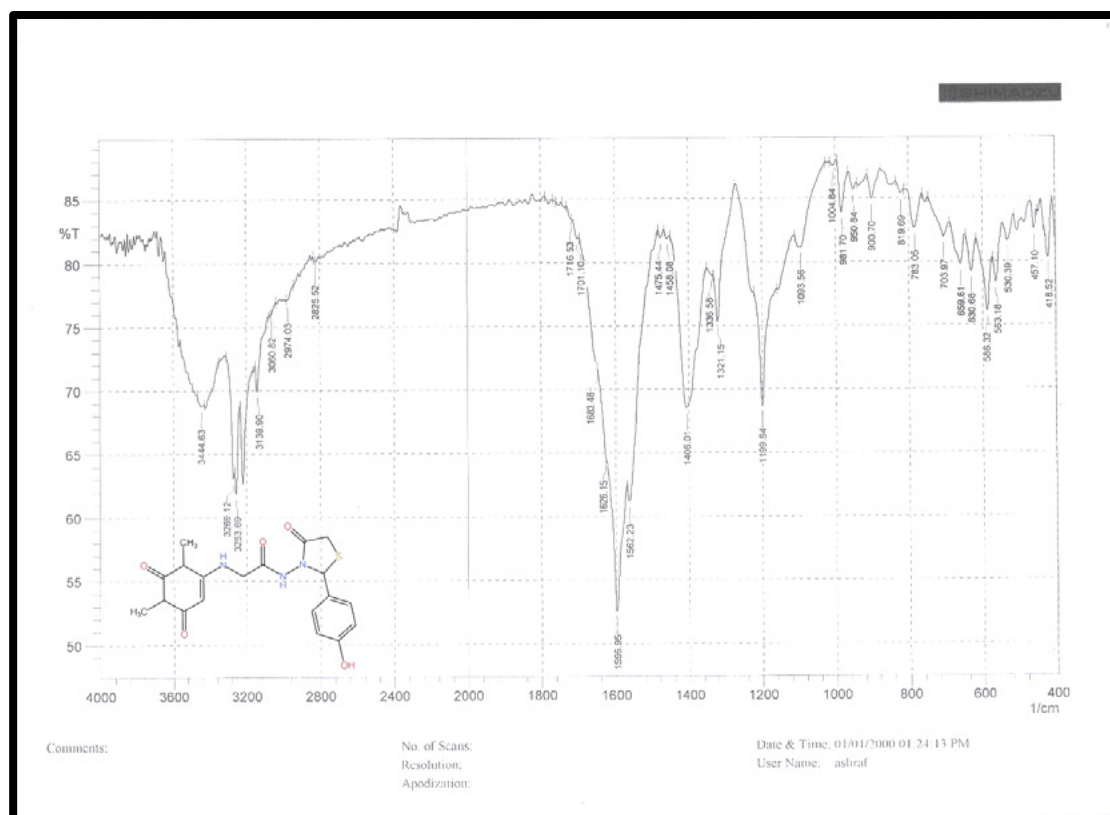


Figure 14. FTIR Soectrum of Compound (14)

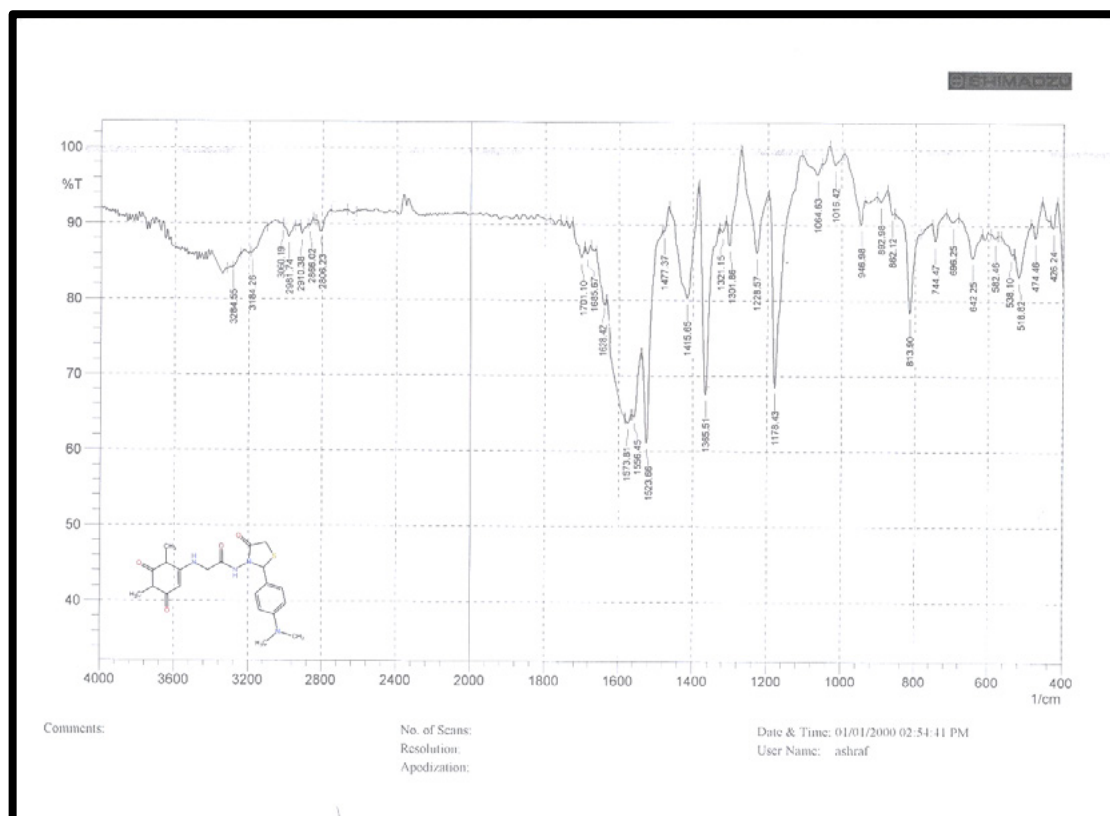


Figure 15. FTIR Soectrum of Compound (15)

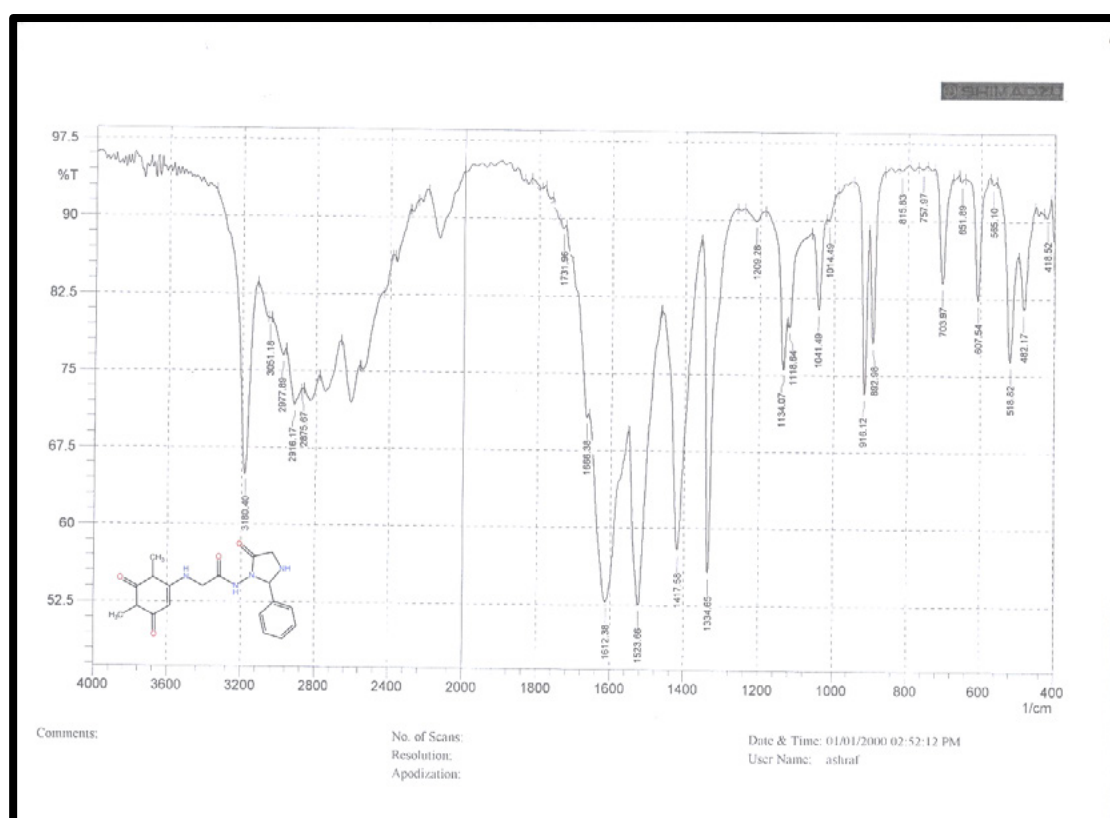


Figure 16. FTIR Soectrum of Compound (16)

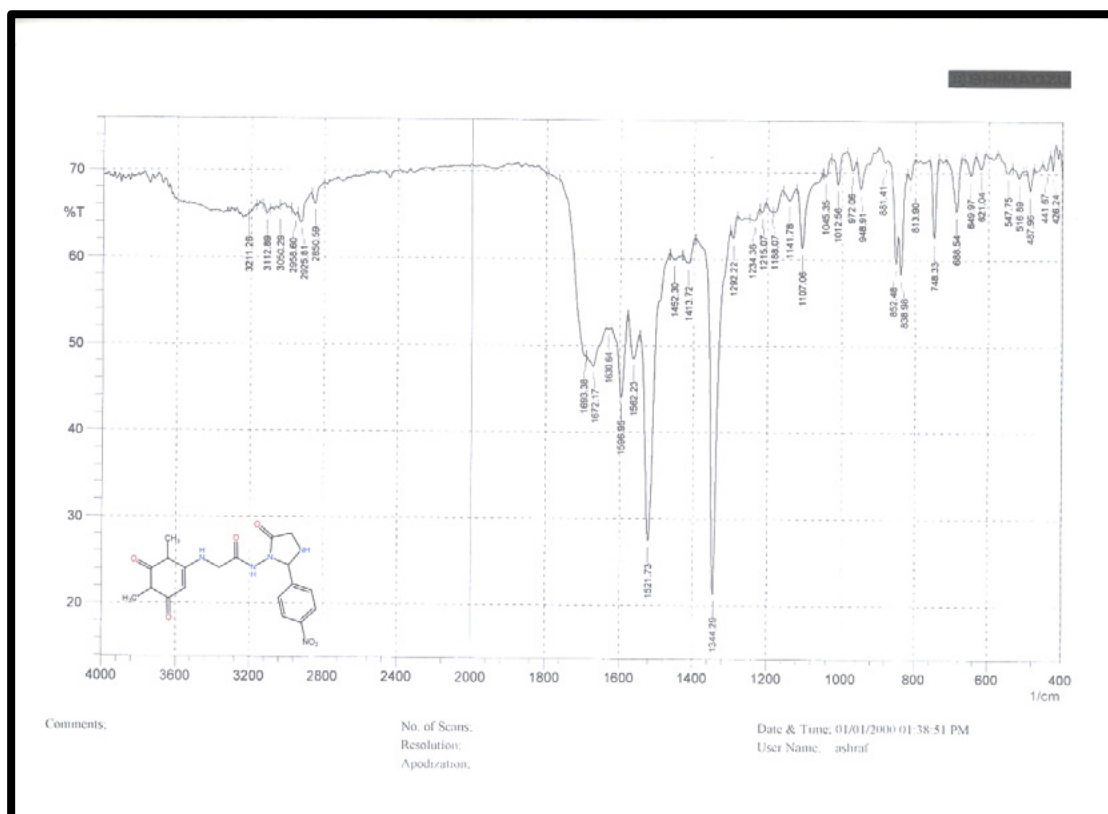


Figure 17. FTIR Soectrum of Compound (17)

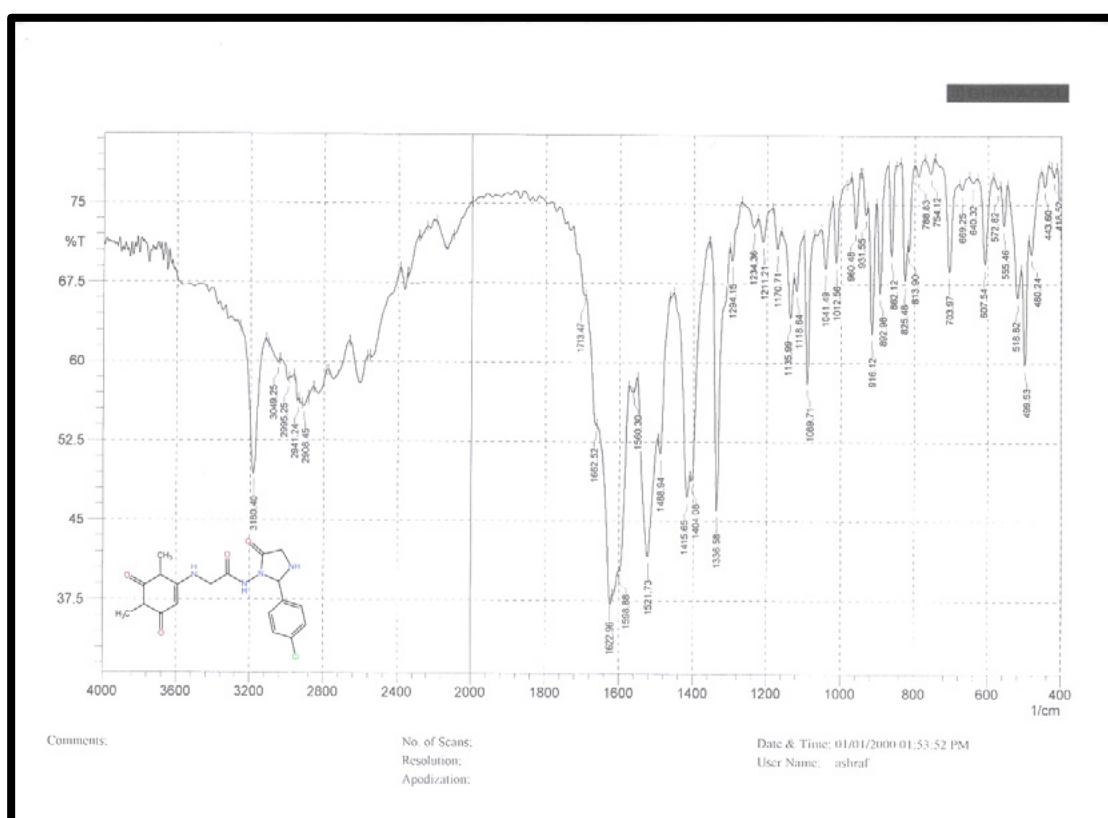


Figure 18. FTIR Soectrum of Compound (18)

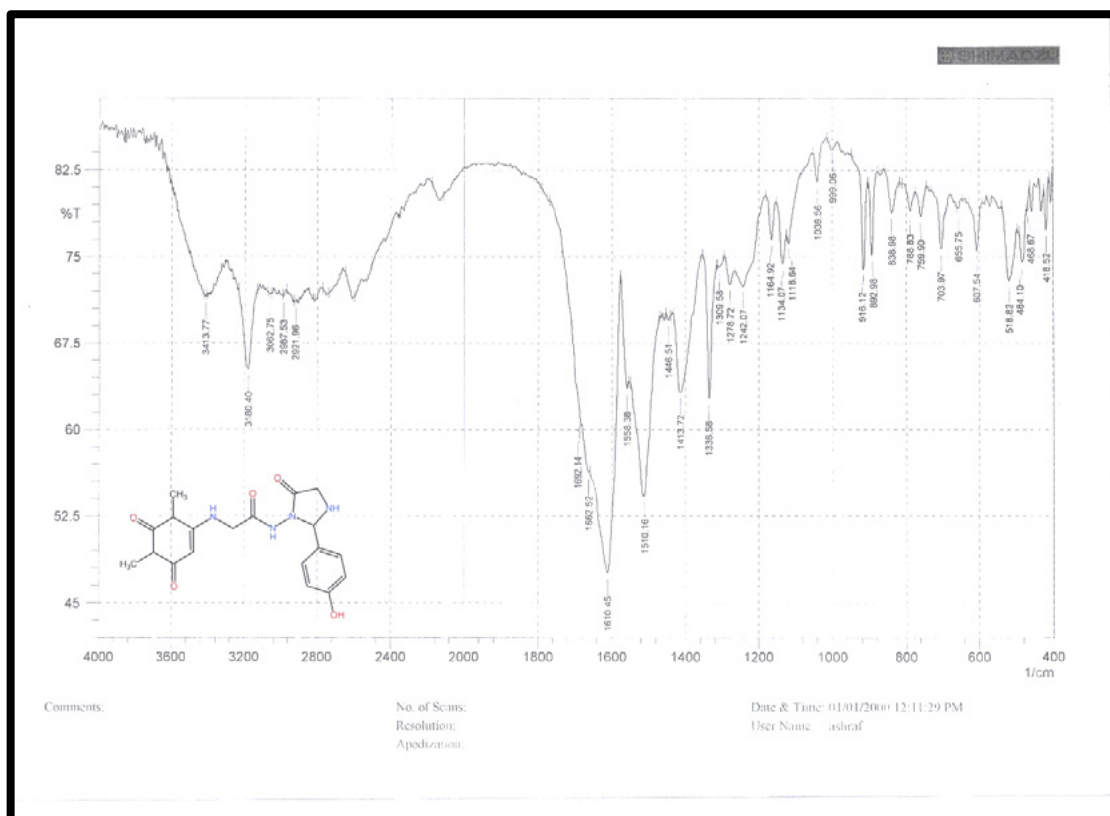


Figure 19. FTIR Soectrum of Compound (19)

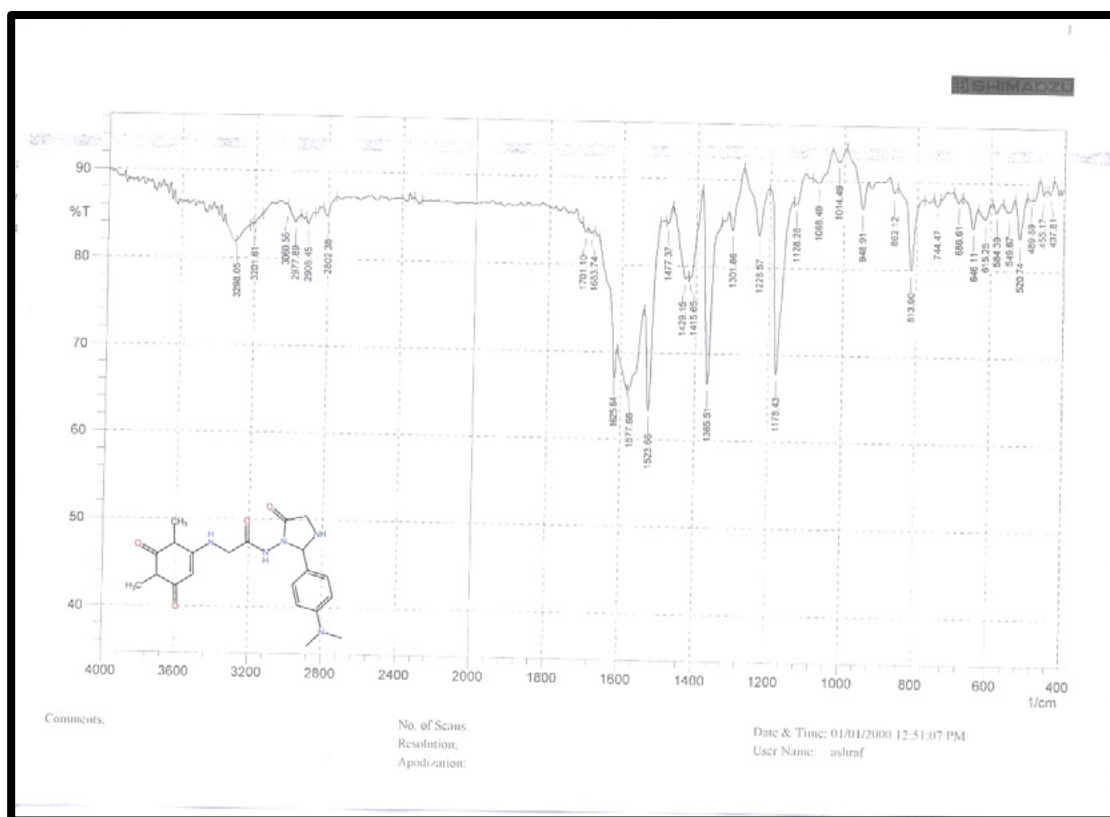
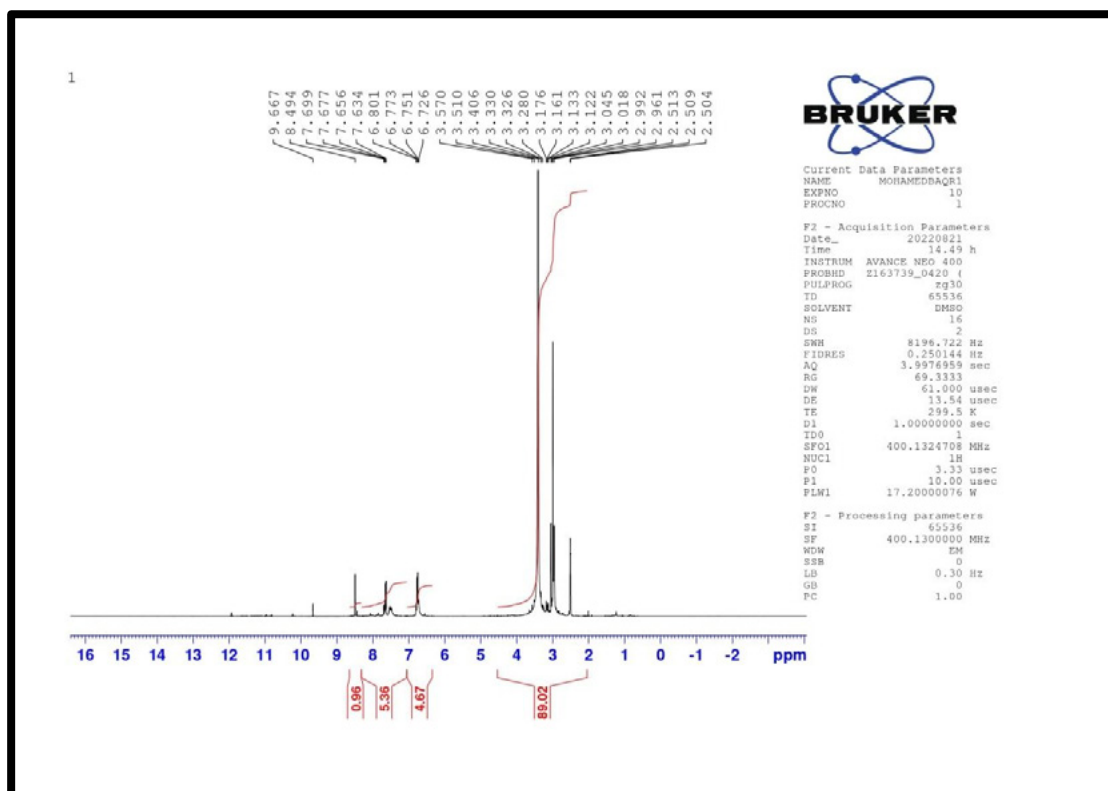
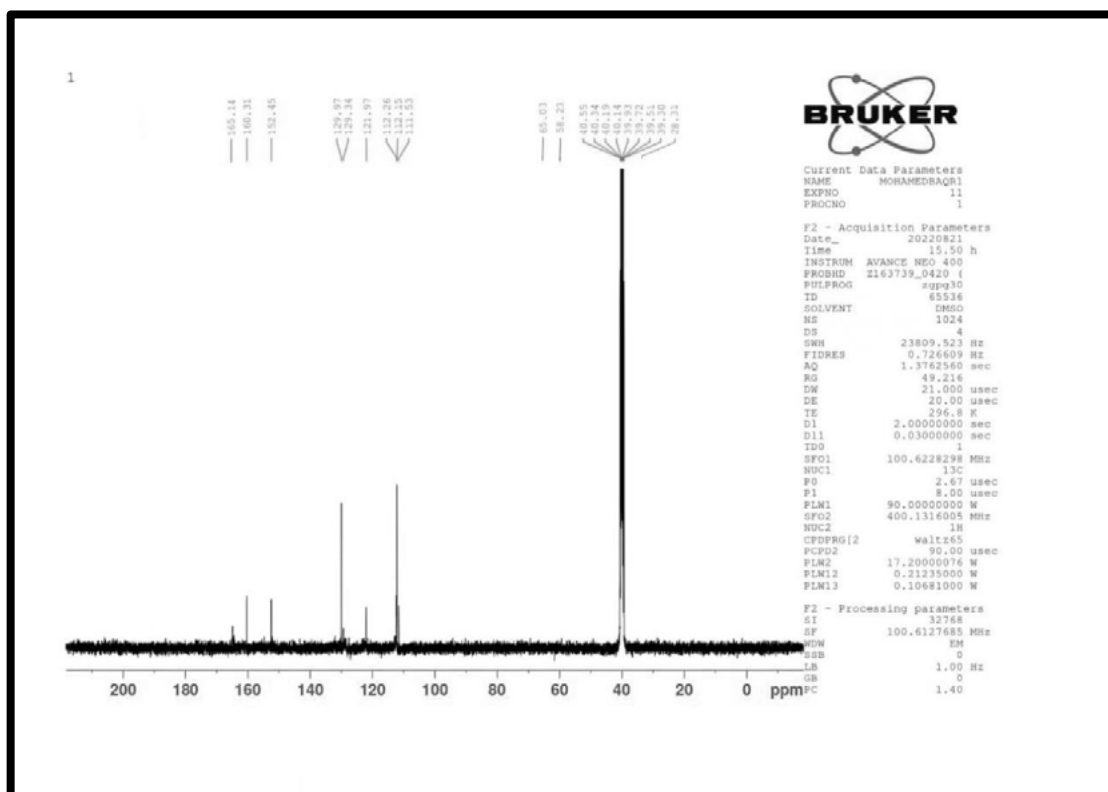
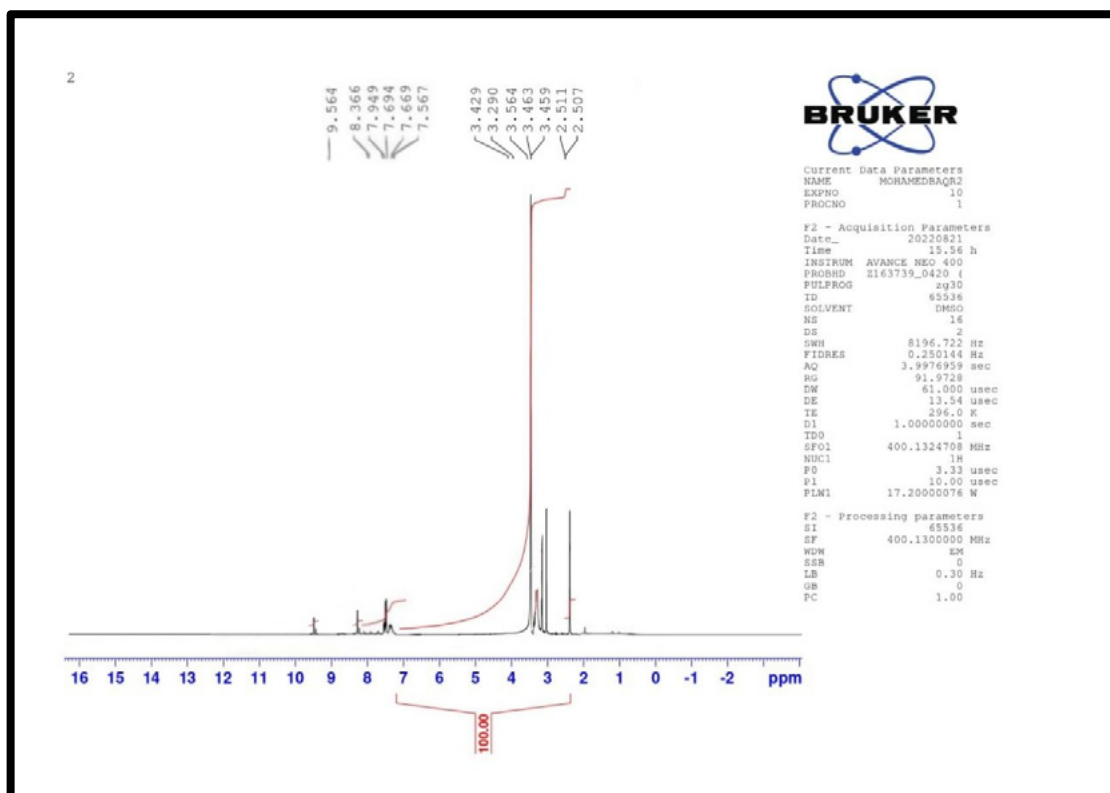
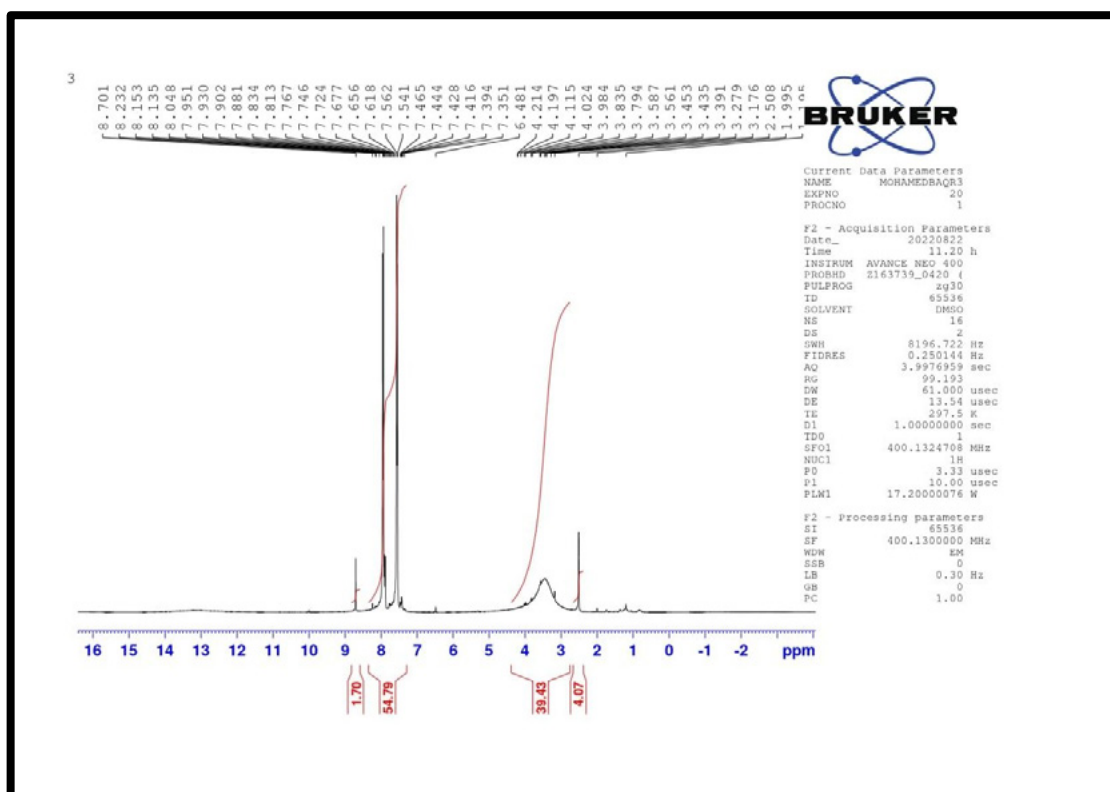
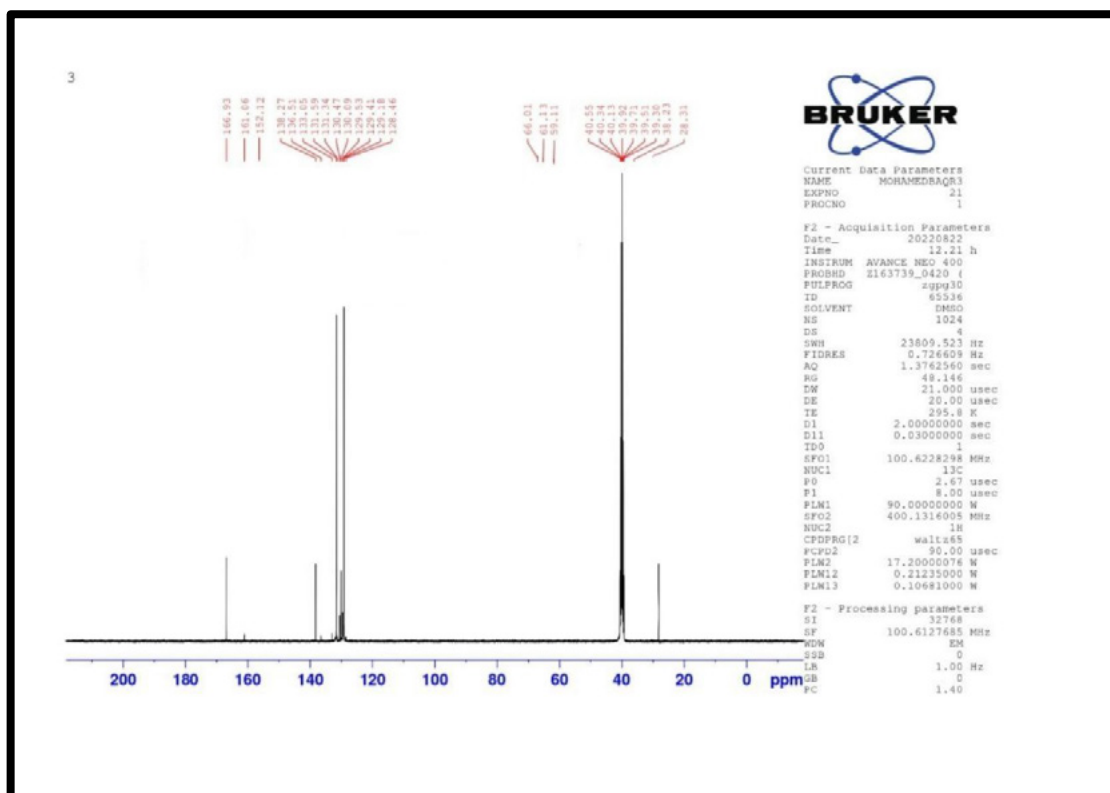
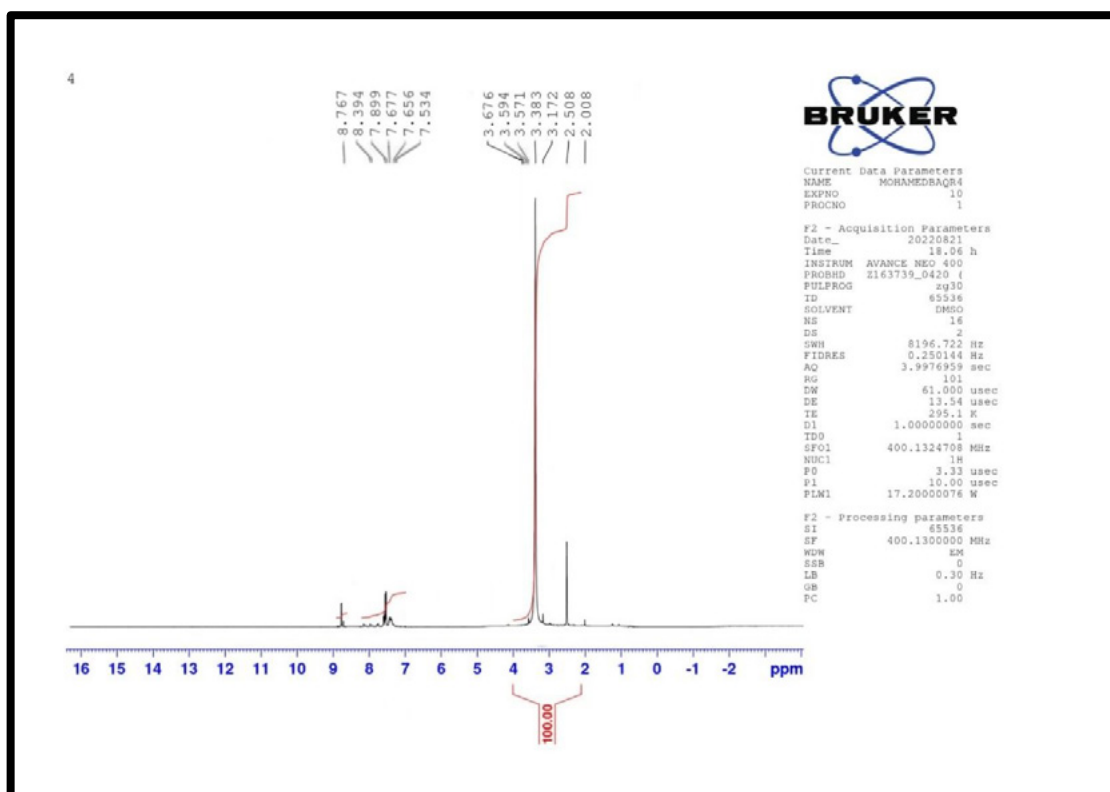


Figure 20. FTIR Soectrum of Compound (20)

Figure 21. ¹H-NMR of compound (5)Figure 22. ¹³C-NMR of compound (5)

Figure 23. ¹H-NMR of compound (7)Figure 24. ¹H-NMR of compound (13)

Figure 25. ¹³C-NMR of compound (13)Figure 26. ¹H-NMR of compound (16)

3.2. DPPH SCAVENGING ACTIVITY

All of the produced compounds (1-20) were either as active as the ordinary ascorbic acid or somewhat less active. The quantities of 50, 100, and 150 g /ml were used in a (2,2-diphenyl-1-picrylhydrazyl) test. The ultimate result is stoichiometric in terms of the number of electrons caught, It can be differentiated from others by either a changing in the dark violet hue of its exterior (DPPH) or a complete loss of color. We see a clear decline in efficacy with decreasing concentration in these prepared samples. Antioxidant activity was highest for component (11) at a concentration of (150 g/ml), as was out by reviewing the various results. An illustration of the newly synthesized compound's DPPH scavenging activity (1-20) is shown in Figure 27.

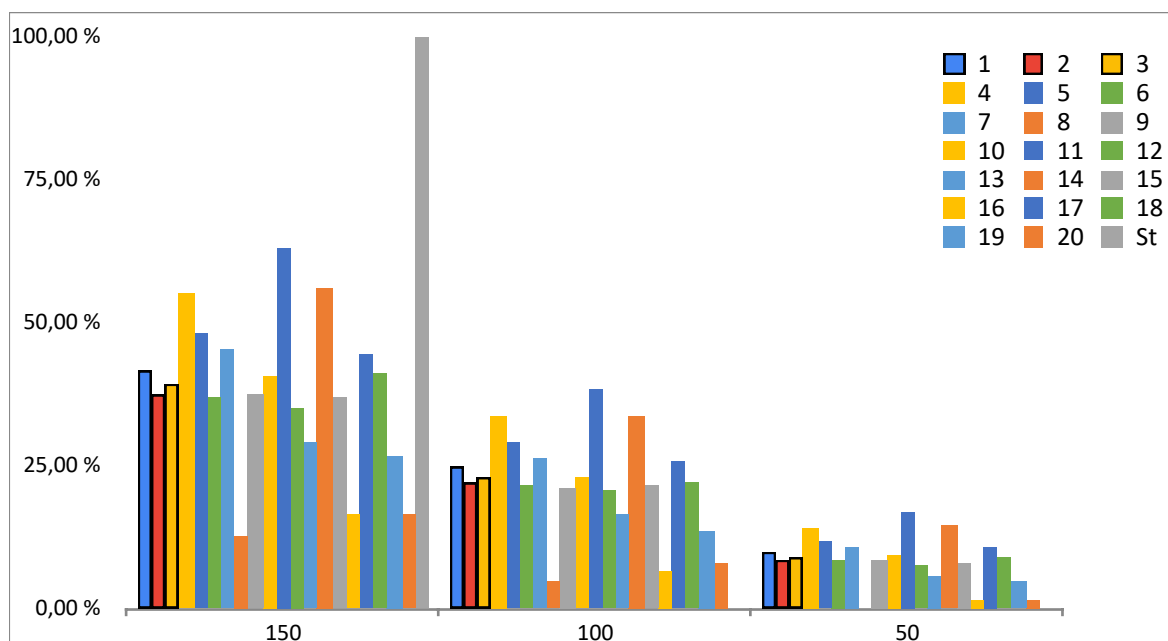


Figure 27. New compound's DPPH-scavenging action(1-20)

3.3. QUANTITATIVE MEASURE OF ANTIOXIDANT CAPACITY

The phosphomolybdenum method was used to calculate the combined antioxidant power of all synthesized compounds (1–20). This technique relies on the ability of synthesized compounds to convert colorless 70 Molybdenum(VI) to colored Molybdenum(V) via the formation of a green phosphate - Mo(V) complex at acidic pH. The chemical was found to have significantly higher antioxidant activity than ascorbic acid. Among the recently synthesized uracil derivatives, compounds (1-20) exhibit a low antioxidant ability against decreased Mo(VI) to Mo(V), as depicted in Figure 28.

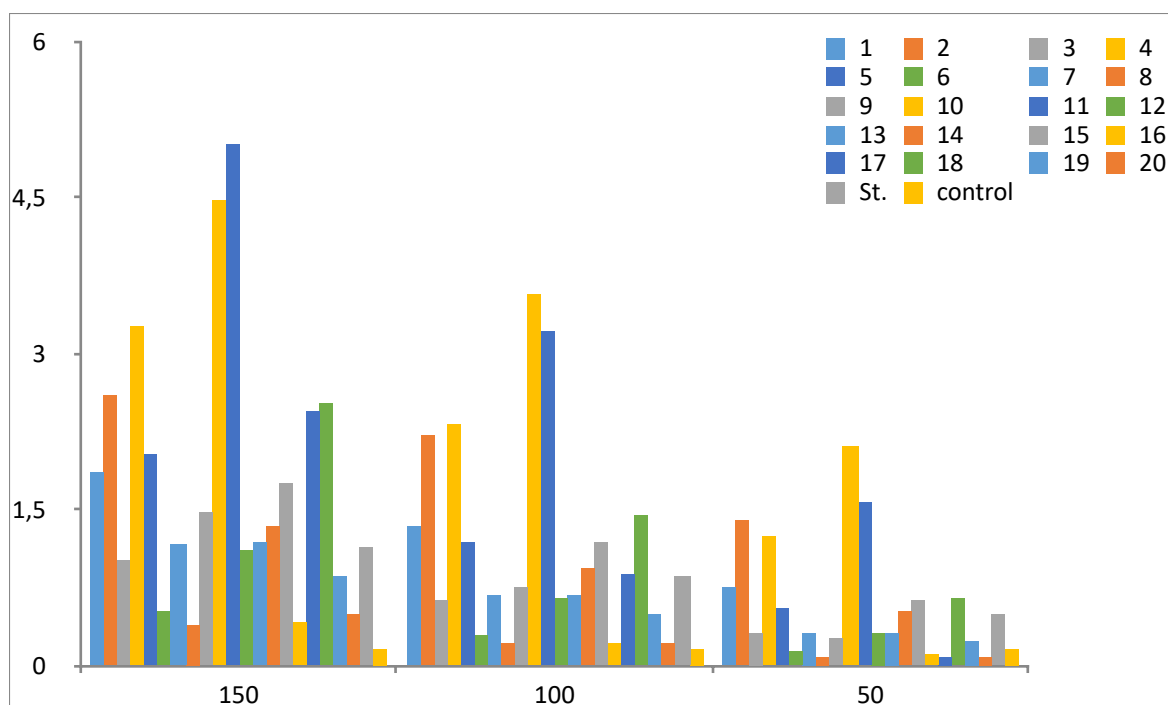


Figure 28. Total antioxidant capacity of the newly synthesized compound (1-20)

3.4. DOCKING STUDIES

To provide light on why synthetic substances have antioxidant properties (1-4, 6-11 and 13-20). Aromatase, an enzyme protein implicated in breast cancer etiology and induction, was one of many pharmaceutical targets subjected to docking studies. The crystal structure of Aromatase's crystal structure (PDB id: 3S7S) in association with the reference drug Exemestane was obtained from the Protein Data Bank (EXM).

There are docking studies shown in Table 5. Compared to the reference medication Exemestane, compounds (1-4, 6-11, and 13-20) showed a more stable fit into the aromatase binding pocket through interactions with critical residues ARG 115, PHE 221, TRP224, ASP309, MET374, HIE 480, and HEM600.

When compared to the reference compound (-3.657 kcal/mol) in table-7, compound (14) has a dock score of -7.139 kcal/mol. The docking score is higher here than it is for co-crystalline.

So, these relationships help to clarify the decline in aromatase activity. This work adds to the growing body of evidence that the synthesized chemicals have potential as a new class of chemotherapeutic medications for the treatment of breast cancer and other associated illnesses. Several compounds' structures are shown in Figure 29.

Table 7. Consequences of molecular docking of compound (1-4, 6-11, and 13-20)

| Compounds | Types of residues | Docking score | Glide Energy |
|-----------|------------------------------------|---------------|--------------|
| 1 | PHE 221, HIE 480 | 0.740 | -16.33 |
| 2 | ARG 115, PHE 221, MET 374, HIE 480 | 0.767 | -10.996 |
| 3 | HEM 600 | -1.735 | -37.043 |
| 4 | TRP 224, MET 374, HEM 600 | -5.530 | -24.171 |
| 6 | PHE 221, TRP 224, MET 374, HEM 600 | -6.486 | -44.412 |
| 7 | MET 374, HEM 600 | -1.045 | -48.6 |
| 8 | ASP 309, MET 374, HEM 600 | -3.503 | -30.517 |
| 9 | PHE 134, MET 374, HEM 600 | -4.456 | -31.474 |
| 10 | MET 374, HEM 600 | -2.910 | -39.268 |
| 11 | TRP 224 | -5.786 | -37.608 |
| 13 | HEM 600 | -3.900 | -39.437 |
| 14 | MET 374, HEM 600 | -7.139 | -29.686 |
| 15 | HEM 600 | -1.166 | -24.856 |
| 16 | TRP224, MET 374, HEM 600 | -5.548 | -43.625 |
| 17 | ARG 115, HEM 600 | -3.685 | -35.37 |
| 18 | MET 374, HEM 600 | -5.050 | -26.56 |
| 19 | HEM 600 | -4.892 | -34.777 |
| 20 | MET 374, HEM 600 | -5.181 | -47.623 |
| Standard | MET 374 | -3.657 | -18.206 |

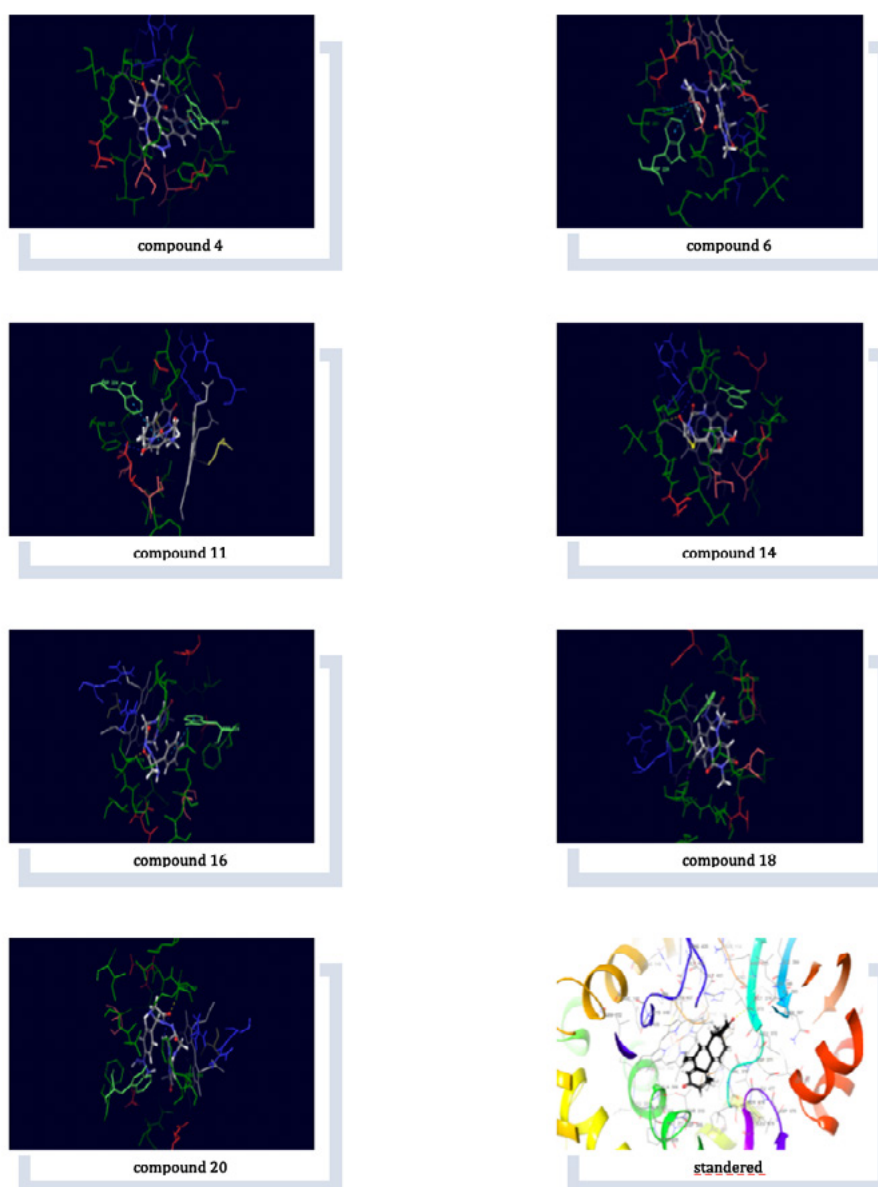


Figure 29. View docking Molecular of some compounds and standard

4. CONCLUSION

In this work, synthesis new heterocyclic compounds from reaction uracil derivatives with sodium azide, 2-mercapto acid & 2-amino acetic acid to produce five-membered heterocyclic rings includes: tetrazoline-1yl, thiazolidin-4-one and imidazolidin-4-one derivatives respectively. This compounds was measured biological activity by two types of anti-oxidant activity DPPH and phosphomolybdenum at three concentration (50, 100 150) ppm Results shown the phosphomolybdenum is batter worked of this compounds and the highest Values at 5.023 of compound (11) compare with standard 1.142 in concentration 150 ppm and study molecular docking shown Results The effectiveness of these compounds for the treatment of breast cancer and other associated diseases.

REFERENCES

- (1) Diab, H. M., Salem, M. E., Abdelhamid, I. A., & Elwahy, A. H. (2021). **Aminouracil and aminothiouracil as versatile precursors for a variety of heterocyclic systems.** *ARKIVOC: Online Journal of Organic Chemistry*, 2021.
- (2) Nayab, R. S., Maddila, S., Krishna, M. P., Titinchi, S. J., Thaslim, B. S., Chinthi, V., ... & Chamarthi, N. R. (2020). **In silico molecular docking and in vitro antioxidant activity studies of novel α -aminophosphonates bearing 6-amino-1, 3-dimethyl uracil.** *Journal of Receptors and Signal Transduction*, 40(2), 166-172.
- (3) Pałasz, A., & Cieź, D. (2015). **In search of uracil derivatives as bioactive agents. Uracils and fused uracils: Synthesis, biological activity and applications.** *European Journal of Medicinal Chemistry*, 97, 582-611.
- (4) Tang, J., Yang, P., Yang, H., Xiong, H., Hu, W., & Cheng, G. (2020). **A simple and efficient method to synthesize high-nitrogen compounds: Incorporation of tetrazole derivatives with N5 chains.** *Chemical Engineering Journal*, 386, 124027.
- (5) Wang, T., Gao, H., & Shreeve, J. N. M. (2021). **Functionalized tetrazole energetics: A route to enhanced performance.** *Zeitschrift für anorganische und allgemeine Chemie*, 647(4), 157-191.
- (6) Yu, Q., Imler, G. H., Parrish, D. A., & Shreeve, J. N. M. (2019). **Challenging the limits of nitro groups associated with a tetrazole ring.** *Organic letters*, 21(12), 4684-4688.
- (7) Wu, J. T., Zhang, J. G., Yin, X., & Wu, K. (2015). **Energetic Oxygen-Containing Tetrazole Salts Based on 3, 4-Diaminotriazole.** *Chemistry—An Asian Journal*, 10(5), 1239-1244.
- (8) Sampada, P., G. Kavita, and M. Renuka. (2022). **Synthesis of some new novel thiazolidinone from chalcone and their anti-microbial activity.** *International Journal of Reserches in Biosciences, Agricuture and technology*, 35-42.
- (9) Li, W., Zhang, J., He, J., Xu, L., Vaccaro, L., Liu, P., & Gu, Y. (2020). **I₂/DMSO-Catalyzed Transformation of N-tosylhydrazones to 1, 2, 3-thiadiazoles.** *Frontiers in Chemistry*, 8, 466.
- (10) Abdullah, J. A., Aldahham, B. J., Rabeea, M. A., Asmary, F. A., Alhajri, H. M., & Islam, M. A. (2021). **Synthesis, characterization and in-silico assessment of novel thiazolidinone derivatives for cyclin-dependent kinases-2 inhibitors.** *Journal of Molecular Structure*, 1223, 129311.
- (11) Sercel, Z. P., Sun, A. W., & Stoltz, B. M. (2021). **Synthesis of Enantioenriched gem-Disubstituted 4-Imidazolidinones by Palladium-Catalyzed Decarboxylative Asymmetric Allylic Alkylation.** *Organic letters*, 23(16), 6348-6351.
- (12) Souissi, S., Gabsi, W., Echaieb, A., Roger, J., Hierso, J. C., Fleurat-Lessard, P., & Boubaker, T. (2020). **Influence of solvent mixture on nucleophilicity parameters: the case of pyrrolidine in methanol–acetonitrile.** *RSC advances*, 10(48), 28635-28643.
- (13) Swain, S. P., & Mohanty, S. (2019). **Imidazolidinones and Imidazolidine-2, 4-diones as Antiviral Agents.** *ChemMedChem*, 14(3), 291-302.

- (14) Smolobochkin, A. V., Gazizov, A. S., Otegen, N. K., Voronina, J. K., Strel'nik, A. G., Samigullina, A. I., ... & Pudovik, M. A. (2020). **Nucleophilic Cyclization/ Electrophilic Substitution of (2, 2-Dialkoxyethyl) ureas: Highly Regioselective Access to Novel 4-(Het) arylimidazolidinones and Benzo [d] [1, 3] diazepinones.** *Synthesis*, 52(21), 3263-3271.
- (15) Murinov, Y. I., Grabovskii, S. A., & Kabal'nova, N. N. (2019). **Pro-and antioxidant properties of uracil derivatives.** *Russian Chemical Bulletin*, 68, 946-954.
- (16) Al-Adhami, H., & Al-Majidi, S. M. (2021). **Synthesis, Characterization of Thiazolidin-4-one, Oxazolidin-4-one and Imidazolidin-4-one Derivatives from 6-Amino-1, 3-dimethyluracil and evaluation of their Antioxidant and Antimicrobial Agent.** *Al-Qadisiyah Journal Of Pure Science*, 26(4), 59-72.
- (17) Nassar, I. F., Farargy, A. F. E., Abdelrazek, F. M., & Hamza, Z. (2020). **Synthesis of new uracil derivatives and their sugar hydrazones with potent antimicrobial, antioxidant and anticancer activities.** *Nucleosides, Nucleotides & Nucleic Acids*, 39(7), 991-1010.
- (18) Długosz-Pokorska, A., Pięta, M., Kędzia, J., Janecki, T., & Janecka, A. (2020). **New uracil analog U-332 is an inhibitor of NF-κB in 5-fluorouracil-resistant human leukemia HL-60 cell line.** *BMC Pharmacology and Toxicology*, 21(1), 1-10.
- (19) Sanduja, M., Gupta, J., Singh, H., Pagare, P. P., & Rana, A. (2020). **Uracil-coumarin based hybrid molecules as potent anti-cancer and anti-bacterial agents.** *Journal of Saudi Chemical Society*, 24(2), 251-266.
- (20) Al-Majidi, S. M., & Al-Adhami, H. J. (2016). **Synthesis and Evaluation Antibacterial Activity of Some New Substituted 5-Bromoisatin Containing Five, Six Heterocyclic Ring.** *Baghdad Science Journal*, 13(2).
- (21) Lu, G. Q., Li, X. Y., Wang, D., & Meng, F. H. (2019). **Design, synthesis and biological evaluation of novel uracil derivatives bearing 1, 2, 3-triazole moiety as thymidylate synthase (TS) inhibitors and as potential antitumor drugs.** *European journal of medicinal chemistry*, 171, 282-296.
- (22) Zhao, S., Li, K., Jin, Y., & Lin, J. (2018). **Synthesis and biological evaluation of novel 1-(aryl-aldehyde-oxime) uracil derivatives as a new class of thymidine phosphorylase inhibitors.** *European Journal of Medicinal Chemistry*, 144, 41-51.
- (23) Brel', A. K., Spasov, A. A., Lisina, S. V., Popov, S. S., Kucheryavenko, A. F., Litvinov, R. A., ... & Rashchenko, A. I. (2019). **Uracil Hydroxybenzamides as Potential Antidiabetic Prodrugs.** *Pharmaceutical Chemistry Journal*, 53, 511-515.
- (24) Al-Adhami, H., & Al-Majidi, S. M. (2021). **Synthesis, Characterization of Thiazolidin-4-one, Oxazolidin-4-one and Imidazolidin-4-one Derivatives from 6-Amino-1, 3-dimethyluracil and evaluation of their Antioxidant and Antimicrobial Agent.** *Al-Qadisiyah Journal Of Pure Science*, 26(4), 59-72.
- (25) Al-Azzawi, A. M., & Raheem, A. A. A. K. (2017). **Synthesis and antibacterial screening of new Schiff bases based on N-(4-acetophenyl) succinimide.** *Iraqi Journal of Science*, 1790-1801.

- (26) Al Khuzaie, M. G., & AL MAJIDI, A. (2019). **Synthesis and characterization of some new Pyrazolin, Triazolin and Tetrazolin derivatives of 1, 8 naphthal imide and evaluate their antimicrobial activity.** *International Journal of Pharmaceutical Research*, 11(4).
- (27) Al-Sultani, K. T., Al-Majidi, S. M., & Al-Jeilawi, O. H. (2016). **Synthesis, Identification and Evaluation Biological Activity for Some New Triazole, Triazoline and Tetrazoline Derivatives From 2-Mercapto-3-phenyl-4 (3H) Quinazolinone.** *Iraqi Journal of Science*, 57(1B), 295-308.
- (28) Al Khuzaie, M. G., & AL MAJIDI, A. (2019). **Synthesis and characterization of some new Pyrazolin, Triazolin and Tetrazolin derivatives of 1, 8 naphthal imide and evaluate their antimicrobial activity.** *International Journal of Pharmaceutical Research*, 11(4).
- (29) IBRAHIM, H., AL-MAJIDI, S. M., & AL-ISSA, Y. A. (2020). **Synthesis, and identification. of some, new N.-substituted quinazoline-. 4-one, thiazine-4-one and, tetrazoline rings, incorporating. N-ethyl-2-(benzylthio), benzimidazole acetate, and: study, their, application, as: anti-oxidant, agent.** *International Journal, of. Pharmaceutical. Research*, 12(3).
- (30) Al-Joborry, N. M., & Kubba, R. M. (2020). **Theoretical and Experimental Study for Corrosion Inhibition of Carbon Steel in Salty and Acidic Media by A New Derivative of Imidazolidine 4-One.** *Iraqi Journal of Science*, 1842-1860.
- (31) Ali, M., Ali, S., Khan, M., Rashid, U., Ahmad, M., Khan, A., ... & Latif, A. (2018). **Synthesis, biological activities, and molecular docking studies of 2-mercaptobenzimidazole based derivatives.** *Bioorganic chemistry*, 80, 472-479.
- (32) Shah, S. S., Shah, D., Khan, I., Ahmad, S., Ali, U., & Rahman, A. (2020). **Synthesis and antioxidant activities of Schiff bases and their complexes: An updated review.** *Biointerface Res. Appl. Chem*, 10, 6936-6963.
- (33) AL-Tamimi, M. B. W., & Al-Majidi, S. M. **Synthesis, identification of some new 1, 2, 4-triazole derivatives from 6-amino-1, 3-dimethyluracil and evaluation of their molecular docking, Anti-oxidant and experimental.**
- (34) Shriner, R. L., Hermann, C. K., Morrill, T. C., Curtin, D. Y., & Fuson, R. C. (2003). **The systematic identification of organic compounds.** *John Wiley & Sons*.
- (35) Kirgiz, M. S., de Sousa Galdino, A. G., Kinuthia, J., Khitab, A., Hassan, M. I. U., Khatib, J., ... & Tiwary, C. S. (2021). **Synthesis, physico-mechanical properties, material processing, and math models of novel superior materials doped flake of carbon and colloid flake of carbon.** *Journal of Materials Research and Technology*, 15, 4993-5009. <https://doi.org/10.1016/j.jmrt.2021.10.089>

/06/

EFFECT OF METHOD NANO APPLICATION WITH NPK FERTILIZER ON THE VEGETATIVE GROWTH OF TWO GRAPE CULTIVARS (VITIS VINIFERA L.)

Nabil Mohammed Ameen Alimam

Department of Horticulture and Landscape Design – College of Agriculture and Forestry – University of Mosul – Iraq

nabemo56@uomosul.edu.iq

Sarah Ahmed Mokeem Hasan

Department of Horticulture and Landscape Design – College of Agriculture and Forestry – University of Mosul – Iraq



Reception: 08/11/2022 **Acceptance:** 29/12/2022 **Publication:** 23/02/2023

Suggested citation:

A.A., Nabil Mohammed and M.H., Sarah Ahmed. (2023). **Effect of method nano application with NPK fertilizer on the vegetative growth of two grape cultivars (Vitis Vinifera L.).** *3C TIC. Cuadernos de desarrollo aplicados a las TIC*, 12(1), 118-131. <https://doi.org/10.17993/3ctic.2023.121.118-131>

ABSTRACT

This studied the effect of method's and efficiency application of nano- NPK fertilizer (0, 1 and 2. l⁻¹) in addition to the soil or foliar spray on the vegetative growth of Olivetti noier and Thompson Seedless young grapevines grown under Nineveh Governorate during 2021 season. Applications three levels of nano- NPK 0, 2 and 4gm. as soil addition either alone or in combination with foliar application of nano- NPK sprayed three times at 0, 1 and 2.l⁻¹ significantly promoted all vegetative growth traits, height and diameter of the main stem, number of leaves, chlorophyll concentration in leaves, leaf area and leaf area. Moreover, these treatments resulted of vegetative growth parameters compared with untreated (control). Result showed that fertilization with the addition of 4 gm. Nano NPK.l⁻¹, led to a significant increase in the rates of height and diameter of the main stem, number of leaves, chlorophyll concentration in leaves. Foliar fertilization with 2 gm. Nano NPK l⁻¹, led to a significant improving main stem diameter of seedling, leaf area, leaf area of seedling, chlorophyll concentration in leaves. Spray with 1 gm. Nano NPK l⁻¹ led to a significant increase in the height of the main stem and the number of leaves per seedling. Thompson Seedless grape cv. over Olivetti noier cv. in height and diameter of the main stems, leaf area and the leaf area of the seedling.

KEYWORDS

Nano, NPK, Fertilizer, Grape.

PAPER INDEX

ABSTRACT

KEYWORDS

1. INTRODUCTION

3. RESULTS AND DISCUSSION

3.1. HEIGHT OF THE MAIN STEM OF GRAPE SEEDLINGS (CM)

3.2. MAIN STEM DIAMETER (MM):

3.3. NUMBER OF LEAVES / SEEDLINGS

3.4. LEAF AREA (CM²)

3.5. THE LEAF AREA OF THE SEEDLING (CM².SEEDLING-1)

3.6. TOTAL CHLOROPHYLL IN THE LEAVES (MG.G-1F.W)

4. CONCLUSION

REFERENCES

1. INTRODUCTION

Grape was one of the oldest fruits planted by man, and commercially the most cultivated and widespread fruit crop in the world, which was mentioned in the holy books, and the cultivation of grapes in Iraq is as old as the settlement of people in Mesopotamia (Childers et al. 1995 and Alsaidi, 2014).

In recent years, a lot of studies and research have appeared that dealt with the introduction of nanotechnology in the agricultural field, which is called Agro-Nanotechnology, which has significant effects on the global economy. The nano fertilizers are characterized by having a great ability to dissolve in water in addition to the speed of penetration into the plant cell, in addition to the possibility of adding such fertilizers to the soil or spraying on the vegetative system of the plant (Chinnamuthu and Boopathi, 2009 ; Sabir et al,2014).

Fertilization is one of the horticultural process that must be performed in the nurseries and vineyard orchards in order to give the requirements of growth and development of grape vines as a result of the depletion of the nutrients necessary from the soil. Among these elements nitrogen, phosphorus and potassium are the important nutrients of the plants, (Epstein and Bloom, 2005 and Marschner, 2012).

The aim of this research to study the efficiency of nano NPK fertilization on the vegetative growth, mineral content, response of the cultivars to nano-fertilizers and determining the best way to application of nano-fertilizer of grape seedlings.

2. MATERIALS AND METHODS

The present investigation was carried out during 2021 season on two young grape cultivars including Olivetti noier and Thompson were one year old, planted at 2×3 meters apart in the grape orchard of the Department of Horticulture and Landscape - College of Agriculture and Forestry - University of Mosul - Iraq. The soil was loam soil, full description of the tested soil is given in Table 1.

Table 1. Physical and chemical properties of the experimental soil.

| Item | Value | Available nutrients | Value |
|-----------|-------|----------------------|-------|
| Sand % | 34.8 | N g.Kg ⁻¹ | 0.121 |
| Silt % | 25.45 | P g.Kg ⁻¹ | 3.01 |
| Clay % | 39.75 | K g.Kg ⁻¹ | 49.76 |
| Texture | Loam | O.M. % | 1.20 |
| E.C. ds/m | | 0.2 | |

Factorial experiment with the complete randomized block design was applied with three replicates, two young vines per each. The treatments were as follows by three factors:

The first factor: Cultivars on Olivette noire and Thompson Seedless Grape.

The second factor: Fertilization by adding nano-NPK (20:20:20) at three levels: 0, 2 and 4 gm. Young vine⁻¹

The third factor: foliar application with three concentrations of the nano-NPK at 0, 1 and 2 gm.l⁻¹ on vegetative growth till runoff.

Three levels of nano- NPK were added when the shoots reached 10 cm in the length on April 12, 2021, and the second addition was a month after the first addition. While the nano-NPK was sprayed on the vegetative growth in three times the first was on April 19, 2021, and the second spray was a month after the first and the third was a month after the second spray. Tween 80 as wetting agent was applied at 0.1% to all spray solutions and the young vines were sprayed solution till runoff and control vines were sprayed water containing Tween 80. Vegetative parameter such as height and diameter of the main stem, number of leaves / young vine, Leaf area (cm²), The leaf area of the young vine (cm². Young vine) and the total chlorophyll concentration in the leaves were measured on 1 Oct. 2021.

3. RESULTS AND DISCUSSION

3.1. HEIGHT OF THE MAIN STEM OF GRAPE SEEDLINGS (CM)

The data in Table (2) showed that the seedling height of the Thompson Seedless cv. were significantly superior (165.99cm.) compared with the Olivette noire cv. (148.50cm). It's evident from the data in the same table that the height of grape seedlings were affected by nano NPK application, especially when adding 4g.seedlings⁻¹ of nano NPK and reached 169.28cm. which provided the maximum value (169.28cm.) compared with the lowest value of height of seedling steam (156.77) in control treatment.

Table 2. Effect the method of nano application with NPK fertilizer on height of the main stem of seedlings (cm) of Olivette noire and Thompson Seedless grape cultivars.

| cultivars | Adding nano NPK (g.seedling ⁻¹) | Foliar nano NPK (mg.l ⁻¹) | | | CV. × NPK | Mean Effect of cultivar |
|--------------------------------|--|---------------------------------------|-----------|-----------|-----------------------------------|-------------------------------|
| | | 0 | 1 | 2 | | |
| Olevitte noire | 0 NPK | 139.83 f | 145.55 ef | 143.67 ef | 142.83 d | 148.50 b |
| | 2 NPK | 121.33 g | 154.17 ed | 135.33 f | 136.94 e | |
| | 4 NPK | 166.67 cd | 168.00 c | 162.50 cd | 165.72b | 165.99 a |
| Thompson Seedless | 0 NPK | 136.30 f | 229.50 a | 146.33 ef | 170.71a | |
| | 2 NPK | 135.83 f | 168.50 c | 159.00 cd | 154.44 c | |
| | 4 NPK | 139.33 f | 191.50 b | 187.67 b | 172.83 a | |
| Olevitte noire | | 142.61 ed | 155.72 c | 147.16 d | Main effect of adding nano NPK | |
| Thompson Seedless | | 137.16 e | 196.50 a | 164.33 b | | |
| Adding × Foliar nano NPK | 0 NPK | 137.16 e | 196.50 a | 164.33 b | 156.77 b | |
| | 2 NPK | 138.07 e | 187.25 a | 145.00 de | 145.69 c | |
| | 4 NPK | 128.58 f | 161.33 c | 141.17 d | 169.28 a | |
| Mean effect foliar nanoNPK | | 139.88 c | 176.11 a | 155.75 b | | |

Means with the same letter are not significantly different according to Duncan multiple ranges test at 5% level.

Spraying with 1 g.l⁻¹ of nano-NPK was significantly superior in the height of the main stem of grape seedlings, which amounted to (176.11) cm, while the control treatment gave the lowest value were (139.88cm.) for the average height of the main stem.

The data in Table (2) also indicates that the binary, especially triple, interactions between the studied factors made clear significant differences between the treatments of adding 0 nano NPK + spraying with 1gm. nano NPK. l⁻¹ for Thompson Seedless cv. was gave the highest values in the average height of the main stem and amounted to 229.50cm, which significantly outperformed all treatments, while the lowest height of the main stem was recorded when adding 2 g nano NPK. seedlings⁻¹ + spraying with 0gm. nano NPK.l⁻¹ for Olivette noire cv. which amounted to 121.33 cm.

3.2. MAIN STEM DIAMETER (MM):

It is noticed from the data of Table (3) that there are significant differences between the two grape cultivars in the main stem diameter, especially the Thompson Seedless cv. (14.67mm.) was superior than Olivette noire cv. (12.32 mm.). It is also evident from the data of the same table that addition 4gm. of nano NPK are significant superior in

the main stem diameter (14.64 mm.), than control treatment which amounted to 12.24 mm.

It is also noted that spraying with 2gm. nano NPK.l⁻¹ has a clear effect which achieved the highest significant increase in the average diameter of the main stem of grape seedlings (14.99 mm), while the control treatment recorded the lowest value for this trait, which amounted to 11.92 mm. It is also evident from the data of the same table that addition 4gm. of nano NPK are significant superior in the main stem diameter (14.64 mm.), than control treatment which amounted to 12.24 mm.

It is also noted that spraying with 2gm. nano NPK.l⁻¹ has a clear effect which achieved the highest significant increase in the average diameter of the main stem of grape seedlings (14.99 mm), while the control treatment recorded the lowest value for this trait, which amounted to 11.92 mm. It is also noted in the data of Table (4) that the interactions between the factors under this study achieved a significant increase in the average diameter of the main stem diameter of grape seedlings, especially when adding 4 gm. nano NPK + spraying with 2gm. nano NPK fertilizer for Thompson Seedless grape cv. which achieved the highest average for the main stem diameter (16.67 mm), while the comparison treatment for Olivette noire grape cv. recorded the lowest values for this trait, which amounted to (7.79 mm).

Table 3. Effect the method of nano application with NPK fertilizer on stem diameter of seedlings (mm) of Olivette noire and Thompson Seedless grape cultivars.

| Cultivars | Adding nano NPK (g.seedling ⁻¹) | Foliar nano NPK (mg.l ⁻¹) | | | CV. × NPK | Mean Effect of Cultivar |
|--------------------------------|--|---------------------------------------|-------------|----------|---|-------------------------------|
| | | 0 | 1 | 2 | | |
| Olevitte noire | 0 NPK | 7.79 f | 11.49 ed | 16.03 ab | 11.77 e | 12.32 b |
| | 2 NPK | 10.88 e | 12.38 d | 12.48 d | 11.91 e | |
| | 4 NPK | 12.46 d | 12.71 d | 14.66 cd | 13.28 c | |
| Thompson Seedless | 0 NPK | 10.76 e | 12.98 d | 14.40 c | 12.72 b | 14.67 a |
| | 2 NPK | 14.51 bc | 15.60 abc | 15.71abc | 15.27 b | |
| | 4 NPK | 15.12 abc | 16.26 a | 16.67 a | 16.01 a | |
| Olevitte noire | | 10.38 e | 12.19 d | 14.39 b | Main effect of adding nanoNPK | |
| Thompson Seedless | | 13.46 c | 14.95 ab | 15.54 a | | |
| Adding × Foliar nano NPK | 0 NPK | 9.28 e | 12.23 d | 15.22 ab | 12.24 c | |
| | 2 NPK | 12.69 d | 13.99 c | 14.09 c | 13.59 b | |
| | 4 NPK | 13.79 c | 14.48 bc | 15.66 a | 14.64 a | |
| Mean effect foliar nanoNPK | | 11.92 c | 13.57 b | 14.99 a | | |

Means with the same letter are not significantly different according to Duncan multiple ranges test at 5% level.

3.3. NUMBER OF LEAVES / SEEDLINGS

The data in Table (4) indicate the clear discrepancy in number of leaves for the two grape cultivars under study. The Olivette noire grape cv. (164.17 leaves, seedlings⁻¹) were significantly outperformed compared with Thompson Seedless grape cv. (153.06 leaves, seedlings⁻¹).

It is also noted from the data of the same table that the addition of nano-fertilizer was significantly superior to the average number of leaves per seedling for treatments 4 and 2 g. seedling⁻¹ were significantly over the comparison treatment (176.77, 176.24 and 122.81) leaves. seedling⁻¹, respectively.

Table 4. Effect the method of Nano application with NPK fertilizer on number of leaves of seedlings of Olivette noire and Thompson Seedless grape cultivars.

| Cultivars | Adding nano NPK (g.seedling ⁻¹) | Foliar nano NPK (mg.l ⁻¹) | | | CV. × NPK | Mean Effect of cultivar |
|------------------------------------|--|---------------------------------------|-----------|-----------|---|-------------------------------|
| | | 0 | 1 | 2 | | |
| Olevitte noire | 0 NPK | 100.33 jk | 121.33 h | 119.03 hi | 113.56 f | 164.17 b |
| | 2 NPK | 182.33 cd | 201.13 a | 166.66 ef | 183.37 b | |
| | 4 NPK | 187.33 bcd | 198.83 ab | 198.83 ab | 195.55 a | |
| Thompson Seedless | 0 NPK | 95.00 k | 108.16 ij | 108.16 cd | 132.06 e | 153.05 b |
| | 2 NPK | 178.83 de | 182.16 cd | 182.16 cd | 169.11 c | |
| | 4 NPK | 131.50 h | 183.50 cd | 183.30 cd | 158.00 d | |
| Olevitte noire | | 156.66 c | 174.32 a | 161.51 bc | Main effect of adding nanoNPK | |
| Thompson Seedless | | 135.11 d | 166.12 b | 157.94 c | | |
| Adding × Foliar nano NPK | 0 NPK | 97.66 e | 157.18 c | 113.60 d | 122.81 b | |
| | 2 NPK | 18.58 b | 173.73 b | 174.41 b | 176.24 a | |
| | 4 NPK | 159.41 c | 179.75 b | 191.16 a | 176.77 a | |
| Mean effect foliar nanoNPK | | 145.88 c | 170.22 a | 159.72 b | | |

Means with the same letter are not significantly different according to Duncan multiple ranges test at 5% level.

The data of Table (4) shows the significant superiority of the treatment of spraying with 1 gm. nano NPK l⁻¹ over treatments (2 and 0 gm. nano NPK. l⁻¹), as well as the superiority of the spraying treatment with 2 gm. nano NPK. l⁻¹ was significantly on the comparison treatment. The treatment of triple interaction between the factors in this study when adding 2 gm.l⁻¹ of nano NPK + spraying with 1 gm. nano NPK l⁻¹ was

significantly outperformed most of the treatments, which amounted to 201.13 leaves. seedlings⁻¹, while the treatment of adding zero gm.seedling⁻¹ of nano fertilizer for Thompson Seedless grape cultivar recorded the lowest values for the average number of leaves, which amounted to 95.00 leaves. Seedlings⁻¹.

3.4. LEAF AREA (CM²)

It is evident from the data of Table (5) that Thompson Seedless cv. was significantly outperformed the average leaf area (101.10 cm².leaf⁻¹) over the Olivette noire cv. (66.69 cm².leaf⁻¹). It is noted from the data of the same table showed that the addition of nano NPK fertilizer had a clear effect on increasing the leaf area, as the treatment of adding 2 gm. nano NPK. Seedlings⁻¹ was significantly (90.15 gm. leaf⁻¹) over the comparison treatment (73.30 gm. leaf⁻¹).

Table 5. Effect the method of nano application with NPK fertilizer on leaf area (cm²) of Olivette noire and Thompson Seedless grape cultivars.

| Cultivars | Adding nano NPK (g.seedling ⁻¹) | Foliar nano NPK (mg.l ⁻¹) | | | CV. × NPK | Mean Effect of Cultivar |
|--------------------------------|--|---------------------------------------|-----------|----------|----------------------------------|-------------------------------|
| | | 0 | 1 | 2 | | |
| Olevitte noire | 0 NPK | 29.82 j | 62.83 ghi | 66.68 gh | 53.11 e | 66.69 b |
| | 2 NPK | 57.04 hi | 78.17 ef | 84.52 ed | 73.24 d | |
| | 4 NPK | 63.28 ghi | 88.31 de | 69.50 fg | 73.69 d | |
| Thompson Seedless | 0 NPK | 54.47 i | 87.83 de | 138.18 a | 93.49 c | 101.10 a |
| | 2 NPK | 125.10 b | 102.27 c | 93.82 cd | 107.06 a | |
| | 4 NPK | 93.43 cd | 92.98 cd | 121.78 b | 102.73 b | |
| Olevitte noire | | 50.05 d | 76.43 c | 73.57 c | Main effect of adding nanoNPK | |
| Thompson Seedless | | 91.00 c | 94.36 b | 117.93 a | | |
| Adding × Foliar nano NPK | 0 NPK | 42.14 d | 75.33 c | 102.43 a | 73.30 b | |
| | 2 NPK | 91.07 b | 90.22 b | 89.17 b | 90.15 a | |
| | 4 NPK | 78.36 c | 90.65 b | 95.64 b | 88.21 a | |
| Mean effect foliar nanoNPK | | 70.52 c | 85.40 b | 95.75 a | | |

Means with the same letter are not significantly different according to Duncan multiple ranges test at 5% level.

The data of Table (6) also showed that spraying with 2 gm.l⁻¹ nano NPK fertilizer (95.71 cm².leaf⁻¹) had a significantly increase in the leaf area compared with the other treatments. In addition to the significant superiority of spraying at a concentration of 1 gm nano NPK.l⁻¹ over the control treatment (70.52 cm².leaf⁻¹).

The triple interactions between the factors studied in Table (5), it is also showed that the addition 0 gm. seedling⁻¹ of nano NPK + foliar spray with 2 gm. l⁻¹ of the same

fertilizer for Thompson Seedless cv. ($138.18 \text{ cm}^2.\text{leaf}^{-1}$) was significantly superior to all treatments, while the comparison treatment of Olivette noire cv. was recorded the lowest values ($29.82 \text{ cm}^2.\text{leaf}^{-1}$) for this trait.

3.5. THE LEAF AREA OF THE SEEDLING ($\text{CM}^2.\text{SEEDLING}^{-1}$)

The data in Table (6) indicates that Thompson Seedless cv. ($15657.2 \text{ cm}^2.\text{seedling}^{-1}$) was significantly superior to the Olivette noire cv. in the seedling leaf area which reached $11345.2 \text{ cm}^2.\text{seedling}^{-1}$. It is noted from the data of the same table that the addition of $2 \text{ gm}.\text{seedling}^{-1}$ of nano NPK fertilizer ($15764.8 \text{ cm}^2.\text{seedling}^{-1}$) achieved a significant superiority over the control treatment ($9276.0 \text{ cm}^2.\text{seedling}^{-1}$).

Spraying at a concentration of $2 \text{ gm}.\text{l}^{-1}$ of nano NPK fertilizer on caused a significant increase in the seedling leaf area ($15036.3 \text{ cm}^2.\text{seedling}^{-1}$) compared to the treatment of $0 \text{ gm}.\text{l}^{-1}$ of nano fertilizer ($10845.4 \text{ cm}^2.\text{seedlings}^{-1}$).

Table 6. Effect the method of nano application with NPK fertilizer on seedling leaf area ($\text{cm}^2.\text{seedling}^{-1}$) of Olivette noire and Thompson Seedless grape cultivars.

| Cultivars | Adding nano NPK (g.seedling ⁻¹) | Foliar nano NPK (mg.l ⁻¹) | | | CV. × NPK | Mean Effect of cultivar |
|-----------------------------|--|---------------------------------------|------------|------------|-----------------------------|-------------------------------|
| | | 0 | 1 | 2 | | |
| Olevitte noire | 0 NPK | 2996.0 k | 7619.7 i | 7920.3 i | 53.11 e | 11345.2 b |
| | 2 NPK | 10392.3 h | 15731.0 cd | 14089.7de | 73.24 d | |
| | 4 NPK | 11860.3 gh | 17706.3 b | 13791.3 ef | 73.69 d | |
| Thompson Seedless | 0 NPK | 5186.0 j | 16946.3 bc | 14987.7 de | 93.49 c | 15657.2 a |
| | 2 NPK | 22353.3 a | 14941.7 de | 17080.7 bc | 107.06 a | |
| | 4 NPK | 12284.3 fg | 14786.7 de | 22348.3 a | 102.73 b | |
| Olevitte noire | | 8416.2 e | 13685.7 c | 11933.8 d | Main | |
| Thompson Seedless | | 13274.6 c | 15558.2 b | 18138.9 a | effect of adding nanoNPK | |
| Adding × Foliar nano NPK | 0 NPK | 4091.0 d | 12283.0 c | 11454.0 c | 9276.0 b | |
| | 2 NPK | 16372.8 b | 15336.3 b | 15585.2 b | 15764.8 a | |
| | 4 NPK | 12072.3 c | 16246.5 b | 18069.8 a | 15462.9 a | |
| Mean effect foliar nanoNPK | | 10845.4 b | 14621.9 a | 15036.3 a | | |

Means with the same letter are not significantly different according to Duncan multiple ranges test at 5% level.

Studying the effect of the triple interaction between the studied factors, it is clear showed the data in Table (7) that the treatment of adding $4 \text{ gm}.\text{ nano NPK}.\text{ seedlings}^{-1}$ + spraying with $2 \text{ gm}.\text{ nano NPK}.\text{l}^{-1}$ for Thompson Seedless grape cultivar gave the highest values for seedling leaf area ($22348.3 \text{ cm}^2.\text{seedling}^{-1}$), which was significantly

superior to all treatments, while the comparison treatment of grape cultivar olivette noire (2996.0 cm².seedling⁻¹) recorded the lowest values for this trait.

3.6. TOTAL CHLOROPHYLL IN THE LEAVES (MG.G⁻¹F.W)

The results presented in Table (7) showed that there weren't any different between the cultivars in the total chlorophyll content of the leaves in this study. However, fertilization with 4gm.nano NPK.seedling⁻¹ gave the highest value of chlorophyll content 1.31 mg.g⁻¹F.W which surpassed significantly compared with the addition of 0 nano NPK.seedling⁻¹. The lowest value of chlorophyll content was 0.934 mg.g⁻¹ F.W.

Table 7. Effect the method of nano application with NPK fertilizer on total chlorophyll in leaves (mg.g⁻¹F.W) of Olivette noire and Thompson Seedless grape cultivars.

| Cultivars | Adding nano NPK (g.seedling ⁻¹) | Foliar nano NPK (mg.l ⁻¹) | | | CV. × NPK | Mean Effect of cultivar |
|-----------------------------|--|---------------------------------------|-----------|---------|---|-------------------------------|
| | | 0 | 1 | 2 | | |
| Olevitte noire | 0 NPK | 0.81 b | 0.92 b | 0.96 b | 0.90 a | 1.02 a |
| | 2 NPK | 0.86 b | 0.98 b | 1.06 b | 0.97 a | |
| | 4 NPK | 0.98 b | 1.2400 ab | 1.37 ab | 1.19 a | |
| Thompson Seedless | 0 NPK | 0.93 b | 0.98 b | 0.99 b | 0.96 a | 1.18a |
| | 2 NPK | 0.95 b | 1.26 ab | 1.29 ab | 1.17 a | |
| | 4 NPK | 1.03 b | 1.45 ab | 1.77 a | 1.42 a | |
| Olevitte noire | | 0.88 b | 1.05 ab | 1.13 ab | Main effect of adding nanoNPK | |
| Thompson Seedless | | 0.97ab | 1.23 ab | 1.35 a | | |
| Adding × Foliar nano NPK | 0 NPK | 0.87 b | 0.95 b | 0.97 b | 0.93 b | |
| | 2 NPK | 0.90 b | 1.12 ab | 1.17ab | 1.07 ab | |
| | 4 NPK | 1.00 b | 1.34ab | 1.57a | 1.31 a | |
| Mean effect foliar nanoNPK | | 0.92 b | 1.14 ab | 1.24 a | | |

Means with the same letter are not significantly different according to Duncan multiple ranges test at 5% level.

Foliar application of 2gm.l⁻¹ nano-NPK was a significant increases in leaf chlorophyll content giving the highest significant value of 1.242 mg.g⁻¹ F.W compared to the lowest value of chlorophyll content was shown in the control treatment of 0.928 mg.g⁻¹ F.W.

Regarding the interactions between all factors, the results showed a combination of fertilization with 4gm nano-NPK.seedling⁻¹ + spraying with 2gm.l⁻¹ nano-NPK.l⁻¹ with Thompson Seedless cv. was reached 1.77 mg.g⁻¹ F.W and gave the highest content of

chlorophyll compared with control treatment, which gave the lowest value 0.813 mg. g⁻¹ F.W. for the total chlorophyll concentration in the leaves.

It is clear from the data of the results that the cultivar has a major role in the vegetative growth characteristics of grape seedlings (young vines). This variation is due to the genetic factor between the cultivars and according to their strength and the efficiency of the biological processes that take place in each cultivar, especially the variation of the genetic structures of each cultivar and the extent of their interaction with the different environmental conditions and fertilizer treatments, which works to vary the efficiency of the photosynthesis process and the use of its products in the growth processes and increase the vegetative growth of seedlings of different grape cultivars (Alimam, 1998; Mangel and Kirkby, 2001; Hopkins and Huner 2004 and Aljubori et al., 2022).

Through the study of the effect of nano NPK fertilizer on increasing the vegetative growth of grape seedlings shown in Tables (2,3,4,5,6 and 7), the efficiency of the surfaces of particles in ion exchange of nano fertilizer increases the chances of the absorption of nutrients by the root and vegetative systems and high speed of nanoparticles in the leaves of seedlings to meet the requirements of vegetative growth by increasing enzymatic activity and speed of reactions (Morteza et al., 2013 and Aljubori et al., 2022).

Nitrogen increases the vitality and activity of the meristem areas of seedlings by increasing the biosynthesis of auxins, amino acids, nucleic acids, chlorophyll, and many enzymatic facilities that increase the efficiency and elongation of cell divisions for different plant organs, in addition to the role of physiology of phosphorous in increasing vegetative growth, which includes its entry into vital energy compounds, especially phospholipids and nucleic acids and its role in building cell membranes that have a major role in increasing the activity and effectiveness of seedlings to carry out photosynthesis, respiration that lead to increase seedling height, diameter, number of leaves.

In addition to the physiological role of potassium in the processes of regulating the osmotic effort of cells and its clear role in increasing and activating enzymes related to photosynthesis (Yasin, 2001, Taiz and Zeiger 2001, and Marschner, 2003 and Aljubori et al., 2022) and that all these roles of nutrients were reflected in increasing the vegetative growth of grape seedlings (Alimam and Alsaidi, 2003; Cheng et al. 2010; Barad et al. 2010 and Aljubori, et al., 2022).

Although the foliar spraying of major nutrients such as nitrogen, phosphorous and potassium as a method is highly efficient in absorbing these elements through spraying techniques with nano-fertilizers. Which increasing the efficiency of absorption of major nutrients, which resulted in the response of grape seedlings in increasing vegetative growth spraying with nano-fertilizers (Mengel and Kirkby,2001and Alimam, and Al-Qasim, 2022).

4. CONCLUSION

The results of this study showed that the cultivar had a clear role in the average height and diameter of the main stem of the seedling, the area of one leaf and the leaf area of the seedling, especially for the grape cultivar Thompson Seedless, compared with the Olivette noire cv.. The addition of nano NPK fertilizer at 4g.seedlings⁻¹ or foliar spraying with 2g.l⁻¹ with nano NPK fertilizer singly or overlap with each other caused a significant increase in the rates of length and diameter of the main stem of seedlings, leaf area of seedlings, chlorophyll and protein content in leaves and carbohydrate in branches and the concentration of nutrients nitrogen, phosphorous and potassium in the petioles of the leaves.

REFERENCES

- (1) Al-Imam, N. M. (1998). **Effect of foliar application of iron, zinc and compound fertilizer (NPK) on growth and yield of Halwani Lebanon and Kamali Grape Cultivars (*Vitis vinifera* L.)**. Ph. D. Thesis. College of Agriculture and Forestry. University of Mosul. Iraq.
- (2) Aljubori, Y.M.S.;N.M.A. Alimam and S.M.AL-Atrushy (2022). **Effect of nano and chemical fertilization with NPK and chelated zinc on vegetative growth of Taifi and Kamali grape cultivars**. *Iraqi J. of Agric.Sci. (IJAS)*, 55(3), 1-10.
- (3) Alimam, N. M. A. (2003). **Effect of boliar application of iron and NPK fertilization on flowering, setting and vegetative growth of halwani lubnan and kamali grape cultivars (vitis vinifera)**. *Damascus university journal for the agricultural sciences*, (19)2, 131-148.
- (4) Alimam, N. M. A. A., & Al-Qasim, M. G. S. (2022). **The effect of compound fertilizer (NPK) and gibberellic acid on the growth of two transplants grape cultivars Zarik and Thompson seedless (*Vitis vinifera* L.)**. *Journal of Genetic and Environmental Resources Conservation*, 10(2), 138-145.
- (5) Al-Saeedi, I. H. M. (2014). **Grapes Classification**. Dar Al-Wadah Publishing and Ishtar for Cultural Investments, The Hashemite Kingdom of Jordan, Amman.
- (6) Barad, A. V., Nandre, B. M., & Sonwalkar, N. H. (2010). **Effect of NPK levels on gerbera cv. Sangria under net house conditions**. *Indian Journal of Horticulture*, 67(3), 421-424.
- (7) Cheng, L., Fuchigami, L. H., & Breen, P. J. (2000). **Light absorption and partitioning in relation to nitrogen content inFuji'apple leaves**. *Journal of the American Society for Horticultural Science*, 125(5), 581-587.
- (8) Childers, N. F., Morris, J. R., & Sibbett, G. S. (1995). **Modern fruit science. Orchard and small fruit culture**. *Modern fruit science. Orchard and small fruit culture*, (Ed. 10).
- (9) Chinnamuthu, C. R., & Boopathi, P. M. (2009). **Nanotechnology and agroecosystem**. *Madras Agricultural Journal*, 96(1/6), 17-31.
- (10) Epstein, E. and A.J. Bloom. (2005). **Mineral Nutrition of Plants: Principles and Perspectives**. Sunderland, MA: Sinauer Associates.
- (11) Hopkins, W. G. & N. P. A. Hüner. (2004). **Introduction of plant physiology**. 3rd Edition. John Wiley & Sons, Inc. U.S.A.

- (12) Marschner, H., P. Marschner. (2012). **Marschner's Mineral nutrition of higher plants**. *Third edition, Elsevier/Academic Press, Amsterdam*, 651.
- (13) Mengel, K., Kirkby, E. A., Kosegarten, H., & Appel, T. (2001). **Principles of plant nutrition**. *Edition Kluwer academic publishers*, 51-52.
- (14) Morteza, E., Moaveni, P., Farahani, H. A., & Kiyani, M. (2013). **Study of photosynthetic pigments changes of maize (*Zea mays* L.) under nano TiO₂ spraying at various growth stages**. *SpringerPlus*, 2, 1-5.
- (15) Sidra Sabir, Muhammad Arshad, Sunbal Khalil Chaudhari. (2014). **Zinc Oxide Nanoparticles for Revolutionizing Agriculture: Synthesis and Applications**. *The Scientific World Journal*, 2014, 8 pages, Article ID 925494. <https://doi.org/10.1155/2014/925494>
- (16) Taiz, L. and E. Zeiger. (2010). **Plant physiology**. *Sinaure Associates. Inc. Publishers. Sunderland*.
- (17) Yassin, B. T. (2001). **Fundamentals of plant physiology**. *Qatar University - Doha*.

/07/

ANALYSIS OF THE IMPACT OF LAKE ENVIRONMENTAL WATER POLLUTION ON THE HEALTH OF OUTDOOR SWIMMERS BASED ON STIRPAT ENVIRONMENTAL IMPACT ASSESSMENT MODEL

Xiaogang Gong*

Information and Communication Branch of State Grid Zhejiang Electric Power Co.,
Hangzhou, Zhejiang, 310000, China

gongxiaogang@foxmail.com

Xinyu Wu

Information and Communication Branch of State Grid Zhejiang Electric Power Co.,
Hangzhou, Zhejiang, 310000, China

Xuxiang Zhou

Information and Communication Branch of State Grid Zhejiang Electric Power Co.,
Hangzhou, Zhejiang, 310000, China



Reception: 14/11/2022 **Acceptance:** 16/01/2023 **Publication:** 02/03/2023

Suggested citation:

G., Xiaogang, W., Xinyu and Z. Xuxiang. (2023). **Analysis of the impact of lake environmental water pollution on the health of outdoor swimmers based on STIRPAT environmental impact assessment model.** *3C TIC. Cuadernos de desarrollo aplicados a las TIC*, 12(1), 132-150. <https://doi.org/10.17993/3ctic.2023.121.132-150>

ABSTRACT

With the continuous development of China's economy, outdoor swimming has become an indispensable sport for Chinese people thereupon. However, the pollution of the outdoor water environment is capable of directly affecting the physical health of outdoor swimming lovers. Given the above, this paper uses the Stochastic Impacts by Regression on Population, Affluence, and Technology (STIRPAT) model to analyze the environmental water pollution of lakes and study the influencing factors and degree of physical health of outdoor swimming crowds. Moreover, this paper also identifies the causes of water pollution in two respects, namely water pollution and human pollution and analyzes from the perspectives of water quality monitoring environment survey and questionnaire survey. The results show that the primary factors affecting water quality contain weather, swimming crowd density and environmental pollution around water areas, lake waters have direct and indirect effects on human health, and the incidence of eye inflammation, itchy skin, stuffy nose, sore throat, stomachache, nausea, earache, diarrhea, fever and vomiting are 36.4%, 30.3%, 29.5%, 26.5%, 21.2%, 20.1%, 20.1%, 17.0%, 14.8% and 12.9% respectively.

KEYWORDS

Water environment pollution; Outdoor swimming; Sports crowd; Influence study; Water quality monitoring.

PAPER INDEX

ABSTRACT

KEYWORDS

1. INTRODUCTION
 2. MATHEMATICAL MODELS AND DATA SOURCES
 - 2.1. STIRPAT model
 - 2.2. Data sources
 3. CHARACTERISTICS AND CAUSES OF WATER POLLUTION
 - 3.1. Characteristics of water environment pollution
 - 3.2. Analysis of causes of water environment pollution
 - 3.2.1. Water pollution
 - 3.2.2. Human pollution
 4. RESULTS AND ANALYSIS
 - 4.1. Water quality monitoring and environmental survey results
 - 4.1.1. Water quality monitoring methods
 - 4.1.2. Environmental survey results
 - 4.2. Questionnaire survey and results
 - 4.2.1. Questionnaire survey method
 - 4.2.2. Influence on the Health of the swimming population
 - 4.2.3. Logistic regression analysis of risk factors affecting the health status of the swimming population
 5. DISCUSSION
 6. CONCLUSION
 7. DATA AVAILABILITY STATEMENT
 8. CONFLICT OF INTEREST
- REFERENCES

1. INTRODUCTION

With the continuous progress of science and technology, the ability of human beings to intervene in nature is getting stronger and stronger. The natural environment on which human beings depend for survival and development is also under enormous pressure [1]. Various activities of human society discharge pollutants into the environment, which not only seriously threaten human health, cause property loss, but also damage the environmental resources themselves [2-3].

In recent years, the number of environmental pollution damages caused by water pollution has risen sharply [4-5]. Such as the cadmium pollution incident in Beijing, Guangdong in December 2005, the arsenic pollution incident in Yueyang, Hunan in September 2006, the arsenic pollution incident in Yangzonghai in September 2008, the Yancheng pollution incident in Jiangsu in February 2009, and the arsenic pollution incident in July 2010. Zijin Mining Pollution Incident and Dalian Oil Spill Incident [6-7].

According to reports from the State Environmental Protection Administration system, yearbooks, journals, literature and online media, between 2005 and 2010, 95 major environmental pollution accidents were committed. Water pollution incidents caused by pollutant discharge have become an important type of accident that causes damage to the water environment [8-9].

In recent years, a large number of scholars at home and abroad have carried out related research on water environment pollution. Literature [10] has some innovations in the overall theory of water environmental pollution. They break the traditional way of thinking about water governance and use the theory of sustainable development to explore new water pollution management models. They believe that achieving effective protection and sustainable development is the focus of water pollution control and improvement. They pointed out that to achieve water pollution control, we must carry out the overall system and institutional innovation. Literature [11] and [12] put forward the following viewpoints from the perspective of comprehensive management: they believe that the management of water environment pollution is an important part of human production activities. Comprehensive treatment is the most powerful weapon for water pollution control. Literature [13] introduced the market governance method into the process of water environment governance, emphasizing the coordinated governance of various departments. Emission trading theory is a theoretical development in the process of water environment pollution control. In terms of governance methods, the literature [14] and [15] creatively put forward a new concept. He believed that the previous water environment pollution control was an all-powerful government-style governance. In the process of water pollution control, the role of market participation has been emphasized. The main role of the people is emphasized here, and it is hoped that the public can actively participate in water pollution control. Literature [16] focuses more on the idea that the government guides the whole society to govern, and believes that the degree of cooperation and coordination between all parties in the society is an important factor affecting the realization of high efficiency. References [17] and [18] believe that a government, market, enterprises, farmers and social organizations can be constructed to participate in the network governance mechanism of water pollution. Reference [19]

introduces an environmental penalty function based on the evolutionary game model analysis. Using this model, the distribution of water pollution loads in the Zarjub River in northern Iran was analyzed. Reference [20] analyzes the influencing factors of rural water pollution from the legal level. They argue that there is a Chinese rural water pollution legislation dependent on the cities. References [21] and [22] compared the investment in urban and rural environmental pollution control in 2013, and found that the focus of water environmental pollution control is in cities, while the rural water environment pollution control lacks investment. The study also shows that the uneven distribution of urban and rural areas leads to significant differences in the effects of urban and rural water pollution control. Literature [23], from the perspective of urban development, believes that the acceleration of urbanization has changed the quality and spatial distribution of water resources. Reference [24] took Hanji Township, Hubei Province as a case study object, and tested the water quality of Hanji Township. The main causes of water pollution are agricultural pollution, industrial pollution, domestic sewage, and waste pollution. Finally, the management countermeasures and suggestions are put forward. Reference [25] focuses on the current situation of rural drainage facilities and proposes that the lack of rural drainage facilities leads to improper sewage treatment, resulting in serious damage to the rural water environment. Reference [26] starts from the institutional mechanism of rural water environmental protection and proposes that the current rural water environmental protection mechanism has gradually become rigid. Reference [27] starts with the current situation of rural residents' understanding of water law and finds that rural residents lack access to knowledge of water law. It can be seen that scholars from all over the world regard water environment pollution as a major problem that affects the sustainable development of society and economy and affects people's life and health. Therefore, while promoting social and economic development, we must also do a good job in the protection of the water environment. This has become an important theme of economic development and reform in the new era [28-30].

With the rapid development of China's economy, people pay more and more attention to the spiritual world. Outdoor sports have become indispensable sport for the Chinese people. Outdoor swimming is especially sought after by outdoor sports enthusiasts. Therefore, whether the water environment is polluted or not will directly affect the health of outdoor swimming enthusiasts. This paper takes the water environment of a suburban lake in a city in China as an example to study the impact of typical water environment pollution on outdoor tourism and sports people. The purpose is to analyze the pollution of the lake water environment in the suburbs of a city and to study the impact on the outdoor swimming population after the water environment is polluted.

2. MATHEMATICAL MODELS AND DATA SOURCES

In studying the influencing factors of water environmental pollution, some researchers use different models to demonstrate. Different scholars have analyzed the influencing factors and their degree of influence. In recent years, the research on the STIRPAT model has become more and more extensive, and it is mainly applied to

environmental problems caused by carbon emissions and energy consumption. In the research on water environment pollution, some scholars have used the STIRPAT model to analyze the influence factors and degree of influence of water environment pollution on the health of the outdoor swimming population.

2.1. STIRPAT MODEL

The STIRPAT model refers to an extensible and random environmental impact assessment model. This paper will use this model in the subsequent empirical analysis to empirically analyze the environmental pollution of lakes in the suburbs of a city, the factors that affect the health of outdoor swimming people and their degree of influence. The STIRPAT model is an extension of the IPAT model. The initial form of the model can be expressed as:

$$I = P \times A \times T \quad (1)$$

In the above formula, I is the environmental pressure, P is the number of swimmers, A is the wealth of a city, and T is the technological progress.

The model believes that the environmental pressure I is determined by the scale of the number of swimmers P , the affluence of a city A , and technological progress T . Due to the limitations of this model in the application, many scholars have modified the nonlinear regression model STIRPAT model obtained by the IPAT model. The standard form of the model can be expressed as:

$$I = aP^bA^cT^de \quad (2)$$

The above formula, I, P, A and T respectively represent the same meaning as formula (1), a, b, c and d the model influence coefficient and the index of each variable respectively, e is the random error term. In practical applications, to reduce the influence of heteroscedasticity, logarithm processing is performed on both sides of the formula (2). To facilitate the expression of each coefficient, it is expressed by β . After processing, a linear model is obtained. The linear model can be expressed as:

$$\ln I = \beta_0 + \beta_1 \ln P + \beta_2 \ln A + \beta_3 \ln T + e \quad (3)$$

The above linear model was used to realize the analysis of factors affecting the health of the outdoor swimming population by water environment pollution.

2.2. DATA SOURCES

Water pollution is mainly caused by population growth, rapid social and economic development, and accelerated urbanization [31]. To comprehensively study the influencing factors and degree of influence of China's water environment pollution, this paper adds industrial structure, water consumption structure, urbanization and other indicators based on formula (3), so formula (3) is further extended to formula (4), that is, the extended linear regression equation of the STIRPAT model can be expressed as:

$$\ln I = \beta_0 + \beta_1 \ln P + \beta_2 \ln A + \beta_3 \ln T + \beta_4 \ln ur + \beta_5 \ln st + \beta_6 \ln cs \quad (4)$$

Formula (4), I is the water environment quality. In this paper, the total amount of wastewater discharge, COD value and ammonia nitrogen discharge is used as water pollution indicators; P is the population size; A is the wealth level, expressed by per capita GDP; T is the technical level, expressed by the intensity of wastewater discharge; ur is the urbanization rate, expressed by the proportion of the urban population to the total population; st is the water consumption structure, expressed by the proportion of domestic water consumption to total water; cs is the industrial structure, expressed by the industrial output value Expressed as a percentage of GDP.

When China studies water pollution, the main statistical indicators include total wastewater discharge, COD discharge and ammonia nitrogen discharge [32]. According to the research on water environment pollution by Chinese scholars, this paper uses the total amount of wastewater discharge, COD discharge, and ammonia nitrogen discharge as indicators to measure China's water environment pollution, and conducts model test analysis with various water environment pollution factors. The degree of influence of environmental pollution factors on water pollution [33]. The water environment pollution evaluation index system is shown in Table 1.

Table 1. Evaluation index system of water environment pollution

| Criterion layer | Indicator layer | Interpretation of indicators |
|------------------------------|--|--|
| Outdoor swimmers on the rise | Number of people swimming outdoors (P) | Minimum number of swimmers |
| Socioeconomic development | Urban affluence (A) | GDP per capita |
| | Technique level (T) | Wastewater discharge intensity |
| | Urbanization rate (ur) | The proportion of the number of swimmers to the total number of people |
| | Industrial structure (cs) | Industrial output as a share of GDP |
| Swimmers swimming habits | Swimming habits (st) | The proportion of domestic water consumption in total water |

The data comes from the 2009-2018 "China Statistical Yearbook", "China Environmental Statistical Yearbook" and the statistical yearbooks of various provinces, municipalities and autonomous regions.

3. CHARACTERISTICS AND CAUSES OF WATER POLLUTION

3.1. CHARACTERISTICS OF WATER ENVIRONMENT POLLUTION

The water pollutants in the lake area in the suburbs of a city are mainly phosphorus and nitrogen indicators. Judging from the monitoring results of the four factors of total phosphorus, total nitrogen, transparency and PH value, which are the evaluation indicators of the nutritional status of the lake, the lake water in the suburban lake area of a certain city is still in a state of eutrophication, with the appearance of periodic intensive growth of aquatic plants and peculiar smell in the water body, resulting in the deterioration of the lake water environment quality in the suburban lake area of a city and affecting the landscape of the lake area [34]. In terms of time distribution, the pollution degree in the suburban lake area of a certain city has strong regularity, and it mostly occurs between May and July every year, in terms of spatial distribution, artificial lakeshore areas are the main areas.

3.2. ANALYSIS OF CAUSES OF WATER ENVIRONMENT POLLUTION

3.2.1. WATER POLLUTION

Water eutrophication is a phenomenon of water pollution caused by excessive nitrogen, phosphorus and other nutrients in the water body. Crazy growth destroys the flow of material and energy in the system and gradually deteriorates the water ecosystem.

In the water body of a suburban lake area of a city, the external input of nutrient salts and the release of nutrients in the bottom of the lake area are important factors that cause the water quality in the lake area on the outskirts of a city to show a rich state, and at the same time, the eutrophication of natural water bodies is related to the changes in physical factors such as light, temperature, and dissolved oxygen [35].

The water in a lake area in the suburbs of a city is eutrophic, which mostly occurs from May to July every year (usually during stratification in summer). At this time, there is sufficient sunshine and the highest ambient temperature during the day is generally maintained in the range of 25°C-33°C, basically meeting the external climatic conditions of water eutrophication.

Nutrients such as phosphorus, nitrogen, etc. in the lake water body mainly come from the following aspects:

(1) The phosphorus released by the dead aquatic organisms and the decaying rhizomes of aquatic plants in the lake, and its humus is deposited on the bottom of the water, resulting in the enrichment of nutrients, and released under specific environmental conditions, resulting in the water quality of the lake area is rich in nutrients, this phenomenon is especially directly affected by phosphorus. In the water body of a lake area on the outskirts of a city, the change in phosphorus content will directly dominate the production of a certain type or several types of aquatic plants, and when phosphorus is the limiting factor, the increase of phosphorus will create favorable conditions for the large reproduction of aquatic organisms such as aquatic plants, directly affecting the degree of eutrophication of water quality [36].

(2) The mass reproduction and death of aquatic organisms such as aquatic plants will consume a large amount of oxygen in the water body, resulting in further deterioration of water quality. The decrease of dissolved oxygen in various water layers in the lake area was significantly related to the increase in total phosphorus content. Nutrients at all levels in the lake will release nitrogen and phosphorus when they secrete, excrete, and transform and release organic matter, which is also the source of nutrients. During the transformation and release of organic matter, at the same time as bacteria decompose them, it is returned to water bodies and sediments to be released under specific environmental conditions. The faster the aquatic plants reproduce and the more vigorous the activity, the more they will promote the release of nitrogen and phosphorus in the substrate.

(3) The supply of lakes and lakes in the suburbs of a city mainly comes from the surface water in the suburbs of a city, and the water also contains excess nitrogen, which mainly comes from the excessive application of fertilizers, agricultural wastes and domestic pollutants in agricultural production. Surface water mainly exists in the form of phosphate [37].

(4) Some tourists have uncivilized travel habits. Tourists throw bait and garbage into the lake area at will and artificially add phosphorus and nitrogen to the lake area.

3.2.2. HUMAN POLLUTION

Pollution is caused by the swimmer's secretions, excrement, etc. to the water body when swimming. In addition, it also includes that after people with certain infectious diseases or bacteria (viruses) enter the swimming pool, pathogenic factors are brought into the swimming pool, mainly from the digestive tract and body surface of the swimmer. Such as saliva, sweat, urine, tears and other secretions and excretions. The specific sources are the following:

(1) Urinary leakage occurs when the bladder contracts involuntarily due to cold contraction, and the amount of urine leakage for adults is generally 50ml. According to the survey, those who urinate during swimming account for about 3.5~5.0% of the swimmers, that is, one person urinates for every 20 swimmers. The more swimmers in the pool, the higher the urination rate, so urine is one of the main sources of swimming pool water pollution [38-39].

(2) Swimmers spit the water from the entrance into the pool together with saliva from time to time when swimming. The saliva may contain pathogenic bacteria or viruses, thus causing the pollution of the swimming pool water quality.

(3) Sweat is also a source of pool water pollution. According to Japan's Liuye report, the average person sweats 100ml/h when swimming in summer, and the amount of sweat increase with the increase of exercise. Although the amount of tear and other secretions is small, because there are often a variety of pathogenic factors such as germs and viruses in these secretions, it is also an important factor in polluting the water environment.

(4) In addition, the CO₂ in the exhaled breath of the swimmer, together with the secretions and excrement of the human body, can change the PH value of the water quality in the water environment, thus affecting the sanitation of the water quality.

4. RESULTS AND ANALYSIS

To analyze the impact of water environmental pollution on the outdoor swimming population, this paper conducted a water quality test on the lake waters in the suburbs of a city and investigated the waters and the surrounding environment. At the same time, the outdoor swimming population was divided into a swimming group and a non-swimming group, and a questionnaire survey and statistical analysis were carried out for these two groups.

4.1. WATER QUALITY MONITORING AND ENVIRONMENTAL SURVEY RESULTS

4.1.1. WATER QUALITY MONITORING METHODS

According to the "Technical Regulations for Lake Water Environment Monitoring" (2002), 3 monitoring points are set up in the suburban lake waters, among which monitoring point 1 is a peripheral point susceptible to pollution, monitoring point 2 is a crowded area, and monitoring point 3 is a less polluted area. In deep water points, 2 parallel samples were collected from each monitoring point. From 3 to 5 pm from May 28 to June 3, 2021, by GB 17378.4-1998 "Lake Monitoring Specification Part 4: Lake Water Analysis", sampling and microbial and physical index analysis was carried out, using C200 type automatic water quality analysis Instrument for general chemical index analysis. Detection indicators include fecal coliforms, color, transparency, PH, dissolved oxygen, salinity, floating matter and chemical oxygen consumption (COD).

4.1.2. ENVIRONMENTAL SURVEY RESULTS

There is basically no industrial and agricultural sewage discharge near the lakes in the suburbs of a city, and there is scattered non-point source pollution, which is mainly

caused by the domestic garbage brought by restaurants and tourists washed by rainwater. Therefore, changes in weather conditions and the number of tourists are the main reasons for the changes in pollutant discharge. The maximum number of people during the investigation period is 500-800 person-times, and the minimum is 100-200 person-times. 42 lake water samples were collected, and the lake water chromaticity was normal. The chromaticity of monitoring points 1, 2, and 3 were (15.00 ± 3.90) , (14.28 ± 1.20) , and (11.42 ± 1.45) NTU, from near-land point to deep water. The point gradually becomes smaller; the PH value is 8.01~8.10; the salinity is 31‰~33‰; the transparency is >30cm, the water temperature is normal, and there is no thermal pollution source around. Table 2 shows the water quality test results of each monitoring point in the suburban lakes of a city.

Table 2. The water quality test results of each monitoring point in the suburban lakes of a city

| Monitoring points | PH value | Chroma (NTU) | Dissolved oxygen (mg/L) | Nitrate nitrogen (mg/L) | COD (mg/L) | Inorganic nitrogen (mg/L) | Fecal coliforms (pcs/L) |
|--------------------|-----------------|------------------|-------------------------|-------------------------|-----------------|---------------------------|-------------------------|
| Monitoring points1 | 8.10 ± 0.08 | 15.00 ± 3.90 | 6.51 ± 2.16 | 0.16 ± 0.02 | 2.70 ± 0.14 | 0.21 ± 0.02 | 36.0 ± 7.60 |
| Monitoring points2 | 8.09 ± 0.07 | 14.28 ± 1.20 | 5.60 ± 2.01 | 0.17 ± 0.03 | 3.40 ± 0.14 | 0.19 ± 0.02 | 36.0 ± 6.07 |
| Monitoring points3 | 8.01 ± 0.10 | 11.42 ± 1.45 | 6.71 ± 1.90 | 0.16 ± 0.03 | 3.05 ± 0.09 | 0.21 ± 0.03 | 35.0 ± 6.69 |

Table 2 shows that in terms of dissolved oxygen and oxygen-consuming substance content, the dissolved oxygen content of monitoring points 1 and 3 are (6.51 ± 2.16) and (6.71 ± 1.90) mg/L, respectively, reaching the lake water quality class I standard. Monitoring point 2, the dissolved oxygen content is (5.60 ± 2.01) mg/L, which meets the II water quality standard. The chemical oxygen consumption (COD) of monitoring points 1, 2, and 3 were (2.70 ± 0.14) , (3.40 ± 0.14) and (3.05 ± 0.09) mg/L in turn, reaching the lake water quality class II standard.

In terms of nitrogen content, inorganic nitrogen can indicate the status of lake water being polluted by domestic wastewater, etc., and ammonia nitrogen exceeding the standard indicates the existence of new pollution. The inorganic nitrogen of 2 samples exceeded the standard of class II lake water, and the exceeding rate was 4.7%, indicating that the seawater was recently polluted. The nitrate nitrogen content of monitoring points 1, 2 and 3 is 0.16 mg/L~0.17 mg/L, and the inorganic nitrogen content is 0.05 mg/L~0.45 mg/L.

In terms of biological indicators, there is no suspended matter in the lake water in the suburbs of a certain city, and there is white suspended matter in the lake water at certain times, mainly jellyfish, which are unique to the region in May and June. Fecal coliforms <156/L, reaching the class I standard of lake water quality.

The results of this survey show that the inorganic nitrogen in the lake water reaches the standard of lake water category II and meets the requirement of swimming water. Dissolved oxygen, fecal coliform and PH value can reach the standard of lake water category I. The results of the environmental survey of the lake water show that there

is surface source pollution such as the catering industry in the lake area, and the dissolved oxygen content in the water is (1.63 ± 0.63) mg/L. The density of swimmers at monitoring point 2 is the largest, and the dissolved oxygen content in its water is the lowest, at (5.60 ± 2.01) mg/L. Therefore, the weather, the density of swimmers and the environment around the lake water are the main factors affecting water quality.

4.2. QUESTIONNAIRE SURVEY AND RESULTS

4.2.1. QUESTIONNAIRE SURVEY METHOD

The field population in a suburban lake was taken as the survey object, and the questionnaire was formulated and revised according to the actual situation. The questionnaire contains a total of 42 individual choices, which are divided into two parts: the on-site questionnaire survey and the follow-up questionnaire after 7 days. The contents of the investigation included whether there were any changes in the respiratory tract, digestive tract, eyes, ears, nose, chest tightness, tinea pedis, skin infection symptoms and changes in mental state, which were completed within 2 consecutive days. The follow-up questionnaire was conducted by telephone, E-mail, QQ group, WeChat group, etc., and was conducted 7 days after the on-site investigation.

The investigators of this questionnaire survey are all trained and qualified medical students. Before the survey, 60 members of the swimming association and 50 students of the school were organized to conduct a preliminary survey, and the questions in the survey questionnaire were improved. Unify the standards during the investigation, and eliminate abnormal data during data entry. Monitoring data are represented by $\bar{x} \pm s$. Through the above STIRPAT environmental impact assessment model, the health influencing factors and influence degree of the outdoor swimming population were assessed. SPSS 10.0 statistical software was used for data entry, and χ^2 test and Logistic regression analysis was performed. The difference was statistically significant $P < 0.05$.

4.2.2. INFLUENCE ON THE HEALTH OF THE SWIMMING POPULATION

A total of 500 questionnaires were distributed in this survey, 491 were recovered, 408 were valid questionnaires, and the response rate was over 90%. In this paper, the population was divided into swimming and non-swimming groups, and on-site questionnaires were administered to the swimming and non-swimming groups, respectively. Follow-up questionnaires were conducted again after 7d. The results of the survey were summarized for both groups and finally, the number of people in both groups who developed symptoms and the incidence were analyzed. A comparison of the incidence of different symptoms in the swimming and non-swimming groups is shown in Figure 1.

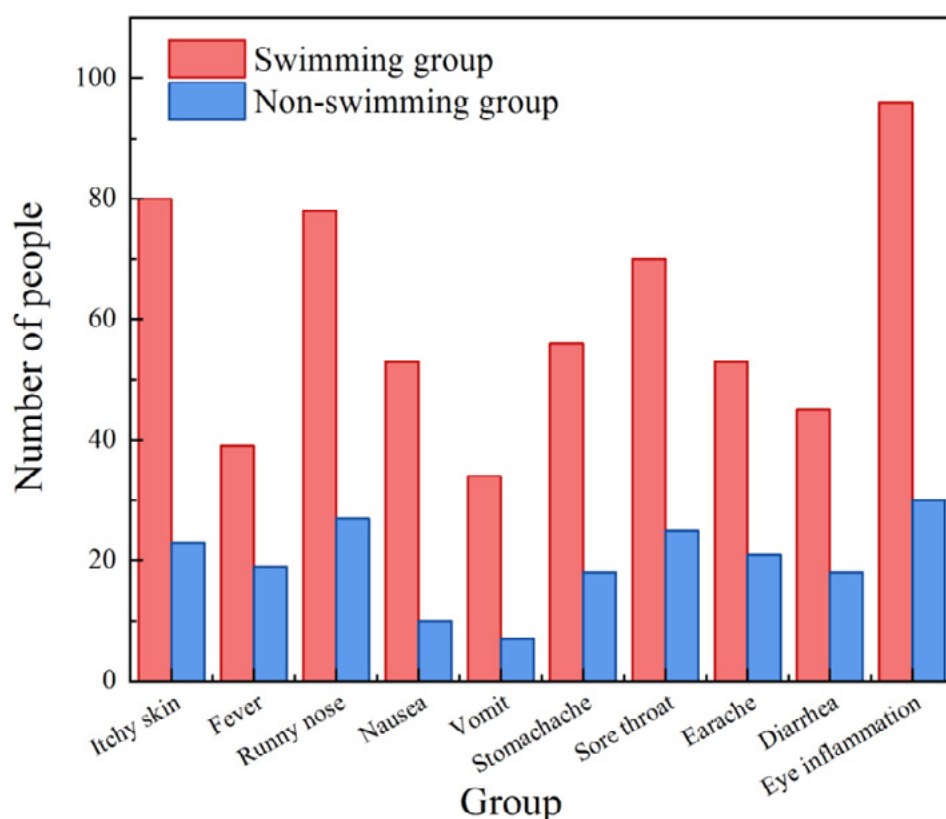


Figure 1. Comparison of the incidence of different symptoms between the swimming group and the non-swimming group.

As can be seen from Figure 1, 264 people in the swimming group suffered from itchy skin, fever, nasal congestion, runny nose, nausea, vomiting, stomach pain, sore throat, earache, diarrhea and eye inflammation, while the number of people in the non-swimming group found such symptoms for 144 people. In addition, the number and incidence of any symptom in the swimming group were higher than those in the non-swimming group. The most obvious one was: in terms of skin itching symptoms, the number and incidence of the swimming group were 57% higher than those in the non-swimming group. people, 14.3%. In terms of nasal congestion and runny nose, the number and incidence of the swimming group were 51 and 10.7% higher than those of the non-swimming group. In terms of symptoms of nausea, the number and incidence of the swimming group were 43 and 13.2% higher than those of the non-swimming group. In terms of inflammation, the number and incidence of the swimming group were 57 and 14.3% higher than those of the non-swimming group, respectively.

According to the above data, the number and incidence of skin itching, fever, nasal congestion, runny nose, nausea, vomiting, stomach pain, sore throat, earache, diarrhea and eye inflammation in the swimming group were higher than those in the non-swimming group. The incidences of itching, nasal congestion and runny nose, nausea, vomiting, stomach pain, sore throat, eye inflammation and diarrhea were significantly different ($P < 0.05$ or $P < 0.01$), while there was no statistical difference

in the incidence of fever and earache between the two groups. academic significance ($P < 0.05$).

4.2.3. LOGISTIC REGRESSION ANALYSIS OF RISK FACTORS AFFECTING THE HEALTH STATUS OF THE SWIMMING POPULATION

Taking the symptoms of the population (whether there is the respiratory tract, digestive tract, eyes, ears, nose, chest tightness, tinea pedis, skin infection symptoms and mental state, etc.), wearing earplugs, swimming goggles, etc.) were used as independent variables, and a two-class logistic regression analysis was performed. The logistic regression multivariate analysis of the risk factors for the health status of the swimming population is shown in Table 3.

Table 3. Logistic regression multivariate analysis of risk factors for the health status of the swimming population

| Symptom | Influencing factors | β value | SE | Wald value | P value | OR value | 95%CI |
|------------------|----------------------------|---------------|-----|------------|---------|----------|-------------|
| Itchy skin | Swim | 1.367 | 389 | 12.337 | 0 | 3.925 | 1.830-8.417 |
| | Swallow lake water | 1.392 | 424 | 10.771 | 1 | 4.023 | 1.752-9.236 |
| Eye inflammation | Swim | 0.93 | 317 | 8.618 | 3 | 2.535 | 1.362-4.718 |
| | Not wearing diving glasses | 889 | 332 | 7.193 | 7 | 2.433 | 1.271-4.661 |

Table 3 shows that the main risk factors for skin itching symptoms in the population include swimming (OR value 3.925, 95%CI: 1.830-8.417) and swallowing lake water (OR value: 4.023, 95%CI: 1.752-9.236). Statistical significance ($P < 0.01$), which indicates that swimming and swallowing lake water sentences can increase the risk of skin itching in the population; the risk factors for eye inflammation in the population include swimming (OR value: 2.535, 95%CI: 1.362~4.718) and swimming Without diving glasses (OR value: 2.433, 95% CI: 1.271-4.661), the difference was statistically significant ($P < 0.01$), indicating that swimming and swimming without diving glasses can increase the risk of eye inflammation in the population.

5. DISCUSSION

The disposal of water environmental pollution incidents, especially the restoration and assessment of water environmental damage, is a blank field in China, and there is a lack of systematic research on the relevant assessment method systems. This paper takes the water environment of a lake in the suburbs of a city as an example to study the impact of the polluted water environment of the lake on the health of outdoor

sports swimmers. However, it does not involve the process of China's disposal of water pollution incidents, as well as the related content of the concept and assessment method of environmental damage assessment. Therefore, in the future research direction, it is mainly China's research on the disposal process of water environmental pollution incidents, the concept and assessment method of environmental damage assessment, which has important theoretical significance and technical support for the establishment of environmental damage restoration and assessment method system, the development of environmental damage assessment method practice, and the construction of environmental economic policy system. The protection of the water environment not only protects human survival, social progress and economic development, but also sustains the need for a good ecological environment. Lake bathing is best to wear waterproof goggles as well as ear plugs, etc., use water to rinse the whole body immediately after bathing and use eye drops and ear drops for prevention if necessary. At the same time, we should strengthen the monitoring of the density of the swimming crowd and control the surface source pollution to protect the physical and mental health of the crowd.

6. CONCLUSION

This paper takes the water environment of a suburban lake in a city as an example to study the impact of the polluted water environment on the health of outdoor sports swimmers. And analyzed from two aspects of water quality monitoring and questionnaire survey. Finally, the influencing factors of water environment pollution on the outdoor tourism population are studied:

(1) Judging from the results of water quality monitoring and environmental investigation, the inorganic nitrogen in the waters of the lake reaches the class II standard of lake water, which meets the requirements for swimming water. Dissolved oxygen, fecal coliform and PH value can reach the class I standard of lake water. The survey results of the lake water environment show that there is non-point source pollution such as food and beverages near the lake waters, especially on rainy days, and the dissolved oxygen content in the water is (1.63 ± 0.63) mg/L. The density of swimmers at monitoring point 2 was the highest, and the dissolved oxygen content in its water was the lowest, which was (5.60 ± 2.01) mg/L, which shows that weather, swimming population density and environmental pollution around the water are the main factors affecting water quality.

(2) According to the questionnaire survey, lake waters have direct and indirect effects on people's health (including skin, respiratory tract, stomach, eyes, ears, etc.). The main symptoms are itchy skin, fever, nasal congestion, runny nose, nausea, vomiting, stomach pain, sore throat, earache, diarrhea, and eye inflammation.

(3) The results of the questionnaire survey show that polluted lake waters can have adverse effects on the health of the population. The main manifestations were eye inflammation at 36.4%, skin itching at 30.3%, nasal congestion and runny nose at 29.5%, sore throat at 26.5%, stomach pain at 21.2%, and nausea at 20.1%, the

incidence of ear pain was 20.1%, the incidence of diarrhea was 17.0%, the incidence of fever was 14.8%, and the incidence of vomiting was 12.9%.

It can be seen that the impact of lake water quality on the health of the population is related to the swimming habits of the swimming population. Lake bathing is best to wear waterproof goggles as well as ear plugs, etc., use water to rinse the whole body after bathing and use eye drops and ear drops for prevention if necessary. At the same time, we should strengthen the monitoring of the density of the swimming crowd and control the surface source pollution to protect the physical and mental health of the crowd.

7. DATA AVAILABILITY STATEMENT

The original contributions presented in the study are included in the article/ supplementary material, further inquiries can be directed to the corresponding author.

8. CONFLICT OF INTEREST

The authors declare that the research was conducted in the absence of any commercial or financial relationships that could be construed as a potential conflict of interest.

REFERENCES

- (1) Tang W, Pei Y, Zheng H, et al. (2022). **Twenty years of China's water pollution control: Experiences and challenges**. *Chemosphere*, 295, 133875.
- (2) Ren L, Lu Z, Xia X, et al. (2022). **Metagenomics reveals bacterioplankton community adaptation to long-term thermal pollution through the strategy of functional regulation in a subtropical bay**. *Water Research*, 216, 118298.
- (3) He J, Zhang Y, Ni F, et al. (2022). **Understanding and characteristics of coagulation removal of composite pollution of microplastic and norfloxacin during water treatment**. *Science of The Total Environment*, 831, 154826.
- (4) Yang J, Stokal M, Kroeze C, et al. (2022). **What is the pollution limit? Comparing nutrient loads with thresholds to improve water quality in Lake Baiyangdian**. *Science of The Total Environment*, 807, 150710.
- (5) Riedel T, C Kübeck, Quirin M. (2022). **Legacy nitrate and trace metal (Mn, Ni, As, Cd, U) pollution in anaerobic groundwater: Quantifying potential health risk from "the other nitrate problem"**. *Applied Geochemistry*, 139, 105254.
- (6) Yan C, Qu Z, Wang J, et al. (2022). **Microalgal bioremediation of heavy metal pollution in water: Recent advances, challenges, and prospects**. *Chemosphere*, 286(3), 131870.
- (7) Niu Y H, Wang L, Wang Z, et al. (2022). **High-frequency monitoring of neonicotinoids dynamics in soil-water systems during hydrological processes**. *Environmental Pollution*, 292, 118219.

- (8) Yu X, Huang W, Wang Y, et al. (2022). **Microplastic pollution in the environment and organisms of Xiangshan Bay, East China Sea: An area of intensive mariculture.** *Water Research*, 212, 118117.
- (9) Yang Q, Liu Y, Wang L, et al. (2022). **Cerium exposure in Lake Taihu water aggravates microcystin pollution via enhancing endocytosis of *Microcystis aeruginosa*.** *Environmental Pollution*, 292, 118308.
- (10) Liu Y, Wang P, Gojenko B, et al. (2021). **A review of water pollution arising from agriculture and mining activities in Central Asia: Facts, causes and effects.** *Environmental Pollution*, 291, 118209.
- (11) Zhou, Z., Liu, J., Zhou, N., Xu, J., He, L., & Jiang, X. (2021). **Does the "10-Point Water Plan" reduce the intensity of industrial water pollution? Quasi-experimental evidence from China.** *Journal of Environmental Management*, 295, 113048.
- (12) Wang, H., Yang, Q., Ma, H., Zou, Z., & Wang, L. (2021). **Chemical compositions evolution of groundwater and its pollution characterization due to agricultural activities in Yinchuan Plain, northwest China.** *Environmental Research*, 200, 111449.
- (13) Dai, L., Lu, Q., Zhou, H., & Jiang, L. (2021). **Tuning oxygenated functional groups on biochar for water pollution control: A critical review.** *Journal of Hazardous Materials*, 420(Part 1), 126547.
- (14) Zhang, Q. Q., Xing, C., Cai, Y. Y., Yu, K., & Liu, X. (2021). **How much do human and livestock actually contribute to steroids emission and surface water pollution from past to the future: A global research.** *Science of The Total Environment*, 772, 145558.
- (15) Ishii, E., Watanabe, Y., Agusa, T., Fujihara, J., Yasuda, T., & Mizukawa, K. (2021). **Acesulfame as a suitable sewer tracer on groundwater pollution: A case study before and after the 2016 Mw 7.0 Kumamoto earthquakes.** *Science of The Total Environment*, 754, 142409.
- (16) Ranjbar, R., Shariati, F. P., Tavakoli, O., & Dorraji, M. S. (2021). **Fabrication of a new reactor design to apply freshwater mussel *Anodonta cygnea* for biological removal of water pollution.** *Aquaculture*, 737077.
- (17) Meng, X., Peng, X., Xue, J., Gao, C., & Liu, Y. (2021). **A biomass-derived, all-day-round solar evaporation platform for harvesting clean water from microplastic pollution.** *Journal of Materials Chemistry A*, 9.
- (18) Haskins, D. L., Brown, M. K., Qin, C., Adams, L., & Hecker, M. (2021). **Multi-decadal trends in mercury and methylmercury concentrations in the brown watersnake (*Nerodia taxispilota*).** *Environmental Pollution*, 274, 116722.
- (19) Oehler, T., Ramasamy, M., George, M. E., & Reniers, A. J. (2021). **Tropical Beaches Attenuate Groundwater Nitrogen Pollution Flowing to the Ocean.** *Environmental Science and Technology*, 55(12).
- (20) He, S., Wu, J., Wang, D., & Wen, Y. (2021). **Predictive modeling of groundwater nitrate pollution and evaluating its main impact factors using random forest.** *Chemosphere*, 290(2), 133388.
- (21) Xia C, Liu G, Wang Z, et al. Distribution of hydrogen and oxygen stable isotopes and pollution indicators in water during a monsoon transitional period in Min River Basin[J]. *Science of The Total Environment*, 2021:146780.

- (22) Kumar S. **Water resources pollution associated with risks of heavy metals from Vatukoula Goldmine region, Fiji.** *Journal of Environmental Management*, 2021.
- (23) Payus C, Geoffrey I, Oliver A. (2018). **Retracted: Determination of free chlorine content in indoor and outdoor swimming pool sports complex.**
- (24) Smith, C. C., Löf, G., & Jones, R. (2019). **Measurement and analysis of evaporation from an inactive outdoor swimming pool.** *Solar Energy*, 53(1), 3-7.
- (25) Simard, S., Tardif, R., & Rodriguez, M. J. (2017). **Variability of chlorination by-product occurrence in water of indoor and outdoor swimming pools.** *Water research: A journal of the international water association*.
- (26) Yao, S. (2020). **An investigation of haloacetic acid occurrence in indoor and outdoor swimming pools in Beijing China.** *IOP Conference Series: Earth and Environmental Science*, 467(1), 012136 (7pp).
- (27) Pérez, P. A., Ballesteros-Gómez, A., Crespo-Lopez, M. E., et al. (2022). **The role of outdoor and indoor air quality in the spread of SARS-CoV-2: Overview and recommendations by the research group on COVID-19 and particulate matter (RESCOP commission).** *Environmental Research*.
- (28) Allen, J. M., Plewa, M. J., Wagner, E. D., et al. (2021). **Making Swimming Pools Safer: Does Copper-Silver Ionization with Chlorine Lower the Toxicity and Disinfection Byproduct Formation?** *Environmental Science & Technology*, 55(5).
- (29) Anugerah, A. R., Muttaqin, P. S., & Purnama, D. A. (2021). **Effect of Large-Scale Social Restriction (PSBB) during COVID-19 on Outdoor Air Quality: Evidence from Five Cities in DKI Jakarta Province, Indonesia.** *Environmental Research*, 197(Special Issue), 111164.
- (30) Belosi, F., Conte, M., Gianelle, V., et al. (2021). **On the concentration of SARS-CoV-2 in outdoor air and the interaction with pre-existing atmospheric particles.** *Environmental Research*, 193, 110603.
- (31) Li M, Lana C C, Tan C S, et al. (2021). **Association of time outdoors and patterns of light exposure with myopia in children.** *British Journal of Ophthalmology*.
- (32) Hamid N A, Alexander N, Suer R, et al. (2020). **Targeted outdoor residual spraying, autodissemination devices and their combination against Aedes mosquitoes: field implementation in a Malaysian urban setting - ERRATUM.** *Bulletin of Entomological Research*, 110(6), 1.
- (33) Rozema A D, Mathijssen J, Van K, et al. (2019). **Results of outdoor smoking bans at secondary schools on adolescents smoking behaviour: a quasi-experimental study.** *The European Journal of Public Health*, 29(4).
- (34) Gartrell B D, Battley P F, Clumpner C, et al. (2019). **Captive husbandry and veterinary care of seabirds during the MV Rena oil spill response.** *Wildlife Research*, 46(7), 610.
- (35) Magalhaes S, Baumgartner J, Weichenthal S. (2018). **Impacts of exposure to black carbon, elemental carbon, and ultrafine particles from indoor and outdoor sources on blood pressure in adults: A review of epidemiological evidence.** *Environmental Research*, 161(FEB.), 345-353.

- (36) Wyse A, Rodrigues A, dos Santos A, et al. (2017). **Pregnancy swimming causes short- and long-term neuroprotection against hypoxia-ischemia in very immature rats.** *Pediatric Research*.
- (37) Yoon I J, Hong J W. (2017). **Safety Equipment for Swimming Beaches in Korea: Implications for Management.** *Journal of Coastal Research*, 79, 1-5.
- (38) Juárez, F. F., Esenarro, D., Díaz, M., & Frayssinet, M. (2021). **Model based on balanced scorecard applied to the strategic plan of a peruvian public entity.** *3C Empresa. Investigación y pensamiento crítico*, 10(4), 127-147. <https://doi.org/10.17993/3cemp.2021.100448.127-147>
- (39) Chen, H., Peng, X., & Chen, C. (2022). **Corporate social responsibility fulfilment, product-market competition and debt risk: Evidence from China.** *Applied Mathematics and Nonlinear Sciences*, 7(2), 757-772. <https://doi.org/10.2478/AMNS.2021.2.00163>

/08/

CALCULATION AND ANALYSIS OF THE IMPACT OF MICROSOFT SECURITY- ASSISTED PHYSICAL EDUCATION MODEL ON COLLEGE BASKETBALL TEACHING IN THE INTERNET INFORMATION ERA

Chenjing Zhou*

School of Economics and Management, Xianyang Normal University, Xianyang,
Shaanxi, 712000, China

12552121255@xync.edu.cn



Reception: 12/11/2022 **Acceptance:** 16/01/2023 **Publication:** 14/03/2023

Suggested citation:

Z., Chenjing. (2023). **Calculation and analysis of the impact of Microsoft security-assisted physical education model on college basketball teaching in the Internet information era.** *3C TIC. Cuadernos de desarrollo aplicados a las TIC*, 12(1), 152-174. <https://doi.org/10.17993/3ctic.2023.121.152-174>

ABSTRACT

With the rapid development of information technology in China in recent years, the network-sharing function in social software such as "WeChat" has begun to serve as a safety aid for educational work and promote the emergence of a new teaching model, so this paper proposes a new idea of basketball teaching based on the WeChat safety-aided sports model. Firstly, under the method of research, the importance of the practical part of the teaching content of the basketball specialization course is analyzed by principal component analysis; then the suitability of basketball teaching theory under WeChat safety-assisted is analyzed according to the correlation reliability test, measurement ANOVA and post hoc test of score rate; based on Kinect sensing technology, a basketball teaching model based on Kinect motion capture and joint construction is constructed; finally Obtain weights according to different weight calculation methods and construct a basketball teaching quality evaluation system based on fuzzy synthesis. The results showed that the experimental class achieved 3.16 ± 1.609 (pcs) and 82.38 ± 8.450 (points) in the 4-meter fixed distance passing into the zone; 35.18 ± 9.167 (sec) and 84.72 ± 10.798 (points) in the half-court dribbling and folding marching layup; 4.8-meter fixed distance one-handed over-the-shoulder basketball in the experimental class. The experimental class achieved the standard score of 3.63 ± 2.282 (one) and the technical evaluation score of 82.28 ± 7.857 (points) for the 4.8m fixed distance one-handed over-the-shoulder shot.

KEYWORDS

Weight calculation method; Microsoft safety-assisted sports; Teaching model; Fuzzy evaluation system; College basketball teaching

PAPER INDEX

ABSTRACT

KEYWORDS

1. INTRODUCTION

2. THE CURRENT SITUATION AND INNOVATION OF TEACHING CONTENT OF BASKETBALL SPECIALIZATION COURSES IN COLLEGES AND UNIVERSITIES

2.1. Investigation and analysis of the importance of the practical part of the teaching content of the basketball specialization course

2.2. STUDY ON THE ADAPTABILITY OF THE THEORETICAL PART OF BASKETBALL TEACHING WITH THE ASSISTANCE OF WECHAT SECURITY

2.3. Building a basketball teaching model based on Kinect motion capture and joints

2.4. Basketball teaching quality evaluation system based on the fuzzy synthesis

3. OVERALL EXPERIMENTAL SCHEME DESIGN

3.1. Experimental subjects and grouping

3.2. Macro and microstructural design of WeChat safety-assisted campaign education model

3.3. Content schedule of teaching experiments

3.4. Teaching procedures of traditional teaching method and reciprocal teaching method with the assistance of Microsoft security

3.5. Schematic diagram of teacher-student communication styles for different teaching methods

3.6. Analysis of experimental results

3.6.1. Comparative analysis of two-handed chest pass performance

3.6.2. Comparative analysis of marching layup performance

3.6.3. Comparative analysis of one-handed over-the-shoulder shooting performance

4. CONCLUSION

DATA AVAILABILITY

CONFLICTS OF INTEREST

REFERENCES

1. INTRODUCTION

With the advent of the information age and the rapid development of wireless communication and network, the Internet has become closely connected with people's life, work and study [1]. WeChat, as an instant messaging software, is not limited by time and space, and it is not only widely used for socializing, but also becomes a communication medium and a safety aid for educational work, which has become a new and generally recognized educational approach driven by information technology [2-3]. WeChat has various functions, for example, the WeChat group function can provide a platform for communication between teachers and students and WeChat public number is an effective and fast way to obtain learning resources [4]. Teachers can capture high-quality graphics and explain micro-videos before class and publish them through the WeChat platform, and they can also make online classroom tasks.

In recent years, more and more research on WeChat safety-assisted physical education has been conducted, and its application in different sports has achieved good teaching results. sport education model (SE) model or sports education model, SE model is based on the theory of sports education, which is developed from game theory and game education theory [5-6]. zhu et al. [7] integrated WeChat into the teaching of yoga and found that the WeChat platform could help teachers reasonably arrange the time, intensity, and frequency of practice, and was also beneficial to the improvement of skills and the formation of exercise habits. The experimental study found that the combination of the WeChat platform and PBL teaching was beneficial to the improvement of students' motor skills, and the safety assistance of the WeChat platform could reduce the time of classroom lectures and demonstrations so that students had more time to practice. The students' participation motivation is also greatly improved.

Liu et al [9-11] combined previous research experience on the sports education model to integrate the WeChat platform into the sports education model, taking into account the advantages of both for teaching design, emphasizing the importance of both giving full play to the advantages of online teaching on the WeChat platform and strictly following the teaching structure process of the sports education model to make an effective interface between the two. Wang et al [12] proposed an adaptive analysis based on Kinect of running posture and Meng et al [13-14] proposed that the MU safety-assisted sports education model can solve the problem of students' weak knowledge of sports items and also provide an online channel to solve in-class problems as a way to ensure that the game process is not interrupted while solving students' in-class problems.

In summary, WeChat plays a great role as a safety aid in physical education, and researchers have designed and verified its advantages in teaching through WeChat safety aid teaching. Some scholars have incorporated WeChat into the basketball teaching mode, and the research results found that WeChat can be incorporated into the basketball teaching mode more conveniently and effectively to promote students' overall development and independent learning. This paper addresses the shortcomings of the traditional basketball teaching model in the information age, proposes basketball teaching ideas based on the WeChat safety-assisted sports

model, constructs a basketball teaching model based on Kinect action analysis, and uses a fuzzy evaluation system to classify and discriminate the proposed method. The SE model is used to emphasize the development of students' sports knowledge, culture and students' initiative. Finally, by understanding the role of the WeChat platform for physical education, and drawing on the experience of previous people in integrating the WeChat platform with other teaching models, the advantages of both are combined and integrated, and basketball teaching in colleges and universities is designed and applied through macro and micro, to be able to provide new teaching ideas and solutions for basketball teaching.

2. THE CURRENT SITUATION AND INNOVATION OF TEACHING CONTENT OF BASKETBALL SPECIALIZATION COURSES IN COLLEGES AND UNIVERSITIES

2.1. INVESTIGATION AND ANALYSIS OF THE IMPORTANCE OF THE PRACTICAL PART OF THE TEACHING CONTENT OF THE BASKETBALL SPECIALIZATION COURSE

Investigations show that basketball specialization courses tend to overemphasize the transmission of existing skills, tactics, and theoretical knowledge and ignore the innovation of existing basketball culture, so the teaching content focuses on the transmission of existing knowledge, skills, and experience. Some teachers of basketball specialization courses take book knowledge as the only teaching content, teaching is simplified to "teaching", learning is equivalent to "learning from books", and teaching activities are limited to experience and cognitive activities [15-16].

Table 1. Questions, structure and reliability test of the questionnaire of the practical part of the teaching content of the basketball specialization course

| Title | Component | |
|---|-------------------|-------------------------------|
| | Practical ability | Technical and tactical skills |
| Teaching the game | 895 | |
| Practice of field command and refereeing | 745 | |
| Basketball special physical training | 741 | |
| Basketball tactics teaching and training | 667 | 514 |
| Teaching and training of basketball techniques | | 895 |
| Teaching and training skills practice | | 480 |
| Characteristics Root | 2.416 | 1.377 |
| Cumulative explanation rate of variance (62.555%) | 40.271 % | 22.284 % |
| Cronbach's alpha coefficient (0.730) | 751 | 464 |

Using principal component analysis with Varimax orthogonal rotation [17], two factors with characteristic roots greater than 1 were extracted to explore the structure of the practical part of the teaching content of the basketball specialization course.

In the 2-factor structure, the Kaiser-Meyer-Olkin value for the 6 topics was 0.671 and Bartlett's Test of Sphericity Approximate (15) = 100.197 ($p < 0.001$), indicators that the topics are suitable for exploratory factor analysis. The cumulative variance explained by the 2 factors reached 62.555%. The topic of basketball tactical instruction and training was highly loaded in both factors, but basketball tactical instruction and training was categorized as the second factor based on previous teaching experience. 2 factors measured the practical part of the basketball specialization course content in terms of f1 practical ability and f2 technical and tactical ability, respectively.

The total score of each factor is then calculated, followed by the normalized score of the factor score according to the following algorithm: $\text{normalized score} = (x - \min) / (\max - \min)$; the normalized score takes the value of each factor score to be between 0 and 1, which is the scoring rate of each factor.

Practical ability is $1 = (\text{practical ability} - 3) / 12$. There are 3 questions in this factor, each question has a minimum value of 1 point and a maximum value of 5 points, so the minimum value of this factor is 3 points and the maximum value is 15 points.

Technical and tactical ability is $1 = (\text{technical and tactical ability} - 3) / 12$. There are 3 questions in this factor, each question has a minimum value of 1 point and a maximum value of 5 points, so the minimum value of this factor is 3 points and the maximum value is 15 points.

The mean value after normalization was 0.10417, and the practical ability was significantly greater than the technical and tactical ability, with p less than 0.001. The three topics consisting of practical ability of teaching and competition, the practice of clinical command and refereeing, and basketball special physical fitness training were relatively favored by basketball special teachers. The three topics of teaching and training of basketball tactics, teaching and training of basketball techniques and practice of teaching and training ability, which consisted of technical and tactical ability, were relatively unpopular, and the reasons for this may be related to the training objectives of basketball specialization courses in each school, where teachers pay more attention to the cultivation and education guidance of students' practical ability.

2.2. STUDY ON THE ADAPTABILITY OF THE THEORETICAL PART OF BASKETBALL TEACHING WITH THE ASSISTANCE OF WECHAT SECURITY

Table 2. Questions, structure and reliability test of the questionnaire of the theoretical part of the teaching content of the basketball specialization course

| Title | Component | | |
|---|-----------------------|----------------------|--------------------------------------|
| | 1 Quality of athletes | 2 Athlete management | 3 Athlete Theory Basketball Injuries |
| Basketball sports scientific research work | 908 | | |
| Nutrition and recovery of basketball players | 837 | | |
| Mental training of basketball players | 819 | | |
| Basic quality and coaching requirements for senior basketball coaches | 737 | | 624 |
| Basic quality and development of high-level referees | 676 | | |
| Basketball awareness and its cultivation | 644 | | 815 |
| Organization and management of basketball competition | 606 | | |
| Basketball rules and referee law | | 831 | |
| Selection and training of children and youth basketball players | | 877 | |
| Theory and methods of basketball teaching | | 631 | 901 |

The structure of the theoretical part of the teaching content of the basketball specialization course was explored by using principal component analysis with Varimax orthogonal rotation and extracting three factors with characteristic roots greater than one.

In the 3-factor structure, the KAISER-MEYER-OLKIN value for 13 questions was 0.838 and Bartlett's Test of Sphericity Approximate (78) = 541.460 ($p < 0.001$), indicating that the questions were suitable for exploratory factor analysis. The cumulative variance explained by the 3 factors reached 70.992%. f1 Athlete quality, f2 Athlete management and f3 Athlete theory were measured in 3 aspects of the theoretical part of the basketball specialization course content. Factor 1 Athlete quality consists of 7 topics such as basketball injury, prevention and rehabilitation, scientific research work in basketball, nutrition and recovery of basketball players, psychological training of basketball players, basic quality and coaching requirements of senior basketball coaches, basic quality and development of high-level referees and basketball awareness and its development, which require students to have high advanced quality in research and training [18-20]. Factor 2 Athlete management, on the other hand, consists of three topics such as organization and management of basketball competitions, basketball rules and officiating law and selection and training of children and youth basketball players, requiring students to be able to be not only a qualified referee, but also to approach management-oriented personnel for youth

selection and training. Factor 3 Athlete Theory is composed of three topics such as basketball teaching theory and methods, basic basketball theory and basketball training theory and methods, etc. Factor 3 tends to the theoretical knowledge of basketball teaching and training.

Then, based on the above factors, the total score of each factor is calculated, and then the normalized score of each factor is calculated according to the following algorithm: Normalized score = $(x - \min) / (\max - \min)$; the normalized score takes the value of each factor score to be between 0 and 1, which is the scoring rate of each factor.

The athlete quality is $1 = (\text{athlete quality} - 7) / 28$. There are 7 questions in this factor, and each question has a minimum value of 1 point and a maximum value of 5 points, so the minimum value of this factor is 7 points and the maximum value is 35 points.

Athlete Management $1 = (\text{Athlete Quality} - 3) / 12$. There are 3 questions in this factor, each question has a minimum value of 1 point and a maximum value of 5 points, so the minimum value of this factor is 3 points and the maximum value is 15 points.

Athlete Theory $1 = (\text{Athlete Quality} - 3) / 12$. There are 3 questions in this factor, each question has a minimum value of 1 point and a maximum value of 5 points, so the minimum value of this factor is 3 points and the maximum value is 15 points.

Table 3. Descriptive statistics of the three factors of the theoretical part of the teaching content.

| Factor 1 | Mean value | Standard deviation |
|--------------------|------------|--------------------|
| Athlete Quality | 247 | 25 |
| Athlete Management | 152 | 20 |
| Athlete Theory | 128 | 17 |

Table 4. Repeated-measures ANOVA for the mean score rate of the three factors

| Error source | Sum of squares | df | mean square | F | Sig. |
|-----------------------|----------------|-----|-------------|--------|------|
| Intra-group variation | 505 | 2 | 253 | 19.032 | 0 |
| Error variation | 1.672 | 126 | 13 | | |

Table 5. Post hoc test of the mean score rate of the three factors

| (I) Factor 1 | (J) Factor 1 | Difference of means (I-J) | Standard error | Sig.b |
|--------------|--------------|---------------------------|----------------|-------|
| 1 | 2 | 94 | 20 | 0 |
| | 3 | 119 | 22 | 0 |
| 2 | 3 | 25 | 20 | .629 |

Table 3 shows that the highest mean value is the athlete quality factor and the lowest mean value is the athlete theory factor; the repeated measures ANOVA in Table 4 shows that there is a significant difference between at least one pair of the three-factor means in the two-way comparison; the two-way post hoc comparison in Table 5 shows that there is a significant difference between the mean values of Factor 1 and Factor 2 and Factor 3, and there is no significant difference between the mean values of Factor 2 and Factor 3.

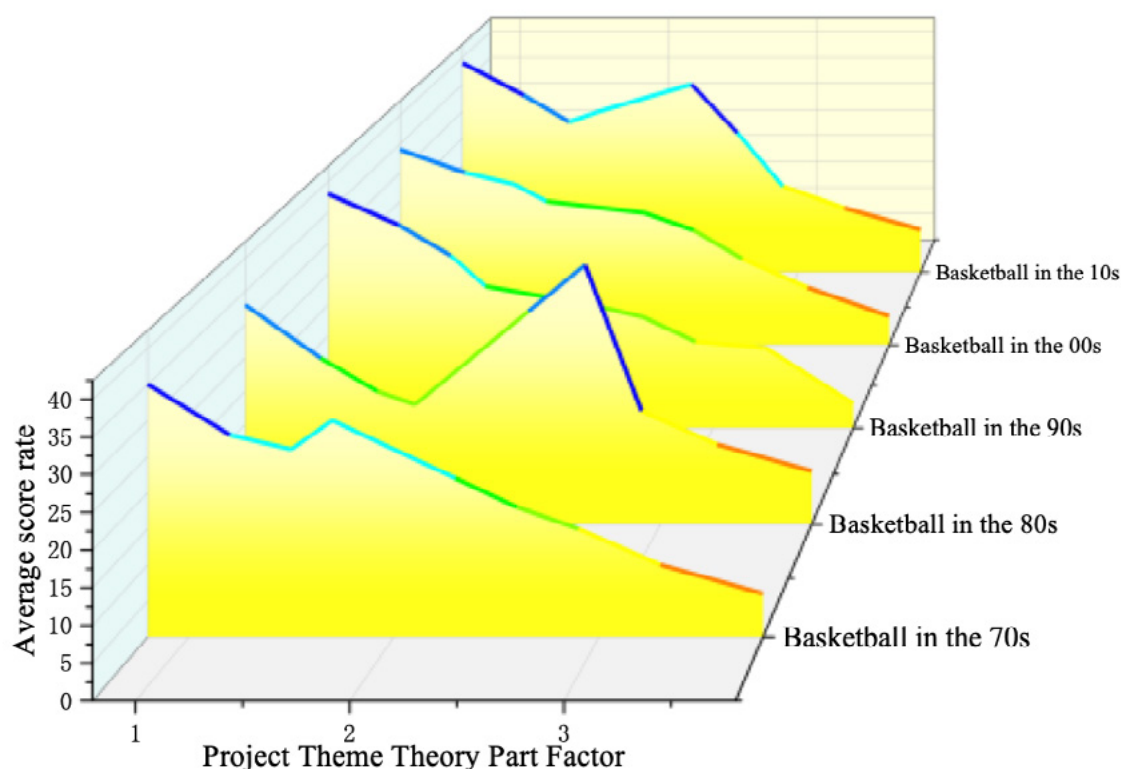


Figure 1. The trend of the average score of the factor of the theoretical part of the teaching content of the basketball specialization course

To sum up, we can see that the factor of athlete quality is very important content for basketball teachers in the teaching process. In different basketball eras, along with the rapid development of social and political economy, the demand of society for talent tends to be diversified, and no longer stays in single talent demand. Factor 2 and factor 3, on the other hand, are old-fashioned contents, which is less and less valued by teachers and students.

2.3. BUILDING A BASKETBALL TEACHING MODEL BASED ON KINECT MOTION CAPTURE AND JOINTS

The Kinect sensor uses Prime Sense's illumination encoding technique to acquire depth information, Light Coding uses infrared light to measure space, and CMOS sensors to read the encoding of light. These encodings are then analyzed by chip decoding calculations to eventually produce a depth image information [21-22]. Light

Coding differs from traditional TOF and structured light measurement techniques by using light waves instead of the previous pulses, and no special photosensitive chip is required, only a common CMOS photosensitive chip, a change that reduces the cost of the solution. Light Coding uses light waves to measure a specific region of space, so Light Coding is essentially a structured light technique [23-24]. However, unlike conventional structured light, the light emitted is not a periodic variation of image coding, but an encoded light source with three-dimensional depth [25].

To build an efficient basketball teaching and training safety aid system, image processing techniques can be used to mark the joint points of the arm and analyze the athletes' movement trajectory to recover the athletes' technical movements and obtain the required parameters. Therefore, athlete modeling consists of 2 stages as described above. In stage (1), focus on the shot preparation, raising the arm, squatting and extending; in stage (2), mark the speed and angle of the shot. The optimal shot data can be calculated so that the same shot data can be used to continuously train the athlete to develop muscle memory and can effectively improve shot accuracy [26-27]. The pitcher's arm joint model is shown in Figure 2.

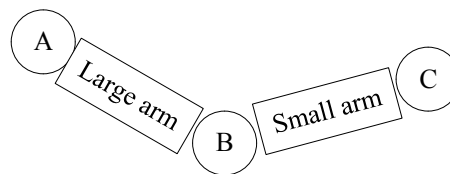


Figure 2. Arm joint model

Assume that the shoulder joint A, elbow joint B and wrist joint C are represented by $M_i (i = 1, 2, 3)$. The pixel area of each marker is represented by $G_i (i = 1, 2, 3)$, and the number of pixel points of the corresponding pixel block $L_i (i = 1, 2, 3)$. The pixel block G_i is as follows:

$$G_i = \{(x_1, y_1), (x_2, y_2), (x_3, y_3), \dots, (x_n, y_n)\} \quad (1)$$

In the above equation, x_i and y_i represent the coordinates of the pixels marked in the video image, respectively. The coordinates of the center of mass of each pixel block can be used as the coordinates of the 3 joints in the shooting process. The formula is as follows:

$$P_m(x, y) = C(x_c, y_c) \quad (2)$$

$$X_c = \frac{1}{n_i} \sum_{i=1}^{n_i} x_i \quad (3)$$

$$Y_c = \frac{1}{n_i} \sum_{i=1}^{n_i} y_i \quad (4)$$

Y_c Change over time:

$$y_c = f(t) \quad (5)$$

According to the above equation, the objective function is defined as:

$$\arg \max \|y_0\|_1 \text{ s.t. } \|y_c - y_0\|_2 < \varepsilon \quad (6)$$

Where, ε represents the residual error and $\|y_0\|_1$ represents the regular term. It can be obtained by differential equations, matching tracking, etc. y_0 . The time from preparation to shooting can be expressed by the following equation:

$$t_0 = \int^{-1}(y_0) \quad (7)$$

where \int^{-1} indicates an inverse take. In the training safety aid system, the number of frames should be an integer. In the coordinate axis system, the maximum number of frames, T , on the axis y is denoted as $\int^{-1}(y_0)$.

$$T = g(t_0) + 1 \quad (8)$$

For the recognition and characterization of human curves, the Hough transform algorithm is used [28-29]. The Hough transform algorithm is a parametric aggregation algorithm for voting through the point-to-point pairwise and Hough parameter spaces in image space, which transforms image detection into a parametric computational problem, thus making the problem more intuitive and accurate. The Hough transform algorithm has been widely used in video image processing, and after years of research, the application range is even wider. It plays an important role not only in video image processing, but also in access control systems, industrial inspection and even military activities. It can effectively reduce the influence of external factors such as noise and solve the problem of incomplete and interrupted video. For example, the equation of the circle is as follows:

$$(x-a)^2 + (y-b)^2 = r^2 \quad (9)$$

a and b are the centers of the circle, while r is the radius. In the coordinate system of the safety-assisted training system, the point (x, y) is unknown. And (a, b) and radius r are the input conditions, then the equation of the above circle can be rewritten as:

$$(a-x)^2 + (b-y)^2 = r^2 \quad (10)$$

In the above equation, there is an exchange between (x, y) and (a, b) , while (a, b) and r are unknown, so (x, y) is converted to a known number. It is known by calculation that in the whole image space, when there are valid feature points (x, y) , there exists a cone space with corresponding threshold values. Each effective feature point (x, y) in the image space corresponds to a cone in the parameter space. The difference at the same point in the image space corresponds to the cone in the parameter space, and the two cones will inevitably intersect at the same point. The process records the variables of repeated points with the same parameters by initializing the 3D accumulator in the parameter space.

2.4. BASKETBALL TEACHING QUALITY EVALUATION SYSTEM BASED ON THE FUZZY SYNTHESIS

First, the set of evaluation indicators (thesis domain) Y , which describes the indicators or criteria for the comprehensive evaluation of various evaluation factors, denoted as:

$$Y = (y_1, y_2, \dots, y_n) \quad (11)$$

Where y_1, y_2, \dots, y_n is each evaluation indicator or criterion and n is the number of evaluation indicators.

The set of evaluation metrics can also be a collection of multilevel recursive structures [30-31].

For different evaluation indicators, the weight F domain can be calculated according to different weight calculation methods, such as hierarchical analysis, weighted average method, Delphi method, expert estimation method, etc., and the weight F domain is noted as

$$F = (f_1, f_2, \dots, f_n) \quad (12)$$

Second, the set of evaluation scales G , which describes the scale used to evaluate each evaluation indicator, is denoted as

$$G = (g_1, g_2, \dots, g_m) \quad (13)$$

Where m is the number of evaluation scales in the evaluation scale set.

The grading of the evaluation scale can be done in a graded manner or a score manner, such as

$$G = (0.8, 0.6, 0.4, 0.2) \quad (14)$$

Third, the affiliation degree v_{ij}^s , describes the degree of possibility of making an evaluation scale g_j with an evaluation index y_i for the evaluation factor A_s . The affiliation degrees of all evaluation indicators for the scenario A_s from the affiliation matrix V_s , which is a fuzzy relationship matrix, denoted as

$$V_s = \begin{bmatrix} V_{11}^s & V_{12}^s & V_{1j}^s & V_{1m}^s \\ V_{21}^s & V_{22}^s & V_{2j}^s & V_{2m}^s \\ V_{i1}^s & V_{i2}^s & V_{ij}^s & V_{im}^s \\ V_{n1}^s & V_{n2}^s & V_{nj}^s & V_{nm}^s \end{bmatrix} \quad (15)$$

In the matrix V_s , the element v_{ij}^s can be calculated based on the evaluation results made by the experts participating in the evaluation, i.e.

$$v_{ij}^s = \frac{b_{ij}^s}{b} \quad (16)$$

where b denotes the number of experts participating in the evaluation, and b_{ij}^s denotes the number of experts who make g_j evaluation scales for the i -th evaluation indicator y_i of the program A_s . Obviously, $\sum_{j=1}^m v_{ij}^s = 1$.

3. OVERALL EXPERIMENTAL SCHEME DESIGN

3.1. EXPERIMENTAL SUBJECTS AND GROUPING

The pre-tests of basic basketball skills and physical fitness were conducted in two classes of public physical education basketball elective course of Inner Mongolia Normal University in the first semester of academic years 2021-2022, and 32 healthy students, without special diseases and with no statistically significant differences in basic basketball skills and physical fitness were selected as experimental subjects in the two classes respectively. The two classes were randomly divided into the control group and the experimental group for teaching experiments, and the experimental group adopted the reciprocal teaching method with the assistance of WeChat security, while the control group adopted the traditional teaching method for teaching experiments[32-33].

3.2. MACRO AND MICROSTRUCTURAL DESIGN OF WECHAT SAFETY-ASSISTED CAMPAIGN EDUCATION MODEL

The physical education teaching process is a structure and procedure for carrying out various effective teaching activities in a planned and purposeful manner to achieve the teaching objectives. The design of the teaching process directly affects the implementation of the teaching model, therefore, the effectiveness of teaching depends on the scientific and operational design of the teaching process. In the process of the theoretical exploration of the SE model, Gao Rong made the top-level design from macro and micro levels to enhance the operability of the model to make it more in line with the actual situation of Chinese school sports, and this study will also make the top-level and detailed design from both macro and micro aspects. From the macro perspective, the SE model differs from the conventional teaching model in the setting of teaching units. The sports education model divides the whole semester teaching into several phases, which is the setting of the sports season in the SE model, and the sports season includes 5 phases, which are sports season preparation, pre-game season, in-game season, post-game season and celebration activities. The micro perspective mainly includes the setting of classroom teaching structure, the allocation of classroom teaching time in different teaching phases of the sports season, the design of the sports season teaching plan, the design of teaching evaluation and the preparation of lesson plans.

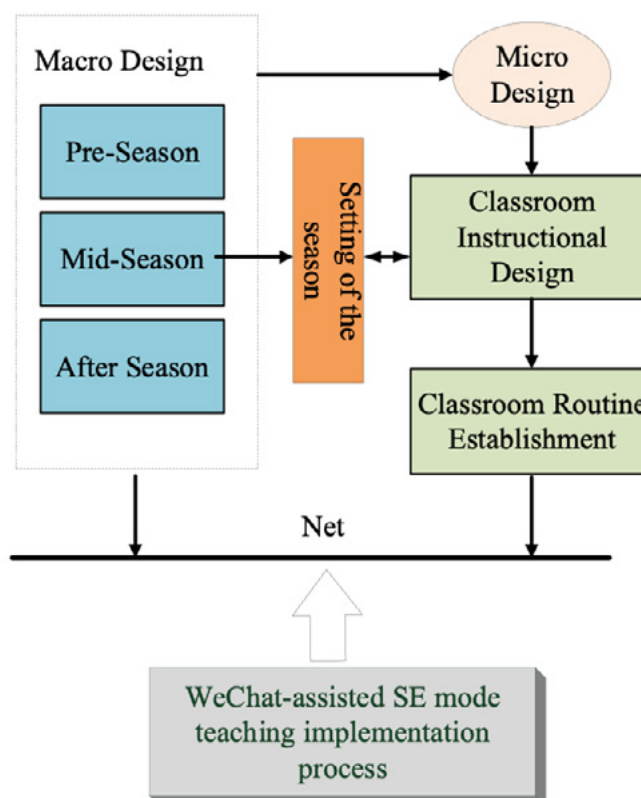


Figure 3. Teaching structure of WeChat safety-assisted movement education model

3.3. CONTENT SCHEDULE OF TEACHING EXPERIMENTS

In addition to the test week, the design of the teaching experiment includes basketball skills practice, physical fitness class practice, etc. The total number of 10 weeks of the teaching experiment, the detailed arrangement of the teaching lesson plan is as follows:

1. Physical fitness pre-test (30s push-ups, standing long jump, five-lane folding run on the basketball court).
2. basic basketball skills test (30s double pass and catch, half-court folding and dribbling, 1min shooting from outside the reasonable rushing zone).
3. Ballistic exercises, newly taught learning principles of two-handed chest passing and catching.
4. Learning to pass the ball in situ with both hands on the ground, physical drills.
5. Introduction to learning the two-handed chest pass between rows.
6. Learning in situ one-handed over-the-shoulder shooting.
7. Review the marching one-handed over-the-shoulder shot.
8. Review of the in-situ one-handed shoulder shot.
9. Physical fitness post-test, classroom contextual interest survey.

3.4. TEACHING PROCEDURES OF TRADITIONAL TEACHING METHOD AND RECIPROCAL TEACHING METHOD WITH THE ASSISTANCE OF MICROVIDEO SECURITY

The traditional teaching method and the reciprocal teaching method with the assistance of micro-video security are similar in terms of organization and method in the early stage of the class, mainly the teacher organizes the formation and explains and demonstrates, but the biggest difference between the two is mainly in the organization of students' practice and the correction and guidance of wrong movements.

(1) In the traditional teaching method, when teaching technical movements, teachers first explain and demonstrate and then let students imitate and practice, correct errors and help, and finally teach through reinforcement exercises, students mainly practice collectively in groups and independently, and teachers' feedback to students is mainly language tips and individual error cases focused on explaining.

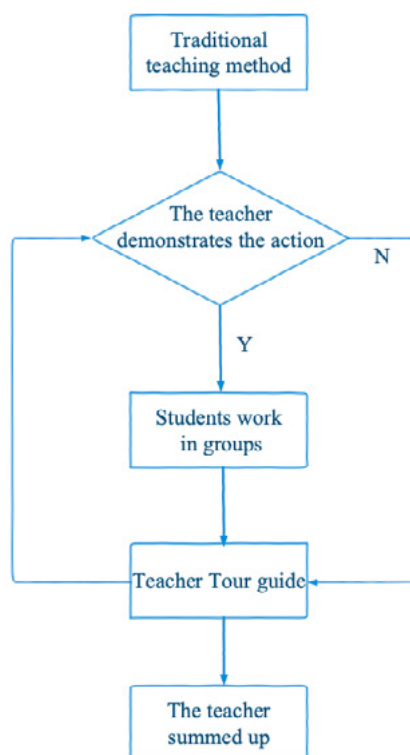


Figure 4. Flow chart of traditional model teaching

(2) Under the teaching method of reciprocal teaching method with the aid of micro-video safety, the teacher first conducts a centralized demonstration and explanation of technical movements during the teaching process, and after the students carry out collective consolidation exercises to deepen their memory, the teacher distributes the standard movement videos designed in advance according to the teaching content to the students, and explains to them how to use the standard movement videos, introduces the roles of students and teachers, and then organizes the students to

practice according to The teacher will then organize students to practice in free teams according to the learning content. This is shown in Figure 5.

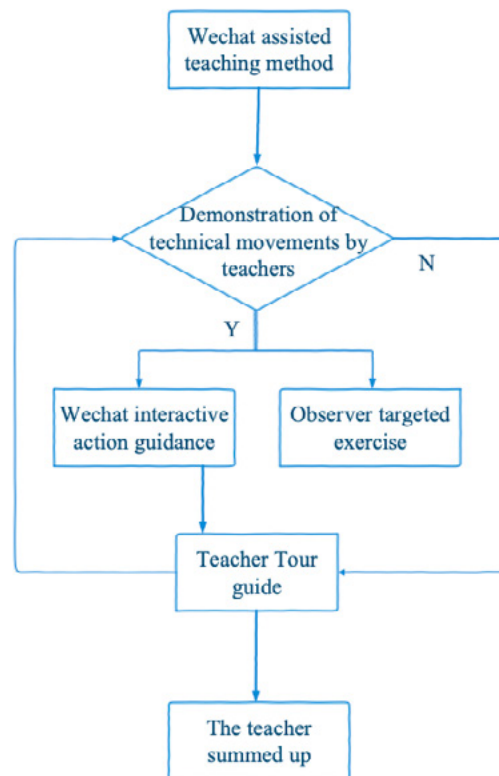


Figure 5. Flowchart of teaching and learning under WeChat security-assisted campaign

3.5. SCHEMATIC DIAGRAM OF TEACHER-STUDENT COMMUNICATION STYLES FOR DIFFERENT TEACHING METHODS

In traditional teaching methods, the teacher usually communicates directly with the practitioner and gives direct feedback to the student on the problems that arise during practice. Students are usually divided into groups of two or more, and given the roles of practitioner and observer. During the practice, the teacher walks around and communicates with the observer, and the observer gives feedback to the practitioner based on his or her observation and communication with the teacher. The specific communication style is shown in Figure 6:

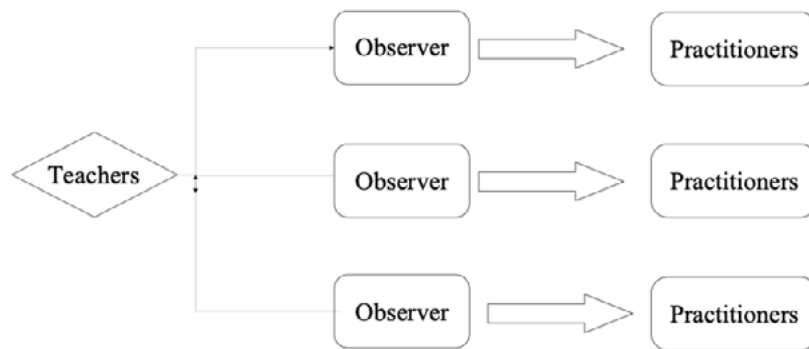


Figure 6. Diagram of teacher-student communication style

3.6. ANALYSIS OF EXPERIMENTAL RESULTS

3.6.1. COMPARATIVE ANALYSIS OF TWO-HANDED CHEST PASS PERFORMANCE

From the data in Figure 7, we can see that the experimental class achieved 3.16 ± 1.609 (passes) and 82.38 ± 8.450 (points) in the 4-m fixed distance pass into the zone, while the control class achieved 2.19 ± 1.401 (passes) and 77.88 ± 8.958 (points). t number=2.067, t technical evaluation=2.569; P number=0.043<0.05, P technical evaluation=0.013<0.05. In conclusion, there were significant differences between the experimental class and the control class in the experimental post-test scores of the two-handed chest pass technique, both in terms of standard scores and technical evaluation scores, and the experimental class had better scores than the control class.

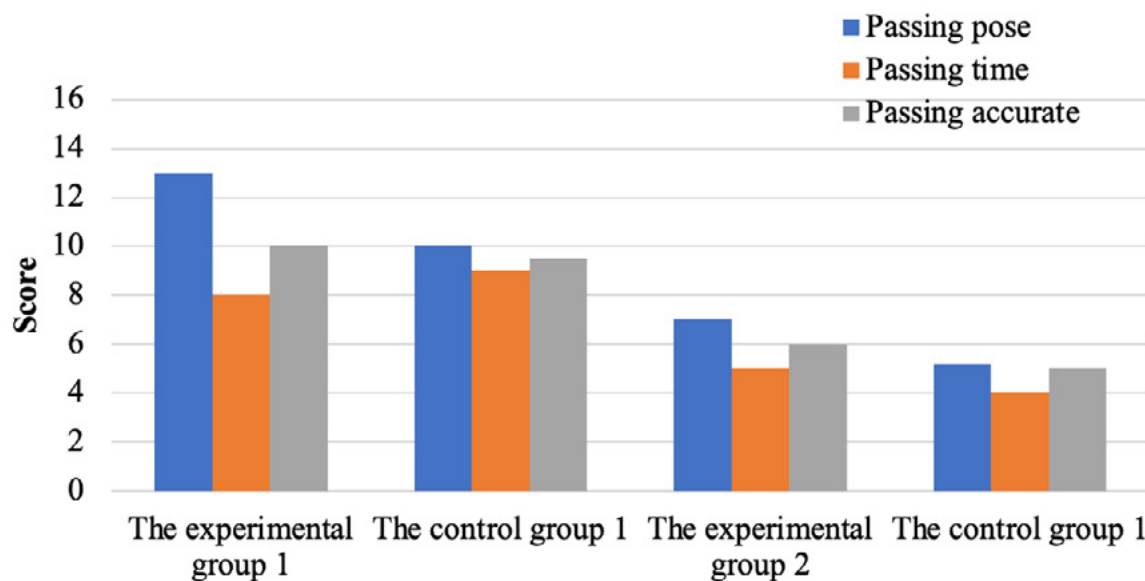


Figure 7. Comparison of two-handed chest pass performance

The ratio of males to females in the experiment is 1:3, with more girls. For girls, it is difficult to pass the basketball into the hoop flatly and quickly by upper limb strength alone, so the three technical aspects of stirrups, extensions and paddles must be consistent to fully transform the power of lower limb stirrups into the power of passing, and then improve the power, direction and speed of passing. In the traditional teaching method, students can only think about the technical movements from the practitioner's perspective, but in the reciprocal teaching method, students can learn the technical movements from different perspectives and have a deeper understanding of the technical movements while observing their teammates' practice, which has a good promotion effect on mastering the power and coherence of the technical movements of the passing ball.

3.6.2. COMPARATIVE ANALYSIS OF MARCHING LAYUP PERFORMANCE

After the experiment, the learning effect of marching one-handed over-the-shoulder shooting in the experimental and control classes was tested by using half-court dribble folding marching layup as the test index, and the specific test results were tested by SE independent sample t-test as shown in Figure 8:

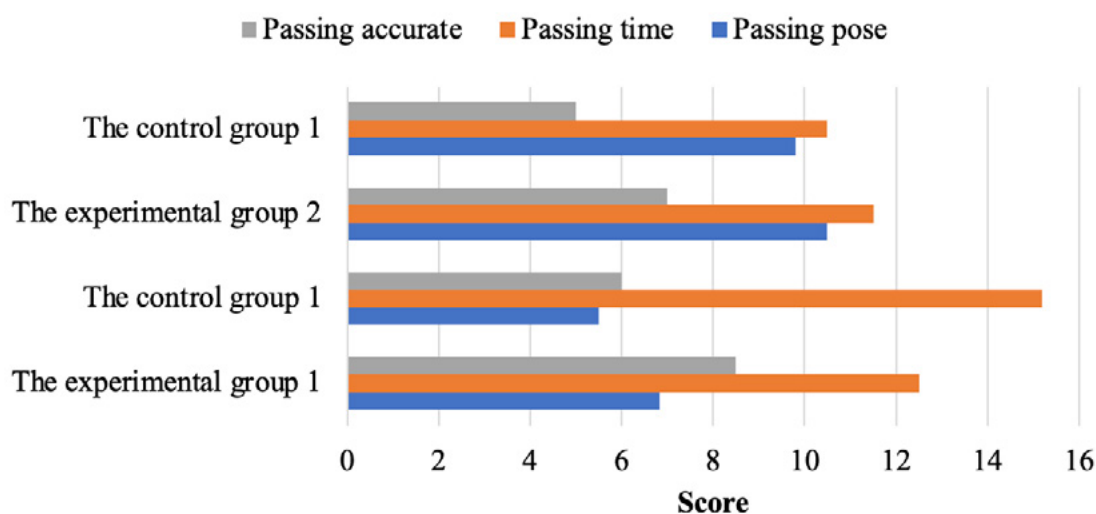


Figure 8. Comparison chart of marching layup scores

The data in Figure 8 shows that the experimental class achieved 35.18 ± 9.167 (seconds) and 84.72 ± 10.798 (points) in the half-court dribbling fadeaway layup, while the control class achieved 41.27 ± 11.723 (seconds) and 78.63 ± 11.370 (points). t values were $t_{\text{time}} = -2.316$, $t_{\text{technical evaluation}} = 2.198$, $t_{\text{time}} = 0.024 < 0.05$, $t_{\text{technical evaluation}} = 0.032 < 0.05$. In conclusion, there were significant differences between the experimental class and the control class in the experimental post-test scores of the marching lay-up technique, both in the attainment scores and the technical evaluation scores, and the experimental class had better scores than the control class.

Due to the limited practice time, the teacher can only correct some students or collectively correct them according to the common problems in the process of practice, which makes some students' problems in the process of practice not solved in time, and at the same time, students' attention may be distracted in the independent practice, so the frequency of violation or poor hit rate in the final test is higher than that of the experimental class, resulting in lower average scores in the standard and technical evaluation than the experimental class.

3.6.3. COMPARATIVE ANALYSIS OF ONE-HANDED OVER-THE-SHOULDER SHOOTING PERFORMANCE

The data in Figure 9 shows that the experimental class achieved 3.63 ± 2.282 (shots) and 82.28 ± 7.857 (points) for the 4.8 m fixed distance one-handed over-the-shoulder shot, while the control class achieved 3.09 ± 1.957 (shots) and 74.72 ± 8.224 (points). t number=1.000, t technical evaluation=3.757. This shows that there is a statistically significant difference between the technical evaluation scores of the experimental class and the control class in the post-test of one-handed over-the-shoulder shooting, and the experimental class has better scores than the control class; however, there is no statistically significant difference between the attainment scores of the experimental class and the control class, so the students are learning the one-handed over-the-shoulder shooting technique. However, there was no statistically significant difference between the experimental class and the control class in terms of attainment scores.

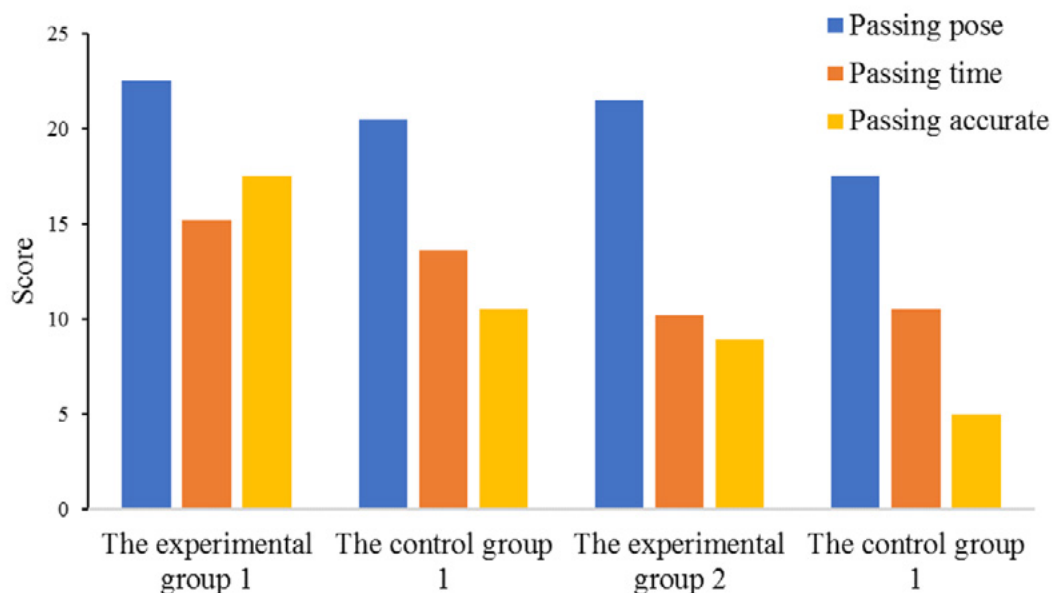


Figure 9. Comparison of one-handed over-the-shoulder shooting performance

The one-handed shoulder shot has the advantage of a high shooting point and is not easy to be targeted by the defense, but it is also the most difficult to learn. The one-handed shoulder shot consists of several technical aspects such as basic

standing posture, bending knee and stirrups, top elbow, arm extension and wrist paddle, etc. The technical aspects are interconnected, and any disconnection in the shooting process will lead to deformation of the shooting action, which will affect the shooting action. The standardization of the shooting action is affected. The study confirmed that timely feedback among students in learning basketball one-handed over-the-shoulder shooting can significantly improve students' performance in shooting skills.

4. CONCLUSION

This paper addresses the shortcomings of the traditional basketball teaching model in the Internet era, proposes a new idea of basketball teaching based on the WeChat safety-assisted sports model, constructs a basketball teaching model based on Kinect motion capture and joint behavior, and uses a fuzzy evaluation system to classify and discriminate the proposed method. Analysis using multiple experimental control groups shows that the Microsoft safety-assisted sports education model proposed in this paper has stronger motivation for students to learn basketball compared with the traditional teaching model; students learn to understand and master basketball through teamwork, team communication and role-playing strengthen students' emotional experience; the creation of real game atmosphere and game creation enrich students' game experience. All of these are conducive to meeting students' basic psychological needs, thus contributing to the enhancement of internal motivation and the internalization of motor motivation.

DATA AVAILABILITY

The data used to support the findings of this study are available from the corresponding author upon request.

CONFLICTS OF INTEREST

The author declares that there is no conflict of interest regarding the publication of this paper.

REFERENCES

- (1) Guo, X., Xu, M., Chen, G., & Li, X. (2021). **Research on team performance prediction method considering synergistic effect--a basketball team member combination as an example.** *Systems Engineering Theory and Practice*, 41(3), 565-573.
- (2) Yang, S., Xin, Y., Wang, Y., & Zhang, F. (2016). **Design and implementation of a mobile platform for universities based on WeChat Enterprise.** *Journal of Huazhong University of Science and Technology (Natural Science Edition)*, 44(S1), 158-161. <https://doi.org/10.13245/j.hust.16S132>

- (3) Li, Z. (2021). **The relationship between tribological analysis of basketball court and youth basketball training.** *Journal of Tribology*, 41(5), 793.
- (4) Zhou, Y. (2021). **Analysis of the effect of friction on track and field speed on the plastic track in high school sports.** *Journal of Tribology*, 41(5), 795.
- (5) Ren, Y., Luo, J., & Liang, X. P. (2021). **An algorithm for detection of obscured basketball players based on adaptive key point heat map.** *Journal of Computer-Aided Design and Graphics*, 33(9), 1450-1456.
- (6) Zhou, G., & Li, J. (2021). **The introduction of physical biomechanics educational resources in competitive sports with reference to.** *Journal of Tribology*, 41(4), 596.
- (7) Zhu, H., Zhang, S., Jin, Z., & Yan, X. (2019). **Research on coupled network knowledge dissemination model between WeChat group and offline communication.** *Systems Engineering Theory and Practice*, 39(7), 1796-1806.
- (8) Zhu, H., Hu, Q., Yang, M., & Chen, Y. (2022). **The application of PBL teaching method in teaching sports human science courses in general undergraduate colleges and universities.** *Neijiang Science and Technology*, 43(7), 147-148+117.
- (9) Liu, Y., Xue, P., Li, F., & Wang, C. X. (2021). **A review of deep learning-based nodal behavior recognition.** *Journal of Electronics and Information*, 43(6), 1789-1802.
- (10) Deng, Z., Wang, D., Cai, J., Jiang, X., & Chen, Z. (2020). **Moral judgment of college basketball players based on dual processing theory: abstract reasoning or emotional control?** *Science Bulletin*, 65(19), 2010-2020.
- (11) Li, X., Huang, B., & Shen, L. (2020). **WeChat marketing strategy of apparel brands.** *Journal of Textiles*, 41(12), 130-136. <https://doi.org/10.13475/j.fzxb.20200302607>
- (12) Wan, C., Yang, K., Wang, W., Qian, Y., & Zhu, Y. (2019). **Kinect-based adaptive treadmill walking speed estimation method.** *Journal of Instrumentation*, 40(10), 219-226. <https://doi.org/10.19650/j.cnki.cjsi.J1905384>
- (13) Meng, H., Yin, W., Li, H., & Guo, Y. (2019). **Fingertip detection-tracking-supervision algorithm based on depth information.** *Journal of Instrumentation*, 40(6), 171-180. <https://doi.org/10.19650/j.cnki.cjsi.J1905207>
- (14) Zhou, H., & Zhang, J. (2019). **Diffusion of Self-media network opinion diffusion based on the forwarding effect.** *Control and Decision Making*, 34(03), 572-580. <https://doi.org/10.13195/j.kzyjc.2017.1398>
- (15) Wang, C., Qu, J., Zhang, F., Wang, Y., & Fu, Y. (2017). **Direct teaching of humanoid Using Kinect.** *Robotics*, 39(05), 697-703. <https://doi.org/10.13973/j.cnki.robot.2017.0697>
- (16) Ni, T., Zhao, Y.J., Zhang, H.Y., Liu, X.F., & Huang, L.T. (2017). **Real-time positional control system for robotic arm based on Kinect dynamic gesture recognition.** *Journal of Agricultural Machinery*, 48(10), 417-423+407.
- (17) Li, X., Wang, G., Xu, T., & Huang, W. (2013). **Factor analysis algorithm based on maximum variance rotation.** *Nanotechnology and Precision Engineering*, 11(06), 557-561. <https://doi.org/10.13494/j.npe.2013.092>

- (18) Zhang, T., Yu, J., Liao, B., Guo, B., Bian, C., Wang, Y., & Liu, Y. (2016). **Research on the construction and analysis of GraphX-based passing network.** *Computer Research and Development*, 53(12), 2729-2752.
- (19) Yang, S., Xin, Y., Wang, Y., & Zhang, F. (2016). **Design and realization of mobile platform based on WeChat Enterprise.** *Journal of Huazhong University of Science and Technology (Natural Science Edition)*, 44(S1), 158-161. <https://doi.org/10.13245/j.hust.16S132>
- (20) Chen, W., Zhu, W., Mason, S., Hammond-Bennett, A., & Colombo-Dougovito, A. (2016). **The effectiveness of quality physical education to improve students' manipulative skills.** *Journal of Sport and Health Science*, 5(02), 231-238+257.
- (21) Xiao, Z. G., Zhou, M. X., Yuan, H. B., Liu, Y. A. D., Fan, C., & Cheng, M. (2021). **Effect of illumination intensity on the accuracy of Kinect v2 depth data measurement.** *Journal of Agricultural Machinery*, 52(S1), 108-117.
- (22) Liu, Y., Xue, P., Li, H., & Wang, C. (2021). **A review of deep learning-based nodal behavior recognition.** *Journal of Electronics and Information*, 43(06), 1789-1802.
- (23) Drake, K. M., Longacre, M. R., MacKenzie, T., Titus, L. J., Beach, M. L., Rundle, A. G., & Dalton, M. A. (2015). **Gender differences in high school students' participation in sports programs.** *Journal of Sport and Health Science*, 4(03), 282-288+210.
- (24) Lundvall, S. (2015). **Physical literacy in the field of physical education - challenges and opportunities.** *Journal of Sport and Health Science*, 4(02), 113-118+212+216.
- (25) Ennis, C. D. (2015). **Knowledge, knowledge transfer and innovation in physical literacy curricula.** *Journal of Sport and Health Science*, 4(02), 119-124+213+216.
- (26) Silverman, S., & Mercier, K. (2015). **Instructional design and physical education teacher education in physical literacy education.** *Journal of Sport and Health Science*, 4(02), 150-155+213+216.
- (27) Castelli, D. M., Barcelona, J. M., & Bryant, L. (2015). **The challenge of integrating physical literacy in school settings.** *Journal of Sport and Health Science*, 4(02), 156-163+213+217.
- (28) Wu, J. P., Chen, K., & Liu, Y. (2022). **Real-time vanishing point detection by fusing random sampling consistency and Hough transform.** *Journal of Computer-Aided Design and Graphics*, 1-14.
- (29) Quan, Y. H., Chen, M. D., Ruan, F., Gao, X., Li, Y. C., & Xing, M. D. (2019). **An anti-dense dummy target interference algorithm with shortcut conversion combined with Hough transform.** *Journal of Electronics and Information*, 41(11), 2639-2645.
- (30) Liu, Y., Zhang, W., & Wang, X. (2018). **Access control scheme based on multi-attribute fuzzy trust evaluation in cloud manufacturing environment.** *Computer Integrated Manufacturing Systems*, 24(02), 321-330.
- (31) Yang, A.-M., Gao, F., Bian, M.-H., & Yang, S.-L. (2016). **Cloud computing security assessment and countermeasures based on hierarchical analysis-fuzzy evaluation.** *Journal of Communication*, 37(S1), 104-110.

- (32) Juárez, F. F., Esenarro, D., Díaz, M., & Frayssinet, M. (2021). **Model based on balanced scorecard applied to the strategic plan of a Peruvian public entity.** *3C Empresa. Investigación y pensamiento crítico*, 10(4), 127-147. <https://doi.org/10.17993/3cemp.2021.100448.127-147>
- (33) Chang, Y., Gao, W., Karim, C., & Ahmed K. H., M. (2022). **Performance evaluation of college laboratories based on fusion of decision tree and BP neural network.** *Applied Mathematics and Nonlinear Sciences*, 7(2), 1-14. <https://doi.org/10.2478/AMNS.2022.1.00001>

/09/

APPLICATION OF AR VIRTUAL IMPLANTATION TECHNOLOGY BASED ON DEEP LEARNING AND EMOTIONAL TECHNOLOGY IN THE CREATION OF INTERACTIVE PICTURE BOOKS

Sidan Liu*

College of Education, China West Normal University, Nanchong, Sichuan, 637000,
China

liusidan11@cwnu.edu.cn

Peng Peng

College of Education, China West Normal University, Nanchong, Sichuan, 637000,
China

Lei Cao

College of Education, China West Normal University, Nanchong, Sichuan, 637000,
China



Reception: 11/11/2022 **Acceptance:** 16/01/2023 **Publication:** 11/03/2023

Suggested citation:

L., Sidan, P., Peng and C., Lei. (2023). **Application of AR virtual implantation technology based on deep learning and emotional technology in the creation of interactive picture books.** *3C TIC. Cuadernos de desarrollo aplicados a las TIC*, 12(1), 176-198. <https://doi.org/10.17993/3ctic.2023.121.176-198>

ABSTRACT

In recent years, the field of deep learning has flourished, not only breaking through many difficult problems that are difficult to be solved by traditional algorithms but also bursting with greater vitality when combined with other fields. For example, product emotional design based on deep learning can integrate users' emotional needs into the actual product design. In this paper, we aim to use deep learning and affective technology in the creation of AR interactive picture books to transform the reading process from static to dynamic, enrich visual stimulation, and increase the fun and interactivity of reading. In this paper, based on the three-level theoretical model of emotion, the emotion labeling results are input to a deep neural network for learning, to establish an emotion-based recognition model for picture book images. The results show that the model can well analyze the emotion of images in AR picture books, and the accuracy of prediction is a big improvement compared with traditional machine recognition algorithms. The application of AR virtual implantation technology in interactive picture books on the market is often just a marketing gimmick while combining deep learning and emotional technology can better create diverse interactive picture books to meet children's emotional reading needs, enhance reading engagement, and stimulate children's creativity.

KEYWORDS

Deep learning; affective technology; AR implantation technology; interactive picture book; three-level theory.

PAPER INDEX

ABSTRACT

KEYWORDS

1. INTRODUCTION

2. EMOTIONAL AND DEEP LEARNING

2.1. Emotional design

2.1.1. Sources and classification of emotions

2.1.2. Emotionality in product design

2.1.3. Three-level theoretical model

2.2. Deep Learning

2.2.1. Convolutional neural network

2.2.2. Deep neural network

2.2.3. VGGNet network

3. APPLICATION OF AR VIRTUAL IMPLANTATION TECHNOLOGY IN INTERACTIVE PICTURE BOOKS

3.1. Combined application of AR technology in multiple directions

3.2. Features of AR technology

3.3. Comparison of AR interactive picture books and ordinary picture books

3.4. Use of Deep Learning and Affective Techniques

3.4.1. Emotion decoding and emotion labeling

3.4.2. Emotional deep learning

4. CONCLUSION

DATA AVAILABILITY

CONFLICTS OF INTEREST

REFERENCES

1. INTRODUCTION

In recent years, the continuous development of artificial intelligence algorithms such as deep learning and the emergence of ever-changing new media have contributed to the growth of various emerging technologies that have gradually changed the way information is relayed [1-3]. At the same time, digital technology, as one of the emerging technologies, has also been developing rapidly, and this technology is especially reflected in the field of picture books, creating a new wave that has a profound impact on the way children read. Augmented reality (AR) is a common and popular over-the-top concept, the principle of which is to use computer technology to transfer virtual information into the real environment to achieve the combination of virtual and reality [4-7], in three-dimensional form, the application of AR technology to interactive picture books can improve children's extraction and recognition of information [8-9], allowing children to feel the overlap of virtual and real scenes to enhance the virtual emotional experience and provide a deeper understanding of knowledge. The application of deep learning and emotional technology will strengthen the emotional analysis in the creation of AR picture books and enrich the emotional education function of interactive picture books.

Research on AR books first started with *The Magic Book* by Billinghamurst et al [10-12]. It is essentially a mixed reality application. In this application, by using a handheld display equipped with a small camera, the experimenter can then experience a realistic virtual world through a paper book. Since then many scholars have studied AR books. Professor Hiromichi Kato and Mark Billinghamurst jointly developed the first open-source framework for AR, AR Tool Kit [13-15], through which applications for AR can be easily written to superimpose virtual scenes onto real environments. The literature [16-17] introduces natural feature tracking techniques on AR books. The literature [18-19] focuses on the user interface design and interaction design of AR books. The literature [20-21] focuses on the design and research of interactive 3D books based on AR technology, introducing key technologies and proposing the production process. In the field of AR picture book publishing, Leo Paper Group publishes and designs the augmented reality interactive three-dimensional book *The Search for Wondla* [22], and the German company ArsEdition publishes the augmented reality book *Aliens and UFOs* [23-25]. By installing a special player, it is possible to see the three-dimensional scenes in this children's science fiction story on any camera-equipped computer through the Internet, breaking through the bottleneck of local reading.

In the era of new media, the application of AR interactive picture books is emerging. This paper will analyze the application of augmented reality technology based on deep learning and emotional technology in the creation of interactive picture books with the help of quantitative models based on the concepts of emotional design, deep learning, AR virtual implantation technology and interactive picture books, and explore how deep learning and emotional technology can better serve the application of AR virtual implantation technology in the creation of picture books. This paper establishes a quantitative emotion model based on psychologist Robert Pultchit's emotion wheel and Donald Arthur Norman's three-level emotional design theory. Then we compare

and analyze the algorithmic ideas of several current mainstream deep learning network models, and determine that VGGNet is more suitable for emotion discrimination and prediction of AR picture books. Finally, we establish an AR interactive picture book image sentiment analysis platform through deep learning training in an image sample library.

2. EMOTIONAL AND DEEP LEARNING

This paper uses cutting-edge deep learning techniques to learn product image emotions to promote the development and application of affective design, and affective design and deep learning are the two fundamental cores of this paper. This chapter introduces the concepts and development of these two topics and the lack of research in each of them, to discover the research points of this paper before the specific research is carried out. Among these two topics, affective design is the basic theory of this paper, while deep learning technology is the technical tool of this paper.

2.1. EMOTIONAL DESIGN

People's need for emotion can be found everywhere in life at any time, for example, compared to electronic books, people feel that the paper version is not only more comfortable but there is also a kind of emotional experience that is difficult to imitate with electronic books, perhaps a gentle and solid touch, perhaps a distant memory is touched, perhaps the familiar fragrance of paper brings a sense of freshness. For example, the phone can give me a timely notification of charging when it is out of battery, and give me a warm reminder when the weather is bad, bringing a sense of warmth and surprise. In modern society, machines are becoming more and more common, but people have an innate fear of machines; we feel they are complicated, cold, and even dangerous. Human-to-human communication is the most natural and intimate, so I hope the machine can be more humanized, and realize the humanization of the machine is the main purpose of human-computer interaction research, and the key to humanization is to make the machine have emotion.

Emotional design is the process of making design objects with emotional factors, taking into account the user's physiology and psychology throughout their life cycle, and catering to their innermost emotional needs to induce emotional responses.

2.1.1. SOURCES AND CLASSIFICATION OF EMOTIONS

Emotions were not separated independently long ago and still belonged to the realm of philosophy. It was only in the 19th century that the German psychologist Von Wundt separated the study of human emotions from philosophy and began scientific research. With the development of time and the maturity of theories, the study of human emotion was refined into three major branches, behavioral theory, theory of mind, and cognitive theory.

There are various classifications of human emotions, and the earliest days of psychology used a dichotomy to classify emotions into positive and negative emotions. In 1980 psychologist Robert Pultchlt proposed the emotion wheel to describe the association between emotions [26-27]. Robert Pultchlt's psycho-evolutionary theory of emotions is one of the most influential taxonomies of common emotional responses. He believed that there are eight most basic emotional elements as shown in Figure 1, which are anger, fear, sadness, dislike, surprise, curiosity, acceptance, and cheerfulness.

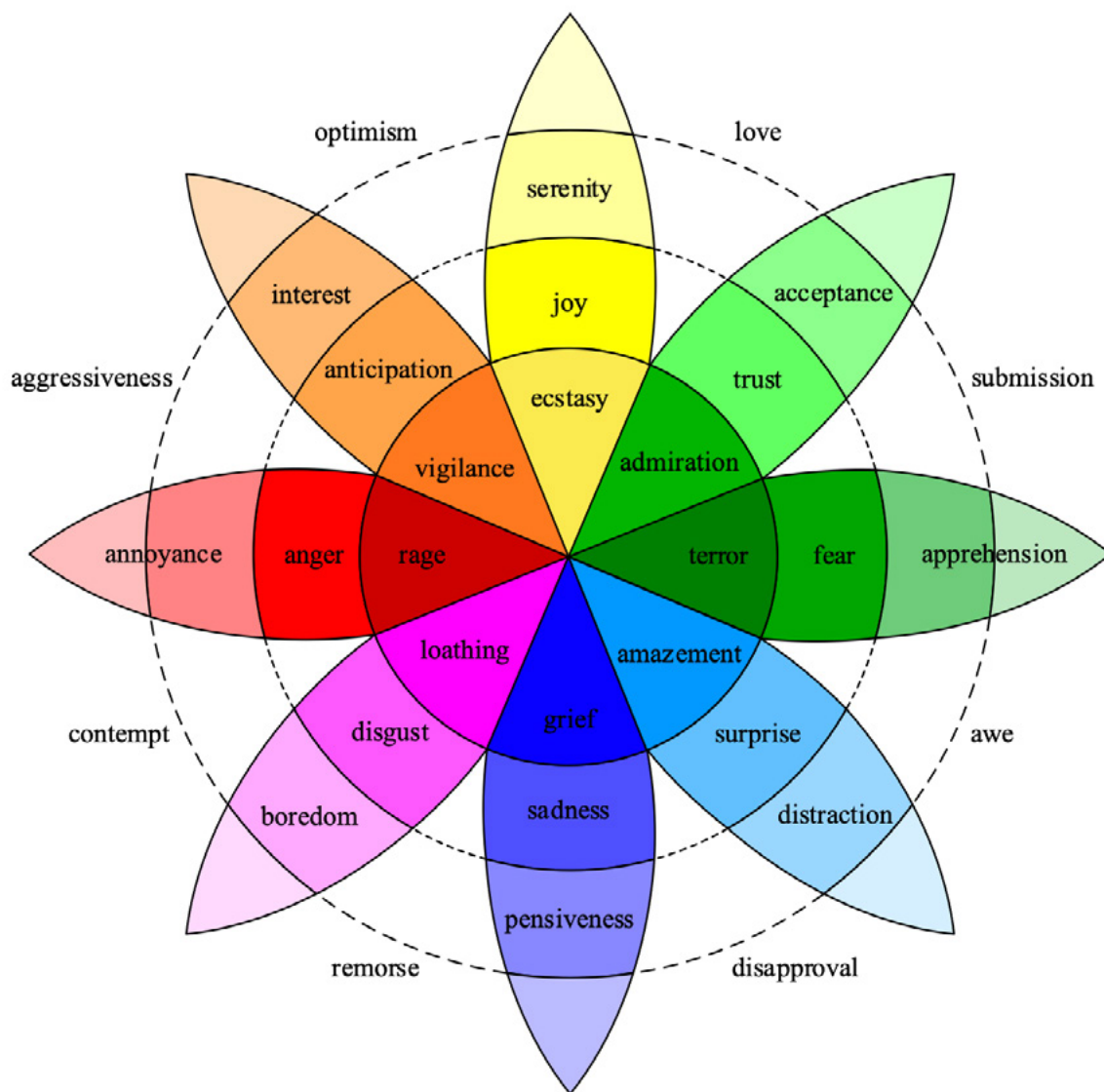


Figure 1. Robert Pultchlt's Emotional Roulette

2.1.2. EMOTIONALITY IN PRODUCT DESIGN

Emotional design is proposed by Donald Arthur Norman, an American cognitive psychologist, and its main idea is to attract users' attention and induce their emotional response through design, to realize the emotional communication and connection between humans and design objects and bring a better experience and deeper impression to users.

The purpose of emotional design is to bring positive emotions or complex emotions dominated by positive emotions. Talking about emotion from the perspective of design can even be extended to the category of style. For example, simplicity is style, which can also be said to be an emotion, because it reflects not only the properties of the design itself but also the psychological feelings of the viewer.

Emotions have objective and subjective aspects. The objective aspect refers to the emotional factors embedded in objective things or phenomena, while the subjective aspect refers to the subjective feelings and understanding received by the viewer or experienter. For design works, the objective aspect is the creator's use of design principles (such as composition principles), combined with psychology, to integrate colors, shapes, and materials to form a complete system to trigger a specific emotional response in the experience, which is the process of injecting emotions into the creator. The subjective aspect of emotion is influenced by the individual differences of the experience, such as the aesthetics, experience, and preferences of different experiences, so each person may have very different emotions towards the same work. It is also influenced by the different states of the same experience, such as the mood at the time. Even so, due to human commonalities, there is a strong convergence in the perception of a particular phenomenon, as evidenced by the research of Dacher Keltner's team.

2.1.3. THREE-LEVEL THEORETICAL MODEL

In Emotional Design, Professor Donald A. Norman divides the emotional design into three levels: instinctive, behavioral, and reflective [28-29]. The instinctive layer of design is concerned with the human sensory experience of the material characteristics of a specific product, which are usually visible or palpable, such as the structure, color, material, and form of the product. The instinctive layer is the most basic part and the first to attract people's attention. The behavioral layer of design is concerned with the interaction process between the product and the user, focusing on the efficiency and enjoyment of the operation, including the functionality, performance and usability of the product. The behavioral layer is about the design of product use so that the function of the product can conform to human behavior to the maximum extent, in this level of design, the shape of the product and design principles are not the most important, the most important is the performance of the product. The reflection layer is essentially also due to the role of the first two levels, but in the three levels is the most difficult to achieve, need to start from the user's common culture and information, resonate with the user, but the impact on the user is far-reaching, which is also the reason why a large number of the current market to give the product a certain quality and story, to create a different and evocative feeling to the user. However, in the actual design process, the three levels of emotional design are not completely independent, but intertwined and difficult to distinguish, as shown in Figure 2 a diagram of the relationship between the three levels, only for different levels of design focus will be different. Instinctive design is the human-computer dialogue of intuitive feeling, behavioral design is the human-computer dialogue in the process of

use, and reflective design is a dialogue of deep consciousness activity shown between humans and products.

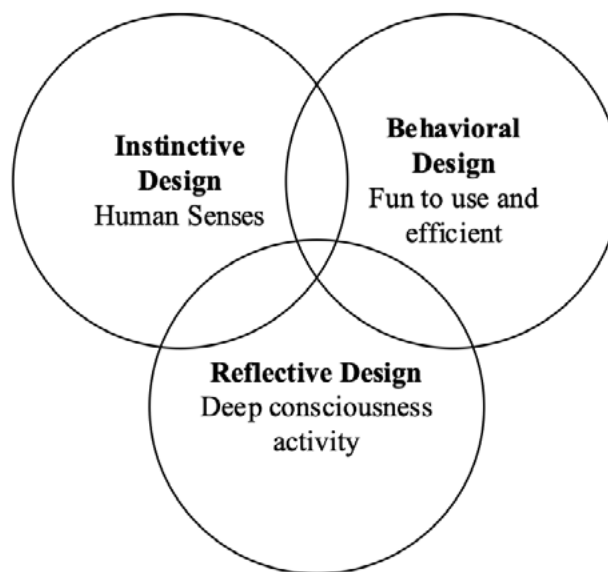


Figure 2. Emotional design three levels of relationship diagram

2.2. DEEP LEARNING

Emotions can be learned. There has been a lot of research using machine learning techniques to perform sentiment analysis for various types of image content. Machine learning is the process of training a model with data, allowing the machine to find patterns and use the knowledge learned to analyze and judge new data. The core part of this process is to design algorithms that allow the computer to learn automatically, so that the whole learning process "comes to life", and to continuously optimize the feature weights through backpropagation to improve the learning effect. With the rise of deep learning, more and more work is being done using deep learning features instead of traditional hand-designed features for analysis. Among them, deep learning is a data-driven feature extraction process. Under the premise of ensuring data quality, the more training samples there are, the deeper features can be obtained and the more ideal the training effect is. Compared with traditional algorithms, the expressiveness of deep learning is significantly more efficient and accurate, and the obtained abstract features are much better in terms of robustness and generalization, and the whole training process is end-to-end, so there is no need for human intervention in the middle.

One of the most important technologies for deep learning is neural networks. A neural network, which mimics the human brain, relies on neurons to transmit and process information, and the entire network is a system that includes a large number of neurons. A neuron is a simple classifier that is used to identify object features.

2.2.1. CONVOLUTIONAL NEURAL NETWORK

Convolutional neural network (CNN) [30-31] is arguably the most typical structure of deep learning networks. 1998 LeNet-5, proposed by Lecun et al. is the first real multi-layer network, and its convolutional network structure is shown in Figure 3. It uses convolutional structure to obtain one-dimensional or spatial data, for example, temporal data is a one-dimensional form of data, while pictures are a two-dimensional form of data, and convolutional neural network is especially good at processing picture-like two-dimensional structure data. The process of convolutional data extraction is a special mathematical operation, and convolutional kernels have been used in research related to image content processing for a long time.

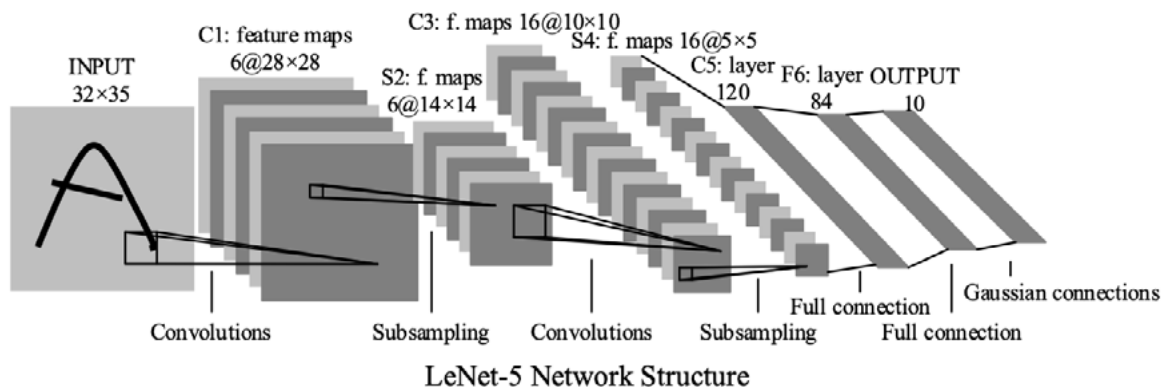


Figure 3. Structure of LeNet-5

The network starts with an input layer, which is typically an image. Next are successive alternating convolutional and pooling layers. The convolutional layer consists of multiple feature maps, i.e., feature maps in Figure 2, and each feature map consists of multiple neurons, which are connected to some local block of the previous layer's feature map by the weights of the convolutional kernel. The convolution kernel is a matrix of weights, for example, it can be 3×3 or 5×5. The extraction of features is performed by the convolution operation of the convolution kernel with the feature maps of the previous layer, and as the number of convolution layers deepens, the feature maps obtained become more abstract. In the same feature map, the weights of the filters are the same, called weight sharing, which has the advantage of reducing the complexity of the model on the one hand and capturing the local features of the input on the other. The locally weighted sum of each convolution kernel after convolution with the previous layer is passed to a nonlinear function (called the activation function) to obtain the output of the convolutional layer. The activation function is an indispensable feature of convolutional neural networks to enhance the expressiveness of the network. The commonly used activation functions are the sigmoid function, tanh function, ReLU function, etc. The calculation formula is as follows.

$$\text{sigmoid}(x) = \frac{1}{1 + (1 + e^{-x})} \quad (1)$$

$$\text{tanh}(x) = \frac{2}{1 + e^{-2x}} - 1 \quad (2)$$

$$\text{ReLU}(x) = \max(0, x) \quad (3)$$

The learning effect of a convolutional neural network can be defined by the loss function. And the training goal of the convolutional neural network is to minimize the loss of function. The common loss functions are the 0-1 loss function, square loss function, logarithmic loss function, etc. Suppose the input is given as X , the true value is Y , and the predicted value of the convolutional neural network model is $f(x)$, then the squared loss function $L(Y, f(X))$ is

$$L(Y, f(X)) = (Y - f(X))^2 \quad (4)$$

The training process is divided into two processes: forward propagation and backward propagation. First, forward propagation is performed, and the prediction result $f(x)$ is calculated layer by layer according to the given input X . Then the corresponding loss is calculated according to the defined loss function, and then the backpropagation of the gradient is performed according to the loss using the stochastic gradient descent algorithm. The bias of the loss to each parameter in the network is calculated by the chain rule of derivatives, and then the weights are updated, and the update formula is

$$\omega_i \leftarrow \omega_i - \eta \frac{\partial L(Y, f(X))}{\partial \omega_i} \quad (5)$$

where ω_i is one of the weights in the network and η is the learning rate, which is used to control the intensity of the weight update.

2.2.2. DEEP NEURAL NETWORK

A deep neural network (DNN) is a feedforward neural network with multiple hidden layers [32-33], also known as MLP, and its structure is shown in Figure 4. This DNN has a total of $L+1$ layers, where layer 0 is the input layer, layers 1 to $L-1$ are the hidden layers, and layer L is the output layer, and adjacent layers are connected by a feedforward weight matrix.

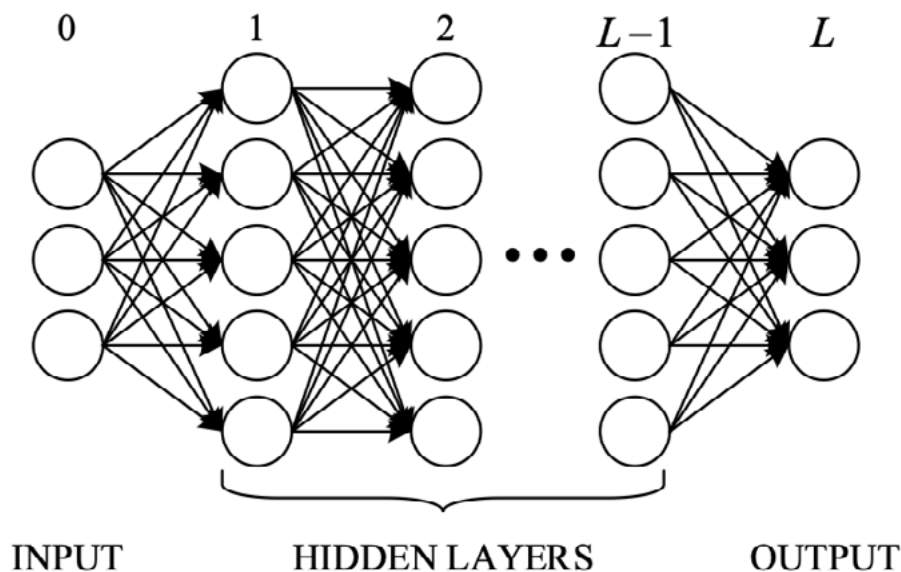


Figure 4. DNN structure schematic

Assuming that layer l has n_l neurons, the vector consisting of the inputs of these neurons is $z^{(l)}$ and the vector consisting of the outputs is $h^{(l)}$. Also, we let $u = h^{(l)}$ to distinguish the final output of the DNN from the output of the hidden layer, given a training sample with the feature x , at this point there is $h^{(0)} = z^{(0)} = x$. According to the rules of DNN computation

$$z^{(l)} = W^{(l)}z^{(l-1)} + b^{(l)}, l = 1, 2, \dots, L \quad (6)$$

where $W^{(l)} \in \mathbb{R}^{n_l \times n_{l-1}}$ is the matrix of weights from layer $l-1$ to layer l and $b^{(l)} \in \mathbb{R}^{n_l}$ is the bias vector of the layer l . Then there is

$$h^{(l)} = f_l(z^{(l)}) \quad (7)$$

The activation function of the output layer depends on the nature of the problem to be solved by the DNN. Linear activation functions or sigmoid functions are usually used for regression problems, sigmoid functions are usually used for binary classification problems, and for multi-classification problems, the most commonly used is the softmax function, which takes the following form.

$$u = \text{softmax}(z^{(L)}) = \frac{\exp(z^{(L)})}{\sum_{k=1}^{n_L} \exp(z^{(L,k)})} \quad (8)$$

$z^{(L,k)}$ denotes the k rd component of the vector $z^{(L)}$.

Combined with the above process, the features x of the training samples are first sent to the input layer, then propagated through each hidden layer in the direction of the arrow in the figure and finally reach the output layer to obtain the final network output, a process called forward propagation.

DNN can also be trained with a backward propagation algorithm, and the parameters of DNN are

$$\theta = \{W^{(l)}, b^{(l)} | l = 1, 2, \dots, L\} \quad (9)$$

The features of the training sample set used are denoted as

$$\chi = \{x_i \in \mathbb{R}^{n_0} | i = 1, 2, L, S\} \quad (10)$$

The corresponding label is noted as

$$R = \{r_i | i = 1, 2, L, S\} \quad (11)$$

The loss function on the training set is

$$E(\theta, \chi, R) = \frac{1}{S} \sum_{i=1}^S E(\theta, x_i, r_i) \quad (12)$$

$E(\theta, x_i, r_i)$ is the loss function corresponding to the training sample X_i . The goal of training is to minimize the training set loss function. To obtain satisfactory performance, model optimization is often performed using large-scale data, so the method often used for DNN training is stochastic gradient descent.

Firstly, \mathbf{x} is sent to the DNN input layer to complete the forward propagation and $E(\theta, x_i, r_i)$ is calculated based on the output and the label r . Define the error signal of the layer l as

$$\mathbf{e}^{(l)} = \left. \frac{\partial E(\theta, \mathbf{x}, r)}{\partial \mathbf{z}^{(l)}} \right|_{\theta = \theta^{(t)}} \quad (13)$$

The error signal $\mathbf{e}^{(L)}$ of the output layer can be easily calculated according to the loss function, and for the hidden layer according to the chain rule of derivation

$$\begin{aligned} \mathbf{e}^{(l)} &= \left. \frac{\partial E(\theta, \mathbf{x}, r)}{\partial \mathbf{h}^{(l)}} \right|_{\theta = \theta^{(t)}} \odot \frac{\partial \mathbf{h}^{(l)}}{\partial \mathbf{z}^{(l)}} \\ &= \frac{\partial \mathbf{z}^{(l+1)}}{\partial \mathbf{h}^{(l)}} \cdot \left. \frac{\partial E(\theta, \mathbf{x}, r)}{\partial \mathbf{z}^{(l+1)}} \right|_{\theta = \theta^{(t)}} \odot f'_l(\mathbf{z}^{(l)}) \\ &= \mathbf{W}^{(l+1)^T} \cdot \mathbf{e}^{(l+1)} \odot f'_l(\mathbf{z}^{(l)}) \end{aligned} \quad (14)$$

where \odot denotes element-by-element multiplication. From this calculation process, it can be seen that the error signal is propagated from layer L to layer 1 through the weight matrix in the opposite direction of forward propagation, hence the name backward propagation. Finally, according to the chain rule, we can get

$$\left. \frac{\partial E(\theta, \mathbf{x}, r)}{\partial \mathbf{W}^{(l)}} \right|_{\theta = \theta^{(t)}} = \frac{\partial E(\theta, \mathbf{x}, r)}{\partial \mathbf{z}^{(l)}} \cdot \frac{\partial \mathbf{z}^{(l)}}{\partial \mathbf{W}^{(l)}} = \mathbf{e}^{(l)} \cdot \mathbf{h}^{(l)^T} \quad (15)$$

$$\left. \frac{\partial E(\theta, \mathbf{x}, r)}{\partial \mathbf{b}^{(l)}} \right|_{\theta = \theta^{(t)}} = \frac{\partial E(\theta, \mathbf{x}, r)}{\partial \mathbf{z}^{(l)}} \cdot \frac{\partial \mathbf{z}^{(l)}}{\partial \mathbf{b}^{(l)}} = \mathbf{e}^{(l)} \quad (16)$$

Based on the above derivation process of forward and backward propagation, it can be found that the training of DNN involves a large number of matrix operations, which are well suited to speed up the computation by using graphics processing units (GPUs). The development of GPU technology is credited with driving the deep learning research boom. Since GPUs are suitable for large-scale matrix operations, to give full play to their power, in actual training, we use the mini-batch SGD algorithm, i.e., for each iteration, a small number of samples are randomly taken from the training samples to form a mini-batch, and the gradients corresponding to all the samples in it are calculated at the same time, and this gradient information is used to update the model parameters in this round. the use of SGD can greatly accelerate the training of DNN The use of SGD can greatly accelerate the DNN training speed.

2.2.3. VGGNET NETWORK

In 2014, Simonyan and Zisserman, scholars from Oxford University, proposed the famous VGG family of models (including VGG-11/VGG-13/VGG-16/VGG-19) [34-35] and achieved second place in the classification competition and first place in the localization competition at the ImageNet competition that year. VGGNet, with its good generalization performance, VGGNet has been widely used in the field of computer vision.

The network structure of VGGNet is shown in Table 1. VGGNet replaces five convolutional layers with five groups of convolutions, adding the previous part consisting of five convolutional layers superimposed with an activation function, so that each part does not consist of one convolutional layer plus an activation function, but multiple such combinations, with pooling operations between each part[36-37].

Table 1. Architecture of VGGNet

| A | A-LRN | B | C | D | E |
|----------------------------|-----------|------------------|------------------|------------------|------------------|
| 11 Layers | 11 Layers | 13 Layers | 16 Layers | 16 Layers | 19 Layers |
| Input (224×224 RGB) Image | | | | | |
| conv3-64 | conv3-64 | conv3-64 | conv3-64 | conv3-64 | conv3-64 |
| | LRN | conv3-64 | conv3-64 | conv3-64 | conv3-64 |
| Maximum pooling layer | | | | | |
| conv3-128 | conv3-128 | conv3-128 | conv3-128 | conv3-128 | conv3-128 |
| | | conv3-128 | conv3-128 | conv3-128 | conv3-128 |
| conv3-256 | conv3-256 | conv3-256 | conv3-256 | conv3-256 | conv3-256 |
| conv3-256 | conv3-256 | conv3-256 | conv3-256 | conv3-256 | conv3-256 |
| | | | conv1-256 | conv3-256 | conv3-256 |
| | | | | | conv3-256 |
| Maximum pooling layer | | | | | |
| conv3-512 | conv3-512 | conv3-512 | conv3-512 | conv3-512 | conv3-512 |
| conv3-512 | conv3-512 | conv3-512 | conv3-512 | conv3-512 | conv3-512 |
| | | | conv1-512 | conv3-512 | conv3-512 |
| | | | | | conv3-512 |
| Maximum pooling layer | | | | | |
| conv3-512 | conv3-512 | conv3-512 | conv3-512 | conv3-512 | conv3-512 |
| conv3-512 | conv3-512 | conv3-512 | conv3-512 | conv3-512 | conv3-512 |
| | | | conv1-512 | conv3-512 | conv3-512 |
| | | | | | conv3-512 |
| Maximum pooling layer | | | | | |
| Fully connected layer-4096 | | | | | |
| Fully connected layer-4096 | | | | | |
| Fully connected layer-1000 | | | | | |
| Softmax layer | | | | | |

VGGNet has the following main advantages.

1. VGGNet uses convolutional kernels with small sensory fields instead of those with large sensory fields, which can reduce the number of network parameters. Since the number of parameters is greatly reduced, one convolutional layer with a large sensory field can be replaced by multiple convolutional layers with a small sensory field, thus increasing the nonlinear expression capability of the network.
2. Starting from VGG-16, VGGNet introduces a convolutional layer with 1×1 kernel size, which enhances the nonlinear expression ability of the network without affecting the size of the feature map.

3. APPLICATION OF AR VIRTUAL IMPLANTATION TECHNOLOGY IN INTERACTIVE PICTURE BOOKS

Augmented Reality (AR) is a branch of VR technology, which is currently used in various fields such as design and life. With the maturity and progress of AR technology, AR technology has been gradually applied to new fields such as education, with a wide range of radiation, such as medical systems, cultural heritage preservation, games and entertainment, children's publishing books, etc. AR technology system extends from a simple desktop to a complex interactive experience and gradually expands to touch screen and portable convenience.

3.1. COMBINED APPLICATION OF AR TECHNOLOGY IN MULTIPLE DIRECTIONS

Currently, in the context of AR technology being widely used in other fields, the technology has also begun to be applied in the book publishing industry. In the process of application, it will also fully combine other forms of technology, such as digital technology, multimedia technology, etc. The use of these technologies provides more possibilities for augmented display technology so that it can be applied to more fields. The static and single content expression is presented in a realistic and three-dimensional way.

3.2. FEATURES OF AR TECHNOLOGY

AR technology is to fuse virtual impact and real impact, and enhances reality to achieve real-time interaction, and through three-dimensional registration to complete the realization of AR products.

1. Virtual reality fusion refers to the enhancement of realistic scenes with the superimposition of virtual objects and realistic environments. Augmented reality technology provides an intermediate transition state for children, this transition state is partly virtual imaginary and partly real, the emergence of this transition state can alleviate children's anxiety due to cognitive uncontrollability after age enhancement and constant exposure to the external world. Potential space, as a kind of

intermediary in the transition space, can prompt children to enter reality from the fantasy world, participate in reality and cognize the object.

2. Real-time interaction means that people can interact and operate with the enhanced reality environment machinery through the device. This interaction should meet real-time requirements. Augmented reality technology can convert the static content of science-based children's picture books into a huge network linked by keywords, consisting of graphic images, animation, sound effects and text and other media to form an independent text. Children interact with AR picture books and can get a new reading experience with the help of clicking, touching and hearing, which is incomparable to traditional picture books.
3. Three-dimensional registration (also called three-dimensional alignment) is a one-to-one fusion correspondence between the computer-generated virtual image and the real environment, and maintains accurate positioning and correspondence, while the correspondence between virtual objects and the real environment must be perfectly integrated to facilitate users to use their portable cell phones to use the camera to aim at the QR code for identification, to identify the information materials that match the QR code.

3.3. COMPARISON OF AR INTERACTIVE PICTURE BOOKS AND ORDINARY PICTURE BOOKS

AR interactive picture books and traditional picture books are communication mediums to convey information in the form of images. AR picture books are based on traditional picture books, integrated with augmented reality technology, cell phones scan the picture of the book in three-dimensional presentation. The traditional picture book display form becomes more diversified. It can be said that AR picture books are developed based on traditional picture books, and AR picture books can meet more needs of children. The comparison of the two is shown in Table 2.

Table 2. Comparison table of traditional picture books and AR picture books

| | Traditional picture books | AR picture books |
|-------------------------|--|---|
| Vision | Traditional picture books convey information through pictures, the output of knowledge points is more homogeneous. | (1) Cell phones scan the picture of this book, a three-dimensional model and animation display appears on the screen, more vivid image, enhance the emotional experience of children. (2) Augmented reality technology allows the presentation of models' diversification. |
| Aural | Without parents around to explain, children can only can read with their own understanding. | The content of the science is equipped with audio commentary, subtitles, etc. more memorable for children. |
| Haptics | Hand-turned book touch only, no interactive operation interaction. | (1) interacting with the model inside the phone screen. through gesture operations can achieve zoom in, zoom out, pan zoom in, zoom out, pan, rotate, etc., which can enhance children's reading interest in reading. (2) AR picture books, by adding game sessions, can to develop children's thinking in a multi-dimensional way. |
| Other Dimensions | Traditional science picture books do not meet children for digital needs. | AR development supports a wide range of systems to meet the needs of different needs of different models. |

3.4. USE OF DEEP LEARNING AND AFFECTIVE TECHNIQUES

AR interactive picture book is a comprehensive picture, voice, click an interactive multimedia product, combined with deep learning product emotional design can make the AR interactive picture book greatly enhance the expressive power, and interactive effect significantly improved.

3.4.1. EMOTION DECODING AND EMOTION LABELING

The most important medium in picture books is images, and how exactly do the underlying features of images generate high-level abstract emotions? It is difficult to explain clearly even for humans, and the machine learning this process is a huge semantic gap, and the process of deep learning is to bridge this gap, but because of the end-to-end nature of deep learning, the machine learning process in terms of which features are extracted is something that no one can say. One cannot understand what rules are used to map the underlying features to the high-level

sentiment semantics. This is often referred to as the "black box" of deep learning. The current research in the field of computer science has a lot of neural network feature extraction rules and emotion mapping rules, the object of study is the machine, and the study is "how the machine learns emotion".

Starting from the international award-winning works of high quality and reflecting contemporary design trends, and guided by design emotion theory, we selected product design images with more obvious design emotion characteristics and established a preliminary design gallery with 2048 images covering common product categories. Next, we invited design professionals to extract design emotion vocabulary based on design knowledge and experience and learning of the three-level theory, and to label the images in the design emotion gallery with emotion, identifying the typical emotion label for each design image and the design feature label that generates emotion.

As shown in Table 3, the overall distribution of various sentiments of the picture samples was obtained after the aggregation of all data annotations.

Table 3. Sentiment distribution of image samples

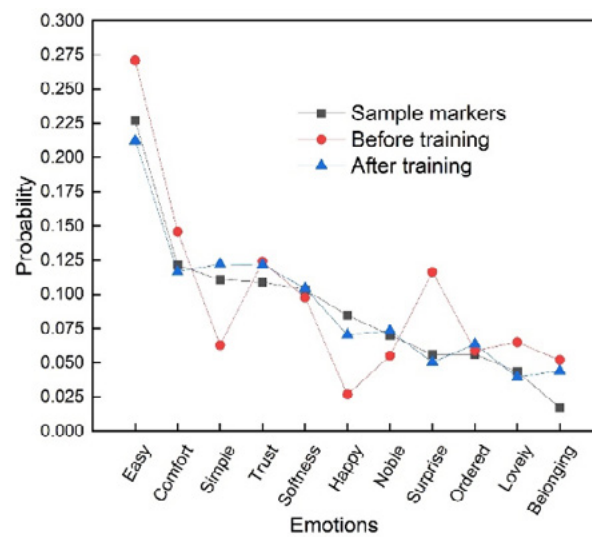
| Emotional name | Emotional share | Level of affiliation |
|----------------|-----------------|----------------------|
| Easy | 22.70% | 2 |
| Comfort | 12.15% | 2 |
| Simple | 11.08% | 1 |
| Trust | 10.91% | 3 |
| Softness | 10.36% | 1 |
| Happy | 8.47% | 1 |
| Noble | 7.03% | 1 |
| Surprise | 5.61% | 1 |
| Ordered | 5.62% | 2 |
| Lovely | 4.37% | 1 |
| Belonging | 1.71% | 3 |

In the emotional labeling of product images, the first level of emotion not only has the largest number of words, but also has the highest total percentage, reaching 46.92%, and the second level also has a total percentage of 40.46%, and the highest percentage of ease of use and comfort belongs to the second level, becoming the most prominent emotional words, which also reflects the current trend of emotional design towards the second level. The third level of emotion not only has the least variety, but also accounts for far less than the first two levels, with only 10.91% and 1.71%, and the sense of belonging has become the most unattractive emotion.

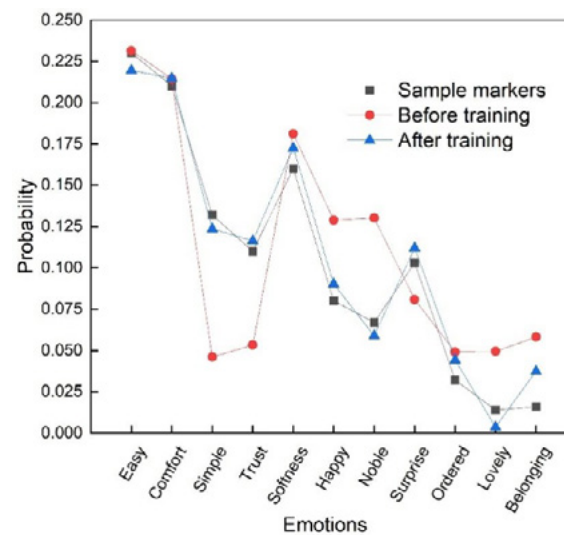
3.4.2. EMOTIONAL DEEP LEARNING

Based on the 2.2.3 VGGNet deep learning network, 1500 of the above 2048 images were used for model training, and the remaining images were used for testing. After the model training is completed, the sentiment with the highest probability for each image is taken as a single label for the test set, the degree of compliance between prediction and actual labeling is compared, and the accuracy is measured in the form of a percentage, which is more intuitive and clear. In this paper, cross-validation is used to calculate the final learning effect. Cross-validation, also known as cyclic evaluation, is done by first dividing the total data set into multiple parts at random, using one part of the data for testing and most of the remaining part for training the model, which can be used to find the prediction accuracy in the test set, and then selecting the second part for testing and the rest for training. This cycle continues until all samples are tested and only tested once, and finally, the average of all predictions is taken. According to this method, we divide more than 2000 images into random equal parts and use one part for testing and the rest for training the model, so that each part is used for prediction once in 10 rounds. The average of the 10 results is taken as the evaluation criterion. The process can also be repeated several times, each time with a different randomly divided sample, to achieve multiple cross-validations for more accurate results.

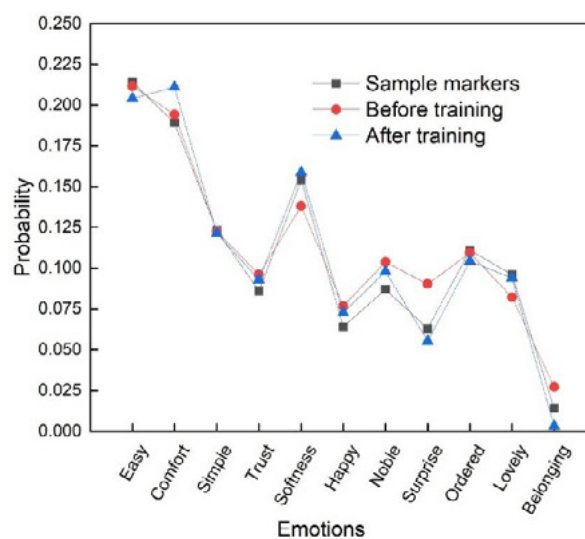
The predicted results of the sentiment probability distribution of the images are shown in Figure 5.



(a) Training samples (1-500)



(b) Training samples (501-1000)



(c) Training samples (1001-1500)

Figure 5. Predicted results of the probability distribution of emotions

With this calculation method, we obtained a final single-label accuracy of 61.02%, which is a very good learning result compared to the 50% to 60% accuracy of single-label classification of emotions by traditional machine learning methods. The horizontal axis of the figure indicates 11 emotion categories: pleasant, cute, surprise, soft, comfortable, trust, plain, easy to use, noble, sense of order, and sense of belonging. The vertical axis shows the proportion of each emotion in each picture. It can be seen that the prediction results of the learning are all improved compared with those before the learning, and the prediction curves fit better and better as the number of learning samples increases. The evaluation of the learning results in this study includes two parts, the evaluation of the loss of multi-label distribution (KL loss) and the evaluation of the accuracy of single-label classification (cross-validation), and the combination of the two aspects can be a good measure of the learning effect. The evaluation results demonstrate the feasibility and superiority of deep learning in emotion recognition and also show that the emotion-based design combined with deep learning can better serve the AR interactive picture book creation.

4. CONCLUSION

As the book industry becomes more and more depressed, traditional paper picture books are slowly forgotten by children and parents, and many children are even addicted to smartphones, iPads and other mobile devices, rarely reading picture books. The combination of AR technology and traditional industry links can well inherit the culture of traditional paper hand-drawn, giving children's picture books a new connotation, such as AR interactive picture books are more dynamic, enhance the reader and the book presents interactivity, increasing the fun of paper books. At the same time, different from paper picture books, AR interactive picture books can strengthen the interactive communication experience based on deep learning algorithms. By analyzing and summarizing the sources and connotations of emotional design, we focus on the three levels of emotional design, highlighting the second and third levels of emotional needs in the creation of interactive picture books. The creation of AR interactive picture books with such new technology, can bring children an emotionally pleasant experience when reading and subtly educate them.

DATA AVAILABILITY

The data used to support the findings of this study are available from the corresponding author upon request.

CONFLICTS OF INTEREST

The author declares that there is no conflict of interest regarding the publication of this paper.

REFERENCES

- (1) Standoli, G., Salachoris, G. P., Masciotta, M. G., et al. (2021). **Modal-based FE model updating via genetic algorithms: Exploiting artificial intelligence to build realistic numerical models of historical structures.** *Construction and Building Materials*, 303, Oct. 11.
- (2) Maduabuchi, C. (2022). **Thermo-mechanical optimization of thermoelectric generators using deep learning artificial intelligence algorithms fed with verified finite element simulation data.** *Applied Energy*, 315, 118943-.
- (3) Gasimova, R. T., & Abbasl, R. N. (2020). **Advancement of the search process for Digital Heritage by utilizing artificial intelligence algorithms.** *Expert Systems with Applications*.
- (4) Dias, L., Coelho, A., Rodrigues, A., et al. (2013). **GIS2R — Augmented reality and 360° panoramas framework for geomarketing.** In *Information Systems & Technologies* (pp. 1-6). IEEE.
- (5) Moretamartinez, R., Mediavillasantos, L., & Pascau, J. (2021). **Combining Augmented Reality and 3D Printing to Improve Surgical Workflows in Orthopedic Oncology: Smartphone Application and Clinical Evaluation.** *Sensors*, 21(4), 1370.
- (6) Laviola, E., Gattullo, M., Manghisi, V. M., et al. (2022). **Minimal AR: visual asset optimization for the authoring of augmented reality work instructions in manufacturing.** *The International Journal of Advanced Manufacturing Technology*, 119(3), 1769-1784.
- (7) Zhang, Z., Li, T., & Yoon, S. (2021). **A Feasibility Study of LiDAR-Enhanced Augmented Reality on a Handheld Device for Collision Detection and Patient Positioning.** *International Journal of Radiation Oncology, Biology, Physics*, 111-3S.
- (8) Frederico, A. (2016). **The future of the reader or the reader of the future: Children's interactive picturebook apps and multiliteracies.**
- (9) Sun, C. (2020). **Interactive Picture Book Read-Alouds to the Rescue: Developing Emerging College EFL Learners' Word Inference Ability.** *Journal of Adolescent & Adult Literacy*, 63.
- (10) Kuswaty, M., & Cahyani, I. (2019). **Analysis of musical drama in and the magic book.** *KnE Social Sciences*.
- (11) Johnson, A. (2021). **Malory's Magic Book: King Arthur and the Child, 1862–1980 by Elly McCausland.** *The Lion and the Unicorn*, 45(1), 124-127.
- (12) Ren, P. (2020). **AR 3D Magic Book: A Healthy Interactive Reading Device Based on AR and Portable Projection.** In *CIPAE 2020: 2020 International Conference on Computers, Information Processing and Advanced Education*.
- (13) Min, X. U., Tong, Q., Chen, D. C., et al. (2015). **Design and Production of Augmented Reality Courseware Based on ARTool Kit.** *Modern Computer*.
- (14) Khan, D., Ullah, S., & Rabbi, I. (2015). **Classification of Markers in the ARTool Kit Library to Reduce Inter-marker Confusion.** In *International Conference on Frontiers of Information Technology* (pp. 257-262). IEEE.
- (15) Simon, B. N., Chandrashekar, C. M., & Simon, S. (2011). **Hamilton's turns as a visual tool-kit for designing of single-qubit unitary gates.** *arXiv preprint arXiv*, 1108.1368.

- (16) Hermawan, H. D., Yuliana, I., Saputri, A., et al. (2021). **How Does ARBook Promotional Media For MSME Crafts Using Augmented Reality Marker Tracking Works?.**
- (17) Chiu, P.-H., Lin, P.-H., Lee, H.-L., et al. (2018). **Interactive Mobile Augmented Reality System for Image and Hand Motion Tracking.** *IEEE Transactions on Vehicular Technology*, 67(6), 5029-5040.
- (18) Chrysanthi, A., Papadopoulos, C., & Frankland, T. (2012). **'Tangible pasts': user-centred design of a mixed reality application for cultural heritage.** *Computer Applications & Quantitative Methods in Archaeology*, 2012, 113-120.
- (19) Grasset, R., Dünser, A., & Billinghamurst, M. (2008). **The design of a mixed-reality book: Is it still a real book?** *In IEEE/ACM International Symposium on Mixed & Augmented Reality* (pp. 73-82). IEEE.
- (20) Barvir, R., Vondrakova, A., & Brus, J. (2021). **Efficient Interactive Tactile Maps: A Semi-Automated Workflow Using the TouchIt3D Technology and OpenStreetMap Data.** *ISPRS International Journal of Geo-Information*, 10(5), 316.
- (21) Guo, C., Hou, Z. X., Shi, Y. Z., et al. (2017). **A virtual 3d interactive painting method for Chinese calligraphy and painting based on real-time force feedback technology.** *Frontiers of Information Technology and Electronic Engineering*, 18(11), 1799-1810.
- (22) Wy, A., Dy, A., Eh, A., et al. (2018). **Acid-activatable oxidative stress-inducing polysaccharide nanoparticles for anticancer therapy.** *Journal of Controlled Release*, 269, 235-244.
- (23) Wright, D. (2020). **Encountering UFOs and aliens in the tourism industry.** *Journal of Tourism Futures*, (aop).
- (24) Boli, J. (2018). **Small planet in the vastness of space: Globalization and the proliferation of UFOs, aliens, and extraterrestrial threats to humanity.** *Discussion Papers, Research Unit: Global Governance*.
- (25) MD Lafayette. (2011). **1520 Things You Don't Know About Ancient Aliens, UFOs, Aliens Technology and U.S. Black Operations** [Ebook].
- (26) Shuman, V., Scherer, K., Fontaine, J., et al. (2015). **The GRID meets the Wheel: Assessing emotional feeling via self-report.** *Oxford University Press*.
- (27) Dubreucq, S., Marsicano, G., & Chaouloff, F. (2015). **Emotional consequences of wheel running in mice: which is the appropriate control?** *Hippocampus*, 21(3), 239-242.
- (28) Zhang, X. (2016). **Research on Ways to Stimulate Students' Interest in Learning Korean: Based on Dornyei Three-level Theory.** *The Science Education Article Collects*.
- (29) Zhao, T., & Zhu, T. (2019). **Exploration of Product Design Emotion Based on Three-Level Theory of Emotional Design.** *Springer, Cham*.
- (30) Cui, F., Ning, M., Shen, J., et al. (2022). **Automatic recognition and tracking of highway layer-interface using Faster R-CNN.** *Journal of Applied Geophysics*, 196,
- (31) Shin, H. C., Roth, H. R., Gao, M., et al. (2016). **Deep Convolutional Neural Networks for Computer-Aided Detection: CNN Architectures, Dataset**

- Characteristics and Transfer Learning.** *IEEE Transactions on Medical Imaging*, 35(5), 1285-1298.
- (32) Kim, S., Kojima, M., & Toh, K. C. (2016). **A Lagrangian–DNN relaxation: a fast method for computing tight lower bounds for a class of quadratic optimization problems.** *Mathematical Programming*, 156(1-2), 161-187.
- (33) Li, J., Zhao, R., Huang, J. T., et al. (2014). **Learning Small-Size DNN with Output-Distribution-Based Criteria.** *In Conference of the International Speech Communication Association. ISCA.*
- (34) Wang, L. (2015). **Places205-VGGNet Models for Scene Recognition.** *Computer Science.*
- (35) Rao, B. S. (2020). **An Accurate Leukocoria Predictor Based On Deep VGG-Net CNN Technique.** *IET Image Processing*, 14(5).
- (36) Singh, A. K., & Sora, M. (2021). **An optimized deep neural network-based financial statement fraud detection in text mining.** *3C Empresa. Investigación y pensamiento crítico*, 10(4), 77-105. <https://doi.org/10.17993/3cemp.2021.100448.77-105>
- (37) Yan Kang, Jinling Song, Mingming Bian, Haipeng Feng, & Salama Mohamed. (2022). **Red tide monitoring method in coastal waters of Hebei Province based on decision tree classification.** *Applied Mathematics and Nonlinear Sciences*, 7(1), 43-60. <https://doi.org/10.2478/AMNS.2022.1.00051>

/10/

INNOVATION OF COLLEGE POP MUSIC TEACHING IN TRADITIONAL MUSIC CULTURE BASED ON ROBOT COGNITIVE-EMOTIONAL INTERACTION MODEL

Hua Zhou*

School of Electronic Engineering, Xi'an Shiyou University, Xi'an, Shaanxi, 710065, China

Shanghai Salvage, Shanghai, 201914, China

211122@126.com



Reception: 13/11/2022 **Acceptance:** 06/01/2023 **Publication:** 21/03/2023

Suggested citation:

Z., Hua. (2023). **Innovation of college pop music teaching in traditional music culture based on robot cognitive-emotional interaction model.** *3C TIC. Cuadernos de desarrollo aplicados a las TIC*, 12(1), 200-220. <https://doi.org/10.17993/3ctic.2023.121.200-220>

ABSTRACT

Emotional computing and artificial psychology is a new research direction that has received increasing attention in the field of harmonious human-computer interaction and artificial intelligence and is also a new intersection of mathematics, information science, intelligence science, neuroscience, physiology, psychological science and other multidisciplinary intersection. The current problems and drawbacks in the teaching of popular music in colleges and universities, and the search for methods and measures to reform and innovate popular music education in colleges and universities are the difficulties of current music teaching work. In this paper, we try to apply a robot cognitive-emotional interaction model to college pop music teaching, and establish an emotional interaction model based on reinforcement learning with the help of cognitive-emotional computing of human-computer interaction, to be able to integrate emotional interaction in pop music teaching and to make an accurate emotional analysis of students' singing effect. Different from traditional music teaching methods, the robot-based cognitive-emotional interaction model established in this paper can establish an innovative teaching model for college pop music teaching and optimize the teaching effect.

KEYWORDS

Robot cognition; Emotional interaction; Popular music; University teaching; Optimization and innovation

PAPER INDEX

ABSTRACT

KEYWORDS

1. INTRODUCTION

2. EMOTIONAL DESCRIPTION AND EMOTIONAL INTERACTION

2.1. Affective description model

2.1.1. Dimensional sentiment description model

2.1.2. A discrete sentiment description model

2.2. Cognitive-emotional computing for human-computer interaction

3. THE COGNITIVE-EMOTIONAL INTERACTION MODEL FOR ROBOTS BASED ON REINFORCEMENT LEARNING

3.1. Cognitive-emotional computing based on reinforcement learning

3.2. Emotional interaction model based on reinforcement learning

3.2.1. Status

3.2.2. Behavior

3.2.3. Discount factor

3.2.4. Rewards

3.2.5. Strategies

3.2.6. Model Optimization

3.2.7. Emotional interaction process simulation

3.3. Robot Emotional State Update

4. INNOVATION OF POPULAR MUSIC TEACHING IN COLLEGES AND UNIVERSITIES

4.1. Popular music and traditional music culture

4.2. The Role of cognitive-emotional interactive robots in music teaching

5. CONCLUSION

DATA AVAILABILITY

CONFLICTS OF INTEREST

REFERENCES

1. INTRODUCTION

As human communication is natural and contains multiple emotions, it is also natural to expect computers to have the ability of emotional cognition in human-computer interaction. How to enable computers to recognize, understand, and generate human-like emotions has received widespread attention from disciplines such as computer science, brain science, and psychology, and has given birth to the intersection of cognitive-emotional computing [1-3]. As an important way to reflect the application value of artificial intelligence technology, the research of human-computer interaction systems has received common attention from academia and industry, and human-computer interaction products have gradually entered people's daily life. Influenced by the great satisfaction of material needs, people have begun to desire and pursue the sense of fit brought by human-robot interaction at the emotional level, and hope that robots can have the cognitive-emotional computing ability to generate advanced anthropomorphic emotions while satisfying daily interaction needs [4-5]. The study of cognitive-emotional computation for robots is the key to realizing advanced human-robot interaction technology with organic integration of emotions, which has important practical significance and high research value. The applications of robotic cognitive-emotional interaction models are also becoming more and more multifaceted. In the field of popular music teaching in colleges and universities, this paper is devoted to making innovations with the help of cognitive-emotional interaction robots for its disadvantages such as backward teaching model, preaching by the book and lack of vitality [6].

Intelligent human-robot dialogue systems, as an intuitive manifestation of intelligence in artificial intelligence technology, have become an important research component for achieving natural and harmonious human-robot interaction. In recent years, to improve robot anthropomorphism in human-robot interaction systems and create a harmonious and friendly human-robot interaction environment, researchers have conducted a lot of research around cognitive-emotional computing of robots in open domains, and numerous cognitive-emotional interaction models with important reference values have emerged. The literature [7-8] proposed an affective interaction model based on a guided cognitive reappraisal strategy to emotionally regulate external affective stimuli and promote the positive affective expression of the robot to some extent. In the literature [9-10], the cognitive emotion model of the robot is integrated into the smart home environment, and the cognitive reassessment strategy guided by positive emotion is obtained by optimizing and analyzing the cognitive emotion model of the service robot in the smart home environment using simulated annealing algorithm, and the probability of transferring emotional states is updated based on the cognitive reassessment strategy. Literature [11-12] proposed the multi-emotion dialogue system MECS, which tends to generate coherent emotional responses in dialogue and selects the most similar emotion as the robot response emotion. The literature [13-14] proposes emotional chat machines that can produce appropriate responses not only in terms of content relevance and syntax but also in terms of emotional coherence. In response to the teaching of popular music in colleges and universities, the American Education Act explicitly proposes that music

education in schools should break with tradition and no longer be limited to the teaching and development of traditional resources, but expand to all aspects of popular music and contemporary music [15]. German universities believe that both elegant music and modern music should be actively drawn from the advantageous factors of these musicians in the teaching and development of universities so that students can have a richer musical vision from them and can be exposed to richer musical content [16]. With the continuous development of music education, the application of popular music in college education has become more and more extensive, making the music classroom in colleges and universities more colorful and further highlighting the function and value of popular music teaching.

Establishing and maintaining social connections with others is a basic human need in interpersonal relationships, and when users use more anthropomorphic robots as partners and establish relationships with them, they have a better willingness to continue interacting with these robots for a longer period than with those robots that are more rigid in their expression. As robots become more anthropomorphic, the user experience increases and the trust and dependence on the robot increase. In this paper, we investigate the application of emotional robots to the teaching of popular music in universities. First, we quantify the emotion analysis of human-robot interaction by multi-dimensional emotion description, which makes it possible for the robot to compute emotion. Then, the emotional input and output of human-robot interaction are simulated based on reinforcement learning algorithms, to establish its complete cognitive-emotional interaction model. Finally, the model is practiced in college pop music teaching, and a pop music teaching model that makes innovations in traditional music culture is proposed.

2. EMOTIONAL DESCRIPTION AND EMOTIONAL INTERACTION

2.1. AFFECTIVE DESCRIPTION MODEL

The ultimate goal of robotic cognitive emotion computing can be interpreted as giving human-like artificial emotions to robots in interactive systems by simulating human emotion processing to build trust between humans and machines. The main research content includes three parts: emotion recognition, emotion modeling and emotion understanding. Due to the complexity and abstraction of actual emotion, before establishing the robot cognitive emotion interaction model, it is necessary to recognize and quantify the emotion of the user interaction input content, and convert it into an emotion state vector that can be recognized and processed by the computer, and at present, according to its different ways of emotion description, the methods for emotion recognition and quantification. The current methods for emotion recognition and quantification can be divided into dimensional emotion description models and discrete emotion description models.

2.1.1. DIMENSIONAL SENTIMENT DESCRIPTION MODEL

The dimension-based emotion description model describes emotions as coordinate points in a state space composed of Cartesian product operations, each dimension in the state space corresponds to a psychological attribute of emotion, and the magnitude of the value on the dimension reflects the strength of the emotional characteristics corresponding to the psychological attribute, and the emotion description capability of this space covers all emotions [17-18]. In other words, that is, there is a one-to-one mapping relationship between the emotions that exist in reality and the coordinate points in the state space. At the same time, the similarities and differences between different emotions can be quantified and analyzed by calculating the distance between coordinate points. The basis of emotion calculation is to find this mapping dimensional theory, which regards the transition between different emotions as a continuous and smooth state transfer process. The dimensionality-based model of emotion description has received a lot of attention from scholars because it combines the characteristics of continuity and complexity of human emotion distribution. According to the different ways of dividing emotional attributes in psychology, dimension-based emotion description models have one-dimensional, two-dimensional, three-dimensional and more multi-dimensional spatial theories. Currently, the widely used dimensional description models are the two-dimensional activation-valence spatial theory (AV), where the Arousal axis is the activation dimension, representing the degree of pleasantness-unpleasantness, and the Valence axis is the valence dimension, representing the degree of agitation-calmness. The three-dimensional Pleasure-Activation-Dominance (PAD) spatial theory, in which the Pleasure axis is the Pleasure dimension, representing the degree of positive and negative affective states, and the Arousal axis is consistent with the Arousal axis in the AV spatial theory, representing the individual's level of neurophysiological activation. The AV spatial theory is shown in Figure 1, from which we can see that the emotional labels that exist in daily life can be mapped to coordinate points in space, and the magnitude of the corresponding coordinate values in each dimension varies according to the strength of each emotional attribute.

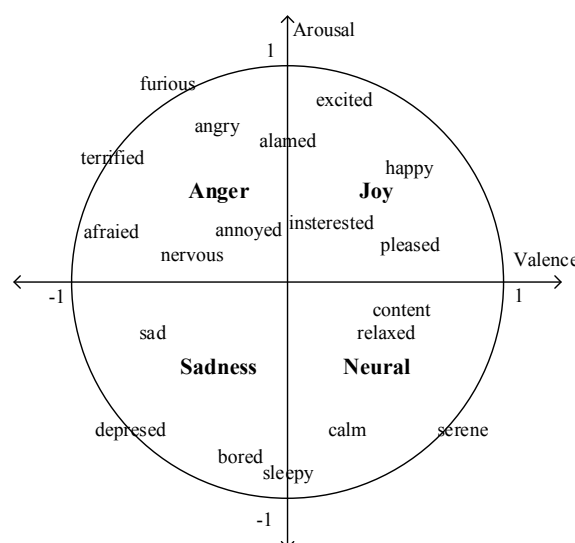


Figure 1. Activation Degree-Validity emotional space

2.1.2. A DISCRETE SENTIMENT DESCRIPTION MODEL

Discrete models of emotion description describe emotions in the form of a finite number of adjective labels and are widely used in people's daily lives, as well as in early computational research on emotions. Rich linguistic labels can describe a large number of affective states, but which classifications are of higher research value? This question can be attributed to the classification of basic affective states based on adjectival labels [19-21]. In general, the categories of emotions that can cross different races and cultures and are shared by humans and socially oriented mammals are the basic emotions. Table 1 lists the definitions and classifications of basic emotions by different scholars.

Table 1. Definition of basic emotions by different scholars

| Scholars | Basic emotions |
|---------------------------|---|
| Weiner, Graham | Happiness, Sadness |
| Watson | Fear, Love, Rage |
| James | Fear, Grief, Love, Rage |
| Panksepp | Anger, Disgust, Anxiety, Happiness, Sadness |
| Ekman, Friesen, Ellsworth | Anger, Disgust, Fear, Joy, Sadness, Surprise |
| Fridja | Desire, Happiness, Interest, Surprise, Wonder, Sorrow |
| McDougall | Fear, Disgust, Elation, Fear, Subjection, Tender-emotion, Wonder |
| Plutchik | Anger, Interest, Contempt, Disgust, Distress, Fear, Joy, Shame, Surprise |
| Tomkins | Anger, Interest, Contempt, Disgust, Distress, Fear, Joy, Shame, Surprise |
| Arnold | Anger, Aversion, Courage, Dejection, Desire, Despair, Fear, Hate, Hope, Love, Sadness |

In summary, considering the rich and strong emotions of participants in open-domain HCI systems, the continuous model based on the PAD emotion space is chosen for the quantitative analysis of emotions in the open-domain cognitive emotion study of robots [22-24]. In closed-domain HCI systems, the emotions of the participants are simpler, and the discrete emotion model is chosen to classify the emotions into positive, negative and neutral when studying the cognitive emotions of robots for the closed domain.

2.2. COGNITIVE-EMOTIONAL COMPUTING FOR HUMAN-COMPUTER INTERACTION

In the long history of robotics research, researchers have focused more on the design and manufacturing of robots, control systems, drive systems, and content representation, until the introduction of "affective computing" and the gradual shift of

robotics research to intelligent robotics, robot cognitive emotion research has received increasing attention [25-27]. The study of robot cognitive emotion has received increasing attention from researchers [25-27]. Emotion is a subjective response to a valued relationship, which is simply the process of perceiving the impact of external values on oneself, and to facilitate an intuitive understanding of this process, a triad can be used to represent cognitive affective computing formally:

$$SC = (S, C, W) \quad (1)$$

where S denotes the set composed of different types of information carriers such as text, speech and pictures. Different carriers contain different emotional features, and there are large differences between the representations of different features.

C denotes the set composed of different sentiment categories. C can denote a discrete set of sentiment states composed of several basic sentiment states, or a spatial set of sentiment states composed of different sentiment dimensions.

W denotes the set composed of different emotional trait intensities, and the intensities can be initially quantified into basic high, medium and low levels, or further subdivided.

Emotional features combined with intensity features form the core of cognitive sentiment computing. Cognitive sentiment computing first identifies and quantitatively analyzes the data features related to objective things extracted from different information carriers. Secondly, the affective features in the data features are calculated under different polarity dimensions to achieve the subjective affective perception of objective things. Finally, it is fed back to the participant with an appropriate sentiment expression. The cognitive sentiment computation can be further described as a combination of state space composed of S, C and W by Cartesian product operation, i.e:

$$SC = S \times C \times W \quad (2)$$

In recent years, the emergence of smart speakers and other devices has largely promoted the productization of human-robot interaction systems. In the process of cognitive-emotional modeling of robots, existing research has achieved better results in the extraction and recognition of emotional features. With the development of intelligence in various industries, research in AI-related fields has been greatly promoted, and its ultimate development goal is to establish intelligent bodies with the ability to observe the environment and to think and decide independently.

3. THE COGNITIVE-EMOTIONAL INTERACTION MODEL FOR ROBOTS BASED ON REINFORCEMENT LEARNING

3.1. COGNITIVE-EMOTIONAL COMPUTING BASED ON REINFORCEMENT LEARNING

In the process of human emotion generation, individual emotional state responses are not only related to external emotional stimuli but also related to their emotional states and emotional interaction motives. When performing affective state response, we should not only consider the influence of contextual multi-round interaction context on the probability of transferring the current affective state but also consider the influence of the current affective state response on the subsequent interaction relationship. Therefore, to effectively carry out robot emotional strategy learning, this paper proposes to use reinforcement learning features to establish the correlation between contextual multi-round emotional state and current response emotional state, and perform cognitive emotion computation for the robot, and the computational framework is shown in Figure 2.

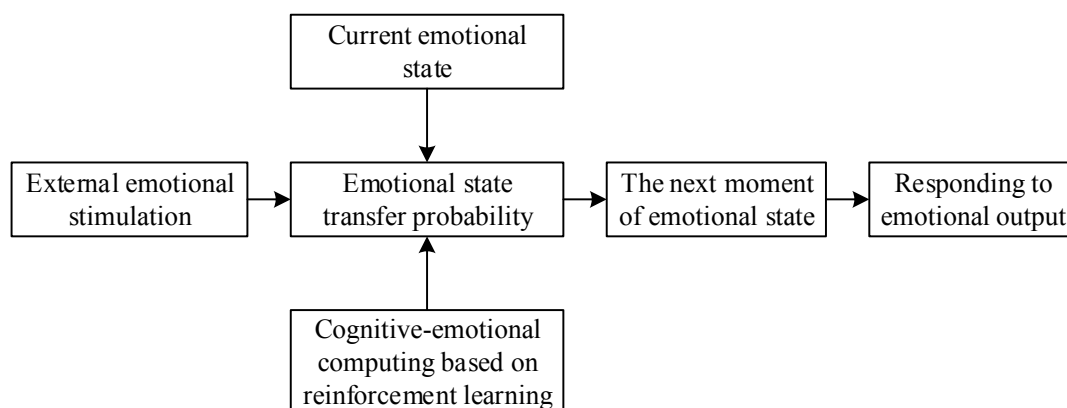


Figure 2. The framework of robotic affective computing

To facilitate the implementation of participant sentiment state tracking, sentiment quantification and state evaluation are performed on the interactive input content. In this paper, we quantify the sentiment of the interactive input content and obtain its corresponding sentiment value $E_i = (p, a, d)$ in the PAD continuous sentiment space. Secondly, the interaction sentiment value vector E_i is evaluated in terms of state, and its sentiment state vector $I(E_i)$ under the action of six basic sentiment states in the PAD continuous sentiment space is obtained. The emotion state evaluation function is defined as:

$$I(E_i) = [i_1, i_2, i_3, i_4, i_5, i_6] \quad (3)$$

$$\left. \begin{aligned} i_j &= \frac{1/h_j}{\sum_{j=1}^6 1/h_j}, & h_j &\neq 0 \\ i_1 = 0, i_2 = 0, 1, \dots, i_j = 1, 2, \dots, i_6 = 0 \end{aligned} \right\} \quad (4)$$

$$h_j = (E_i - E_j)C_j(E_i - E_j)^T, j = 1, 2, \dots, 6 \quad (5)$$

where E_i denotes the interactive input sentiment value. $j = 1, 2, \dots, 6$ denotes the six basic sentiment states of happy, surprised, disgusted, angry, fearful, and sad, respectively; E_j denotes the sentiment value corresponding to basic sentiment j . G_j denotes the covariance matrix of the clustering region of basic sentiment j . h_j denotes the distance between E_i and E_j . then denotes the assessed value of the affective state of E_i under the action of E_j .

3.2. EMOTIONAL INTERACTION MODEL BASED ON REINFORCEMENT LEARNING

The reinforcement learning model is based on the principle that intelligence, in its current state, performs a behavior to interact with the environment and enters a new state, while obtaining the corresponding immediate reward from the environment, and then evaluates this behavior according to the reward, and the reward value increases for behaviors favorable to goal achievement and decays for behaviors unfavorable to goal achievement, and this process continues to cycle until the termination state [28-31].

3.2.1. STATUS

The state s indicates the emotional state in which the intelligent body is, which is usually given by the external environment. To reduce the granularity of emotion division and increase the continuity and delicacy of robot emotion expression, the PAD continuous emotion space containing 151 emotion states is taken as the emotion state space of the intelligent body in this paper, and the emotion state vector of each emotion state in the space under the action of six basic emotion states is taken as the possible interaction input response emotion states.

3.2.2. BEHAVIOR

Behavior a denotes an action executed by the intelligent body in the interactive response process when selecting the next round of response emotional state with the search space of the emotional space size. The activity process of the intelligent body in the emotion space is the Markov transfer process between the emotional states in the emotion space.

3.2.3. DISCOUNT FACTOR

The discount factor γ can be used to calculate the future reward decay of the cumulative rewards of a state sequence when the environment is stochastic. In this paper, we consider that the more distant the future moment is from the current session, the smaller the effect of future rewards on the satisfaction used to measure the affective state of the next round of sessions. Its value is between 0 and 1. The

greater the importance of future rewards is considered, the greater the value of γ , and vice versa the smaller the value of γ .

3.2.4. REWARDS

The reward r can be used to measure the future satisfaction of the obtained affective state after the intelligent body performs the corresponding action a . Both sides of the human-robot interaction have certain emotional motivations during the interaction. Based on the principle of interpersonal attraction in social psychology, the emotional motivation of robot interaction is set to achieve a certain degree of emotional affirmation, emotional guidance and emotional empathy for the participant, and the emotional reward function is constructed accordingly.

1. Similarity emotional reward function: Considering the process of interpersonal interaction, people often hope that the other party can produce similar emotional responses to themselves, to achieve the emotional affirmation of the participant, the cosine similarity is calculated to measure the similarity function between the emotional state vectors as

$$r_1 = S(E_{k+1}, E_k) = \frac{I(E_{k+1}) \cdot I(E_k)}{\|I(E_{k+1})\| \|I(E_k)\|} \quad (6)$$

2. Positive affective reward function: Considering the process of interpersonal interaction, people will achieve some kind of emotional guidance to others by adjusting their emotional expression state. Therefore, to achieve emotional guidance for participants, this paper increases the participants' willingness to interact by setting the robot's emotional positivity guidance. In fact, the higher the positivity, the better, especially when the participant's emotion is negative, it may be counterproductive. The synergistic effect of positivity and similarity can effectively solve the problem of over-guidance. Therefore, in this paper, the positivity of the response emotional state vector is calculated as

$$r_2 = P(E_{k+1}) = P(I(E_{k+1})) = \sum_{j=1}^6 I_j \cdot i_j \quad (7)$$

3. Empathic affective reward function: Consider the process of interpersonal interaction in which interpersonal attraction is not only related to the similarity between individuals but is also influenced by complementary relationships with each other. Complementary relationships are influenced by the fact that people sometimes tend to prefer people who can complement them in some way. In emotional interactions, this can be interpreted as the expectation that the other person has empathy and resonates with them in terms of emotional expression. Therefore, this paper measures emotional empathy by calculating the interrelationships between emotional state vectors

$$r_3 = M(E_k, E_{k+1}) = \frac{1}{1 + \text{rank}(E_{k+1})} \log_2 P(I(E_k) | a) + \frac{1}{1 + \text{rank}(E_k)} \log_2 P(a | I(E_k)) \quad (8)$$

For behavior a , the final reward it receives is the weighted sum of the above 3 reward measures

$$R(a | I(E_k)) = \alpha_1 r_1 + \alpha_2 r_2 + \alpha_3 r_3 \quad (9)$$

where α_1 , α_2 , and α_3 are the corresponding weight parameters, respectively.

3.2.5. STRATEGIES

The policy P is used to represent the probability distribution corresponding to when the intelligence chooses the next emotional state in the current state and can be expressed by the formula

$$\pi(a | s) = P_{RL}(I(E_{k+1}) | I(E_k)) \quad (10)$$

The initial value is the initial transfer probability between affective states. The model is generally optimized using a strategic gradient algorithm, so its value is related to the future reward value available for selecting the next affective state, with a greater probability of occurrence for actions that receive a large future reward value and correspondingly a smaller probability of occurrence for actions that receive a small future reward value.

3.2.6. MODEL OPTIMIZATION

The model update training is achieved by parameterizing the policy through the policy gradient algorithm, to maximize the future cumulative reward expectation by optimizing the model parameters. Therefore, the objective function is to maximize the expected value of future rewards, defined as

$$L_{RL}(\theta) = E_{RH(a_{1:T})} \left[\sum_{k=1}^T R(a_k, I(E_k)) \right] \quad (11)$$

where $R_k(a_k, I(E_k))$ denotes the reward value obtained by acting a_k in the state $I(E_k)$; then the gradient is updated using the likelihood ratio technique

$$\nabla_{\theta} L_{RL}(\theta) = \sum_{k=1}^T \nabla_{\theta} \log_2 P(a_k, I(E_k)) R(a_k, I(E_k)) \quad (12)$$

Finally, the parameter θ is updated using the obtained gradient values

$$\theta_{new} = \theta_{old} + \beta \nabla_{\theta} L_{RL}(\theta) \quad (13)$$

When the cumulative reward expectation is maximized, the sentiment state corresponding to the resulting optimal policy is the optimal response sentiment state for the interaction input.

3.2.7. EMOTIONAL INTERACTION PROCESS SIMULATION

This chapter uses two Agents to simulate the emotional interaction process between the Agent and the external environment by continuously interacting with each other. The interaction process between two Agents can be described as follows: first, Agent 1 is given a random emotional state E_1 , and then Agent 1 converts it into an emotional state vector $(E_1)1$ through emotional evaluation and then transmits this vector to Agent 2 as input, after which Agent 2 converts the corresponding response emotional value E_2 evaluation into an emotional state vector $I(E_2)$ back to Agent 1, and this process is repeated until the maximum number of interaction rounds is simulated. The interaction goal is to be able to select the optimal emotional state with the maximum future reward under the current interaction input emotional state. The emotional interaction process between Agents is shown in Figure 3.

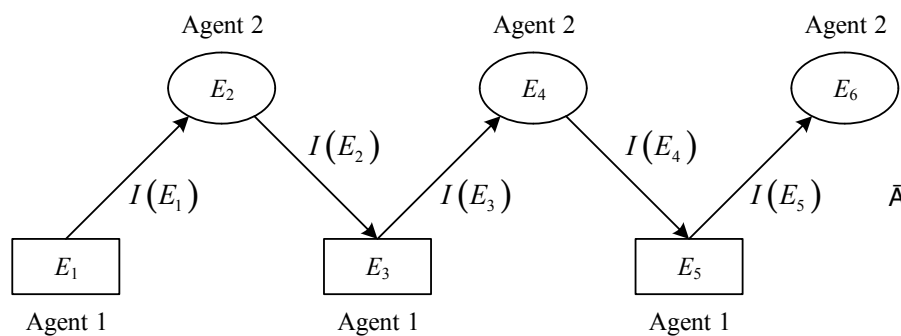


Figure 3. Emotional interaction process

The distance of spatial distance is used to map the similarity between different affective categories in the affective space. The transfer probability between emotional states differs with different distances and similarities between categories. The closer the distance, the greater the state transfer probability; conversely, the farther the distance, the smaller the state transfer probability. Therefore, to facilitate the calculation and analysis of the emotional states in response to external emotional stimuli, this chapter uses the top n emotional states in space that are closest to the Euclidean distance from the external emotional stimulus point as the candidate emotional states for each round of Agent interaction.

3.3. ROBOT EMOTIONAL STATE UPDATE

In this paper, the optimal response emotional value P_{RH}^{k+1} of the robot in continuous emotional space is calculated by combining the six basic emotional values with the probability of emotional state transfer E_{RH}^{k+1} obtained by the robot after being subjected to external emotional stimuli to achieve the emotional state transfer of the robot in

continuous emotional space [32-33]. First, assuming that the optimal response emotional state vector obtained from the reinforcement learning model corresponds to a strategy p , the probability of transferring the response emotional state to the six basic emotional states based on the user input can be obtained as:

$$P(E_{k+1} | E_{HR}^k) = [P(1), P(2), P(3), P(4), P(5), P(6)] = [i_{p1}, i_{p2}, i_{p3}, i_{p4}, i_{p5}, i_{p6}] \quad (14)$$

Second, the $k - 1$ rounds of robot response emotional state transfer probability P_R^{k-1} are updated by combining the $k - 1$ rounds of robot emotional state transfer probability P_{RH}^{k+1} and the k rounds of interactive user input optimal response emotional state transfer probability $P(E_{k+1} | E_{HR}^k)$ with the following equation:

$$P_R^{k+1}(j) = P_{RH}^{k-1}(j) + c_j P(j) \quad (15)$$

$$c_j = \frac{P(j) - \min \{P(E_{k+1} | E_{HR}^k)\}}{\max \{P(E_{k+1} | E_{HR}^k)\} - \min \{P(E_{k+1} | E_{HR}^k)\}} \quad (16)$$

where c_j represents the confidence level of transferring the interaction input response emotional state to the 6 basic emotional states [34-35]. The resulting transfer probability P_R^{k+1} is then normalized to obtain the transfer probability of the $k + 1$ -round interactive robot response emotional state as:

$$P_{k+1}(j) = \frac{P_R^{k+1}(j)}{\sum_{j=1}^6 P_R^{k+1}(j)} \quad \left. \vphantom{\sum_{j=1}^6} \right\} P_{RH}^{k+1} = [P_{k+1}(1), P_{k+1}(2), P_{k+1}(3), P_{k+1}(4), P_{k+1}(5), P_{k+1}(6)] \quad (17)$$

Finally, the coordinate position $(p_{k+1}, a_{k+1}, d_{k+1})$ of the $k + 1$ -round robot optimal response emotional value E_{RH}^{k+1} in the emotional space is calibrated based on the obtained robot emotional state transfer probability P_{RH}^{k+1} , which is calculated as follows:

$$\left. \begin{aligned} p_{k+1} &= \sum_{j=1}^6 p_j P_{k+1}(j) \\ a_{k+1} &= \sum_{j=1}^6 a_j P_{k+1}(j) \\ d_{k+1} &= \sum_{j=1}^6 d_j P_{k+1}(j) \end{aligned} \right\} \quad (18)$$

$$E_{RH}^{k+1} = (p_{k+1}, a_{k+1}, d_{k+1}) \quad (19)$$

Based on the above conditions, the interaction input content emotion is quantified and evaluated based on the PAD emotion space, the user and robot emotion generation process in the human-robot interaction system is modeled using reinforcement learning, the long-term correlation between the current interaction input emotion state and the contextual long-term emotion state is established, and the model parameters are optimized and updated by maximizing the reward value

expectation, and finally, the optimal response emotion state corresponding to the obtained user input is realized by updating the transfer probability of $k + 1$ rounds of robot emotion state, and the optimal response emotion state of the robot in the continuous emotion space can be obtained.

4. INNOVATION OF POPULAR MUSIC TEACHING IN COLLEGES AND UNIVERSITIES

4.1. POPULAR MUSIC AND TRADITIONAL MUSIC CULTURE

In the new era, the traditional music teaching mode is increasingly unable to meet the continuously growing spiritual and cultural needs of students, and pop music teaching in colleges and universities needs to develop in a diversified direction so that students can express their real emotions more intuitively through learning and mastering pop music. Pop music teaching in colleges and universities mainly presents the following characteristics.

1. Both artistic and popular

The teaching of popular music in higher education should be fully based on art education, but on top of that, it should also ensure that it is more significantly popular to ensure that students can understand and accept it in the teaching process. In the teaching of pop music in colleges and universities, it is because of the artistic and popular characteristics that students are more likely to understand and sing it. In conclusion, the teaching of pop music needs to be both popular and artistic. In the process of development, universities should firmly grasp the pulse of the development of art education, distinguish it from other types of music, and make the teaching height continuously improve through more professional control.

2. Tradition and fashion intermingle

The content of popular music teaching in colleges and universities have both characteristics of tradition and fashion. Tradition refers to the unique ideological nature of popular music over the years of development, which can, to a certain extent, pass on the culture and values of the era in which it lives, and has a stronger ideological appeal and influence, and that influence is fundamental to the continuous development of popular music, as well as being a characteristic that needs to be observed in the process of building popular music.

3. Integrating and diversifying at the same time

The reason for this is that the curriculum should take into account the comprehensive quality and development requirements of students, and needs to have a certain degree of comprehensiveness, but also needs to add corresponding special practical courses to fully ensure that students can have a high level of comprehensive quality. In addition, pop music was established late, and it needs to integrate instrumental music, vocal music and music management in the actual teaching process to improve its perfection and become one of the more mature music majors, so it has a more significant comprehensive.

4. Unity and independence are common

Popular music in colleges and universities can also fully reflect the unity and independence of music in the teaching process. Unity mainly refers to the teaching process, teachers set the subject construction plan, curriculum system design and other content based on the curriculum design and other music majors' teaching methods. Based on this, the construction of each music major can maintain a high degree of unity, and the basic construction steps in the implementation process will not have a high degree of deviation, and can jointly promote the orderly development of the overall music major construction.

5. Inheritance and innovation co-exist

Heritage and innovation is one of the characteristics of teaching popular music in colleges and universities, and also the purpose of teaching popular music in colleges and universities. Artistic, popular, traditional and fashionable belong to the characteristics of pop music itself, while inheritance and innovation are based on the artistic level for enhancement. The inheritance of teaching and professional construction of popular music in colleges and universities is mainly reflected in a variety of musical concepts, music construction and inheritance of traditional art music, in addition to the inheritance and expansion of the way of professional construction of conventional music and the development of the experience of art education in colleges and universities. Compared to other contents, the way of building conventional music is the inheritance of methods, while the way of developing popular music mainly targets the innovation level and is the most innovative compared to other characteristics. In actual teaching, the combination of inheritance and innovation can fully reflect the developmental qualities of the professional construction of popular music.

4.2. THE ROLE OF COGNITIVE-EMOTIONAL INTERACTIVE ROBOTS IN MUSIC TEACHING

The form of education is an inherent requirement of educational work, and it is also an inevitable requirement of society and the times for educational work. Educators in general should make more innovative and diligent research in teaching methods and approaches, work with diversified, multi-level and multi-angle music teaching methods, and incorporate the healthy parts and excellent parts of the many traditional music forms in China into the teaching contents, meanwhile, they should widely absorb the advanced teaching experiences at home and abroad, and show the many excellent music forms to students in the teaching process, so that they can It is also beneficial to the promotion and growth of these excellent forms of music to have more choices while relying on popular music.

Cognitive-emotional interactive robots can be used to create an intimate teaching atmosphere of mutual respect, mutual trust and mutual help, thus making the teaching relationship more pleasant and harmonious. In such a relaxed and pleasant atmosphere, students' self-confidence will be improved and they will develop lively, cheerful and positive psychological qualities, which can not only relieve some of the

more common bad emotions such as nervousness and anxiety in the college pop music classroom, but also increase the fun of learning pop music and turn pop music learning into a happy and joyful thing, and face the future with a more positive They will be able to face the present and future with a more positive attitude.

The high school pop music classroom is required to teach specific one-on-one lessons. The teaching process begins with listening to the student's singing of the song, then finely identifying any vocal problems that arise and giving the student specific instructions on how to perform the song. The student then imitates and sings according to the Emotion Robot's analysis and suggestions, while at the same time, the Emotion Robot accurately listens to see if the sound the student is making is up to snuff, similar or consistent with what the Emotion Robot expects, and guides the student to find the correct vocal method for singing.

The classification results of the cognitive-emotional interaction robot are shown in Figure 4 by recording and analyzing 15 pop music singing performances of multiple students.

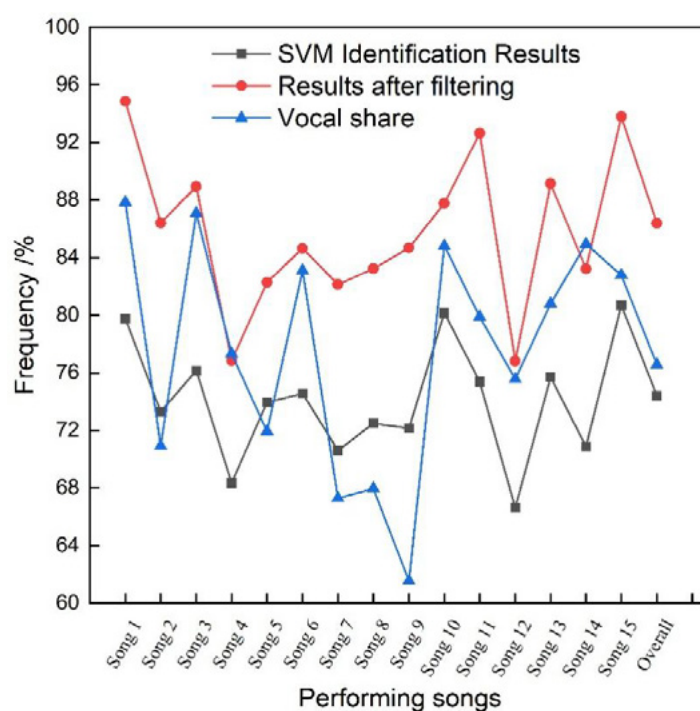


Figure 4. Vocal and musical classification

Figure 4 gives a detailed comparison of the intermediate results of classification based on the SVM classifier and the final classification results after low-pass filtering, as well as the percentage of human voices in each song. It can be seen that the SVM-based classification method and the post-processing filtering mechanism are effective. The first two songs are rap-style songs, which show strong linguistic properties, so MFCC combined with the classical model of traditional speech recognition like SVM has got good results on them. The classification effect of the 4th song and the 12th song is poor, the former as a Cantonese song has a great difference in vocal characteristics from the training data; the latter female voice is more difficult to distinguish from the music and cannot effectively capture the difference between the

human voice and music. In contrast, the classification method of the cognitive-emotional interactive robot is effective in terms of the overall classification effect.

The cognitive-emotional interaction robot was also able to identify the emotion of the student's pop music singing to compare it with the emotional tone of the original song, and the results are shown in Figure 5.

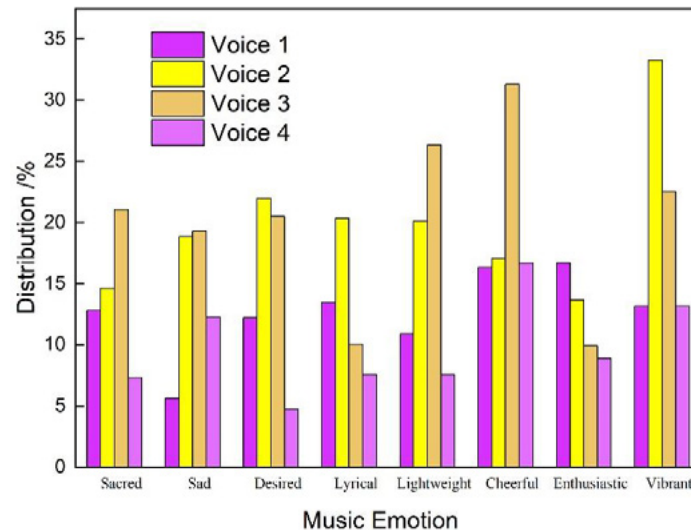


Figure 5. Emotion recognition in music singing

It is not difficult to find that data points of various types of emotions are intertwined on the vector space due to the existence of errors in the data, and since the projection process is a linear transformation, the fusion of data with each other has a small impact on the accuracy of the robot cognitive-emotional discrimination based on reinforcement learning. Based on the basic rhythmic information, the cognitive-emotional interactive robot can perform the initial recognition of basic emotions. Although the recognition results need to be further improved, this conclusion can be applied to musical emotion recognition systems where recognition accuracy requirements are not very stringent. Further, we can use a neural network approach to perform more accurate emotion information recognition using a more adequate set of feature parameters and apply it to improve the recognition rate and robustness of the music recognition system and achieve more human and intelligent human-robot emotion interaction.

5. CONCLUSION

The current intelligent development of human-robot interaction systems has reached a high level, and robotic cognitive-emotional computing has received more and more attention from researchers as an important research component of its intelligent development. In this paper, we carry out research work on the problems of robot cognitive-emotional research in open-domain and closed-domain systems, propose a robot cognitive-emotional interaction model based on reinforcement learning, and apply the model to the innovation of university popular music teaching in traditional music culture. The integration of Chinese traditional music culture in pop music professional education can well cultivate students' traditional music culture

literacy and traditional music culture communication ability. The combination of modern information technology and artificial intelligence technology is in line with the development trend of pop music, and the efficient combination of the two can inject more contemporary vitality into pop music, stimulate the musical creativity of college students, and improve the students' artistic professionalism and social competitiveness.

DATA AVAILABILITY

The data used to support the findings of this study are available from the corresponding author upon request.

CONFLICTS OF INTEREST

The author declares that there is no conflict of interest regarding the publication of this paper.

REFERENCES

- (1) Wang, Y. (2014). **Fuzzy Causal Patterns of Humor and Jokes for Cognitive and Affective Computing**. *International Journal of Cognitive Informatics and Natural Intelligence*, 8(2), 33-45.
- (2) Yang, H., Coddington, D., Mouza, C., et al. (2021). **Broadening Participation in Computing: Promoting Affective and Cognitive Learning in Informal Spaces**. *TechTrends*, 65(3).
- (3) Hsu, D. F. (2013). **Cognitive diversity in perceptive informatics and affective computing**. In *IEEE International Conference on Cognitive Informatics & Cognitive Computing* (pp. 294-297). IEEE.
- (4) Mercadillo, R. E., Sarael, A., & Barrios, F. A. (2018). **Effects of Primatological Training on Anthropomorphic Valuations of Emotions**. *IBRO Reports*, 5, 54-59.
- (5) Takanishi, A., Endo, N., & Petersen, K. (2012). **Towards Natural Emotional Expression and Interaction: Development of Anthropomorphic Emotion Expression and Interaction Robots**. *International journal of synthetic emotions*, 3(2), 47-62.
- (6) Smith, E. K. (2016). **A descriptive analysis of high school choral teachers' inclusion of popular music in current teaching practices**.
- (7) So, J. (2013). **A further extension of the Extended Parallel Process Model (E-EPPM): implications of cognitive appraisal theory of emotion and dispositional coping style**. *Health Communication*, 28(1), 72-83.
- (8) Luo, X., & Min-Jiang, A. I. (2019). **College Students' Cognitive Appraisal, Emotional Identification and Reaction Mode of Online News**. *Journal of Jimei University(Education Science Edition)*.

- (9) Tao, W., & Huang, Y. (2013). **Research on Disposal Station Location Problem Based on Genetic and Simulated Annealing Algorithm.** In *2013 International Conference on Computational and Information Sciences*.
- (10) Meng, X. (2021). **Optimization of Cultural and Creative Product Design Based on Simulated Annealing Algorithm.** *Complexity*, 2021.
- (11) Zhang, A., Wu, S., Zhang, X., et al. (2020). **EmoEM: Emotional Expression in a Multi-turn Dialogue Model.** In *2020 IEEE 32nd International Conference on Tools with Artificial Intelligence (ICTAI)*. IEEE.
- (12) Yang, J., & Wu, C. (2021). **Emotional Response Generation in Multi-Turn Dialogue.** *Journal of Physics: Conference Series*, 1827(1), 012124.
- (13) Sun, X., Peng, X., & Ding, S. (2017). **Emotional human-machine conversation generation based on long short-term memory.** *Cognitive Computation*.
- (14) Christ, N. M., Elhai, J. D., Forbes, C. N., Ford, J. D., & Adams, T. G. (2021). **A machine learning approach to modeling PTSD and difficulties in emotion regulation.** *Psychiatry Research*, 301, 113947.
- (15) Kelly, S. (2009). **Teaching Music in American Society: A Social and Cultural Understanding of Music Education - Steven N. Kelly.** Routledge.
- (16) Schmid, E. V. (2015). **Popular music in music education in Germany - historical, current and cross-cultural perspectives.**
- (17) Qamash, M., Altal, S. M., & Jawaldeh, F. E. (2011). **Dimensional Common Emotional Intelligence for the Student of Higher Education In Princess Alia College At the University of Al Balq'a Applied University In Jordan from the Point of View of the Students.** *European Journal of Social Sciences*.
- (18) Cowie, R., Doherty, C., & McMahon, E. (2009). **Using dimensional descriptions to express the emotional content of music.** In *Affective Computing and Intelligent Interaction and Workshops, 2009. ACII 2009. 3rd International Conference on* (pp. 1-8). IEEE Xplore.
- (19) Selvaraj, J., Murugappan, M., Wan, K., & Yaacob, S. (2013). **Classification of emotional states from electrocardiogram signals: a non-linear approach based on hurst.** *BioMedical Engineering OnLine*, 12(1), 44.
- (20) Martin, Schels, M., Kächele, M., Glodek, M., & Kopp, S. (2013). **Using unlabeled data to improve classification of emotional states in human computer interaction.** *Journal on Multimodal User Interfaces*, 8(1), 169-176.
- (21) Schels, M., Kächele, M., Glodek, M., & Kopp, S. (2014). **Using unlabeled data to improve classification of emotional states in human computer interaction.** *Journal on Multimodal User Interfaces*, 8(1), 169-176.
- (22) Weiguo, W. U., & Hongman, L. I. (2019). **Artificial emotion modeling in PAD emotional space and human-robot interactive experiment.** *Journal of Harbin Institute of Technology*.
- (23) Zafar, Z., Ashok, A., & Berns, K. (2021). **Personality Traits Assessment using P.A.D. Emotional Space in Human-robot Interaction.** In *5th International Conference on Human Computer Interaction Theory and Applications*.
- (24) Song, J., Zhang, X. Y., Sun, Y., & Zhang, B. Y. (2016). **Emotional speech recognition based on PAD emotion model.** *Microelectronics & Computer*.

- (25) Hsieh Y Z, Lin S S, Luo Y C, et al. (2020). **ARCS-Assisted Teaching Robots Based on Anticipatory Computing and Emotional Big Data for Improving Sustainable Learning Efficiency and Motivation.** *Sustainability*, 12. <https://doi.org/10.3390/su12145605>
- (26) Puviani L, Rama S, & Vitetta G M. (2018). **A Mathematical Description of Emotional Processes and Its Potential Applications to Affective Computing.** *IEEE Transactions on Affective Computing*, 9(1), 1-1. <https://doi.org/10.1109/TAFFC.2018.2887385>
- (27) Good J, Rimmer J, Harris E, et al. (2013). **Self-Reporting Emotional Experiences in Computing Lab Sessions: An Emotional Regulation Perspective.** *PPIG*. <https://www.ppig.org/papers/25th-good.pdf>
- (28) Nelson A B, Serena R, Elisa T, et al. (2020). **Neural fatigue due to intensive learning is reversed by a nap but not by quiet waking.** *SLEEP*, 43(4), 1-12. <https://doi.org/10.1093/sleep/zsaa143>
- (29) Cheng J, Sollee J, Hsieh C, et al. (2022). **Correction to: COVID-19 mortality prediction in the intensive care unit with deep learning based on longitudinal chest X-rays and clinical data.** *European Radiology*, 32(1), 1-1. <https://doi.org/10.1007/s00330-022-08680-z>
- (30) Aisling, McMahon, Gabor, et al. (2017). **Intensive care microbiology pearls: learning by 1-500-5-1.** *Medical Education*, 51(5), 541-542. <https://doi.org/10.1111/medu.13289>
- (31) Nousiainen, Markku, Garbedian, et al. (2015). **Toronto Orthopedic boot camp III: Examining the efficacy of student-regulated learning during an intensive, laboratory-based surgical skills course (vol 154, pg 29, 2013).** *Surgery*, 158(6), 1756-1757. <https://doi.org/10.1016/j.surg.2013.05.003>
- (32) Panksepp J, & Watt D. (2011). **What is Basic about Basic Emotions? Lasting Lessons from Affective Neuroscience.** *Emotion Review*, 3(4), 387-396. <https://doi.org/10.1177/1754073911410741>
- (33) Gilead M, Katzir M, Eyal T, et al. (2016). **Neural correlates of processing "self-conscious" vs. "basic" emotions.** *Neuropsychologia*, 80, 207-218. <https://doi.org/10.1016/j.neuropsychologia.2015.12.009>
- (34) L., Wenling (2023). **Deep Learning Network-Based Evaluation method of Online teaching quality of International Chinese Education.** *3C Tecnología. Glosas de innovación aplicada a la pyme*, 12(1), 87-106. <https://doi.org/10.17993/3ctecno.2023.v12n1e43.87-106>
- (35) Liu Hailiang, Hou Chenglong, & Ramzani Sara Ravan. (2021). **Construction and reform of art design teaching mode under the background of the integration of non-linear equations and the internet.** *Applied Mathematics and Nonlinear Sciences*, 7(1), 215-222. <https://doi.org/10.2478/amns.2021.2.00149>

/11/

EXPLORING THE DIRECTION OF THE ENGLISH TRANSLATION OF ENVIRONMENTAL PROTECTION ARTICLES BASED ON THE ROBOT COGNITIVE- EMOTIONAL INTERACTION MODEL

Shuai Song*

Shanghai University of Sport, Shanghai, 200000, China

renlilin666@163.com



Reception: 01/12/2022 **Acceptance:** 16/01/2023 **Publication:** 05/03/2023

Suggested citation:

S., Shuai. (2023). **Exploring the direction of the English translation of environmental protection articles based on the robot cognitive-emotional interaction model.** *3C TIC. Cuadernos de desarrollo aplicados a las TIC*, 12(1), 222-246. <https://doi.org/10.17993/3ctic.2023.121.222-246>

ABSTRACT

To broaden the application area of the cognitive-emotional interaction model for robots. In this paper, an algorithmic model for the English translation of environmental articles based on a cognitive-emotional interaction model for robots is used to model the process of emotion generation using reinforcement learning. Similarly, positivity and empathy are used to quantify the reward function for emotional state assessment, and the optimal emotional strategy selection is derived based on the utility function. In the process of article translation by the robot, Lagrangian factors are introduced to make the translation probability maximum process transformed into the process of obtaining the highest value of the auxiliary function at a random state. Finally, the effectiveness of the robot's cognitive-emotional interaction model in the English translation of environmental protection articles is verified by the Chinese-English parallel question-and-answer dataset. The experimental results demonstrate that this model can not only be used for the English translation of environmental protection articles but also can give the corresponding English translation work similar to human emotions, which can better help people understand the meaning of English. It also provides a basis and direction for the subsequent in-depth application of the robot cognitive-emotional interaction model in various fields.

KEYWORDS

Robot cognitive model; Emotional interaction model; Optimal emotional strategy; Emotional state assessment reward function; Reinforcement learning model

PAPER INDEX

ABSTRACT

KEYWORDS

1. INTRODUCTION

2. A COGNITIVE MODEL OF THE ROBOT WITH EMOTION AND MEMORY MECHANISM

2.1. Cognitive model structure

2.2. EMOTION GENERATION SYSTEM

2.3. Incentive mechanism

3. GAME MODEL BASED ON COGNITIVE-EMOTIONAL INTERACTION MODEL OF ROBOT

3.1. Game Model

3.2. Definition of utility functions

3.3. Optimal emotional strategy selection

3.4. Construction of a cognitive-emotional interaction model for robots

4. ENGLISH TRANSLATION MODEL BASED ON ROBOT COGNITIVE-EMOTIONAL INTERACTION

5. EXPERIMENTAL DESIGN AND ANALYSIS OF RESULTS

5.1. Experimental design

5.2. Emotional Accuracy Analysis

5.3. Retrieving translation validity

5.4. Validation of Interaction Translation

5.5. Model satisfaction assessment

6. CONCLUSION

DATA AVAILABILITY

CONFLICTS OF INTEREST

REFERENCES

1. INTRODUCTION

In recent years, with the introduction and implementation of the concepts of "smart home", "smart community" and "smart city", human-computer interaction has become an indispensable part of the public's daily life [1-4]. People expect robots to have the cognitive-emotional computing ability to generate advanced anthropomorphic emotions while satisfying daily interaction needs [5]. At the same time, as the intersection of psychology, cognitive science, and artificial intelligence has intensified, researchers have found that robot cognition should be reflected in both "intelligence" and "emotional intelligence" [6]. Therefore, robot cognition and computation of emotional interaction models have become a hot topic in the field of intelligent robot research [7].

Emotional interaction cannot be achieved without the technical means of artificial intelligence [8]. For nearly two decades, AI researchers have been trying to empower machines with cognitive abilities to recognize, interpret, and express emotions [9]. Artificial intelligence techniques simulate human emotional cognition and decision-making processes by correlating, analyzing and reconstructing data containing emotional information in different scenarios with each other, and eventually transforming the data into abstracted thoughts that computers can understand [10-12]. The affective interaction process uses the user's modal data to achieve recognition of the user's affective state and uses the feedback information from the affect recognition to perform affective modeling based on cognitive analysis and to guide the interaction behavior [13-14]. Thus, the sentiment recognition process and the sentiment modeling process are the two most important steps of sentiment interaction [15].

In recent years, numerous valuable research approaches have emerged in the field of cognitive and affective interaction modeling for robots. The literature [16] argues that cognitive-emotional computing is about giving computers the human-like ability to observe, understand, and generate various emotional states so that they can interact in a naturally intimate, lively, and interesting way like humans. The literature [17] proposed an emotional interaction model based on guided cognitive reassessment strategies GCRs, which can reduce the robot's dependence on external emotional stimuli and promote positive emotional expression of the robot to some extent. The literature [18] proposed a personalized emotion model based on PAD and established a three-level mapping relationship between personality space, mood space and emotion space to describe the human emotion change pattern. The literature [19] used electrophysiological techniques and MRI to study the expression of cognition and emotion in the brain during behavior. In the literature [20], cognitive feelings were identified as an emotional experience, and this was confirmed by observing changes in the physiological and behavioral representations of validity and arousal in a cognitive task. In [21], a willingness-based interpretable and computational emotion model and CASE, a personality model to measure robot differences, were proposed to improve the performance of multiple robots in pursuit of tasks by using a willingness to quantify the effect of emotional factors on task assignment through an emotional contagion model to compute inter-robot emotional interactions. In the literature [22], by conducting emotion-cognition-related experiments, it was found that emotional

states affect the input of cognitive control in the brain and the associated metacognitive experience. The literature [23] established a multi-emotion dialogue system MECs by multi-task Seq2Seq learning, and after multi-task learning based on question-answer datasets, the candidate answer with the most similar emotion to the input interrogative was selected as the output of the robot, which achieved better results in a single round of dialogue. The literature [24] proposed an integrated framework for emotion computation, which firstly considers personality traits, social content and other factors for the evaluation of external emotional stimuli, secondly considers mood states, internal memories and other factors for the generation of emotions, and finally performs the expression of intelligent behaviors based on the generated emotions. The literature [25] assesses students' interest in learning events based on a combination of OCC affective modeling and fuzzy reasoning, which is a means of using affective modeling as an aid to affect recognition prediction. The literature [26] implements the process of natural change in robot emotions, which for interactive behavior is still based on discrete rules for emotion mapping. The literature [27] uses statistical features of skin electrical signals, ECG signals with body temperature and time-frequency features for global generalized emotion recognition. The literature [28] uses hierarchical support vector machines for reducing the bias of robot cognitive training binary classifiers. The literature [29] proposes an emotion model based on the Pruschik emotional color wheel to enable social robots to mimic human emotional changes and personality traits in entertainment and education to talk naturally with people. The literature [30] builds an affective cognitive model that implements emotion generation based on external event motivation and regulates the flow of information generated by the generated emotions through the competition under different drivers to determine the behavioral output.

In this paper, a reinforcement learning-based cognitive emotional interaction model for robots is proposed [31-32]. First, reinforcement learning is used to model the emotion generation process, and the one-dimensional emotion model theory is used as the emotion state space of the robot, which motivates the robot to improve efficiency in the process of emotional interaction; second, three emotional influencing factors of similarity, positivity and empathy are considered to quantify as the reward function for conducting emotional state assessment, and the optimal emotional strategy selection is derived based on the effectiveness function to realize the interaction motive of emotional support, emotional guidance and emotional empathy for the participants; thirdly, Lagrange factor is introduced in the process of environmental protection English articles translation by the robot, which makes the process of the highest value of machine translation probability transform into the process of obtaining the highest value of the auxiliary function at the random state. The retrieval speed of machine translation is improved, the efficiency of machine translation is enhanced, and high-precision translation results can be obtained more effectively. Finally, the Chinese-English parallel question-and-answer corpus commonly used in environmental protection articles is used as the experimental data set, and the optimal emotional state is combined with the optimal emotional state to update the robot's emotional state transfer probability, to realize the robot's state transfer in the translation process

and ensure the continuity of the translation process. The experiments validate the model's effectiveness in terms of accuracy, MAP and MRR.

2. A COGNITIVE MODEL OF THE ROBOT WITH EMOTION AND MEMORY MECHANISM

2.1. COGNITIVE MODEL STRUCTURE

Different disciplines, such as brain science, cognitive neuroscience, and cognitive psychology, have researched brain structure and its emotional and cognitive principles. The results show that emotional and cognitive functional areas of the brain are mainly concentrated in the thalamus, limbic system, and cerebral cortex. The thalamus, as the sensory transmission center, is responsible for the transmission of external sensory information such as visual, auditory and olfactory information, as well as internal sensory information. The limbic system, as the emotional center, mainly includes the hippocampus, amygdala, and cingulate gyrus. The hippocampus is responsible for emotional memory and learning, the amygdala is responsible for emotion generation, regulation, and recognition, while the anterior lower part of the cingulate gyrus is related to emotional processing and the posterior upper part is related to cognitive functions. These structures are linked to the hypothalamus and the vegetative nervous system and are involved in regulating instinctive responses and emotional behavior; the cerebral cortex is mainly involved in human brain activities such as understanding events, making decisions about goals, and managing the timing of behavior.

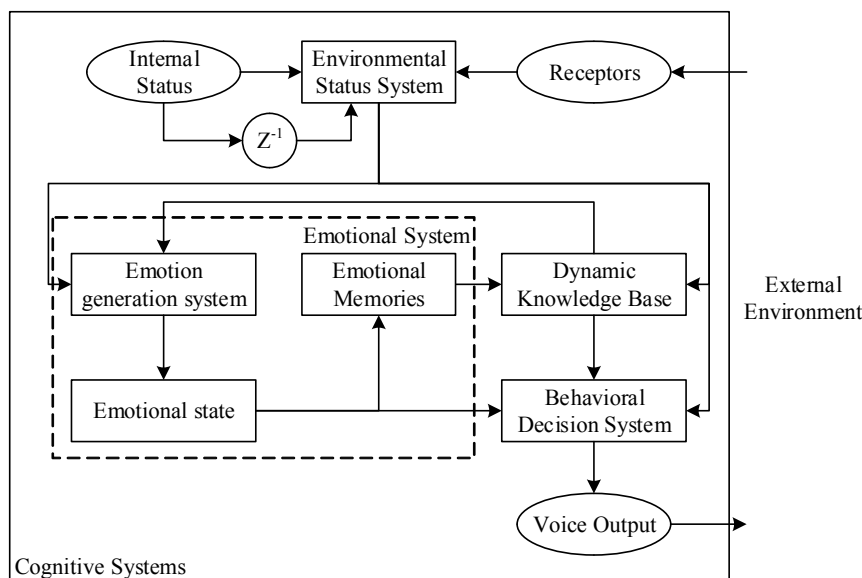


Figure 1. Cognitive model structure

Based on the above cross-disciplinary research foundation, this paper proposes a robot cognitive model, which contains seven parts: receptor, internal state, environmental state system, emotional system, behavioral decision system, dynamic

knowledge base, and execution output, and the model structure is shown in Figure 1. The meanings of each part are as follows:

(1) Receptors: feel all kinds of information from the external environment, and represent the felt information as a triad:

$$PER_ORG = \langle S, A, Ga \rangle \quad (1)$$

Where $S = \{S_i | i = 1, 2, \dots, n_s\}$ is the set of perceptible discrete states, $A = \{A_i | i = 1, 2, \dots, n_s\}$ is the set of optional action subsets corresponding to discrete states, $Ga = \{Ga_i | i = 1, 2, \dots, n_s\}$ is the set of maximum internal energy state replenishment corresponding to discrete states, and 4 is the number of perceptible discrete states.

(2) Internal state: the internal state information of the robot body, such as the internal energy robot and the durability of the robot. The internal state of the robot is the internal energy state $P(t)$, that is:

$$P = \{P(t) | t = 1, 2, \dots, n_t\} \quad (2)$$

Where P is the set of energy states inside the robot body, n_t is the robot task survival time, $t=0$ means the robot is at the task start moment; $t = n_t$ represents the robot body internal energy state is zero or the task completion moment.

(3) Environmental state system: the robot's external environmental information and the body's internal state hub station, denoted as: $\langle PER_ORG, P, G \rangle$. Where $G = \{G(t) | t = 1, 2, \dots, n_t\}$ is the set of internal energy state gains obtained by the robot from discrete states, and the internal energy state gains are defined as follows:

$$G(t) = \begin{cases} P(t) - P(t-1) & Ga(t) \neq 0 \\ G(t-1) & Ga(t) = 0 \end{cases} \quad (3)$$

Where $Ga(t)$ is the maximum internal state replenishment Ga_i corresponding to the discrete state at the time t .

(4) Emotional system: robot emotional state and emotional memory generation center, expressed as a triad:

$$EMO_SYS = \langle E, R_{emo}, R_{mem} \rangle \quad (4)$$

Where $E = \{E(t) | t = 1, 2, \dots, n_t\}$ is the set of emotional states generated by the emotion generation system; $R_{emo} = \{R_{emo}(t) | t = 1, 2, \dots, n_t\}$ is the set of inverse emotional rewards generated by the emotional memory; $R_{mem} = \{R_{mem}(T) | T = 1, 2, \dots, n_T\}$ is the set of periodic emotional rewards generated by the emotional memory, n_T is the robot task survival time internal energy state recharge cycle, $T = 1$ represents the first internal energy state recharge; $T = n_T$ represents the robot internal energy state before zero or the completion of the task maximum energy recharge cycle.

(5) Behavior decision system: Based on the output of the environment state system and the emotion system, we combine the dynamic knowledge base to realize the

robot's behavior decision. It is expressed as a binary group: $\langle \pi, a \rangle$, where $\pi = \{\pi_j | j = 1, 2, \dots, n_j\}$ is the set of behavioral decisions, n_j is the number of behaviors of the translation robot, $a_m = \{m = 1, 2, \dots, n_m\}$ is the set of translation word selection, and n_m is the number of actions of the translation robot. For the English translation task of environmental protection articles requiring "energy replenishment", the robot's behaviors are divided into the search, energy replenishment, and search actions for the selection of $\{north, south, east, west\}$ directions at each node of the article.

(6) Dynamic knowledge base: Knowledge base of English words for robotics and environment, with knowledge elements represented as five-tuples:

$$DYN_KNO = \langle A', EL, D, STA_EGW, STA_PWO \rangle \quad (5)$$

$A' = \{A'_i | i = 1, 2, \dots, n_s\}$ is the set of discrete states corresponding to the best action of energy replenishment; $EL = \{EL(T) | T = 1, 2, \dots, n_T\}$ is the set of word search states; $D = \{D(T) | t = 1, 2, \dots, n_t\}$ is the set of environment search states; $STA_EGW = \langle (Y, U), (Y', U') \rangle = \{(Y_k, U_k), (Y'_c, U'_c) | k = 1, 2, \dots, n_k, c = 1, 2, \dots, n_c\}$ is the set of state-English word memory, (Y, U) records the sequence of states encountered and English word selection during the cycle, n_k represents the total number of discrete states encountered during the cycle, (Y', U') records the last state encountered during the cycle and the sequence of English word selection for that state, n_c , $STA_PWO = \{(Y''_z, B_z) | z = 1, 2, \dots, n_z\}$ is the state-energy memory set, which records the discrete states encountered during the cycle and the internal energy states required to return to the energy recharge point B_z , n_z is the number of discrete states encountered during the search cycle, STA_EGW and STA_PWO reflect the memory function of the robot cognitive model.

(7) Execution output: the robot article translation output actuator and the action actuator are represented as a binary group: $\langle V1, V2 \rangle$. Where $V1 = \{V1_m | m = 1, 2, \dots, n_m\}$ is the first article translation output set; $V2 = \{V2_m | m = 1, 2, \dots, n_m\}$ is the correction article translation output set.

2.2. EMOTION GENERATION SYSTEM

To study robots with emotional mechanisms, first of all, artificial emotions have to be generated, which requires modeling emotions. In this paper, based on the theory of the one-dimensional emotion model, an emotion interaction model is designed for the emotion generation system, which can generate six emotions: happy, surprised, disgusted, angry, fearful and sad, in the following form:

$$E(t) = \frac{G(t)}{k_1} \left[\arctan(P(t) - k_2) + \frac{P(t) - B(t)}{k_3} \right] \cdot e^{-D(t)} \quad (6)$$

$$E(t) = G(t) \cdot e^{\frac{2P(t) - B(t) - k_4}{k_5} - D(t)} - k_6 \quad (7)$$

Where $B(t)$ is the internal energy state value B_z required to return to the energy recharge point corresponding to the discrete state at the time t . The emotional intensity $|E(t)|$ is positively related to the internal state gain $G(t)$ obtained by the robot. When $G(t) > 0$, (6) produces four emotions: happy, surprised, sad, and fearful, with positive happy emotion at $E(t) > 0$ and fearful emotion at $k_7 < E(t) < 0$. When $G(t) < 0$, (7) produces angry emotion at $k_6 < E(t) < k_5$ and disgustful emotion at $k_7 < E(t) < k_6$. $k_1 \sim k_7$ is the emotion model parameters.

2.3. INCENTIVE MECHANISM

In everyday life, rewards are usually sparse. The performer often needs to go through a series of attempts during a task until the task is completed to obtain a reward, and no reward is manifested during the process. However, the human brain possesses a reflective mechanism that can establish a relevant connection between the temporal situation and the target thing and obtain a reward based on the memory mechanism. Therefore, in this paper, while considering affective cognition, we combine memory cognition, based on the framework of reinforcement learning theory, to integrate intra-emotional reward with memory. A reward mechanism is proposed, which consists of environmental reward, reversed affective reward and periodic affective reward. Among them, the reversed affective reward and the periodic affective reward are internal rewards.

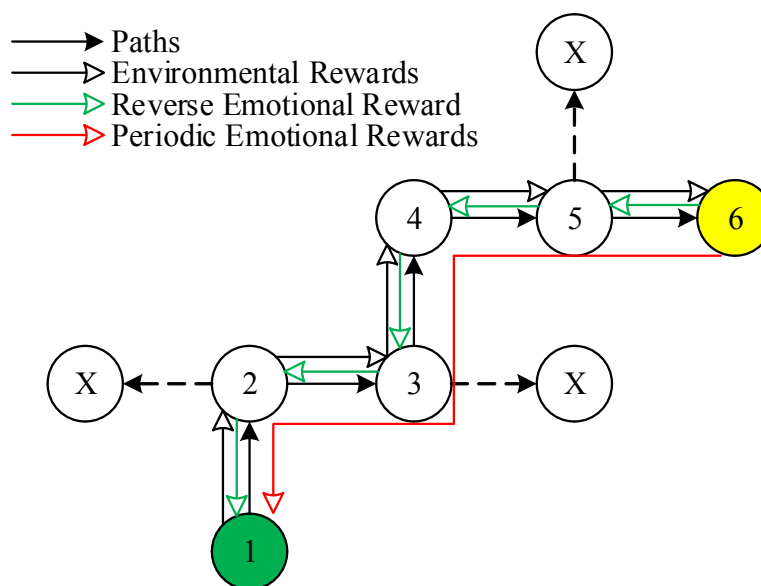


Figure 2. Schematic diagram of the robot cognitive reward mechanism

Figure 2 shows the process of obtaining a search reward for an article to be translated by the article English translation robot (schematic diagram). The robot consumes internal energy during the search process, and translates the word a_m selection according to the optional action subset $A_i \in \{north, south, east, west\}$ of nodes, assuming that node 1 is the energy replenishment point and node X indicates the unsearched point. As shown in Figure 2, the robot search trajectory is:

$1 \rightarrow 2 \rightarrow 3 \rightarrow 4 \rightarrow 5 \rightarrow 6$, if it reaches node 6, the robot must go back to node 1 to replenish the internal energy state to maintain the next search, the return trajectory is: $6 \rightarrow 5 \rightarrow 4 \rightarrow 3 \rightarrow 2 \rightarrow 1$, the robot from the energy replenishment point to search and then back to the energy replenishment point. At this point, the article English translation robot completes a cycle of the search for the article to be translated. The reward mechanism in this process generates rewards $R = \langle R_{env}, R_{emo}, R_{mem} \rangle$, and each reward is shown in Table 1:

Table 1. Schematic diagram of the robot cognitive reward mechanism

| Reward type | Reward collection |
|-------------|--|
| R_{env} | $R_{env1 \rightarrow 2}, R_{env2 \rightarrow 3}, R_{env3 \rightarrow 4}, R_{env4 \rightarrow 5}, R_{env5 \rightarrow 6}$ |
| | $R_{env6 \rightarrow 5}, R_{env5 \rightarrow 4}, R_{env4 \rightarrow 3}, R_{env3 \rightarrow 2}, R_{env2 \rightarrow 1}$ |
| R_{emo} | $R_{emo1 \leftarrow 2}, R_{emo2 \leftarrow 3}, R_{emo3 \leftarrow 4}, R_{emo4 \leftarrow 5}, R_{emo5 \leftarrow 6}$ |
| R_{mem} | $R_{mem6 \rightarrow 5 \rightarrow 4 \rightarrow 3 \rightarrow 2 \rightarrow 1}$ |

Where, $1 \rightarrow 2$ process to node $R_{env1 \rightarrow 2}$, 2 is the external environment reward for node 1 to obtain action toward node 2; $R_{emo1 \leftarrow 2}$ is the reward for node 2 to obtain action toward node 1, i.e., the reverse emotional reward. $6 \rightarrow 5 \rightarrow 4 \rightarrow 3 \rightarrow 2 \rightarrow 1$ the process to node 1, $R_{mem6 \rightarrow 5 \rightarrow 4 \rightarrow 3 \rightarrow 2 \rightarrow 1}$ is the reward for node 6, node 5, node 4, node 3, and node 2 to obtain the tendency to node 1 action step by step, i.e., the periodic affective reward.

The environment bonus is set according to (8). The energy replenishment point is the node where the robot replenishes internal energy during the article translation process; the dead-end node is the node where only the "return" action can be selected when there is a single word that cannot be searched; the trap point is the node where the robot loses additional internal energy at this node; and the normal node is the node with internal state gain $Ga(t) = 0$ and is not a dead-end node. The Q value is updated by (9), s is the current state, a is the current action state of the selected English word, α is the learning rate, and $\max Q(s', a')$ is the maximum gain of the next state after the current state selected action.

$$R_{env}(t) = \begin{cases} 100 & \text{Energy recharge point} \\ 0 & \text{General Node} \\ -5 & \text{Dead end nodes} \\ -1 & \text{Trap point} \end{cases} \quad (8)$$

$$Q(s, a) = (1 - \alpha)Q(s, a) + \alpha[R_{env} + \max Q(s', a')] \quad (9)$$

The reverse sentiment reward is set as in equation (10), and the Q value is updated as in equation (11), with a'' the reverse direction at the time of entering this node state.

$$R_{emo}(t) = \begin{cases} E(t) & E(t) > 0 \\ \frac{1}{|E(t)|} & E(t) < 0 \end{cases} \quad (10)$$

$$Q(s, a'') = R_{emo} \quad (11)$$

The cycle sentiment reward is set according to equation (12), where $E(T)$ is the sentiment state generated at the moment of completion of the T th cycle, and the Q value is updated according to equation (13); this reward is obtained only when the cycle is completed.

$$R_{mem}(T) = \begin{cases} E(T) & T > 0 \\ 0 & T = 0 \end{cases} \quad (12)$$

$$Q(s, a) = (1 - \alpha)Q(s, a) + \alpha[R_{mem} + \max Q(s', a')] \quad (13)$$

3. GAME MODEL BASED ON COGNITIVE-EMOTIONAL INTERACTION MODEL OF ROBOT

3.1. GAME MODEL

Modeling the emotion generation process of the participant and the robot during human-robot interaction, the emotional cognitive interaction model tries to get the optimal emotional response of the robot based on the previous historical emotion and the current interaction input emotion of the participant, which leads to a more natural and harmonious human-robot interaction, i.e., the optimal E_{RH}^{k+1} is obtained by knowing $E_{HR}^l (1 \leq l \leq k)$, as shown in Figure 3 (R denotes the robot and H denotes the participant object).

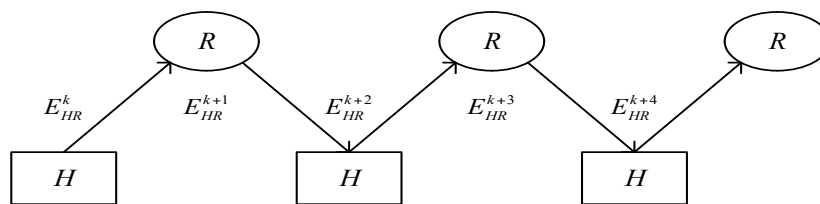


Figure 3. Human-machine interaction process

To facilitate theoretical analysis, as mentioned above, this paper unifies and normalizes the emotional strategies of the participating object and the robot in the human-robot interaction process into six basic emotions. After the robot is stimulated by the external emotion of the participant E_{HR}^k , it then selects the optimal emotion strategy from the six basic emotions. In the process of making the optimal emotion selection, the robot needs to perform the emotion trend prediction for each emotion selection. The prediction of the emotion E_{HR}^{k+2} that will be generated by the participant in $k + 2$ interactions and the emotion that

may be replied to by the participant in $k + 3$ sessions E_{HR}^{k+3} . The emotion strategy selection process of the robot is shown in Figure 4.

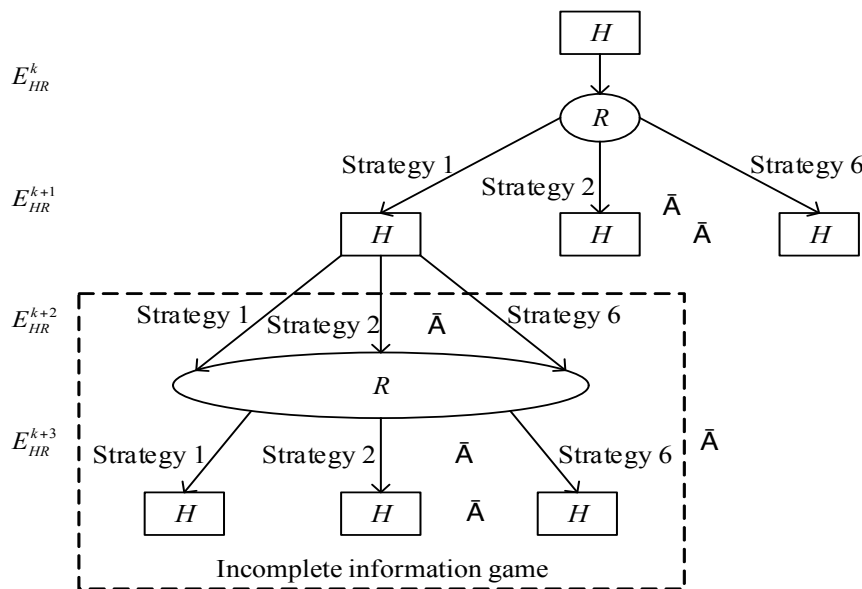


Figure 4. The emotional strategy selection process of the robot

The game model should be judged by 3 elements: the participant, the strategy combination, and the game gain. The participant and the robot constitute the two objects of the game model, and both parties make different strategy choices around subjective satisfaction, and different combinations of these strategies will produce different game outcomes. Considering the human-robot interaction, both the participant and the robot start from their subjective satisfaction, which is a non-cooperative game. In human-robot interaction, emotions are bidirectional, i.e., the subjective satisfaction of the participant is influenced by the robot's reply emotions, and the subjective satisfaction of the robot is also influenced by the participant's reply emotions, and the robot does not know what kind of emotional response it will get from the participant for $k + 1$ sessions, which is an incomplete information game. Therefore, this paper uses an embedding game based on the robot cognitive-emotional interaction model to model the emotion generation process of the participant and the robot.

3.2. DEFINITION OF UTILITY FUNCTIONS

The utility is the subjective satisfaction obtained by the interacting parties during human-computer interaction without loss of generality. Consider the definition of the participant's utility function: $UH(E_{RH}^k, E_{RH}^{k+1}, E_{HR}^{k+2}, E_{HR}^{k+3})$ denotes k session participant interactions with an input sentiment of E_{RH}^k . Assuming that the sentiment value of the $k + 1$ session robot response is E_{RH}^{k+1} , predict the value of subjective satisfaction obtained by the participant if the sentiment value of the $k + 2$ session participant is E_{HR}^{k+2} and the sentiment value of the $k + 3$ session robot is E_{HR}^{k+3} .

In this paper, we define the utility function of a participant based on whether the robot can adjust its self-friendliness according to the change in participant friendliness

and define the utility function of a participant based on whether the value of emotional empathy between the participant and the robot keeps increasing. $UH(E_{RH}^k, E_{RH}^{k+1}, E_{HR}^{k+2}, E_{HR}^{k+3})$ is defined as:

$$UH(E_{RH}^k, E_{RH}^{k+1}, E_{HR}^{k+2}, E_{HR}^{k+3}) = 10 \cdot \left\{ 0.5 \frac{F_{\min}}{F_{\max}} + 0.5(R_2 - R_1) \right\} \quad (14)$$

where F_{\min}/F_{\max} denotes the ratio of the amplitude of change in participant and robot friendliness, and F_{\min}/F_{\max} tends to 1 when the amplitude of change between participants and robots is essentially the same, and vice versa, tends to 0; for F_{\min} and F_{\max} are defined as:

$$\begin{aligned} F_{\min} &= \min(F(k+2) - F(k), F(k+3) - F(k+1)) \\ F_{\max} &= \max(F(k+2) - F(k), F(k+3) - F(k+1)) \end{aligned} \quad (15)$$

R_1, R_2 denote the empathy values between k session participant emotions and $k+1$ session bot emotions, and $k+2$ session participant emotions and $k+3$ session bot emotions, respectively. The multiplication term 10 is to ensure that the values are taken in the range $[0, 10]$.

$$\begin{aligned} R_1 &= R(E_{RH}^k, E_{RH}^{k+1}) \\ R_2 &= R(E_{HR}^{k+2}, E_{HR}^{k+3}) \end{aligned} \quad (16)$$

The definition of the robot utility function $UH(E_{RH}^k, E_{RH}^{k+1}, E_{HR}^{k+2}, E_{HR}^{k+3})$ takes into account, on the one hand, the change in the participant's friendliness, and if the participant's friendliness increases, then the robot's utility value increases; on the other hand, the robot's utility value decreases. On the other hand, the robot's emotional resonance with the participant is considered based on the "principle of increase and decrease in interpersonal attraction", which is similar to the definition of the participant's utility function. Thus, the utility function of the robot is defined as:

$$UH(E_{RH}^k, E_{RH}^{k+1}, E_{HR}^{k+2}, E_{HR}^{k+3}) = 10 \cdot \{0.5[F(k+3) - F(k+1)] + 0.5(R_2 - R_1)\} \quad (17)$$

3.3. OPTIMAL EMOTIONAL STRATEGY SELECTION

Based on the definition of the utility function, the optimal emotional choice strategy of the robot is obtained for the emotional interaction input of the participant with the help of the game model:

(1) The emotional stimuli of k session participants, each emotional strategy of $k+1$ session robots, 6 emotional strategies of $k+2$ session participants, and 6 emotional strategies of $k+3$ session robots form a game matrix, and since $k+1$ session robots share 6 emotional strategies, there are 6 game matrices in total;

(2) Assume that the emotional choice strategy of the robot for $k+1$ sessions is s . Predict the emotional choice strategies of the participants and the robot by finding a

pure strategy Nash equilibrium for the game matrix formed by $k + 2$, $k + 3$ sessions, i.e.:

$$\left. \begin{aligned} &UH(E_{RH}^k, E_{RH}^{k+1}(s), E_{HR}^{k+2}(\cdot), E_{HR}^{k+3}(\cdot)) \\ &\geq UH(E_{RH}^k, E_{RH}^{k+1}(s), E_{HR}^{k+2}(i), E_{HR}^{k+3}(\cdot)), \\ &\exists E_{HR}^{k+2}(\cdot), E_{HR}^{k+3}(\cdot) \in E_l, \forall E_{HR}^{k+2}(i) \in E_l \\ &UH(E_{RH}^k, E_{RH}^{k+1}(s), E_{HR}^{k+2}(\cdot), E_{HR}^{k+3}(\cdot)) \\ &\geq UH(E_{RH}^k, E_{RH}^{k+1}(s), E_{HR}^{k+2}(\cdot), E_{HR}^{k+3}(j)), \\ &\exists E_{HR}^{k+2}(\cdot), E_{HR}^{k+3}(\cdot) \in E_l, \forall E_{HR}^{k+2}(j) \in E_l \end{aligned} \right\} \quad (18)$$

(3) Solving for the optimal affective choice strategy s using the cis-induction method.

$$UH(E_{RH}^k, E_{RH}^{k+1}(s), E_{HR}^{k+2}(\cdot), E_{HR}^{k+3}(\cdot)) \geq UH(E_{RH}^k, E_{RH}^{k+1}(s), E_{HR}^{k+2}(i), E_{HR}^{k+3}(\cdot)), \exists s(\cdot) \in E_l \quad (19)$$

The solution of the static embedded game Nash equilibrium is mainly for the prediction of the next session sentiment trend from the subjective satisfaction of participants and robot self, and the sub-game perfect equilibrium of the embedded game is mainly for obtaining the optimal sentiment selection strategy of the sub-session robot from maximizing the subjective satisfaction of the robot by using the parsimonious induction method to simplify the Nash equilibrium.

3.4. CONSTRUCTION OF A COGNITIVE-EMOTIONAL INTERACTION MODEL FOR ROBOTS

The game model is used to model the emotion generation process of the participant and the robot during human-robot interaction, and the optimal emotional response of the robot is obtained based on the previous historical emotions and the interaction input emotions of the participant. The model construction process is as follows:

Step 1 Input: $k - 1$ post-session friendliness update values $F(k - 1)$ and the probability of transferring the sentiment state of the robot $P_r(k - 1)$, k sessions of participant interaction input sentiment E_{RH}^k ;

Step 2 Output: the sentiment value of the robot at $k + 1$ sessions E_{RH}^{k+1} ;

Repeat:

Step 3 Participant input interaction emotion E_{RH}^k ;

Step 4 Calculate the utility values of the participant and robot under each sentiment strategy choice for $k + 1$ the sessions robot, predicted $k + 2$ sessions participant for each sentiment strategy choice, and $k + 3$ sessions robot for each sentiment strategy according to Eqs. (14)-(17);

Step 5 Solve the emotional choice strategy s of the cognitive model according to Eqs. (18)-(19);

Step 6 The probability of transferring the emotional state of the robot is updated by the optimal emotional strategy s ; the human-robot interaction friendliness is updated such that $k = k + 2$;

Step 7 Until the participant stops entering interactive emotions;

Step 8 End of the HCI session.

During each round of human-computer interaction, the cognitive interaction model is mainly a matrix operation with a time complexity of constant order $O(1)$ in the process of participant interaction input emotion evaluation and robot optimal emotion strategy selection. Assuming that the number of human-computer interaction rounds is n , the time complexity of the model is $O(n)$, which ensures that the response time of the model during human-computer interaction is acceptable.

4. ENGLISH TRANSLATION MODEL BASED ON ROBOT COGNITIVE-EMOTIONAL INTERACTION

Setting any Chinese matrix f and an English sentence e , the probability of e being machine translated into f is $P(e|f)$. The problem of machine translation of f into e can be viewed as the process of solving equation (20):

$$\hat{e} = \arg \max P(e|f) \quad (20)$$

If the lengths of the English string e , as well as the Chinese string, are $f = f_1^m = f_1 f_2 \cdots f_m$ and m , respectively, then we have 1. The alignment can describe the positions of the words within the Chinese sentence corresponding to the words in the English sentence by the presence of the position information of each value, then we have $a = a_1^m = a_1 a_2 \cdots a_m$. Where the value interval of each value is $[0,1]$, then we have :

$$P(f, A|e) = p(m|e) \prod_{j=1}^m p(\alpha_j | a_1^{j-1}, f_1^{j-1}, m, e) \cdot p(f_j | a_1^j, f_1^{j-1}, m, e) \quad (21)$$

In this process, we generate Chinese sentences and alignment process based on English sentences, obtain Chinese sentence length based on English sentences, obtain the link position of the first Chinese word string, and then obtain the first word of Chinese sentences based on English sentences, Chinese sentence length and the position of the English sentence related to the first Chinese word, and loop the process to obtain the overall Chinese sentences.

The English translation model based on robot cognitive-emotional interaction can be implemented to simplify equation (21) and then give the model the ability of emotional interaction, which makes the text more colorful in translation and can keep the semantic and emotional color of the original text. The prerequisites set at the same time are:

(1) If $p(m|e)$ does not correlate with the target language e and the source language length m .

(2) If $p(\alpha_j | \alpha_1^{j-1}, f_1^{j-1}, m, e)$ is related to the target language e length l , then we have:

$$p(\alpha_j | \alpha_1^{j-1}, f_1^{j-1}, m, e) = \frac{1}{l+1} \quad (22)$$

(3) If $p(\alpha_j | \alpha_1^{j-1}, f_1^{j-1}, m, e)$ is related to f_j and f_{al} , then there exists $\varepsilon = P(m|e)$, $t(f_j | e_{al}) = p(f_j | \alpha_1^j, f_1^{j-1}, m, e)$. $t(f_j | e_{al})$ is the probability given e_{al} and f_j .

After incorporating the Lagrangian factors λ_1 , the process of obtaining the highest value of machine translation probability is transformed into the process of obtaining the highest value of the auxiliary function at the random state, then the English machine translation model based on the robot cognitive-emotional interaction model is as follows:

$$h(p, \lambda) = \frac{S}{(l+1)^m} \sum_{al=0}^l L \sum_{al=0}^l \prod_{j=1}^m t(f_j | \alpha_{\theta}) - \sum_{\theta} \lambda_{\theta} (\sum_{\gamma} t(f | e) - 1) \quad (23)$$

The above English machine translation model is transformed into a reverse machine translation model to accomplish accurate machine translation of the English language using the statistical machine method of maximum entropy. The transformation within the model ensures that the machine translation efficiency of the machine translation model is improved by obtaining improved parameter values through the great likelihood prediction method as follows:

$$\hat{\theta} = \arg \max_{\theta} \prod_{s=1}^S p_{\theta}(f_s | e_s) \quad (24)$$

$$\hat{\gamma} = \arg \max_{\gamma} \prod_{s=1}^S p_{\gamma}(e_s) \quad (25)$$

and then obtain the formula:

$$\hat{e}_1^l = \arg \max_{e_1^l} \{p_{\hat{\gamma}}(e_1^l) \cdot P_{\hat{\theta}}(f_1^j | e_1^l)\} \quad (26)$$

After incorporating the new property, $P_{\hat{\theta}}(e_1^j | f_1^l)$ replaces $P_{\hat{\theta}}(f_1^j | e_1^l)$ and the framework of the obtained extended statistical machine translation is:

$$\hat{e}_1^l = \arg \max_{e_1^l} \{p_{\hat{\gamma}}(e_1^l) \cdot P_{\hat{\theta}}(e_1^j | f_1^l)\} \quad (27)$$

Equation (27) enables the implementation of more efficient retrieval and the acquisition of high-quality English machine translation results.

5. EXPERIMENTAL DESIGN AND ANALYSIS OF RESULTS

5.1. EXPERIMENTAL DESIGN

To facilitate the performance analysis and comparison experiments of the robot-based cognitive-emotional interaction model proposed for the text, an English text translation robot based on the robot-based cognitive-emotional interaction model of this paper is built using the open-source chatbot ChatterBot. First, the English translation model is used to match English translation answers of environmental protection articles with the translation robot logic adapter, and the top answers with higher confidence are returned as the candidate answer set; then, the sentiment strategy is evaluated using the model of this paper, and the optimal sentiment strategy is selected. Finally, the candidate answers are optimally ranked based on the response sentiment of this paper's model, and the answer with the highest ranking level is selected as the robot response output. In addition, since the number of emotional states to be explored increases exponentially with the number of interaction rounds, the maximum number of interaction rounds $T=8$ (rounds) for two bits of intelligence and the number of candidate emotional states selected in each round $n=8$ (kinds) are set in this model for emotional state evaluation.

The experimental data uses the sample dataset from the NLPCC2017 shared task Emotional Conversation Generation, which contains a total of 11207 Chinese-English parallel question-and-answer corpus of articles about environmental protection. 6000 question and answer pairs are randomly divided as the validation set, 5000 question and answer pairs as the test set, and the remaining question and answer pairs are used as the training corpus for the chatbot to translate from English to Chinese.

The experiment focuses on the translation and affective accuracy of the English translation of environmental protection articles, as well as the actual effect of human-computer interaction sessions, so the following cognitive models are selected for comparison experiments:

- (1) A single robot cognitive model, Chatterbot, outputs responses based on the high confidence level of each answer in the candidate answer set. Since it does not have cognitive-emotional computing capability, it is only used for model validation comparison experiments;
- (2) Emotional Chat Machine ECM, which can produce appropriate responses in terms of content-related grammar and emotional coherence;
- (3) Adversarial network SentiGAN model, capable of generating generic, diverse and high-quality sentiment texts;
- (4) Two-way asynchronous sentiment session generation method E-SCBA, which can generate text with a logical and emotional degree;

(5) An emotional interaction model based on the guided cognitive reassessment strategy GCRs can reduce the robot's dependence on external emotional stimuli and, to some extent, prompt positive emotional expressions.

5.2. EMOTIONAL ACCURACY ANALYSIS

To avoid the ambiguity of the robot's emotional expression that makes it difficult for the participants to recognize the response emotion state, the response emotion state should have a certain degree of accuracy in the expression of the expected emotion category. To visually evaluate the accuracy of the robot's emotion generation state under the action of each model, the accuracy of the target emotion category of the response emotion is calculated:

$$Acc(E_{RH}^{k+1}) = P_{k+1}(i) - \frac{1}{5} \sum_{j \neq i} P_{k+1}(j) i, j = 1, 2, \dots, 6 \quad (28)$$

The results are shown in Table 2. As can be seen from Table 2, the models in this paper are better than other models in terms of sentiment accuracy, which is mainly because the confidence of the input response sentiment state to each basic sentiment state transfer probability is used as the update factor when the robot sentiment state transfer probability is updated. This is mainly because the confidence of the input response emotional state to each basic emotional state transfer probability is used as the update factor in this paper, which effectively increases the influence of the input response expected emotional category on the robot's emotional state transfer probability.

Table 2. Statistical table of sentiment accuracy for different models

| Cognitive models | Accuracy |
|------------------|----------|
| ECM | 0.785 |
| GCRs | 0.821 |
| E-SCBA | 0.802 |
| SentiGAN | 0.856 |
| This article | 0.895 |

5.3. RETRIEVING TRANSLATION VALIDITY

To facilitate the verification of the effectiveness of model answer retrieval translation, two information retrieval evaluation indexes, MRR and MAP, were used to calculate the sorting accuracy of each model candidate answer, 60 sentences were randomly selected from the test set for the experiment, and the average of the sorting accuracy was taken as the final result of the experiment, and the results are shown in Figure 5.

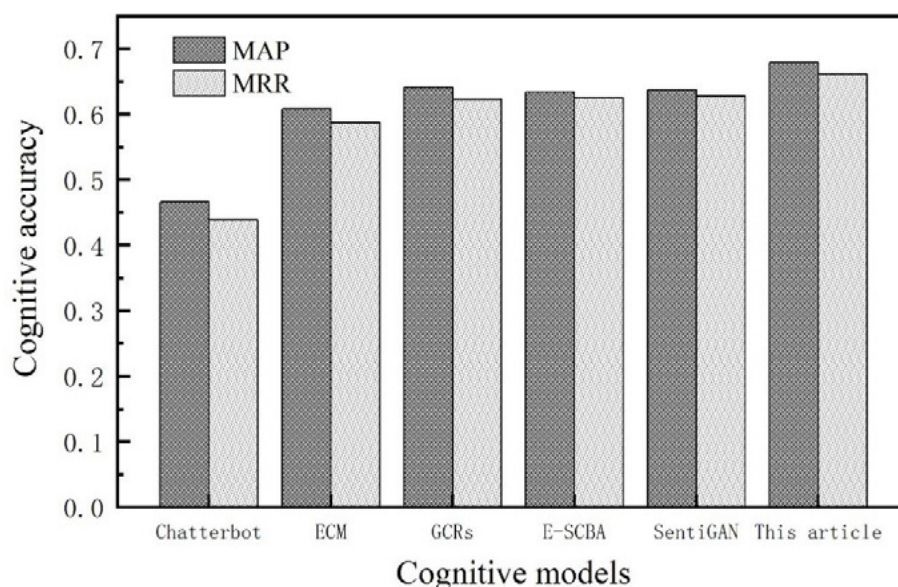


Figure 5. Different models retrieve translation accuracy statistics

Figure 5 shows the statistical results of the average accuracy of retrieving translation ranking for different cognitive model answers ($m=6$), and it can be seen from the table that this paper's model achieves relatively satisfactory results compared with other models. This is because the model in this paper ensures more effective retrieval by combining quantitative evaluation of contextual affective states and quantitative analysis of factors influencing human-like affective states when ranking candidate answers, and transforming the translation model into a reverse machine translation model by incorporating Lagrangian factors in the English translation model, to obtain high-quality English translation results. Reinforcement learning is used to establish the correlations between contextual long-term affective states to achieve a comprehensive and optimal assessment of the following state response with better cognitive affective ability.

5.4. VALIDATION OF INTERACTION TRANSLATION

To effectively evaluate the effectiveness of interactive sessions, 20 volunteers were invited to participate in multiple human-computer interaction translation tests under different models in this paper. At the same time, to increase the objective comparability among the models, each model was subjected to 30 rounds of multi-round human-computer interaction conversation experiments. Thirty English sentences were randomly selected from the test set and used as the initial input for each model to conduct interactive sessions. The average number of conversations and the average interaction time for each model are shown in Table 3.

Table 3. Conversation translation rounds and interaction time statistics table

| Cognitive models | N(rounds) | T(s) |
|------------------|-----------|--------|
| Chatterbot | 7 | 67.51 |
| ECM | 10 | 98.54 |
| GCRs | 15 | 137.51 |
| E-SCBA | 12 | 119.47 |
| SentiGAN | 10 | 107.63 |
| This article | 18 | 152.92 |

As shown in Table 3, this model outperforms other models in terms of the average number of conversation rounds and the average interaction time, which indicates that the translation robot under the effect of this model can better express the meanings expressed in English, can better communicate with people in English, and can effectively extend the human-robot interaction session time. This is because the response emotions obtained from the model in this paper are more diverse, positive and accurate by considering human-like emotion generation in the continuous space of multiple emotion states and combining with the robot's emotion state update, which effectively guides the participants to participate in human-robot interaction.

5.5. MODEL SATISFACTION ASSESSMENT

To evaluate the model satisfaction effectively, this paper conducts questionnaire experiments in two aspects: single-round sentence translation and dialogue subjective satisfaction, and multi-round sentence translation and conversation subjective satisfaction. The evaluation indexes of subjective satisfaction with single-round sentence translation and conversation are rationality, diversity, and empathy. The experiment process is as follows: 100 question-and-answer phrases are randomly selected from the test set for the test, 500 question-and-answer pairs are used in total, and 200 volunteers are invited to conduct the questionnaire survey online and offline through multiple channels. The evaluation indexes of subjective satisfaction of multi-round sessions were fluency, positivity, interestingness and participation. The experimental process is as follows: based on the evaluation indexes, a multi-round session satisfaction survey is conducted for 20 HCI volunteers in the validation of interactive sessions. At the same time, all indicators were evaluated using a three-point scale (0,1,2): 0 indicates a low degree, 1 indicates an average degree, and 2 indicates a high degree. The final statistical results were averaged, and the higher the score the higher the model satisfaction. The results of the model's single-round sentence translation and dialogue subjective satisfaction survey are shown in Figure 6, and the results of the multi-round sentence translation and dialogue subjective satisfaction survey are shown in Figure 7.

As seen in Figure 6, the model in this paper is significantly better than other models in terms of dialogue rationality, diversity and empathy, especially in terms of diversity

of emotional expressions, which is because this paper makes full use of multiple emotional states in the emotional space when making emotional decisions, and the results show that the model in this paper can effectively improve the satisfaction of the robot's single-round dialogue response in many ways.

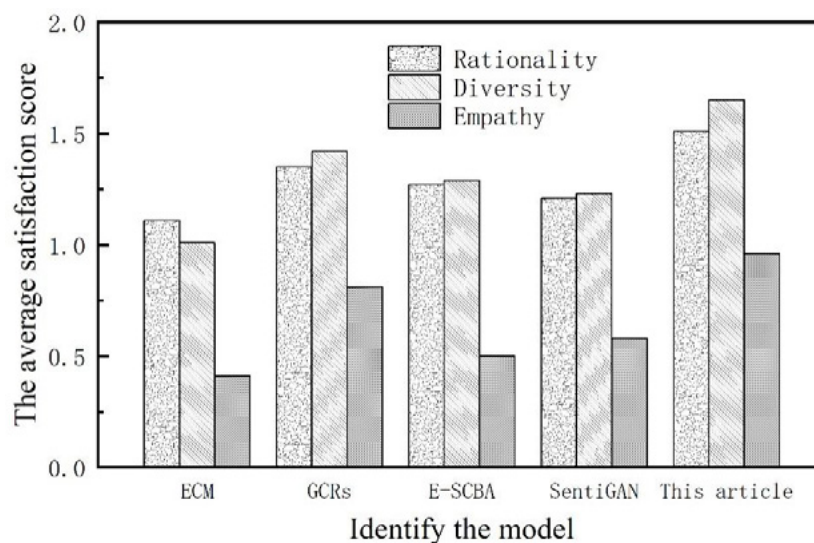


Figure 6. Statistical chart of single-round subjective evaluation data

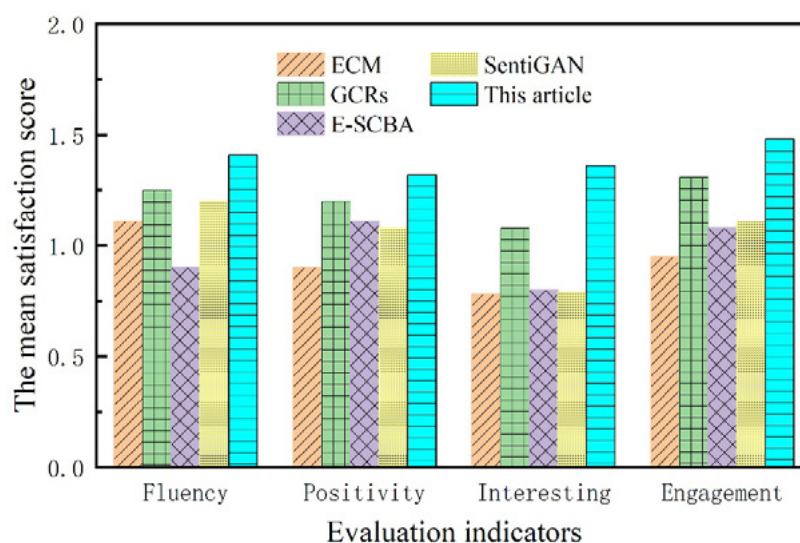


Figure 7. Statistical chart of subjective evaluation data for multiple rounds

As can be seen from Figure 7, the model in this paper has effectively improved the overall fluency and positivity of the robot's emotional utterance translation expression, the interestingness of human-robot interaction, and the participant's involvement compared with other models, indicating that the contextual long-term dependency relationship and the factors influencing emotion generation established in this paper are reasonable and effective in the construction of the emotional interaction model, which can further increase the participant's willingness to interact with human-robot and build a natural and harmonious human-robot interaction relationship.

6. CONCLUSION

Robot cognitive-based affective interaction computing is to give computers the ability to observe, understand and generate various emotional states similar to human beings, so that they can interact naturally and intimately, vividly and interestingly like human beings. In this paper, we propose a reinforcement learning-based emotional interaction model for robot cognition. First, we use reinforcement learning to model the emotion generation process, and use the one-dimensional emotion model theory as the emotion state space of the robot, with small granularity of emotion division and delicate expression, which motivates the robot to improve efficiency in the process of emotional interaction; second, we consider quantifying the three emotional influencing factors of similarity, positivity and empathy as the reward function for conducting reward function for emotional state assessment, and derive the optimal emotional strategy selection based on the utility function to realize the interaction motive of emotional support, emotional guidance and emotional empathy for the participants; thirdly, in the process of environmental protection English articles translation by the robot, the Lagrange factor is introduced, which makes the process of machine translation probability maximum transformed into the process of obtaining the highest value of the auxiliary function at the random state. The retrieval speed of machine translation is improved, the efficiency of machine translation is enhanced, and high-precision translation results can be obtained more effectively. Finally, the Chinese-English parallel question and answer corpus commonly used in environmental protection articles is used as the experimental data set, and the optimal emotional state is combined with the optimal emotional state to update the robot's emotional state transfer probability, to realize the robot's state transfer in the translation process and ensure the continuity of the translation process. The experiments verified the validity of the model in terms of accuracy, MAP and MRR, and also proved that the robot cognitive-emotional interaction model can competently translate environmental protection English articles as a whole with faster translation efficiency and more accurate retrieval translation quality. Due to the complexity of the human emotion generation process and the diversity of factors influencing the probability of emotion state transfer, the model in this paper only considers some of the influencing factors in the process of emotion generation and translation of English articles. Therefore, future work needs to consider all the factors influencing the process of human emotion generation and translation of English texts to further optimize human-like emotion state generation, so that the robot cognitive-emotional interaction model can help people in all aspects of daily life in a real sense.

DATA AVAILABILITY

The data used to support the findings of this study are available from the corresponding author upon request.

CONFLICTS OF INTEREST

The author declares that there is no conflict of interest regarding the publication of this paper.

REFERENCES

- (1) Sovacool, B. K., & Rio, D. (2021). **Corrigendum to "Smart home technologies in Europe: a critical review of concepts, benefits, risks and policies" [Renew Sustain Energy Rev 120 (2020) 109663].** *Renewable and Sustainable Energy Reviews*, 111277.
- (2) Hoskote, M., Le, G., Cherian, R., et al. (2021). **Cancer patient perspectives on survivorship goals from the Smart Patients online community.** *Supportive Care in Cancer*, 29(5), 2375-2384.
- (3) Calp, M. H., Butuner, R., Kose, U., et al. (2022). **IoHT-based deep learning controlled robot vehicle for paralyzed patients of smart cities[J].** *The Journal of Supercomputing*, 78(9), 11373-11408.
- (4) Souza, A., Filho, M. R., & Soares, C. (2020). **Production and evaluation of an educational process for human-computer interaction (HCI) courses[J].** *IEEE Transactions on Education*, PP(99), 1-8.
- (5) Mmab, C., Kr, B., Aga, B., et al. (2020). **Cognitive ability and education: How behavioral genetic research has advanced our knowledge and understanding of their association - ScienceDirect[J].** *Neuroscience & Biobehavioral Reviews*, 111, 229-245.
- (6) Eder, M., Reip, M., & Steinbauer, G. (2021). **Creating a robot localization monitor using particle filter and machine learning approaches[J].** *Applied Intelligence*, 1.
- (7) He, Y., Yang, S., Chan, C. Y., et al. (2020). **Visualization analysis of intelligent vehicles research field based on mapping knowledge domain[J].** *IEEE Transactions on Intelligent Transportation Systems*, PP(99), 1-16.
- (8) Chetan, M. R., Dowson, N., Price, N. W., et al. (2022). **Developing an understanding of artificial intelligence lung nodule risk prediction using insights from the Brock model[J].** *European Radiology*, 32(8), 5330-5338.
- (9) Alghadir, A. H., Gabr, S. A., Al-Momani, M., et al. (2021). **Moderate aerobic training modulates cytokines and cortisol profiles in older adults with cognitive abilities[J].** *Cytokine*, 138, 155373.
- (10) Panahiazar, M., Chen, N., Lituiev, D., et al. (2021). **Empowering study of breast cancer data with application of artificial intelligence technology: promises, challenges, and use cases[J].** *Clinical & Experimental Metastasis*.
- (11) Martinez, E. O., Jorns, J. M., Kong, A. L., et al. (2022). **ASO Visual Abstract: Primary Breast Neuroendocrine Tumors—An Analysis of the National Cancer Database[J].** *Annals of Surgical Oncology*, 29(10), 6349-6349.
- (12) Griebeling, T. L. (2020). **Re: Do Canadian Radiation Oncologists Consider Geriatric Assessment in the Decision-Making Process for Treatment of Patients 80 Years and Older with Non-Metastatic Prostate Cancer? National Survey[J].** *The Journal of Urology*, 204(2), 361-361.

- (13) Kuo, J. Y., Chen, C. H., Roberts, J. R., Chen, L. C., & Yang, C. C. (2020). **Evaluation of the user emotional experience on bicycle saddle designs via a multi-sensory approach.** *International Journal of Industrial Ergonomics*, 80, 103039.
- (14) Arana, S., Marquand, A., Hultén, A., Richiardi, J., Loth, E., & Murphy, D. G. (2020). **Sensory modality-independent activation of the brain network for language.** *The Journal of Neuroscience*, 40(14), 2271-2219.
- (15) Lca, B., Wsa, B., Yu, F., Cai, L., & Li, H. (2020). **Two-layer fuzzy multiple random forests for speech emotion recognition in human-robot interaction.** *Information Sciences*, 509, 150-163.
- (16) Zucco, C., Calabrese, B., & Cannataro, M. (2017). **Sentiment analysis and affective computing for depression monitoring.** In *2017 IEEE International Conference on Bioinformatics and Biomedicine (BIBM)* (pp. 1988-1995). IEEE.
- (17) Liu, X., Xie, L., & Wang, Z. (2017). **Empathizing with emotional robot based on cognition reappraisal.** *China Communications*, 14(9), 100-113.
- (18) Wu, D., Han, X., Yang, Z., Li, B., & Zhang, Y. (2021). **Exploiting transfer learning for emotion recognition under cloud-edge-client collaborations.** *IEEE Journal on Selected Areas in Communications*, 39(2), 479-490.
- (19) Kraljević, N., Schaare, H. L., Eickhoff, S. B., & Nickl-Jockschat, T. (2021). **Behavioral, anatomical and heritable convergence of affect and cognition in superior frontal cortex.** *NeuroImage*, 243, 118431.
- (20) Loev, S. (2022). **Epistemic feelings are affective experiences.** *Emotion Review*, 14(1), 1-11.
- (21) Zhong, Q. B., Fang, B. F., Guo, X. P., Li, Z. J., & Zhang, J. (2021). **Task allocation for affective robots based on willingness.** *IEEE Access*, 9, 80028-80042.
- (22) Culot, C., & Gevers, W. (2021). **Happy is easy: The influence of affective states on cognitive control and metacognitive reports.** *Cognition and Emotion*, 35(12), 1195-1202.
- (23) Zhang, R., Wang, Z., & Mai, D. (2017). **Building emotional conversation systems using multi-task Seq2Seq learning.** In *The Sixth CCF International Conference on Natural Language Processing and Chinese Computing* (pp. 612-621). Springer.
- (24) Rodríguez L. F., Gutiérrez-García, J. O., & Ramos, F. (2016). **Modeling the interaction of emotion and cognition in autonomous agents.** *Biologically Inspired Cognitive Architectures*, 17, 57-70. <https://doi.org/10.1016/j.bica.2016.07.008>
- (25) Fatahi, S., & Moradi, H. (2016). **A fuzzy cognitive map model to calculate a user's desirability based on personality in e-learning environments.** *Computers in Human Behavior*, 63, 272-281.
- (26) Mohsin, M. A., & Beltiukov, A. (2019). **Summarizing emotions from text using Plutchik's wheel of emotions.** In *CY7th Scientific Conference on Information Technologies for Intelligent Decision Making Support (ITIDS2019)* (pp. 291-294). Atlantis Press.

- (27) Ali, M., Al Machot, F., Haj Mosa, A., et al. (2018). **A globally generalized emotion recognition system involving different physiological signals.** *Sensors*, 18(6), 1905.
- (28) Pan, H., Xie, L., Lv, Z., et al. (2020). **Hierarchical support vector machine for facial micro-expression recognition.** *Multimedia Tools and Applications*, 79(41), 31451-31465.
- (29) Qi, X., Wang, W., Guo, L., et al. (2019). **Building a Plutchik's wheel inspired affective model for social robots.** *Journal of Bionic Engineering*, 16(2), 209-221.
- (30) Belkaid, M., Cuperlier, N., & Gaussier, P. (2018). **Autonomous cognitive robots need emotional modulations: Introducing the eMODUL model.** *IEEE Transactions on Systems, Man, and Cybernetics: Systems*, 49(1), 206-215.
- (31) Maqache, N., & Swart, A. J. (2021). **Remotely measuring and controlling specific parameters of a PV module via an RF link.** *3C Tecnología. Glosas de innovación aplicadas a la pyme*, 10(4), 103-129. <https://doi.org/10.17993/3ctecno/2021.v10n4e40.103-129>
- (32) Che Xiangbei, Li Man, Zhang Xu, Alassafi Madini O., & Zhang Hongbin. (2021). **Communication architecture of power monitoring system based on incidence matrix model.** *Applied Mathematics and Nonlinear Sciences*, 7(1), 83-92. <https://doi.org/10.2478/AMNS.2021.1.00098>

/12/

A STRATEGY FOR BUILDING A SMART SPORTS PLATFORM BASED ON MACHINE LEARNING MODELS

Mingchan Gong *

School of design and art, Hunan Institute of Technology, Hengyang, Hunan,
421000, China

2000001200@hnit.edu.cn



Reception: 13/11/2022 **Acceptance:** 08/01/2023 **Publication:** 23/03/2023

Suggested citation:

G., Mingchan. (2023). **A strategy for building a smart sports platform based on machine learning models**. *3C TIC. Cuadernos de desarrollo aplicados a las TIC*, 12(1), Page-Page. <https://doi.org/10.17993/3ctic.2023.121.248-265>

ABSTRACT

With the rapid development of big data technology, it has greatly changed the way people get information, and also improved the speed and quality of information. In this context, smart sports has become a new trend in sports development. This paper creates an intelligent learning environment and builds a smart sports platform through advanced concepts and technical means, which can effectively optimize the integration and sharing of sports resources. Starting from the overall architecture design of smart sports, the key technologies of machine learning model to realize smart sports are sorted out. Through the five basic linking stages with machine learning model as the core, the value innovation path of platform construction structure is analyzed. The current status of sports resources application is studied, and the data mining algorithm is used to calculate the user usage data of the smart sports platform and improve the construction of the smart platform. Through the construction of the smart sports platform, people shift from traditional reading books and watching TV programs to getting information through intelligent mobile terminals, and the proportion of attention to sports information is as high as 58.6%. This shows that by building a smart sports platform, it can provide support and guarantee for the sustainable development of sports.

KEYWORDS

Smart sports; machine learning modeling technology; resource sharing; platform construction; sports information

PAPER INDEX

ABSTRACT

KEYWORDS

1. INTRODUCTION

2. SMART SPORTS PLATFORM CONSTRUCTION

3. SMART SPORTS SERVICES

4. SMART SPORTS PLATFORM DESIGN

5. MACHINE LEARNING MODEL ALGORITHMS

6. PLATFORM CONSTRUCTION ANALYSIS

6.1. Test Environment and Methodology

6.2. System Performance

6.3. Survey Results

7. CONCLUSION

DATA AVAILABILITY

CONFLICT OF INTEREST

REFERENCES

1. INTRODUCTION

Machine learning model analysis has increasingly become an important reference for people's judgment and decision making, and is increasingly known and used. Various analytical tools and analytical methods based on machine learning models have emerged [1-4]. The idea of big data, which itself has undergone the process from experiment to practice and from niche to mass, is also increasingly known [5-8]. The smart sports platform is based on information technology, including machine learning model analysis, Internet of Things, and cloud computing technology, which together build a public basic service platform integrating social, cultural, sports, and environmental factors [9-12]. Its main functions include query service function, data collection function, and data management function. The rapid development of communication technologies such as machine learning models has made the integration and application of resource information the key to the construction of sports informatization [13-15]. The rapid development of science and technology development under machine learning models will promote the application of mobile terminals such as smartphones and tablets in the sports industry [16-18]. Machine learning models are a collection of massive data, the volume of which is particularly huge and cannot be processed by conventional software within a certain period of time. Machine learning models are characterized by massive scale, high-speed flow, and rich form [19-20]. The construction platform on the basis of machine learning models should be unified to manage the collected data, and the multi-channel, multi-level and multi-angle feedback query service window after data analysis. The platform can achieve the sharing of sports information in the province and even in the country or even globally, and build a service network covering the whole province, with the characteristics of intelligence, innovation and extensiveness [21].

The literature [22] mentions that smart cities are the direction and advanced form of future urban development, integrating the functions of digital, knowledge, ecological, and creative cities. Big data is changing people's life, work and thinking, bringing major changes in cities. Huge amount of data exists in all aspects and fields of the city. The establishment of a technical system framework for smart cities based on big data technology is discussed, and the feasibility of this technical system framework is explored. The literature [23] outlines the significance of machine learning modeling techniques in the construction of smart cities. Its important role in further promoting the development of the Zhengzhou Airliner Economic Zone in China and the whole process is analyzed. As well as how it can promote economic transformation and upgrading, it is expected to provide ideas and support for the Zhengzhou Airliner Economic Zone, China, to lead and promote the regional economy of Henan, China, in the future and achieve continuous improvement in sustainable development. Literature [24] et al. Also, a more reliable trust protocol can be established, which is conducive to the implementation of machine learning model applications. The literature [25] and others mention that with the advancement of urbanization and the coordination of urban transportation, municipalities, economic industries.

This paper analyzes the application of machine learning models in the design of smart sports and evaluates the impact of the planning and construction of smart

sports based on machine learning models on economic and social benefits. Through the wide application of machine learning models in building smart sports platforms, the government is able to run more smoothly, conveniently and efficiently in planning, construction, industry, people's livelihood, society and cities. The current situation of sports informatization construction, as well as the advantages and related strategies of the construction plan of the smart sports platform based on big data, are mainly analyzed and discussed.

2. SMART SPORTS PLATFORM CONSTRUCTION

The construction target of the smart sports platform is to gather various types of venues and fitness groups of people's resources, and realize the digital fitness consultation and guidance, sports and fitness activity resources, venue booking, equipment purchase, personalized sports services and sports culture exchange for all people and high social participation through the platform [26-27].

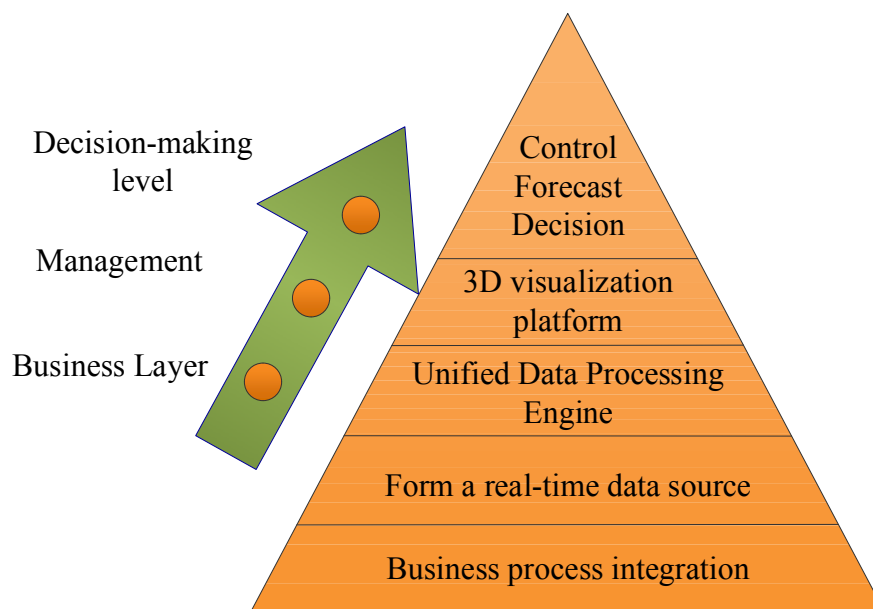


Figure 1. Smart Sports Platform Framework and Structure

The essential difference between smart sports services is the empowerment of "wisdom". It refers to the use of advanced concepts, technology and other means to create an intelligent learning environment, forming a precise, individual and flexible education service system as shown in Figure 1. As can be seen, although "wisdom" has different facets, "wisdom" represents, first of all, positive, innovative and comprehensive capabilities on the outside, and on the inside, value understanding and moral identity for good and common good. In order to better clarify the seven modules of the application service layer, to open up and integrate the storage and computing centered on big data, and to realize the effective operation of the modules and the process of value output.

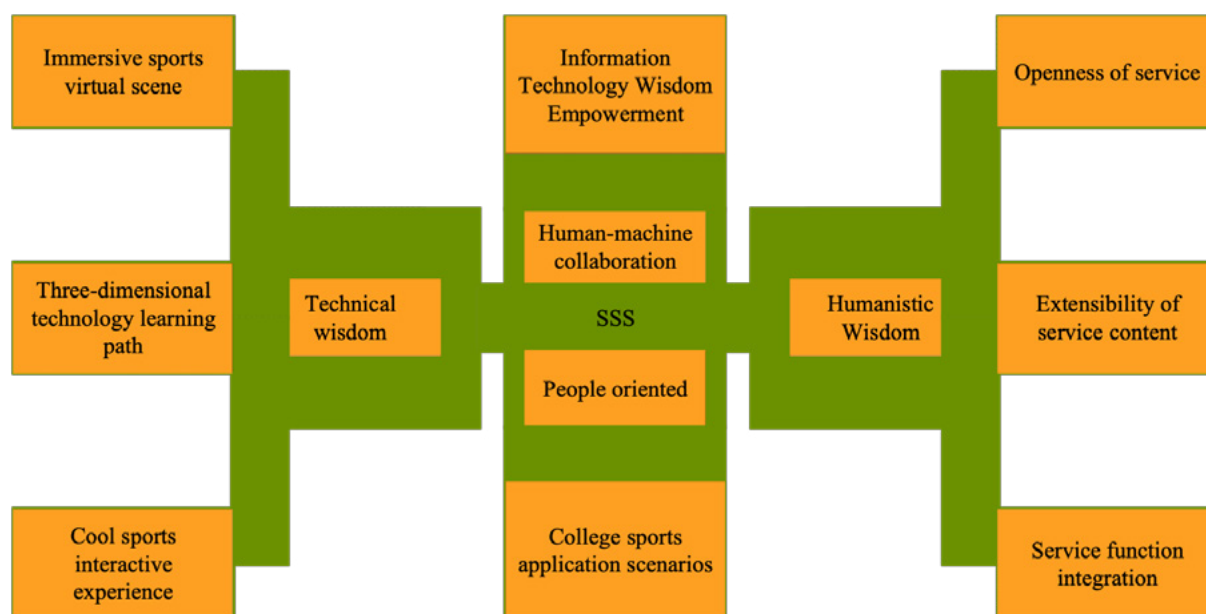


Figure 2. Creating a value innovation path for smart sports with machine learning models at its core

As shown in Figure 2, the module value innovation is analyzed through five basic linking stages with machine learning model as the core.

Demand identification: Based on the collection of basic data such as users' physical health level, sports cognition and technical ability, sports learning demands and sports preferences, the demand instruction for sports course learning is intelligently generated.

Precise Matching: By analyzing and mining the system data, we provide precise matching course learning solutions.

Intelligent push: When personalized learning solutions are intelligently pushed to the platform's user interface, users can operate tasks and learn skills according to the sports process and specific requirements of different scenarios in the module architecture even in fragmented time periods with the help of ubiquitous networks and mobile terminals.

Decision-making and implementation: Once a user enters a certain task point, the coach will synchronously track and instantly share the learning process data through intelligent perception, supervise and control the efficiency of sports implementation, make timely professional assessment in three dimensions of "sports spirit, sports practice and health promotion", and provide personalized counseling and suggestions for non-standard problems, as well as instant evaluation and feedback.

The evaluation of sports completed by users in the client is instantly fed back to the intelligent learning system to promote the quality of subsequent sports activities. In the five basic linking stages, the sports courses through the platform fundamentally stimulate the initiative and motivation of "value co-creation" between the platform and users, and realize the "sports meaningful growth" with technical support in the new era. Through the instant dialogue, two-way communication and joint exploration

between coaches and users, the skills learning willingness of users is fully achieved in the new scenario, and targeted sports activities are effectively promoted.

3. SMART SPORTS SERVICES

From the perspective of service essence, the "wisdom core" of smart sports service is a "people-oriented wisdom". It takes the sports needs of service recipients as the core, and provides the most necessary, suitable, accurate and convenient personalized sports platform services and health management services through the systematic changes of service forms, service contents and service functions, thus manifesting the human-centered service thrust.

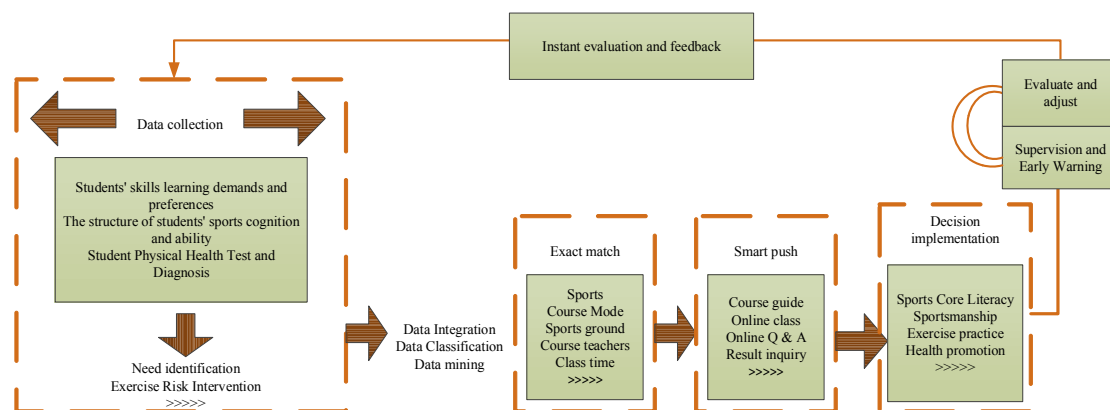


Figure 3. Smart Sports Service Structure

As shown in Figure 3 its performance is specified in:

1. Openness of service form. With the support of modern information technology, users only need to hold smart terminals to seamlessly connect and interoperate to the open, collaborative and shared central system of smart sports service platform, they can get "menu" sports resources and services anytime, anywhere, freely and efficiently, so that sports are everywhere.
2. Wide extension of service content. In terms of content scope, the content of intelligent sports services covers online and offline integrated sports model, sports community interaction, intelligent venue management and other multi-dimensional needs. In terms of content depth, sports skills output is more full and vivid under the conditions of language, image, emotional awareness three-dimensional multi-sensory technology, which can make the sports experience under the resonance of sports thinking and sports psychological immersion more profound.
3. Integration of service functions. It is through the application of intelligent technology and information technology, fully mining and analyzing the full record of data information and automatically generate adapted personalized services to meet the differentiated sports needs of the user body; through portable devices associated with the user's heart rate, blood pressure, pulse oxygen saturation and other physiological indicators, expression behavior recognition technology analysis of sports emotions, perception and other psychological indicators of the dual

assessment feedback, to achieve the scientific norm of the user's sports risk Prevention and control, etc.

4. SMART SPORTS PLATFORM DESIGN

While leading sports reform and innovation, smart sports services are bound to bring great impact and challenges to the traditional sports learning mindset, sports management model and sports cultural environment.

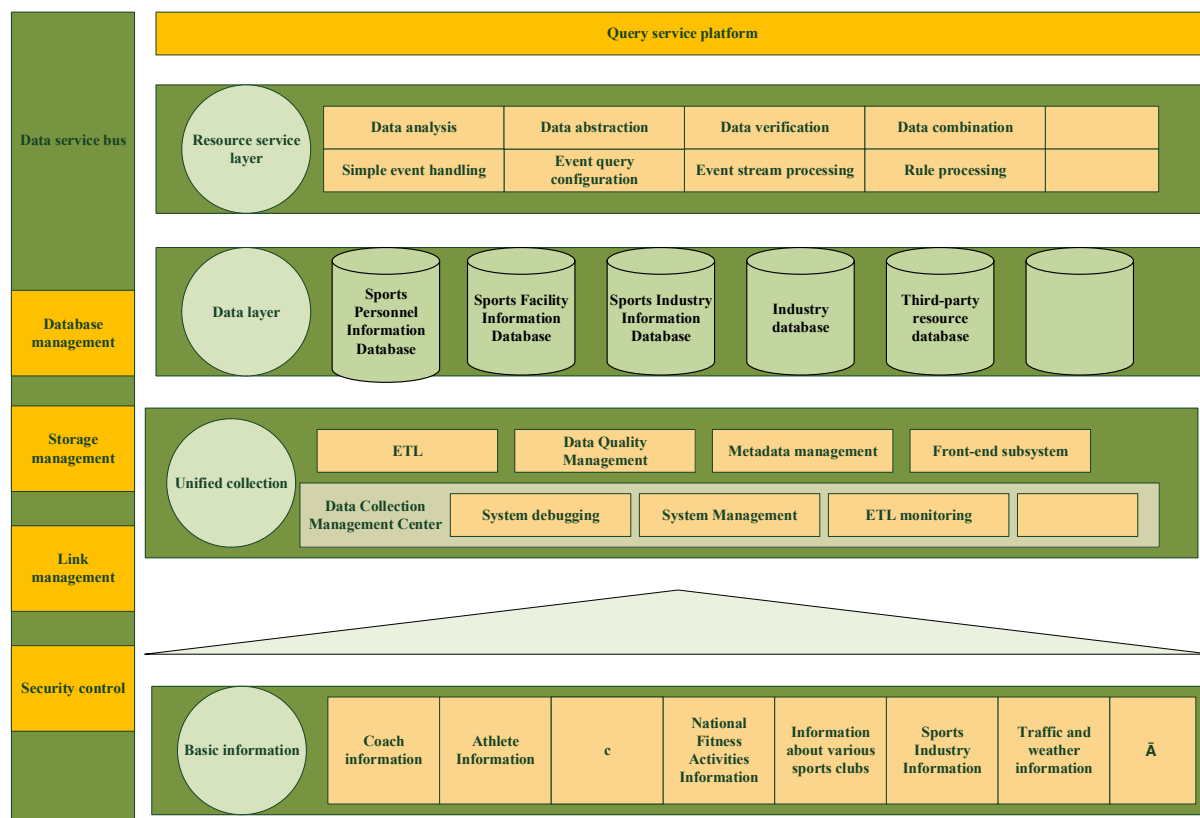


Figure 4. Logical framework design for smart sports platform

As shown in Figure 4, the resource service layer refers to the application functions based on the realization of data processing, mainly through modeling, to realize the analysis, abstraction, verification, combination and other processing of data extracted from the database, and the functions for event processing include brief event processing, event query configuration, event flow processing, rule processing, etc.

The data layer, i.e. database, is a warehouse for organizing, storing and managing data according to the data structure, and as the basic data storage area of the whole platform, and guarantee the integrity and convenience of data extraction by users.

As the convergence layer of the platform data, the unified collection realizes the convergence, filtering and data conversion of sports-related information such as sports activities personnel, and then submits them to the front subsystem for temporary storage, and submits them to the storage.

Users complete the selection of self-chosen content for sports courses within a specified period of time through the Smart Sports Platform. The platform sets the

course content name for users to choose, and users choose the course with their own situation and interest points. Users can also give feedback on courses that are not set up through the platform's comment section and text the reasons for applying for the course. The platform will give feedback to the sports coach, and the sports coach will try his best to provide appropriate advice to support his own situation. This way not only realizes the interaction between coaches and students, but also improves the efficiency of communication.

5. MCHINE LEARNING MODEL ALGORITHMS

The data mining algorithm utilized in this paper contains a clustering analysis algorithm and a BP neural network model algorithm, and the two are organically combined to achieve data analysis of the construction of a smart platform. Thus, the user usage data of the smart sports platform is calculated, which can better improve the platform information and grasp the psychological needs of users.

Firstly, the data is classified and calculated using the K-means algorithm for the measurement technique step. Its main steps for analyzing big data are:

1. K centroids are randomly extracted from different sample data to select the initial cluster centroids.
2. Divide the sample cluster points by allocating each different data point to the center nearest to that data point. In this step, the distance formula is introduced to obtain:

$$d(x, y)^2 = \sum_{i=1}^n (x_i - y_i)^2 = \|x - y\|_2^2 \quad (1)$$

Based on the selected centroids of the clustered samples of each data, the distance between each database sample data and these central sample parameters is calculated using Equation (1), and the corresponding large data are re-classified according to the minimum distance.

(3) Based on the mean value of each clustered sample data object, the distance between each object and these central objects is calculated, and the corresponding objects are re-divided according to the minimum distance recalculating the mean value of the distance from the point in each class to the centroid of that class, assigning each data to its nearest centroid. Forming the matrix D with the minimum data calculated each time, then:

$$D = \begin{pmatrix} x_{11}, x_{12}, \dots, x_{1n} \\ x_{21}, x_{22}, \dots, x_{2n} \\ \dots \\ x_{k1}, x_{k2}, \dots, x_{kn} \end{pmatrix} \quad (2)$$

where x_{ij} is the set of the found minimum values.

(4) In big data processing, by using K-means algorithm can obtain the clusters with the smallest error criterion function of big data. By centering K sample data points in

the space and clustering them, the information big data closest to the different samples is finally categorized.

After using the K-means algorithm output results, then use the BP network algorithm model algorithm to continue mechanical learning, training. It is able to map and handle the more complex nonlinear relationships in the data samples in a timely manner. In adjusting the BP neural network model, the following formula is followed: where the adjustment formula for the output layer power system is:

$$\Delta\omega_{ij} = \eta O_k^p (1 - O_k^p) (t_k^p - O_k^p) O_i^p \quad (3)$$

The adjustment formula for the implied layer weight factor is:

$$\Delta\omega_{ij} = \eta O_i^p (1 - O_i^p) \sum_{k=1}^L \Delta\omega_{ki} O_j^p \quad (4)$$

The quadratic exact function model for pairs of input patterns in different large data samples is:

$$J_p = \frac{1}{2} \sum_{k=1}^L (t_k^p - O_k^p)^2 \quad (5)$$

Expression for the total accurate function for N different large data samples:

$$J = \sum_{p=1}^N J_p = \frac{1}{2} \sum_{p=1}^N \sum_{k=1}^L (t_k^p - O_k^p)^2 \quad (6)$$

Big data samples are standardized as follows: assuming that the type of input big data information is m and the sample is N , for the input data X_{ij} is standardized according to the steps of the following equation.

$$Z_{ij} = \frac{(x_{ij} - \hat{x}_j)}{\delta_j} \quad (7)$$

$$\hat{x}_j = \frac{1}{N} \sum_{i=1}^N x_{ij} \quad (8)$$

$$\delta_j^2 = \frac{1}{N-1} \sum_{i=1}^N (x_{ij} - \hat{x}_j)^2 \quad (9)$$

In the above equation, $i = 1, 2, \dots, N$; $j = 1, 2, \dots, m$, and Z_{ij} in the above equation are the data after the normalization process. The standardization formula is shown in Equation (10).

$$y'_i = \frac{q(y_i - y_{min} + b)}{(y_{max} - y_{min} + b)} \quad (10)$$

Where: y_i is the output database sample data information; y'_i is the normalized database sample big data; y_{max} and y_{min} is the extreme and extreme small values of the output database sample big data; where $0 < q < 3$; $0 < b < 2$.

In the validation of clustering analysis algorithms, F-measure can be chosen as the evaluation criterion for determination, and here, two parameters, accuracy and recall, are cited. Accuracy and recall are able to evaluate the accuracy rate of clustering classification algorithms and are calculated as follows:

The accuracy rate is calculated as follows:

$$precision(i, j) = \frac{n_{ij}}{n_j} \quad (11)$$

Recall rate calculation formula.:

$$recall(i, j) = \frac{n_{ij}}{n_i} \quad (12)$$

Solve to obtain the value of F:

$$FI = \sum_i \frac{n_i}{n} \max\{F(i, j)\} \quad (13)$$

Through the above-mentioned calculation process, the data mining algorithm can make the weights and thresholds in the neural network gradually adjusted to gradually approximate the results precisely needed for the test system, and timely discover all kinds of data information in the use of the intelligent sports platform. The data mining computing service is a platform service that strips the business logic from the computing application and provides the platform support service required by the business logic to the developer. Corresponding to the node part of the application, it provides data input adaptation and data pre-processing services, the processing node part provides streaming data analysis, complex event processing and business rule processing services, and the output node part provides data output adaptation services. Combining the above algorithms, the SCS model is proposed. Developers can define a streaming computing application that can run on the streaming computing service system based on the elements of the SCS model.

6. PLATFORM CONSTRUCTION ANALYSIS

6.1. TEST ENVIRONMENT AND METHODOLOGY

The construction of smart sports platform meets the practical needs and greatly improves the level of informationization of sports. In particular, universities should reasonably build a platform under the framework of smart sports based on machine learning model technology. In order to better build this platform, we should effectively share the standardized data, create a "one-stop" service platform, do a good job of data statistics and analysis, and provide a solid and reliable basis for decision-making.

After the above machine learning model algorithm, this part uses the Storm application execution entity to test the dynamic adjustment of parallelism, and then verifies the feasibility and effectiveness of the streaming SCS definition tool and SCS execution engine by application examples.

In the test of Storm application execution entity parallelism dynamic adjustment algorithm, there are four virtual machines in the test cluster. One of them is used as a Nimbus node and Zookeeper is installed on the Nimbus node, while the other three are used as Supervisor nodes. All four virtual machines are installed with Ubuntu 12.04 OS, Open JDK 64-bit 1.8.0_45, Storm version 0.94, and Zookeeper version 3.4.7.

The test environment for the dynamic tuning of the Storm application execution entity parallelism is shown in Table 1:

Table 1. Application execution entity parallelism dynamic test environment table

| Name/IP | CPU/Memory/Disk | Use |
|-----------------------|---|------------------------|
| Dclab-1/192.168.1.252 | Intel(R) Xeon(R) CPU E5-2660 0 @ 2.20GHz / 3.6GB/42G | Storm clouds zookeeper |
| Dclab-2/192.168.1.254 | Intel(R) Xeon(R) CPU E5-2660 0 @ 2.20GHz / 3.6GB/42G | Tutor |
| Dclab-3/192.168.1.238 | Intel(R) Xeon(R) CPU E5-2660 0 @ 2.20GHz / 3.6GB/42G | Tutor |
| Dclab-4/192.168.1.242 | Intel(R) Xeon(R) CPU E5-2660 0 : @ 2.20GHz / 3.65GB/42.2G | Tutor |

The first step is to verify that the Parallelism Dynamic Adjustment module can dynamically adjust the parallelism ratio between components with sequential order according to the component execution events, and the second step is to verify that the Parallelism Dynamic Adjustment module can optimize resource utilization by dynamically adjusting the parallelism of each component. In our experiments, we set the statistical interval of Storm to 5 seconds, set the topology builtin. metrics.bucket size secs item in the configuration file of Storm.yaml as follows, set the high threshold to 92%, the low threshold to 32%, and the count period to 10. For the test of dynamic adjustment of entity parallelism of the Storm application execution, we validate it by three different applications General1, General2 and General3, which all correspond to a Topology containing three nodes, i.e., one Spout and two Bolt nodes. The structure diagram is shown in Fig.



Figure 5. Test application architecture diagram

The code logic for each of the three test applications is as follows:

In General1:Hibernate for 1 second in the execute method of Bolt1, hibernate for 1 second in the execute method of Bolt2, and set the initial parallelism of Spout, Bolt1, and Bolt2 to 1; In General2:Hibernate 1 second in the execute method of Bolt1, hibernate 3 seconds in the execute method of Bolt2, and set the initial parallelism of

Spout, Bolt1, and Bolt2 to 1; General3:Hibernate for 3 seconds in the execute method of Bolt1, hibernate for 1 second in the execute method of Bolt2, set the initial parallelism of Spout to 1, and set the initial parallelism of Bolt1 and Bolt2 to 3. Submit each of the above three Topologies to Storm for execution.

6.2. SYSTEM PERFORMANCE

In order to test the optimization of the parallelism dynamic adjustment module on the use of system resources, we changed the Storm cluster to a single machine for testing, and then we sampled the system information in 12 time periods. The first 6 sampling points Jmeter opened 2000 threads, and the last 6 sampling points Jmeter opened 500 threads to send data. Then we record the CPU usage and memory usage of the system at each of these 12 sampling points. First, we run Storm on the machine without the parallelism dynamic adjustment module to sample the machine usage, and then replace Storm with Storm with the parallelism dynamic adjustment module and run it under the same conditions as before.

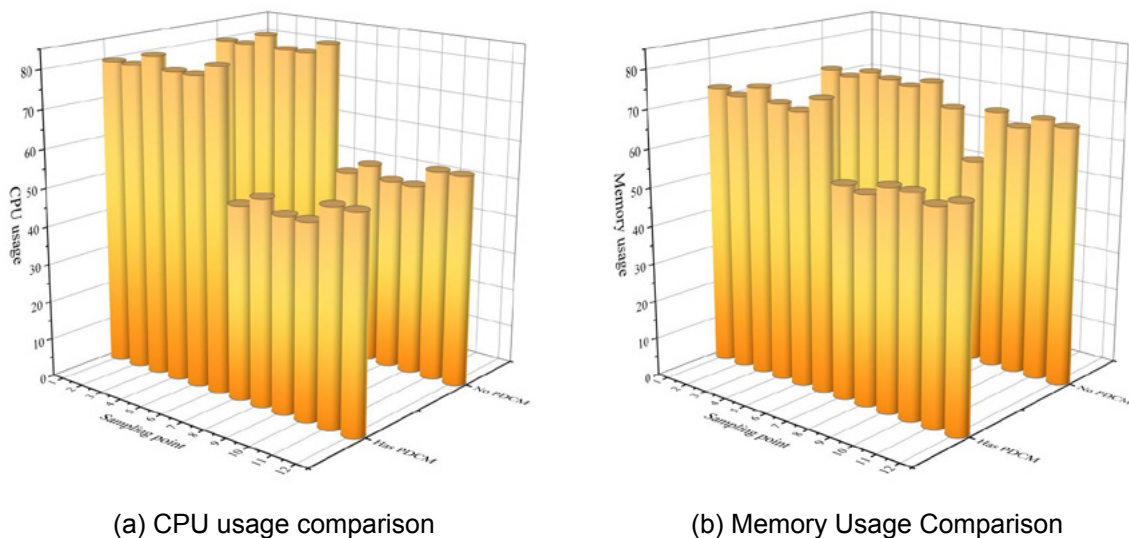


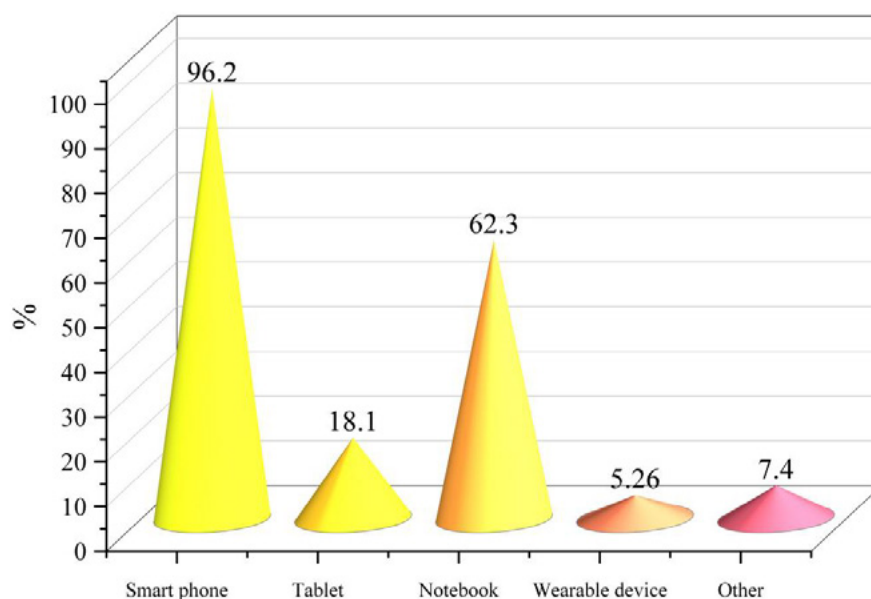
Figure 6. Usage Comparison Chart

As shown in Figure 6, in General1, the processing time of two Bolts is the same, so the parallelism ratio should be the same; in General2, the processing time of Bolt1 is one-third of the processing time of Bolt2, and the parallelism ratio should be roughly 1:3; in General3, the processing time of Bolt1 is three times of the processing time of Bolt2, and the parallelism ratio should be roughly 3:1. According to the change of the number of Executors in the three applications in the figure: General1 remains the same, and the ratio is still 1:1; General2 increases by two, presumably because the parallelism of Bolt2 increases from 1 to 3, and the ratio is 1:3; General3 decreases by two, presumably because the parallelism of Bolt2 decreases from 3 to 1, and the ratio is 3:1. That is, the parallelism between execution entities with sequential relationship is dynamically adjusted according to the processing time proportionality. The parallelism of execution entities is dynamically adjusted in the actual execution process. By introducing the parallelism dynamic adjustment module (PDCM), the CPU

usage and memory usage of the system increase (<2%) but not very significantly, but when the real-time data volume is small, the parallelism dynamic adjustment module can release the free memory resources (8%-11%) by stopping the idle Executor. Through the smart sports platform route, on the one hand, users can independently choose their favorite sports for physical exercise, which improves their motivation to exercise independently; on the other hand, it facilitates the update of the sports platform content.

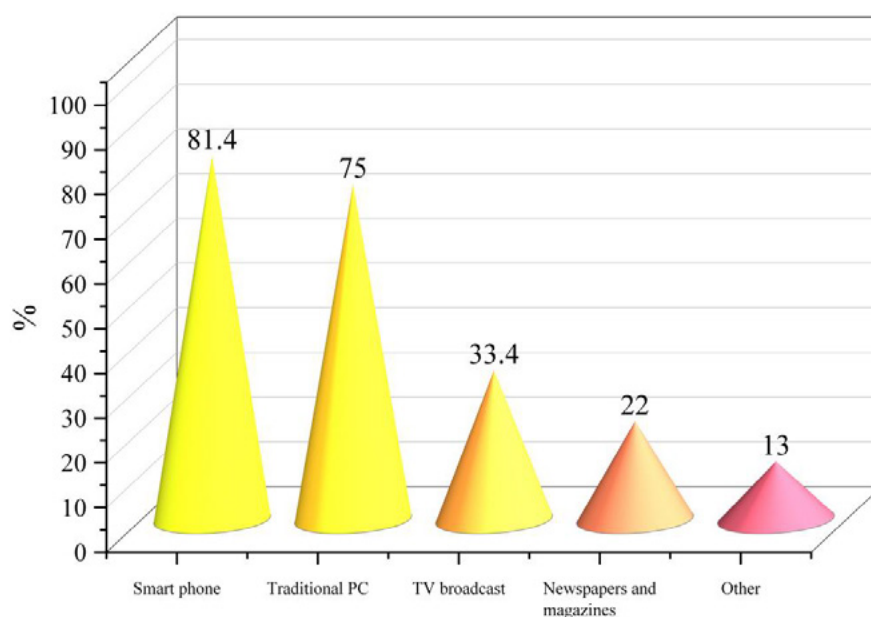
6.3. SURVEY RESULTS

Through the construction of a smart sports platform, students are used as experimental subjects in order to fully test the performance of the built platform. The issue of individualization and differences of students is emphasized by giving students the right to choose their own courses. At the same time, through the university's smart sports platform, teachers can make timely adjustments to their teaching programs and teaching plans to facilitate the completion of teaching tasks and teaching objectives.



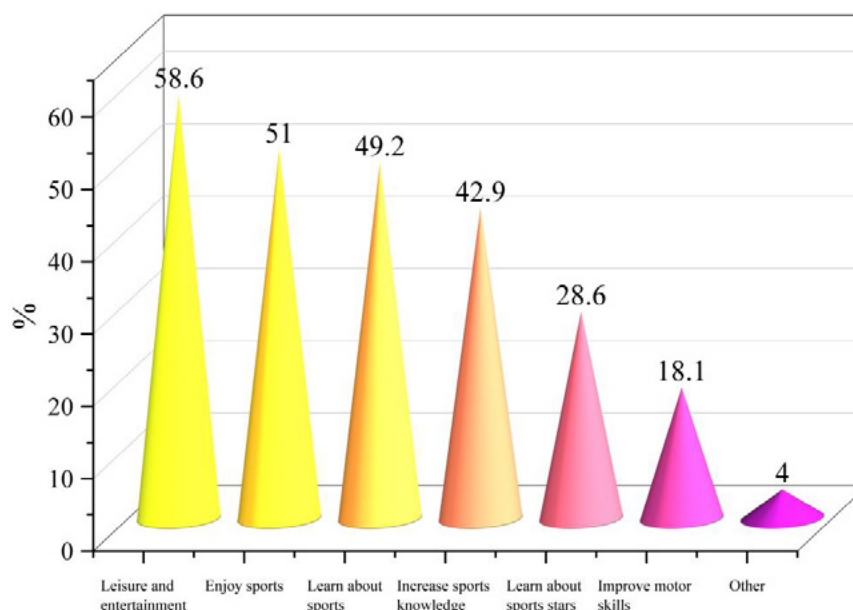
Statistical analysis of mobile terminal devices owned by college students

(a) Statistical analysis of college students' ownership of mobile mobile terminal devices



A survey of college students' access to sports information

(b) Survey on college students' access to sports information



The purpose of college students' attention to sports information

(c) Survey on the purpose of college students' attention to sports information

Figure 7. College students' access to and purpose of sports information survey analysis chart

From Figure 7(a), it can be seen that among the mobile terminal devices owned by college students, smart phones rank first, with almost one smart phone per person, while the proportion of students who own laptops also reaches 62.30%. It can be seen that the Internet access by smart mobile terminals has become one of the main

lifestyles of college students at present. From Fig. 7(b), it can be seen that through building the intelligent sports platform in colleges and universities, the way of college students getting information has changed dramatically, from traditional reading books and watching TV programs to getting information through intelligent mobile terminals. From Fig. 7(c), it can be seen that leisure and entertainment is the main purpose for college students to pay attention to sports information, accounting for 58.6%, and enjoying sports competition is another main purpose for college students to pay attention to sports information, accounting for 51.00%; another more important reason is to understand sports news, accounting for 49.2%. Thus, it can be seen that through building a smart sports platform, college students start to become concerned about sports information.

7. CONCLUSION

The emergence of smart sports to better provide convenient services for participants. With a mobile client such as a smartphone or sports watch, people can get reasonable sports advice anytime and anywhere. The smart sports platform changes the way users exercise, and through interaction users can get more reasonable and standardized exercise intensity and exercise combinations by inputting their physical conditions and exercise patterns. In this paper, students are taken as the experimental subjects, and according to the platform statistics it is known that sports competition is the focus of college students' attention to sports information, with a percentage of 51.00%. The percentage of understanding sports dynamics is 49.2%. Let more students understand the fun of physical education and physical exercise through the smart sports platform under the machine learning model, and also let teachers inspire more teaching inspiration through the platform and generate good teaching interaction with students. Therefore, carrying out research on the overall architecture and key technologies of smart sports, and seeking to translate and apply its results in the fields of competitive sports and national fitness will certainly play an important and positive role in the development of sports.

DATA AVAILABILITY

The data used to support the findings of this study are available from the corresponding author upon request.

CONFLICT OF INTEREST

The authors declare that the research was conducted in the absence of any commercial or financial relationships that could be construed as a potential conflict of interest.

REFERENCES

- (1) Wei, Y., Pan, D., Taleb, T., Han, Z., & Chen, X. (2016). **An unlicensed taxi identification model based on big data analysis**. *IEEE Transactions on Intelligent Transportation Systems*, 17(6), 1703-1713.
- (2) R. A. de Assis, R. Pazim, M. C. Malavazi, P. P. da C. Petry, L. M. E. de Assis and E. Venturino (2020). **A Mathematical Model to describe the herd behaviour considering group defense**. *Applied Mathematics and Nonlinear Sciences*, 5(1), 11-24. <https://doi.org/10.2478/amns.2020.1.00002>
- (3) Nallaperuma, D., Nawaratne, R., Bandaragoda, T., Singh, A. K., & Yang, B. (2019). **Online incremental machine learning platform for big data-driven smart traffic management**. *IEEE Transactions on Intelligent Transportation Systems*, PP(99), 1-12.
- (4) Jinxiang Xue. (2022). **Design of language assisted learning model and online learning system under the background of artificial intelligence**. *Applied Mathematics and Nonlinear Sciences*, (aop). <https://doi.org/10.2478/amns.2022.1.00027>
- (5) Mora-Sanchez, O. B., Lopez-Neri, E., Cedillo-Elias, E. J., & Rodriguez-Molano, J. I. (2020). **Validation of IoT infrastructure for the construction of smart cities solutions on living lab platform**. *IEEE Transactions on Engineering Management*, PP(99), 1-10.
- (6) Yukong Zhang, Hongwei Li and John D. Clark (2020). **Experimental simulation of mathematical learning process based on 'chunk-objective'**. *Applied Mathematics and Nonlinear Sciences*, 5(2), 425-434. <https://doi.org/10.2478/amns.2020.2.00061>
- (7) Xiang, Y., Tian, X., Zhou, S., & Li, Y. (2020). **Construction and application of digital creative platform for digital creative industry based on smart city concept**. *Computers & Electrical Engineering*, 87, 106748.
- (8) Liu, Y. (2022). **Analysis of government public management information service and computer model construction based on smart city construction**. *Mathematical Problems in Engineering*, 2022.
- (9) Yilin Fan, Zheng Huo and Yaxin Huang (2022). **Fed-UserPro: A user profile construction method based on federated learning**. *Applied Mathematics and Nonlinear Sciences*, (aop). <https://doi.org/10.2478/amns.2021.2.00188>
- (10) Su, L. X., Lyu, P. H., Yang, Z., Li, Y., & Cai, J. (2015). **Scientometric cognitive and evaluation on smart city related construction and building journals data**. *Scientometrics*.
- (11) Kang, J., & Wang, X. (2020). **The organizational structure and operational logic of an urban smart governance information platform: Discussion on the background of urban governance transformation in China**. *Complexity*, 2020.
- (12) Hui Jia, Islam Nassar and Sarp Erkir (2022). **English Learning Motivation of College Students Based on probability Distribution**. *Applied Mathematics and Nonlinear Sciences*, (aop). <https://doi.org/10.2478/amns.2022.2.0127>
- (13) Mora-Sanchez, O. B., Lopez-Neri, E., Cedillo-Elias, E. J., et al. (2020). **Validation of IoT Infrastructure for the Construction of Smart Cities Solutions on Living Lab Platform**. *IEEE Transactions on Engineering Management*, PP(99), 1-10.

- (14) Cho, O. (n.d.). **Impact of Physical Education on Changes in Students' Emotional Competence: A Meta-analysis.** *International Journal of Sports Medicine*.
- (15) Chen, C., Peng, X., Li, Y., et al. (2021). **Smart city community governance based on blockchain big data platform.** *Journal of Intelligent and Fuzzy Systems*, 2021(2), 1-7.
- (16) Xiang, Y., Tian, X., Zhou, S., et al. (2020). **Construction and application of digital creative platform for digital creative industry based on smart city concept.** *Computers & Electrical Engineering*, 87, 106748.
- (17) Pal, A., & Hsieh, S. H. (2021). **Deep-learning-based visual data analytics for smart construction management.** *Automation in Construction*, 131(November 2020), 103892.
- (18) Machado, V. R., & Saldanha, M. (2015). **The impact of sports mega-events on health and environmental rights in the city of Rio de Janeiro, Brazil.** *Cadernos De Saude Publica*, 31 Suppl 1(suppl 1), 39-50.
- (19) Escamilla-Fajardo, P., Alguacil, M., & García-Pascual, F. (2021). **Business model adaptation in Spanish sports clubs according to the perceived context impact on the social cause performance.** *Sustainability*, 13.
- (20) Kaga, H. (2016). **Positive Research on the Developmental process of Modern Sports in Japan: on the Militarization of Meiji Jingu Athletic Meeting.** *Computers & Geosciences*, 91(194), 405-9.
- (21) Zhuang, H., Zhang, J., Sivaparthipan, C. B., et al. (2020). **Sustainable Smart City Building Construction Methods.** *Sustainability*, 12.
- (22) Guan, S. (2020). **Smart E-commerce logistics construction model based on big data analytics.** *Journal of Intelligent and Fuzzy Systems*, 40(2), 1-9.
- (23) Li, W. (2019). **Research on Intelligent Urban Management Information System Framework Based on Big Data.**
- (24) Ma, Q., & Yang, Y. (2021). **Research on the Construction of Smart Cities by the Big Data Platform of the Blockchain.** *Journal of Physics: Conference Series*, 1883(1), 012144 (6pp).
- (25) Zhao, Z., & Zhang, Y. (2020). **Impact of Smart City Planning and Construction on Economic and Social Benefits Based on Big Data Analysis.** *Complexity*, 2020(4), 1-11.
- (26) Horani, M. O., Najeeb, M., & Saeed, A. (2021). **Model electric car with wireless charging using solar energy.** *3C Tecnología. Glosas de innovación aplicadas a la pyme*, 10(4), 89-101. <https://doi.org/10.17993/3ctecno/2021.v10n4e40.89-101>
- (27) Chen, S., & Ren, Y. (2021). **Small amplitude periodic solution of Hopf Bifurcation Theorem for fractional differential equations of balance point in group competitive martial arts.** *Applied Mathematics and Nonlinear Sciences*, 7(1), 207-214. <https://doi.org/10.2478/AMNS.2021.2.00152>

/13/

RECONSTRUCTION OF PHYSICAL DANCE TEACHING CONTENT AND MOVEMENT RECOGNITION BASED ON A MACHINE LEARNING MODEL

Lei Li

Football College, Wuhan Sports University, Wuhan, Hubei, 430079, China

Tingting Yang*

School of Journalism and Communication, Wuhan Sports University, Wuhan,
Hubei, 430079, China

ytt342784081@163.com



Reception: 14/11/2022 **Acceptance:** 17/01/2023 **Publication:** 05/03/2023

Suggested citation:

L., Lei and Y., Tingting (2023). **Reconstruction of physical dance teaching content and movement recognition based on a machine learning model.** *3C TIC. Cuadernos de desarrollo aplicados a las TIC*, 12(1), 267-285. <https://doi.org/10.17993/3ctic.2023.121.267-285>

ABSTRACT

With the technological development of movement recognition based on machine learning model algorithms, the content and movements for physical dance teaching are also seeking changes and innovations. In this paper, a set of three-dimensional convolutional neural network recognition algorithms based on a machine learning model is constructed through the collection to recognition of sports dance movement data. By collecting the skeleton information of typical movements of physical dance, a typical movement dataset of physical dance is constructed, which is recognized by the improved 3D convolutional neural network recognition algorithm under the machine learning model, and the method is validated on the public dataset. The experimental results show that the 3D CNNs in this paper can produce relatively satisfactory results for sports dance action recognition with high accuracy of action recognition, which verifies the feasibility of the 3D convolutional neural network action recognition algorithm under the machine learning model for the acquisition to recognition of sports dance actions. It illustrates that the future can be better to open a new direction of physical dance education content through machine learning models in this form.

KEYWORDS

machine learning model; sports dance movements; DDPG algorithm model; 3D convolutional neural network movement recognition algorithm; movement skeleton information dataset

PAPER INDEX

ABSTRACT

KEYWORDS

1. INTRODUCTION

2. MACHINE LEARNING MODELS

2.1. The DDPG algorithm model used for machine learning

2.2. Observed and rewarded values of machine learning model algorithms

2.3. THREE-DIMENSIONAL CONVOLUTIONAL NEURAL NETWORK

3. METHODS OF RECONSTRUCTING THE CONTENT AND MOVEMENT IDENTIFICATION OF PHYSICAL DANCE TEACHING

3.1. Physical dance movement data pre-processing

3.2. Experimental data analysis methods

4. EXPERIMENTAL RESULTS AND ANALYSIS

5. CONCLUSION

DATA AVAILABILITY

CONFLICT OF INTEREST

REFERENCES

1. INTRODUCTION

With the boom of artificial intelligence, academics have begun to explore the research use of machine learning models in various fields in the hope of reducing human costs and improving output efficiency through these techniques [1-2]. In the era of big data, machine learning models that can model relevant variables with complex relationships will surely become the mainstream of scientific research in the future [3]. Machine learning models are a top science and technology that specializes in how computers can simulate or implement human learning behaviors [4]. Machine learning models are trained to acquire new knowledge or skills and reorganize the existing knowledge structure to continuously improve their performance [5]. With the advent of the third wave of artificial intelligence, machine learning models, which are the core of artificial intelligence, have started to appear frequently in the limelight [6]. Machine learning models are models that make predictions about unknown data based on known data [7]. Machine learning models usually divide the original data set into a training set and a test set. The data are then fitted and optimized several times in the training set to build the model that best reflects the characteristics of the data, and finally, the performance of the model is evaluated in the test set to verify the generalization ability and reliability of the model [8-11].

In recent years, machine learning models have been applied to various fields with remarkable results and their predictive reliability has been widely recognized by researchers. In the literature [12], two sets of classification models were developed to predict students' academic performance at graduation using individual course grades and GPA, respectively. Logistic regression, random forest and plain Bayesian algorithms in machine learning were used to build prediction models for academic performance. The literature [13-14] proposed that when machine learning models were used to predict students' academic performance, the prediction of students' academic performance was more accurate when combining multiple factors compared to a single factor. The literature [15] used machine learning methods to predict changes in major depressive and generalized anxiety disorder symptoms from pre-treatment to 9-month follow-up. The literature [16] revealed the relationship between Internet use behaviors and academic performance and used machine learning models to predict the academic performance of college students with these behavioral data. The literature [17] studied a review of different machine learning algorithms and their application in cardiovascular diseases and found that the application of machine learning can increase the understanding of different types of heart failure and congenital heart disease. The literature [18] proposed a multidimensional approach based on GPS measurements and machine learning to predict injuries in professional soccer. It also provided a simple and practical method to assess and interpret the complex relationship between sports injury risk and training performance in professional soccer. The literature [19] analyzed how to predict and prevent financial losses through public news and historical prices in the Brazilian stock market through a machine learning model. The literature [20] uses Recurrent Neural Networks (RNN) for stock market forecasting. RNN is a machine learning model dedicated to time series, which can take into account past correlation

series when predicting future trends, and the authors introduced the model to the analysis of financial time series and tested it on the Nikkei index, proving the usefulness of the approach. The literature [21] uses oil price movements, gold and silver price movements, and foreign exchange movements as features to demonstrate that the KSE-100 index can be predicted by machine learning algorithms and that the multilayer perceptron outperforms the other algorithms among the machine learning algorithms used. The literature [22] applied machine learning algorithms such as deep learning, random forests, neural networks, and support vector regression machines to stock index prediction in the UK stock market and found that deep learning gave the best prediction results and support vector machines gave the second best results. The literature [23] used the XGBoost algorithm for stock index futures forecasting and compared it with LSTM and traditional autoregressive time series processing methods, and the empirical results showed that the XGBoost algorithm was superior in determining the ups and downs. Research on dance moves also abounds, and the literature [24] proposes a modern deep architecture for C3D that can learn on large-scale datasets. And the C3D method based on linear classifiers outperforms or approaches the current state-of-the-art methods in both recognition accuracy of action videos. The literature [25] uses convolutional neural networks (CNNs) for the classification of Indian classical dance movements. Two hundred dance poses and gestures were collected from online videos and offline recordings, respectively, and the experiments were compared with the results of other classification algorithms on the same dataset, finally obtaining a recognition rate of 93.33%. In [26], six Greek folk dance movements were collected using a Kinect sensor, and four common classifiers were used to directly classify the movements on the raw data to compare the classification results, and the effect of different body joints on the recognition rate was also investigated. The literature [27] studied motion data acquisition devices, among which the Kinect depth vision sensor device has the advantages of high depth map resolution, low cost, and the ability to directly track the human skeleton motion trajectory.

In this paper, the typical movement dataset of sports dance was constructed by collecting the skeleton information of the typical movement of sports dance. This dataset was identified using a 3D convolutional neural network recognition algorithm based on a machine learning model, and the original data recorded in this dataset was checked for missing skeleton point data. In the case that the skeleton point data was lost in the experiment and could not be recorded, the missing skeleton point data of a frame was filled with the skeleton data of the previous frame to reduce the influence of the subsequent machine learning model on the judgment of different movements. The frame rate of the few skeletal sequences of typical sports dance movements obtained is 30 fps. The duration of each movement in the dataset is different, and the corresponding number of frames is also different. The sequence length of each movement sequence in the dataset is unified, and the maximum number of frames of the samples in the dataset is obtained. The remaining movement samples with less than the maximum number of frames are copied to the last frame and supplemented to the maximum number of frames for subsequent input into the machine learning model for training Learning. After the dataset is completed, it is input

into the machine learning model, and the 3D convolutional neural network recognition algorithm is used to train the dataset. The experimental results show that the 3D CNNs in this paper have greater recognition advantages and accuracy compared with several other action recognition algorithms, which can help the innovative development of physical dance teaching contents and also make another perspective of physical dance teaching methods. It is verified that the 3D convolutional neural network action recognition algorithm under the machine learning model is feasible in the acquisition to recognition of physical dance actions, which can better open a new direction of physical dance education content through this form of machine learning model and provide an optional path for the reconstruction of physical dance teaching content and action recognition.

2. MACHINE LEARNING MODELS

With the development of information technology, intelligent algorithms represented by reinforcement learning are increasingly used in the field of robot control with their adaptive characteristics. In recent years, DQN algorithms combining deep neural networks and reinforcement learning have been proposed to solve the problem of high-dimensional input to machine learning models. However, DQN is still an algorithm oriented to discrete control and has insufficient capacity to handle continuous actions. In the practical control of machine learning models, the angular output of each joint is a continuous value, and if the range of values taken for each joint angle is discretized, the number of behaviors grows exponentially with the number of degrees of freedom. If this accuracy is further improved, the number of values taken will grow exponentially [28-29].

2.1. THE DDPG ALGORITHM MODEL USED FOR MACHINE LEARNING

DDPG is an Actor-Critic based algorithm in reinforcement learning, the core idea of which is to use the Actor-network to generate the behavior policy of the intelligence, and the Critic network to judge the good and bad actions and guide the updated direction of the actions.

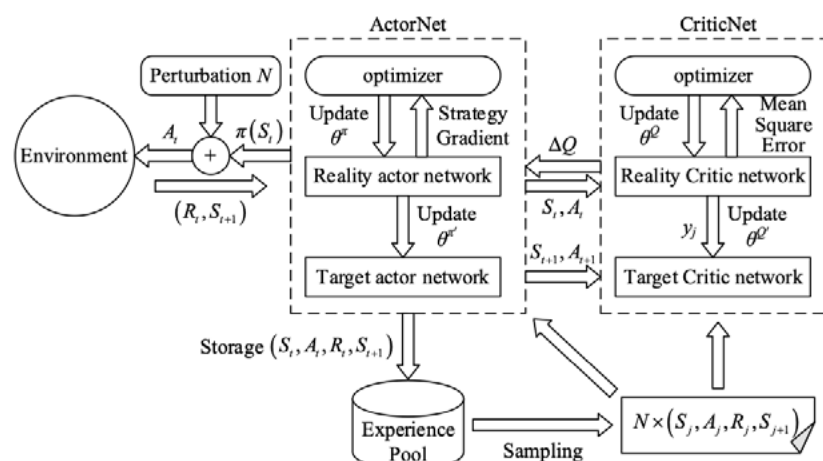


Figure 1. DDPG algorithm structure

As shown in Figure 1, the DDPG algorithm structure contains an Actor-network with parameters and a Critic network with a parameter to compute the deterministic policy and action-value function, respectively. Since the learning process of a single network is not stable, the Actor-network and the Critic network are subdivided into a realistic network and a target network, respectively, drawing on the successful experience of DQN fixed target networks. The Actor-network and the Critic network are each subdivided into a realistic network and a target network. The real network and the target network have the same structure, and the target network parameters are softly updated by the real network parameters with a certain frequency.

The loss function of the realistic Critic network is:

$$J(\theta^Q) = \frac{1}{m} \sum_{j=1}^m \omega^j (y^j - Q(S_t^j, A_t^j, \theta^Q))^2 \quad (1)$$

Among them:

$$y^j = \begin{cases} R^j, end^j \\ R^j + \gamma Q(S_{t+1}^j, A_{t+1}^j, \theta^Q), not\ end^j \end{cases} \quad (2)$$

m is the number of samples, ω^j is the weight of the different samples used, $Q(S_t^j, A_t^j, \theta^Q)$ is the action value calculated by the realistic Critic network when sample j takes action A_t at the state S_t , y^j is the target action value calculated by the samples and derived from the target Critic network, R^j is the immediate reward obtained by sample j for taking action A_t at the state S_t , and γ is the discount factor.

The loss function of a realistic Actor network is :

$$J(\theta^\pi) = \frac{1}{m} \sum_{j=1}^m Q(S_t^j, A_t^j, \theta^Q) \quad (3)$$

Which, finding the minimal value of this loss function $J(\theta^\pi)$ by the gradient descent method is equivalent to the process of maximizing the action value $Q(S_t^j, A_t^j, \theta^Q)$.

The target Critic network and target Actor network parameters are updated in the following way:

$$\theta^{Q'} \leftarrow \tau \theta^Q + (1 - \tau) \theta^{Q'} \quad (4)$$

$$\theta^{\pi'} \leftarrow \tau \theta^\pi + (1 - \tau) \theta^{\pi'} \quad (5)$$

τ is the update coefficient, and the range is 0.01~0.1 to avoid excessive parameter changes.

When a machine learning model has a high degree of freedom, an additional class of exploration strategy, maximum a posteriori policy optimization, is needed to enhance the efficiency of the machine learning model based on the use of the DDPG algorithm model. The maximum a posteriori policy optimization approach models the reinforcement learning problem as an inference problem from a probabilistic point of

view. Assuming the probability of completing the task, the probability, according to the inference problem, is:

$$\begin{aligned}\log p_{\pi}(O=1) &= \log \int p_{\pi}(\tau) p(O=1|\tau) d\tau \\ &\geq \int q(\tau) \left[\log p(O=1|\tau) + \log \frac{p_{\pi}(\tau)}{q(\tau)} \right] d\tau\end{aligned}\quad (6)$$

Let the loss function :

$$J(q, \pi) = E_q \left[\sum_t r_t / a \right] - KL(q(\tau) \| p_{\pi}(\tau)) \quad (7)$$

where: $q(\tau)$ is the proposed distribution. the optimization problem can be solved by the EM method, and the optimal proposed distribution $q(\tau)$ is obtained in step E. The non-parametric optimization solution in this step is:

$$q_i(a|s) \propto \pi(a|s, \theta_i) \exp\left(\frac{Q_{\theta_i}(s, a)}{\eta^*}\right) \quad (8)$$

where the optimal temperature term η^* can be optimized according to equation (9):

$$g(\eta) = \eta \varepsilon + \eta \int \mu(s) \log \int \pi(a|s, \theta_i) \exp\left(\frac{Q_{\theta_i}(s, a)}{\eta}\right) da ds \quad (9)$$

In the M-step, the optimal proposal distribution is used to update the neural network strategy:

$$\max_{\theta} J(q_i, \theta) = \max_{\theta} E_{\mu_q(s)} [E_{q(a|s)} [\log \pi(a|s, \theta)]] + \log p(\theta) \quad (10)$$

2.2. OBSERVED AND REWARDED VALUES OF MACHINE LEARNING MODEL ALGORITHMS

To give full play to the performance advantages of the DDPG algorithm, this paper takes into account the motion state of the machine learning model, the processing efficiency of the intelligent body, the environment and other factors, and selects some observations as shown in Table 1.

Table 1. Learning process observations

| Parameter | Symbol |
|-----------------------------------|--|
| Machine learning model location | $[x, y, z]$ |
| Machine learning model pose angle | $[roll, pitch, yaw]$ |
| Machine learning model speed | $[v_x, v_y, v_z]$ |
| Contact force | $[F_{N_l}, F_{N_r}]$ |
| Joint torque output | $[t_{hip_l}, t_{hip_r}, t_{knee_l}, t_{knee_r}, t_{tire_l}, t_{tire_r}]$ |
| Last joint moment output | $[t'_{hip_l}, t'_{hip_r}, t'_{knee_l}, t'_{knee_r}, t'_{tire_l}, t'_{tire_r}]$ |

and the following weighted reward values r are designed based on the observed values, where $k_1 \sim k_9$ are the weights.

(1) The speed reward value r_v , which is to encourage the machine learning model to move forward, is shown in equation (11):

$$r_v = k_1 \cdot v_x \quad (11)$$

where: v_x is the velocity of the machine learning model on the x axis.

(2) The stability reward value r_s , lies in rewarding the machine learning model for completing smooth motions in both instantaneous and global decisions, as shown in equation (12):

$$r_s = -(y - y_{init})^2 - k_3(z - z_{init})^2 - k_4 roll^2 - k_5 pitch^2 - k_6 yaw^2 \quad (12)$$

where: y, z denotes the current position of the machine learning model on the y, z axis, y_{init}, z_{init} denotes the position of the machine learning model on the y, z axes, $roll, pitch, rolll, pit yaw$ denote the attitude angle (roll angle, pitch angle, yaw angle) of the machine learning model.

(3) The joint stability bonus value r_3 , which lies in improving the energy utilization efficiency of the robot, is shown in equation (13):

$$r_{js} = -k_7 \sum_i (t'_i - t_i)^2 \quad (13)$$

where: t_i and t'_i represent the output of each joint torque and its torque output at the previous time.

(4) The value of touchdown reward r_F , lies in rewarding the machine learning model for controlling the same contact force between its own two feet and the ground, reducing the probability of training to generate singular motion poses, as shown in equation (14):

$$r_F = -k_8 (F_{N_l} - F_{N_r})^2 \quad (14)$$

where: F_{N_l}, F_{N_r} denotes the contact forces between the left and right feet of the machine learning model and the ground, respectively.

(5) The motion duration reward value r_c , lies in encouraging the machine learning model to keep moving, as shown in equation (15):

$$r_c = k_9 T \quad (15)$$

where T is a constant and takes any value.

2.3. THREE-DIMENSIONAL CONVOLUTIONAL NEURAL NETWORK

Compared with other traditional deep learning methods, 3D convolutional neural networks are not limited to the input of 2D single-frame images, and can better extract features from the temporal and spatial dimensions and extract motion information of

multiple consecutive frames after reinforcement learning algorithms by machine learning models.

The three-dimensional deep convolutional neural network used in this paper includes four convolutional layers, two downsampling layers, two fully connected layers and one Softmax classification layer, and the downsampling layer uses Max-pooling with a kernel size of $3 \times 3 \times 3$ and a step size of 1, as shown in Figure 2.

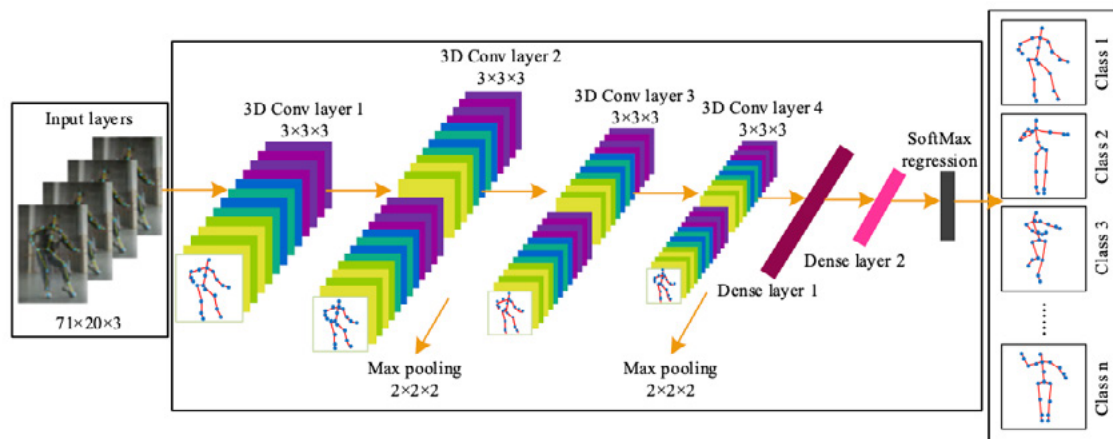


Figure 2. Three-dimensional convolutional neural network framework

To capture the sports dance movement information in multiple consecutive frames, the features are calculated from the spatial and temporal dimensions, the value of the cell with position coordinates (x, y, z) in the j th feature map of the i th layer is given by the following equation:

$$V_{ij}^{xyz} = f \left(b_{ij} + \sum_r \sum_{l=0}^{l_i-1} \sum_{m=0}^{m_i-1} \sum_{n=0}^{n_i-1} \omega_{ijr}^{lmn} v_{(i-1)r}^{(x+l)(y+m)(z+n)} \right) \quad (16)$$

The time dimension of the 3D convolution kernel is n_i , and the weight value of the convolution kernel connected to the r th feature map at position (l, m, n) is ω_{ijr}^{lmn} .

The ReLU function is the most commonly used activation function in deep machine learning models, which keeps the original feature value unchanged when the input feature value is greater than 0, and sets it to 0 when it is less than 0. This is the unilateral inhibition of the activation function, which allows the model parameters to become sparse and thus reduces the risk of overfitting to some extent. In addition, the derivative of the activation function is very simple to compute, which can speed up the computation to a certain extent, and the derivative is always 1 when the input is positive, so it can effectively alleviate the problem of gradient disappearance, the ReLU activation function is defined as:

$$f(x) = \max(0, x) = \begin{cases} 0, & (x \leq 0) \\ x, & (x > 0) \end{cases} \quad (17)$$

Pooling is also known as downsampling, where, unlike the processing of 2D images, the information of the video in the temporal dimension is taken into account;

by pooling, the feature map is reduced, the dimensionality of the data is reduced, and the number of calculations is reduced, making it easier to train and improve accuracy:

$$V_{x,y,z} = \max_{0 \leq i \leq s_1, 0 \leq j \leq s_2, 0 \leq k \leq s_3} (\mu_{x \times s + i, y \times t + j, z \times r + k}) \quad (18)$$

The Softmax function is often used in the last layer of a classification task to map an n-dimensional vector x to a probability distribution such that the probability of the correct category tends to 1 and the probability of the other categories tends to 0, and the sum of the probabilities of all categories is 1.

The Dropout strategy is to temporarily discard the neurons in the deep model from the network and disconnect them according to a certain probability when the model is trained so that the closed neurons do not participate in the calculation of forward propagation and the update of weights by the backward gradient. Therefore, Dropout can be considered as an integration method, i.e., averaging different model architectures over several iterations, thus significantly reducing the risk of overfitting.

3. METHODS OF RECONSTRUCTING THE CONTENT AND MOVEMENT IDENTIFICATION OF PHYSICAL DANCE TEACHING

At present, there are many action recognition methods based on deep learning, and the commonly used classical action recognition algorithms are the C3D algorithm, P3D ResNet algorithm, and ConvLSTM algorithm, and these algorithms have a good effect on action recognition. To realize the recognition of physical dance teaching content movements, this paper firstly constructs a physical dance movement dataset, which needs to record the skeleton information of dancers, using the skeleton information for recognition can be processed faster and reduce the storage space. Secondly, based on the machine learning model and 3D convolutional neural network, an improved model is proposed for the recognition of physical dance movements. In this paper, the Dropout technique is also used to reduce the overfitting phenomenon, and Dropout is experimentally compared by setting different ratios.

This experiment uses the 5-fold cross-validation method, in which the pre-processed sports dance typical movement dataset is randomly divided into 5 groups, of which 4 groups are used as the training set and 1 group is used as the test set, and then the results of 5 times are averaged as the recognition rate.

3.1. PHYSICAL DANCE MOVEMENT DATA PRE-PROCESSING

To reduce the impact of the subsequent machine learning model on the judgment of different movements, the missing skeletal data of a certain frame was filled with the skeletal data of the previous frame to check the missing skeletal data of the recorded raw data. To reduce the redundant information, only one frame out of every five frames of the original data was kept, and the maximum number of frames for each action in the dataset is shown in Table 2, The remaining action samples with less than

the maximum number of frames are copied to the last frame to be added to the maximum number of frames for subsequent input into the machine learning model for training and learning.

Table 2. Sports Dance Motion Dataset Motion Name and Maximum Number of Frames

| Dance type | Serial number | The action name | The maximum number of frames |
|--------------|---------------|------------------------------|------------------------------|
| Modern dance | 1 | Next to the T-step step | 62 |
| | 2 | Z-step | 37 |
| | 3 | Pendulum | 60 |
| | 4 | Side-click steps | 30 |
| | 5 | Single step | 33 |
| Waltz | 6 | Step back | 50 |
| | 7 | Lift the step | 40 |
| | 8 | One-handed one-handed step | 42 |
| | 9 | Single step | 36 |
| Tango | 10 | Cats wash their faces | 25 |
| | 11 | Alternate cover hands | 30 |
| | 12 | Flick your fingers | 35 |
| Latin dance | 13 | Flat step | 48 |
| | 14 | Drag | 31 |
| | 15 | Shrug | 40 |
| | 16 | Crankulated arms | 38 |
| Samba | 17 | High shake hands | 35 |
| | 18 | Alternate waving hands | 32 |
| | 19 | Wave your hands | 50 |
| | 20 | Draw circles with both hands | 24 |

3.2. EXPERIMENTAL DATA ANALYSIS METHODS

Using the test set in the dataset, the recognition results of each method for 20 typical sports dance movements are evaluated in terms of accuracy. the recognition results of the experiments using the 3D convolutional neural network recognition method under the machine learning model of this paper are calculated, which can clearly express the categories and numbers of correct and incorrect recognition of each movement, and then the recognition accuracy of three different types of recognition methods are calculated, namely, the UTKinect dataset, the MSRAction3D

dataset and the TYYDance dataset of this paper under the recognition algorithm. MSRAction3D dataset and the sports dance action TYYDance dataset of this paper are then calculated for the overall dance action recognition accuracy under the recognition algorithm, and finally, the method of this paper is compared with the classical algorithm, and the corresponding recognition results and conclusions are drawn.

4. EXPERIMENTAL RESULTS AND ANALYSIS

First, to alleviate the overfitting phenomenon, the Dropout technique was used, and the Dropout ratios were set to 0.2, 0.4, 0.5, 0.6, and 0.8 and the experiments were conducted on the dataset of this paper, and the results of the validation set are shown in Figure 3. After 50 iterations, the recognition accuracy of the Dropout ratio of 0.5 is slightly higher than that of the ratio of 0.4.

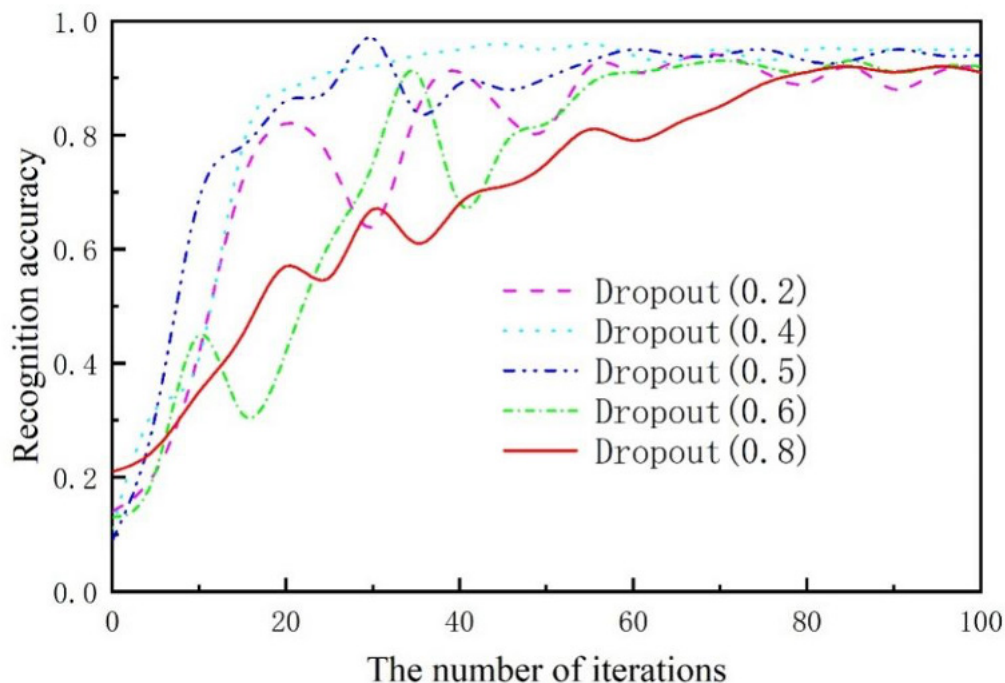


Figure 3. Experimental results of different Dropout ratios

To verify the effectiveness of the 3D convolutional neural network dance movement recognition method based on the machine learning model proposed in the text, experiments were conducted on the public dataset UTKinect dataset, MSRAction3D dataset and the sports dance movement TYYDance dataset of this paper. The UTKinect dataset contains 10 types of movements with 220 movement samples, the MSRAction3D dataset contains 20 types of movements with 540 movement samples, and the dance movement dataset in this paper contains 20 types of dance movements with 640 movement samples, The dance movement dataset in this paper contains 20 types of dance movements, with a total of 640 movement samples.

Figure 4 shows the recognition accuracy of the training set and Figure 5 shows the recognition accuracy of the test set. 82% recognition rate was obtained on the

UTKinect dataset, 90% recognition rate was obtained on the MSRActon3D dataset, and 96% recognition rate was obtained on the TYYDance dataset. The reasons for the better recognition results are as follows: (1) in the selection process of the typical movements of sports dance, the dance movements with relatively large differences in movements are selected; (2) more dance movements are collected.) more samples of movements were collected, and more deep learning data were obtained; (3) the collected dance movements had more duration than the general movements, and more movement representations were also obtained.

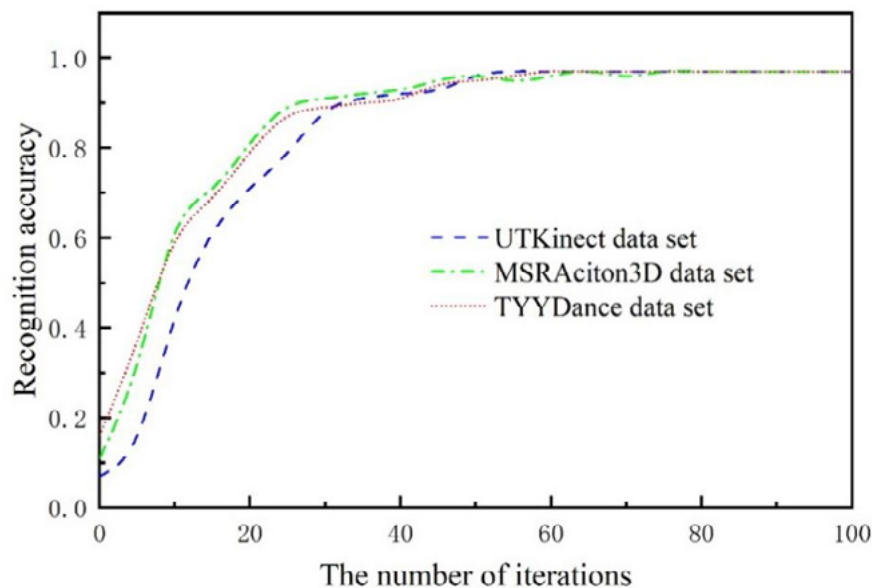


Figure 4. The training recognition rate of three data sets

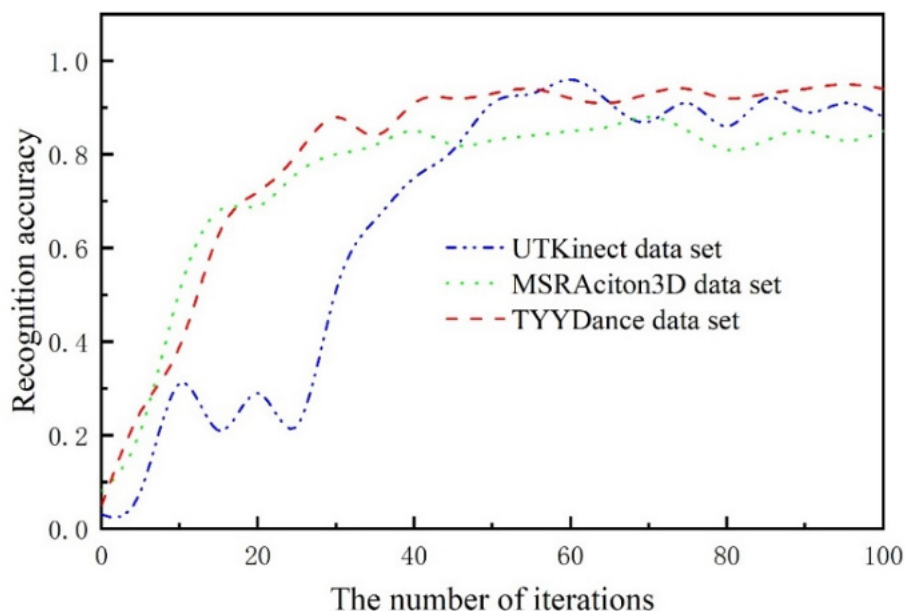


Figure 5. The test recognition rate of three data sets

In the experimental process, the 3D convolutional neural network action recognition algorithm under the machine learning model was trained on the training and validation sets of all subjects, and the loss function curves were obtained as shown in Figure 6.

In the figure, the vertical coordinate is the loss value, and the horizontal coordinate is the number of iterations; from Figure 6, we can see that after 45 iterations, the loss gradually stabilizes at about 0.016, which is the best training effect of the model.

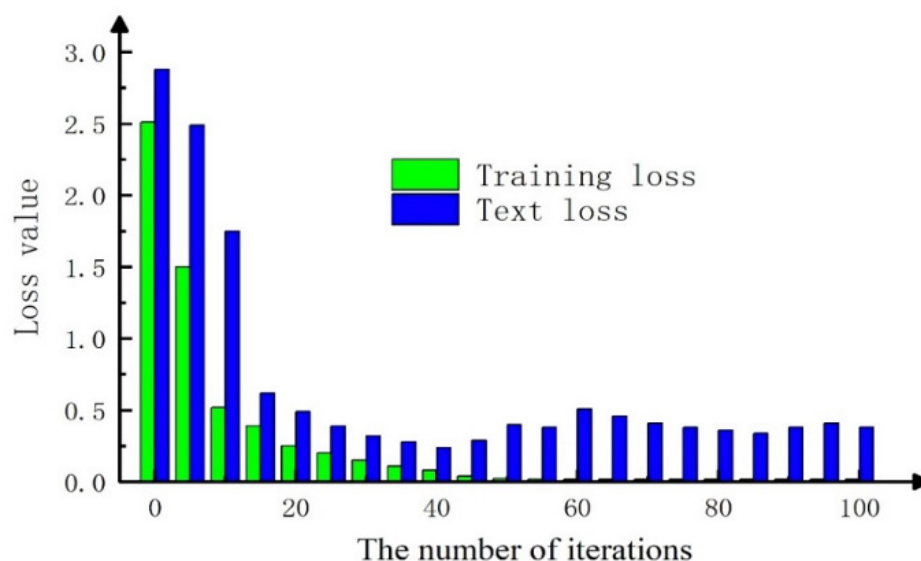


Figure 6. The loss function of the training set and test set

As shown in Figure 7, the graphs of the recognition accuracy functions of the training and validation sets are obtained experimentally. In the graph, the recognition rate of the training set reaches 99.74% after 45 iterations of model training, and then the curve remains stable, reaching the best recognition effect of the model.

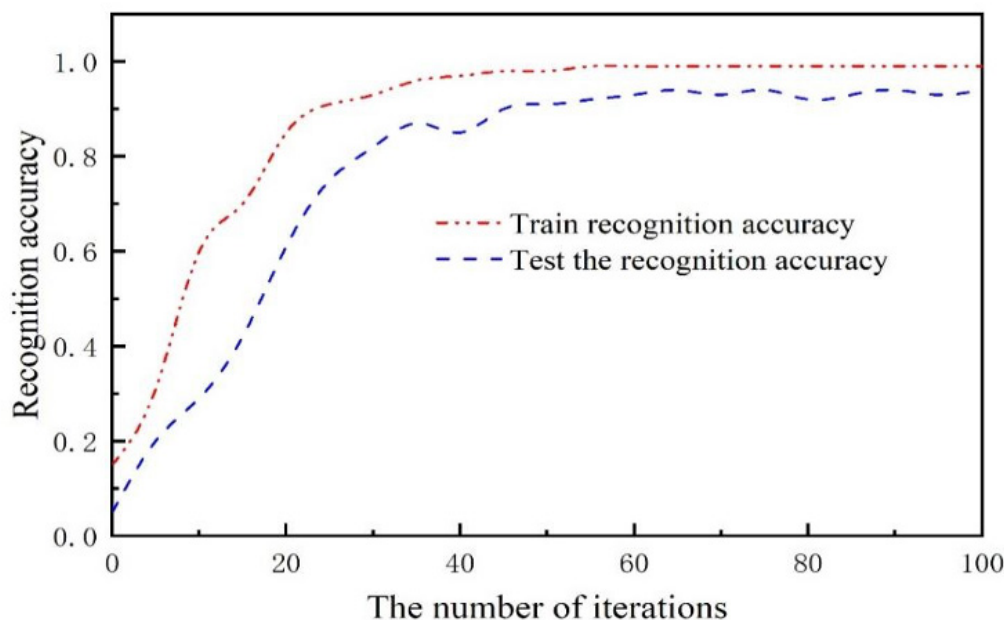


Figure 7. The loss function of the training set and test set

Other classical algorithms also use skeleton data input, and compared with the 3D convolutional neural network action recognition algorithm based on the machine learning model, the results are shown in Table 3, the model used in this paper has

higher recognition accuracy in the dataset of this paper, which is slightly higher than P3D, about 6% higher than ConvLSTM, and about 3.5% higher than C3D(1net).

Table 3. Compare results with other methods

| Methods | Recognition accuracy |
|---------------|----------------------|
| C3D(1 net) | 91.27% |
| P3D ResNet | 94.29% |
| ConvLSTM | 90.13% |
| 3D CNNs(ours) | 96.91% |

From the experimental results, we can see that using human skeleton information can occupy less storage space to obtain good recognition results, so each model has good recognition results in the dataset of this paper. Compared with the C3D recognition algorithm model, this paper follows the convolutional kernel small and large $3 \times 3 \times 3$, but there are 8 convolutional layers in C3D, and the data volume is too large for the data set in this paper, so this paper adjusts the number of layers and the number of convolutional kernels in the model to obtain better recognition results. This is one of the reasons why the skeleton information of sports dance movements is collected in this paper, and the good results obtained from the experiments in this paper validate the experimental movement collection, as well as the data pre-processing and the rationality of this data set.

5. CONCLUSION

Each kind of sports dance has its own unique culture and spirit, and dance is a way for human beings to use body language to express emotions and convey their feelings, which is a common language for human beings regardless of borders and race. In this paper, a complete process from dance movement data collection to movement recognition is realized, and the typical movement data set is constructed by collecting the typical movement skeleton information of physical dance, excluding the interference of background, lighting and other factors. The experimental results show that the 3D CNNs in this paper can produce satisfactory results for sports dance movement recognition, and validate the feasibility of the 3D convolutional neural network movement recognition algorithm based on a machine learning model in the acquisition to recognition of sports dance movements, which can better open up the content of sports dance education through machine learning model. However, there are still some deviations in the recognition results of a few movements with high similarity, and only some typical movement fragments were collected as data samples for the construction of the dataset, and there is still a lot of research space for the whole performance. Therefore, the next research direction is to use more optimized deep learning algorithms to optimize the recognition of sports dance movements, collect more sports dance movement data to expand the dataset, and to recognize different dance movements in longer dance performances.

DATA AVAILABILITY

Data for this study are available from the authors upon request.

CONFLICT OF INTEREST

The authors declare that the research was conducted in the absence of any commercial or financial relationships that could be construed as a potential conflict of interest.

REFERENCES

- (1) Lou, R., Lv, Z., Dang, S., Li, S., Zhang, Y., & Li, L. (2021). **Application of machine learning in ocean data.** *Multimedia Systems*, 1-10.
- (2) Guo, J. X., & Huang, C. (2020). **Feasible roadmap for CCS retrofit of coal-based power plants to reduce Chinese carbon emissions by 2050.** *Applied Energy*, 259, 114112.
- (3) Zounemat-Kermani, M., Matta, E., Cominola, A., Giuliani, M., & Castelletti, A. (2020). **Neurocomputing in Surface Water Hydrology and Hydraulics: A Review of Two Decades Retrospective, Current Status and Future Prospects.** *Journal of Hydrology*.
- (4) Waring, J., Lindvall, C., & Umeton, R. (2020). **Automated Machine Learning: Review of the State-of-the-Art and Opportunities for Healthcare.** *Artificial Intelligence in Medicine*, 104, 101822.
- (5) Bougie, N., & Ichise, R. (2020). **Skill-based curiosity for intrinsically motivated reinforcement learning.** *Machine Learning*, 109(3), 493-512.
- (6) Horton, M. B., Brady, C. J., Cavallerano, J., et al. (2020). **Practice Guidelines for Ocular Telehealth-Diabetic Retinopathy, Third Edition.** *Telemedicine and e-Health*, 26(4).
- (7) Shuntaro, C., Kenjirowelq, L., Narin, S., et al. (2021). **eSkip-Finder: a machine learning-based web application and database to identify the optimal sequences of antisense oligonucleotides for exon skipping.** *Nucleic Acids Research*.
- (8) Mangold, C., Zoretic, S., Thallapureddy, K., et al. (2021). **Machine Learning Models for Predicting Neonatal Mortality: A Systematic Review.** *Neonatology*, 1-12.
- (9) Hindson, J. (2022). **Proteomics and machine-learning models for alcohol-related liver disease biomarkers.** *Nature Reviews Gastroenterology & Hepatology*, 19(8), 488.
- (10) Hasan, M. S., Kordijazi, A., Rohatgi, P. K., et al. (2022). **Machine learning models of the transition from solid to liquid lubricated friction and wear in aluminum-graphite composites.** *Tribology International*, 165.
- (11) Sun, Z. Y., Herold, F., Cai, K. L., et al. (2022). **Prediction of Outcomes in Mini-Basketball Training Program for Preschool Children with Autism Using Machine Learning Models.** *International Journal of Mental Health Promotion*, 24(2), 143-158.

- (12) Tatar, A. E., & Distegor, D. (2020). **Prediction of Academic Performance at Undergraduate Graduation: Course Grades or Grade Point Average?** *Applied Sciences*, 10(14), 4967.
- (13) Lau, E. T., Sun, L., & Yang, Q. (2019). **Modelling, prediction and classification of student academic performance using artificial neural networks.** *SN Applied Sciences*, 1(9), 1-10.
- (14) Oyedele, A. O., Salami, A. M., Folorunsho, O., et al. (2020). **Analysis and prediction of student academic performance using machine learning.** *Journal of Information Technology and Computer Engineering*, 4(1), 10-5.
- (15) Jacobson, N. C., & Nemesure, M. D. (2021). **Using artificial intelligence to predict change in depression and anxiety symptoms in a digital intervention: Evidence from a transdiagnostic randomized controlled trial.** *Psychiatry research*, 259, 113618.
- (16) Xu, X., Wang, J., Peng, H., et al. (2019). **Prediction of academic performance associated with internet usage behaviors using machine learning algorithms.** *Computers in Human Behavior*, 98, 166-173.
- (17) Mathur, P., Srivastava, S., Xu, X., et al. (2020). **Artificial intelligence, machine learning, and cardiovascular disease.** *Clinical Medicine Insights: Cardiology*, 14, 1179546820927404.
- (18) Rossi, A., Pappalardo, L., Cintia, P., et al. (2018). **Effective injury forecasting in soccer with GPS training data and machine learning.** *PloS one*, 13(7), e0201264.
- (19) Duarte, J. J., Gonzalez, S. M., & Jr JC C. (2020). **Predicting stock price falls using news data: Evidence from the Brazilian market.** *Computational economics*, 57(2), 311-340.
- (20) Yoshihara, A., Fujikawa, K., Seki, K., et al. (2014). **Predicting stock market trends by recurrent deep neural networks.** *In Pacific Rim International Conference on Artificial Intelligence* (pp. 759-769). Springer, Cham.
- (21) Usmani, M., Adil, S. H., Raza, K., et al. (2016). **Stock market prediction using machine learning techniques.** *In 2016 3rd International Conference on Computer and Information Sciences (ICCOINS)* (pp. 322-327). IEEE.
- (22) Nikou, M., Mansourfar, G., & Bagherzadeh, J. (2019). **Stock price prediction using deep learning algorithm and its comparison with machine learning algorithms.** *Intelligent Systems in Accounting, Finance and Management*, 26(4), 164-174.
- (23) Hah, D. W., Kim, Y. M., & Ahn, J. J. (2019). **A study on KOSPI 200 direction forecasting using XGBoost model.** *The Korean Data & Information Science Society*, 30(3), 655-669.
- (24) Tran, D., Bourdev, L., Fergus, R., et al. (2015). **Learning spatiotemporal features with 3D convolutional networks.** *In Proc of IEEE International Conference on Computer Vision* (pp. 4489-4497). Washington DC: IEEE Computer Society.
- (25) Kishore, P. V. V., Kumar, K. V. V., Kiran Kumar, E., et al. (2018). **Indian classical dance action identification and classification with convolutional neural networks.** *Advances in Multimedia*, 2018.

- (26) Protopapadakis, E., Grammatikopoulos, A., Doulamis, A., et al. (2017). **Folk dance pattern recognition over depth images acquired via Kinect sensor.** *The International Archives of Photogrammetry, Remote Sens.*
- (27) Li, G., & Li, C. (2020). **Learning skeleton information for human action analysis using Kinect.** *Signal Processing: Image Communication*, 84, 115814.
- (28) Frayssinet, M., Esenarro, D., Juárez, F. F., & Díaz, M. (2021). **Methodology based on the NIST cybersecurity framework as a proposal for cybersecurity management in government organizations.** *3C TIC. Cuadernos de desarrollo aplicados a las TIC*, 10(2), 123-141. <https://doi.org/10.17993/3ctic.2021.102.123-141>
- (29) Chen, S., & Ren, Y. (2021). **Small amplitude periodic solution of Hopf Bifurcation Theorem for fractional differential equations of balance point in group competitive martial arts.** *Applied Mathematics and Nonlinear Sciences*, 7(1), 207-214. <https://doi.org/10.2478/AMNS.2021.2.00152>

/14/

FABRIC YARN DETECTION BASED ON IMPROVED FAST R-CNN MODEL

Haiyan Xu*

Business School, Yangzhou Polytechnic Institute, Yangzhou, Jiangsu, 225127, China

hyxu_ypi@163.com



Reception: 16/11/2022 **Acceptance:** 09/01/2023 **Publication:** 06/03/2023

Suggested citation:

X., Haiyan (2023). **Fabric yarn detection based on improved fast R-CNN model.** *3C TIC. Cuadernos de desarrollo aplicados a las TIC*, 12(1), 287-306. <https://doi.org/10.17993/3ctic.2023.121.287-306>

ABSTRACT

With the rapid development of modern computer technology, and gradually combined with the textile industry, the application of modern computer technology in the field of textile is increasingly extensive, which makes textile production gradually move towards the road of automation development. This paper proposes an automatic detection method of simple weave fabric density based on computer image vision. Computer vision and digital image processing technology are used to analyze and identify the simple weave fabric's warp and weft yarn information and calculate the fabric density. To avoid the phenomenon of warp and weft yarn skew, a method of fabric skew correction based on the Radon transform is proposed. The optimal decomposition order of these four fabrics is $k = 2$, $k = 5$, and $k = 3$. The decomposition series is k . It is found that the relative error of both warp and weft density is about 1.00%. Most of the data obtained by the method of correlation coefficient curve to determine the optimal decomposition series are consistent with the results of the energy curve method. The relative error of the density test results of No. 3 fabric, No. 6 fabric, and No. 7 fabric is higher than 10%, and the relative error of No. 3 fabric is the highest, reaching 66%. This shows serious errors in these three fabrics' warp and weft density. To solve the problems of simple weave fabric density detection, the corresponding algorithm is used to solve the problems. Finally, good results are obtained, which verifies the feasibility of this method. It is significant to realize the automatic measurement of fabric density in textile factories.

KEYWORDS

Fabric yarn; Fast R-CNN algorithm; Visual inspection; Image processing; Wavelet decomposition.

PAPER INDEX

ABSTRACT

KEYWORDS

1. INTRODUCTION

2. IMPROVED FAST R-CNN ALGORITHM

2.1. Basic structure and characteristics of convolution neural network

2.2. R-CNN series algorithm

2.3. Yolo algorithm

3. SIMPLE WEAVE FABRIC DENSITY DETECTION BASED ON WAVELET TRANSFORM

3.1. Wavelet transform

3.2. Wavelet transform of simple weave fabric

3.3. Determination of optimal wavelet decomposition series of fabric image

4. SIMPLE WEAVE FABRIC DENSITY TEST RESULTS AND ANALYSIS

4.1. Calculation of warp and weft density of simple weave fabric processed by computer

4.2. Analysis of experimental results

5. CONCLUSION

DATA AVAILABILITY

CONFLICT OF INTEREST

REFERENCES

1. INTRODUCTION

With the rapid development of modern computer technology, and gradually combined with the textile industry, the application of modern computer technology in the field of textile is increasingly extensive, which makes textile production gradually move towards the road of automation development. The structure parameters such as fabric texture, density, and color yarn arrangement are important in detecting and controlling textile quality. Currently, most factories and enterprises in the textile industry mainly rely on manual sample analysis and detection of fabric texture with the aid of fabric lenses, which is subjective, time-consuming, labor-intensive, and prone to errors. Therefore, the use of computer image processing technology to effectively replace manual to achieve intelligent fabric density detection, improve industrial production efficiency, achieve automation, and intelligent production of textile products is of great significance.

In recent years, the rapid development of computers has made computer vision technology into people's field of vision and has been much attention. Under our research and exploration, computer vision continues to develop and progress, and image processing technology has been widely used. Especially in textile testing, computer vision technology is also used, which makes the textile industry more intelligent and efficient. Shukla et al. Collected the transmission image and reflection image of fabric sample by optical principle, calculated the autocorrelation value of each row and column of the image with the autocorrelation function after preprocessing, and processed and analyzed the transmission image and reflection image respectively to obtain the relevant information of fabric texture parameters [1]. Finally, the fabric structure is determined by the length and weft of each row, and the fabric structure is determined by scanning the length and weft of each row[2]. Raj et al. Reduced the gray image level through histogram equalization, then constructed the gray level co-occurrence matrix according to the pixel spacing and angle changes, calculated its eigenvalue, and obtained the fabric density parameter through its periodic calculation [3]. Used autocorrelation function to determine the position, density, and weave point position of fabric warp and weft yarn. Later, the data of the organization point area was input into the neural network to output the fabric structure, which was trained repeatedly. Finally, the fabric structure was identified by a neural network [4]. Wu and Cao used the gray projection method to get the gray projection curve in the warp and weft direction of the fabric image[5,6]. The warp and weft yarns were separated according to the position and quantity of the gray projection curve peak and valley, and the fabric warp and weft density was calculated. Trafton et al. First calculated the weft density of twill and satin fabrics was by the gray projection method and then calculated the warp density of twill and satin fabrics was through the relationship between the density of twill and satin fabrics and the fabric texture. Later, the study found that fabric warp and weft yarn inclination was easy to occur when image processing was used to detect the density of fabric warp and weft [7-9]. Monfared and XZ et al. Proposed using Hough transform to obtain the fabric tilt angle, then making a gray projection on the fabric along the tilt direction, and finally judging

the yarn gap according to the wave crest of the projection curve to calculate the fabric warp and weft density [10,11].

Qin uses MATLAB language to carry out a series of preprocessing for woven fabric images, then carry out wavelet decomposition and reconstruction to separate and extract the information of warp and weft yarn, and then carry out binarization and smoothing processing to obtain the distribution image of warp and weft yarn. Finally, the warp and weft density of the woven fabric is obtained through program calculation [12-15]. Shi et al. Carried out multi-layer wavelet decomposition on woven fabric image through wavelet transform, reconstructed single-layer signal and calculated average brightness value of warp and weft yarn direction image, and finally calculated warp and weft density according to periodic change of brightness signal [16,17]. Combined image processing technology with time-frequency transform theory, transformed woven image from the time domain to frequency domain through Fourier transform, selected characteristic region to filter and separate single group of warp and weft yarn images. Finally, the adaptive threshold method was used to locate yarn, count the number of warp and weft yarn, and calculate woven fabric's warp and weft density [18-20]. Obtained the frequency spectrum of the fabric through a two-dimensional fast Fourier transform and calculated the fabric warp and weft density through the correlation between the characteristic change of the frequency spectrum and the fabric warp and weft density [21]. Using the Halcon algorithm library and machine vision technology, Niu processed the fabric image by Fourier transform, analyzed it by Gabor transform, and finally calculated the fabric warp and weft density through wavelet transform results [22]. Barreto and Shi use Fourier transform and wavelet transforms to process fabric images, analyze spectrum characteristics, process interference information, and then transform them into spatial domain through inverse transformation. Finally, fabric warp and weft density can be calculated by spatial domain detection or correlation between frequency spectrum features and warp and weft yarn density [23,24]. Le obtains the power spectrum of woven fabric image by Fourier transform, then processes the threshold value and calculates the fabric warp and weft density by using the relationship between the spatial domain and frequency domain. Secondly, it uses wavelet transform to separate the warp and weft sub-images of woven fabric. After processing, the ideal warp and weft yarn density information is obtained. Finally, a computer program automatically calculates the fabric warp and weft density. Others use the wavelet transform to reconstruct the fabric spatial domain image according to the spectrum characteristics of the fabric image to detect the fabric warp and weft density [26,27]. Some also use the deep learning method to train many samples to obtain stable automatic detection of fabric density after Fourier transform or wavelet transform processing of fabric [28].

To sum up, there have been a lot of research and achievements in the automatic detection of fabric warp and weft density, but there are still some problems that have not been solved perfectly, and so far, it has not been well applied to actual industrial production. This paper proposes a warp and weft yarn detection method based on the improved fast R-CNN algorithm, which is of great significance to realize the automation and intelligent production of textile products.

2. IMPROVED FAST R-CNN ALGORITHM

The current deep learning algorithm uses a convolutional neural network to recognize yarn features, and when the number of training samples of the network is enough, its recognition accuracy and robustness are better than the traditional image processing technology, so it has a good application prospect.

2.1. BASIC STRUCTURE AND CHARACTERISTICS OF CONVOLUTION NEURAL NETWORK

A convolutional neural network (CNN) is a feedforward neural network with a depth structure. It can complete the local sampling and image-sharing task using a neural network. Since the convolutional neural networks can collect the spatial and channel information of feature graphs simultaneously, it is mostly used in the backbone network of the algorithm to achieve feature extraction tasks[29-30]. CNN structure is generally divided into the following layers: convolution, pooling, activation, and full connection layer. The algorithm's core is to adaptively and update the convolution kernel parameters iteratively through the computer's automatic learning, so the convolution layer's calculation is particularly important. The main purpose of the convolution layer is to extract features of different receptive fields by convolution kernels of various sizes.

CNN differs from the common neural network in that the neurons in the previous layer are only partially connected with the current layer. This connection structure greatly reduces the number of branches in the network. A convolution kernel is a local region. Let the convolution kernel go through the whole characteristic graph.

Weight sharing means that a single parameter controls multiple connections without considering the position relationship of input data. A convolution kernel with fixed internal weight parameters is used to process the whole graph by a convolution operation. The convolution kernel is equivalent to the weight of the traditional network. Each neuron of the traditional network has different weights, but the same set of convolution kernels is used in feature processing, so the parameters of the convolution neural network are shared.

Pooling is an important downsampling operation. Its principle is to do some simple operations on the neurons in the convolution layer through the local correlation and take the results as the input values of the neurons in the pooling layer. This operation not only reduces the amount of calculation but also retains valuable information. Common pooling operations include maximum pooling and average pooling. We can select different pooling techniques according to the actual situation to prevent model overfitting and improve network robustness.

The full connectivity layer (FC) is located at the end of the network hierarchy. Its function is to connect the feature maps of the previous layer output and map all the features distributed in the front layer network to the output sample space to reduce the influence of the target location on classification accuracy. The full connection layer can

be completed in the actual network by convolution, and all feature expressions can be mapped to one output value by a convolution operation.

2.2. R-CNN SERIES ALGORITHM

In the development of deep learning, R-CNN is the first industrial-level target recognition and detection algorithm, which has become an important research direction in the target recognition and detection field. Fast R-CNN, fast R-CNN, and other algorithms are based on R-CNN, aiming at the shortcomings of the previous generation of algorithms for continuous optimization expansion research. Through training and calculation, the R-CNN algorithm filters the targets in the candidate region, filters out the invalid feature regions and then completes the corresponding classification according to the task requirements. Compared with the one-stage target recognition and detection algorithm, the recognition error rate and miss recognition rate of the series of algorithms are relatively low, but the recognition speed is relatively slow. We can choose different algorithms for different target recognition and detection requirements in practical applications.

It overcomes the limitation of traditional machine learning methods. The biggest contribution of the Alex net network is the introduction of the activation function of the modified linear unit (re Lu). The introduction of the re Lu activation function can not only effectively prevent the overfitting phenomenon but also shorten the training period due to the reduction of calculation.

The target classification method of the R-CNN algorithm is to use SVM to classify the extracted features and then use the non-maximum suppression algorithm (NMS) to evaluate the feature area. The high-score region is identified as the target area, and the overlapping, redundant area is removed to obtain the region with the highest possibility of the target. An important factor that affects the performance of the target recognition and detection model is whether the object can be located accurately. Because the inaccuracy of the target candidate frame region will cause the overlap area error, it is necessary to modify and regress the candidate frame and then generate the final prediction frame.

The fast R-CNN algorithm is an efficient target recognition and detection algorithm based on the R-CNN algorithm and uses a deep neural network. Because of the shortcomings R-CNN algorithm, the fast R-CNN algorithm has made corresponding improvements. The fast algorithm uses the output of the intermediate convolution layer of the vgg-16 network.

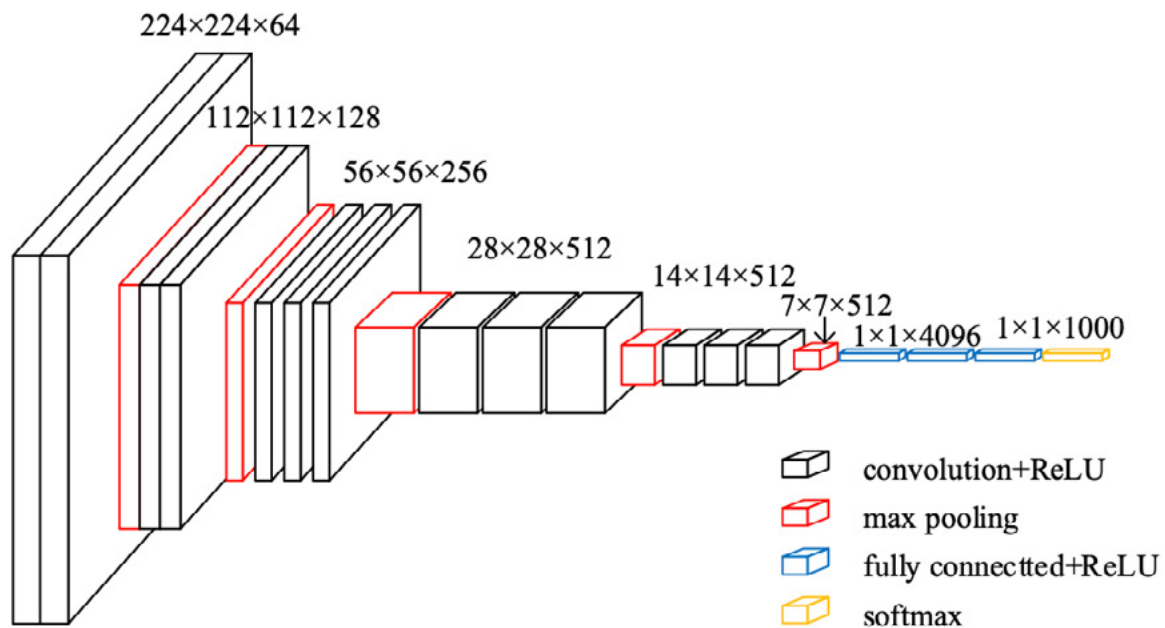


Figure 1. Structure of vgg-16 network model

The fast R-CNN algorithm can complete the task of feature extraction, detection frame regression, and classification at the same time. The efficiency of this algorithm is far higher than that of other algorithms of the R-CNN series. The fast R-CNN algorithm does not need distributed training and testing. Firstly, it proposes a series of anchors with preset sizes through the regional recommendation network (RPN), then adjusts the anchor's size several times through the training network and outputs the final target detection regression box. Since this paper will optimize the fast R-CNN algorithm, the principle of the algorithm is analyzed in detail from three aspects: network architecture, RPN structure, and algorithm loss function.

$$L(\{p_i\}\{t_j\}) = \frac{1}{N_{cls}} \sum L_{cls}(p_i, p_i^*) + \lambda \frac{1}{N_{reg}} \sum_i p_i^* L_{reg}(t_i, t_i^*) \quad (1)$$

2.3. YOLO ALGORITHM

Yolo (you only look once) is a target recognition and detection framework based on suggestion region. Yolo algorithm is different from the two-stage recognition and detection idea. Yolo algorithm first divides the given image into $S \times S$ cells, which cell is responsible for detecting the center of each target. Compared with the two-stage detection algorithm, $S \times S$ cells are equivalent to the target region of interest, so there is no need to generate candidate regions through the network similar to RP, and the detection task can be completed in one step.

$$C_j^i = \text{pr}(\text{object}) * \text{IOU}_{\text{pred}}^{\text{truth}} \quad (2)$$

Next, the C conditional category probabilities are predicted by the segmented grid, and the redundant boundary boxes are removed by non-maximum suppression (NMS) to get the best result

$$pr(class_i / object) = \frac{pr(class_i \times object)}{pr(object)} \quad (3)$$

$$pr(class_i / object) * pr(object) * IOU_{prad}^{truth} = pr(class_i \cdot object) * IOU_{prad}^{truth} \quad (4)$$

Yolo is a simple and fast end-to-end algorithm, but the accuracy of Yolo recognition and detection is not high, and the object positioning is not accurate enough. It is not good enough for small targets and dense target recognition and detection.

Table 1. Comparison of advantages and disadvantages of target recognition algorithm

| Algorithm name | advantage | shortcoming |
|----------------|---|--|
| R-CNN | 1. CNN is proposed to extract features 2. Map on Pascal VOC increased from 35.1% to 53.7% | 1. The training process is divided into stages, and the recognition speed is slow 2. Consumes disk space |
| Fast R-CNN | 1. Using the full winder network, the ROI pooling, all feature maps can be predicted only once 2. The problem of image distortion and redundant computation is reduced | 1. The method of extracting candidate regions is computationally expensive and repetitive 2. The end-to-end training is not implemented |
| Faster R-CNN | 1. Propose RPN network 2. Real end-to-end detection model 3. Recognition accuracy and speed have been greatly improved | 1. ROI pooling operation results in precision loss 2 |
| YOLOv3 | 1. Faster speed 2. End to end model | 1. There is the deviation in the accuracy of object position recognition 2. Low recall rate |

3. SIMPLE WEAVE FABRIC DENSITY DETECTION BASED ON WAVELET TRANSFORM

Wavelet transform is the inheritance and development of the traditional Fourier transform. Wavelet transform has good adaptability for time-frequency windows. Different from Fourier transform, the window size cannot change with the change in frequency. Wavelet can be used for multi-scale analysis, feature extraction, and analysis of the object's high-frequency and low-frequency information, a new image

processing method. This study uses the wavelet transform to detect simple weave fabric images' warp and weft density.

3.1. WAVELET TRANSFORM

Compared with the Fourier transform, the wavelet transform has better time-frequency window characteristics, which has attracted many experts and scholars to study. In the past ten or twenty years, wavelet transform has developed rapidly and widely in many scientific and technological fields. Wavelet transform decomposes the signal into a series of wavelets by scaling and shifting the original wavelet. Compared with Fourier transform, the wavelet transform overcomes its three shortcomings: first, Fourier coefficients cannot change with frequency, but wavelet coefficients can; Two wavelet transforms can well reflect the signal frequency change with time; Wavelet transform - Fourier transform can solve the problem of variable window size. Wavelet transforms mainly include continuous wavelet transform and discrete wavelet transform.

$$C_{\Psi} = \int_{-\infty}^{+\infty} \frac{|\Psi'(x)|^2}{x} dx < \infty \quad (5)$$

$$W_f(k, t) = \langle f(x), \Psi_{k,t}(x) \rangle = \frac{1}{\sqrt{k}} \int_{\mathbb{R}} f(x) \Psi^* \left(\frac{x-t}{k} \right) dx \quad (6)$$

Where k is the decomposition series, and t is the displacement $\Psi(x)$ length. The basic wavelet function can be obtained $\Psi(x)$ based on the wavelet transform. The wavelet sequence function after displacement and decomposition is as follows:

$$\Psi_{k,t}(x) = \frac{1}{\sqrt{k}} \Psi \left(\frac{x-t}{k} \right), k, t \in \mathbb{R}; k > 0 \quad (7)$$

When the decomposition series K and the displacement length T are continuous variables, the above wavelet transform process is called continuous wavelet transform (CWT). There is another form of discrete wavelet transform (DWT). In many cases, the decomposition series K and the displacement length t need to be discretized by the power series.

$$W_f(m, n) = \langle f(x), \Psi_{m,n}(x) \rangle = \frac{1}{\sqrt{k_0^m}} \int_{\mathbb{R}} f(x) \Psi^* \left(\frac{x - nt_0}{k_0^m} \right) dx \quad (8)$$

The discrete wavelet sequence function is as follows:

$$\Psi_{m,n}(x) = \frac{1}{\sqrt{k_0^m}} \Psi \left(\frac{x - nt_0}{k_0^m} \right) \quad (9)$$

3.2. WAVELET TRANSFORM OF SIMPLE WEAVE FABRIC

The fabric image can be decomposed into approximate and detailed image information by one-dimensional wavelet transform on two-dimensional images, low-frequency, and high-frequency parts. Then the high-frequency part can continue to be decomposed into a group of high-frequency and low-frequency components, and the low-frequency part can be further decomposed into another group of high-frequency and low-frequency components. Finally, a two-dimensional image is decomposed into four parts by wavelet transform. Compared with one-dimensional wavelet transform, two-dimensional wavelet transform decomposes the high-frequency information component more carefully along the horizontal and vertical directions and further decomposes the high-frequency part into horizontal detail component, vertical detail component, and diagonal detail component. Therefore, four parts can be obtained after the first level decomposition: approximate detail component, horizontal detail component, vertical detail component, and diagonal detail component. In theory, the decomposition process can be continued for a long time.

After the multi-scale decomposition of fabric images, wavelet transform can reconstruct and output approximate and detailed image information according to the demand. Wavelet has good decomposition and reconstruction ability, so it can obtain clear and complete fabric structure information and detail information without losing important information and eliminating interference information.

The principle of automatic detection of fabric warp and weft density is that the horizontal high-frequency detail component and vertical high-frequency detail component, which match the height of warp and weft yarn, are obtained by wavelet decomposition and reconstruction, and the number of warp and weft threads is calculated to obtain the fabric warp and weft density. The horizontal high-frequency detail component and vertical high-frequency detail component obtained by different scales are completely different. The matching degree of detail component and yarn number is also completely different. Therefore, the decomposition scale of wavelet decomposition directly affects the horizontal and vertical detail component information obtained and the accuracy of the fabric warp and weft density information reflected by the image. To obtain the most complete warp and weft yarn information to obtain the warp and weft yarn number information matching the image height, the wavelet decomposition scale has directly impacted the fabric's accuracy. Knowing which scale is processed is necessary to obtain the reconstructed detail image, which is highly matched with the fabric image details. We call this wavelet decomposition scale the optimal decomposition series. Therefore, the research on determining the optimal decomposition series is of great significance for the automatic calculation and detection of warp and weft density.

3.3. DETERMINATION OF OPTIMAL WAVELET DECOMPOSITION SERIES OF FABRIC IMAGE

The correlation coefficient is used to study the degree of linear correlation between two variables. The curve of the correlation coefficient can reflect the correlation

between two variables, but it is unclear about the degree of correlation, so it is a kind of uncertain relationship. To determine the optimal wavelet decomposition series by the method of correlation coefficient curve is to compare the correlation degree between the fabric image reconstructed by wavelet decomposition and the fabric image before decomposition and reconstruction, and calculate the correlation coefficient of the two images, and take the decomposition series corresponding to the maximum correlation coefficient as the optimal decomposition series. Then the fabric is decomposed into high-frequency details and series to get the optimal fabric density. The concept of the correlation coefficient is that assuming that there are two matrices of the same dimensions, A and B, the correlation coefficient of a and B is calculated as follows:

$$r = \frac{\sum_m \sum_n (A_{mn} - \bar{A})(B_{mn} - \bar{B})}{\sqrt{\left(\sum_m \sum_n (A_{mn} - \bar{A})^2\right) \left(\sum_m \sum_n (B_{mn} - \bar{B})^2\right)}} \quad (10)$$

Where m and N represent the rows and columns of the matrix, respectively.

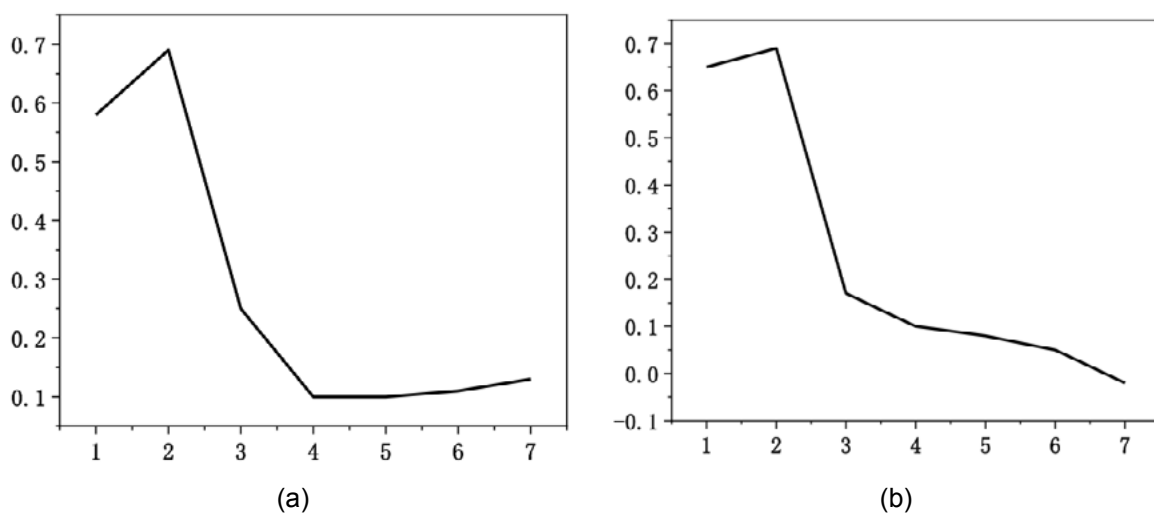


Figure 2. Sample correlation coefficient curve

From the correlation coefficient curve in the above figure, it can be seen that the correlation coefficient curve of each sample fabric has a maximum peak value, which indicates that the reconstructed image obtained by wavelet decomposition and reconstruction under the corresponding decomposition series is most similar to that before fabric image processing. Therefore, the maximum peak value of correlation coefficient curve is selected as the optimal decomposition series of wavelet decomposition and reconstruction. From the curve in the figure above, the maximum correlation coefficients of fabrics 1, 2, 3, and 4 are 2, 2, 5, and 3, respectively, which means that the optimal decomposition order of the four fabrics obtained by the method of correlation coefficient curve is $k = 2$, $k = 2$, $k = 5$, $k = 3$, that is, for fabric 1 at decomposition scale 2, for fabric 2 at decomposition scale 2, for fabric 3 at decomposition scale 5, and for fabric 4 at decomposition scale 3.

and vertical high-frequency detail components matching the number of warp and weft yarns can be obtained by wavelet decomposition and reconstruction respectively.

In the study of determining the optimal decomposition order by the correlation coefficient, it is found that the results obtained by some fabrics are not very ideal. In the process of a large number of experimental studies, the optimal decomposition order determined by the maximum correlation coefficient is still inaccurate. For example, in the treatment of fabric 3 above, the maximum correlation coefficient is 5. After processing, the matching degree between the detail component and the warp and weft yarn of the fabric is not large, so a more stable and accurate method to determine the optimal decomposition order is studied. Solving the optimal decomposition series is to obtain the optimal detail components after decomposition and reconstruction. Through the in-depth study and analysis of all the component information obtained from many experiments, it is found that there is a certain relationship between the optimal wavelet decomposition series and the information of all components obtained after decomposition and reconstruction.

In this paper, the concept of energy curve is introduced to determine the optimal decomposition series of wavelet decomposition and reconstruction. The energy values among the approximate, vertical, horizontal, and diagonal components obtained by wavelet decomposition and reconstruction are calculated using the energy calculation function energy. The program operation formula is: $[a, h, V, D] = \text{wenergy2}(C, s)$. A is the approximate low-frequency component of the image after decomposition and reconstruction, h is the horizontal high-frequency detail component after decomposition and reconstruction, V is the vertical high-frequency detail component after decomposition and reconstruction, and D is the diagonal high-frequency detail component after decomposition and reconstruction. The energy curve is used to determine the optimal wavelet decomposition series. The wavelet coefficient square is used for each component after decomposition and reconstruction by the energy function, and then the energy of each component is obtained by summation, and then the energy proportion of each component is calculated by normalization. Finally, the relative gradient change of energy is calculated, and the energy curve is drawn to observe the change of the energy curve. The lowest peak value of the energy curve is taken as the optimal decomposition order of the wavelet, and the fabric image is processed by wavelet transform.

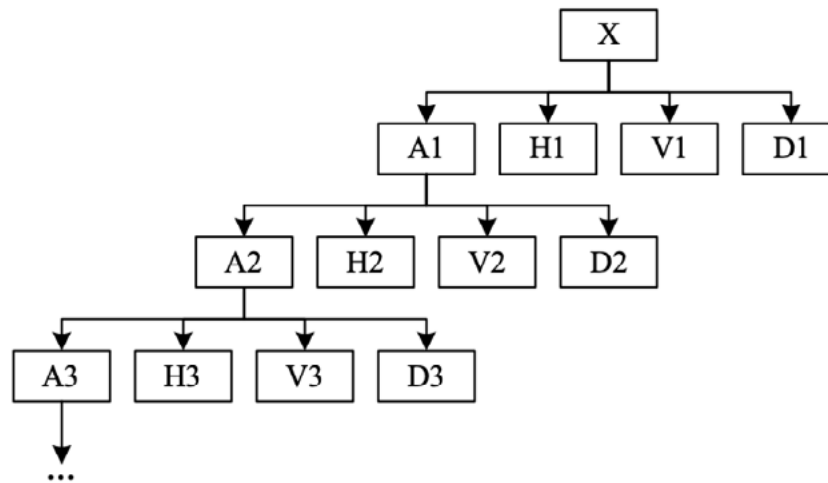


Figure 3. Wavelet decomposition tree

The two-dimensional signal x (fabric image) is decomposed into four components: A_1 , H_1 , V_1 , and D_1 , after the first-order wavelet decomposition. The second-order decomposition further decomposes A_1 into four components, namely A_2 , H_2 , V_2 , and D_2 . The third-order decomposition decomposes A_2 into four components: A_3 , H_3 , V_3 , and D_3 . The subsequent decomposition is carried out according to this law, and the whole wavelet decomposition process is like branching out. Therefore, the decomposition process and the resulting components can be represented in a tree view.

From the above wavelet decomposition tree, we can know that all the components obtained from the two-dimensional image after K (k is a natural number greater than 0) level decomposition include approximate image component A_k , horizontal detail component H_1 , H_2 , H_k , vertical detail component V_1 , V_2 , V_k , and diagonal detail component D_1 , D_2 , D_k . If each component of the output after decomposition and reconstruction is regarded as a matrix, then the information contained in the component is stored in the matrix data. Assuming that there are n data in each matrix, each component is written into a matrix in the form of:

$$A_k = \begin{bmatrix} a_{k1} & a_{k2} & a_{k3} & \dots & a_{kn} \end{bmatrix} \quad (11)$$

$$H_k = \begin{bmatrix} h_{k1} & h_{k2} & h_{k3} & \dots & h_{kn} \end{bmatrix} \quad (12)$$

$$V_k = \begin{bmatrix} v_{k1} & v_{k2} & v_{k3} & \dots & v_{kn} \end{bmatrix} \quad (13)$$

$$D_k = \begin{bmatrix} d_{k1} & d_{k2} & d_{k3} & \dots & d_{kn} \end{bmatrix} \quad (14)$$

4. SIMPLE WEAVE FABRIC DENSITY TEST RESULTS AND ANALYSIS

Simple fabric is the original fabric, which is also called basic fabric. It includes plain weave, twill weave, and satin weave. All fabrics can not be separated from warp and

weft. This paper's fabric density detection method can monitor all fabrics containing warp and weft. However, there is a problem of high relative error in the density monitoring of individual fabrics. To get a better result of fabric design, we need to use the computer to calculate the fabric density automatically.

4.1. CALCULATION OF WARP AND WEFT DENSITY OF SIMPLE WEAVE FABRIC PROCESSED BY COMPUTER

From the analysis in the previous section, it can be seen that clear warp and weft density yarns are arranged. The black horizontal line represents the yarn, and the white horizontal line represents the gap between the yarn and the yarn. Therefore, the warp and weft density of the simple woven fabric is required. The number of warp and weft yarns can be obtained by calculating the number of black transverse lines in the vertical and horizontal directions. Then the warp and weft yarn density is calculated. The vertical detail component diagram of fabric represents the arrangement of warp yarn, alternately arranged between warp and blank space. In the image, the alternate arrangement of black pixels and white pixels is shown; The horizontal detail component of the fabric represents the weft arrangement of the fabric.

Similarly, the alternate arrangement of the weft and the blank space means that the black pixels and white pixels in the vertical direction of the image are arranged alternately. Therefore, black and white pixels alternate once, representing a yarn. To calculate the number of yarns in the detail image, we can get it by calculating the number of consecutive black pixels in the image.

Taking the vertical detail component of fabric as an example, the unit length of fabric is set as 10cm, the unit of fabric density is the national standard unit "root / 10cm", and the image width of fabric is d (unit is a pixel). Counting the total number of consecutive black pixels in a row of vertical detail component maps, the yarn number S_j in the horizontal direction can be obtained. The total number of continuous black pixels S_j is divided by the width of fabric image D . According to the parameters of the CCD industrial camera, the camera's resolution can be obtained. Through the resolution, the number of pixels per centimeter P (in pixels/cm) can be obtained. Finally, the warp density converted into a standard unit can be obtained by multiplying M_j and P and multiplying by unit length 10. The calculation formula of fabric warp density P_j is as follows:

$$M_j = S_j \div d \quad (15)$$

$$P_j = M_j \times p \times 10 \quad (16)$$

If the contour curve is marked as $f(\rho)$, and all the peak positions of the drop curve are recorded as $\rho_i, i = 0, \dots, M-1$ and M are the total number of peaks, the weft density formula of the fabric is expressed as:

$$D_{weft} = \frac{r \times (M-1)}{2.54 \times (\rho_{M-1} - \rho_0)} \quad (17)$$

In the formula, r is the resolution of the image, and the unit of weft density D_{weft} is/cm.

After the same preprocessing process, the correlation coefficient curve and energy curve are used to determine the optimal wavelet decomposition series and the optimal decomposition series is used to decompose and reconstruct the sample fabric image. After reconstruction, the vertical and horizontal detail components are optimized, and the fabric warp and weft density detected by the two methods are calculated.

Table 2. shows the measurement results of the optimal decomposition series determined by the correlation coefficient curve

| Fabric number | Warp density (PCS / 10cm) | | | |
|---------------|---------------------------|-----------------|------------|---------------|
| | for the first time | The second time | third time | average value |
| 1 | 351.20 | 355.58 | 350.12 | 352.30 |
| 2 | 769.48 | 771.72 | 775.19 | 772.13 |
| 3 | 104.11 | 107.93 | 103.14 | 105.06 |
| 4 | 308.56 | 311.69 | 310.56 | 310.27 |
| 5 | 215.24 | 210.70 | 213.09 | 213.01 |
| 6 | 241.82 | 236.17 | 240.12 | 239.37 |
| 7 | 527.67 | 535.18 | 538.30 | 537.05 |
| 8 | 407.66 | 401.97 | 407.68 | 405.77 |
| 9 | 682.00 | 681.43 | 675.13 | 679.52 |
| 10 | 637.11 | 640.15 | 634.85 | 637.11 |

No. 1 is a woven fabric, No. 2 is a knitted fabric, and No. 3 is knitted fabric; No. 4 is non-woven fabric, No. 5 is three-way fabric, No. 6 is multi-directional fabric, No. 7 is composite fabric, No. 8 is a twill fabric, No. 9 is plain fabric, and No. 10 is checkered fabric. In manual testing, we use a direct method to measure simple weave fabric's warp and weft density. Use fabric density. The number of yarns in 5cm length is measured by analyzing the mirror, and the warp (weft) yarn density is obtained by multiplying the number of yarns by 2. Each piece of fabric is measured three times, and the average value of the three values is taken as the final measurement result of warp and weft density.

4.2. ANALYSIS OF EXPERIMENTAL RESULTS

For the convenience of measuring the fabric density and weft, we will use the method of measuring the fabric density and going direct. The accuracy and reliability of the two methods are analyzed to verify the feasibility of the computer automatic detection method for the warp and weft density of simple woven fabrics.

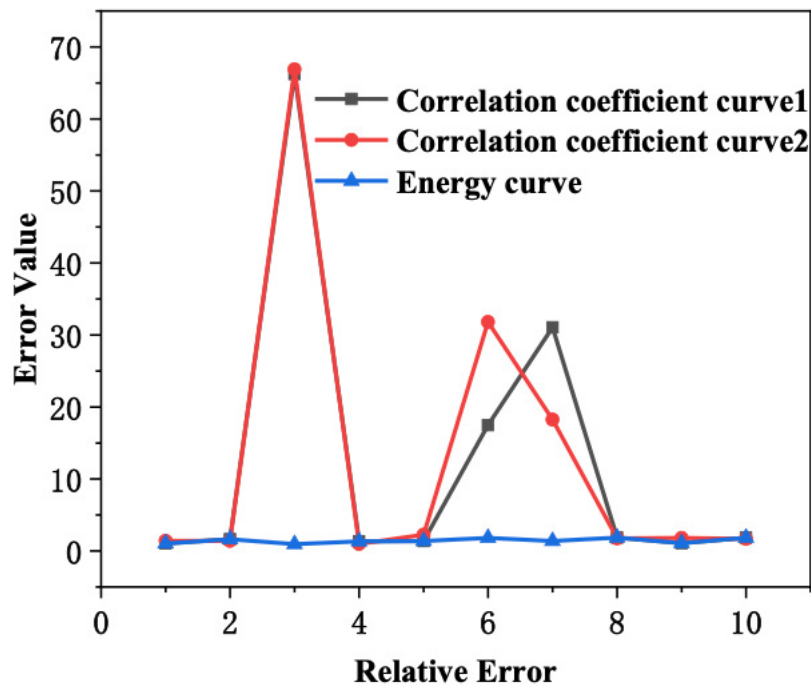


Figure 4. Relative error results

The results show that the relative error of warp and weft density of simple weave fabric is about 1.00% by using the method of energy curve to determine the optimal decomposition series. It is found that the relative error of both warp and weft density is about 1.00%. The results show that this method is feasible. However, most of the data results of the correlation coefficient curve method for determining the optimal decomposition series are consistent with the results of the energy curve method. The relative error of the density test results of No. 3 fabric, No. 6 fabric, and No. 7 fabric is higher than 10%, and the relative error of No. 3 fabric is the highest, reaching 66%. This shows a serious error in these three fabrics' warp and weft density. That is to say, the decomposition order determined by the three fabrics' correlation coefficient curves is not the fabric's optimal decomposition series. Therefore, the fabric warp and weft density results calculated by the vertical and horizontal detail components obtained by the wavelet decomposition and reconstruction of the fabric by using this decomposition series will be so different from the real density of the fabric. This group of experimental results also further shows that when using wavelet decomposition and reconstruction methods to detect the fabric warp and weft density, the determination of the optimal wavelet decomposition series is very important. The results of different series decomposition and the real warp and weft density of fabric may be greatly different. Such a large deviation will also greatly impact the subsequent production of fabrics. Compared with the correlation coefficient curve, the accuracy of the energy curve method is better. However, in the experiment, it is also found that the processing error of simple weave fabric with large warp and weft density or complex pattern and color of the fabric itself may be large, which needs further research and improvement.

5. CONCLUSION

This paper aims to use computer vision and digital image processing technology to replace manual identification and automate simple weave fabric production detection. This research combines textile knowledge, computer technology, and image processing technology and achieves the integration of subject knowledge, which is of great significance for bringing innovative results. To solve the problems existing in the previous research on the automatic detection of fabric warp and weft density, this paper puts forward the corresponding algorithm. The main research contents and innovations are as follows

1. The method in this paper combines the correlation coefficient curve method to determine the optimal decomposition order of fabrics, which are respectively $k=2$, $k=2$, $k=5$, $k=3$. When the decomposition scale of fabric 1 is 2, the decomposition scale of fabric 2 is 2, the decomposition scale of fabric 3 is 5, and the decomposition scale of fabric 4 is 3. Therefore, this method can effectively avoid warp and weft skew.
2. Only the fabric density detection method in this paper is used. The relative error of the warp and weft density of the simple woven fabric detected is 1%, which is consistent with the curve with the most decomposition sequence, indicating that the relative error detected by the fabric density detection method in this paper is the smallest and the accuracy is the highest.
3. In this paper, the fabric density detection method decomposes and reconstructs the horizontal, vertical, and high-frequency detail components and approximate detail components of the fabric image. Most of the data from the optimal decomposition sequence determined by the correlation coefficient curve method are consistent with the results obtained by the energy curve method. However, there is a problem of high relative error in the density monitoring of individual fabrics.

DATA AVAILABILITY

The data used to support the findings of this study are available from the corresponding author upon request.

CONFLICT OF INTEREST

The authors declare that the research was conducted without any commercial or financial relationships that could be construed as a potential conflict of interest.

REFERENCES

- (1) Shukla, K., Ahmad, A., Ahluwalia, B. S., et al. (2022). **Finite element simulation of transmission and reflection of acoustic waves in the ultrasonic transducer.** *Japanese Journal of Applied Physics*.

- (2) Elemmi, M. C., Anami, B. S., & Malvade, N. N. (2021). **Defective and nondefective classification of fabric images using shallow and deep networks.** *International Journal of Intelligent Systems.*
- (3) Raj, A., Sundaram, M., & Jaya, T. (2020). **Thermography based breast cancer detection using self-adaptive gray level histogram equalization color enhancement method.** *International Journal of Imaging Systems and Technology.*
- (4) Ojo, J. F., & Olanrewaju, R. O. (2021). **Review of Family of Autoregressive Integrated Moving Average Models in the Comportment of Autocorrelation Function for Non-Seasonal Time Series Data.** *International Journal of Mathematical Sciences & Applications*, 19(1), 79-89.
- (5) Wu, D., & Tang, Y. (2020). **An improved failure mode and effects analysis method based on uncertainty measure in the evidence theory.** *Quality and Reliability Engineering*, (1).
- (6) Cao, Y., You, J., Shi, Y., et al. (2021). **Research on the Green Competitiveness Index of Manufacturing Industry in Yangtze River Delta Urban Agglomeration.** *Problemy Ekorozwoju*, 16(1), 143-156.
- (7) Trafton, K., & Giachetti, T. (2021). **The morphology and texture of Plinian pyroclasts reflect their lateral sourcing in the conduit.** *Earth and Planetary Science Letters*, 562.
- (8) Le, B., Troendle, D., & Jang, B. (2021). **Detecting fabric density and weft distortion in woven fabrics using the discrete fourier transform.**
- (9) Kaplan, V. (2021). **Detection of Remote Sensing Warp Tension during Weaving on Plain Twill and Satin Fabric.** *Fibres and Textiles in Eastern Europe*, 29(1(145)), 35-39.
- (10) Monfared, S. S., & Sedef, B. (2021). **Road Lane detection through image and video processing using edge detection and Hough transform for autonomous driving purposes.**
- (11) Xz, A., Gla, B., Zya, B., et al. (2020). **Parameter estimation based on Hough transform for airborne radar with conformal array - ScienceDirect.** *Digital Signal Processing*, 107.
- (12) Qin, T., Cao, P., Zhang, Y., et al. (2021). **Underwater magnetic target signal denoising based on modified wavelet decomposition and reconstruction algorithm.** *Journal of Physics: Conference Series*, 1738(1), 012019 (8pp).
- (13) Yan Y, Liu Y, Yang M, et al. (2020). **Generic wavelet-based image decomposition and reconstruction framework for multi-modal data analysis in smart camera applications.** *IET Computer Vision*, 14(7), 471-479.
- (14) Lgt, A., Mld, B., & Jgg, C. (2022). **Picking out the warp and weft of the Ediacaran seafloor: Paleoenvironment and paleoecology of an Ediacara textured organic surface.** *Precambrian Research*, 369, 106539-.
- (15) Wang, X., Wang, S., Guo, Y., et al. (2020). **Research on improved sharpening algorithm based on closed operation and binarization.** *Journal of Physics Conference Series*, 1629, 012019.
- (16) Shi, J., Wang, Y., Zhang, X., et al. (2021). **Extraction method of weak underwater acoustic signal based on the combination of wavelet transform**

- and empirical mode decomposition.** *International Journal of Metrology and Quality Engineering.*
- (17) Nugroho, P.C., Widadi, R., & Zulherman, D. (2021). **Hand and Foot Movement of Motor Imagery Classification Using Wavelet Packet Decomposition and Multilayer Perceptron Backpropagation.** *In 2nd Borobudur International Symposium on Science and Technology (BIS-STE 2020).*
 - (18) Pavićić, I., Brievac, Z., et al. (2021). **Geometric and fractal characterization of pore systems in the upper Triassic dolomites based on image processing techniques example from umberak mts nw Croatia.** *Sustainability*, 13.
 - (19) Pang, K., Alam, M. Z., Zhou, Y., et al. (2021). **Adiabatic Frequency Conversion Using a Time-Varying Epsilon-Near-Zero Metasurface.** *Nano Letters.*
 - (20) Tang, S.C., Wang, X.Y., Yang, L.L., et al. (2020). **Design of Slotted Dielectric Patch Antenna with Filtering Characteristic.** *In 2019 International Symposium on Antennas and Propagation (ISAP). IEEE.*
 - (21) Tutatchikov, V. (2020). **Application of parallel version two-dimensional fast Fourier transform calculating algorithm with an analogue of the Cooley-Tukey algorithm.** *In 2020 International Conference on Information Technology and Nanotechnology (ITNT).*
 - (22) Niu, H., Wu, B., Wang, Q., et al. (2020). **Research on steel barrel flattened seam recognition based on machine vision.** *Journal of Physics Conference Series*, 1633, 012014.
 - (23) Barreto, M., Reis, J., Muraoka, T., et al. (2021). **Diffuse reflectance infrared Fourier transform spectroscopy for a qualitative evaluation of plant leaf pigment extraction.**
 - (24) Shi J, Wang Y, Zhang X, et al. (2021). **Extraction method of weak underwater acoustic signal based on the combination of wavelet transform and empirical mode decomposition.** *International Journal of Metrology and Quality Engineering.*
 - (25) Le B, Troendle D, Jang B. (2021). **Detecting fabric density and weft distortion in woven fabrics using the discrete Fourier transform.**
 - (26) Tabunschik V. A., T. M. Chekmareva, & Gorbunov R. V. (2020). **Spectral characteristics of some agricultural crops in different phenological phases of vegetation.** *Plant Biology and Horticulture Theory Innovation*, 152, 56-70.
 - (27) Cooney G. S., Barberio M., Diana M., et al. (2020). **Comparison of spectral characteristics in human and pig biliary system with hyperspectral imaging (HSI).**
 - (28) Bo C., Polatkan G., Sapiro G., et al. (2020). **The hierarchical beta process for convolutional factor analysis and deep learning.** *In ICML.*
 - (29) Kaseng, F., Lezama, P., Inquilla, R., & Rodriguez, C. (2020). **Evolution and advance usage of Internet in Peru.** *3C TIC. Cuadernos de desarrollo aplicados a las TIC*, 9(4), 113-127. <https://doi.org/10.17993/3ctic.2020.94.113-127>
 - (30) Liu Chunguang. (2021). **Precision algorithms in second-order fractional differential equations.** *Applied Mathematics and Nonlinear Sciences*, 7(1), 155-164. <https://doi.org/10.2478/AMNS.2021.2.00157>

/15/

THE OPTIMIZATION PATH OF HIGHER EDUCATION RESOURCE ALLOCATION IN CHINA BASED ON FUZZY SET THEORY

Yuqi Zhao*

Academy of Music, Introduction of Henan University, Kaifeng, Henan, 475000,
China

vivizhaoqiqi@163.com



Reception: 26/11/2022 **Acceptance:** 13/01/2023 **Publication:** 07/03/2023

Suggested citation:

Z., Yuqi. (2023). **The Optimization Path of Higher Education Resource Allocation in China Based on Fuzzy Set Theory.** *3C TIC. Cuadernos de desarrollo aplicados a las TIC*, 12(1), 308-328. <https://doi.org/10.17993/3ctic.2023.121.308-328>

ABSTRACT

The use of fuzzy set theory to adjust the educational resource allocation model is the optimal path to achieve the allocation of educational resources. The optimal path realized by fuzzy set theory promotes the healthy development of education and addresses the current important and urgent tasks in the field of higher education in China. This study utilizes the basic theory of fuzzy sets and analyzes dynamic fuzzy set theory, fuzzy relations and fuzzy matrices. The indexes of optimal allocation are selected according to the classification of higher education resources, the fuzzy set multi-objective planning model is designed, and finally, the combination of factors of education production in colleges and universities is optimized. The experiment proves that: the average allocation efficiency of excellent colleges and universities is 0.186, and the average improvement is 35.41% after optimization. The average allocation efficiency of ordinary colleges and universities is 0.174, which is improved by 22.12% on average after optimization. It can be found that the resource allocation efficiency of excellent colleges and universities is generally higher than that of ordinary colleges and universities, and the role of excellent colleges and universities with more abundant resources themselves is greater after the optimization of college resource allocation. It indicates that by adjusting the quantity and structure of educational resources according to the optimization path, the optimization of educational resource allocation can be achieved. This verifies that: the emergence of optimal paths for solving resource allocation realized by fuzzy set theory has greatly expanded the application of fuzzy methods in the field of higher education and provided a new theoretical tool for solving resource allocation.

KEYWORDS

Fuzzy set theory; optimization path; dynamic fuzzy set; resource allocation efficiency; fuzzy matrix

PAPER INDEX

ABSTRACT

KEYWORDS

1. INTRODUCTION

2. A PATH GENERATION MODEL FOR RESOURCE ALLOCATION OPTIMIZATION BASED ON FUZZY SET THEORY

2.1. Fuzzy sets, fuzzy relations and fuzzy matrices

2.2. Classification of higher education resources

2.3. Resource allocation optimization modeling

2.3.1. Selection of capital indicators

2.3.2. Multi-objective planning model

2.3.3. Optimization of the combination of production factors in higher education

2.3.4. A generative model of the optimized path

3. EXPERIMENTS AND ANALYSIS OF OPTIMAL PATHS UNDER THE FUZZY SET THEORY

3.1. Faculty staffing resources

3.2. Resource utilization efficiency

3.3. Resource allocation efficiency

4. CONCLUSION

DATA AVAILABILITY

CONFLICT OF INTEREST

REFERENCES

1. INTRODUCTION

Using fuzzy set theory to adjust the educational resource allocation model is the optimal path to achieve the allocation of educational resources. The optimal allocation of higher education resources in China refers to the integration and rational arrangement of educational resources in the area to be determined according to the principles of sustainability and resource sharing to achieve maximum benefits [1-4]. The priority allocation of educational resources is a condition and prerequisite for the development of education; without sufficient and compliant educational resources, the universalization of education and the improvement of educational standards cannot be discussed [5-9]. The allocation of educational resources reflects the degree of education adapting to social development in a certain period and also reflects the level of efficiency and fairness of education. Entering the era of the knowledge economy and talent competition, the development of colleges and universities affects all aspects of social and economic life, and the construction of talent in colleges and universities has been a problem that cannot be ignored in any country or region [10-11]. Educational activities consist of four factors, which are the objectives of educational activities, the basic principles or norms of educational activities, the conditions of educational activities, and the means of educational activities [12-14]. In summary, they can be divided into two categories: subjective factors and objective factors. Subjective factors include the goals and norms of educational activities, which are reflected in the meaning and value of educational activities [15-19]. Objective factors include the objective conditions and means of educational activities, which are the ways and means to achieve educational activities [20]. Higher education resource allocation reflects this characteristic. On the one hand, resource allocation is a subjective activity with strong purposefulness. On the other hand, it strictly depends on certain objective methods and is carried out with the help of certain means [21-23]. This is an important path in the analysis of higher education resource allocation and is of great significance for the study of the value theory of higher education resource allocation [24].

Fuzzy set theory is generally used to express inexact evaluation data and information in a fuzzy language in numerous decision problems with multiple attributes and multiple dimensions. This is because when solving decision problems, the use of fuzzy language can more accurately and efficiently reflect the information about the decision maker's preferences for each attribute in the decision solution. The literature [25] used fuzzy set theory to estimate the cognitive (or fuzzy) uncertainty that arises due to limited data samples when measuring small field output factors. The literature [26] conducted a questionnaire survey in which a total of 169 questionnaires were sent to participants using Google Forms based on the results of the literature review and interviews. The results of the linguistic fuzzy set approach identified three main conditions that influence the wage level in the automotive industry in Mexico City, including unskilled labor, the neoliberal economic model, and political and trade reforms. On the other hand, organizational conditions were not considered relevant for determining wage levels. Based on the findings, several recommendations were made. The literature [27] explored all necessary and sufficient combinations of the

presence or absence of outcomes in the fuzzy dataset. Necessary causal conditions are those that produce an outcome, while sufficient combinations are those that always lead to a given outcome. Many face images feature extraction and dimensionality reduction algorithms, such as local graph embedding-based algorithms or fuzzy set algorithms, have been proposed in the literature [28] for linear and nonlinear data. However, the above algorithms are not very effective for face images because they always suffer from overlaps (outliers) and sparse points in the database. To solve these problems, a new effective dimensionality reduction method for face recognition is proposed: sparse graph embedding fuzzy sets for image classification. The purpose of this algorithm is to construct two new fuzzy Laplace scattering matrices using local graph embedding and fuzzy k-nearest neighbors. Finally, the optimal discriminative sparse projection matrix is obtained by adding elastic network regression. Many problems have been solved in the above literature using the basic theory of fuzzy sets with good results.

The construction of human resources education in colleges and universities has become a problem that cannot be ignored in any country or region. To be able to use resource allocation optimization to solve education construction problems, this study uses the basic theory of fuzzy sets and analyzes dynamic fuzzy set theory, fuzzy relations and fuzzy matrix. It elaborates to give specific higher education resource classification, and selects indicators for optimal allocation of education resources in Chinese universities according to education resource classification. And design the fuzzy set multi-objective planning model according to the known allocation indexes, and finally realize the combination optimization of higher education production factors and determine the optimal path of higher education resources allocation based on fuzzy set theory. Integrating fuzzy set theory into the construction of the optimal path of resource allocation can not only provide a theoretical basis for solving the dynamic fuzzy problem and create an important path for the value analysis of college teaching evaluation but also lay the foundation for the value theory research of college teaching evaluation.

2. A PATH GENERATION MODEL FOR RESOURCE ALLOCATION OPTIMIZATION BASED ON FUZZY SET THEORY

2.1. FUZZY SETS, FUZZY RELATIONS AND FUZZY MATRICES

Let a map be defined on the domain U of the argument:

$$\left(\overleftarrow{A}, \overrightarrow{A} \right) : \left(\overleftarrow{U}, \overrightarrow{U} \right) \rightarrow [0,1] \times [\leftarrow, \rightarrow], \left(\overleftarrow{u}, \overrightarrow{u} \right) \rightarrow \left(\overleftarrow{A} \left(\overleftarrow{u} \right), \overrightarrow{A} \left(\overrightarrow{u} \right) \right) \quad (1)$$

Recorded as:

$$\left(\overleftarrow{A}, \overrightarrow{A} \right) = \overleftarrow{A} or \overrightarrow{A} \quad (2)$$

Then call $(\overleftarrow{A}, \overrightarrow{A})$ the fuzzy set on $(\overleftarrow{U}, \overrightarrow{U})$, or *DFS* for short, and call $(\overleftarrow{A}(\overleftarrow{u}), \overrightarrow{A}(\overrightarrow{u}))$ the subordination of the subordination function to $(\overleftarrow{A}, \overrightarrow{A})$.

Note: Any number $a \in [0,1]$, can be fuzzy a to

$a \stackrel{DF}{=} (\overleftarrow{a}, \overrightarrow{a})$, $a \stackrel{DF}{=} \overleftarrow{a}$ or \overrightarrow{a} , $\max(\overleftarrow{a}, \overrightarrow{a}) \triangleq \overrightarrow{a}$, $\min(\overleftarrow{a}, \overrightarrow{a}) \triangleq \overleftarrow{a}$. So that we can visualize the development trend of a the state. If the teaching quality is good, it means good or bad, good means good teaching quality but with a downward trend, and bad means bad teaching quality and with an upward trend. The fuzzy theory can not only represent the fuzzy degree of the data but also can visualize the trend of the fuzzy data.

There can be more than one *DF*-set on the theoretical domain U , and the whole of the *DF*-set U is $DF(U)$ as shown in Equation (3):

$$\begin{aligned} DF(U) &= \left\{ (\overleftarrow{A}, \overrightarrow{A}) \mid (\overleftarrow{A}, \overrightarrow{A}), (\overleftarrow{u}, \overrightarrow{u}) \rightarrow [0,1] \times [\leftarrow, \rightarrow] \right\} \\ &= \left\{ (A \times (\leftarrow, \rightarrow)) \mid (A \times (\leftarrow, \rightarrow)), (u \times (\leftarrow, \rightarrow)) \rightarrow [0,1] \times [\leftarrow, \rightarrow] \right\} \end{aligned} \quad (3)$$

There is a one-to-one correspondence between fuzzy relations and fuzzy matrices, and fuzzy matrices are an important tool for studying fuzzy relations. Let $(\overleftarrow{X}, \overrightarrow{X})$ and $(\overleftarrow{Y}, \overrightarrow{Y})$ are both fuzzy data, then the relationship between $(\overleftarrow{X}, \overrightarrow{X})$ and $(\overleftarrow{Y}, \overrightarrow{Y})$ is defined as follows:

If equation (4) holds, then $(\overleftarrow{R}, \overrightarrow{R})$ is a type *L* type *DF* relation from $(\overleftarrow{X}, \overrightarrow{X})$ to $(\overleftarrow{Y}, \overrightarrow{Y})$.

$$(\overleftarrow{R}, \overrightarrow{R}) \in DF_L(\overleftarrow{X}, \overrightarrow{X}) \times (\overleftarrow{Y}, \overrightarrow{Y}) \quad (4)$$

If equation (5) holds, then $(\overleftarrow{R}, \overrightarrow{R})$ is the *DF* relation from $(\overleftarrow{X}, \overrightarrow{X})$ to $(\overleftarrow{Y}, \overrightarrow{Y})$.

$$L = \left[(\overleftarrow{0}, \overrightarrow{0}), (\overleftarrow{1}, \overrightarrow{1}) \right] \quad (5)$$

Let the *DF*-relationship from $(\overleftarrow{X}, \overrightarrow{X})$ to $(\overleftarrow{Y}, \overrightarrow{Y})$ be a *DF*-matrix and expressed as Equation (6).

$$\left\{ (\overleftarrow{X}_n, \overrightarrow{X}_n) \right\}, (\overleftarrow{Y}, \overrightarrow{Y}) = \left\{ (\overleftarrow{y}_1, \overrightarrow{y}_1), \dots, (\overleftarrow{y}_n, \overrightarrow{y}_n) \right\} \quad (6)$$

2.2. CLASSIFICATION OF HIGHER EDUCATION RESOURCES

All the elements that can play an influence and role in the allocation of educational resources in higher education can become educational resources, and their content

composition is relatively complex and can be classified according to their different qualities. As shown in Table 1.

Table 1. Classification of higher education resources

| Classification category | Higher education resources |
|-------------------------|----------------------------|
| Own attribute | Land space resources |
| | Financial resources |
| | Equipment resources |
| | Time resources |
| | Human resources |
| | Information resources |
| Existential form | Dominant resources |
| | Recessive resources |
| Time node | Traditional resources |
| | Real resources |
| | Future resources |

The higher education resources under different classification levels are detailed below:

1. Land and space resources: Land and space resources are the most traditional resources and the most basic elements that enable education and teaching to take place. It mainly includes natural resources such as suitable teaching land and teaching space [29-30]. However, with the development of the times and the advancement of network technology, its basic role has not changed but its importance is weakening.
2. Financial and material resources: The progress of all disciplines needs financial and material support. Financial resources refer to the financial investment to support the development of university education, including research funds and public funds. Financial resources are characterized by the diversity of sources, continuity of supply and professionalism of management. Physical resources refer to all material elements that support the development of university education, including teaching places, libraries, dormitory buildings, logistic facilities and so on. There are man-made and natural physical resources, and this paper refers to physical resources in a narrow sense.
3. Equipment resources: This resource refers to the sum of various teaching equipment that assists teaching and learning to be carried out effectively, with the characteristics of the times, and the complete teaching equipment has begun to play and will continue to play its important role in today's teaching. Equipment resources mainly include advanced multimedia teaching facilities, abundant library

materials and retrieval equipment, experimental equipment, etc. It provides more possibilities for the development of big data teaching.

4. Time resources: Time resources are a more important factor than space resources because they control the trajectory of all human development, and time is also our wealth. The improvement of an idea is an accumulative process, so time and resources must play a very important role and are one of important factors for educational development.
5. Human resources: Broadly speaking, it refers to all the people involved in the educational process to achieve the educational goals, including the implementers of the goals and the goal bearers. For example, teachers, counselors, administrators and all students in the university.
6. Information resources: Information resources are the collective term for all information that has a positive impact on the achievement of educational purposes and can be used. Educational information resources are characterized by the wide range of sources, the timeliness of dissemination, and the comprehensiveness of content.
7. Explicit resources: Explicit resources are all the public and direct educational processes conducted by education for college students. They undertake the main task of systematic and formalized teaching, and the theoretical nature of the information they contain cannot be replaced by other resources.
8. Implicit resources: Implicit resources generally refer to all the resources that have indirect educational effects on students in education. Generally speaking, we call all resources other than "two courses" teaching in colleges and universities that can have a positive effect on the improvement of students' thinking level as hidden educational resources in colleges and universities.
9. Traditional resources: Traditional resources refer to the rich human heritage that has been accumulated in history and can be utilized by educational disciplines. Our traditional culture is extremely rich and provides a constant source of cultural support and inspiration for educational teaching.
10. Realistic resources: Realistic resources are the general term for the resources that are updated from the traditional resources in the context of the new era. Real resources generally cover the healthy spiritual achievements formed in the process of socialist modernization.
11. Future resources: Future resources are the sum of all resources that will be needed and used by the future society and can be predicted to be used in education and teaching. With the acceleration of globalization, the exchange of information is everywhere, and the earth has become a "village", which creates conditions for the exchange of educational resources between countries of different regions.

2.3. RESOURCE ALLOCATION OPTIMIZATION MODELING

2.3.1. SELECTION OF CAPITAL INDICATORS

In this paper, we measure the efficiency of educational resources allocation in colleges and universities according to the attributes of Chinese educational resources in 2.2.1 and finally determine six indicators: x_1 teacher-student ratio (%), x_2 average management-teacher ratio (%), x_3 the total value of teaching instruments and equipment assets (million yuan), x_4 the average amount of special funds invested (million yuan), x_5 the average area of practice platform room (m²) and x_6 average area of the educational base (m²). To quantify the allocation efficiency, the values of the above indicators are used to calculate the resource utilization efficiency of universities, and the calculation formula is shown in Equation (8):

$$S = C_1 * \underline{A}_1 + C_2 * \underline{A}_2 + C_3 * \underline{A}_3 + C_4 * \underline{A}_4 + C_5 * \underline{A}_5 + C_6 * \underline{A}_6 \quad (7)$$

where \underline{A}_i is the rating of A_i and c_i is ($i = 1, 2, \dots, 6$). Since the determination of weights is subjectively influenced by individuals, this paper de-quantifies some indicators and establishes a fuzzy set multi-objective planning model.

2.3.2. MULTI-OBJECTIVE PLANNING MODEL

According to the fuzzy set correlation theory in Section 2.1, suppose $f(x) = (f_1(x), f_2(x), \dots, f_9(x))$ denotes the vector of objective functions of nine indicators of higher education resources, and $g(x) = (g_1(x), g_2(x), \dots, g_9(x))$ denotes the vector of constraint functions of each indicator. The problem of optimal allocation of resources can be transformed into the following fuzzy set planning model, as shown in Equation (9):

$$\max = \{ (Z_1 = f_1(x), Z_2 = f_2(x), \dots, Z_9 = f_9(x)) \} \quad (8)$$

In the feasible domain as shown in Eq. (10):

$$Z = \{ z \in R^n \mid z_1 = f_1(x), z_2 = f_2(x), \dots, z_9 = f_9(x) \} \quad (9)$$

where S^m is the feasible domain of decision space and R^n is the feasible domain of target space.

2.3.3. OPTIMIZATION OF THE COMBINATION OF PRODUCTION FACTORS IN HIGHER EDUCATION

Higher education resources are influenced by multiple factors such as time, geography and social structure, and the problem of their allocation is not a simple linear distribution. Among the factors of production, quality is the life and ultimate measure of higher education, and its ultimate goal is to maximize the benefits in terms of student output, knowledge output and social output. Assuming that z is the quantity of educational output and x is the different forms of the factors, then:

$$P = \sum_{j=1}^m Z_j / \sum_{i=1}^n X_i \quad (10)$$

Where, P , X and Z_j denote the input-output ratio, the combination of different educational factors and the quantity of educational output respectively. From the above equation, it can be seen that when P is larger, the combination of educational production factors is more reasonable, so the combination with the largest input-output ratio should be selected. However, at the same time, as the input increases, the cost of education will also increase. Therefore, it is also necessary to consider the cost issue.

2.3.4. A GENERATIVE MODEL OF THE OPTIMIZED PATH

The objective function is obtained from the above analysis as:

$$\max R_1 = \sum_{i=1}^n x_f / \sum_{i=1}^n y_f \quad \max R_2 = \sum_{i=1}^n y_f / \sum_{i=1}^n z_f \quad \max R_3 = \sum_{i=1}^n D_f / \sum_{i=1}^n y_f \quad (11)$$

$$\max R_4 = \sum_{i=1}^n E_f / \sum_{i=1}^n y_f \quad \max R_5 = \sum_{i=1}^n F_f / \sum_{i=1}^n x_f \quad \max R_6 = \sum_{i=1}^n x_f \quad (12)$$

Where: $X_{uv}, Y_{uv}, D_{uv}, E_{uv}, F_{uv}, H_{uv} \geq 0, \forall uv$ The following constraints should be satisfied at the same time:

$$\text{S.t. } \alpha_{11} \leq \sum_{i=1}^{n_j} x_{ij} \leq \alpha_{12} \quad \alpha_{21} \leq \sum_{i=1}^{n_j} y_{ij} \leq \alpha_{22} \quad \alpha_{31} \leq \sum_{i=1}^{n_j} y_{ij} \leq \alpha_{32} \quad (13)$$

$$\alpha_{41} \leq \sum_{i=1}^{n_j} y_{ij} \leq \alpha_{42} \quad \alpha_{51} \leq \sum_{i=1}^{n_j} y_{ij} \leq \alpha_{52} \quad (14)$$

The above model is developed for each indicator of higher education in China. Where, n_j denotes the number of colleges and universities in j regions, and other indicators in j regions are represented by annual totals \sum . The different meanings of these optimization indicators are represented in Table 2.

Table 2. Representative meanings of optimization path indicators based on fuzzy set theory

| Value of U | Representative meaning |
|------------|--|
| X | Total number of students in school |
| Y | Total number of annual management teachers |
| Z | Total assets of teaching instruments and equipment |
| D | Annual special fund input |
| E | Annual floor area of practice platform |
| F | Annual education base area |

3. EXPERIMENTS AND ANALYSIS OF OPTIMAL PATHS UNDER THE FUZZY SET THEORY

Six excellent colleges and universities and six general local colleges and universities in a province are used as research samples to integrate the optimization objective functions and constraints of multi-objective higher education resource allocation in China. The multi-objective planning model based on fuzzy set theory is used to calculate the optimal path of the combination of higher education production factors. When the configuration optimization model tends to be stable and the fitness function tends to the minimum value, the six sets of optimal paths obtained at this time are shown in Table 3. The optimal paths 1-3 indicate the highest efficiency of educational resource utilization and allocation when the educational resources of general colleges and universities are allocated in such a ratio. The optimal paths 4-6 indicate that when the educational resources of excellent colleges and universities are allocated in this way, the educational resources are used and allocated with the highest efficiency.

Table 3. Optimization path of higher education resource allocation in China based on fuzzy set theory

| Measurable index | Optimal path 1 | Optimal path 2 | Optimal path 3 | Optimal path 4 | Optimal path 5 | Optimal path 6 |
|---|----------------|----------------|----------------|----------------|----------------|----------------|
| Teacher student ratio/% | 1:220 | 1:215 | 1:213 | 1:201 | 1:198 | 1:189 |
| Ratio of management teachers per student/% | 1:320 | 1:311 | 1:300 | 1:298 | 1:290 | 1:287 |
| Total assets of teaching instruments and equipment per student/10000 yuan | 0.0895 | 0.0845 | 0.0823 | 0.0811 | 0.0802 | 0.0800 |
| Special fund input per student/10000 yuan | 0.0095 | 0.0091 | 0.0084 | 0.0082 | 0.0080 | 0.0071 |
| Room area of practice platform per student/m ² | 1.15203 | 1.15201 | 1.15198 | 1.15186 | 1.15166 | 1.1502 |
| Area of education base per student/m ² | 0.3860 | 0.3854 | 0.3823 | 0.3811 | 0.3802 | 0.3799 |

To illustrate the positive utility of the optimization path in depth, further analysis is conducted in three aspects: faculty staffing resources, resource utilization efficiency, and resource allocation efficiency, respectively.

3.1. FACULTY STAFFING RESOURCES

To be able to use resource allocation optimization to solve the problem of equipping resources for faculty in educational construction, the average number and structure of faculty in educational resource allocation in 12 universities were analyzed according

to the classification of higher education resources using the resource allocation optimization model of fuzzy set theory, and the following analysis results were obtained:

1. In terms of the overall number of teaching and research staff on board and the number of different titles, the total number of teaching and research staff has steadily increased from 2017 to 2021, and the number of the four titles has tended to stabilize. Among them, the number of associate professors tends to increase slightly, the number of professors and lecturers remains unchanged, and the number of assistant professors gradually decreases, as shown in Figure 1.

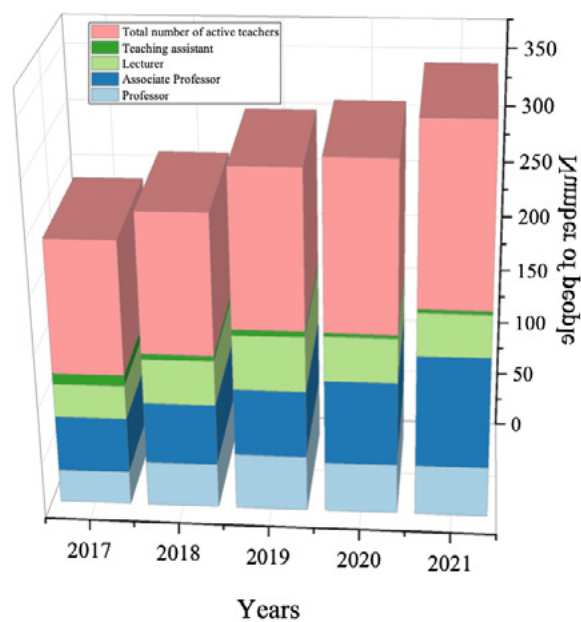


Figure 1. Statistics on the number of active teaching and research staff in the optimization path

2. The situation of student-teacher ratio shows a general downward trend. Due to the adjustment of enrollment policy, it leads to the increase in the number of undergraduate and master students in 2018-2019, while it returns to a stable state in 2020, and the student-teacher ratio decreases to 20:1. The ratio of the total number of graduate students to the total number of professors and associate professors decreases to 15:1 from more than 20:1 in previous years. The ratio of doctoral students to professors is higher than 20, which is caused by the expansion of universities in the early stage on the one hand, and the lack of faculty on the other hand. The ratio of Ph.D. The specific situation is shown in Table 4.

Table 4. Percentage of students and faculty under the optimized pathway (Unit:%)

| | Student-teacher ratio | Ratio of students to the number of professors, associate professors and lecturers | Ratio of graduate students to the number of professors and associate professors | Ratio of the number of doctoral students to professors |
|------|-----------------------|---|---|--|
| 2017 | 23 | 22 | 25 | 21 |
| 2018 | 23 | 22 | 20 | 23 |
| 2019 | 21 | 24 | 22 | 25 |
| 2020 | 20 | 23 | 25 | 21 |
| 2021 | 22 | 25 | 20 | 22 |

3. In terms of the title structure of the active faculty and researchers, the share of professors remained unchanged from 2017 to early 2021, the share of associate professors increased, while the share of lecturers and assistant professors decreased. The details are shown in Table 5.

Table 5. Structure of teaching and research staff titles in the optimization path (unit:%)

| | Professor | Associate Professor | Lecturer | Teaching Assistants |
|------|-----------|---------------------|----------|---------------------|
| 2017 | 0.25 | 0.38 | 0.25 | 0.08 |
| 2018 | 0.27 | 0.38 | 0.26 | 0.07 |
| 2019 | 0.27 | 0.38 | 0.25 | 0.09 |
| 2020 | 0.27 | 0.45 | 0.26 | 0.07 |
| 2021 | 0.25 | 0.38 | 0.25 | 0.07 |

4. In terms of the academic structure of the teaching and research staff in post, as shown in Figure 2, 67% of the total number of teaching and research staff have doctoral degrees. Among them, 56% of the professors have Ph. D.s, 72% of the associate professors and 80% of the lecturers. Since the current policy stipulates that faculty and researchers who stay in the university must have a doctoral degree, the academic structure at the beginning of 2021.

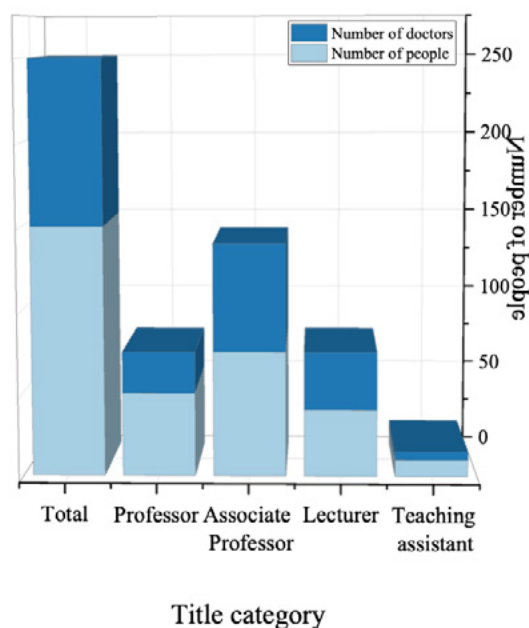


Figure 2. Statistics on the educational structure of faculty and researchers in the optimization path

5. Looking at the age structure of the faculty and research staff with a reasonable allocation of higher education resources in China, it is shown in Figure 3. 46% of the faculty and research staff are less than 40 years old. Thirty-five percent of the teaching and research staff are between 40 and 50 years old, and only 15% of them are older than 50 years old, and they are mainly professors. Professors are all older than 40 years old, and 50% of them are older than 50 years old. The age of associate professors is mainly below 50 years old, among which 46% and 47% of associate professors are above and below 40 years old respectively. Lecturers and assistant professors are relatively younger, generally under 40 years old. In terms of age structure, the age distribution is relatively reasonable.

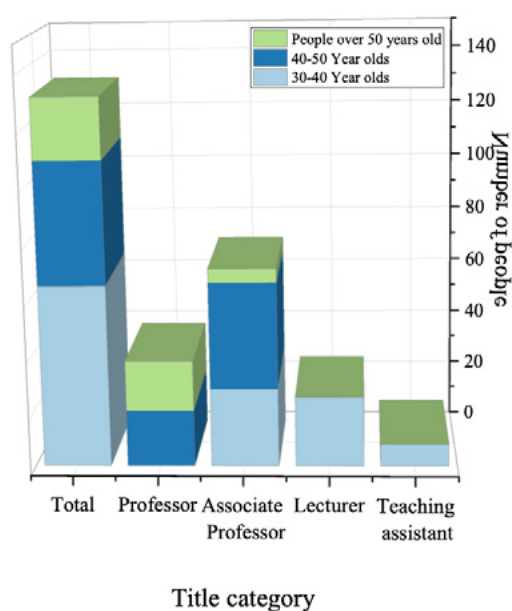


Figure 3. Statistics on the age structure of faculty and researchers in the optimization path

6. The gender structure of in-service Chinese higher education researchers with reasonable resource allocation is shown in Figure 4. Women account for 35%. Among them, 21% of professors are female, 40% of both associate professors and lecturers are female, and 33% of assistant professors are female.

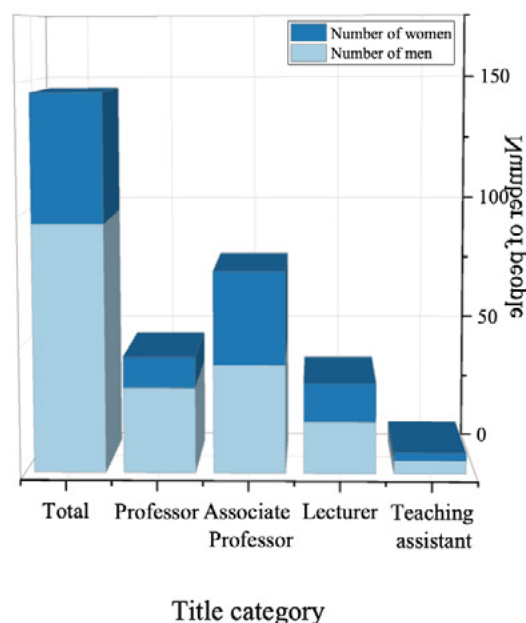
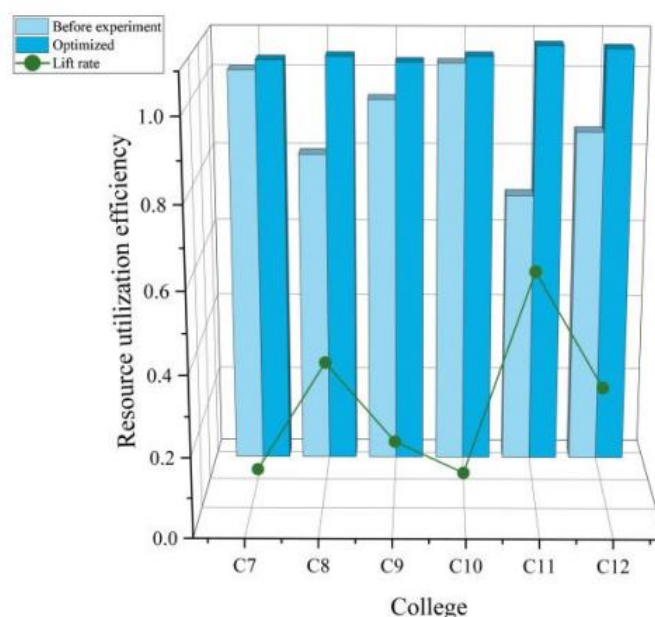


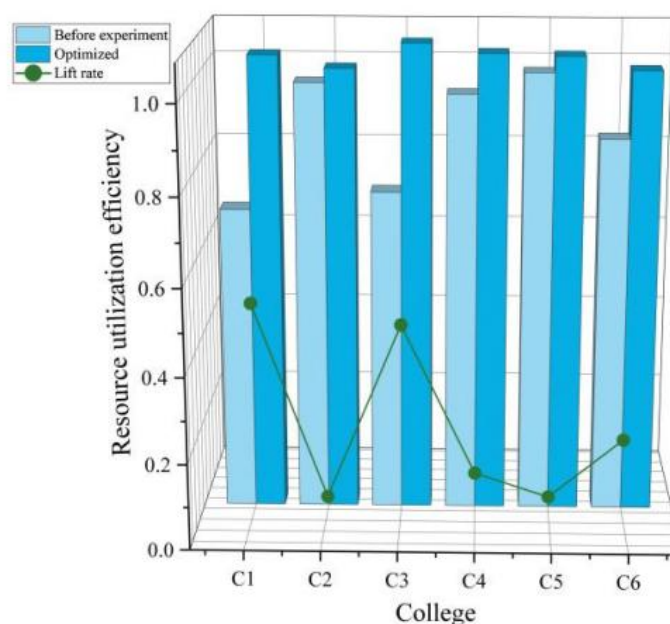
Figure 4. Statistics on the gender structure of Faculty and Researchers in the optimization path

3.2. RESOURCE UTILIZATION EFFICIENCY

Six excellent universities and six general local universities in a province were used as the research samples, and the data of China's higher education resources from 2017-2021 were counted. To verify whether the resource allocation optimization path generated by the fuzzy set multi-objective planning model improves the resource utilization efficiency, optimal path 1 and optimal path 3 are used as examples for the analysis of experimental results. According to the calculation of the resource utilization efficiency of each university before and after the experiment, it is found that the resource utilization efficiency of each university before and after the experiment has improved, with an average increase of 18.25%, and the resource utilization efficiency of each university tends to be in a balanced state. The experimental resource utilization efficiency of excellent schools is shown in Figure 5(a), and the resource utilization rate of ordinary colleges and universities is shown in Figure 5(b). The resource utilization efficiency of excellent colleges and universities and general colleges and universities are improved from 48.302 and 0.523 before optimization to 1.057 and 1.068, respectively, with an improvement rate of 32.3% and 52.4%. It can be found that the resource utilization rate of ordinary colleges and universities is generally higher than that of excellent colleges and universities, which indicates that resource allocation optimization is more useful for ordinary colleges and universities with scarce resources.



(a) Resource utilization rate of excellent universities



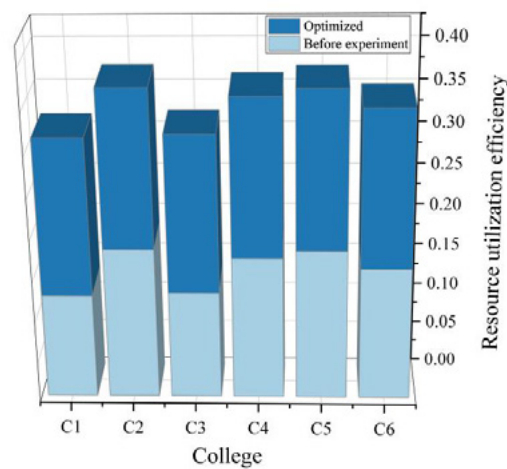
(b) Resource utilization rate of general universities

Figure 5. Comparison of resource utilization of universities before and after the implementation of the optimized path

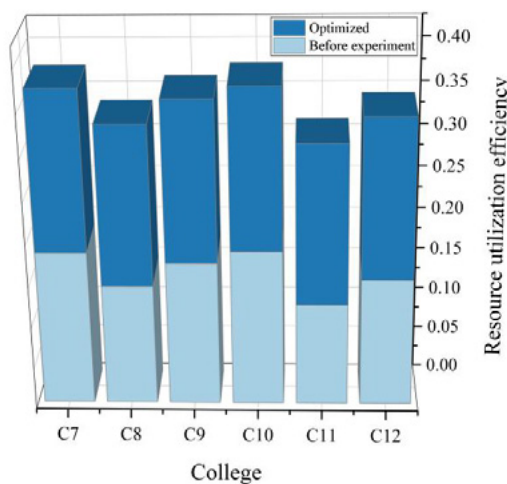
3.3. RESOURCE ALLOCATION EFFICIENCY

To verify whether the optimized paths generated by the fuzzy set multi-objective planning model improve the resource allocation efficiency, the overall resource allocation efficiency of the original data and the optimized allocation solutions (optimal path 1 and optimal path 3) of each university are calculated before and after

optimization, respectively. The resource allocation efficiency of excellent universities is shown in Figure 6(a), and the resource allocation efficiency of ordinary universities is shown in Figure 6(b).



(a) Excellent university resource allocation efficiency



(b) Resource allocation efficiency of general universities

Figure 6. Comparison of resource allocation efficiency of universities before and after the implementation of the optimized path

As can be seen from Figure 6, the difference in resource allocation efficiency between excellent universities and ordinary universities before implementing the optimized path is large, with a minimum value of 0.125 and the maximum value of 0.192. The average allocation efficiency of excellent universities after optimization is 0.186, with an average improvement of 35.41%. The average allocation efficiency of ordinary colleges and universities is 0.174, with an average increase of 22.12%. It can be found that the resource allocation efficiency of excellent colleges and universities is generally higher than that of ordinary colleges and universities, and after the optimization of college resource allocation, the role of excellent colleges and universities with more abundant resources themselves is greater. It indicates that

adjusting the quantity and structure of educational resources according to the optimization path can achieve the optimization of educational resource allocation.

4. CONCLUSION

Using fuzzy set theory to adjust the education resource allocation mode is the optimal path to achieve education resource allocation. This paper analyzes dynamic fuzzy set theory, dynamic fuzzy relationship and dynamic fuzzy matrix according to the basic theory of fuzzy sets. Combined with the classification of higher education resources, indicators for the optimal allocation of educational resources in Chinese universities are selected and a fuzzy set multi-objective planning model is designed. Based on the combination optimization form of higher education production factors and the fuzzy set multi-objective planning model, the fuzzy model for generating the optimal path is structured. The research results obtained are as follows:

1. The content composition of educational resources is relatively complex and can be classified according to their different qualities. First, according to the different attributes of ideological and political education resources, they can be classified into various kinds of resources with different attributes. Secondly, educational resources are classified into explicit resources and implicit resources according to their different forms of existence. Thirdly, according to the different times of their existence, they can be divided into traditional, real and future resources.
2. The average resources of excellent colleges and universities and the resource utilization efficiency of general colleges and universities are improved from 48.302 and 0.523 before optimization to 1.057 and 1.068, respectively, with an improvement rate of 32.3% and 52.4%. It can be found that the resource utilization efficiency of ordinary colleges and universities is generally higher than that of excellent colleges and universities, which indicates that resource allocation optimization is more useful for ordinary colleges and universities with scarce resources.
3. The average allocation efficiency of excellent colleges and universities is 0.186, and the average improvement after optimization is 35.41%. The average allocation efficiency of ordinary colleges and universities is 0.174, which is improved by 22.12% on average after optimization. It can be found that the resource allocation optimization path generated by the adjustment of the multi-objective planning model based on the fuzzy set theory makes the excellent colleges and universities with more abundant resources get higher resource allocation efficiency.

DATA AVAILABILITY

The data used to support the findings of this study are available from the corresponding author upon request.

CONFLICT OF INTEREST

The authors declare that the research was conducted in the absence of any commercial or financial relationships that could be construed as a potential conflict of interest.

REFERENCES

- (1) Cui, J. (2021). **Optimal allocation of higher education resources based on fuzzy particle swarm optimization.** *International Journal of Electrical Engineering Education*, 002072092098355.
- (2) Zhang, X., & Venkateswaran, N. (2022). **The Influence of Mobile Learning on the Optimization of Teaching Mode in Higher Education.** *Wireless Communications and Mobile Computing*.
- (3) Ahmed, A., Mateo-Garcia, M., Arewa, A., et al. (2021). **Integrated Performance Optimization of Higher Education Buildings Using Low-Energy Renovation Process and User Engagement.** *Energies*, 14(5), 1475.
- (4) Shao, C., & Li, Y. F. (2021). **Multistage Attack–Defense Graph Game Analysis for Protection Resources Allocation Optimization Against Cyber Attacks Considering Rationality Evolution.** *Risk Analysis*.
- (5) Liu, J., & Zhu, L. (2021). **Joint Resource Allocation Optimization of Wireless Sensor Network Based on Edge Computing.** *Complexity*.
- (6) Liu, B., Zhu, Q., & Zhu, H. (2020). **Trajectory optimization and resource allocation for UAV-assisted relaying communications.** *Wireless Networks*, 26(1), 739-749.
- (7) Baa, B., Bgk, A., Na, C., et al. (2020). **Application of binary PSO for public cloud resources allocation system of video on demand (VoD) services.** *Applied Soft Computing*.
- (8) Wang, Y., Shan, X., Wang, H., et al. (2022). **Ticket Allocation Optimization of Fuxing Train Based on Overcrowding Control: An Empirical Study from China.** *Sustainability*.
- (9) Yuan, Z., Chen, H., & Li, T. (2022). **Exploring interactive attribute reduction via fuzzy complementary entropy for unlabeled mixed data.** *Pattern Recognition*, 127.
- (10) Liang, G., Xu, L., & Chen, L. (2021). **Optimization of Enterprise Labor Resource Allocation Based on Quality Optimization Model.** *Complexity*, 2021(5), 1-10.
- (11) Jiang, L., & Wang, X. (2020). **Optimization of Online Teaching Quality Evaluation Model Based on Hierarchical PSO-BP Neural Network.** *Complexity*, 2020(7), 1-12.
- (12) Jitta, S. R., Bhaskaran, N. A., Salwa, et al. (2022). **Anti-oxidant Containing Nanostructured Lipid Carriers of Ritonavir: Development, Optimization, and In Vitro and In Vivo Evaluations.** *AAPS PharmSciTech*, 23(4), 1-15.
- (13) Liu X. (2022). **Optimization of College Students' Mental Health Education Based on Improved Intelligent Recognition Model.** *Mathematical Problems in Engineering*, 2022.

- (14) Wang, J., & Li, W. (2021). **The Construction of a Digital Resource Library of English for Higher Education Based on a Cloud Platform.** *Scientific Programming*, 2021, 2021, 1-12.
- (15) Sun, J., Li, H., Zeng, B., et al. (2020). **Parameter Optimization on the Three-Parameter Whitenization Grey Model and Its Application in Simulation and Prediction of Gross Enrollment Rate of Higher Education in China.** *Complexity*, 2020, 2020(1), 1-10.
- (16) Ghanbari-Adivi, E., Ehteram, M., Farrokhi, A., et al. (2022). **Combining Radial Basis Function Neural Network Models and Inclusive Multiple Models for Predicting Suspended Sediment Loads.** *Water Resources Management*, 36(11), 4313-4342.
- (17) Vinayaki, V. D., & Kalaiselvi, R. (2022). **Multithreshold Image Segmentation Technique Using Remora Optimization Algorithm for Diabetic Retinopathy Detection from Fundus Images.** *Neural Processing Letters*, 54(3), 2363-2384.
- (18) Wilson, P. K., & Jeba, J. R. (2022). **A developed framework for multi-document summarization using softmax regression and spider monkey optimization methods.** *Soft Computing*, 2022.
- (19) Tanji, K., Zouheir, M., Naciri, Y., et al. (2022). **Visible light photodegradation of blue basic 41 using cobalt doped ZnO: Box-Behnken optimization and DFT calculation.** *Journal of the Iranian Chemical Society*, 2022, 1-16.
- (20) Wang, J. B., Yang, H., Cheng, M., et al. (2020). **Joint Optimization of Offloading and Resources Allocation in Secure Mobile Edge Computing Systems.** *IEEE Transactions on Vehicular Technology*, PP(99), 1-1.
- (21) Suo, M., Xia, F., & Fan, Y. (2022). **A Fuzzy-Interval Dynamic Optimization Model for Regional Water Resources Allocation under Uncertainty.** *Sustainability*, 14.
- (22) Liu, Y., Dong, H., Wang, H., et al. (2021). **Multi-objective titanium alloy belt grinding parameters optimization oriented to resources allocation and environment.** *The International Journal of Advanced Manufacturing Technology*, 113(6), 1-15.
- (23) Singh, B. (2020). **Fairness criteria for allocating scarce resources.** *Optimization Letters*, 14(6), 1533-1541.
- (24) Naghdi, S., Bozorg-Haddad, O., Khorsandi, M., et al. (2021). **Multi-objective optimization for allocation of surface water and groundwater resources.** *Science of The Total Environment*, 776(12), 146026.
- (25) Chaudhary R K, Kumar R, Sharma S D, et al. (2021). **Computation of epistemic uncertainty due to limited data samples in small field dosimetry using Fuzzy Set Theory.** *British Journal of Radiology*, 94(1121), 20190561.
- (26) Lozano C, & Chiatchoua C. (2022). **Conditions Influencing Salary of the Automotive Industry in Mexico City—A Linguistic Fuzzy-Set Approach.** *Sustainability*, 14.
- (27) Liu H, Zhou Y, Zhang Y, et al. (2021). **A rough set fuzzy logic algorithm for visual tracking of blockchain logistics transportation labels.** *Journal of Intelligent and Fuzzy Systems*, 41(12), 1-8.
- (28) Liu F, Wu J, Mou L, et al. (2020). **Decision Support Methodology Based on Covering-Based Interval-Valued Pythagorean Fuzzy Rough Set Model and**

Its Application to Hospital Open-Source EHRs System Selection.*Mathematical Problems in Engineering*, 2020.

- (29) Frayssinet, M., Esenarro, D., Juárez, F. F., & Díaz, M. (2021). **Methodology based on the NIST cybersecurity framework as a proposal for cybersecurity management in government organizations.** *3C TIC. Cuadernos de desarrollo aplicados a las TIC*, 10(2), 123-141. <https://doi.org/10.17993/3ctic.2021.102.123-141>
- (30) Guo, Z., & Alghazzawi, D. M. (2021). **Optimal solution of fractional differential equations in solving the relief of college students' mental obstacles.** *Applied Mathematics and Nonlinear Sciences*, 7(1), 353-360. <https://doi.org/10.2478/AMNS.2021.1.00095>

/16/

QUANTIZATION AND APPLICATION OF LOW-RANK TENSOR DECOMPOSITION BASED ON THE DEEP LEARNING MODEL

Jia Zhao*

- 1.- School of Tourism, Shanghai Normal University, Shanghai, 200234, China.
- 2.- School of Hospitality and Culinary Arts Management, Shanghai Institute of Tourism, Shanghai, 201418, China.

vivienne_yangyu@163.com



Reception: 20/11/2022 **Acceptance:** 13/01/2023 **Publication:** 27/02/2023

Suggested citation:

Z., Jia. (2023). **Quantization and application of low-rank tensor decomposition based on the deep learning model.** *3C TIC. Cuadernos de desarrollo aplicados a las TIC*, 12(1), 330-350. <https://doi.org/10.17993/3ctic.2023.121.330-350>

ABSTRACT

Watching the presentation of a large-scale network is very important for network state tracking, performance optimization, traffic engineering, anomaly detection, fault analysis, etc. In this paper, we try to develop deep learning technology to solve the defect problem of tensor filling based on inner product interaction. To solve the limitations of the existing tensor-filling algorithms, a new neural tensor-filling (NTC) model is proposed. NTC model can effectively type the third-order communication between data landscapes through outer creation operation. It creates the third-order interaction mapping tensor. On this basis, the interaction between local features of the 3D neural network is studied. In this paper, another fusion neural tensor filling (Fu NTC) model is proposed to solve the problem that the NTC model can only extract the nonlinear complex structural information between potential feature dimensions. In the framework of the neural network, the NTC model and tensor decomposition model share the same potential feature embedding. It can effectively extract nonlinear feature information and linear feature information at the same time. It achieves higher precision data recovery.

KEYWORDS

Tensor filling; Sparse network monitoring; Deep learning; matrix; modeling

PAPER INDEX

ABSTRACT

KEYWORDS

1. INTRODUCTION

2. NEURAL TENSOR FILLING MODEL FOR PRECISE NETWORK MONITORING

2.1. description of the NTC model

2.2. detail of the NTC model

2.3. theoretical analysis

2.4. 2.4 experimental simulation of the real data set

2.5. Real network platform experiment

3. FUSION NEURAL TENSOR FILLING MODEL FOR MORE COMPREHENSIVE FEATURE EXTRACTION

3.1. solution overview

3.2. detail of Fu NTC model

3.3. real data set experimental simulation

3.4. real network platform experiment

4. SUMMARY

5. DATA AVAILABILITY

6. CONFLICT OF INTEREST

REFERENCES

1. INTRODUCTION

The rapid development and wide application of modern multimedia technology and information science. We need a higher level of technology to achieve data collection, storage, processing, and analysis. Massive data brings convenience to our life. Its scale is increasing. Its structure is becoming more and more complex. The data we collected may be incomplete. In addition, in the recommendation system, we also need to use the known data to infer the unknown data[1]. It can also be transformed into the problem of missing data recovery.

The estimation of missing values from the very limited information of an unknown matrix has attracted extensive attention in many fields. In practical applications, the target matrix is usually low rank or approximately low rank. For example, natural image data has a low-rank structure [2]. Therefore, a hypothesis is often used in the matrix filling: the matrix to be restored as a low-rank or near-low-rank structure [3-5]. The above problem is called the rank minimization problem [6]. Because the rank function is nonconvex and discontinuous. The solution to the above problem is the NPHard problem [7]. The original algorithm which can calculate the lowest rank solution of all instances needs at least an exponential time of matrix dimension [8]. In reference [9], Wei et al. Proposed two heuristic algorithms for approximate RMP based on convex optimization. And it proved that the kernel norm (i.e., the sum of singular values). The heuristic method is optimal in the sense of minimizing the convex envelope of rank functions. Subsequently, a series of theoretical studies were carried out to prove that. The kernel norm is a good convex proxy for the minimization of rank functions [10]. Yang et al. [11] proved that the kernel norm is the most compact convex lower bound of the rank function. And the relationship between kernel norm and matrix rank is similar to that between the L1 norm and l0 norm of the vector. Therefore, many scholars have implemented the rank kernel function as a surrogate matrix. The fixed-point extension and approximate singular value decomposition algorithm for solving the rank minimization problem of large-scale matrices [12] proposed by Qiao et al. Ahn et al. Provide a boundary for the number of elements needed to reconstruct a low-rank matrix. It is optimal in the range of a small numerical constant and a logarithmic factor [13-15]. In addition, some studies have shown that, under certain constraints, the minimum kernel norm can be filled by partial observation elements of the matrix [16].

The kernel norm minimization problem was first proposed. One of the most advanced semi-definite programming algorithms, to solve the problem. The algorithm is based on the interior point method. It needs to solve a large number of linear equations to calculate Newton's direction. When the matrix scale is large. The algorithm is not suitable. Ai proposed the singular value threshold algorithm (SVT) for the approximate solution of the kernel norm minimization problem in 2010. It proved that the method is suitable for large-scale matrix-filling problems [17]. In addition, Saeedi et al. Proposed a fast approximate gradient descent method for solving kernel norm regularized linear least squares problems [18]. In practical applications, the above-mentioned kernel norm algorithm and some other kernel norm algorithms may only obtain suboptimal solutions. A large number of iterative converge is required [19].

An important reason for this is that the kernel norm cannot approximate the rank function well in practical applications. Specifically, in the rank function, all non-zero singular values are treated equally. The kernel norm is to add all singular values. It leads to different singular values in the process of optimization. In addition, the theoretical requirements of heuristic kernel norms are difficult to meet in practical applications [20]. Therefore, some kernel norm extension algorithms have been proposed. Zhang et al. Used joint minimization of Schatten PNorm and LPNorm is used to recover the incomplete noise matrix. And it is applied to actual scenarios such as collaborative filtering and social network link prediction in the recommendation system [21]. CHEN et al. Proposed to use truncated kernel norm to better approximate matrix rank function. The truncated kernel norm is obtained by subtracting the sum of the largest singular values from the kernel norm [22]. At the same time, a new matrix-filling algorithm is proposed to minimize the truncated kernel norm of the matrix. At the same time, three effective iterative algorithms are developed to solve the truncated kernel norm minimization model: TNNRADMM、TNNRAPGL、TNNRADMMAP. The first type (TNNRADMM is an alternative multiplier method (ADMM). Firstly, according to a new ADMM update rule, the adaptive penalty parameter is used to accelerate the convergence speed. Among them, the ADMM method has also been widely used in image processing, such as non-local low-rank regularization [23] compressed sensing and matrix decomposition based on dual kernel norm for occluded image restoration [24], imprecise low rank and structural sparse decomposition [25]. Subsequently, the TNN algorithm has been successfully applied in many fields by many scholars. Liu et al. Proposed a matrix-filling TNN algorithm based on weighted residuals [26]. Liu proposed a more efficient TNN algorithm to deal with the matrix filling of high dynamic range images [27]. In addition, the reference research [28] further shows that TNN can be used as a better alternative to the rank function.

In the field of computer vision and signal processing, a large number of multidimensional data need to be analyzed and processed. In particular, multidimensional arrays (i.e., tensors) provide a natural representation of these data. Tensor is considered a generalization of a multivariate linear matrix or vector. Since tensor is a mathematical model which can establish multi-dimensional data structure. The study and research of tensors have attracted great attention. In recent years, more and more people use it in computer vision [29], machine learning [30], signal processing [31], pattern recognition [32], and other fields. However, due to technical limitations, the tensors we observe in real life are usually incomplete. It makes the application of tensors a challenging problem.

Because of previous studies, the goal of this paper is to recover the original data from partially lost observation matrix and tensor data. And apply them to practical applications, such as spectral data recovery, image/video data, text analysis, multitask learning, recommendation system, etc.

2. NEURAL TENSOR FILLING MODEL FOR PRECISE NETWORK MONITORING

In the modern data center, there are tens of thousands of servers. And the network scale is constantly expanding. Network monitoring, monitoring equipment, and communication costs will be a huge challenge. To effectively reduce the measurement cost. It measures the network performance data of some nodes and paths. It reconstructs other unmeasured networks. Therefore, in the case of sampling. How to reconstruct and infer the unmeasured network performance data. And how to ensure the push. The accuracy of measurement has become a prominent problem in network monitoring.

2.1. DESCRIPTION OF THE NTC MODEL

To solve the limitations of the existing tensor filling algorithms. A new neural tensor filling (NTC) model is proposed. The multi-layer architecture is adopted. And the output of the previous layer is used as the input of the next layer to model the source node target node time interaction. **Figure.1** is the overall framework of the NTC model. From bottom to top, there are five main functional modules: input sheet, inserting layer, interactive mapping sheet, feature abstraction layer, and prediction layer.

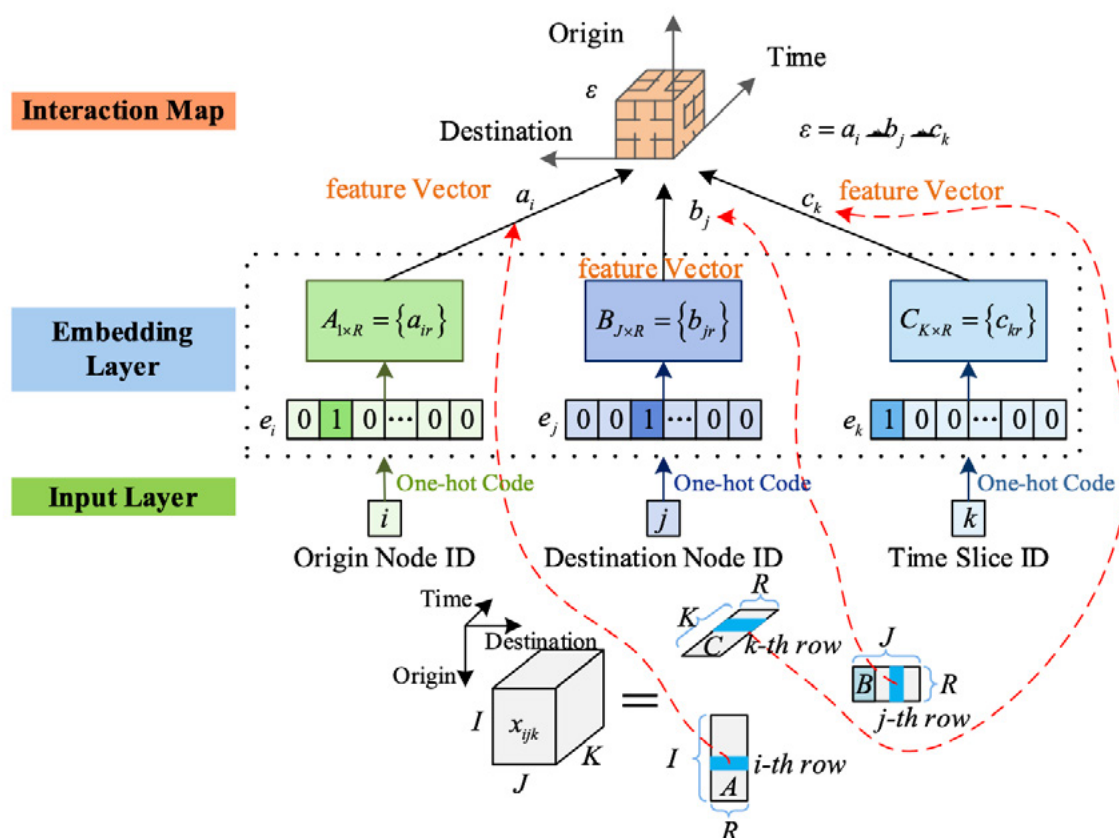


Figure 1. The overall framework of the NTC model

At the lowest input sheet, there are three indicator vectors e_i, e_j, e_k . The source node i , target node j , and moment hole k are described separately. Next, the embedded sheet is fully associated. It designs the source node, target node, and time hole onto a feature direction respectively.

$$\min_{\mathbf{A}, \mathbf{B}, \mathbf{C}, \Theta_f^C, \Theta_f^M} \sum_{i,j,k \in \Omega} \left(x_{ijk} - f(\mathbf{e}_i \mathbf{A}, \mathbf{e}_j \mathbf{B}, \mathbf{e}_k \mathbf{C} \Theta_f^C, \Theta_f^M) \right)^2 + \alpha \|\mathbf{A}\| + \beta \|\mathbf{B}\| + \gamma \|\mathbf{C}\| \quad (1)$$

Among them, $\mathbf{A} \in R^{I \times R}$, $\mathbf{B} \in R^{J \times R}$, $\mathbf{C} \in R^{K \times R}$. The potential characteristic matrix represents the source node, target node, and time respectively. e_i, e_j and e_k is a unique hot code vector indicating the source node i , the target node j , and the time slot k , respectively. α, β and γ is the regularization coefficient.

2.2. DETAIL OF THE NTC MODEL

Inspired by this, the input and embedding layers of a neural network are designed to obtain a potential eigenvector of the source node, target node, and time slot. Given the ID of the source node i , target node j , and slot k , their embedding vectors can be obtained by the formula a_i, b_j and c_k :

$$\mathbf{a}_i = \mathbf{e}_i \mathbf{A}, \mathbf{b}_j = \mathbf{e}_j \mathbf{B}, \mathbf{c}_k = \mathbf{e}_k \mathbf{C} \quad (2)$$

Among them, $e_i \in R^{1 \times I}$, $e_j \in R^{1 \times J}$ and $e_k \in R^{1 \times K}$. The unique hot ID indication vectors of the source node i , target node j , and slot k are represented respectively. On top of the embedded layer, 3D interactive mapping is recommended to represent the interaction between potential features.

$$\varepsilon = \mathbf{a}_i \circ \mathbf{b}_j \circ \mathbf{c}_k \quad (3)$$

Among them, ε was an $R \times R \times R$. In the 3D measurement of R , each of its values (x, y, z) could be calculated. This was the main project of the NTC model to safeguard the authenticity of the NTC model's data speculation. The main compensations of using this 3D communication map to express the communication between features were:

1. Compared with the traditional inner product operation, the outer product of the 3D interactive mapping tensor can capture the interaction between dimensions more effectively. Because the embedded dimensions of the inner product are independent of each other.
2. The 3D interaction and map structure were good for high-level relevant models. And they could be regarded as a kind of tornado in the depth. He could use the powerful 3D CNN to learn the complicated structure concealed in the nursing data. So that he could restore the missing data more accurately.

To extract the potential information from the net checking data, a simple key was to use the MLP net. Although MLP was hypothetically certain to have a robust aptitude to express information. It had the shortcoming of a large number of arguments that could not be ignored.

To solve the shortcomings of MLP, it is suggested to use 3D CNN to extract hidden features on a 3D interactive map. 3D CNN stacks layers in the way of local connection and limits distribution. It uses much fewer limits than the MLP network. It makes it possible to build a hidden 3D CNN model than an MLP network [33-34]. The hidden 3D CNN typically can better learn the high-order correlation between embedded dimensions, thus bringing higher accuracy for the recovery of missing data.

In the design of 3D CNN, there were L roll-up layers and a full connect sheet. The input of 3D CNN was the 3D communication map $\varepsilon \in R^{R \times R \times R}$. It seemed that he was not going to give up. In each layer, there were T-packing cores (or filters). On each floor, the three-dimensional operation of the crumple core and the Re LU was performed first. And then a deviation was added. Using the re Lu as the activation function, the three-dimensional transformation was carried out. And a new one was obtained. The structure design of 3D CNN was to cutting potential topographies from the 3D communication map. It was achieved through the three-dimensional operation between the purification cores. The various layers of the input Hebe. Because one of the two kinds of cores could only excerpt one kind of topographies from the input Hebe. To excerpt more kinds of topographies. T (t) and 1 (more than one) of the 3D CNN were used. Therefore, there were T feature maps on each layer of the tornado. And each of them stored the data extracted by a core of the tornado. In the simulation test, how the number of the spiral core T would affect the performance was displayed. And the data was set according to the test.

In each convolution sheet, the input of the first sheet can be expressed as a ε^{l-1} . When $l = 1$, its contribution is a 3D interactive mapping tensor ε^{l-1} . After convolution, the i -th feature chart extracted from the L -th convolution sheet can be expressed as follows:

$$S_i^l = \text{ReLU} \left(G_i^l \otimes E^{l-1} + b_l \right) \quad (4)$$

Among them, S_i^l represents the i -th chin record extracted on the L -th complication sheet. \otimes represents the convolution operation, b_l represents deviation. The (x, y, z) term of the i -th typical diagram of the layer l can be obtained by the following formula:

$$\begin{cases} e_{xyz}^{li} = \text{ReLU} \left(b_{li} + \sum_{p=0}^{l_R-1} \sum_{q=0}^{l_R-1} \sum_{r=0}^{l_R-1} g_{pqr}^{li} e_{(x+p)(y+q)(z+r)}^0 \right), l = 1 \\ e_{xyz}^{li} = \text{ReLU} \left(b_{li} + \sum_{m=0}^{T-1} \sum_{p=0}^{l_R-1} \sum_{q=0}^{l_R-1} \sum_{r=0}^{l_R-1} g_{pqr}^{lim} e_{(x+p)(y+q)(z+r)}^{(l-1)m} \right), l > 1 \end{cases}$$

Among them, e_{xyz}^0 means the (x, y, z) item of the 3D communication chart. b_{li} means the deviation term of the i -feature map of level l . l_R was the scope of the spiral core beside the source node, the target node. And the time direction. g_{pqr}^{li} and g_{pqr}^{lim} is the (p, q, r) term of the i layer of the l sheet.

The latter sheet of the NTC model was the prediction sheet. It accepted the production of the previous chin-extracting sheet. Then the final deduction data was generated. On this floor, he first inputs into a single-sheet observation device. And then used the Sigmoid function $\sigma(\cdot)$ to calculate \hat{x}_{ijk} :

$$\hat{x}_{ijk} = \sigma(\mathbf{w}_{out}^T \mathbf{s} + b) \quad (6)$$

Among them, $\mathbf{W}_{out}^R \in R^R$ a vector is a weight. $\mathbf{s} \in R^R$ is the expansion vector of 3D CNN output. b is a deviation term.

2.3. THEORETICAL ANALYSIS

The NTC model is assumed to have a half-barbican structure. The convolution kernel is $2 \times 2 \times 2$.

$$k_1 = 3(l + 1) \quad (7)$$

The theorem is proved by mathematical induction.

The input layer maps the tensor (e , each of its entries) for 3D interactively e_{xyz} . It encodes the third-order interaction between embedded dimensions $[x; Y; Z]$. In this case, $l = 0$, $K_0 = 3$.

When $l = 1$, the size of the convolution kernel is $2 \times two \times 2$. convolution layer L captures 2 of the input 3D interactive mapping tensor. It can capture the sixth-order features of the input layer. The entries in the first feature map of the first convolution layer depend on the eight elements of the previous layer, namely, the 3D interactive mapping tensor.

When $Kt = 1$, the feature can be captured. When $Kt = 1$, the convolution layer $T + 1$ captures 2 of the convolution layers $t \times two \times 2$. The feature of the local region, and the term of the i -th feature map of the $(T + 1)$ layer $e_{xyz}^{(t+1)i}$. The interaction between embedded dimensions $[x; X + 1; Y; y + 1; Z; Z + 1]$ can be captured. Where the interaction between embedded dimensions $[x + 1; y + 1; Z + 1]$ is new to the $(T + 1)$ level of convolution. And $[x; Y; Z]$ can be inherited from the previous level t . $re, K(M203) = 3 + KT = 3 + 3(T + 1) = 3((T + 1) + 1)$.

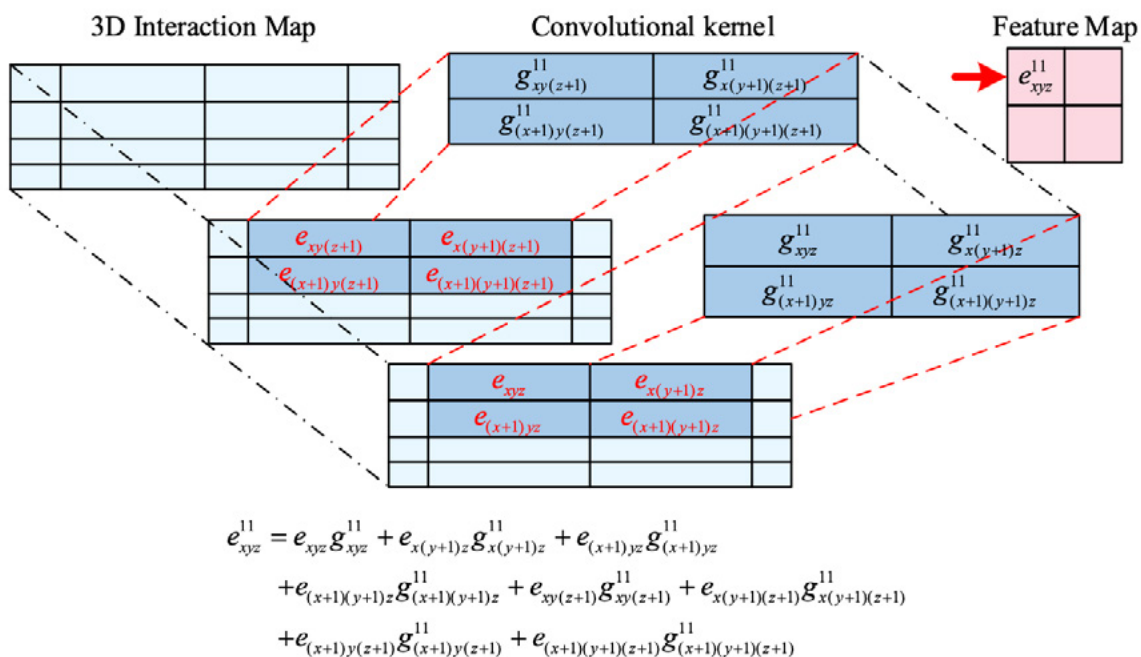


Figure 2. Example of high-order feature extraction

CP disintegration was the most common way to solve the problem. It was widely studied. It showed how to interpret the CP division as an exception to the NTC model. The internal product function was used as the interaction function in the CP disintegration. The internal product of a_i , b_j , and CK were the elements on the diagonally opposite side of the a_i , b_j , and CK . If one wanted to express the standard CP decomposed model with the NTC model, he needed to do the following:

1. By deleting the feature extracting layer based on 3D CNN, the three-dimensional interaction map layer in NTC was connected with the prediction layer directly.
2. The diagonally opposite three-dimensional interaction map was unfolded, forming the input of the prediction layer, and then projected the input to the prediction layer.

$$\hat{x}_{ijk} = a_{out}(\mathbf{h}^T \mathbf{h}) \quad (8)$$

Among them, V was the unfolded arrow, a_{out} and h respectively showed the activation functions and parameters of the prediction layer. To put it bluntly, if a_{out} constant functions of out and h were set to 1. So the revised NTC has filled in the model based on the CP disintegration.

2.4.2.4 EXPERIMENTAL SIMULATION OF THE REAL DATA SET

Represent raw data as $\chi \in R^{I \times J \times K}$ about x_{ijk} . To process the data more effectively, we use the inverse function of σ . They represent matrix and variance respectively

$$x_{ijk} = \mu + \sqrt{2\sigma \operatorname{erfinv}}(2x_{ijk} - 1) \quad (9)$$

Performance index: in the experimental simulation, four evaluation indexes are used to evaluate the performance of the NTC model: training error ratio (SER).

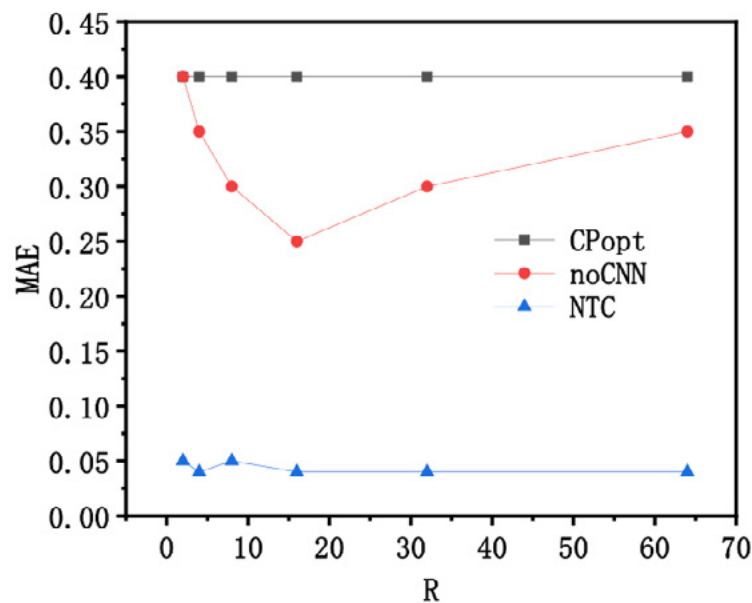
$$SER = \frac{\sqrt{\sum_{i,j,k \in \Omega} (x_{ijk} - \hat{x}_{ijk})^2}}{\sqrt{\sum_{i,j,k \in \Omega} x_{ijk}^2}} \quad (10)$$

$$TER = \frac{\sqrt{\sum_{i,j,k \in \bar{\Omega}} (x_{ijk} - \hat{x}_{ijk})^2}}{\sqrt{\sum_{i,j,k \in \bar{\Omega}} x_{ijk}^2}} \quad (11)$$

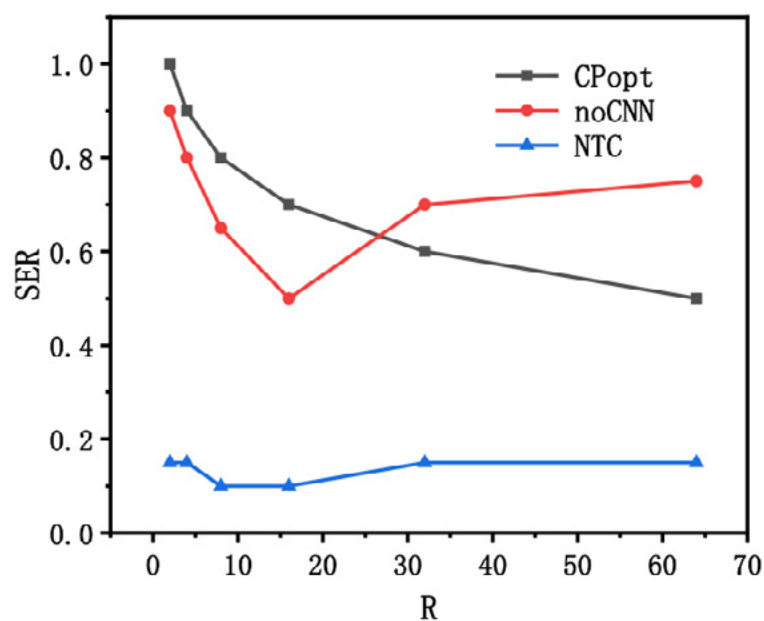
$$MAE = \frac{1}{m} \left(\sum_{i,j,k \in (\Omega + \bar{\Omega})} |x_{ijk} - \hat{x}_{ijk}| \right) \quad (12)$$

$$RMSE = \sqrt{\frac{1}{m} \sum_{i,j,k \in (\Omega + \bar{\Omega})} (x_{ijk} - \hat{x}_{ijk})^2} \quad (13)$$

x_{ijk} and \hat{x}_{ijk} represent the monitoring data tensors respectively χ . The (I, J, K) original monitoring data and predictive monitoring data. Only the training error ratio SER was calculated for the sampled data set. And the test error ratio TER was calculated for the non-sampled data set. The mean absolute error MAE and root mean square error $RMSE$ was calculated for all data items.



(a)



(b)

Figure 3. The influence of spatial dimension (R) on potential features

Effects of CNN mode. In this comparative experiment, in addition to 3D CNN, 2dcnn was implemented to extract potential features of missing data. As expected, 3D CNNs have much better recovery performance than 2D CNNs. The convolution of 3D

CNNs in the depth direction explicitly captures higher-order features of network monitoring data in time. 2D CNNs cannot achieve in such an unambiguous way.

Table 1. Recovery performance of Abilene

| Model | TER | | | | | | MAE | | | | | |
|---------|------|------|------|------|------|------|------|------|------|------|------|------|
| | 1 % | 3 % | 5 % | 7 % | 9 % | 11 % | 1 % | 3 % | 5 % | 7 % | 9 % | 11 % |
| CP-als | 0.99 | 0.98 | 0.96 | 0.95 | 0.94 | 0.93 | 0.55 | 0.55 | 0.54 | 0.53 | 0.52 | 0.52 |
| CP-nmu | 0.96 | 0.98 | 0.96 | 0.95 | 0.93 | 0.93 | 0.5 | 0.5 | 0.54 | 0.53 | 0.52 | 0.51 |
| CP-opt | 0.99 | 0.98 | 0.96 | 0.95 | 0.94 | 0.93 | 0.55 | 0.55 | 0.54 | 0.53 | 0.52 | 0.52 |
| No-CNN | 1.99 | 1.12 | 0.11 | 0.07 | 0.06 | 0.05 | 0.89 | 0.51 | 0.54 | 0.53 | 0.52 | 0.52 |
| No-OUT | 0.05 | 0.04 | 0.03 | 0.03 | 0.03 | 0.03 | 0.03 | 0.02 | 0.02 | 0.01 | 0.01 | 0.01 |
| NTC | 0.01 | 0.03 | 0.03 | 0.02 | 0.02 | 0.02 | 0.02 | 0.01 | 0.01 | 0.01 | 0.01 | 0.01 |
| Advance | 21 | 27 | 31 | 32 | 33 | 33 | 26 | 36 | 40 | 43 | 43 | 44 |

Table 2. Recovery performance of ws-dream

| Model | TER | | | | | | MAE | | | | | |
|---------|------|------|------|------|------|------|------|------|------|------|------|------|
| | 1 % | 3 % | 5 % | 7 % | 9 % | 11 % | 1 % | 3 % | 5 % | 7 % | 9 % | 11 % |
| CP-als | 0.99 | 0.97 | 0.95 | 0.93 | 0.91 | 0.90 | 0.52 | 0.51 | 0.50 | 0.49 | 0.48 | 0.48 |
| CP-nmu | 0.99 | 0.97 | 0.95 | 0.93 | 0.91 | 0.90 | 0.52 | 0.51 | 0.50 | 0.49 | 0.48 | 0.48 |
| CP-opt | 0.99 | 0.97 | 0.95 | 0.93 | 0.91 | 0.90 | 0.52 | 0.51 | 0.50 | 0.49 | 0.48 | 0.48 |
| No-CNN | 2.85 | 0.95 | 0.72 | 0.60 | 0.40 | 0.25 | 1.20 | 0.85 | 0.44 | 0.33 | 0.23 | 0.21 |
| No-OUT | 0.15 | 0.14 | 0.14 | 0.11 | 0.11 | 0.10 | 0.06 | 0.06 | 0.05 | 0.04 | 0.04 | 0.03 |
| NTC | 0.12 | 0.11 | 0.11 | 0.10 | 0.10 | 0.02 | 0.06 | 0.04 | 0.04 | 0.04 | 0.03 | 0.03 |
| Advance | 8 | 8 | 9 | 9 | 9 | 9 | 9 | 11 | 12 | 12 | 13 | 14 |

2.5. REAL NETWORK PLATFORM EXPERIMENT

To more effectively verify the accuracy of the proposed NTC model for missing data recovery of a network monitoring system, the NTC model will be applied to the network monitoring center in the later stage of the experiment. The algorithm of the NTC model will be integrated into the network monitoring platform. Large-scale actual network deployment will be carried out. Then, experiments are carried out in a real network environment to evaluate, verify and improve the proposed algorithm.

It is proposed to adopt the software. The hardware-integrated platform of high-performance data packet collection and intelligent analysis. It can realize high-speed packet capture and obtain the latest data sets of the backbone network and service

requests of operators. It includes the following aspects: one-way delay, round-trip delay (QoS), round-trip delay (QoS), packet loss rate (QoS), packet loss rate (QoS), packet loss rate (QoS), packet loss rate (QoS), packet loss rate.

In the actual deployment of the NTC model, a small and medium-sized LAN is proposed to collect monitoring data every 10 minutes to continuously measure the network performance data for 7 days, mainly measuring network delay and bandwidth. The measured data of this week were taken as the total sample of NTC model training. In the subsequent validation of the NTC model, the first task is to train the parameters of the NTC model in this real network monitoring platform, including the dimension of latent feature space (R) and the number of convolution kernels (T). In the previous real data set simulation experiments, we can see that there are generally a better R -value and t -value in the data, not that the larger the R -value and t -value, the better. After training the optimal R -value and t -value, to verify that the NTC model can also have good recovery accuracy in the case of a large data loss rate, a random collection of 1% to 10% of the total sample data for model training and missing data recovery. Finally, the performance of the proposed NTC model is evaluated and verified by comparing it with the real data.

Because the deployment of the NTC model in a real network monitoring platform is not enough to evaluate the performance of the NTC model. It is planned to implement all the comparison algorithms on the platform. To evaluate the effectiveness of the NTC model through comparative analysis.

3. FUSION NEURAL TENSOR FILLING MODEL FOR MORE COMPREHENSIVE FEATURE EXTRACTION

One model based on tensor filling uses a linear kernel to extract potential features from data. And the other model based on a neural network uses a nonlinear kernel to learn interaction functions in data. However, the actual network monitoring data may contain both linear and nonlinear features. Therefore, it is not comprehensive to adopt a single linear kernel or a nonlinear kernel. Then, to better improve the recovery performance of network monitoring data unmeasured data, the next problem is how to integrate the model based on tensor filling. And the model is based on a neural network. So that they can enhance each other. To better model the complex data interaction. It improves the information extraction of data.

3.1. SOLUTION OVERVIEW

To fuse linear and nonlinear frameworks, a simple solution is to take one of the models as the main one and express the other model under its framework. To fuse them. The NTC model is a typical non-linear model. It can be expressed and extended by other algorithms in its framework. It is proved that the tensor filling model based on CP decomposition is a special case of NTC. Therefore, a simple solution is to use a neural network to represent CP and let NTC and CP share the same embedding layer. That is a potential eigenvector. And then combine the output of their interaction

function to predict the recovery data. This method is similar to the famous neural tensor network (NTN).

The model combines the inner product and outer product of potential features to realize the fusion of linear and nonlinear latent features. Therefore, the model is defined as a fusion neural tensor completion (Fu NTC) model. The structure of the Fu NTC model is similar to that of the NTC model. It also adopts multi-layer hierarchical architecture.

3.2. DETAIL OF FU NTC MODEL

The essential purpose of input and inserting layer operations is to represent the potential characteristics of source node i , target node j , and time k by the ID of source node i , target node j , and time k , respectively

$$\mathbf{a}_i = \mathbf{e}_i \mathbf{A}, \mathbf{b}_j = \mathbf{e}_j \mathbf{B}, \mathbf{c}_k = \mathbf{e}_k \mathbf{C} \quad (14)$$

Among them, the potential eigenvectors of the source node i , target node j , and time k are a_i , b_j and c_k . $A \in R^{I \times R}$, $B \in R^{J \times R}$ and $C \in R^{K \times R}$. The feature nodes are embedded in the feature matrix of the source node. And the target node respectively. The latent characteristic matrices A , B , and C contain the features of the whole network monitoring data. It is the key point of the whole model training.

In theory, the performance of the fusion model may be limited if the linear model. And the nonlinear model shares the same embedding layer. Because this means that the linear model. Because the nonlinear model must use the same size as the embedding vector. For the two models with large changes in the optimal embedding dimension, the optimal feature extraction may not be obtained. Moreover, using the same embedding layer, the fusion model is not flexible enough.

The feature extraction layer of the Fu NTC model is divided into two parts: linear feature extraction and nonlinear feature extraction. The nonlinear feature extraction follows the NTC model. And it uses the outer product of the potential feature vector as the interaction function to generate a 3D interactive mapping tensor. And then it uses 3D CNN to extract high-order features. The nonlinear model can extract effective information from network measurement data. And the recovery performance of unmeasured data is also verified in the simulation experiment in the previous chapter. However, linear feature extraction is the representation of CP decomposition in the neural network. Different from the traditional CP decomposition, the result of the inner product is not added at this time. Instead, it is extended into a tensor to facilitate the fusion operation of the feature fusion layer.

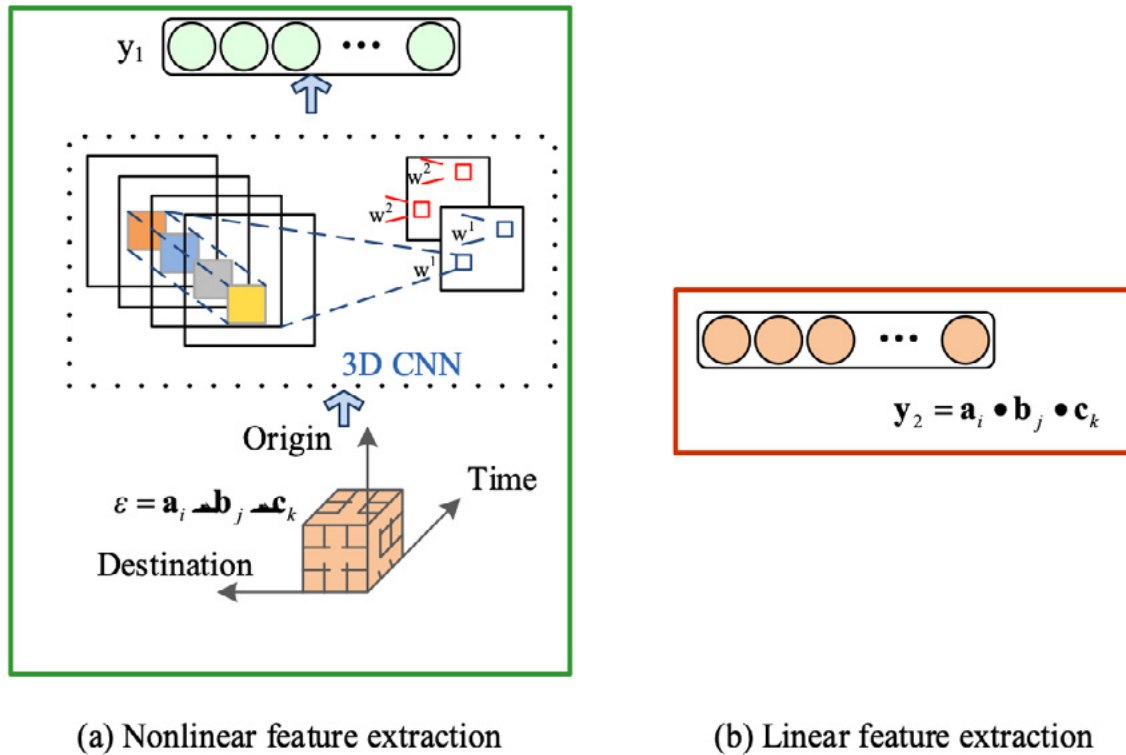


Figure 4. Linear feature extraction and nonlinear feature extraction

In the feature fusion layer, the feature vector y_1 is obtained from the nonlinear model. It is spliced with the feature vector y_2 obtained from the linear model to form a fusion vector

$$\mathbf{z} = \begin{bmatrix} \mathbf{y}_1 \\ \mathbf{y}_2 \end{bmatrix} \quad (15)$$

Where $\begin{bmatrix} \end{bmatrix}$ represents the vector splicing operation. The feature vector \mathbf{z} contains both nonlinear features and linear features. During the network training, the reverse update operation will adjust the nonlinear model and the linear model synchronously. To realize the synchronous extraction of nonlinear features and linear features for the whole model.

It is only different from the NTC model which only uses single-layer MLP. The number of MLP layers in the Fu NTC model needs to be adjusted dynamically.

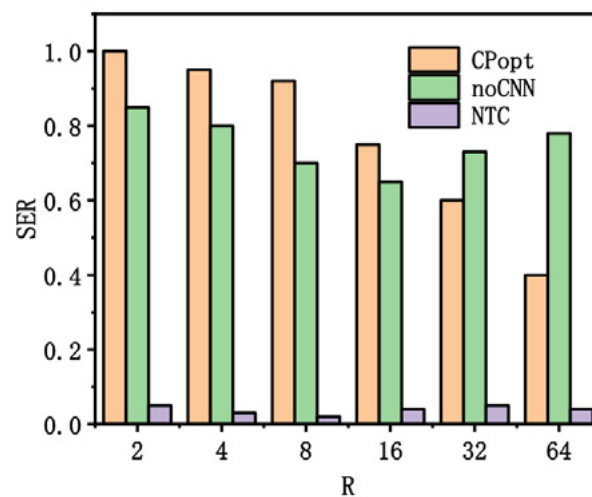
3.3. REAL DATA SET EXPERIMENTAL SIMULATION

An equally large number of experiments were performed in this study to answer the following questions:

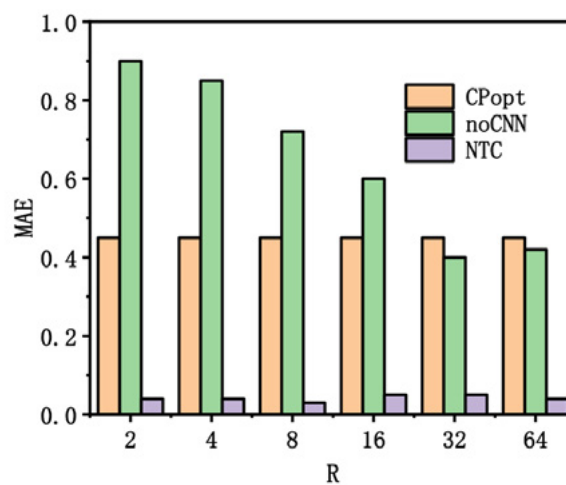
1. Effect of key hyperparameters (i.e., potential feature space dimension (R), number of convolution kernels (T), and number of convolution layers (L)) on the performance of the Fu NTC model.
2. Whether the CNN-based mode has an impact on the recovery performance of Fu NTC.

3. The performance of the Fu NTC model can surpass the current optimal NTC model.

The influence of latent feature space dimension (R). R is the number of hidden features captured. In the NTC model, R directly affects the size of the 3D interactive mapping tensor, while in the Fu NTC model, r not only affects the extraction of nonlinear features. That is the size of the 3D interactive mapping tensor of the outer product. But also, affects the extraction of linear features. That is the size of the vector formed by the inner product. The performance of the Fu NTC model is better than other contrast algorithms in all kinds of R . It shows that no matter how much R . It is, the fused neural tensor filling model is better than the single (linear or nonlinear) feature extraction model in mining potential features in the data. This shows that. The optimal number of latent features for nonlinear feature extraction is also the best latent feature data for linear feature extraction. It also effectively proves the rationality of sharing embedded layers between nonlinear models. And the linear model in the previous model design.



(a)



(b)

Figure 5. The influence of spatial dimension (R) on potential features

The influence of the number of convolution kernels (T). The number of convolution kernels is an important factor affecting the feature extraction performance of the 3D CNN model. NTC model will be affected by hyperparameter t . And Fu NTC model will also be affected by T . Because the nonlinear feature extraction part of the Fu NTC model still adopts the frame structure of 3D CNN. In the experimental algorithm, only Fu NTC, NTC, and not out (special cases of NTC) use 3D CNN to extract information. The recovery performance of the Fu NTC model is better than that of the NTC and no-out algorithm, especially in the comparison between the NTC model and the NTC model. It shows that the NTC model only extracts nonlinear information is not enough, even using the 3D CNN framework. It is very effective for feature extraction. The effectiveness of the tensor filling model is also demonstrated. Similarly, the performance trend of the Fu NTC model increases first and then decreases with the increase of the T value. It indicates that the number of convolution kernels is not better. According to the experimental results, the number of convolution kernels of the Fu NTC model in Abilene is set to $t = 32$, and that of WS-dream is set to $t = 64$.

The influence of CNN mode. Different CNN patterns affect the effectiveness of feature extraction. As we have known before. 3D CNN has one more convolution dimension than 2D CNN. It means that 3D CNN can simultaneously extract features from three dimensions of data: source node, target node, and time, while 2D CNN cannot. Experiments on the NTC model and Fu NTC model verify the effect of 3D CNN. In the two models, the recovery performance of 3dcnn is always better than that of 2D CNN. And Fu NTC model has always been better than the NTC model. Whether in 3D CNN mode or 2D CNN mode. It also shows the effectiveness of the Fu NTC model.

In the experimental simulation, the performance of the seven missing data recovery algorithms increases with the increase in sampling rate. In particular, the performance of the Fu NTC model is slightly improved compared with the NTC model. This means that the fusion neural tensor-filling model can extract more features than the neural tensor-filling model. It only extracts nonlinear features. When the sampling rate is 1%. The term of the Fu NTC model is about 0.04 and 0.11. What are the 24 and 8 areas of the best CP. It is based tensor filling algorithm except for the NTC model.

3.4. REAL NETWORK PLATFORM EXPERIMENT

The real network platform and NTC model adopt the same platform. The Fu NTC model is integrated into the network monitoring platform. And the performance of the proposed Fu NTC model is evaluated. It is verified in the real network environment.

The performance of the small network was monitored by NTC for 10 minutes every day. Then all the comparison algorithms and the Fu NTC model are tested. And the recovery performance of the Fu NTC model for missing data is verified through the analysis of the experimental results.

4. SUMMARY

Through the new neural network framework, the NTC model and CP inner product model share the embedded layer. And then splice the output of their respective interaction functions to speculate the missing data. The experimental results show that. The fusion neural tensor filling model has better data recovery performance than the traditional tensor filling algorithm and NTC model. In this paper, for the large-scale network monitoring system based on the new sparse network monitoring technology. We make the following contributions to improving the prediction accuracy of unmeasured data

1. In this paper, a 3D interactive mapping tensor is proposed to explicitly show the feature interaction between the source node, target node, and time. The interactive mapping tensor uses the outer product operation to model tensor filling to capture the complex correlation between feature dimensions.
2. To extract hidden features and recover lost data more accurately, this paper proposes a 3D CNN framework based on a 3D interactive mapping tensor. It proves theoretically that. CNN can be used to study the great-order correlation between feature scopes from local scope to global scope.
3. To excerpt the potential features unseen in the network performance statistics more comprehensively. This paper proposes a new fusion neural tensor filling model (funtc). It can extract both nonlinear and linear features.
4. In this paper, comprehensive experiments are carried out on two open actual network checking statistics sets to calculate and verify the efficacy of NTC and Fu NTC. The experimental results show that NTC and Fu NTC can realize better retrieval precision even at a very low selection rate.

5. DATA AVAILABILITY

The data used to support the findings of this study are available from the corresponding author upon request.

6. CONFLICT OF INTEREST

The authors declare that the research was conducted in the absence of any commercial or financial relationships that could be construed as a potential conflict of interest.

REFERENCES

- (1) Chen, J., Gao, W., & Wei, K. (2021). **Exact matrix completion based on low rank Hankel structure in the Fourier domain.** *Applied and Computational Harmonic Analysis*, 55(2-3), 301-320.

- (2) Yadav, S. K., & George, N. V. (2020). **Fast Direction-of-Arrival Estimation via Coarray Interpolation Based on Truncated Nuclear Norm Regularization.** *IEEE Transactions on Circuits and Systems II: Express Briefs*, 67(6), 1206-1210.
- (3) Ti, A., Av, B., & Rg, A. (2021). **Ranking recovery from limited pairwise comparisons using low-rank matrix completion.** *Applied and Computational Harmonic Analysis*, 54, 227-249.
- (4) Douik, A., & Hassibi, B. (2021). **Low-Rank Riemannian Optimization for Graph-Based Clustering Applications.** *IEEE Transactions on Pattern Analysis and Machine Intelligence*, 43(7), 2558-2572.
- (5) Wang, P., & Zhang, J. (2021). **A Singular Value Thresholding Based Matrix Completion Method for DOA Estimation in Nonuniform Noise.** *Journal of Beijing Institute of Technology*, 30(4), 368-376.
- (6) Dragomir, R. A., Giannessi, F., & Hull, D. G. (2021). **Quartic First-Order Methods for Low-Rank Minimization.** *Journal of Optimization Theory and Applications*, 189(4), 1216-1248.
- (7) Kao, S. Y., Katsumi, S., Han, D., et al. (2020). **Postnatal Expression and Possible Function of RANK and RANKL in the Murine Inner Ear.** *Bone*, 136, 115837.
- (8) Zhang, F., Hou, J., Wang, J., et al. (2020). **Uniqueness Guarantee of Solutions of Tensor Tubal-Rank Minimization Problem.** *IEEE Signal Processing Letters*, 27, 540-544.
- (9) Wei, H., Qu, Z., Wu, X., et al. (2021). **Decentralized Approximate Newton Methods for Convex Optimization on Networked Systems.** *IEEE Transactions on Control of Network Systems*, 8, 2792-2802.
- (10) Dai, S., Jin, M., & Zhang, X. (2020). **Kernel affine projection p-norm (KAPP) filtering under alpha-stable distribution noise environment.** *International Journal of Pattern Recognition and Artificial Intelligence*, 34(2), 2059006.
- (11) Yang, Y., Yang, Z., Li, J., et al. (2020). **Foreground-Background Separation via Generalized Nuclear Norm and Structured Sparse Norm Based Low-Rank and Sparse Decomposition.** *IEEE Access*, 8, 222957-222970.
- (12) Qiao, W., & Yang, Z. (2020). **An Improved Dolphin Swarm Algorithm Based on Kernel Fuzzy C-Means in the Application of Solving the Optimal Problems of Large-Scale Function.** *IEEE Access*, 8, 2073-2089.
- (13) Ahn, H. S., Park, S. H., & Ye, J. C. (2020). **Quantitative susceptibility map reconstruction using annihilating filter-based low-rank Hankel matrix approach.** *Magnetic Resonance in Medicine*, 83(3).
- (14) Huang, Y., Zhang, X., Guo, H., et al. (2020). **Phase-constrained reconstruction of high-resolution multi-shot diffusion weighted image.** *Journal of Magnetic Resonance*, 312, 106690-.
- (15) Arridge, S., Fernsel, P., & Hauptmann, A. (2020). **Joint Reconstruction and Low-Rank Decomposition for Dynamic Inverse Problems.**
- (16) Huang, C., & Yang, C. F. (2020). **An Empirical Approach to Minimize Latency of Real-Time Multiprocessor Linux Kernel.** *In 2020 International Computer Symposium (ICS).*

- (17) Yang, H. J., Lei, Y. X., Wang, J., et al. (2022). **Tensor decomposition based on the potential low-rank and p-shrinkage generalized threshold algorithm for analyzing cancer multiomics data.** *Journal of Bioinformatics and Computational Biology*, 20(02).
- (18) Saeedi, T., & Rezaghi, M. (2020). **A Novel Enriched Version of Truncated Nuclear Norm Regularization for Matrix Completion of Inexact Observed Data.** *IEEE Transactions on Knowledge and Data Engineering*, PP (99), 1-1.
- (19) Zhang, C. J., & Qin, Y. U. (2020). **Spatiotemporal RPCA algorithm for moving target detection in complex scene.** *Computer Engineering and Design*.
- (20) Zhao, H., & Zheng, S. (2020). **Joint Extreme Channels-Inspired Structure Extraction and Enhanced Heavy-Tailed Priors Heuristic Kernel Estimation for Motion Deblurring of Noisy and Blurry Images.** *IEICE Transactions on Fundamentals of Electronics Communications and Computer Sciences*, E103.A(12), 1520-1528.
- (21) Zhang, X., Zheng, J., Yan, Y., et al. (2019). **Joint Weighted Tensor Schatten p-Norm and Tensor lp-Norm Minimization for Image Denoising.** *IEEE Access*, 1-1.
- (22) Chen, W. G., & Peng, L. I. (2019). **Truncated sparse approximation property and truncated q-norm minimization.** *Applied Mathematics: A Journal of Chinese Universities*.
- (23) Chen, J., Lin, Z., Ren, J., et al. (2020). **Distributed multi-scenario optimal sizing of integrated electricity and gas system based on ADMM.** *International Journal of Electrical Power & Energy Systems*, 117, 105675-.
- (24) Rava, R. A., Mokin, M., Snyder, K. V., et al. (2020). **Performance of angiographic parametric imaging in locating infarct core in large vessel occlusion acute ischemic stroke patients.** *Journal of Medical Imaging*, 7(1), 1.
- (25) Liu, J., He, D., Zeng, X., et al. (2019). **ManiDec: Manifold Constrained Low-Rank and Sparse Decomposition.** *IEEE Access*, PP(99), 1-1.
- (26) Vitali, V., Chevallier, F., Jinaphanh, A., et al. (2021). **Eigenvalue separation and eigenmode analysis by matrix-filling Monte Carlo methods.** *Annals of Nuclear Energy*, 164, 108563-.
- (27) Liu, Y., Zhou, D., Nie, R., et al. (2020). **Construction of High Dynamic Range Image Based on Gradient Information Transformation.** *IET Image Processing*, 14(6).
- (28) Xue, Z., Dong, J., Zhao, Y., et al. (2019). **Low-rank and sparse matrix decomposition via the truncated nuclear norm and a sparse regularizer.** *The Visual Computer*, 35(11), 1549-1566.
- (29) Guo, M.-H., Xu, T.-X., Liu, J.-J., Liu, Z.-N., Jiang, P.-T., Mu, T.-J., Zhang, S.-H., Martin, R. R., Cheng, M.-M., & Hu, S.-M. (2022). **Attention mechanisms in computer vision: A survey.** *Computational Visual Media*, 8(03), 331-368.
- (30) Battisti, R., Claumann, C. A., Manenti, F., Machado, R. A. F., & Marangoni, C. (2021). **Machine learning modeling and genetic algorithm-based optimization of a novel pilot-scale thermosyphon-assisted falling film distillation unit.** *Separation and Purification Technology*, 259.

- (31) Chung, Y., Lee, S., & Kim, W. (2021). **Latest Advances in Common Signal Processing of Pulsed Thermography for Enhanced Detectability: A Review.** *Applied Sciences*, 11(24).
- (32) Pekedis, M., Ozan, F., Koyuncu, S., & Yildiz, H. (2022). **The finite element method-based pattern recognition approach for the classification of patient-specific gunshot injury.** *Proceedings of the Institution of Mechanical Engineers. Part H, Journal of Engineering in Medicine*, 236(5).
- (33) Dewani, A., Memon, M. A., & Bhatti, S. (2021). **Development of computational linguistic resources for automated detection of textual cyberbullying threats in Roman Urdu language.** *3C TIC. Cuadernos de Desarrollo Aplicados a las TIC*, 10(2), 101-121. <https://doi.org/10.17993/3ctic.2021.102.101-121>
- (34) Mei, D. (2022). **What does students' experience of e-portfolios suggest.** *Applied Mathematics and Nonlinear Sciences*, 7(2), 15-20. <https://doi.org/10.2478/AMNS.2021.2.00166>

/17/

THE ROLE OF SOCIAL NETWORKING SITES IN PROMOTING THE CULTURE OF IRAQI RURAL WOMEN AND EMPOWERING THEM

Dr. Haider Falah Zaeid*

Thi-Qar University, College of Media, Department, journalism.

Haiderfah91@utq.edu.iq

Noor Kareem Yasir

Thi-Qar University, College of Media, Department, Radio, and T.V.

Dr. Saad Ibrahim Abbas

Thi-Qar University, College of Media, Department, Radio, and T.V.

Reception: 14/11/2022 **Acceptance:** 15/01/2023 **Publication:**11/03/2023

Suggested citation:

F.Z., Haider, K.Y., Noor and I.A., Saad (2023). **The role of social networking sites in promoting the culture of Iraqi rural women and empowering them.** *3C TIC. Cuadernos de desarrollo aplicados a las TIC*, 12(1), 352-376. <https://doi.org/10.17993/3ctic.2023.121.352-376>

ABSTRACT

Social networking sites are highly effective in serving the community and empowering it cognitively and politically because of its impact on its users and visitors through the information and ideas it provides, mostly free of it without a political, social or inappropriate agenda, Its goal was to advance the knowledge and scientific aspects of the visitors of these sites, and this in itself is a positive step, calculated for those in charge of it.

In his research entitled "The role of social networking sites in promoting the culture of Iraqi rural women and empowering them, the researcher seeks to identify the role of social networking sites in serving rural women, and how Iraqi rural women use these sites, and how it helps them

to communicate with others, and how useful it is for rural women to enhance their culture and empower them intellectually and politically.

The researcher hopes to discuss the role of social media in the effective empowerment of rural women in an academic manner through modern and considered sources, as well as asking a number of questions through the questionnaire form to Iraqi rural women and identifying the role of social networking sites in empowering them, in order to reach results that serve the objectives of the conference and scientific research.

KEYWORDS

Social networking sites, women's culture, women's empowerment, Iraqi rural women.

PAPER INDEX

ABSTRACT

KEYWORDS

INTRODUCTION

1. THE METHODOLOGICAL FRAMEWORK

- 1.1. The research problem.
- 1.2. The importance of research
- 1.3. Research Objectives
- 1.4. Research Hypothesis
- 1.5. Research Methodology and Tools
- 1.6. Research Limits
- 1.7. Definition of Terms
- 1.8. Previous studies
 - 1.8.1. Athamna Study 2017
 - 1.8.2. Study by Halima Lakhal and Rabiha Zaidi 2017
- 1.9. Commenting on previous studies

2. THEORETICAL FRAMEWORK

- 2.1. The role of social networking sites in the effective empowerment of rural women

3. SOCIAL NETWORKING SITES AND IRAQI RURAL WOMEN

- 3.1. Analyzing the results of the questionnaire
- 3.2. Demographic variables
 - 3.2.1. Age
 - 3.2.2. Marital status
 - 3.2.3. Academic achievement
- 3.3. The use of social networking sites and its role in the culture and empowerment of rural women
 - 3.3.1. Use of social networking sites
 - 3.3.2. The most used sites
 - 3.3.3. Extent of use
 - 3.3.4. Tim Average
 - 3.3.5. The role of social networking sites
 - 3.3.6. Developing rural women cognitively and politically
 - 3.3.7. Social networking sites and women's relationship with their social environment
 - 3.3.8. The effect of social networking sites
 - 3.3.9. The family's follow-up of the girls' use of social networking sites

3.3.10.The help of social networking sites for women

3.3.11.The reason for using social networking sites

3.3.12.Social networking sites and their contribution to conveying the voice of women

3.3.13.The nature of using the name on social networking sites

3.3.14.Use of sites and customs in villages and rural areas

3.4. The most important results:

3.5. Recommendations:

REFERENCES

Arabic and translated books

Theses and Dissertations

Published Research

INTRODUCTION

Today, social networking sites has changed the situation and reality of many societies after using it and introducing it to the surrounding developed peoples through this carrier medium, which

helped developing countries, rural women in particular, as a result of the difficult social situation that this class suffers from, represented by some customs and traditions that are practiced in Iraqi villages and countryside.

Today, social networking sites have empowered Iraqi rural women and formed their political and cognitive awareness, and they have become aware of their rights and practiced them effectively, as is the case of city women, and now we see them in schools, universities, and jobs after they were deprived of their rights for hundreds of years as a result of the clan character, in addition to the difficult financial situation that made them share with men Agriculture and farming business.

Today, websites have become important in the lives of peoples and rural women in particular at the present time because of their widespread reach, as well as their attainment of the highest level in achieving the desired goals in the educational, political, social, economic and cultural aspects of the life of rural women in particular.

The sites are turning point for many societies because of the advantages that these sites possess that made them play an effective role in the lives of individuals, in addition to that, these sites have turned the world into a small village in the hands of its users

1. THE METHODOLOGICAL FRAMEWORK

1.1. THE RESEARCH PROBLEM.

The researcher seeks to know the role of social networking sites for rural women, and the extent to which social networking sites contribute to the promotion and development of their culture, as well as identifying their external environment.

Accordingly, the research problem can be formulated with the following main question: What is the role of social networking sites in promoting the culture of Iraqi rural women and empowering them?

From this question, several sub-questions emerge:

1. Do social networking sites contribute to the cultural and political empowerment of rural women?
2. What are the favorite social networking sites for rural women?
3. Is there an effect of social networking sites on women?
4. What are the reasons for women's use of social networking sites?
5. To what extent do rural women use social networking sites?

1.2. THE IMPORTANCE OF RESEARCH

The importance of the research lies in the importance of the topic that it deals with (the role of social networking sites in promoting the culture of Iraqi rural women and empowering them). In addition, this research is one of the pioneering modern researches in the field of digital media that deals with the issue of Iraqi rural women, conveying their suffering and highlighting them by communicating voice and to alleviate their suffering and empower them culturally and politically.

This research is one of the important sources for subsequent research, as it discusses the issue of social networking sites and its contribution to promoting the culture of Iraqi rural women, due to the scarcity in this field, according to the researcher's knowledge, in addition to the novelty of its topic, as it discusses the variable of social networking sites with rural women.

1.3. RESEARCH OBJECTIVES

The research aims at the following:

1. To reveal the contribution of social networking sites to the cultural and political empowerment of rural women.
2. Identifying the favorite social networking sites of rural women.
3. Access to the impact of social networking sites on women.
4. Investigating the reasons for women's use of social networking sites.
5. Detecting the duration of rural women's use of social networking sites.

1.4. RESEARCH HYPOTHESIS

The research hypothesizes that the researcher deduced from the dependence theory are as follows:

1. Social networking sites enhance the culture of Iraqi rural women and empower them intellectually and politically.
2. Rural women use social networking sites to communicate and promote their culture.
3. The heavy use of social networking sites affects the relationship of rural women with their surroundings.

1.5. RESEARCH METHODOLOGY AND TOOLS

The scientific method is defined as "a set of general rules that define scientific procedures and mental processes that follow to reach the truth with regard to various phenomena, whether natural or human ,in the light of the method, it is possible to start

collecting information and data, classifying and tabulating them, and then analyzing them in order to formulate the results that the researcher seeks.¹

The researcher relied on the survey method through the questionnaire form that was distributed to the respondents, and the survey method used by the researcher "is considered one of the most prominent approaches used in media curricula to obtain data and information that target the scientific phenomenon itself."²

As for the society, the research was represented by women from Dhi Qar Governorate who live in villages and rural areas who use social networking sites, and the researcher relied on the intentional sample to reach only women who use social networking sites in villages and rural areas closely in order to obtain realistic answers that we reach the goals of the research, the sample members reached (100) respondents, the questionnaire was distributed to them.

Among the tools used by the researcher is scientific observation in tracking social networking sites and identifying techniques that may serve the public when using the sites, and identifying the negative aspects of social networking sites in order to put questions about them in the questionnaire and obtain answers that are compatible with the nature of the use of these sites by the researched sample, as well as this was used by the researcher in order to determine the main and sub-questions in the questionnaire that is presented to the researched sample.

The researcher also used the questionnaire form, which included a number of closed and open questions to obtain information about the role of social networking sites in promoting the culture of rural women and empowering them, and this is demographic , scientific and personal information related to social networking sites and their role in empowering women, before distributing the questionnaires to the sample, they were presented to a group of experts³, in the field of media, to ensure the integrity of the questionnaire and its questions, and the extent of their validity, and it obtained their approval and considered it valid for use and achieving the objectives of the research

¹ Mohammed Abdul Hamid, Scientific Research in Media Studies, Cairo, World of Books, 2000, p. 65.

² Saad Salman Al-Mashhadani, Media Research Methods, University Book House, United Arab Emirates, 2017, p. 163.

³ Prof. Dr. Hadi Flaih Hassan , Faculty of Media , Dhi Qar University, Prof. Dr. Abdul Razzak Al-Dulaimi _ Middle East University Jordan, Prof. Dr. Assist.-Saad Abdul Rahman Makki _ 8th May ^h University May Algeria, prof. Dr. Saad Ibrahim Abbas - College of Media , Dhi Qar University, Prof. Dr. Mohammed Shaker Mahmoud Al-Shammari_ College of Media, Dhi Qar University.

1.6. RESEARCH LIMITS

The research limits are as follows:

- A. Time limits: The limits in which the research was completed in 2021-2022.
- B. Human limits: Women of villages and rural areas in Dhi Qar Governorate.
- C. Spatial limits: Iraq, Dhi Qar Governorate.

1.7. DEFINITION OF TERMS

1. **Social networking sites:** It is a set of pages that allow subscribers to subscribe to it by creating special pages via e-mail and phone number, and then linking it through an electronic social system with other members.⁴
2. **Women's culture:** It means the set of information and ideas that women obtain through their environment, whether through education and family or through their external environment, women's culture is an awareness through which they form multiple cognitive trends.⁵
3. **Empowerment:** It is the process by which women are able to gain experience in various fields in order to be able to manage their affairs in life.⁶

1.8. PREVIOUS STUDIES

1.8.1. ATHAMNA STUDY 2017⁷

The research problem is represented by the following main question: What is the impact of social networks on the social values of university students?

The objectives of the research centered on identifying the impact of social networks on the social values of university students, such as Facebook, Twitter and YouTube, and their impact on the system of social values that control individual behavior.

This study falls within the descriptive studies and relied on the descriptive and survey approach as it is in the process of studying a social phenomenon, and this

⁴ Ghazal Maryam and Shaoubi Nour Al-Huda, the impact of social networking sites on the development of political awareness among university students, an unpublished master's thesis, Kasdi Merbah University - Ouargla, Faculty of Humanities and Social Sciences, Department of Human Sciences, Division: Media and Communication Sciences, 2014. p.3

⁵ Dr. Abdul Ghani Imad, Sociology of Culture, Center for Arab Unity Studies, Beirut, 2006, p. 37.

⁶ Ministry of Planning, Central Statistical Agency, The Reality of Rural Women in Iraq, Central Agency Press, 2016, p. 2.

⁷ Naziha Athamna: The impact of social networks on the social values of university students, a field study on a sample of students at the University of M'sila, unpublished master's thesis, Faculty of Humanities and Social Sciences, Department of Media and Communication Sciences, Mohammed Boudiaf University, M'sila, Algeria, 2017, p. 7.

requires to analyze, describe and interpret, and its sample was intentional, through the results of the research, the study showed that the majority of university students are exposed to social networking sites with a non-selective tradition, without taking into account the contents they provide that are inconsistent with their established habits, and this can be explained by their negative role on the system of social values of university students.

It presents contents that are inconsistent with their established habits, and this can be explained through its negative role on the system of social values of university students.

1.8.2. STUDY BY HALIMA LAKHAL AND RABIHA ZAIDI 2017⁸

The research problem revolved around the following question: What is the impact of the use of social networking sites on family relations, Facebook as a model? The researchers followed the survey method, and the sample studied was intentional, and through that, the researchers reached through the results of the field study and presented its results and analyzed them and reached to the following:

1. The "Facebook" website is an unlimited field that allows its users to form relationships and friendships, and opens the way for them to communicate and interact without moving, which makes them spend most of their time in front of them without realizing it.
2. Excessive use of the "Facebook" account is an addiction that the individual neglects his responsibilities at the expense of sitting in front of Facebook.
3. Social networking sites Facebook has contributed to creating problems within the family, including the absence of dialogue between husband and wife, forgetting occasions, and not providing an appropriate family atmosphere.

1.9. COMMENTING ON PREVIOUS STUDIES

The researcher developed only two studies as previous studies for the research, due to the lack of a study linking the variable of social networking sites and its role in promoting the culture of women and rural women in particular, according to the limits of the researcher's knowledge, therefore, he was satisfied with these two studies, which he believes are the closest to his topic with the variable of social networking sites and the impact on society that includes women. definitely a part of the community.

⁸ Halima Lakhal and Rabiha Zaidi: The impact of the use of social networking sites on family relations, Facebook as a model, an unpublished master's thesis, Zayan Ashour University, Djelfa, Faculty of Humanities and Social Sciences, Department of Sociology and Demography, 2017.

2. THEORETICAL FRAMEWORK

2.1. THE ROLE OF SOCIAL NETWORKING SITES IN THE EFFECTIVE EMPOWERMENT OF RURAL WOMEN

The social networking site plays an important role in empowering people intellectually and politically because of its cultural, political, social, and economic content, this content is available permanently and renewed as a result of the increasing use of these sites by members of society of different scientific disciplines, as well as the geographical difference of users of social networking sites.⁹

The researchers indicate that the difference in the environment of users of social networking sites has a leading role in cultural intermarriage between its visitors from different countries, and informing users of publications that published by scientific pages and personal pages of experts and intellectuals in various disciplines, making the pioneers of these sites in full communication with knowledge without restrictions and barriers, watching scientific experiments in developed countries, and viewing publications makes the individual of great cultural value that serves him in his daily and scientific life, which makes him a strong empowered personality.¹⁰

Social networking sites today are among the main sources in empowering Iraqi rural women because of its diverse content that is able to stand against discrimination between men and women on the one hand, and rural women who live in cities on the other hand, and the sites give women a great role as we see many pages of female artists and media women have a large and distinguished presence to defend the rights of rural women and others, to stand up to violence against women, and to work to take their role naturally in all areas of life, including professional and political cases¹¹.

Social networking sites were characterized by the intensity of confrontation, enthusiasm, and their diverse style, and their continuing role in broadcasting ideas and information around the clock, these sites helped women take their role by providing them with effective methods to promote culture and information in greater depth, and the ability of mutual interaction between them and the surrounding and virtual community, today, social networking sites are extremely important in popular

⁹ Naziha Athamna: The Impact of Social Media Networks on the Social Values of University Students, A Field Study on a Sample of University of M'sila Students, Unpublished Master's Thesis, Faculty of Humanities and Social Sciences, Department of Media and Communication Sciences, Mohammed Boudiaf University, M'sila, Algeria, 2017.

¹⁰ Halima Lakhal and Rabiha Zaidi, The impact of using social networking sites on family relations, Facebook as a model, an unpublished master's thesis, Zayan Ashour University, Djelfa, Faculty of Humanities and Social Sciences, Department of Sociology and Demography, 2017.

¹¹ Haider Faleh Zayed, The role of advertisements and news on the websites of government institutions to facilitate the procedures of auditors, "Dhi Qar University as a model", previous source, p. 399.

circles as a result of her depth and weight because of the great influence the on society.¹²

These sites are a type of digital media that presents its content in a digital and interactive form, and depends on the fusion of text, image, video and audio, and can be accessed through smart phones of all kinds, as well as the computer as its main mechanism in the production and presentation process. Social networking sites that help Women and their cognitive empowerment are as follows:¹³

1. The Internet (Online) and its applications such as Facebook, Twitter, YouTube, blogs, chat sites, and e-mail. For the media, it represents the fourth system added to the three classic systems.
2. Applications based on various portable tools, including smart phones, personal digital assistants, and others.

Rural women began to take on their role after they used social networking sites and entered the virtual world from its widest gates through these sites that have no restrictions, rural women can be defined as those who live in villages and rural areas, and who work in those areas that depend on natural resources and agriculture for their livelihood, and they constitute more than a quarter of the total world population and in developing countries, and rural women represent about %43 of the agricultural labor force.¹⁴

Social networking sites also help women to get to know and open up to all cultures and customs, especially rural women who live in an atmosphere of (closeness) and pressure as a result of customs and traditions that prevent them from exercising their freedom and rituals, as is the case with women in developed cities, therefore, social networking sites are the appropriate place to express her opinion and personality , It is also a suitable place to receive cultures and empower them cognitively and politically, as a result of obtaining information from others, through the various published content and through communication with scientific, political and academic personalities, elites, etc. that have accounts on these sites.¹⁵

In addition, the sites help the individual to enhance his culture, especially rural women, in shaping their awareness and culture in a large extent due to the diversity of published content within the corridors of these sites, and the sites help the individual by making him master of the art of speech, and arranging ideas, phrases, and sentences frequently, and that makes him able to establishing relationships with those

¹² Abdul Amir Al-Faisal, *Studies in Electronic Media*, Emirates, University Book House, 2014, p. 124.

¹³ Dr.. Bushra Jamil Al-Rawi, *The role of social networking sites in change*, previous source, pg. 97.

¹⁴ Khalid Walid Mahmoud, *Social Networks and the Dynamics of Change in the Arab World*, Beirut, Dar Madrak, 2011, p. 85.

¹⁵ Haider Faleh Zayed, *The role of advertisements and news on the websites of government institutions to facilitate the procedures of auditors*, "Dhi Qar University as a model", *Dhi Qar Journal of Arts*, 2018, p. 383

around him, in addition to that, the sites contribute to the formation of new cultures for him.¹⁶

In fact, social networking sites are controversial, due to the overlapping of opinions and trends in its study, reflecting this concept, and the technical development that occurred in the use of technology, and it called everything that can be used by individuals and groups on the giant web as a result of the abundance of information in it and the diversity of content.¹⁷

The content on social networking sites is usually characterized by a personal nature, and is transmitted between two parties, one of whom is a sender and the other a receiver, through this social medium, with the freedom of the message to the sender, and the freedom to respond by the receiver, and this is what distinguishes it in that its user obtains the freedom to receive the information he needs.¹⁸

These sites are among the new ways for rural women to obtain information, immunize them, and empower them cognitively and politically, the sites allow rural women to access diverse groups in which there are individuals of different races and countries, which allows for the exchange of information in a timely and immediate manner through interactions and dialogues.¹⁹

Social networking sites have played a role in empowering rural women because of the advantages and characteristics that distinguish them from other means, these characteristics are as follows:²⁰

1. **Sharing:** It allows people to share and comment on the content they follow.
2. **Openness:** It helped openness and universality to facilitate the communication of individuals with others, overcoming all barriers, and exchanging information and opinions.
3. **Conversation:** Allowing for conversation, participation and interaction with the event, news and provided information.

¹⁶ Amer Ibrahim Qandilji and Hassan Reda Al-Najjar, Information Science, Systems and Technologies, Dar Al-Masirah for Publishing, Distribution and Printing, Amman, Jordan, 2015, p. 92.

¹⁷ Osama bin Sadiq Tayeb, Knowledge of Social Networks, a series of studies, King Abdulaziz University, Saudi Arabia, 2012, p. 30.

¹⁸ Dr. Hosni Awad, The impact of social networking sites on the development of social responsibility among young people, the experience of the Allar Youth Council as a model, Al-Quds Open University, Social and Family Development Program, 2011, p. 10.

¹⁹ Dr.. Bushra Jamil Al-Rawi, The Role of Social Networking Sites in Change, Media Researcher Magazine, Issue 18, College of Information, University of Baghdad, 2012, p. 96

²⁰ Dr.. Ibrahim Ahmed Al-Dawy, Social Networks, Arab Red Crescent and Red Cross Organization, 2015, p. 7

4. **Sending messages:** It allows sending messages between users with direct or indirect relationships.²¹
5. **Community:** Allows local communities to connect with international communities on common concerns or interests.
6. **Groups:** It allows the creation of groups of interest under a name and with specific goals, in what is like a discussion forum on a very large scale.
7. **Interdependence:** It is a social network that is interconnected with each other through the connections and links that it provides

In addition, social networking sites are not without negatives and defects for their users, especially those who are addicted to them, these defects are as follows:²²

1. Addiction and social isolation: as it is attractive and leads to addiction, which leads to isolation from society to launch into the virtual society.
2. The emergence of new habits and language among users: The language used in social networks is understandable only to network users, in addition to the emergence of slogans and the so-called trend, most of whose content contradicts societal values.
3. Absence of oversight and some users' lack of responsibility.
4. Spreading false news and inaccurate reporting of events.
5. Lack of privacy that leads to psychological damage and defamation of personalities.

3. SOCIAL NETWORKING SITES AND IRAQI RURAL WOMEN

3.1. ANALYZING THE RESULTS OF THE QUESTIONNAIRE

This topic includes analyzing the results of the questionnaire distributed to the sample chosen by the researcher, which is represented by women from villages and rural areas in Dhi Qar Governorate who use social networking sites closely, the researcher distributed the questionnaire to (100 women), after fulfilling all scientific conditions.

The questionnaire, which was distributed on two important axes, included axis one, the demographic variables of the respondents, and axis two, which included the use of social networking sites and its role in the culture and empowerment of rural women. The results showed in the following:

²¹ Ghazal Maryam and Shaoubi Nour Al-Huda, the impact of social networking sites on the development of political awareness among university students, an unpublished master's thesis, University of Kasdi Merbah - Ouargla, Faculty of Humanities and Social Sciences, Department of Human Sciences, Department of Media and Communication Sciences, 2014, p.3.

²² Amer Ibrahim Qandilji, Electronic Media, Dar Al Masirah, Jordan, Amman, 2017, p. 68.

3.2. DEMOGRAPHIC VARIABLES

3.2.1. AGE

Table 1. shows the distribution of sample members according to age.

| Question | Category | Repetition | Ratio |
|----------|------------------|------------|-------|
| Age? | From (18-27) | 82 | 82 % |
| | From (28-37) | 12 | 12 % |
| | From (38-47) | 6 | 6 % |
| | From (48 - 57) | 0 | 0 % |
| | (58 - and above) | 0 | 0 % |
| | Total | 100 | 100 % |

The results of the above table indicate that the percentage of the respondents differed according to age, as it was for the age group (18-27 years) with (82) repetitions, with a rate of (%82), and for the age group (28-37 years) with (12) repetitions, with a rate of (%12) and for the age group (38-47 years) with (6) repetitions at a rate of (6%), and for the age group (48-57 years) with (0) repetitions at a rate of (0%), and for the age group (58 years and over) with (0) repetitions at a rate of (0%). We conclude from this that the age group (18-28) is the highest and most uses social networking sites, being the most open and understanding of the questionnaire matters, reading and writing, and has knowledge in social networking sites, see Figure (1).

3.2.2. MARITAL STATUS

Table 2. shows the distribution of sample members according to marital status.

| Question | Category | Repetition | Ratio |
|-----------------|----------|------------|-------|
| Marital status? | Single | 78 | 78 % |
| | Married | 20 | 20 % |
| | Widow | 0 | 0 % |
| | Discrete | 0 | 0 % |
| | Divorced | 2 | 2 % |
| | Total | 100 | 100 % |

The percentage of the respondents varied according to the marital status, as it came to a single paragraph with a rate of (78) repetitions at a rate of (%78), for a married woman at a rate of (20) repetitions at a rate of (%20), a widow with a rate of (0) repetitions at a rate of (%0), and a separated woman at a rate of (0). repetitions

(%0), and divorced women (2) repetitions at a rate of (2%). We infer from this that unmarried women are the most frequent users of social networking sites as a result of the lack of family and social obligations, see Figure (2).

3.2.3. ACADEMIC ACHIEVEMENT

Table 3. shows the distribution of sample members according to academic achievement.

| Question | Category | Repetition | Ratio |
|----------------------|---------------------|------------|-------|
| Academic achievement | Read and write | 3 | 3 % |
| | Primary | 1 | 1 % |
| | secondary school | 20 | 20 % |
| | Bachelor's degree | 74 | 74 % |
| | Postgraduate degree | 2 | 2 % |
| | Total | 100 | 100 % |

The results of the above table show that the percentage of respondents for the reading and writing category is (3) repetitions at a rate of (%3%), for a primary category at (1) repetitions at a rate of (%1), for a secondary category at (20) repetitions at a rate of (%20), and for a bachelor's category at ((74) repetitions, at a rate of (%74), and for the category of higher degrees, at a rate of (2) repetitions, at a rate of (%2). It becomes clear that the higher percentage of the sample are educated and holders of certificates, and this is a good indication that the answers are realistic as a result of the educational level of the respondents, see Figure (3).

3.3. THE USE OF SOCIAL NETWORKING SITES AND ITS ROLE IN THE CULTURE AND EMPOWERMENT OF RURAL WOMEN

3.3.1. USE OF SOCIAL NETWORKING SITES

Table 4. shows the use of social networking sites.

| Question | Category | Repetition | Ratio |
|-------------------------------------|-----------|------------|-------|
| Do you use social networking sites? | Often | 86 | 86 % |
| | Sometimes | 12 | 12 % |
| | Rarely | 2 | 2 % |
| | Total | 100 | 100 % |

The results of Table (4) showed that the percentage of the sample that uses social networking sites often is (86) repetitions (%86), sometimes (12) repetitions with the

rate of (12%), and rarely (2) repetitions (2%). We conclude from this that the sample uses social networking sites at a very high rate, and this gives us a good indication that the answers of the respondents are accurate, stemming from an understanding of this communication medium and its importance and identifying its positives and negatives.

3.3.2. THE MOST USED SITES

Table 5. shows the most used sites by the sample

| Question | Category | Repetition | Ratio |
|--------------------------------|-----------|------------|-------|
| Which of your most used sites? | Facebook | 8 | 8 % |
| | Twitter | 0 | 0 % |
| | Instagram | 82 | 82 % |
| | Tik Tok | 3 | 3 % |
| | YouTube | 7 | 7 % |
| | Others | 0 | 0 % |
| | The total | 100 | 100 % |

The results of the above table show that the most used sites by the researched sample were for the Facebook category with (8) repetitions, with a rate of (%8), for Twitter, with (0) repetitions, with a rate of (%0), and for Instagram with (82) repetitions, with a rate of (%82). For TikTok, with (3) repetitions, with a rate of (%3), for YouTube, with (7) repetitions, with a rate of (%7), and for other sites with (0) repetitions, with a rate of (%0). It is clear from this that women use Instagram more than other websites as a result of its content, which abounds in pictures, short clips, and offers of cosmetics and accessories, and this is what women prefer, whether in the countryside or the city.

3.3.3. EXTENT OF USE

Table 6. shows the extent to which the respondents use social media

| Question | Category | Repetition | Ratio |
|--|----------------------|------------|-------|
| How much do you use social networking sites? | Once daily | 1 | 1 % |
| | More than once a day | 52 | 52 % |
| | Daily all week | 47 | 47 % |
| | Total | 100 | 100 % |

The results of the above table indicate that the researched sample uses social networking sites once a day at (1) repetitions at a rate of (%1), more than once a day at (52) repetitions at a rate of (%52), and daily throughout the week at a rate of (47)

repetitions at a rate of (%47), and we infer from that the researched sample who use social networking sites a lot.

3.3.4. TIM AVERAGE

Table 7. shows the time average spent by the sample on the use of social networking sites

| Question | Category | Repetition | Ratio |
|---|-------------------------|------------|-------|
| How much time do you spend using social networking sites? | Less than an hour a day | 4 | 4 % |
| | From 1-3 hours per day | 11 | 11 % |
| | From 4-6 hours | 10 | 10 % |
| | More than 6 hours | 17 | 17 % |
| | According to free time | 58 | 58 % |
| | Total | 100 | 100 % |

The results of the above table show that the sample spends time using social networking sites for less than an hour a day, at a rate of (4) repetitions, at a rate of (%4), and from (1-3) hours a day at a rate of (11) repetitions, at a rate of (%11), and from (4-6) hours a day with (10) repetitions, at a rate of (10%), and more than 6 hours per day, at a rate of (17) repetitions, at a rate of (%17), according to free time, at a rate of (58) repetitions, at a rate of (%58), and we conclude from this that the sample follows social networking sites when free time without specific time .

3.3.5. THE ROLE OF SOCIAL NETWORKING SITES

Table 8. shows the sample's opinion of social networking sites in promoting women's culture

| Question | Category | Repetition | Ratio |
|---|-----------|------------|-------|
| Do you think there is a role for social networking sites in promoting the culture of rural women and empowering them? | Yes | 75 | 75 % |
| | No | 2 | 2 % |
| | Sometimes | 23 | 23 % |
| | Total | 100 | 100 % |

The results of the above table indicate that the researched sample believes that there is a role for social networking sites in promoting the culture of rural women and empowering them for the category of yes by (75) repetitions (75%), for the category of No by (2) repetitions by (%2), and for the sometimes category by (23).) repetitions and by (%23), we infer from the results of table (9) that social networking sites have a role in promoting the culture of rural women and empowering them, this result is a good indication of the importance of the research topic, and the extent to which it was chosen accurately, and these sites were defined by the researchers as a group of pages that allow subscribers to participate in it by creating special pages via email

and phone number, and then linking it through an electronic system with other members, and the researcher agrees With this definition, what he sees is identical to the use way of social networking sites.²³

3.3.6. DEVELOPING RURAL WOMEN COGNITIVELY AND POLITICALLY

Table 9. shows the opinion of the sample on social networking sites to empower women cognitively and politically

| Question | Category | Repetition | Ratio |
|---|-----------|------------|-------|
| Does social networking sites have a role in empowering rural women cognitively and politically? | Yes | 70 | 70 % |
| | No | 2 | 2 % |
| | Sometimes | 27 | 27 % |
| | Total | 100 | 100 % |

The results of the above table indicate that social networking sites have a role in empowering rural women cognitively and politically, according to the opinion of the sample, by (70) frequency, by (70%), and those who do not see social networking sites as a role, according to the sample, by (2) repetitions, by (2%), and for the category sometimes by (27) repetitions at a rate of (70%), and we discern from that that social networking sites are of great importance in shaping knowledge and empowering women politically, and empowering women cognitively and politically means a set of information and ideas that women obtain through their environment, whether through education and the family or through her external environment, and the culture of women, is an awareness through which she forms multiple cognitive directions²⁴. It is the process by which women become able to acquire experiences in various fields in order to be able to manage their affairs in life²⁵.

²³ Abbas Mustafa Sadiq, New Media Concepts, Methods and Applications, Dar Al-Shorouk for Publishing and Printing, 2008, p. 218.

²⁴ Dr. Abdul Ghani Imad, Sociology of Culture, Center for Arab Unity Studies, Beirut, 2006, p. 37.

²⁵ Ministry of Planning, Central Statistical Agency, The Reality of Rural Women in Iraq, Central Agency Press, 2016, p. 2.

3.3.7. SOCIAL NETWORKING SITES AND WOMEN'S RELATIONSHIP WITH THEIR SOCIAL ENVIRONMENT

Table 10. shows the sample's opinion of social networking sites and the woman's relationship with her social environment

| Question | Category | Repetition | Ratio |
|---|-----------|------------|-------|
| Is there an effect of social networking sites on rural women's social relationship with their surroundings? | Yes | 47 | 47 % |
| | No | 15 | 15 % |
| | Sometimes | 38 | 38 % |
| | Total | 100 | 100 % |

The results of the above table of social networking sites show an impact on the relationship of rural women with their social environment for Yes category with (47) repetitions and at a rate of (%47), for the No category with (15) repetitions with a rate of (15%), and for the sometimes category with (38) repetitions with a rate of (%38) ,we conclude that social networking sites have an impact on women's relationship with their social environment as a result of addiction to these sites.

3.3.8. THE EFFECT OF SOCIAL NETWORKING SITES

Table 11. Shows the impact of social networking sites on rural women

| Question | Category | Repetition | Ratio |
|---|--------------|------------|-------|
| What is the impact of social networking sites on rural women? | Positive | 70 | 70 % |
| | Negative | 12 | 12 % |
| | I don't know | 18 | 18 % |
| | Total | 100 | 100 % |

The results of the above table show that social networking sites have a positive effect with a rate of (70) repetitions, with a rate of (70%), and a negative effect with a rate of (12) repetitions, with a rate of (12%). This result shows that social networking sites have a positive impact on rural women.

3.3.9. THE FAMILY'S FOLLOW-UP OF THE GIRLS' USE OF SOCIAL NETWORKING SITES

Table 12. shows the opinion of the sample regarding the follow-up of girls in the use of social sites or not.

| Question | Category | Repetition | Ratio |
|---|--------------|------------|-------|
| Do you encourage Iraqi families to follow girls when using social networking sites? | Yes | 71 | %71% |
| | No | 29 | 29 % |
| | I don't know | 0 | 0 % |
| | Total | 100 | 100 % |

The results of the above table indicate that the sample encourages the Iraqi families to follow- up girls when using social networking sites for the Yes category with a rate of (71) repetitions, and a rate of (71%), and those who do not encourage the follow-up of girls and a category of No with a rate of (29) repetitions, and a rate of (29%), and for the category of I do not know (0) repetitions, and at a rate of (0%). We discern from this that there is a danger when girls use social networking sites, according to what the sample indicated that it is necessary to follow up on girls' use of social networking sites.

3.3.10. THE HELP OF SOCIAL NETWORKING SITES FOR WOMEN

Table 13. shows the help of social networking sites for rural women.

| Question | Category | Repetition | Ratio |
|--|--------------|------------|-------|
| Did social networking sites help rural women to see the world around them and the outside? | Helped | 86 | 86 % |
| | Didn't help | 2 | 2 % |
| | I don't know | 12 | 12 % |
| | Total | 100 | 100 % |

The above results showed that social networking sites help rural women to learn about the outside world and their surroundings by (86) repetitions,, with a rate of (%86), and for a category that did not help, by (2) repetitions,, by (2%), and those who do not know from the sample by (12) repetitions, at a rate of (12%), and we are guided by that social networking sites have a role in informing rural women of their external environment, as a result of the wide spread of social networking sites and its importance in all surrounding countries, which made its content diverse and its users knowledgeable.

3.3.11. THE REASON FOR USING SOCIAL NETWORKING SITES

Table 14. Shows the reasons for the sample's use of social networking sites

| Question | Category | Repetition | Ratio |
|---|--|------------|---------|
| What are the reasons for your use of social networking sites? You can choose more than one alternative. | To communicate with friends | 78 | % 27.73 |
| | For leisure and entertainment | 62 | % 21.91 |
| | To get to know new people | 19 | % 6.17 |
| | To get the news | 44 | % 15.60 |
| | To enhance my culture and empower me politically | 42 | %14.84 |
| | To view the latest cosmetics and accessories | 37 | % 13.12 |
| | Total | 282 | 100 % |

The results of the above table indicate that the reasons for the researched sample's use of social networking sites are for the category of communication with friends with a rate of (78) repetitions, with a rate of (%27.73), and for the category of leisure and entertainment, with a (62) repetitions, with a rate of (%21.91), and for the category of getting to know new people with a rate of (19). repetitions with (%6.17), and for the category of obtaining news by (44) repetitions, with (%15.60), and for the category to promote the culture of the sample and its political empowerment by (42) repetitions, with (%14.84), and for the category of viewing the latest cosmetics and accessories by (37)) repetitions, at a rate of (%13.12), and we infer from that the use of social networking sites by the researched sample is multi-use, the most important of which is to communicate with friends.

3.3.12.SOCIAL NETWORKING SITES AND THEIR CONTRIBUTION TO CONVEYING THE VOICE OF WOMEN

Table 15. shows the extent to which communication sites contribute to conveying the voice of rural women and their suffering.

| Question | Category | Repetition | Ratio |
|---|-----------|------------|-------|
| Did social networking sites contribute to the voice of rural women and their suffering? | Yes | 79 | 79 % |
| | No | 17 | 17 % |
| | sometimes | 4 | 4 % |
| | Total | 100 | 100 % |

Through the above results, social networking sites contribute to conveying the voice of rural women and their suffering by (79) repetitions, at a rate of (79%), and these sites did not contribute to convey of their voice by (17) repetitions, at a rate of (17%), and for a category, the sites sometimes contribute by (4) repetitions, at a rate

of (4%), we can see from this that social networking sites contribute greatly to conveying women's voice and suffering.

3.3.13.THE NATURE OF USING THE NAME ON SOCIAL NETWORKING SITES

Table 16. shows the nature of the use of name by the sample in social networking sites

| Question | Category | Repetition | Ratio |
|---|----------|------------|-------|
| Do you use social networking sites by name? | Frank | 72 | 72 % |
| | Borrowed | 28 | 28 % |
| | Total | 100 | 100 % |

The above results indicate that the researched sample uses the real name on social networking sites with a rate of (72) repetitions, at a rate of (%72), and those who use a pseudonym at a rate of (28) repetitions, with (%28), and we infer from that that the largest percentage uses the real name, and this indicates on the acceptance of women's use of social networking sites in rural areas.

3.3.14.USE OF SITES AND CUSTOMS IN VILLAGES AND RURAL AREAS

Table 17. shows the sample's use of sites and the extent to which the rural community accepts it.

| Question | Category | Repetition | Ratio |
|--|-----------|------------|-------|
| Does the use of social networking sites by women violate the customs and traditions in your regions and affect their reputation? | Yes | 6 | 6 % |
| | No | 58 | 58 % |
| | sometimes | 36 | 36 % |
| | Total | 100 | 100 % |

The results of the above table show that the use of social networking sites in rural areas is considered by some to violate customs and traditions by (6) repetitions, and those who consider that the use of sites did not constitute a violation of traditions by (58) repetitions, with a rate of (%58), and for sometimes category by (36)) repetitions , with a rate of (%36), and we infer from that that the use of websites is no longer in violation of customs and traditions by rural women.

3.4. THE MOST IMPORTANT RESULTS:

1. The age group (18-28) topped the researched sample with a rate of (%82), and in the marital status, the single category topped the other categories, and its

percentage was (%78), and in academic achievement, the percentage of bachelors was (%74) of other certificates.

2. The sample uses social networking sites with (%86), and it is considered a heavy use of social sites.
3. The sample mentioned that they use Instagram with (%82), among other sites.
4. The sample confirmed that they use social networking sites more than once a day at a rate of (%52), and throughout the week daily at a rate of (%47).
5. The sample showed that the rate of using social networking sites according to free time was (%58).
6. The sample stated that social networking sites have a role in promoting the culture of rural women and empowering them by (%75).
7. The sample confirmed that social networking sites have a role in empowering rural women cognitively and politically at a rate of (%70).
8. The results revealed that there is an impact of social networking sites on rural women's social relationship with their surroundings by (47%).
9. The results showed that the impact of social networking sites on rural women was positive with (%70).
10. The results showed that the sample encourages Iraqi families to follow girls when using social networking sites with (%71).
11. The results showed that social networking sites helped rural women to learn about the surrounding and outside world with (%86).
12. The results revealed that the reasons for the sample's use of social networking sites to communicate with friends with (%27.73).
13. The sample confirmed that social networking sites contributed to conveying the voice of rural women and their suffering by (79%).
14. The sample mentioned that they use the real name in their personal accounts on social networking sites with (%72).
15. The sample indicated that the use of social networking sites by women is contrary to the customs and traditions of villages and rural areas and does not affect their reputation with (%58).

3.5. RECOMMENDATIONS:

According to the results of the research, the researcher recommends the following:

1. Developing social networking sites in terms of form and content to be in line with the aspirations of rural women.
2. Monitoring publications on social media that call for violence against women and rural women in particular.

3. Stopping the racial discrimination between men and women that is being raised on social networking sites.
4. Paying attention to the contents of social networking sites and making them more targeted and focused to serve rural women and to promote their culture and to develop and empower them intellectually and politically, since rural women follow social networking sites closely.
5. Follow-up of Iraqi families of young girls when using social networking sites because of their great influence on this class, as a result of the presence of undisciplined posts on it.
6. Do not use social networking sites all the time, as they cause addiction and social isolation.

REFERENCES

ARABIC AND TRANSLATED BOOKS

- (1) Mahmoud, K. W. (2011). **Social Networks and the Dynamics of Change in the Arab World.** Beirut, Lebanon: Dar Madrak.
- (2) Al-Dawy, I. A. (2015). **Social Networks, Arab Red Crescent and Red Cross Organization.**
- (3) Imad, A. G. (2006). **Sociology of Culture.** Beirut, Lebanon: Center for Arab Unity Studies.
- (4) Al-Mashhadani, S. S. (2017). **Media Research Methods.** United Arab Emirates: University Book House.
- (5) Qandilji, A. I., & Al-Najjar, H. R. (2015). **Information Science, Systems and Technologies.** Amman, Jordan: Dar Al-Masirah for Publishing, Distribution and Printing.
- (6) Qandilji, A. I. (2017). **Electronic Media.** Amman, Jordan: Dar Al Masirah.
- (7) Sadiq, A. M. (2008). **New Media Concepts, Methods and Applications.** Dar Al-Shorouk for Publishing and Printing.
- (8) Al-Faisal, A. A. (2014). **Studies in Electronic Media.** United Arab Emirates: University Book House.
- (9) Abdul Hamid, M. (2000). **Scientific Research in Media Studies.** Cairo, Egypt: World of Books.

THESES AND DISSERTATIONS

- (10) Awad, H. (2011). **The impact of social networking sites on the development of social responsibility among young people, the experience of the Allar Youth Council as a model.** *Al-Quds Open University, Social and Family Development Program.*
- (11) Maryam, G., & Shaoubi, N. A. (2014). **The impact of social networking sites on the development of political awareness among university students**

[Unpublished master's thesis]. *Kasdi Merbah University-Ouargla, Faculty of Humanities and Social Sciences, Department of Human Sciences, Department of Media and Communication Sciences.*

- (12) Athamna, N. (2017). **The Impact of Social Media Networks on the Social Values of University Students, A Field Study on a Sample of University of M'sila Students** [Unpublished master's thesis]. *Faculty of Humanities and Social Sciences, Department of Media and Communication Sciences, Mohamed Boudiaf University, M'sila, Algeria.*
- (13) Lakhal, H., & Zaidi, R. (2017). **The impact of using social networking sites on family relations, Facebook as a model** [Unpublished master's thesis]. *Zayan Ashour University, Djelfa, Faculty of Humanities and Social Sciences, Department of Sociology and Demography.*

PUBLISHED RESEARCH

- (14) Ministry of Planning, Central Statistical Agency. (2016). **The reality of rural women in Iraq.** *Central Agency Press.*
- (15) Tayeb, O. B. S. (2012). **Knowledge of social networks: A series of studies.** *King Abdulaziz University.*
- (16) Al-Rawi, B. J. (2012). **The role of social networking sites in change.** *Media Researcher Magazine*, (18), College of Information, University of Baghdad.
- (17) Zayed, H. F. (2018). **The role of advertisements and news on the websites of government institutions to facilitate the procedures of auditors, "Dhi Qar University as a model".** *Dhi Qar Journal of Arts.*

/18/

PARTICULATE MATTER LEVELS CLASSIFICATION USING MODIFIED AND COMBINED RESNET MODELS WITH LOW FEATURES EXTRACTION

Rayan Awni Matloob

University of Duhok, College of Engineering, Electrical and Computer
Department, Zakho Street 38, Kurdistan Region (Iraq).

<https://orcid.org/0000-0001-7406-8196>

Mohammed Ahmed Shakir*

University of Duhok, College of Engineering, Electrical and Computer
Department, Zakho Street 38, Kurdistan Region (Iraq)

Mohammed.shakir@uod.ac



Reception: 29/01/2023 **Acceptance:** 09/04/2023 **Publication:** 28/04/2023

Suggested citation:

A.M., Rayan and A.S., Mohammed. (2023). **Particulate Matter Levels Classification Using Modified and Combined ResNet Models with Low Features Extraction.** *3C TIC. Cuadernos de desarrollo aplicados a las TIC*, 12(1), 378-398. <https://doi.org/10.17993/3ctic.2023.121.378-398>

ABSTRACT

Smog is a serious environmental problem. It is an atmospheric pollutant that, if inhaled frequently, can lead to lung diseases such as asthma and bronchitis. One of the most dangerous air pollutants is particulate matter with a diameter of fewer than 2.5 micrometers (PM2.5), which may be breathed into the body and cause major health issues by introducing dangerous compounds deep into the lungs and bloodstream. In this research, a new convolutional neural network is proposed, by upgrading and parallelly stacking the two pre-trained models ResNet18 and ResNet50 to form a new modified-combined convolutional model (C-DCNN). Besides, we stacked another two columns of layers to extract the low features of ResNet18 and ResNet50 separately, to create finally four stacked columns of layers. The new model classifies images into different classes based on their PM2.5 concentration levels. To assess the suggested approach, an image augmentation is applied, then divided the images randomly (80% for the training progress, 20% of the used training data for validation, and 20% for testing). The experimental results demonstrate that the proposed method increased the accuracy of level estimation with an accuracy increment equal to (6.25% at LR=0.0007) compared to ResNet50.

KEYWORDS

Deep Learning, Combined Convolutional Neural Network, ResNet, Image Classification, Air Quality, Particulate Matter.

PAPER INDEX

ABSTRACT

KEYWORDS

1. INTRODUCTION

2. RELATED WORKS

2.1. COMPARISON WITH OTHER MACHINE LEARNING WORKS

3. CONTRIBUTIONS AND MATERIAL

3.1. CONTRIBUTIONS

3.2. DATASET AND AUGMENTATION

4. METHODOLOGY

4.1. TRANSFER LEARNING FOR TRAINING DEEP LEARNING MODELS

4.2. RESNET18 ARCHITECTURE

4.3. RESNET50 ARCHITECTURE

4.4. COMBINING MODELS AND ADDED LAYERS

4.4.1. DROPOUT LAYER

4.4.2. 2D MAX POOLING AND AVERAGE LAYERS

4.4.3. FLATTEN LAYER

4.4.4. LSTM LAYERS (LONG SHORT-TERM MEMORY)

5. EXPERIMENTATION SETTINGS

5.1. IMAGES CLASSIFICATION RESULTS

6. CONCLUSION AND FUTURE WORK

REFERENCES

1. INTRODUCTION

The act of polluting the air with toxins that are harmful to living beings and humans, or that degrade the environment or materials is referred to as "air pollution" [1]. Humans may suffer from sicknesses or allergies, or even pass away as a result of it. In addition, it can impact the built environment (as a result of factors like ozone depletion, climate change, or habitat degradation) as well as other living things like food crops and animals, such as acid rain [2]. With anthropogenic ozone and PM_{2.5} causing 2.1 million fatalities per year, outdoor air pollution from the combustion of fossil fuels alone is one of the leading causes of mortality in people [3, 4]. Particles or as also called Particulate matter are minute solid or liquid particles suspended in a gas, commonly known as (PM), atmospheric particulate matter (APM), or fine particles [4]. The 2.5 refers to the size range of particles. A particle considered to be PM_{2.5} has a diameter between 1 and 2.5 micrometers (which is about 1/30th of the width of a human hair) [3, 4]. Some of the biggest cities such as China and Taiwan installed PM_{2.5} monitoring stations, but due to the expensive and the required resources it is not always the best idea, due to the need of installing more than one station for the large cities due to coverage limitation. The use of deep learning to forecast air quality by picture classification or regression is one of the better methods in this sector. Image-based automated information extraction has been the subject of a lot of work in machine learning and computer vision. The use of the image is an efficient and easy method because of the widespread of smartphones and the ability of every person to capture an image whenever he wants and wherever he is. This study introduced an image-based PM_{2.5} analysis technique that uses a deep learning network to categorize the PM_{2.5} concentration levels of outdoor images. The method suggested in this study leverages the cutting-edge CNN algorithm for image analysis in contrast to image feature-based PM_{2.5} analysis methodologies. Due to the CNN's explicit end-to-end design and ability to automatically extract both low-level and high-level picture characteristics. The Shanghai dataset (1052 photos, one scene) from [5] was used to test our methodology. The rest of this study is divided into the following sections. We describe some earlier work on machine learning for image categorization in Section 2. We discuss the contributions of our study and the provisions relating to the experiments in Section 3 of this article. We provide our suggested approach to concatenated neural convolution networks in Section 4. The experimental findings in Section 5 demonstrate how well our strategy performed. In Section 6, we draw to a close this essay, and finally, the references in Section 7.

2. RELATED WORKS

In [6] they merged meteorological data and images to predict PM_{2.5} indices of outdoor photos, using support vector regression (SVR) and deep learning techniques. Their suggested approach employs two datasets gathered from Beijing and Shanghai city in China besides a constructed SVR model to integrate the PM_{2.5} predicted by the CNN with two meteorological parameters, wind speed, and humidity, to provide the expected outcomes towards the end of the PM_{2.5} index. For the Shanghai

dataset, the proposed model reduced the RMSE by 26.08% and the R-squared increased by 24.57%. For the Beijing dataset, the proposed model reduced the reduced RMSE by 5.27% to 56.03 and increased the R-squared by 8.4% to 0.6046.

The authors of [7], Using an ensemble of deep neural network-based regression, the researchers estimated the PM2.5 concentrations based on photos taken outside. Using a feedforward neural network and a dataset of 1460 pictures for performance analysis, they merged the PM2.5 predictions from three convolutional neural networks ResNet50, Inception-v3, and VGG-16, to generate the final PM2.5 forecast of the image. As a consequence of their experimental findings, which show that the meta trainer can effectively aggregate the PM2.5 predictions from base learners and provide a better prediction than any single base learner utilized, the suggested technique is suitable for monitoring PM2.5 pollution. Based on a study of a substantial number of outdoor pictures accessible for Beijing, Shanghai (China), and Phoenix, the researchers calculated PM air pollution. Six picture elements were taken from the photographs and combined with additional pertinent information, such as the sun's position, the date, the time, the location, and the weather, to forecast the PM2.5 index.

The researchers in [8], have proposed an image-based deep learning model (CNN-RC, under VGG schemes and ResNet with some layers). That combines a convolutional neural network with a regression classifier. By shots extraction feature and feature categorization into air quality categories. This model is capable of calculating the air quality at specified places. The models were tested after training on datasets, comprising different combinations of the current image, HSV (hue, saturation, value), characteristics, and the baseline image, to boost model dependability and estimation accuracy. The Linyuan air quality monitoring station in Kaohsiung City, Taiwan, collected a total of 3549 hourly air quality datasets, including images, PM2.5, and the air quality index (AQI), to quickly produce an accurate image-based estimation of multiple pollutants at once using just one deep learning model. According to their test findings, the estimation accuracy for R2 for PM2.5 using day (night) photos is 76%.

In the manuscript of [9], they integrated two deep convolutional neural networks (DCNNs) utilizing transfer learning to extract distinctive picture properties, running the previously trained Inception and Xceptions models concurrently. Before feeding the final fully linked layers for classification, the feature maps are merged and reduced by dropout. The system uses maximum likelihood and majority voting criteria to classify sub-images first, then the entire picture. Breast cancer is classified as having four tissue malignancy levels: invasive carcinoma, in situ carcinoma, benign, and normal. The experiments were conducted using the BACH, Breast Cancer Histology dataset, and they used 4800 photos to obtain an accuracy of roughly 95%.

2.1. COMPARISON WITH OTHER MACHINE LEARNING WORKS

Predicting the air quality using image-based machine learning has a huge role, as it reduces the dependence on the huge amount and expensive equipment. In addition to being available at hand, for ease of use by smartphone devices. The accuracy of

any image-based CNN model depends on the size of the used dataset (is it enough to learn the model or not?) and how good the model is for training correctly. Besides, the number of classes for classifying the problem at hand is important with the classification model. For the same dataset, increasing the number of classes used means decreasing the number of images in each class, which may reduce the accuracy or cause an overfitting problem. The results comparison demonstrates that the proposed new model significantly achieved reasonable accuracy increment compared to the ResNet50, despite the small dataset and the number of classes that are categorized by it. It is noteworthy that the used models in [6], and [9] have higher accuracy as they are owning a large number and a clear difference of images in the dataset. Any increment in the number of images per class has a significant effect on increasing the accuracy as clarified in.

3. CONTRIBUTIONS AND MATERIAL

3.1. CONTRIBUTIONS

The following is a summary of our work's significant contributions:

- This paper uses two pre-trained CNN models for air quality (PM2.5 levels) using one scene image. Instead of creating a new model and solving the issue of the little amount of accessible dataset, this study tries to improve the performance of learning.
- The main goal of this study is to provide a comprehensive classification that considers the following five categories of pollutants: Level 1, Level 2, Level 3, Level 4, and Level 5.
- This work develops a model based on parallel convolutional neural networks, to consolidate the machine learning training process. This architecture assembles the architecture of two conventional networks: ResNet18 and ResNet50 models.

As far as we are aware, no study has been done using ResNet18 and ResNet50 with their low features to show this design.

3.2. DATASET AND AUGMENTATION

With the use of the AQI index, the daily air quality is provided. It lets you know if the air is clean or dirty, and it alerts you to any potential health risks. The AQI focuses on potential health effects that may occur hours or days after inhaling polluted air. The four primary air pollutants specified by the Clean Air Act are used to calculate the AQI: carbon monoxide, sulfur dioxide, ground-level ozone, and particle pollution. The amount of air pollution and health concern is inversely correlated with the AQI value. This paper considered the air quality using photos taken at fixed locations in Shanghai [10] with its corresponding PM2.5 [11]. The images have been divided into five classes based on the number of micrograms (the mass or weight) per cubic meter of air as ($\mu\text{g}/\text{m}^3$), In this work, the level of PM2.5 images start with Level 1 class and a

concentration between (0 to 18.5) and end with the Level 5 class with concentrations greater than 59.9 as shown in Table (1)

Table 1. PM2.5 classes and concentration.

| Class Level | PM2.5 concentration (μg) |
|-------------|---------------------------------------|
| Level 1 | ≤ 18.4 |
| Level 2 | 18.5 - 30.4 |
| Level 3 | 30.5 - 40.4 |
| Level 4 | 40.5 - 59.9 |
| Level 5 | ≥ 60 |

The Shanghai PM2.5 dataset is available online through Figshare and contains about 1954 images with different air quality levels during daylight. The images are 389 by 584-pixel resolution. To use the images with ResNet, and as its first layer of size (224, 224, 3), we resized the image to fit the input layer. besides, for image augmentation, we flipped all the images horizontally to get a total image equal to 2104 images. The images number in each class are shown in Table (2), (some images are not considered to ensure data balancing between the classes). According to [12], using a pre-trained model, 150-500 images per class is sufficient to achieve reasonable classification accuracy (Reasonable, not the best).

Table 2. The number of images in each class.

| Class | No. of images |
|---------------------|---------------|
| Level 1 | 320 |
| Level 2 | 411 |
| Level 3 | 492 |
| Level 4 | 472 |
| Level 5 | 409 |
| All classes' images | 2104 |

4. METHODOLOGY

In this part, we presented a novel categorization scheme for air-quality photographs. The design is built on transfer learning by utilizing ResNet18 (Depth=18, layers =71, Size=44MB, Parameters =11.7 million, input size, 224, 224, 3) and ResNet50 (Depth=50, layers =177, Size=96MB, Parameters =25.6 million, input size, 224, 224, 3) and. The new proposed model consists of 260 layers and 35.4 million parameters, and its size is 249 MB. ResNet18 and ResNet50, two pre-trained convolutional neural networks, are upgraded and utilized without the final layers (fully connected, Softmax, and classification layers). Their role is to perform high-feature

extraction (dense presentations of the input images). This means, to this point, we will have two lines of stacked layers both starting with the input layers and ending with a ReLU layer, with some in between layers according to each model architecture. The ResNet18 and ResNet50 are upgraded then, by adding two important layers, (Flatten and LSTM layers). In addition to the two models, we stacked another two lines of layers called (Low_R18 and Low_R50) to extract the low image features from ResNet18 and ResNet50 respectively.

Low_R18, started by the ResNet18 layer number (18), while Low_R50, started by the ResNet50 layer number (36), with no layers in between for both. The Low_R18 and Low_R50 columns are designed by feeding them (from their starting layers) directly into a dropout layer with a probability equal to 0.5 to reduce the overfitting (A dropout layer randomly sets some input elements to zero with a given probability). Then to a “2-D max pooling” layers, with (pool size = 4,4, strid = 4,4. Each output of the “2-D max pooling” layer is fed to a 2-D average pooling layer with (pool size = 2,2, strid = 2,2). After that, we entered the output of both columns (Low_R18, and Low_R50) to a flattened layer, followed by Long short-term memory (LSTM) layer with several hidden units equal to (10). The two outputs of columns (ResNet18 and Low_R18) are added using an additional layer. Also, the two outputs of columns (ResNet50 and Low_R50) are added using another additional layer.

The outputs from the two additional layers are concatenated using the concatenation layer and passed again to another dropout layer with a probability of 0.5, and finally passed to the last dense layer followed by a Layer normalization layer.

The strategy's conceptual underpinnings include:

- Initial pre-processing for image resizing.
- Image augmentation with horizontal flip to the right.
- ResNet18 and ReNet50 upgrading.
- Low and high feature extraction based on transfer learning, by the newly added columns of layers (Low_18 and Low_50).

Figures (1 and 2), which depict the upper and bottom portions of the newly proposed model, respectively, exhibit the block diagram of the suggested technique. The suggested models and the added layers will be covered in detail in the sections below. The proposed model will add the high features of the modified ResNet18 with the low features of the ResNet18 after stacking some useful layers (Low_R18). And the same for ResNet50, it will add the high features of the modified ResNet50 with the low features of the ResNet50 after stacking some useful layers (Low_R50).

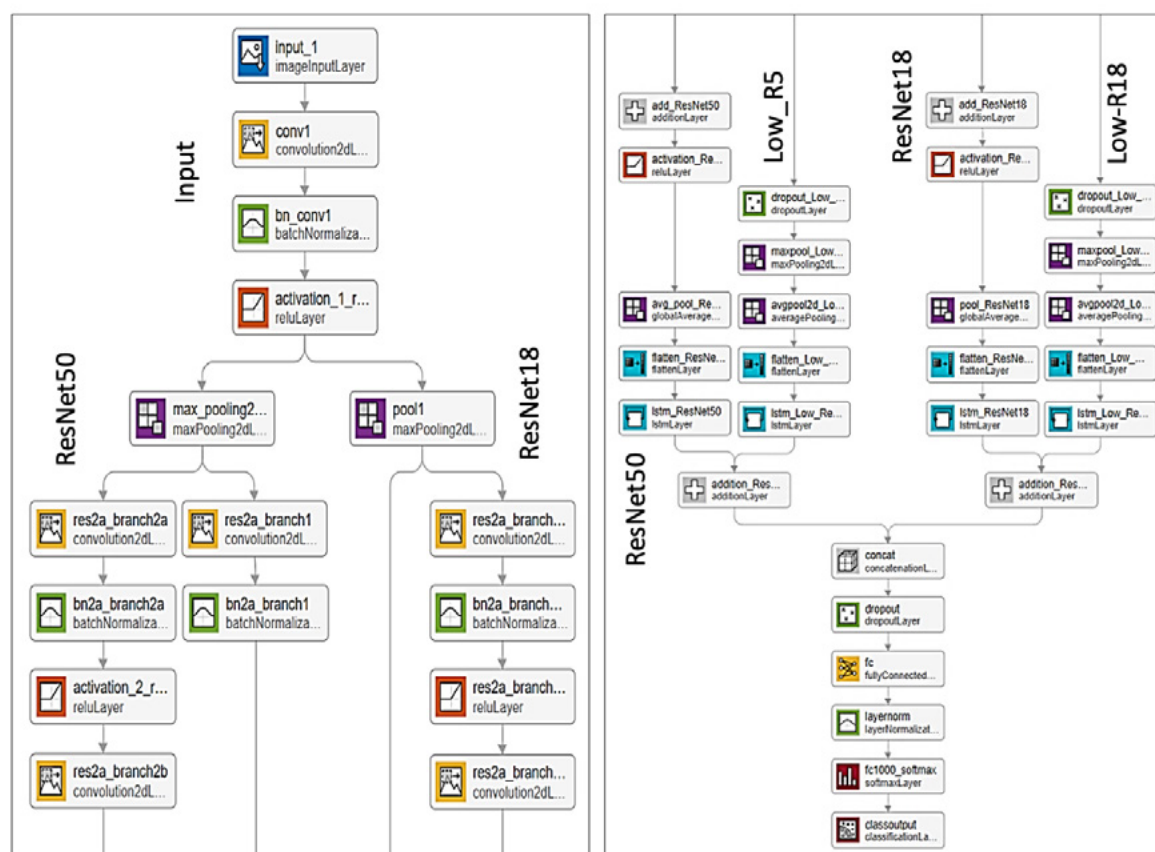


Figure 1. The upper layers of the new model **Figure 2.** The lower layers of the new model

4.1. TRANSFER LEARNING FOR TRAINING DEEP LEARNING MODELS

A model that has been trained for one job is utilized as a starting point for a model that completes a related task in the transfer learning method of deep learning [13]. Transfer learning may often update and retrain a network more quickly and easily than starting from scratch. Transfer learning is a well-liked approach because: It allows you to reuse well-liked models that have already been trained on huge datasets, allowing you to train models with less labeled data. Training and testing data for traditional machine learning often share the same input feature space and data distribution. The performance of a predictive learner may suffer when the distribution of data between training and test sets differs [14]. In some circumstances, it might be challenging and expensive to find training data that fits the test data's feature space and projected data distribution properties. A high-performance learner for a target domain is thus required, and it must be taught from a comparable source domain. The drive behind transfer learning is this. On the other hand, combined deep convolutional neural networks (C-DCNN) eliminate the requirement to extract complex features before training the classifier and allow for the learning of high-level and advanced features from the training dataset [9]. Convolutional layers for feature extraction give the classification system effective field knowledge. CNNs enable the reduction of the field knowledge required to create a classification system, followed by layer pooling. As a result, the approach's performance is less influenced by the dataset that was utilized,

and comparable network topologies can produce positive outcomes for a variety of issues. When used to estimate air quality, the C-DCNN has improved pollutant concentration predictions [15]. The performance of the created learning model heavily depends on the accessibility of the learning dataset. Due to their small datasets, certain classification problems cannot conduct the necessary deep learning. Additionally, data gathering is costly and may need a complex capture procedure and professional annotation. Transfer learning seeks to solve the dataset availability issue by using a pre-trained model on a sizable, labeled dataset of a generic context. To meet the new setting, only a minor training change is necessary [9]. The massive Imagenet dataset, which includes more than a million photos belonging to a thousand different object categories, is used to train ResNet50 and ResNet18. The accuracy of the two models on the Imagenet dataset is good. The following is a description of the two CNNs' structures:

4.2. RESNET18 ARCHITECTURE

ResNet18 has 18 layers with a 7x7 kernel as 1st layer. It has four layers of ConvNets that are identical. Each layer is made up of two residual blocks. Each block is made up of two weight layers with a skip connection connected to the output of the second weight layer with a ReLU. If the result is equal to the input of the ConvNet layer, then the identity connection is used. But, if the input is not similar to the output, then a convolutional pooling is done on the skip connection. ResNet18 also used two pooling layers throughout the network one at the network's inception and the other at its conclusion. The input size taken by it is (224, 224, 3), where 224 is the width and height, and 3 represents the RGB channel. The output is a fully connected layer that gives input to the sequential layer [16, 17].

4.3. RESNET50 ARCHITECTURE

ResNet-50 is a pre-trained model that won the 2015 ImageNet Large-Scale Visual Recognition Challenge (ILSVRC) competition. It was trained on a portion of the ImageNet database. The model can classify photos into 1000 item categories and is trained on more than a million photographs. It contains 177 layers in total, which corresponds to a 50-layer residual network (224, 224, 3) [18]. The ResNet architecture (figure 3) is considered to be among the most popular Convolutional Neural Network architectures around. Residual Networks (abbreviated ResNet) were first described by Xiangyu Zhang, Kaiming He, Jian Sun, and Shaoqing Ren in their 2015 computer vision research paper titled "Deep Residual Learning for Image Recognition" [18]. ResNet was later introduced by Microsoft Research in 2015 and set numerous records.

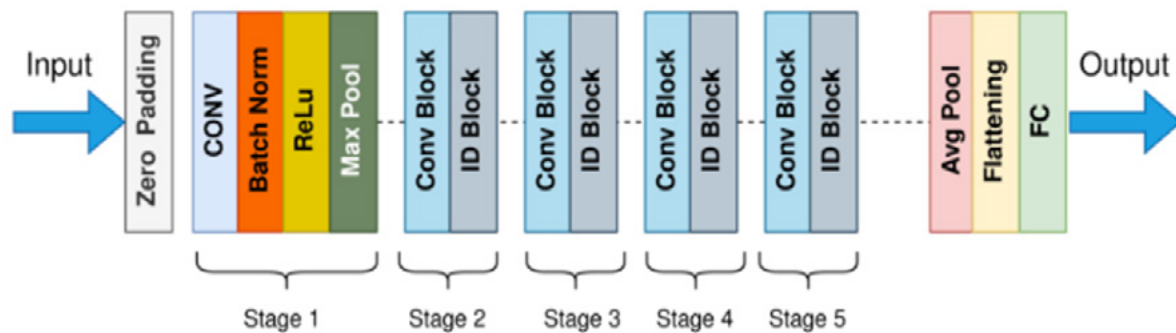


Figure3. ResNet architecture.

A significant drawback of convolutional neural networks is the "Vanishing Gradient Problem." Weights scarcely change as a result of the considerable fall in radiant value that occurs during backpropagation. ResNet is employed to get around this. It employs "SKIP CONNECTION," which, as illustrated in Figure (4) [18], adds the original input to the convolutional block's output. The authors of Xiao Tian [19] provide many common convolutional neural networks, including VGG16, VGG19, Inception, Xception, and ResNet50, which are utilized to determine the constellation's modulation pattern. Through trials, it has been shown that among other models, the ResNet50 network works best and has the greatest accuracy. Numerous more studies, including [20] and [21], demonstrate ResNet50's superior accuracy performance.

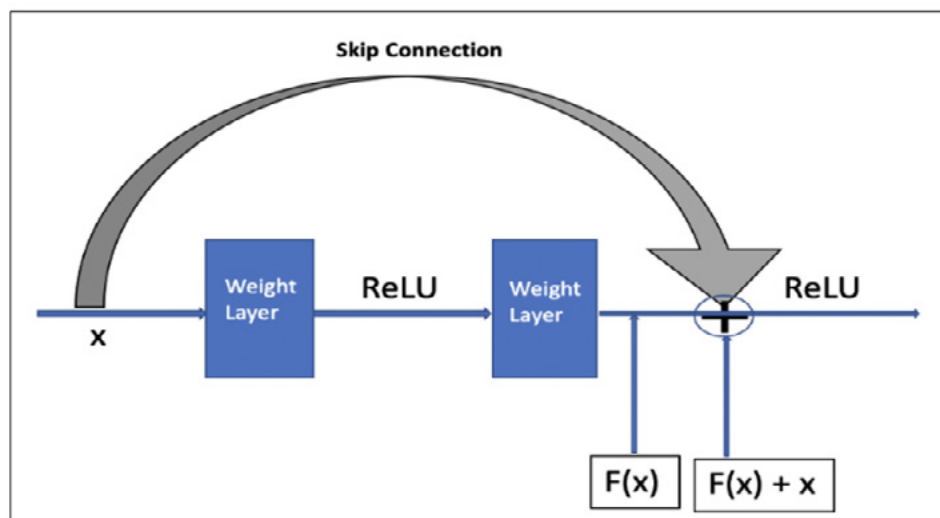


Figure 4. ResNet skip connection.

4.4.COMBINING MODELS AND ADDED LAYERS

Next in sections (4.4.1 to 4.4.5), we will describe the added layers to ResNet18 and ResNet50, and the layers added to extract the ResNet18 low features and ResNet50 low features (Low_R18 and Low_R50 respectively), to build the whole proposed model.

4.4.1. DROPOUT LAYER

Problems with training time and learning overfitting are frequent in deep learning, particularly in C-DCNN. Additionally, it costs a lot of computation to combine the outputs of several trained models [22]. To address these issues, the feature vector should be dropped out before being fed into the max pooling layers. Dropout [23] is a newly suggested regularizer to combat the overfitting problem. It is a regularization technique that stochastically adjusts the hidden unit activations for each training example to zero during training. Other stochastic model averaging techniques like stochastic pooling [24], drop-connect [25], and maxout networks [26] were influenced by dropout. The following figure (5) illustrates how the dropout layer affected the Low R50 and Low R18 input features.

Adding a dropout layer before the first max pooling layer row [27] demonstrate that sampling activation based on a multinomial distribution with an adjustable parameter p is equal to utilizing max-pooling dropout at training time (the retaining probability). This method, which is only carried out during training time, has a major impact on cutting down on training time and preventing overfitting. The following layer for columns (Low R50 and Low R18) is a max pooling layer based on that.

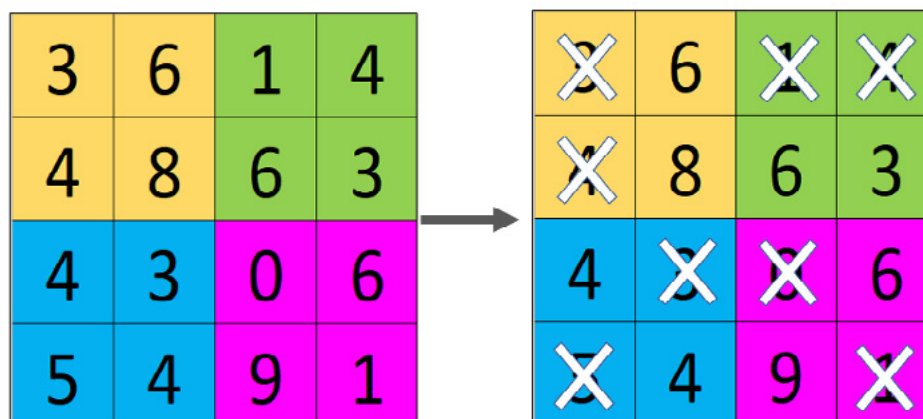


Figure 5. Dropout layer with probability = 0.5

4.4.2. 2D MAX POOLING AND AVERAGE LAYERS

The output feature vectors of each dropout are fed into a “2-D max pooling” row layer and symbolized as “maxPooling2dLayer”, with (pool size = 4,4, stride = 4,4). This layer is used to perform downsampling separately on columns (Low_R50 and Low_R18), by breaking the layer’s input into square or rectangle areas according to the pool size, then finding each area’s maximum value. The used pool size refers to the width and height of the rectangular regions and the stride represents the stride dimensions which is the steps that the rectangular region will move as shown in Figure (6).

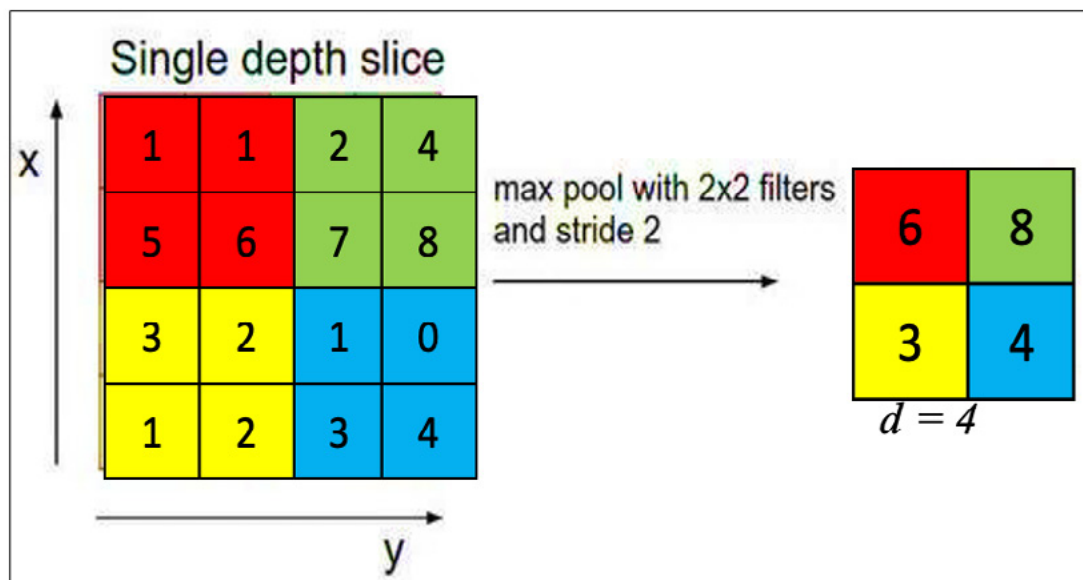


Figure 6. Max pooling layer.

The pooling zones overlap if the stride dimensions are smaller than the corresponding pooling dimensions [28]. To overcome this problem, we have to choose a size equal to or greater than the pooling size (in our model we used a stride size equal to the pooling size), to prevent the overfitting issue by reducing the number of parameters. Each $(x \times y)$ area represents a feature map, for example, the green area to the left of the figure is changed to a single number (the green area with the number '4' in the right of the figure tallied as the max of $[x \ y]$ values). The resultant feature is an array with d values, where d is the number of filters. Introduced in [28], maxPooling2dLayer provides a more accurate classification. Additionally, the Max pooling layer offers the key functionality (i.e., edges), Additionally, it is more adept at handling the extraction of the extreme characteristics. This implies that feature mapping truly uses all values [29].

The same is for the 2D average pooling layer shown in Figure (7) which downsamples the pooled area by splitting the features into the square area and calculating the average of that area.

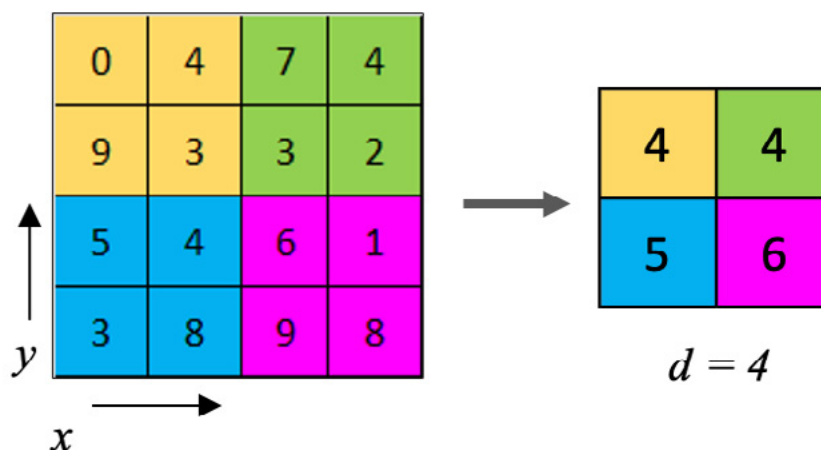


Figure 7. 2D average pooling layer.

4.4.3. FLATTEN LAYER

The square or rectangle input features are converted into a single dimension by a flattened layer since rectangular or cubic forms cannot be used as direct inputs (convert images to feature vectors). Figure (8) shows a flattened layer applied on a pooled feature map.

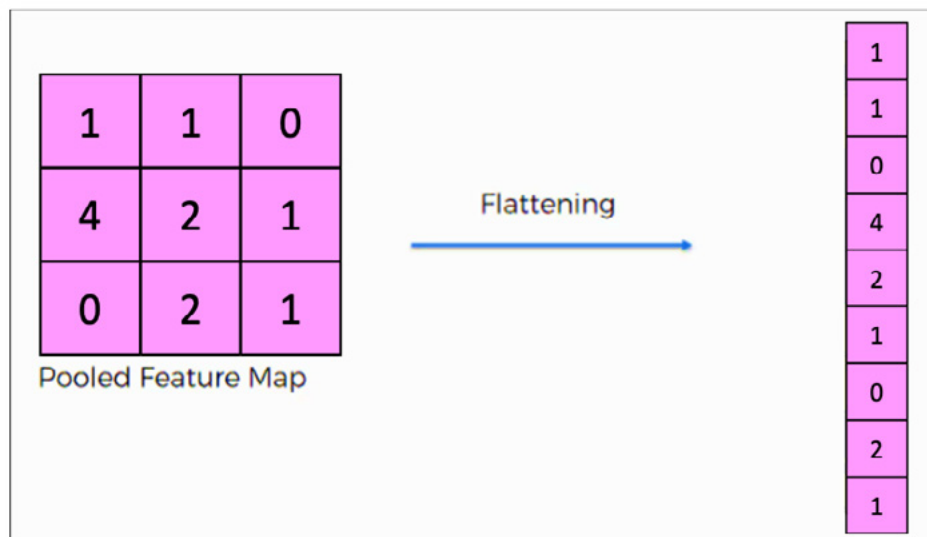


Figure 8. Applying a flattened layer.

The reason for flattening the intermediate outputs (feature maps) is: After the pooling layer, we will get a feature map with different heights and widths for each column as shown in the activation of Table (3), which is already obtained from images after passing through a lot of layers. Flatten layers allow us to add features of different lengths.

Table 3. Activations properties of each column.

| Column | Activations | After flattening |
|----------|-----------------------|------------------|
| ResNet50 | 1(S) x 1(S) x 2048(C) | 4048(C) |
| ResNet18 | 1(S) x 1(S) x 512(C) | 512(C) |
| Low_R18 | 7(S) x 7(S) x 256(C) | 12544(C) |
| Low_R50 | 7(S) x 7(S) x 64(C) | 3136(C) |

For our problem we have only five classes, so, we have to flatten the output of each pooling layer and pass through a neural network that has the number of output layers corresponding to the number of classes (5). In the imaging context, these are referred to as linear layers. In other words, the convolution layer acts as a feature extractor which helps a fully connected layer to do the task of classifying the images. A 1D array is used by these fully connected layers to carry out the categorization. To facilitate smooth 1D array operations, we flatten the data as we analyzed the images.

4.4.4. LSTM LAYERS (LONG SHORT-TERM MEMORY)

The long-term relationships between time steps in time series and sequence data are learned by an LSTM layer. The additive interactions carried out by this layer during training may aid in enhancing gradient flow over lengthy periods. Recurrent neural networks of the (LSTM) kind can learn order dependency in sequence prediction tasks, and complicated problem domains demand this behavior. It contains feedback connections, which means that aside from single data points like photos, it can interpret the complete sequence of data. The theory of LSTM is shown in the following figure (9).

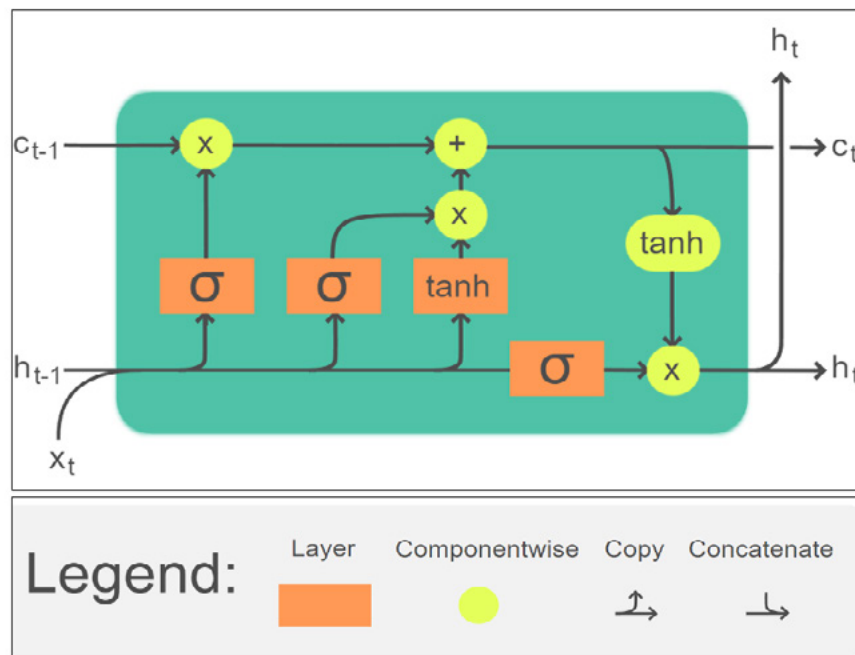


Figure 9. LSTM layer architecture

An important role in an LSTM model is played by a memory cell known as a "cell state" that maintains its state across time. The horizontal line that passes across the top of the aforementioned figure indicates the cell state. It may be seen as a conveyor belt across which data simply and unaltered passes. Information removal from or addition to the cell state is controlled by the LSTM layer gates. These gates could let data through and out of the cell. It has a sigmoid neural network layer and a pointwise multiplication operation that support the technique shown in Figure (10). The sigmoid layer generates numbers ranging from 0 to 1, where 0 denotes that nothing should be let through and 1 denotes that everything should be allowed through. Simple addition or multiplication operations that pass-through cell states are used by LSTM to make little changes to the data. The LSTM selectively forgets and recalls information in this way. The quantity of data remembered in between time steps (the hidden state) is configured to match the number of hidden units (10). Regardless of the duration of the series, the concealed state can contain data from every previous time step.

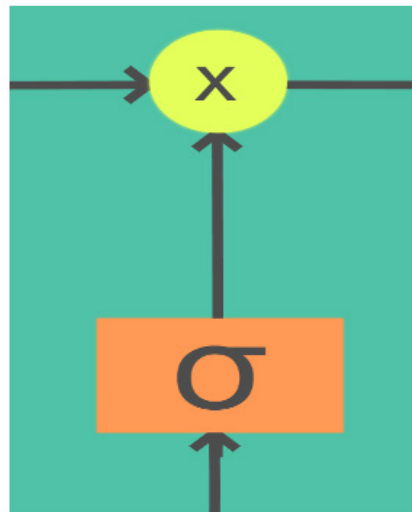


Figure 10. Multiplication operation and a sigmoid neural netlayer

4.4.5. DENSELY CONNECTED LAYERS

Finally, the output features of the concatenation layer are fed again to a dropout layer, then to a densely connected layer (fully connected layer) followed by a “layer normalization layer and”, then to a Softmax logistic regression layer. The reason behind using the layer normalization layer is to speed up the training of recurrent and multilayer perceptron neural networks and reduce the sensitivity to network initialization. After normalizing progress, the input to the layer is scaled with a factor γ called “learnable scale” and then it is shifted by the learnable offset β (which are left as their default values).

5. EXPERIMENTATION SETTINGS

The five classes are presented with several images as in Table (2). The images are in (.jpg) format and have a size of 389 by 584 pixels. Figure 11 highlights the variability of the five classes. Before the learning and classification steps, the input images are used directly after resizing them to (224, 224, 3), with no other previous filtering or pre-processing. The combination of the two models with the low features allows for achieving an improvement in air quality prediction by about 6.31% (with a learning rate $LR=0.0007$). The dataset was expanded through image data augmentation and obtained using Python programming language and achieved by flipping the images horizontally to one side only (right). We specified No special parameters in Matlab for image data augmentation. For columns (Low_R18 and Low_R50), a dropout of 0.5 is used to prevent the overfitting of the training process. Followed by two rows of 2D_max pooling and 2D average pooling layers. From this point, all the columns, then are passed to flatten layers to convert the features map into vector form followed by LSTM layers. The experiments were set with the following parameters (option of training): Solver for training network = sgd (use the stochastic gradient descent with momentum optimizer), This work, tried different learning rates (0.007, 0.0007, and 0.00007), with tested batch sizes equal to 10 and 60 epochs. The number of iterations per epoch was 149 of a total of 8940 iterations. The loss function

computes the cross-entropy loss between the labels and predictions for the training set and the validation set.



Figure 11. A variability of the five classes starting with Level 1, Level 2, Level 3, Level 4 and Level 5.

The proposed model is trained first on 80% of the dataset while 20% of the training data are used for the validation step and 20% for testing. That led to 65% of the data for training, 15% for validation, and 20% for testing. The statistics about the training, test, and validation for the sub-images datasets are detailed in Table (4).

Table 4. Datasets statistics for training, validation, and testing.

| Set | Percentage | No. of images |
|------------|------------|---------------|
| Training | 65 % | 1368 |
| Validation | 15 % | 316 |
| Test | 20 % | 420 |

The environment for the experiment used along with MATLAB R2022a is as follows:

- System Manufacturer: LENOVO LEGION5
- OS Name: Microsoft Windows 11 Home
- System Type: x64-based PC
- Processor: Intel(R) Core (TM) i7-10750H CPU @ 2.60GHz, 2592 Mhz, 6 Core(s), 12 Logical Processor(s)
- Installed Physical Memory (RAM): 16.0 GB

5.1. IMAGES CLASSIFICATION RESULTS

As the number of images is limited and too low, two pre-trained models are used. dataset augmentation, learning transfer, allows for to prevent or reduce the overfitting issue by dataset increasing and enhance the training process. The classes are created by splitting the utilized image dataset (each of size 389 by 584) into five classes each of size (224 by 224). The estimated level of the five sub-images classes is obtained using the presented deep model. In this paper, first, a zero-weight ResNet50 is used, to test a model that hasn't been trained before to show if using a small image dataset could achieve reasonable accuracy or not. It is found that the zero-weight ResNet50 could not exceed 28% of accuracy, whatever the learning rate

is. Then the pre-trained ResNet50 along with the three learning rates (LR= 0.007, 0.0007, and 0.00007) is applied, without any changes on its layers. It is found that the system achieved an average accuracy (tested three times with the same model options) equal to (68.61%, 70.86%, and 67.44% respectively with the LR). Also, the average accuracy using the test part of the image gave a close accuracy to the validation accuracy which is a clue that the system has not overfitted, as shown in Table (5).

Table 5. ResNet50 accuracies to LR.

| ResNet50 | | | |
|---------------|----------------------|----------------|-----------------|
| Learning rate | Avg. Validation acc. | Avg. test acc. | Avg. total time |
| 0.007 | 68.49 | 67.64 | 51.34 |
| 0.0007 | 70.92 | 70.88 | 54.59 |
| 0.00007 | 66.91 | 67.52 | 58.54 |

net50 achieved the best accuracy (70.86%) with LR = 0.0007 with an average time equal to 52 minutes and 85 seconds. Then the new model with the same previously mentioned training options is applied, three times on each of the three learning rates to calculate the average validation accuracy. The experimental results show that the new model can achieve an average validation accuracy equal to (72.92%, 77.17%, and 73.54% respectively with the LR= 0.007, 0.0007, and 0.00007) as shown in Table (6).

Table 6. The new model accuracies for LR.

| The New Proposed Model | | | |
|------------------------|----------------------|----------------|-----------------|
| Learning rate | Avg. Validation acc. | Avg. test acc. | Avg. total time |
| 0.007 | 72.92 | 71.88 | 82.84 |
| 0.0007 | 77.17 | 75.31 | 81.21 |
| 0.00007 | 73.54 | 73.27 | 88.41 |

The new model achieved the highest accuracy with LR=0.0007, it is also clear that the model has a test accuracy very close to the validation accuracies. Compared to a fresh model like the zero-weight ResNet50, the system achieved a very big jump in accuracy close to 50%. Compared to the pre-trained ResNet50, the new model achieved a reasonable increment in accuracy with about (6.31%) for the learning rate (0.0007), while it achieved about (4.31% and 6.1%) for learning rates (0.007 and 0.00007). From tables (5 and 6). it is noticed that the new model takes longer time for learning, which is because the new model has a higher number of layers and extracts the features four times.

6. CONCLUSION AND FUTURE WORK

In this work, a deep architecture for the classification of air quality based on PM2.5 concentration levels images is proposed. The new proposed model allows for the discrimination of the low and high features. Compared to existing research, the performance of our approach outperforms state-of-the-art methods. From the results, because the new models have a higher number of layers and extract the features four times, the new models take a longer time per epoch for learning. The new proposed model achieved an accuracy increment of about (6.31% at LR=0.0007), while it achieved (4.31% and 6.1% with LR=0.007 and 0.00007 respectively) as clarified in Tables (5 and 6). In the future, our approach can be extended by adding other models to the proposed one in this paper, or by utilizing other pre-trained models. Also, a multi-scene image dataset can be used next.

REFERENCES

- (1) Silva, L. F. O., Oliveira, M. L. S., Neckel, A., Maculan, L. S., Milanes, C. B., Bodah, B. W., & Dotto, G. L. (2022). **Effects of atmospheric pollutants on human health and deterioration of medieval historical architecture (North Africa, Tunisia)**. *Elsevier BV*. <https://doi.org/10.1016/j.uclim.2021.101046>
- (2) Brook, R. D., Brook, J. R., & Rajagopalan, S. (2003). **Air pollution: The “heart” of the problem**. *Springer Science and Business Media LLC*. <https://doi.org/10.1007/s11906-003-0008-y>
- (3) Landrigan, P. J. (2017). **Air pollution and health**. *Elsevier BV*. [https://doi.org/10.1016/s2468-2667\(16\)30023-8](https://doi.org/10.1016/s2468-2667(16)30023-8)
- (4) Zheng, S., Wu, X., Lichtfouse, E., & Wang, J. (2022). **High-resolution mapping of premature mortality induced by atmospheric particulate matter in China**. *Springer Science and Business Media LLC*. <https://doi.org/10.1007/s10311-022-01445-6>
- (5) Liu, C., Tsow, F., Zou, Y., & Tao, N. (2016). **Particle Pollution Estimation Based on Image Analysis (H. Liu, Ed.)**. *Public Library of Science (PLOS)*. <https://doi.org/10.1371/journal.pone.0145955>
- (6) Won, T., Eo, Y. D., Sung, H., Chong, K. S., Youn, J., & Lee, G. W. (2021). **Particulate Matter Estimation from Public Weather Data and Closed-Circuit Television Images**. *Springer Science and Business Media LLC*. <https://doi.org/10.1007/s12205-021-0865-4>
- (7) Rijal, N., Gutta, R. T., Cao, T., Lin, J., Bo, Q., & Zhang, J. (2018). **Ensemble of Deep Neural Networks for Estimating Particulate Matter from Images**. *Presented at the 2018 IEEE 3rd International Conference on Image, Vision and Computing (ICIVC)*. <https://doi.org/10.1109/icivc.2018.8492790>
- (8) Kow, P.-Y., Hsia, I.-W., Chang, L.-C., & Chang, F.-J. (2022). **Real-time image-based air quality estimation by deep learning neural networks**. *Elsevier BV*. <https://doi.org/10.1016/j.jenvman.2022.114560>
- (9) Elmannai, H., Hamdi, M., & AlGarni, A. (2021). **Deep Learning Models Combining for Breast Cancer Histopathology Image Classification**. *Springer Science and Business Media LLC*. <https://doi.org/10.2991/ijcis.d.210301.002>

- (10) Liu, Chenbin; Tsow, Francis; Zou, Yi; Tao, Nongjian (2016): **Particle pollution estimation based on image analysis**. *figshare. Figure*. <https://doi.org/10.6084/m9.figshare.1603556.v2>
- (11) Airnow.gov. (n.d.). **U.S. Embassies and Consulates - China - Shanghai**. Retrieved April 20, 2023, from [https://www.airnow.gov/international/us-embassies-and-consulates/#China\\$Shanghai](https://www.airnow.gov/international/us-embassies-and-consulates/#China$Shanghai)
- (12) Shahinfar, S., Meek, P., & Falzon, G. (2020). **“How many images do I need?” Understanding how sample size per class affects deep learning model performance metrics for balanced designs in autonomous wildlife monitoring**. *Elsevier BV*. <https://doi.org/10.1016/j.ecoinf.2020.101085>
- (13) Weiss, K., Khoshgoftaar, T. M., & Wang, D. (2016). **A survey of transfer learning**. *Springer Science and Business Media LLC*. <https://doi.org/10.1186/s40537-016-0043-6>
- (14) Shimodaira, H. (2000). **Improving predictive inference under covariate shift by weighting the log-likelihood function**. *Elsevier BV*. [https://doi.org/10.1016/S0378-3758\(00\)00115-4](https://doi.org/10.1016/S0378-3758(00)00115-4)
- (15) Gilik, A., Ogrenci, A. S., & Ozmen, A. (2021). **Air quality prediction using CNN+LSTM-based hybrid deep learning architecture**. *Springer Science and Business Media LLC*. <https://doi.org/10.1007/s11356-021-16227-w>
- (16) Ramirez, O. J. V., Cruz de la Cruz, J. E., & Machaca, W. A. M. (2021). **Agroindustrial Plant for the Classification of Hass Avocados in Real-Time with ResNet-18 Architecture**. *Presented at the 2021 5th International Conference on Robotics and Automation Sciences (ICRAS)*. <https://doi.org/10.1109/icras52289.2021.9476659>
- (17) Li, Y., Huang, J., & Luo, J. (2015). **Using user generated online photos to estimate and monitor air pollution in major cities**. *Presented at the ICIMCS '15: International Conference on Internet Multimedia Computing and Service*. <https://doi.org/10.1145/2808492.2808564>
- (18) He, K., Zhang, X., Ren, S., & Sun, J. (2016). **Deep Residual Learning for Image Recognition**. *Presented at the 2016 IEEE Conference on Computer Vision and Pattern Recognition (CVPR)*. <https://doi.org/10.1109/cvpr.2016.90>
- (19) Tian, X., & Chen, C. (2019). **Modulation Pattern Recognition Based on Resnet50 Neural Network**. *Presented at the 2019 IEEE 2nd International Conference on Information Communication and Signal Processing (ICICSP)*. <https://doi.org/10.1109/icicsp48821.2019.8958555>
- (20) Yang, X., Yang, D., & Huang, C. (2021). **An interactive prediction system of breast cancer based on ResNet50, chatbot and PyQt**. *Presented at the 2021 2nd International Seminar on Artificial Intelligence, Networking and Information Technology (AINIT)*. <https://doi.org/10.1109/ainit54228.2021.00068>
- (21) Kumar, D., Sharma, P., Anupama, A., & Sharma, P. (2022). **A Performance Study on Deep Learning Covid-19 Prediction through Chest X-Ray Image with ResNet50 Model**. *Presented at the 2022 Second International Conference on Advances in Electrical, Computing, Communication and Sustainable Technologies (ICAECT)*. <https://doi.org/10.1109/icaect54875.2022.9807920>

- (22) Garbin, C., Zhu, X., & Marques, O. (2020). **Dropout vs. batch normalization: an empirical study of their impact to deep learning**. *Springer Science and Business Media LLC*. <https://doi.org/10.1007/s11042-019-08453-9>
- (23) Hinton, G. E., Srivastava, N., Krizhevsky, A., Sutskever, I., & Salakhutdinov, R. R. (2012). **Improving neural networks by preventing co-adaptation of feature detectors (Version 1)**. *arXiv*. <https://doi.org/10.48550/ARXIV.1207.0580>
- (24) Zeiler, M. D., & Fergus, R. (2013). **Stochastic Pooling for Regularization of Deep Convolutional Neural Networks (Version 1)**. *arXiv*. <https://doi.org/10.48550/ARXIV.1301.3557>
- (25) Santos, C. F. G. dos, Roder, M., Passos, L. A., & Papa, J. P. (2022). **MaxDropoutV2: An Improved Method to Drop Out Neurons in Convolutional Neural Networks**. *Springer International Publishing*. https://doi.org/10.1007/978-3-031-04881-4_22
- (26) do Santos, C. F. G., Colombo, D., Roder, M., & Papa, J. P. (2021). **MaxDropout: Deep Neural Network Regularization Based on Maximum Output Values**. *Presented at the 2020 25th International Conference on Pattern Recognition (ICPR)*. <https://doi.org/10.1109/icpr48806.2021.9412733>
- (27) Wu, H., & Gu, X. (2015). **Max-Pooling Dropout for Regularization of Convolutional Neural Networks**. *Springer International Publishing*. https://doi.org/10.1007/978-3-319-26532-2_6
- (28) Fouad, M. M., Mostafa, E. M., & Elshafey, M. A. (2020). **Detection and localization enhancement for satellite images with small forgeries using modified GAN-based CNN structure**. *Universitas Ahmad Dahlan, Kampus 3*. <https://doi.org/10.26555/ijain.v6i3.548>
- (29) Ma, Z., Chang, D., Xie, J., Ding, Y., Wen, S., Li, X., ... Guo, J. (2019). **Fine-Grained Vehicle Classification With Channel Max Pooling Modified CNNs**. *Institute of Electrical and Electronics Engineers (IEEE)*. <https://doi.org/10.1109/tvt.2019.2899972>

